Energy, Mines and Resources Canada
Énergie, Mines et Ressources Canada

CANMET
Canada Centre for Mineral and Energy Technology
Centre canadien de la technologie des minéraux et de l'énergie

CANMET CONTRACT REPORT

No. ISQ83-00162

DEVELOPMENT OF A UNIFIED THEORY FOR PREDICTING THE BEHAVIOUR OF GLASSY WASTE PRODUCTS (FLY ASH, FUMED SILICA AND SLAGS) IN CONCRETE AND TO DEVELOP NEW COMPOSITIONS OF CONCRETE FOR OFFSHORE APPLICATIONS

Prepared by
M. van Roode and R.T. Hemmings
Materials Division
Glass and Ceramics Centre
Ontario Research Foundation

Work on this project was conducted under the auspices of the
Canada Centre for Mineral and Energy Technology,
Energy, Mines and Resources Canada

412 pp

MAR 3 1986
MICROMEDIA

JULY 1985

Canadä

DEVELOPMENT OF A UNIFIED THEORY FOR PREDICTING THE BEHAVIOUR OF GLASSY WASTE PRODUCTS (FLY ASH, FUMED SILICA AND SLAGS) IN CONCRETE AND TO DEVELOP NEW COMPOSITIONS OF CONCRETE FOR OFFSHORE APPLICATIONS

BY

M. van Roode and R.T. Hemmings
Materials Division
Glass and Ceramics Centre
Ontario Research Foundation

Work on this project was conducted under the auspices of the Canada Centre for Mineral and Energy Technology (CANMET), Energy, Mines and Resources Canada.

DSS FILE NUMBER	:	15SQ23440-3-9193
DSS CONTRACT SERIAL NUMBER	:	1SQ83-00162
CANMET PROJECT NUMBER	:	303702
CANMET SCIENTIFIC AUTHORITY	:	V.M. Malhotra and E. Douglas

1SQ
This report should be cited as Contract Report No.: ~~15Q~~83-00162

JULY 1985

MAR 3 1986
MICROMEDIA

412 pp

TABLE OF CONTENTS

Page

SUMMARY
1. INTRODUCTION 1
2. OBJECTIVES 2
3. MAJOR TASKS 2
4. LITERATURE ASSESSMENT 3
5. EXPERIMENTAL METHODS 4

5.1 Source Materials 4
5.2 Chemical Analysis of the Source Materials 4
5.3 Density Determinations 5
5.4 Particle Size Analysis - Wet Sieving 5
5.5 Particle Size Analysis - Sedigraph Analysis 5
5.6 Surface Area Analysis - Blaine 5
5.7 Surface Area Analysis - B.E.T. 5
5.8 X-Ray Powder Diffraction Measurements 6
5.9 Fourier Transform Infrared Spectroscopy 6
5.10 Optical Examination-McMaster Technique 6
5.11 Optical Examination - Image Analysis 7
5.12 Electron Optical Investigation 7
5.13 Model Glasses for X-Ray Diffraction 7
5.14 Preparation of Melilite and Merwinite for QXRD Studies 10
5.15 Preparation of Cordierite Glass and α-Cordierite for X-Ray Diffraction Studies 10
5.16 Preparation of Glassy and Redevitrified Analogues of Fly Ashes and Slags 10
5.17 Preparation of Model Glass for Hydration Studies 11
5.18 Hydration Studies 12

6. RESULTS 13

6.1 Chemical Analysis 13
6.2 Specific Gravity Determinations 13
6.3 Particle Size Analysis Wet Sieving 13

TABLE OF CONTENTS (contd)

Page

6.4 Particle Size Analysis - Sedigraph Analysis 13
6.5 Surface Area Analysis - Blaine 14
6.6 Surface Area Analysis - B.E.T. 14
6.7 Glass Content Methodology(1): Optical Examination-Image Analysis 14
6.8 Glass Content Methodology(2): Electron Optical Investigation 14
6.9 Glass Content Methodology(3): McMaster Technique 15

6.10 Glass Content Methodology(4): Quantitative X-Ray Diffraction Method (QXRD) 16
  6.10.1 Introduction 16
  6.10.2 Feasibility of Approach-Model Study on the Cordierite System 17
  6.10.3 The QXRD Method Applied to Fly Ashes - Rapid Scans 18
  6.10.4 Improvements to the QXRD Method 19
  6.10.5 The QXRD Method Applied to Blast Furnace Slags 24

6.11 Glass Content Methodology(5): Non-Crystalline Scattering Method (NCXRD) 25
  6.11.1 Introduction 25
  6.11.2 Feasibility of Approach-Model Study on the Cordierite System 25
  6.11.3 The QXRD Method Applied to Fly Ashes-Rapid Scans 26
  6.11.4 Improvements to the QXRD Method 27
    6.11.4.1 Cordierite System 27
    6.11.4.2 Fly Ashes and Slags 28

6.12 Glass Content Methodology(6): Differential Intensity Method (DIXRD) 28
  6.12.1 Introduction 28

TABLE OF CONTENTS (contd)

Page

6.12.2 Feasibility of Approach-Model Study on the Cordierite System 29
6.12.3 The DIXRD Method Applied to Wabamun Fly Ash 30

6.13 Glass Content Methodology(7): The Amorphous Hump Method (AHXRD) 31
6.14 Glass Content Methodology(8): Density Approach 32
6.15 Structural Evaluation Using X-Ray Diffraction 33
6.16 Fourier Transform Infrared (FTIR) Spectroscopy 33

6.17 Hydration Studies in H_2O 33
6.17.1 Studies on As-Received Fly Ashes and Slags 33
6.17.2 Particle Size Effect 33
6.17.3 Leaching of Glassy Analogues of Fly Ashes and Slags 34
6.17.4 Leaching of Redevitrified Analogues of Glassy Waste Materials 34
6.17.5 Leaching of Glasses 35
6.17.6 X-Ray Diffraction Patterns 36
6.17.7 Chemical Analysis of Leachates 37

6.18 Hydration Studies in NaOH 37

7. DISCUSSION 39

7.1 Chemical Analysis 39
7.2 Specific Gravity 40
7.3 Particle Size and Surface Area 40

7.4 Glass Content Methodologies 41
7.4.1 Introduction 41
7.4.2 Comparison of the QXRD and NCXRD Methods 42

TABLE OF CONTENTS (contd)

Page

7.5 Electron Optical Investigation 45

7.6 X-Ray Diffraction Studies 47
- 7.6.1 Introduction 47
- 7.6.2 Na_2O-SiO_2 Glasses and SiO_2 48
- 7.6.3 Na_2O-CaO-SiO_2, CaO-SiO_2, CaO-Al_2O_3 and CaO-Al_2O_3-SiO_2 Glasses 49
- 7.6.4 Commercial Glasses 49
- 7.6.5 Fly Ashes, Slags and Vitreous Analogues 49
- 7.6.6 Correlation of Results 51
- 7.6.7 Summary 55

7.7 Fourier Transform Infrared (FTIR) Spectroscopy 56
- 7.7.1 Introduction 56
- 7.7.2 FTIR Spectra of Fly Ashes and Slags 59
- 7.7.3 Summary 64

7.8 Hydration Studies in H_2O 64
- 7.8.1 Introduction 64
- 7.8.2 Studies on As-Received Fly Ashes and Slags 64
- 7.8.3 Particle Size Effect 70
- 7.8.4 Leaching of Glassy and Redevitrified Analogues of Fly Ashes and Slags 71
- 7.8.5 Leaching of Model Glasses 74

7.9 Hydration Studies in NaOH 74

8. SUMMARY AND CONCLUSIONS 76
9. RECOMMENDATIONS 80
10. ACKNOWLEDGEMENTS 83

References 84

TABLE OF CONTENTS (contd)

List of Tables

		Page
Table 1	Nucleation/Crystallization Parameters	87
Table 2	Composition of Fly Ashes and Granulated Blast Furnace Slags	88
Table 3	Specific Gravities of the Source Materials	89
Table 4	Densities, Particle Sizes and Surface Areas of the Source Materials	90
Table 5	Particle Size Distribution by Sedigraph Analysis - Numerical data accompanying the Sedigraph traces of Figure 1	91
Table 6	Comparison of Concentrations of Selected Oxides from SEM/EDXA Analysis and Chemical Analysis	103
Table 7	EDXA Oxide Analysis of Wabamun Fly Ash in Cross-Section	104
Table 8	Results of Modified McMaster Individual Particle Analysis on Standard and Atlantic Slags	105
Table 9	Mineralogy of Canadian Fly Ashes and Slags	106
Table 10	X-ray Data for 4 Crystalline Phases and NaCl	107
Table 11	Intensity Ratios for Four Phases and NaCl	108
Table 12	The Crystalline and Glass Content of Seven Canadian Fly Ashes	109
Table 13	Contents of Crystalline Phases and Glass in Seven Canadian Fly Ashes	116
Table 14	Settling Parameters	117
Table 15	Composition of Mixtures (in.g) Prepared for the Standard Curves	118
Table 16	Peaks Scanned for the Standard Curves	119
Table 17	α-Quartz Content of 8 Canadian Fly Ashes	120
Table 18	Mullite Content of 8 Canadian Fly Ashes	122
Table 19	Magnetite Content of 8 Canadian Fly Ashes	124
Table 20	Hematite Content of Canadian Fly Ashes	126
Table 21	Crystalline and Glass Content of 8 Canadian Fly Ashes	128
Table 22	Composition of the Mixtures (in.g) Prepared for Standard Curves for Melilite and Merwinite	129

ORF

TABLE OF CONTENTS (contd)

Page

List of Tables (contd)

Table 23 Peaks Scanned for the Standard Curves for Melilite and Merwinite 130

Table 24 Crystalline and Glass Contents of 2 Glast Furnace Slags 131

Table 25 XRD Data for Cordierite Non-Crystalline Scattering Method 132

Table 26 XRD Data for Wabamun Fly Ash (Non-Crystalline Scattering Method) 133

Table 27 XRD Data for Sundance Fly Ash (Non-Crystalline Scattering Method) 134

Table 28 XRD Data for Forestburg Fly Ash (Non-Crystalline Scattering Method) 135

Table 29 XRD Data for Nanticoke Fly Ash (Non-Crystalline Scattering Method) 136

Table 30 XRD Data for Lakeview Fly Ash (Non-Crystalline Scattering Method) 137

Table 31 XRD Data for Lingan Fly Ash (Non-Crystalline Scattering Method) 138

Table 32 XRD Data for Estevan Fly Ash (Non-Crystalline Scattering Method) 139

Table 33 XRD Data for Thunder Bay Fly Ash (Non-Crystalline Scattering Method) 140

Table 34 XRD Data for Standard Slag (Non-Crystalline Scattering Method) 141

Table 35 XRD Data for Atlantic Slag (Non-Crystalline Scattering Method) 142

Table 36 Scattering Intensities of Cordierite Glass (I_a), α-Cordierite (I_c) and a Mixture of 20% Cordierite Glass and 80% of α-Cordierite (I_u) 143

Table 37 Scattering Intensities of Cordierite Glass (I_a), α-Cordierite (I_c) and a Mixture of 70% Cordierite Glass and 30% of α-Cordierite (I_u) 145

TABLE OF CONTENTS (contd)

Page

List of Tables (contd)

Table 38 Scattering Intensities of Wabamun Fly Ash Glass (I_a), its Redevitrified Analogue (I_u) and Wabamun Fly Ash (I_u) 147

Table 39 Glass Contents Determined with the Differential Intensity Method 149

Table 40 Specific Gravities of Three Fly Ashes and Analogues Determined by Pycnometry 150

Table 41 Composition (wt.%) and Diffraction Maxima ($2\Theta_{Imax}$) of Glasses 151

Table 42 Composition (wt.%) and Diffraction Maximum ($2\Theta_{Imax}$) of Commercial Glasses 152

Table 43 XRD $2\Theta_{Imax}$ for 9 Fly Ashes, 2 Slags and Their Glassy Analogues 153

Table 44 Mass Changes Observed for Fly Ashes and Slags after Leaching for 24 hrs in Deionized Distilled H_2O 154

Table 45 Summary of Observations Made During Leaching of Fly Ashes and Slags 156

Table 46 Mass Changes Observed in Various Derived Materials During Leaching in Deionized H_2O 157

Table 47 Summary of Observations Made During Leaching of Fly Ash and Slag Derivatives 159

Table 48 Chemical Compositions of Five Model Glasses 160

Table 49 XRD Patterns of Selected Materials Subjected to Leaching in Deionized Water 161

Table 50 Results of DCP Analysis on Leaching Solutions of 1.00 g of Wabamun Fly Ash 162

Table 51 Glass Content Values (%) Determined by Various Methods 163

Table 52 Regions of Absorption (cm^{-1}) Corresponding to Metal-Oxygen Stretching for Tetrahedral and Octahedral Co-ordination 164

Table 53 Vibrational Frequencies (cm^{-1}) of Atomic Groups in Minerals Containing Oxygen 165

TABLE OF CONTENTS (contd)

Page

List of Tables (contd)

Table 54 Intensity Maximum of the 1300-750 cm^{-1} Band and Modifier Contents 166

Table 55 Leaching in H_2O: Correlation Between pH and Compositional Parameters or Physical Properties 167

List of Figures

Figure 1 Particle Size Distribution by Sedigraph Analysis - Sedigraph Traces (a)-(k) 168

Figure 2 Particle Size Distribution by Sedigraph Analysis - Histograms (a)-(k) 180

Figure 3 Optical micrograph (mag. 137x) of a Wabamun fly ash sample in an Elvacite medium 192

Figure 4(a) SEM micrograph of Wabamun fly ash in an Elvacite medium (mag. 20μ) 193

Figure 4(b) Detail of 4(a) (mag. 10μ) 193

Figure 5 EDXA analysis for selective locations (A-H) on Figure 4(a) 194

Figure 6 Cross section of Wabamun fly ash after ion etching 203

Figure 7 Cross section of Wabamun fly ash after ion etching 204

Figure 8 SEM micrograph of location 3 in Figure 7 at higher magnification 205

Figure 9 SEM micrograph of a plerosphere 206

Figure 10 SEM micrograph of location 4 in Figure 7 at higher magnification 207

Figure 11 XRD patterns for cordierite glass-α-cordierite mixtures for glass content determination 208

Figure 12 Intensity ratios for cordierite glass-α-cordierite mixtures vs. glass content 209

Figure 13 Standard curve for α-quartz (a)-(f) 210

Figure 14 Standard curve for Mullite (a)-(h) 216

TABLE OF CONTENTS (contd)

Page

List of Figures (contd)

Figure 15 Standard curve for Magnetite (a)-(f) 224

Figure 16 Standard curve for Hematite (a)-(f) 230

Figure 17 Standard curve for Melilite 236

Figure 18 Standard curve for Merwinite (a)-(d) 237

Figure 19 XRD patterns for cordierite glass-α-cordierite mixtures for glass content determination 241

Figure 20 Intensity ratio of glassy halo at 24^0 2θ vs. glass content for cordierite glass-α-cordierite mixtures 242

Figure 21 XRD patterns of mixtures of Vitrified and redivitrified Forestburg fly ash 243

Figure 22 Intensity ratio of glassy halo at 25^0 2θ vs. glass content for Forestburg glass and redevitrified glass mixtures 244

Figure 23 Scattering intensity vs. glass content for cordierite glass 245

Figure 24 Scattering intensity vs. glass content for Wabamun fly ash 246

Figure 25 Scattering intensity vs. glass content for Sundance fly ash 247

Figure 26 Scattering intensity vs. glass content for Forestburg fly ash 248

Figure 27 Scattering intensity vs. glass content for Nanticoke fly ash 249

Figure 28 Scattering intensity vs. glass content for Lakeview fly ash 250

Figure 29 Scattering intensity vs. glass content for Lingan fly ash 251

Figure 30 Scattering intensity vs. glass content for Estevan fly ash 252

Figure 31 Scattering intensity vs. glass content for Thunder Bay fly ash 253

ORF

TABLE OF CONTENTS (contd)

List of Figures (contd)

		Page
Figure 32	Scattering intensity vs. glass content for Standard slag	254
Figure 33	Scattering intensity vs. glass content for Atlantic slag	255
Figure 34	I_u-I_a for the 20% cordierite glass/80% α-cordierite mixture	256
Figure 35	I_u-I_a vs. I_c-I_a for the 70% cordierite glass/ 30% α-cordierite mixture	257
Figure 36	Reconstructed XRD scans for the cordierite system	258
Figure 37	I_u-I_a vs. I_c-I_a for Wabamun fly ash	259
Figure 38	Reconstituted XRD scans for the Wabamun fly ash	260
Figure 39	Intensity ratio of amorphous hump vs. NaCl standard	261
Figure 40	X-ray diffraction patterns of glasses in Na_2O-SiO_2 system	262
Figure 41	X-ray diffraction patterns of glasses in $Na_2O-CaO-SiO_2$ and other systems	263
Figure 42	X-ray diffraction patterns of some commercial glasses	264
Figure 43	FTIR spectra of fly ashes and slags	265
Figure 44	FTIR spectrum of Sundance fly ash in the 4000-400cm^{-1} range	266
Figure 45	pH vs. time curves for the leaching of fly ashes and slags in dionized distilled H_2O	267
Figure 46	pH vs. time curve for two fly ashes of different particle size ranges	270
Figure 47	pH vs. time curves for the leaching of glassy analogues of fly ashes and slags	271
Figure 48	pH vs. time curves of redevitrified analogues of fly ashes and one slag	273
Figure 49	pH vs. time curves for nucleated and crystallized Wabamun glass	275

ORF

TABLE OF CONTENTS (contd)

Page

List of Figures (contd)

Figure 50	pH vs. time curves of synthetic glasses with compositions similar to those of the glassy phases of five fly ashes	276
Figure 51	XRD pattern of leached Sundance fly ash glass	277
Figure 52	XRD patterns of Wabamun fly ash glass	278
Figure 53	pH vs. time curves for Wabamun and Dalhousie fly ashes and Standard slag (a)-(e)	279
Figure 54	Positions of glass X-ray maxima vs. analytical CaO contents for 16 fly ashes	284
Figure 55	2θ maxima for the Na_2O-SiO_2 glasses	285

APPENDIX A: Minutes of the Meeting of the Steering Committee held January 16, 1984
APPENDIX B: Work Statement
APPENDIX C: Literature Assessment

SUMMARY

Nine Canadian fly ashes and two blast-furnace slags have been characterized by chemical and mineralogical composition, density, particle size distribution surface area, glass content and their structures have been investigated with X-ray powder diffraction and Fourier Transform Infrared Spectroscopy. Hydration studies have been carried out in deionized H_2O and aqueous NaOH solutions.

A literature assessment was carried out which included chapters on Sources, Availability and Compositions of Glassy Waste Materials, Glass Content Methodology, and Hydration Kinetics and Mechanisms of Glassy Waste Materials. On the basis of this assessment nine techniques were identified which could be potentially useful for the determination of glass content. Five of these nine techniques have been investigated for their applicability.

Chemical analysis gave CaO levels from 1.29 - 13.0%, SiO_2 levels from 37.1 - 58.6% and Al_2O_3 levels from 12.3 - 23.2% for the fly ashes. The CaO level of the slags were 35.1 and 40.1% respectively. B.E.T. surface areas ranged from 0.4 - 4.4 $m^2.g^{-1}$, Blaine surface areas were ~0.2 $m^2.g^{-1}$. B.E.T. (Krypton) was found to give surface areas which would be more meaningful for hydration studies. The average particle size was found to be between 5.2 and 20.0 μm.

Quantitative X-ray diffraction (QXRD) gave glass content values in the 53.5 - 94.5% range while Non-Crystalline Scattering X-Ray Diffraction (NCXRD) gave glass content values from 42.8 - 99.3%. The average over the two techniques was in the 65.6 - 86.9% range.

Electron optical examination in conjunction with energy dispersive X-ray analysis (SEM/EDXA) indicated the presence of four different particle types and substantial compositional variation between particles and to a lesser extent within a particle.

X-ray diffraction studies on model glasses showed the presence of two diffraction maxima for most compositions. It was proposed that a change in the relative intensities of the scattering at these two maxima is responsible for the sudden shift in the amorphous halo fly ashes with high CaO content (>20%) reported by Diamond.

FTIR spectroscopy showed an inverse relationship between the frequency maximum of the dominant silicate-aluminate stretch and the total matrix modifier content. The implications for the reactivity of the glassy waste materials have been discussed.

Preliminary hydration studies in deionized H_2O showed that most glassy waste materials exhibited a rapid rise in pH to alkaline values followed by a decline. A correlation between maximum pH and $\sum(SiO_2 + 2Al_2O_3)$ was observed. A high-Fe fly ash showed a drop in pH to acidic values. The implications for alkalie-aggregate reactivity have been discussed.

ORF

1. INTRODUCTION

The development of new concrete compositions that can better withstand the impact of the severe climatic conditions of Canada's offshore and Arctic regions is a mandatory task if this country is to move closer to self-sufficiency in its energy requirements in the years ahead. It is with this objective in mind that Energy, Mines and Resources Canada (CANMET) has supported the present program that would enhance the understanding of the fundamental processes involved in the formation of high performance concrete using admixtures of fly ash, silica fume or slags.

It has been known for some time that these industrial by-products impart desirable properties such as increased mechanical strength and durability and it is believed that the glassy nature of these waste materials is largely responsible for the observed performance characteristics. However, a theoretical basis for these observations is lacking. The program entitled "Development of a Unified Theory for Predicting the Behaviour of Glassy Waste Products (Fly Ash, Silica Fume and Slags) in Concrete and to Develop New Compositions of Concrete for Offshore Applications" (DSS File No. 15SQ.23440-3-9193, DSS Contract No. 1SQ83-00162) was initiated to study the properties of these waste materials and their role in concrete formation. The data obtained during this program would provide the basis for a theoretical frame-work which would explain the hydration kinetics of the glassy waste materials from a unified perspective.

Phase I of the program was initiated in November 1983 and was completed in December 1984. The investigations carried out during that period focussed on a characterization of nine Canadian fly ashes and two blast furnace slags to provide base data for subsequent hydration studies. The emphasis of the research effort was on the development of glass content methodology in the belief that both the concentration and nature of the glass are crucial for a unified understanding of the waste materials in concrete formation.

The results of these investigations which include the in-depth development of two X-ray diffraction methods for glass content determinations are discussed in this final report for the preliminary program.

2. OBJECTIVES

The overall objectives of the program are summarized as follows:

(i) To develop a unified theory to predict the behaviour of glassy waste products (fly ash, silica fume, and slags).

(ii) On the basis of the formulated theory, to develop new compositions of concrete for offshore and other marine applications.

The specific objective of the first phase is to study the kinetics and mechanism pertaining to the reaction of glassy waste materials with leaching agents including water, alkalies, and other solutions.

3. MAJOR TASKS

The major tasks shown below were agreed upon during the Steering Committee Meeting for the project held January 16, 1984.

(a) The determination of the glassy content of the waste material.

(b) The determination of the composition and structure of the glassy portion of the waste material.

(c) A study of the hydration behaviour of synthetic analogues of the waste material.

(d) A study of hydration kinetics, mechanisms and energetics of the glassy waste material.

A review of the progress on the project on September 21, 1984, led to the recommendation that the efforts during the remainder of the program be fully directed towards glass content methodology assessment and development.

The minutes of the review meetings are attached as Appendix A. The work statement for the program based on the directions provided at the meeting of January 16, 1984, is given in Appendix B.

4. LITERATURE ASSESSMENT

A literature review and assessment was carried out consisting of the following chapters:

1. Sources, Availability and Compositions of Glassy Waste Materials.
2. Glass Content Methodology.
3. Hydration Kinetics and Mechanisms of Glassy Waste Materials.

The literature assessment is attached to this report as Appendix C.

5. EXPERIMENTAL METHODS

5.1 Source Materials

Seven Canadian fly ashes labelled Wabamun, Sundance, Forestburg, Nanticoke, Lakeview, Lingan and Dalhousie, blended and homogenized under the supervision of Dr. G. Carette of Energy, Mines and Resources Canada (CANMET), were shipped in quantities of about 100 lbs to ORF in early February, 1984. Two additional fly ashes labelled Estevan and Thunder Bay and two granulated blast-furnace slags labelled Standard and Atlantic were procured with the assistance of R. Suderman of Canada Cement Lafarge Co. in May, 1984. Quantities of about 5 lbs were received for each of the source materials of the second shipment. These samples were grab samples that were rehomogenized prior to shipment.

5.2 Chemical Analysis of the Source Materials

The seven Canadian fly ashes received directly from EMR-CANMET were sent for chemical analysis to X-Ray Assay Laboratories of Mississauga. The analysis was performed as follows: Na_2O, MgO, Al_2O_3, SiO_2, P_2O_5, K_2O, CaO, TiO_2, Fe_2O_3, Cr_2O_3 and MnO_2 by X-ray fluorescence (XRF); B_2O_3, PbO and ZnO by Direct Current Plasma (DCP); SO_3 by a wet technique. The loss on ignition (LOI) was also determined.

The second set of raw materials (two fly ashes and one blast furnace slag) was also analyzed by X-Ray Assay Laboratories. XRF analysis was carried out for Na_2O, MgO, Al_2O_3, SiO_2, P_2O_5, K_2O, CaO, TiO_2, Fe_2O_3 and MnO. Loss on ignition (LOI) values were also determined for this set.

Total carbon content determination for all samples was carried out by the LECO technique.

Chemical analysis of fly ash leaching solutions was carried out by DC plasma emission spectrophotometry.

5.3 Density Determinations

Specific gravities of the source materials were determined by pycnometry and by the Le Chatelier method. The specific gravities were determined on "as-received" samples and on samples ground for 30 min. in an automatic grinder.

5.4 Particle Size Analysis - Wet Sieving

Particle size analysis by wet sieving was carried out as follows. The source materials were rehomogenized prior to testing. A mass of 10g of each sample was washed with distilled water until no more fines were passed through a 45 µm sieve. The percentage by mass retained on the 45 µm sieve was calculated.

5.5 Particle Size Analysis - Sedigraph Analysis

The source materials were analyzed for particle size analysis (by mass) using a Sedigraph 5000D which employs the X-ray sedimentation technique. Densities used were determined by pycnometry. Due to the presence of some magnetic material a glass stir rod arrangement was used to ensure sample homogeneity.

5.6 Surface Area Analysis - Blaine

Blaine surface area analysis was carried out for Wabamun and Dalhousie fly ashes. Specific gravities were co-determined using the Le Chatelier method with ethanol displacement.

5.7 Surface Area Analysis - B.E.T.

Samples of Reynolds Al_2O_3 (known surface area: 8.0 $m^2.g^{-1}$) and the source materials were characterized by specific surface area analysis (B.E.T. triple point method). The samples were outgassed overnight at room temperature. Two of the samples (Reynolds Al_2O_3 and Wabamun fly ash) were subsequently analyzed using nitrogen as the adsorbing gas. Since the results for Reynolds Al_2O_3 were lower than expected measurements were also carried out using krypton as the adsorbing gas. Outgassing was carried out for 60 hrs at room temperature. The result for Reynolds Al_2O_3 showed better agreement with the expected value. Krypton was subsequently used for all other samples.

5.8 X-Ray Powder Diffraction Measurements

X-ray powder spectra were recorded using a Philips diffractometer equipped with goniometer, using a nickel-filtered CuK_α radiation at 40KV and 30mA. The range of measurements was $2\theta=6^\circ$ to 71° and the scan speed for rapid scans was 2°/min. Peak intensities for glass content determinations were also determined using slow scanning and stationary (point) counting.

5.9 Fourier Transform Infrared Spectroscopy

Infrared spectra were measured of the "as-received" source materials using the ORF Analect 6160 Fourier Transform Infrared spectrometer. The samples were run as KBr pellets. The Thunder Bay fly ash was also run using photo-acoustic spectroscopy. It was found that the FTIR reflectance spectrum measured with the latter technique was similar to the FTIR absorbance spectrum using KBr pellets. Since absorption spectra are easier to prepare it was decided to use this technique for the samples.

5.10 Optical Examination-McMaster Technique

The modified McMaster Individual Particle Analysis Method (CSA A363-M1983) was used to determine glass contents of the two blast- furnace slag samples of this study. The granulated "as-received" slags were wet sieved to provide a fraction -63/+45 µm sieve. Immediately before examination, a small amount of sample is placed on a glass slide and a drop of ethylene glycol or camphorated oil is applied. A cover plate is placed on top and sheared to spread the fluid and to obtain a uniform, single layer of particles.

5.11 Optical Examination - Image Analysis

Slurries of homogenized fly ash samples were prepared using a 10% solution of Elvacite in isopropanol. The slurries were pressed in a tablet, 2.5 cm in diameter using a specimen mount press (Buchler) at 9,000 psi. The tablets were left to dry for a 24 hr period prior to optical examination. Image analysis was carried out using a Quantimet 720 Image Analyzer.

5.12 Electron Optical Investigation

An extensive electron optical investigation was carried out on a selected (Wabamun) fly ash. The sample in an Elvacite medium (see 5.11) without any further application of a coating was subjected to scanning electron microscopic examination (SEM) in conjunction with energy dispersive X-ray analysis (EDXA).

A more extensive electron optical investigation was carried out using Wabamun fly ash in epoxy. Initial examination was carried out on cut discs, 2.5 cm in diameter. To obtain information on the interior of the fly ash particles the samples were cut to 1 mm thick slices. The specimens were subsequently subjected to argon ion-milling for approximately 8 hours. The etched samples were carbon-coated prior to SEM examination.

5.13 Model Glasses for X-Ray Diffraction

A series of synthetic glasses in the Na_2O-SiO_2, CaO-SiO_2, Na_2O-CaO-SiO_2 and CaO-Al_2O_3-SiO_2 systems were prepared for an X-ray diffraction study using the following approach:

(a) Starting Materials

The starting materials used were Na_2CO_3 "Baker Analyzed" reagent grade; silica powder (240 mesh) supplied by the Fisher Scientific Company, New Jersey, USA; and Al_2O_3 and $CaCO_3$ reagent grade supplied by Anachemia Ltd, Montreal and Toronto.

(b) Glass Preparation

The preparation of the synthetic glasses was carried out by wet mixing of the batch materials in a glass mortar. After drying at 110°C for 1 hr the mixtures were melted in Pt crucibles.

Glasses in the Na_2O-SiO_2 system were prepared on a 20g scale by melting between 1320 and 1360°C for 1 hr and quenched on a stainless steel plate in air. The glass was crushed and remelted for an additional 1 hr and quenched in the same manner. The glass with composition $0.5Na_2O/0.5SiO_2$ devitrified when prepared on a 20g scale. It was, therefore, prepared on a 2g scale and the Pt crucible containing the melt was partially quenched in water to prevent devitrification.

Glasses in the $CaO-SiO_2$, $CaO-Al_2O_3$, $CaO-Al_2O_3-SiO_2$ and $Na_2O-CaO-SiO_2$ systems were prepared on a 5g scale. Melting was carried out at 1600°C for 15 to 30 minutes. The melts were quenched by partial quenching of the Pt crucibles in cold water.

(c) X-Ray Measurements

X-ray powder patterns were collected of the ground samples (-75 µm) following the procedure outlined in Section 5.8. Patterns were also collected of a series of commercial glasses.

5.14 Preparation of Melilite and Merwinite for QXRD Studies

Melilite, a solid solution of akermanite (C_2MS_2) and gehlenite (C_2AS), and merwinite (C_3MS_2) were synthesized for use in admixtures needed for the preparation of standard curves for QXRD measurements as follows:

Melilite:

A melilite composition was chosen based on 70% C_2MS_2 and 30% C_2AS. This oxide composition is:

CaO, 41.0%; MgO, 10.4%; Al_2O_3, 11.2%; and SiO_2, 37.5%.

$CaCO_3$ and $MgCO_3$ were used as sources of CaO and MgO, respectively. The batch materials were thoroughly mixed, ball milled in ethanol for four hours and calcined overnight at 1050°C. Melting was carried out for 2 hrs at a soak temperature of 1450°C. Melting was first attempted in Pt/30% Rh crucibles but severe corrosion led to the choice of clay crucibles for further melts. A partly crystallized glass was produced upon cooling the crucibles in the kiln. The XRD pattern of the crystalline fraction showed strong peaks at d-spacings of 2.87 ($2\theta=31.2$) and 1.76 ($2\theta=51.8$) indicative of a melilite phase. The partly devitrified glass was powdered to -75 μm and heat treated overnight at 1120°C to give a fully crystalline material identified as melilite from the XRD pattern.

Merwinite:

Merwinite was prepared by mixing batch materials with composition:

CaO, 5.11%; MgO, 12.3%; SiO_2, 3.66%

Again $CaCO_3$ and $MgCO_3$ were used as batch materials. These were ball milled for 4 hrs in ethanol and calcined overnight at 1050°C. Melting was carried out at 1420°C for 2 hrs in clay crucibles. A partly devitrified glass was formed as for melilite. X-ray analysis of the devitrified pieces showed the presence of merwinite. The glass was powdered to -75 μm and heat treated at 1100°C overnight to give merwinite as determined by its XRD pattern.

Reduction of Particle Size:

Ball milling for 4 days in ethanol using a corundum medium was used to reduce the particle size of the melilite and merwinite. Powders had been prepared prior to ball milling by crushing and sieving to give a -200 mesh material. Settling experiments as described in Section 6.10.4 were used to collect fine crystallites. The fraction <6 µm was collected since there were not sufficient particles <5 µm.

5.15 Preparation of Cordierite Glass and α-Cordierite for X-Ray Diffraction Studies

Cordierite ($2MgO.2Al_2O_3.5SiO_2$) was synthesized for XRD studies using the following oxide composition:

MgO : 13.78%
Al_2O_3 : 34.86%
SiO_2 : 51.36%

Reagent grade magnesium carbonate, alumina and silica flour, in the stoichiometric proportions 2:2:5 were ball milled for 30 minutes in ethanol in porcelain ball mill jars using a corundum medium. The dried powders were heated to 1625°C and soaked at this temperature for 10 minutes in a platinum crucible. The melt was cast into bars in a mould pre-heated to 600°C. The bars were annealed at 700°C.

α-Cordierite was prepared by crystallizing glass bars at 1000°C for two days. The XRD pattern of the crystalline polymorph was in good agreement with literature data.

5.16 Preparation of Glassy and Redevitrified Analogues of Fly Ashes and Slags

Glassy and redevitrified analogues of fly ashes and slags were prepared for glass content and hydration studies. Table 1 gives relevant data pertaining to the 11 source materials of this study.

The fly ashes and slags were melted at the melting temperature for period between 1 and 2 hours, followed by rapid quenching. XRD patterns were measured of the quenched glass to establish that complete vitrification had indeed occurred.

One fly ash, Dalhousie, which has a high iron oxide content could not be fully vitrified. Two other fly ashes, Nanticoke and Lakeview could initially not be fully vitrified either but subsequent extension of the melting time produced the fully vitreous analog of the fly ash.

Some of the source materials of selected source materials was cast in bars and annealed at 750°C for 16 hrs. Specimens 2 in. long were cut from the annealed bars for measurement of the dilatometric softening point (DSP) and coefficient of thermal expansion (CTE). DSP and CTE values for selected source materials are given in Table 1.

Powders of the quenched fly ashes and slags (-45 μm) were heat-treated according to the nucleation/crystallization schedule in Table 1. XRD patterns were obtained from the heat treated powders to ensure that full devitrification had occurred. One fly ash, Lingan, showed residual glass which could not be fully redevitrified even if the crystallization stage was further extended.

5.17 Preparation of Model Glass for Hydration Studies

A series of model glasses was prepared based on seven major oxides detected in the fly ashes of this study (SiO_2, Al_2O_3, Fe_2O_3, CaO, MgO, Na_2O, K_2O). The compositions of these glasses were chosen in such a way that they were identical to the average composition of the glassy phase of Wabamun, Nanticoke, Lakeview, Dalhousie and Estevan. The glasses were prepared by mixing reagent grade chemicals (SiO_2, Al_2O_3, Fe_2O_3, $CaCO_3$, $MgCO_3$, Na_2CO_3, K_2CO_3) in clay crucibles, ball milling for 2 hrs in ethanol and calcining at 600°C overnight. The glasses were melted for 2 hrs at a temperature between 1420 and 1550°C and quenched in water. X-ray diffraction was used to confirm the glassy nature of these materials.

5.18 Hydration Studies

Hydration studies have been carried out in deionized distilled H_2O and NaOH for the fly ashes and slags, their glassy and redevitrified analogues. Leaching was carried out by suspending a predetermined mass of the material to be leached in 250 mL of deionized distilled H_2O. The suspension was agitated by stirring. In a typical experiment the pH was determined with a pH-meter (Sargent Welch Scientific Company) every 5 minutes for the first hour. Subsequent pH-determinations were carried out at half hour intervals for the next 7 hours and a final reading was taken at the 24 hour mark. Mass losses were determined after the run had been completed and the remaining sample was dried. No efforts were made to control the temperature.

6. RESULTS

6.1 Chemical Analysis

Table 2 shows the results of chemical analysis for the 9 fly ashes and 2 blast-furnace slags investigated in this study. The composition has been expressed for the common oxides of the major elements. Loss on ignition values and carbon contents are also shown.

6.2 Specific Gravity Determinations

Table 3 shows specific gravities of the source materials. Both pycnometry and the Le Chatelier technique were used for 7 Canadian fly ashes. Since pycnometry was found to be more reliable this technique was the only one used for the remaining samples. Specific gravities for the first set of samples were shown for the "as received" samples as well as for samples ground for 30 min. in an automatic grinder.

6.3 Particle Size Analysis-Wet Sieving

The results of wet sieving of the source materials are shown in Table 4. The data give the percentage by mass retained on a 325 mesh (45 µm) sieve.

6.4 Particle Size Analysis - Sedigraph Analysis

All source materials were analyzed for particle size distribution by mass using a Sedigraph 5000D which employs the X-ray sedimentation technique. Sedigraph Traces are shown in Figure 1. The numerical data accompanying the traces are given in Table 5. Histograms accompanying the numerical data are shown in Figure 2. Distributions were calculated using the densities of the "as received" samples determined by pycnometry (Table 2). Distributions were also measured using densities obtained after grinding the sample for 30 min. in a glass mortar. The two data sets only showed minor differences. Only the distributions calculated with the densities of "as received" samples have been reported here.

6.5 Surface Area Analysis - Blaine

Blaine surface areas in $m^2.g^{-1}$ for Wabamun and Dalhousie fly ashes are listed in Table 4.

6.6 Surface Area Analysis - B.E.T.

Table 4 lists the surface areas determined for the 11 source materials of this study using the B.E.T. (triple point) technique with krypton as the adsorbing gas. B.E.T. measurements using nitrogen gave values of 7.3 $m^2.g^{-1}$ for Reynolds Al_2O_3 and 1.4 $m^2.g^{-1}$ for Wabamun fly ash.

6.7 Glass Content Methodology(1): Optical Examination by Image Analysis

Figure 3 shows an optical micrograph (magnification 137x) of a Wabamun fly ash in an Elvacite medium prior to image analysis. The sample showed predominantly spherical beads, some white opaque and some transparent, in the darker medium. Several spherical fly ash beads were identified as being hollow (cenospheres). Several crushed beads could also be observed.

Image Analysis was carried out using a Quantimet 720 Image Analyzer. The medium content of the fly ash tablet was estimated at 12% in good agreement with the mass content of the Elvacite medium. Assuming that the opaque white areas represented devitrified material the content of crystalline manner was determined at 6.6%. The glass content was computed as 93.4%, by difference.

6.8 Glass Content Methodology(2): Electron Optical Investigation

An electron optical investigation was carried out for Wabamun fly ash. The first step was an examination of a cut disc prepared for optical examination and image analysis. Figures 4(a) and 4(b) show SEM micrographs at different magnifications. Several spherical fly ash particles can be distinguished as well as some crushed material. The latter may represent fly ash as well as the medium.

Figures 5(a) - (h) represent EDXA analysis for the spots marked A-H on Figure 4(a). Table 6 lists the concentration range observed for selected oxides as well as the concentrations of these oxides in the fly ash overall.

Subsequently, the SEM study was continued on a Wabamun sample mounted in epoxy and polished by ion-etching. Fig. 6 shows a view of the sample cross-section in secondary electron (a) and back-scatter modes (b). Fig. 7 shows another view of the sample. Fig. 8 shows a close up of location 3 in Fig. 7 at higher magnification. Fig. 9 is an SEM micrograph of a cross-section through a spherical fly ash particle at location 3 showing smaller particles in the interior (plerosphere). Fig. 10 is an SEM micrograph of a non-spherical particle at location 4 on Fig. 7. EDXA analysis was carried out at several points in the particles. The results have been summarized in Table 7. EDXA data are also shown on Figs. 6-10.

The SEM investigation was conducted with the primary objective to establish whether an electron optical approach could be used to establish the glass content of fly ashes and slags. It was hoped that enough contrast in the sample cross-sections would be available to discern the crystalline phases from the glassy phase in the particle quantitatively by image analysis. An examination of the cross-sections showed no clear demarcation between the glassy phase and the remainder. The SEM approach was therefore abandoned for glass content methodology development.

6.9 Glass Content Methodology(3): McMaster Technique

The two blast-furnace slags, Standard and Atlantic, were analyzed by the modified McMaster Individual Particle technique (CSA A363-M1983). This method, developed by Emery and coworkers at McMaster University, distinguishes between clear glassy particles, birefringent crystalline particles and opaque, milky particles. Particles that glow milky white but not with definite birefringence under crossed polars should be considered crystalline (generally opaque in plane light).

The problem which arises with the McMaster method is the interpretation of what to count as glass or crystalline, and the estimation of their relative percentages in a given particle. The percentage estimations should not vary appreciably between observers, but the actual assigning of glass or crystalline to particles or sections of particles does, in some cases, depend on the operator. Particles or sections of particles which either stay dark under crossed polars or exhibit definite birefringent colour changes on stage rotation under crossed polars pose no problem and can be estimated fairly accurately for glass content. The problem arises with two other types of particles. The first are those that appear opaque or stained under plane polarized light and exhibit a milky, translucent glow under crossed polars. According to the instructions for the McMaster Method these should be considered as crystalline. The second group are those which are centrally dark with a fringe of either milky or translucent brightness around their edges.

The various determinations of glass content have been compiled in Table 8. There is a great deal of variation between the results obtained by different operators. In the data sets collected by operator A particles that looked opaque under plane light but black under crossed polars were not included for the calculation of the glass content. Operators B and C included these same particles as 100% crystalline. Both these operators used the gypsum plate for their glass content estimations. It appears then that operator A will tend to observe higher glass contents than either operator B or operator C. Table 8 shows this to be the case.

6.10 Glass Content Methodology(4): Quantitative X-Ray Diffraction Method (QXRD)

6.10.1 Introduction

The literature assessment of glass content methodology (Appendix

C) showed this technique to be one of the potentially more useful methods. An account of the scope of this method is given in Section 2.3.2 of the literature assessment.

The method is a direct route to a quantitative determination of the content of a particular crystalline phase. The combined amounts of the crystalline phases enables, indirectly, calculation of the glassy content by difference. The mass present for each crystalline phase is computed from the characteristic peak intensity of this crystalline phase as a ratio to the peak intensity of an added internal standard. The mass fraction of each phase is then determined by comparison of the intensity ratio in the sample to the intensity ratio for pure synthetically produced phases.

6.10.2 Feasibility of Approach - Model Study on the Cordierite System:

To demonstrate the feasibility of using the QXRD method a glass/glass-ceramic system was chosen based on cordierite. This substance has the formula $2MgO.2Al_2O_3.5SiO_2$ and its composition by mass (MgO:13.78%, Al_2O_3:34.86%, SiO_2:51.36%) bears some resemblance to the glassy waste materials of this study if one substitutes MgO for CaO. Cordierite which occurs as a natural mineral and as the substrate for low expansion ceramics, has been extensively characterized. Mixtures of glassy cordierite and the α-cordierite crystalline polymorph were prepared (Section 5.15) to demonstrate the feasibility of the QXRD technique.

Preliminary Evaluation:

A preliminary evaluation of the QXRD method involved the determination of selected peak intensities in the XRD patterns of cordierite glass/α-cordierite mixtures to which NaCl had been added as an internal standard. Mixtures were prepared containing 100%, 75%, 50%, 25%, and 0% glassy cordierite, respectively. XRD spectra for the mixtures are shown in Figure 11.

The following peaks were selected for the calculations (NaCl: 31.7°, 2.821; 45.5°, 1.994) α-Cordierite: 21.7°, 4.09; 26.3°, 3.39; 28.5°, 3.13; 29.6°, 3.02). The relative peak intensities versus α-cordierite content are graphically depicted in Figure 12. It can be seen that the intensity ratio:

$$\frac{(I_{Cor,2\theta}/I_{NaCl,2\theta'})}{(I_{Cor,2\theta}/I_{NaCl,2\theta'})_{100}} \times 100\%$$

versus α-cordierite content is a straight line. Linear regression gives:

$$y = 0.9961x + 2.3 \quad (r = 0.9981)$$

Thus, the correlation is highly significant.

6.10.3 The QXRD Method Applied to Fly Ashes - Rapid Scans

Having demonstrated the feasibility of the QXRD method for the cordierite system, the method was used to calculate the crystalline and glassy content of the first set of fly ashes as follows:

Identification of Major Crystalline Phases in the Fly Ashes:

Table 9 lists the source materials of this study and the major crystalline phases identified from their XRD patterns. All fly ashes have quartz as one of their crystalline components, most contain mullite and a few contain magnetite or hematite. This preliminary investigation did not attempt to characterize trace phases.

Selection of Standard:

NaCl was chosen as a standard since it was found that this compound had two strong peaks (d-spacings 2.821 and 1.994) at least one of which did not interfere with the major peaks of each of the above four phases. The line positions from the X-ray data for the four phases and NaCl are listed in Table 10.

ORF

Quantitative Determination of Crystalline Phases and Glass Content:

A preliminary quantitative determination of each of the four phases identified in the seven Canadian fly ashes was carried out as follows:

(a) XRD patterns were recorded for each of the four phases (α-quartz, mullite, magnetite, hematite) with NaCl. The amount of NaCl reference added was 10% by mass. From the XRD spectra the intensity ratios of each of the lines selected for the phases (two or three) with each of two lines of NaCl was computed. The intensity ratio:

$$\frac{I_{\text{phase}}{}^{X,\ 2\theta}}{I_{\text{NaCl}',\ 2\theta'}}$$

corresponds to a mass ratio of 9g phase X/g NaCl. The intensity ratios for the four phases are listed in Table 11.

(b) As for the pure phases the intensity ratios for the various line combinations for a specific phase have been calculated for the seven Canadian fly ashes. The mass of each phase is then calculated as an average over the various line combinations. The results are listed in Table 12.

(c) The percentages by mass of the four crystalline phases and the glass content for the 7 Canadian fly ashes have been compiled in Table 13.

$$\text{Glass Content} = 100\% - \sum\text{crystalline phases} - \text{LOI}$$

6.10.4 Improvements to the QXRD Method

Based on these findings, it is considered that the QXRD technique can be further improved as follows:

ORF

- Choice of internal standards. Important considerations are that the standard:
  - be readily obtainable in high purity;
  - gives sharp diffraction lines;
  - provides strong diffraction lines near the strong lines of the phases of interest to be determined;
  - not be superimposed by the phases of interest or by other materials commonly found within the glassy waste material.

- Since NaCl is somewhat hygroscopic, standards other than this compound could be considered.

- More accurate measurements can be performed by reducing the crystallite size to <5 µm by extended grinding.

- The accuracy can be increased by carrying out multiple scans for each composition.

- The accuracy can also be increased by increasing the scanning time per peak.

- Instead of using only 2 points (intensity ratio at 9g phase/g NaCl and 0,0) a larger number of intensity ratios corresponding to a series of crystalline phase/standard compositions could be measured. This would give a more accurate standard curve.

Selection of CaF_2 Standard:

CaF_2 was selected as an internal standard since it is less hygroscopic and it has at least one line which does not interfere with the lines of the four crystalline phases found in the fly ashes.

Reduction of Particle Size:

Klug and Alexander (2) discussed the effect of crystallite size on the reproducibility of intensity data. It was found that the mean deviation in intensity over 10 values for 15-50 µm powder was 18.2% whereas for a <5 µm powder this was only 1.2%. Care was therefore taken to use crystalline powders with a particle size of less than 5 µm. Particles of this size range were prepared by settling trials.

According to Stokes' Law:

$$V_f = \frac{d^2 g\ (\rho s - \rho L)}{18\ \mu}$$

where, V_f = velocity (cm s^{-1})
g = gravitational constant: 980 cm s^{-2}
ρ_s = density solid (g cm^{-3})
ρ_L = density liquid (g cm^{-3})
d = diameter particle (cm)
μ : viscosity of the liquid (P)

On the basis of the velocity, V_f, the average time can be calculated for a 5 µm particle to settle over a specified distance. Particles <5 µm will require more time. The procedure is to suspend the crystalline powders in a suitable solvent in a graduated cylinder and leave the suspension for the calculated time. The relevant parameters for selected materials for this study are listed in Table 14. The top 20 cm of the suspension were syphoned off and dried at 60°C for 16 hrs. Some error is expected to be introduced into this technique as a result of the presence of particles of varying specific gravity in fly ash*.

Preparation of Standard Curves:

Standard Curves were prepared for α-quartz, mullite, hematite and magnetite with CaF_2 as an internal standard and a glass (composition: CaO, 15.62%; MgO, 2.55%; SiO_2, 65.98%; Al_2O_3, 15.84%) as diluent. The compositions of the mixtures used for the standard curves are listed in Table 15. A number of lines were selected for each phase as well as for

---

* ORF internal research communication.

CaF_2 for intensity determinations. Table 16 lists the peaks and ranges scanned for the various crystalline phases.

The system α-quartz-glass-CaF_2 was used to establish basic methodological parameters. Initially, a series of 10 slow scans were carried out on a mixture of α-quartz, diluent and CaF_2, to determine the number of duplicate scans required to obtain acceptable intensity values. It should be noted that the preparation of the standard curves is extremely time consuming and this investigation was aimed at achieving a reasonable trade off between accuracy of the intensity values obtained and the number of duplicate scans required to achieve a certain precision. Statistical treatment showed that 3 consecutive scans were sufficient to produce results generally within 2% of the average value. Standard curves were subsequently produced by determining the intensities of selected characteristic peaks and calculating for each scan the ratio of characteristic peaks of α-quartz and CaF_2:

$$\text{IR (Intensity Ratio)} = \frac{I_{Q,2\theta}}{I_{F,2\theta'}}$$

where: $I_{x,2\theta}$: intensity of a characteristic peak of α-quartz at 2θ.

$I_{F,2\theta'}$: intensity of a characteristic peak of CaF_2 at $2\theta'$.

The procedure followed in computing the Intensity ratios was as follows:

(a) For a freshly packed sample specimen all peaks were scanned sequentially. Each peak intensity determination involved three measurements (area under the peak, starting intensity and end intensity). The peak area was scanned for 100s, the starting and end intensities were scanned for 40s each. The peak intensity was calculated as:

Peak Intensity = Peak Area Intensity - (Starting Background + End Background) x 1.25.

(b) The slow scanning was repeated twice with a freshly packed sample. The average peak intensity was then calculated over three consecutive scans. This calculation gave $I_{Q,2\theta}$ and $I_{F,2\theta'}$.

(c) The intensity ratios were then calculated using:

$$IR = \frac{I_{Q,2\theta}}{I_{F,2\theta'}}$$

(d) For each composition the intensity ratios were plotted against the concentration in terms of g α-quartz per g CaF_2. One standard curve was prepared for each combination of α-quartz and CaF_2 peaks. Similar curves were prepared for the other three phases.

Typical standard curves are shown in Figure 13a-f (α-quartz), Figure 14a-h (mullite), Figure 15a-f (magnetite) and Figure 16a-f (hematite).

Crystalline and Glass Content of Fly Ashes:

The QXRD technique was used to determine the content of the four crystalline phases, α-quartz, mullite, magnetite and hematite of 8 Canadian fly ashes (Thunder Bay was not investigated in view of the different mineralogy found for this fly ash compared to that of the other fly ashes as discussed below).

Tables 17-20 give the results of the slow XRD scans for α-quartz, mullite, magnetite and hematite. Table 21 summarizes the crystalline and glass contents for the 8 Canadian fly ashes.

Thunder Bay Fly Ash:

Thunder Bay fly ash showed an XRD pattern which was substantially different from that of the other fly ashes. Peaks attributable to sulfur-bearing phases could be identified. This finding is not unexpected since chemical analysis showed a S content of 6.84%, much higher than that of any of the other fly ashes. The sulfur bearing phases are $CaSO_4$ (anhydrite) and possibly $Na_3Al(SO_4)_3$ and CaS.

ORF

6.10.5 The QXRD Method Applied to Blast Furnace Slags

The QXRD method in its improved form was also used to determine the glass content of two granulated blast furnace slags. Rapid XRD scans showed that Standard slag, produced by National Slag Ltd., Hamilton, Ont., had melilite as the only crystalline phase. The Atlantic slag produced by Atlantic Cement Company, Inc., Stamford, Conn., was found to contain merwinite as its only crystalline phase.

The preparation of the melilite and merwinite crystalline phases had been described in Section 5.14. The fine powders (<6 µm) of these materials were used together with vitrified Standard slag glass and Atlantic slag glass powders (<5 µm) for the standard curves.

Preparation of Standard Curves:

Standard Curves were prepared for melilite and merwinite using CaF_2 as the internal standard and Standard slag glass and Atlantic slag glass as the diluent. The compositions prepared are listed in Table 22. Peaks scanned for the various mixtures are given in Table 23. Standard Curves are shown in Figures 17 (Melilite) and 18(a)-(d) (Merwinite). The intensity ratios were calculated somewhat differently from the procedure described in Section 6.10.4. Intensity ratios were computed by first calculating $I_{M,2\theta}/I_{M,2\theta'}$ values for each individually packed sample and then averaging over the three $I_{M,2\theta}/I_{M,2\theta'}$ values for three consecutively packed samples.

Crystalline and Glass Content of Slags:

Following the preparation of the standard curves, mixtures were prepared of each of the two slags with an appropriate amount of CaF_2. Table 24 demonstrates the calculation of the crystalline and glass contents of each sample.

6.11 Glass Content Methodology(5): Non-Crystalline Scattering Method (NCXRD)

6.11.1 Introduction

This potentially useful X-ray diffraction approach to glass content determination uses the non-crystalline XRD technique described by Ohlberg and Strickler (3). The glassy content is determined by measuring the intensity of the amorphous halo in the XRD pattern of the substance of interest at a suitable 2Θ-value and comparing it with the intensity of the amorphous halo of the vitreous analog of this substance. Unlike the QXRD method this approach leads to a direct measurement of glass content and is, therefore, potentially more accurate.

6.11.2 Feasibility of Approach - Model Study on the Cordierite System

To demonstrate the feasibility of the NCXRD approach mixtures of cordierite glass and α-cordierite were examined. Cordierite ($2MgO.2Al_2O_3.5SiO_2$) was also used to do a preliminary evaluation of the QXRD technique.

Preliminary Evaluation:

The preparation of cordierite glass and α-cordierite has been described in Section 5.15. Mixtures of cordierite glass and α-cordierite containing 0, 25, 50, 75 or 100% glassy material were prepared for XRD analysis. The XRD patterns are shown in Figure 19.

Using the mixtures of cordierite glass and α-cordierite the non-crystalline scattering at $2\Theta = 24^\circ$ was determined. The non-crystalline scattering is a measure of the glass content as follows:

$$\% \text{ Glass} = \frac{I_x - I_B}{I_g - I_B} \times 100\%$$

where, I_x = intensity of the amorphous halo at $2\Theta = 24^\circ$ for the cordierite glass/α-cordierite mixtures.

I_g = intensity of the amorphous halo at $2\theta = 24^{\circ}$ for cordierite glass.

I_B = intensity of the amorphous halo of the fully crystalline α-cordierite.

A plot of the relative intensity versus glass content is shown in Figure 20. The regression data are:

$$y = 1.006x + 0.00280 \qquad (r = 0.9997)$$

The correlation of glass content and intensity ratio for this model system is excellent.

6.11.3 The NCXRD Method Applied to Fly Ashes - Rapid Scans

Following the demonstration of feasibility of the NCXRD method to the cordierite system the method was subsequently applied to a fly ash. The fly ash chosen was Forestburg and the XRD patterns are shown in Fig. 21. The relationship between relative intensity and glass content is shown in Figure 22. At this preliminary stage no fully redevitrified analogue could be obtained. In later experiments, fully crystalline redevitrified Forestburg fly ash glass was used (Section 6.11.4.2). The glass content of the mixtures in the rapid scan experiments described here has been corrected for the residual glass content (38.5%) of the redevitrified fly ash.

The relationship between relative intensity and glass content of the mixtures can be represented by:

$$y = 1.03x + 5.026 \qquad (r = 0.993)$$

Again, the correlation is good. Using the data of Figure 22 the glass content of Forestburg fly ash was found to be 85.0%.

6.11.4 Improvements to the NCXRD Method

As with the QXRD technique, the NCXRD method can be improved in several ways:

- The number of data points can be increased by measuring the non-crystalline scattering of an increased number of mixtures of the glassy and crystalline phases.

- The intensities can be more accurately determined with stationary counting than from rapid scans.

- Intensity data for each mixture should be collected for several freshly packed samples.

- A standard should be run at regular intervals to check the reproducibility of the scattering observed.

These aspects have all been taken into account in the glass content determinations described in this section.

6.11.4.1 Cordierite System

The suggestions in the preceding section were implemented when intensity of a series of cordierite glass/α-cordierite mixtures was redetermined.

Mixtures were prepared containing 0, 10, 20, ... 100% cordierite glass by mass, the balance being α-cordierite. The scattering intensity of each mixture was prepared by counting for 100s at $2\Theta = 24^{0}$. Each mixture was scanned in triplicate using freshly packed samples for each determination. A soda-lime glass reference was run between mixtures as a standard. The data collected and their averages are listed in Table 25. Figure 23 shows a plot of $I_x - I_o$ versus glass content where,

I_x = scattering intensity of a mixture containing x% glass

I_o = scattering intensity of a mixture containing 0% glass

The mixture can be represented by the linear relationship

$$I_x - I_o = 3.44\times10^{-2} \text{ \% glass} - 1.29\times10^{3}$$

The correlation coefficient was found to be 0.9969. Thus, the correlation is highly significant.

6.11.4.2 Fly Ashes and Slags

In order to use the NCXRD method it is required that a fully vitreous analog of the glassy waste material can be prepared. A fully crystalline analogue is, strictly speaking, also required, but this condition is somewhat less severe since the percentage of residual glass can be estimated from the residual scattering intensity at the selected 2Θ value and a suitable base line in the rapid XRD scan. The preparation of glassy and crystalline analogues has been described in Section 5.16.

Mixtures containing 0, 10, ..., 100% fly ash or slag glass with the balance being the redevitrified analogue were then prepared as for cordierite. Intensity ratios were determined for the standard curves. The results have been listed in Tables 26-35. The standard curves are shown in Figs. 24-33.

6.12 Glass Content Methodology(6): Differential Intensity Method (DIXRD)

6.12.1 Introduction

The Differential Intensity X-ray technique (DIXRD) described by Wakelin et al (4) for polymers involves the calculation of the percentage crystallinity from an integral or correlation index. These indices are defined as:

$$\text{Integral Index : } C_i = \frac{\sum_{2\theta_o}^{2\theta_m} (I_u - I_a)}{\sum_{2\theta_o}^{2\theta_m} (I_c - I_a)} \qquad (1)$$

$$\text{Correlation Index : } (I_u - I_a) = C_c\ (I_c - I_a) + B \qquad (2)$$

where, I_u: intensity of the (partly crystalline) sample at designated 2θ-values.

I_a: intensity of the amorphous polymorph at these 2θ-values.

I_c: intensity of the crystalline polymorph at these 2θ-values.

The intensity values are measured over small 2θ-increments (at the most 0.5^o).

In essence this technique estimates the proportion of crystalline matter by observing how closely the diffraction pattern of an unknown substance resembles that of its fully crystalline analogue. The indices give the percentage crystallinity directly, and the glass content, indirectly, by difference. The DIXRD approach differs from the QXRD method in that the total amount of crystalline matter in computed and not the amounts of the individual phases.

6.12.2 Feasibility of Approach - Model Study on the Cordierite System

A preliminary investigation was carried out to determine the feasibility of glass content determinations for fly ashes and slags using the differential intensity XRD method. As for the non-crystalline XRD technique the technique was first used to measure the glass content of systems with a known glass content. Again, the system used was cordierite ($2MgO.2Al_2O_3.5SiO_2$).

From a rapid XRD scan of the glassy polymorph it was determined that the amorphous halo was in the 2θ range of $10.0-40.0^{o}$. Scattering intensities for cordierite glass, α-cordierite and mixtures containing predetermined glass contents are listed in Table 36 and Table 37, respectively.

Percentages crystallinity and glass contents of the two cordierite mixtures (A and B) are given in Table 39. It can be seen that the agreement between the known and the calculated values is good when the correlation index is used but rather poor when using the integral index.

Figures 34 and 35 show graphical representations of I_u-I_a versus I_c-I_a for the mixtures containing 20 and 70% cordierite glass, respectively. Linear relationships can be plotted although the correlation coefficients, $r=0.72$ and 0.77, are not very strong. It can be seen that the scatter in the data is substantial for the more positive values of I_u-I_a and I_c-I_a, i.e. for the 2θ values with significant crystalline scattering. The data are more nearly linear for 2θ values where the crystalline scattering is rather weak.

Figure 36 shows XRD scans reconstituted from the counting intensities of Table 37. It can be seen that the peak positions for the 2θ values with strong crystalline scattering agree closely for the α-cordierite and the glassy-crystalline mixture.

6.12.3 The DIXRD Method Applied to Wabamun Fly Ash

Given the encouraging results for the cordierite system the two differential intensity techniques have been applied to Wabamun fly ash for which fully vitreous and redevitrified analogues had been prepared. Table 38 lists counting intensities while the I_u-I_a versus I_c-I_a relationship and reconstituted XRD scans are shown in Figures 37 and 38, respectively. Table 39 gives crystallinity indices and glass contents. It can be seen that the correlation index which is believed to be the more reliable measure of crystallinity is unreasonable, giving a crystalline content of -1.0%. The correlation coefficient (r=-0.0508) shows that $I_u - I_a$ and $I_c - I_a$ are not correlated.

The reconstituted XRD scans (Figure 38) illustrates the origin of the poor correlation. The crystalline phases in the as-received fly ash and its redevitrified analogue clearly show significant differences.

The correlation index, C_c, was therefore recalculated leaving out the strongly scattering 2θ values of the fly ash and its redevitrified analogue (counting intensities marked with an * in Table 38). The recalculated glass content (83.6%) is close to the value found using the integral index (82.0%). This value is closer to the glass content calculated with the QXRD technique (76.1%) than the value calculated using the Non-Crystalline Scattering Method (62.1%). Clearly, it would be interesting to use the DIXRD method in this modified form to establish glass content values for comparison with alternate techniques.

6.13 Glass Content Methodology(7): The Amorphous Hump Method (AHXRD)

A particular variant on the Non-Crystalline XRD method outlined in Section 6.11 is the "Amorphous Hump" technique. The technique has been used to determine the glass content of pozzolans (5).

The glass content is determined by measuring the ratio of the area under the amorphous halo A_H and a prominent peak of a suitable standard (A_s). The area ratios were estimated from the counting of squares. The ratio:

$$\mathrm{GAH} = \frac{A_H}{A_s}$$

plotted against the glass content should obey a linear relationship. Figure 39 shows the relationship of GAH vs. glass content for the cordierite mixtures of Section 6.11.2. The internal standard was NaCl. Linear regression gives:

$$y = 0.948x + 0.1296 \qquad (r = 0.958)$$

Although acceptable, the correlation coefficient is not nearly as good as is generally found for the NCXRD method (Section 6.11.4.2). The theoretical curve predicts a GAH/GAH_{100} ratio of 0.75 for a glass content of 75%. Using the experimentally obtained relationship of Fig. 39 we find a glass content of 65.4% for $GAH/GAH_{100} = 0.75$. Using the experimentally observed relation of Figure 20 for the preliminary evaluation of Section 6.11.3 we find 74.3%, close to the actual value of 75.0%.

6.14 Glass Content Methodology(8): Density Approach

Since most of the Canadian fly ashes surveyed in this study could be fully vitrified and the quenched glass could be redevitrified, the use of density determinations for glass content measurements was investigated. This technique has been used to determine the degree of crystallinity of polymers (6).

The glassy fraction can be computed as:

$$x_a = \frac{\rho a\ (\rho c - \rho)}{\rho c - \rho a}$$

ρ : density fly ash
ρ_a: density glass
ρ_c: density crystalline material

A preliminary evaluation of this approach was carried out for three fly ashes (Wabamun, Sundance and Forestburg and their vitreous and redevitrified analogues. The results are listed in Table 40. The specific gravities of the fly ashes are pycnometric values measured after grinding (see Table 3). The values for the glassy and crystalline polymorph were measured for -45 µm powders.

It can be seen that the specific gravities of the glassy and crystalline analogues are not very different and that both of these are greater than that of the fly ash itself. It appears that the use of the density method has little potential for glass content determinations of fly ashes.

6.15 Structural Evaluation Using X-Ray Diffraction

Section 5.13 describes the preparation of a series of synthetic glasses in the Na_2O-SiO_2, CaO-SiO_2, Na_2O-CaO-SiO_2 and CaO-Al_2O_3-SiO_2 systems for an X-ray diffraction study. Several commercial glasses have also been included in this study.

The compositions and diffraction maxima of the synthetic and commercial glasses are given in Tables 41 and 42, respectively. Table 43 gives the diffraction maxima of the 9 fly ashes and 2 slags investigated in this study. Also listed in Table 43 are the diffraction maxima of the fully vitreous analogues of the glassy waste materials. Representative XRD patterns are shown in Figures 40-42.

6.16 Fourier Transform Infrared (FTIR) Spectroscopy

Figure 43 shows FTIR spectra in the 1800-400 cm^{-1} range for the 11 source materials. Figure 44 gives FTIR spectra over the 4000-400 cm^{-1} range for Sundance fly ash.

6.17 Hydration Studies in H_2O

6.17.1 Studies on As-Received Fly Ashes and Slags

Figure 45 shows pH versus time curves for leaching studies on "as received" fly ashes and slags in deionized water. Mass changes observed during the leaching trials have been recorded in Table 44. The trends observed have been summarized in Table 45. The results of chemical analysis of leachate solutions are given in Table 50.

6.17.2 Particle Size Effect

It is likely that there is a relationship between the acidity or basicity of the leaching solution and the surface area of the particles exposed. A crude experiment was carried out to establish this factor. One g samples of Wabamun and Dalhousie fly ashes were leached in deionized water. Two particle sizes, -400 and +400 mesh were used, pH versus time curves are shown in Fig. 46. Mass changes are recorded in Table 46. The initial pH of deionized water was 6.0.

The two samples behave quite differently. The -400 mesh fraction of Wabamun achieves a maximum pH of 10.2 after 10 min. while the +400 mesh fraction reaches its pH maximum of 9.2 after the same leaching time. The Dalhousie -400 mesh fraction gives a pH profile starting at 4.0 and rising steadily with time to a maximum of 7.0 after 24 hrs. The Dalhousie +400 mesh fraction, starting from a pH of 3.9 achieves its maximum of 7.4 after 5 hrs after which it remains fairly constant. The mass losses for both fly ashes decrease with increased particle size.

6.17.3 Leaching of Glassy Analogues of Fly Ashes and Slags

A set of leaching trials was carried out in deionized water to establish the effect of the glassy nature of glassy waste materials on their leaching behaviour.

Glassy analogues of fly ashes and slags were prepared following the melting procedures outlined in Section 5.16. The glasses were ground and 1.00g of the -325 mesh fraction was leached over a 24 hr period with deionized water. pH versus time curves for 8 fly ash glasses and 2 slags are shown in Fig. 47. Mass changes are listed in Table 46.

The glasses behave very differently from the parent materials as is shown in the summary of Table 47.

6.17.4 Leaching of Redevitrified Analogues of Glassy Waste Materials

The effect of redevitrification on the leaching of the glassy analogues of fly ashes and slags was also studied. The devitrification of the parent glasses has been described in Section 5.16. pH versus time curves for leaching of 1.00g of the redevitrified analogues (-325 mesh fraction) are shown in Figure 48 and the mass changes have been recorded in Table 46. The leaching results have been summarized in Table 47.

To study the effects of progressive devitrification Wabamun fly ash glass was subjected to a schedule of controlled nucleation and crystallization. Glass powder (-325 mesh) was nucleated at 810°C for periods of 1 hr, 2 hrs, 4 hrs, 8 hrs and 24 hrs. Samples were also nucleated at 810°C for 16 hrs and crystallized at 950°C for 1 hr, 2 hrs, 4 hrs, 8 hrs, 24 hrs and 48 hrs. Selected results are shown in Figure 49 and mass losses are listed in Table 46. The results were as follows.

The pH of the deionized water during the leaching trials of 1.00g of nucleated glass was 5.8. The differences between samples nucleated for different time periods was only very slight. The initial pH was slightly higher for the samples nucleated for a longer time but the final results were very similar. No clear trend was observed for the mass losses.

The leaching behaviour of the samples nucleated at 810°C for 16 hrs and then crystallized for various durations is similar to that of the glasses which were nucleated only. There appears to be no clear trend for Wabamun fly ash glass subjected to varying degrees of heat treatment.

6.17.5 Leaching of Glasses

The QXRD method established that appreciable amounts of crystalline materials are present in the materials studied. This will alter the chemical composition of the glassy phase when compared to the overall composition of the glassy waste material. A series of glasses was, therefore, compounded containing seven oxides which were found to be predominant in their parent fly ashes. The compositions of these glasses was chosen in such a way that they represented the average oxide composition of the glassy phase of their parent fly ashes. These compositions are listed in Table 48. A mass of 1.00g of the -325 mesh fraction of the glasses was leached with deionized water. The pH versus time curves are shown in Figure 50 and the mass changes in Table 46.

The pH of the H_2O was 7.1. The pH during the leaching of the glasses does not change much with time. It is interesting that the Estevan 1 glass which has the highest percentage of modifiers (Σ(CaO + MgO + Na_2O + K_2O) = 28.35%) achieves the highest pH maximum. The mass losses do not show a clear trend.

6.17.6 X-Ray Diffraction Patterns

XRD patterns have been collected of selected materials before and after leaching to determine whether any change has occurred in their crystalline and glassy character. The results have been summarized in Table 49.

Fly Ashes and Slags:

All materials except one (Thunder Bay fly ash) show either no detectable crystalline material or the presence of $CaCO_3$ (calcite) after leaching in addition to the phase present in the parent material. Presumably, the latter compound is formed from dissolved Ca^{2+} ions and CO_2 adsorbed from the atmosphere and dissolved into the solution as carbonate ion. The presence of $CaCO_3$ is detected from a sharp peak at $2\Theta = 29.3^{\circ}$ (d=3.035) in the XRD spectrum as well as some minor peaks. The Thunder Bay fly ash behaves differently. The only crystalline phase remaining is α-quartz. The sulfur bearing phases, possibly anhydride ($CaSO_4$), $Na_3Al(SO_4)_3$, and calcium sulfide (CaS) had disappeared from the XRD pattern.

Fly Ash Glasses:

The Wabamun, Sundance, Forestburg and Lingan fly ash glasses showed the presence of crystalline material upon leaching. It is interesting that these four fly ash glasses (and the Nanticoke derivative) did not show a loss in mass during the leaching experiment. The identity of the crystalline material could not unequivocally be established. There was some resemblance with the XRD patterns of prehnite ($Ca_2Al_2Si_3O_{10}(OH)_2$), glaucophane ($Na_2Mg_3Al_2Si_8O_{22}(OH)_2$), sillimanite

(Al_2SiO_5) and meionite ($Al_6Ca_4(SiO_4)_6$ (SO_4,CO_3)) suggesting that a complex C-A-S-H type material was produced possibly with some additions of minor oxides. A representative XRD pattern is shown in Figure 51.

Devitrified Wabamun Fly Ash Glass:

XRD patterns collected for the devitrified Wabamun fly ash glasses prior to leaching showed that no crystalline material was evident after nucleation at 810°C for times of 1-24 hrs. Substantial amounts of crystalline material were formed upon crystallization at 950°C for 1-48 hrs.

Two representative XRD patterns are shown of the nucleated and crystallized glass (Fig. 52). From a comparison of the intensity of the amorphous hump at $2\Theta = 25^\circ$ it appears that about 20% by mass is still glassy. The emergence of a strong peak at $2\Theta = \sim 4.05$ indicates the presence of SiO_2 (crystobalite). The identity of other phases could not be established.

6.17.7 Chemical Analysis of Leachates

To establish the progression of the leaching 1.00g of Wabamun fly ash was leached in deionized water and the solutions of parallel experiments were subjected to elemental analysis by DC plasma emission spectrophotometry. The concentrations of 5 elements together with the solution pH is shown in Table 50.

6.18 Hydration Studies in NaOH

Hydration studies were carried out on Wabamun and Dalhousie fly ashes and Standard slag using NaOH as a leaching medium. The pH range surveyed was the range pH7 - 11.

Leaching was carried out on 1.00g of the "as received" sample in 100 mL of NaOH solution. The following observations were made:

pH7:

The fly ashes and slags behaved as observed earlier (Section 6.17.1). Wabamun reaches pH~10 within 30 min. which drops after 2 hrs to reach pH~9 after 24 hrs. Dalhousie shows an initial pH<4 which gradually increases to pH>7 after 24 hrs. Standard slag initially behaves like Wabamun but the pH drop is less from 2 to 24 hrs (see Fig. 53(a)).

pH8:

The behaviour is similar to that observed for pH=7 (see Figure 53(b)).

pH9:

Wabamun and Standard Slag behave as for pH7 and pH8. Dalhousie has an initial pH<5 but reaches pH7 within 10 min (see Fig. 53(c)).

pH10:

Wabamun behaves as for pH7-9. The pH for Standard Slag is remarkably constant while Dalhousie reaches a pH7.5 within 10 min, which goes up to pH8 from 40 min to 4-1/2 hrs after which a slight drop to pH7.7 is observed (see Fig. 53(d)).

pH11:

All three curves show very similar behaviour with the pH close to pH11. Dalhousie shows a noticeable drop in pH to reach a value of pH=9.6 after 24 hrs (see Fig. 53(e)).

7. DISCUSSION

7.1 Chemical Analysis

Table 2 shows the results of chemical analysis for the 11 source materials of this study. The major components for the fly ashes are SiO_2 (37.1 - 58.6%), Al_2O_3 (12.3 - 23.2%), Fe_2O_3 (3.33 - 38.9%) and CaO (1.29 - 13.0%). Some of the fly ashes contain significant quantities of other oxides. Thus, Thunder Bay has 6.84% SO_3. Both Estevan and Thunder Bay have ~3% MgO and ~7 - ~8.5% Na_2O, respectively. Nanticoke and Lakeview have relatively high carbon contents and LOI values.

On the basis of the analytical results the fly ashes can be classified as follows (see Fig. 1.4 on p. C10 of Chapter 1 of the literature assessment):

(a) Bituminous coal fly ashes: Nanticoke, Lakeview, Lingan.

(b) Subbituminous and lignitic coal fly ashes: Wabamun, Sundance, Forestburg, Estevan, Thunder Bay.

(c) Dalhousie does not quite fit any of the above categories. If SiO_2 and Al_2O_3 content are lower than commonly associated with a bituminous coal fly ash while its CaO content is too low for the subbituminous/lignitic type. This fly ash has an unusually high Fe_2O_3 content (~39%) which accounts for its unusual composition.

Using the other major classification all fly ashes except Estevan and Thunder Bay have in excess of 70% of ($\Sigma SiO_2 + Al_2O_3 + Fe_2O_3$) and can thus be classified as class F fly ashes. Estevan and Thunder Bay have somewhat less than 70% but still in excess of 50% of the major network formers and can be classified as class C fly ashes. In fact, this classification is not very useful here since the high CaO content normally associated with the C type (15-35%) is not observed for Estevan and Thunder Bay while some of the class F fly ashes have a much higher CaO content often attributed to this group (<5%).

The compositions of the two granulated blast-furnace slags are quite different from the chemical make-up of the fly ashes. SiO_2 and Al_2O_3 contents are much lower while CaO and MgO contents are much higher. The compositions are typical of those anticipated for these materials from North American sources (see Table 1.3 on p. C2 of Appendix C).

7.2 Specific Gravity

The specific gravities of the as-received source materials (see Table 3) vary considerably. There is definitely a correlation with the Fe_2O_3 content for the fly ashes (r = 0.78 for the pycnometric values of the as-received samples).

As expected the pycnometric specific gravities increase after grinding presumably because of the lowering of the amount of voids in the source materials.

Specific gravities determined by the Le Chatelier bottle technique are somewhat erratic with an exceptionally high value found for Lakeview (3.74) and much larger differences for the "as-received" and ground materials. In some instances (e.g. Wabamun, Lakeview) the "as-received" densities were found to be higher than those of the ground materials (due to the presence of lightweight floating particles reducing the apparent volume). Pycnometric values which appear somewhat more reliable have, therefore, been used throughout the remainder of this discussion.

7.3 Particle Size and Surface Area

Pycnometric specific gravities, particle size data and surface areas for the 11 source materials of this study have been listed in Table 4. The following observations were made:

1) The average particle size varies a great deal between the source materials ranging from 5.2 (Thunder Bay) to 20.0 µm (Wabamun).

ii) X-ray sedimentation indicates a much greater fraction of particles <45 µm than measured by wet sieving (325 mesh, 45 µm).

iii) B.E.T. (Krypton) analysis gives substantially greater surface areas compared with X-ray sedimentation. This phenomenon was also observed by Mehta (ref. 79 in Appendix C) for American fly ashes. Since B.E.T. takes pores and crevices of the particulate materials measured into account it is believed that this technique more adequately represents the accessible surface area during the hydration of these waste materials than the Blaine or the X-ray sedimentation technique.

iv) Particle size histograms for the 11 source materials (Figure 2) show that none of the materials is obviously bimodal with the exception perhaps of Dalhousie which shows two maxima in the 10-15 µm and the 23-30 µm ranges. The distributions are broad with substantial quantities of particles larger than the average diameter. An exception is Thunder Bay fly ash for which 85% of the particles are less than 10 µm in diameter. The two slags also have a finer particle size distribution when compared with the fly ashes other than Thunder Bay.

7.4 Glass Content Methodologies

7.4.1 Introduction

Table 51 lists the glass content values for the 11 source materials of this study. Two methods, the QXRD and the NCXRD techniques gave almost complete data sets. No value was obtained for Thunder Bay using the QXRD technique since its mineralogical composition was significantly different from the other materials. Since the preparation of the standard curves was the most time-consuming task for the development of the QXRD technique no attempt was made to evaluate the glass content of Thunder Bay fly ash using this method.

The NCXRD technique could not be applied to Dalhousie fly ash since a fully vitreous analogue of this material could not be prepared, presumably because of its high iron oxide content.

The McMaster Individual Particle technique was used to determine the glass contents of the two slag compositions. This technique which appears to be subject to considerable inter-operator variation could not be extended to fly ashes since the crystallites in the latter cannot be distinguished under the optical microscope and the presence of a number of phases complicates the observations.

The DIXRD technique was only applied to one fly ash. This method deserves a more extensive evaluation.

Image Analysis in conjunction with optical or electron microscopy appears to be troublesome for the same reasons given for the McMaster technique. The distinction between glassy and crystalline phases is not very clear.

The density approach to glass content determinations was not found to be very useful.

7.4.2 Comparison of the QXRD and NCXRD Methods

A comparison between the QXRD and NCXRD techniques shows a rather poor correlation ($r = -0.60$) between the two data sets (Dalhousie and Thunder Bay excluded). The large discrepancies for Nanticoke and Lakeview and for Atlantic slag between the two techniques are noticeable, as well as the substantially lower glass content obtained for Wabamun using the NCXRD technique. Replicate glass content determinations by NCXRD for Wabamun and Atlantic slag gave essentially the same glass contents, indicating good precision and suggesting that the differences are attributable to systematic factors.

At this stage, it is difficult to judge which of the two approaches to glass content determination using X-ray diffraction gives the more accurate values. Both the QXRD and NCXRD approaches have potential sources of error which are summarized below:

QXRD Method:

i) The glass content is essentially computed indirectly by subtracting the sum of the masses of the crystalline phases and the loss on ignition (LOI) from 100%. Errors in each of the crystalline contents and in LOI will propagate and affect the final result. On the other hand, the combined error may average out over the various phases rather than accumulate according to a worst-case scenario.

ii) The accuracy of the standard curves is an important factor in the determination of the content of the crystalline phases. Care was taken during the preparation of the standard mixtures to control crystallite size and to optimize the counting of the scattering intensity. An examination of the standard curves show that linearity is closely observed (Figures 13-18). However, improvements can be made in the composition range chosen. Ideally, the curve should be centered about an intensity of 1 for the peaks corresponding to the crystalline phase and to the standard. Some of the standard curves prepared are outside this optimum range, specifically some of the α-quartz and mullite curves.

iii) Having prepared the standard curves, an amount of the internal standard should be added to the glassy waste material to give an intensity peak ratio of about 1. The amount of CaF_2 added to the fly ashes was generally in excess of what was required for the optimum intensity ratio for a particular peak combination and the intensity ratio values, therefore, are often less than 1. This is particularly the case for the iron oxide phases, hematite and magnetite, which for most fly ashes were only present in amounts of a few percent or less. An adjustment of the mass of CaF_2 so as to give the optimum intensity ratio for a specific peak combination for each crystalline phase can be expected to improve accuracy as well as the precision of the computed crystalline contents.

iv) Finally, the use of the QXRD approach for glass content determinations depends on the initial identification of the crystalline phases present. The preparation of the standard curves, preferably several for each crystalline phase, is a time-consuming affair. It follows, therefore, that the QXRD method will be most useful for the routine determination of glass contents of fly ashes, slags and other waste material from specific sources which are not subject to the variations in chemical and mineralogical compositions observed between samples from different sources.

NCXRD Method:

i) The NCXRD approach provides a direct method for glass content determination based on the intensity of the X-ray scattering of the glassy phase in the source material itself. The accuracy of the NCXRD method is, therefore, to a large extent dependent on its inherent ability to estimate the glass content of the source material. The 2θ-value selected for the glass content determination should be selected in such a way as to minimize interference of the crystalline scattering component of the XRD pattern. Care was taken in this study to select 2θ values located in between peaks, both for the glassy waste material as well as for the compositions used to determine the standard curve. At the same time, the intensity of the non-crystalline scattering should be close to the intensity maximum of the amorphous component, i.e. the 2θ value selected for intensity measurements should be close to the 2θ value with maximum non-crystalline scattering. In all cases, except for the cordierite preliminary evaluation, it was found that a 2θ value of 25^{0} was satisfactory. This value was close to the $2\theta_{Imax}$ value of the source materials for this study.

ii) A second factor affecting the accuracy of this technique stems from a consideration of the structure of the glassy phase. We will discuss in subsequent sections XRD and spectroscopic evidence which can be used in the interpretation of the structures of the glassy waste materials.

The shape and the $2\Theta_{Imax}$ value of the amorphous component of the XRD pattern reflect the structure of the glassy phase. The NCXRD approach is based on a comparison of a selected scattering intensity of the glassy component of the source material and the glassy component of the mixtures used for the preparation of the standard curves. Ideally, these two glassy components should be identical in composition and structure. In fact, they are not exactly the same. The vitrified glass is 100% glassy and its composition (corrected for carbon content) should be that of the source material overall. The composition of the glassy component of the source material will normally not be identical to the overall composition since the precipitation of the crystalline phases will alter the composition of the glassy phase. A comparison of the $2\Theta_{Imax}$ values of the source materials and that of their vitrified analogues (see Table 43) is reassuring since their proximity suggests that the shapes of the amorphous components of the XRD patterns are probably similar. The potential error will likely be minor if the glass content of the source material is high since the composition will be close to that of its vitrified analogue.

Apart from the potential sources of error listed here there are no a priori reasons which suggest that the QXRD method is superior to the NCXRD approach, or vice versa. Both techniques give results which appear to be reasonable in view of results reported on slags in the literature. The aforementioned low glass contents found for Nanticoke and Lakeview (QXRD) and for Atlantic slag (NCXRD) are somewhat puzzling, however, particularly since the alternate approach gives values which are in the range expected. It is noteworthy that the low QXRD values were observed for fly ashes with high LOI and carbon contents. In the absence of clear preferences for one of the two approaches, the average glass content from the QXRD and NCXRD data (see Table 51) will, therefore, be used in the remainder of the discussion.

7.5 Electron Optical Investigation

Section 6.8 mentions the results obtained using a combination of scanning electron microscopy (SEM) and energy dispersive analysis (EDXA) for the characterization of Wabamun fly ash. Although, SEM/EDXA does not appear to be a route for glass content evaluation, much useful information was obtained from the micrographs and EDXA analyses.

A cursory examination of the surface of a cut disc in which Wabamun fly ash particles were embedded in an Elvacite medium shows spherical particles as well as some crushed material (Figs. 4(a) and (b)). Chemical analysis by EDXA carried out at 8 different locations, showed that within one fly ash sample particles are found with vastly different compositions (Table 6, Figs. 4(a) and (b), Fig. 5). For example, a large spherical particle (A in Fig. 4(a)) was found to have SiO_2, Al_2O_3 and CaO contents close to those found for the overall fly ash composition. On the other hand, particles were also observed where the TiO_2 (B in Fig. 4(a)), CaO (D in Fig. 4(a)) or FeO (H in Fig. 4(a)) contents were far in excess of those of the average composition. SEM/EDXA shows a picture of the fly ash which is a very heterogenous material as far as composition is concerned. Table 6 also lists side by side the average of the oxide contents over the location sampled by SEM/EDXA and the overall composition determined by chemical analysis. Except for FeO and CaO, the two sets of figures agree reasonably well. The wide range of concentrations actually observed is certainly not evident from these average values.

Another in-depth look at Wabamun fly ash by SEM/EDXA is given in Figs. 6-10 and Table 7. These polished cross-sectional ~~views~~ shows a variety of particle shapes and a range of compositions. The following particle type could be discerned.

(a) Solid spheres containing gas bubbles that are relatively small compared to the diameter. Analysis of one sphere (A in Fig. 6) showed it to be high in CaO and FeO. These spherical particles are probably predominantly glassy (see R.J. Lauf, J. Am. Ceram. Soc. 61(4), 487-490 (1982)).

(b) Cenospheres, empty spheres in which the wall thickness is relatively small compared to the particle diameter. The wall may contain small bubbles as well. Figure 7 shows a grouping of cenospheres (location 3 and a few neighbouring particles). A close-up is shown in Fig. 8. EDXA analysis at location 3 shows this particle to be mostly an alumino-silicate (Table 7).

(c) Plerospheres, spherical particles containing smaller spherical particles inside. For example, Fig. 9 shows a plerosphere containing smaller solid spheres and cenospheres.

(d) Irregularly shaped particles (see Fig. 7, location 4). A close up and EDXA analysis at 4 different spots in this particle indicates a predominantly alumino-silicate composition with some variation in the content of the other oxides, notably CaO.

In conclusion, SEM/EDXA analysis shows a great deal of variation both in particle shapes and sizes. The composition varies a great deal between individual particles and to a somewhat lesser extent within a particle. These observations suggest that the chemical composition of a glassy waste material such as a fly ash is complex and probably not an easily accessible indicator for performance in concrete formation and related processes.

7.6 X-Ray Diffraction Studies

7.6.1 Introduction

Section 6.15 described the collection of data from an extensive X-ray diffraction study on model glasses, commercial glasses, the 11 source materials of this study and their glassy analogues. This study was sparked by a recent study on the glassy nature by Diamond (7).

While studying the glassy nature of fly ashes Diamond (7) observed that U.S. fly ashes with low (<20 wt.%) CaO content show an amorphous diffraction halo with an intensity maximum centred between 23 and 27° 2Θ. Within that composition range, the angular position of the maximum was found to increase linearly with CaO content. The position of the intensity maximum for fly ashes wither higher (>20 wt.%) CaO content was found at a 2Θ value of about 32°. Diamond attributed the latter maximum to a calcium aluminate structural type.

To elucidate the origin of the intensity maximum of the amorphous halo in the X-ray powder diffraction pattern of fly ashes, the X-ray powder patterns of a number of synthetic glasses in the Na_2O-SiO_2, $CaO-SiO_2$, $Na_2O-CaO-SiO_2$ and $CaO-Al_2O_3-SiO_2$ systems were studied together with X-ray powder patterns of some commercial glasses, and the source materials of this study.

7.6.2 Na_2O-SiO_2 Glasses and SiO_2

Fused silica, SiO_2 (Table 42) has a diffraction maximum at 2Θ =21.3°. Figure 40 shows that the amorphous halo in the X-ray diffraction patterns of Na_2O-SiO_2 glasses contains at least two components centred at 2Θ values of about 24.5° and 30.4-22.5°, respectively.

Valenkov and Porai-Koshits (8) have shown that the XRD patterns of Na_2O-SiO_2 glasses could be constructed by adding together the glassy diagrams of $Na_2O.SiO_2$ (sodium metasilicate) and SiO_2, each diagram being given a weight factor proportional to its relative concentration. It has been suggested by these authors that Na_2O-SiO_2 glasses are not homogeneous but that the two structures exist side by side.

Composition No. 8 in Table 41 has a composition close to that of $Na_2O.SiO_2$. Its diffraction maximum is at 34.0°. It is likely that the two diffraction maxima observed in the X-ray patterns of the Na_2O-SiO_2 glasses result from scattering contributions of distinct structural units. The lower diffraction maximum could arise from a siliceous unit while the higher diffraction maximum could be attributed to a lower polymerized silicate grouping, possibly a metasilicate.

7.6.3 Na_2O-CaO-SiO_2, CaO-SiO_2, CaO-Al_2O_3 and CaO-Al_2O_3-SiO_2 Glasses

An examination of the X-ray patterns of the glasses of these series, some of which are shown in Figure 41, reveal that glasses of widely differing compositions have similar X-ray patterns and similar diffraction maxima (see Table 41). For example, glasses No.9 ($CaO.SiO_2$), No. 14 ($CaO.0.3Al_2O_3.0.4\ SiO_2$) and No. 17 ($C_{12}A_7$) have $2\Theta_{Imax}$ values between 30.0 and 31.0°.

On the basis of the similarity in the diffraction maxima of high calcium fly ashes (CaO>20%) and $C_{12}A_7$ Diamond (7) proposed that a calcium aluminate glass was likely responsible for the diffraction maxima of fly ashes with CaO contents in excess of 20%. The diffraction data presented in this study show that, in fact, a number of glass compositions based on the major oxides likely to be present in fly ashes could be responsible for the diffraction maximum at a 2Θ value of about 32° observed by Diamond.

7.6.4 Commercial Glasses

Table 42 shows the compositions of a series of commercial glasses and the diffraction maxima of their X-ray patterns are shown in Fig. 41. The maxima for all of these glasses lie in the 2Θ-range 21.3-24.0°, similar to the 2Θ values associated with the diffraction maxima of the Na_2O-SiO_2 glasses with high SiO_2 contents. Since the commercial glasses have high SiO_2 contents it is reasonable to assume that the X-ray patterns and the diffraction maxima originate from siliceous structural units. It can be seen that the amorphous haloes of container glass, Corning slide glass and window glass are broadened, presumably because of scattering contributions of lesser polymerized silicate units and borate units.

7.6.5 Fly Ashes, Slags and Vitreous Analogues

Table 43 shows $2\Theta_{Imax}$ values for the 11 source materials of this study and their vitreous analogues. The $2\Theta_{Imax}$ values were found to range from 23.0 to 30.8°. For the glassy analogues values between 24.0 and 29.5° were observed.

The $2\theta_{Imax}$ values versus analytical CaO content have been plotted together with the data of Diamond in Fig. 54. There is a great deal more scatter in the data from this study. Considering the 9 fly ashes only, the relationship between analytical CaO content and $2\theta_{Imax}$ may be represented by:

$$y = 23.2 + 0.17\ x$$

but the correlation is poor ($r = 0.42$). Including the two slags gives:

$$y = 23.0 + 0.20\ x$$

and the correlation is vastly improved ($r = 0.86$). For the vitreous analogues (10 samples) the relationship becomes:

$$y = 24.1 + 0.12\ x$$

and the correlation further improves ($r = 0.89$).

Better correlations are obtained by considering $2\theta_{Imax}$ versus total modifier content (i.e. the major oxides: $CaO + MgO + Na_2O + K_2O$). Considering fly ash glasses only, we find $r = 0.70$. For all 11 source materials $r = 0.92$. And for 10 glassy analogues $r = 0.94$. We conclude that:

(a) A better correlation is obtained when source materials of all available concentrations (up to ~40% CaO).

(b) The correlation is better when the glassy analogues are considered, presumably because there exists a better correlation with the overall composition.

(c) A better correlation still is obtained when the total modifier content is considered.

7.6.6 Correlation of Results

Before correlating the results of the X-ray study on synthetic and commercial glasses with the data and conclusions reported by Diamond (7) for U.S. fly ashes it seem appropriate to raise several points.

In the first place, the data reported in this study suggest that the amorphous halo is the resultant of the scattering of distinct structural units in the glass. Each of these units could be responsible for a distinct diffraction maximum. Structural inferences based on the position of the dominant diffraction maxima could be simplistic since they may exclude additional information available from the amorphous component of the diffraction patterns.

Secondly, it should be noted that fly ashes are complex substances, both chemically and mineralogically. The chemical composition indicates the presence of a number of major elements represented conventionally as the oxides, SiO_2, Al_2O_3, CaO, Fe_2O_3, as well as small amounts of minor elements, such as TiO_2, MnO_2, etc. The major mineral phases are α-quartz, mullite, and iron-containing spinel type phases (9). Even if fly ashes were homogeneous substances, the composition of the glassy phase would be complex and unambiguous assignments difficult.

Thirdly, it is unlikely that the glassy component of the fly ashes has a composition identical to that of the overall composition. The presence of SiO_2-, Al_2O_3- and Fe-oxide rich crystalline phases will tend to give a glassy component depleted in these oxides and enriched in CaO. It would be more appropriate to correlate the CaO content of the glassy phase with the diffraction maximum rather than the CaO content of the fly ash overall.

Finally, it has been shown by Lauf (10), and confirmed by this study (Section 7.1.5), that individual fly ash particles may have a very different chemical and mineralogical make-up. The amorphous halo in the diffraction pattern, therefore, represents the average of the scattering contributions of the individual fly ash particles.

Taking the complicating factors referred to above into account, we will now comment on Diamond's findings (7) against the background of the diffraction data on synthetic and commercial glasses of this study. Diamond concluded that the diffraction maxima between 23° and 27° observed for the low calcium fly ashes (<20 wt.% CaO) were indicative of a siliceous glass structure. The data reported here appear to support this conclusion since the Na_2O-SiO_2 glasses with the higher silica contents and the commercial glasses all have primary intensity maxima in this range. Fused silica was found to have a diffraction maximum slightly below this range.

An examination of the diffraction maxima of fused silica, glass No. 1 (Table 42) and glass No. 2 (Table 41), show increasing $2\Theta_{Imax}$ values of 21.3, 22.5 and 24.5, respectively. The SiO_2 content of these 3 glasses decreases while the Na_2O content increases in this order. In first approximation, it is likely that the positive correlation between CaO content and diffraction maxima observed by Diamond for low calcium fly ashes has a similar origin. Presumably, the upward shift in the $2\Theta_{Imax}$ values can be attributed to increased scattering contributions of more depolymerized silicates for glasses with lower SiO_2 and increased modifier (Na_2O or CaO) content.

The sudden jump in the diffraction maximum to a $2\Theta_{Imax}$ value of about 32° observed by Diamond (7) for high calcium (>20 wt.% CaO) fly ashes also becomes clear from the data in Table 41 and Fig. 55. For most compositions in the Na_2O-SiO_2 series two diffraction maxima are present with the maximum at the higher $2\Theta_{Imax}$ value becoming pre-eminent for glass No.3 (32% Na_2O). We surmise that a similar phenomenon is responsible for the sudden emergence of the high diffraction maximum for the high calcium fly ashes reported by Diamond (7). Presumably, both maxima are present in most fly ashes but it requires a CaO content of about 20% in the fly ash overall before the higher maximum becomes predominant. In view of our third comment made above, it is likely that the effective CaO content in the glassy phase may, in effect, have to exceed 20% before the higher maximum emerges.

The X-ray patterns of the Na_2O-SiO_2 glasses show a slight increase in the higher $2\Theta_{Imax}$ values with decreasing SiO_2 or increasing Na_2O content. Diamond (7) did not observe significant change in the $2\Theta_{Imax}$ value for the high calcium fly ashes. It is possible that slight differences between the fly ashes and the Na_2O-SiO_2 system arise because of compositional variations between the two systems. It is noteworthy, for example, that there is a noticeable shift in $2\Theta_{Imax}$ when going from $Na_2O.SiO_2$ (glass No. 9) to $CaO.SiO_2$ (glass No. 10) where the molar percentages of SiO_2 and modifier are the same.

Wright and Leadbetter (11) have reviewed the literature on X-ray diffraction studies of glass structure. It appears that the structure of multicomponent silicate glasses is complicated and still largely unknown when compared to that of pure silica glass. Recent studies of alkali disilicate and alkali metasilicate glasses (12,13) confirm that the structures of even simple alkali silicate glasses have not been established unequivocally.

Current models of glass structure are largely based on the principles which govern the structures of crystalline silicates. The silicon atoms are tetrahedrally co-ordinated by oxygens. The tetrahedra are linked at the vertices to form a network with the modifying cations, such as alkali and alkaline earth ions occupying the interstices. The oxygens are of two types, those linked to two silicons are termed bridging oxygens. They convect adjacent tetrahedra. Oxygens connected to one silicon are known as nonbridging oxygens (NBOs). The NBOs form the co-ordination polyhedra for the modifiers.

Although conclusive evidence is still lacking, Raman spectral data reported by Brawer and White (14) suggest that alkali disilicate and metasilicate glasses have structures composed of the same units as their crystalline polymorphs. The major difference between the glassy and crystalline analogues appears to be a certain degree of disorder in the former, mainly through fluctuating Si-O-Si angles, distorted tetrahedral angles and Si-O distances, random relative orientations of tetrahedra and fluctuations in the number of NBOs per silicon. $Na_2O.2SiO_2$ glass has been assigned a distorted Si_2O_5-sheet structure with an average of one NBO per silicon while $Na_2O.SiO_2$ will have distorted Si_2O_6-chains with two NBOs per silicon on average.

It is worthwhile to include in this discussion the structural changes that have been inferred for alkali silicates upon substitution of Na_2O by CaO or MgO and SiO_2 by Al_2O_3. Since the CaO content of fly ashes is usually larger than the combined alkali oxide content and substantial amounts of Al_2O_3 are present as well. Raman spectral evidence has shown (15) that partial replacement of Na_2O by CaO in glasses containing up to 50 mol % Na_2O merely acts to increase the degree of disorder without substantial modifications of the network structure. With the reservation that the effect of almost complete substitution of Na_2O by CaO has not been evaluated it appears then that the basic structural features observed for Na_2O-SiO_2 glasses will also apply to Na_2O-CaO-SiO_2 glasses. The similarity in X-ray patterns for glasses Nos. 2 and 10 and glasses Nos.7 and 11 which have similar amount of modifier supports this view.

The effects of the addition of Al_2O_3 to soda silicate and soda lime silicate glasses is complex. The role of Al_2O_3 in glasses is two-fold, it can either act as a network former via four co-ordinate aluminum (Al^{IV}) or as a modifier via six co-ordinate aluminum (Al^{VI}). In the former case its presence will not increase the number of NBO's while in the latter case it will.

Whether aluminum in silicate glasses assumes four or six co-ordination is still a matter of controversy. It is usually assumed that in soda silicates all aluminum is present as Al^{IV} until the Al/Na ratio exceeds unity in which case the excess of aluminum is present as Al^{VI} (16-19). Brawer and White (15) have shown, however, that this model changes for sodium silicate in which Na_2O was partially substituted by CaO. In these glasses where the combined amounts of Na_2O and CaO were well in excess of the amount of Al_2O_3 and, therefore, 2Al/(2Na+Ca) was much lower than unity aluminum was predominantly present as Al^{VI} thereby acting as a modifier.

The effect of aluminum on the amorphous halo in the X-ray patterns of fly ashes is further complicated by the fact that a certain amount of Al_2O_3 is immobilized as mullite. The ratio of Al to the combined total of all monovalent and polyvalent modifying oxides and the extent to which CaO predominates as modifier will influence the proportions of aluminum present as Al^{IV} or Al^{VI}. In any case, it is likely that at least one aluminum is present as the six co-ordinate species and the Al^{VI} can be expected to increase the modifier level in the glass.

It is interesting to note again the remarkable similarity in the X-ray patterns and the diffraction maxima for the $CaO-Al_2O_3-SiO_2$ glasses (see Table 41). There is no evidence for a secondary maximum at lower 2θ values suggesting a structure which is highly depolymerized.

7.6.7 Summary

The major conclusions of the X-ray powder diffraction study carried out on model and commercial glasses, fly ashes and slags are:

i) The amorphous halo may contain several diffraction maxima attributable to different structural units in the glassy component of the source material.

ii) The sudden jump observed in the diffraction maxima of U.S. fly ashes with CaO contents in excess of 20% observed by Diamond (7) is probably attributable to a different 2θ maximum being pre-eminent in these fly ashes.

iii) The assignment of the higher $2\Theta_{Imax}$ value to a calcium aluminate glass of composition $C_{12}A_7$ by Diamond (7) is speculative. It has been shown in this study that a number of different glass compositions may give similar $2\Theta_{Imax}$ value close to the value observed for $C_{12}A_7$.

iv) Better correlations are found for various glassy waste materials if the $2\Theta_{Imax}$ values are considered versus the total modifier content.

7.7 Fourier Transform Infrared (FTIR) Spectroscopy

7.7.1 Introduction

There are a number of factors that ought to be considered when interpreting the FTIR spectra of the fly ashes and slags of these studies.

(i) Overall Composition

Since composition and structure are related the content of the major network formers SiO_2, Al_2O_3, Fe_2O_3, and of the major modifiers CaO, MgO and Na_2O is of importance. Knowing the oxide content the structural features can be deduced by comparing the vibrational spectra of the waste materials studied here with literature data on minerals and glasses of similar compositions.

(ii) Composition of the Individual Particles

SEM work carried out during this project has shown that there is a great deal of variation in the composition of individual particles. Thus, the composition deduced from the vibrational spectra is an average over the entire sample examined. This factor is more important for fly ashes than for slags since the latter category of glassy waste materials can be expected to be more homogeneous in the elemental make-up of its individual particles.

(iii) Glassy and Crystalline Phases

Because of disorder arising from variations in bond distances and bond angles the lines in the infrared and Raman spectra of glasses are usually broadened when compared with their crystalline polymorphs.

For an interpretation of the spectral features of the fly ashes and slags studied here we will use the principles outlined in monographs on vibrational spectroscopy by Farmer (20), Lazarev (21) and Nakamoto (22).

Most minerals and glasses can be formulated as $A_aB_bX_x$ where A and B are cations and X is a monoatomic anion. The anion plays a central role in binding the cations together, it is often the lightest atom and it is involved in the strongest bonds within the structure and participates in the vibrations of the highest frequency. Since these vibrations are largely localized on the X atom the masses of the cation play only a minor role compared to bond strengths in determining frequencies. For all practical purposes, the only anion to be considered for the study of fly ashes and slags is the oxide anion, O^{2-}.

Next to consider is whether in the generalized mineral formula $A_aB_b \ldots .X_x$ the B-X bonds are so much stronger than the A-X bonds that a separate BX_n complex can be considered. Such a complex is obvious for carbonates, phosphates, nitrates and sulfates where both the B-X stretching vibrations and the X-B-X bending vibrations are localized in the anions. The A-X bonds, however, can lead to a considerable modification of the effective symmetry of the anion and in the frequency of its vibrations, compared with those of an isolated anion.

At the other extreme are structures such as the spinels, $A_2^{3+}B^{2+}O_4$ in which A-O and B-O bond strengths and stretching frequencies are comparable and separate BO_4^{6-} tetrahedra or $A_2O_4^{2-}$ units can not be identified.

The distinction between these two extremes is not entirely clear but as a rule of thumb one can assume that a B-O stretching frequency of over 700 cm^{-1} makes it useful to discuss the structure in terms of separate BO_n groupings since A-O stretching frequencies generally lie below 500 cm^{-1} for the common situation where A is a heavily coordinated di- or trivalent cation. Table 52 shows the frequency ranges corresponding to metal-oxygen stretching for tetrahedral and octahedral coordination. Table 53 shows the vibrational frequencies of anionic groups in minerals containing oxygen.

In first approximation, the regions of interest are:

1000-800 cm^{-1} : stretching frequencies of isolated SiO_4 polyhedra.

1200-900 cm^{-1} : stretching frequencies of condensed SiO_4 polyhedra.

550-450 cm^{-1} : bending frequencies of isolated SiO_4 polyhedra.

800-400 cm^{-1} : bending frequencies of condensed SiO_4 polyhedra.

900-700 cm^{-1} : stretching frequencies of condensed AlO_4 polyhedra.

850-700 cm^{-1} : Al-O stretching frequencies in isolated AlO_4 tetrahedra.

550-350 cm^{-1} : Al-O stretching frequencies in isolated AlO_6 octahedra.

650-500 cm^{-1} : Al-O stretching frequencies in condensed AlO_6 octahedra.

This first approximation can be further refined by taking into consideration frequency shifts which arise because of the extent of polymerization in the glass network, the ratio of bridging to non-bridging oxygen atoms in silicate and aluminate tetrahedral groupings, the presence of mixed bridging units (e.g. Si-O-Al), the effect of the size, mass and charge on the cations, etc.

ORF

7.7.2 FTIR Spectra of Fly Ashes and Slags

The FTIR spectra of the 9 Canadian fly ashes and 2 blast furnace slags (see Figure 43) are similar in several respects. They all show a strong dominant broad band centred between 1085 and 928 cm^{-1} and a narrower strong band with an intensity maximum between 453 and 520 cm^{-1}. There are subsidiary peaks between 550 and 800 cm^{-1}, at ~1430 cm^{-1}, and ~1630 cm^{-1}. Finally, these spectra also show a broad asymmetric band located between 3426 and 3462 cm^{-1}. These features and their relevance to the structure of the glassy waste materials will now be discussed in turn.

~3400 cm^{-1}, ~1630 cm^{-1}

The vibrational spectrum of weakly absorbed water is characterized by broad bands at ~3400 cm^{-1} and ~1600 cm^{-1}. These features were invariably found in the FTIR spectra of the materials studied here. Figure 2 shows the spectrum of the Sundance fly ash between 4400 and 400 cm^{-1}. The two H_2O-peaks are clearly distinguishable.

The broad band at ~3400 cm^{-1} can be attributed to the symmetric and asymmetric stretching vibrations of adsorbed water. The ~1630 cm^{-1} band is the deformation vibration (ν_2) of adsorbed water.

The presence of the two water bands is evidence that some H_2O is always found in these fly ashes and glasses. The peak positions indicate that the water is weakly adsorbed rather than chemically bound. The adsorption, presumably takes place through the formation of moderately strong hydrogen bonds (20).

~1430 cm^{-1}

A band at approximately this position was clearly found for the two blast furnace slags but was absent in the FTIR spectra of the fly ashes. Table 52 suggests that this band may be attributable to nitrates, carbonates or borates. Chemical analysis showed that the C-content was quite low (0.76% for Standard slag and 0.04% for Atlantic slag). The position of the band, however, clearly indicates the presence of carbonate (20). It is likely that the band arises because of the presence of $CaCO_3$ formed by the reaction of Ca^{2+} in the slag with atmospheric CO_2. The ~1430 cm^{-1} band is absent for the fly ashes which have a substantially lower Ca^{2+} content.

1300-750 cm^{-1}

The strongest feature in the FTIR spectra is a broad band centred between 1085 and 928 cm^{-1} in this range. The position of the band is indicative of a strong silicate component presumably with a contribution of aluminate and alumino-silicate groupings. It was mentioned in the previous section that isolated SiO_4 polyhedra have stretching frequencies in the 1000-800 cm^{-1} range while condensed SiO_4 polyhedra absorb between 1200 and 900 cm^{-1} (Table 53).

Within each of these categories there are a great number of structures possible, each giving rise to several strong bands. A great deal of information is available from the structures of minerals. Isolated SiO_4 tetrahedra are found for the orthosilicate minerals Ba_2SiO_4, $ZrSiO_4$ (zircon), the olivines (M_2SiO_4, M' = Ca, Mn, Fe, Co, Ni). These minerals give a strong band in the 1000-850 cm^{-1} range which may be split into several sub-bands.

Condensed silicates usually have two sets of bands, one of which is observed at higher frequency than those of the isolated SiO_4 polyhedra attributable to the asymmetric stretching vibrations of Si-O-Si and O-Si-O groupings. For example, bands are found between 1200 and 950 cm^{-1} for chain type silicates $(SiO_3)_n$, which make up the network structures of Li_2SiO_3 and Na_2SiO_3. The ring type silicate found in α-$CaSiO_3$ (pseudo-wollastonite) and $Cu_6Si_4O_{18}$ (dioptase) also absorb in this range.

ORF

The second set of bands associated with the symmetric stretching vibrations of Si-O-Si and O-Si-O groupings can be found at the low end of the isolated SiO_4 range between 900 and 550 cm^{-1}.

Condensed silicates with higher degrees of polymerization such as found in talcs and bentonitic clays follow similar trends as for the chain type silicates. But there usually is a good deal of overlap with the range associated with isolated SiO_4 polyhedra.

Silicate glasses have bands that are usually broadened compared to those of the crystalline compounds of identical composition but the positions of highest intensity are often similar. This suggests that the structures of the glasses are close to those of their crystalline polymorphs.

The presence of Al will not change this picture significantly since Al can replace Si as a network former and Si-O-Al stretching and bending vibrations often absorb in the same range as Si-O-Si equivalents. The ratio of Si:Al in the fly ashes ranges from 3.5:2 to 5:2 for most of the compositions studied. A reasonable description of the main band in this range would be ν_{as} Si-O-Si or ν_{as} Si-O-Al (asymmetric stretch).

Although, the FTIR spectra do not allow a detailed assignment of the structural features and by necessity give an overall or average picture some interesting deductions can be made. First, the frequency at which the dominant band in this range reaches its maximum is an indication of the overall degree of polymerization of the network. In general, a lower frequency maximum will correspond to a lower degree of polymerization, i.e. a network with a lower degree of connectivity.

Thus, Estevan fly ash, Standard slag and Atlantic slag with band maxima between 957 and 928 cm^{-1} will be much less polymerized than, for example, Lakeview fly ash which has a band maximum at 1085 cm^{-1}. It can be expected that a weaker network structure would be more easily broken down under chemical attack. The band maximum in this respect could be correlated with chemical reactivity, i.e. a lower maximum can be expected to correspond with a more reactive waste material.

The ratio of network formers to modifying cations affects the degree of polymerization. An increase in modifier content will tend to cause the rupture of Si-O and Al-O bonds in the network leading to a more depolymerized structure. Table 54 lists the frequency maxima from Figure 43 and the content of CaO as well as the total modifier content.

The correlation coefficients for ν_{Si-O} with CaO content and total modifier content were found to be -0.755 and -0.840, respectively. Thus, a higher modifier content and to a lesser extent a higher CaO content will give rise to a lower band maximum. And as discussed above also a more depolymerized network and a more reactive material. It would be interesting to establish experimentally to which extent the band maximum correlates with the reactivity of these waste materials. One point of caution ought to be raised here. It is possible that Al may partially act as a modifier for these waste materials, particularly when the content of the other modifiers is low. It is beyond the scope of this investigation to establish to what extent this has occurred for this system.

There are some minor features in this range worth noting. First, the decrease in ν_{Si-O} for the three Alberta fly ashes Wabamun, Sundance and Forestburg. This decrease does not correspond to the change in the CaO content observed. However, it becomes understandable when considering the decrease in SiO_2 content and increase in total modifier content.

The Thunder Bay fly ash shows the presence of two minor sharp peaks at 1142 and 1103 cm^{-1} within the main band at 1016 cm^{-1}. This fly ash was also found to have different crystalline phases compared with the other fly ashes (sulfates). The 1103 cm^{-1} band is possibly the ν_3 stretching frequency of the sulfate (SO_4) group. This is likely since the corresponding ν_4 bending vibration can also be discerned at 610 cm^{-1}. The bands at 1142 cm^{-1} (and at 638 cm^{-1} and 676 cm^{-1}) could also originate in sulfate vibrations. Anhydrite ($CaSO_4$) has bands and 1108, 1128 and 1160 (ν_3) and at 609, 628 and 674 (ν_4) (22).

676-795 cm^{-1}

All FTIR spectra show a band in this region. A band in the 800-600 cm^{-1} region has been attributed to ν_3 Si-O-Si or ν_3 Si-O-Al (symmetric vibrations) (20). This band follows the same trend as the corresponding asymmetric stretch (ν_{as}), a decrease in frequency when the network is more depolymerized. The band at 684 cm^{-1} observed in the FTIR spectrum of Dalhousie can possibly be attributed to ν_s Si-O-Fe, since the substitution of Fe for Al lowers the frequency of this band.

520-453 cm^{-1}

The band in this region is centred at ~463 cm^{-1} for most compositions. It can be assigned to the O-Si-O deformation mode of the silicate network. This band increases in frequency when the network is more depolymerized. This is indeed observed for the Standard and Atlantic slags but not for Estevan.

550-571 cm^{-1}

A band at this position is found for Nanticoke, Lakeview, Lingan and Dalhousie. It is possible that this band can be attributed to an Fe-O vibration (see Table 52) since its presence is only noted in glassy waste materials with a high Fe-content.

7.7.3 Summary

Fourier Transform Infrared spectroscopy was found to be a useful technique for the correlation of compositional and structural parameters in fly ashes and slags. In particular, the position of the major silicate-aluminate stretching band can be correlated with the total modifier (CaO + MgO + Na_2O + K_2O) content and to a lesser extent with the CaO content of the glassy waste material. The technique is potentially applicable for the correlation of structure and reactivity of glassy waste materials.

7.8 Hydration Studies in H_2O

7.8.1 Introduction

A substantial number of leaching trials have been carried out on the 11 source materials of this study using distilled deionized H_2O. It was realized from the outset that the information obtained from these trials could not be extrapolated to typical reactions occuring during the hydration of concrete mixtures. The pH values in the latter case will be highly alkaline (typically 13-14) and leached cations and other groupings from the various ingredients other than the glassy waste material will determine the types, concentrations and sites of the hydration products. The leaching studies in H_2O are valuable since they can elucidate which cations and groupings of the waste materials themselves are reactive in the absence of activation by OH^- or other species. The simplification achieved by carrying out a set of leaching experiments in dionized water will enable a study of the differences in reactivity between the source materials of this investigation. The data obtained can be correlated with the known behaviour of inorganic glasses and form the foundation for studies in more complex system to be carried out in future work.

7.8.2 Studies on As-Received Fly Ashes and Slags

Profiles of pH vs time and mass changes observed during leaching of the "as-received" source materials of this study are given in Figure 45 and Table 44, respectively. A summary of trends is given in Table 45. On the basis of their hydration behaviour in H_2O the fly ashes and slags can be categorized as follows:

(a) Wabamun, Sundance, Forestburg, Nanticoke, Lakeview and Estevan show a relatively rapid rise in pH from neutral values (6-7) to the pH maximum from 10-11 which is commonly achieved within the first 30 min. after the start of the experiment. The pH remains constant for a period lasting from 1-5 hrs after which a gradual drop in pH occurs until the final value of pH ~8-9 has been achieved. Increasing the amount of source material leads to an increase in the maximum pH value reached, an extension of the time period over which the pH remains approximately constant, a decrease in the rate at which the pH subsequently drops, and a higher final pH value.

(b) Dalhousie shows quite a different pH versus time behaviour. The initial pH is barely in excess of a value of 4. The pH gradually increases with time to reach a maximum close to neutral value at the 24 hr mark. The differences between the curves for various masses are minimal.

(c) The pH versus time behaviour of Lingan is somewhere in between that of Wabamun, etc. and Dalhousie. The maximum pH value of 8.85 is achieved after 45 min. The pH hovers about the 8.5 mark during most of the experiment to reach a final value of about 8 after 24 hrs. The Forestburg fly ash pH versus time curve resembles that of Wabamun etc. but the maximum pH value is much lower.

(d) The two slag materials again behave somewhat differently. For Standard slag, the pH versus time profile closely resembles that of Wabamun, etc. at the two lowest levels of leached material. The pH maximum, however, is at somewhat lower values. For the two highest slag levels, the pH was observed to increase up to about 4 hrs and to drop only slightly during the remainder of the experiment. The pH versus time curves for Atlantic slag are almost identical at the four levels of slag additions studied. The maximum pH similar to the values found for Wabamun, etc. is achieved after ~1 hr and is maintained throughout the experiment.

Correlations with Compositions:

In order to establish the factors that govern the leaching behaviour of the 11 source materials of this study we have calculated the correlation coefficients for a series of compositional, physical and structural parameters which were determined during this study. The results have been listed in Table 55.

The results are somewhat surprising. One would expect the pH to increase with the content of modifying cations in the glass since the exchange reaction:

$$-\text{Si}-\text{O}^- \; M^+_{(g)} + H_2O_{(1)} \longrightarrow \text{Si}-\text{O}-H_{(g)} + M^+_{(aq)} + OH^-_{(aq)}$$

will increase the maximum pH of the leaching solution. In fact, there was no significant correlation between the modifier content of the glass and the maximum pH during leaching.

Interestingly, the maximum pH in solution is positively correlated with both the SiO_2 and Al_2O_3 content of the fly ashes and negatively correlated with the Fe_2O_3 content. A combined correlation coefficient between maximum solution pH and $\sum(SiO_2 + 2xAl_2O_3-2Fe_2O_3)$ is even better. This correlation is still observed when the slags are included as well.

The correlations of maximum solution pH with glass content B.E.T. surface area or average particle diameter are weak or absent.

In conclusion it was observed that the leaching solution became increasingly alkaline with increased SiO_2 or Al_2O_3 levels (for fly ashes only). The solution became less alkaline, or more acidic, with increased Fe_2O_3 levels for all source materials. It appears also that these factors mutually reinforce each other, e.g. a high SiO_2 and low Fe_2O_3 level will give a higher maximum solution pH than a high SiO_2 level by itself. On the other hand, caution is required when interpreting this limited data set. It is possible that the SiO_2, Al_2O_3 and Fe_2O_3 contents are not independent variables. For example, Dalhousie fly ash has a high Fe_2O_3 content while the SiO_2 and Al_2O_3 contents are significantly lower than those of the other fly ashes, at least partly because of the high Fe_2O_3 content.

The Role of Fe^{3+}

The noticeable drop in pH in the presence of substantial amounts of Fe_2O_3 in the glass can be inferred from the known behaviour of iron oxides, iron hydroxides and related species. The Fe^{3+} ion in aqueous solution can be taken as a model system in this respect. The Fe^{3+} ion in aqueous solution is highly acidic since it can undergo hydrolysis according to:

$$[Fe(H_2O)_6]^{3+} + H_2O \rightleftharpoons [Fe(H_2O)_5(OH)]^{2+} + H_3O^+ \qquad (K_1 = 10^{-3.05})$$

$$[Fe(H_2O)_5(OH)]^{2+} + H_2O \rightleftharpoons [Fe(H_2O)_4(OH)_2]^{+} + H_3O^+ \qquad (K_2 = 10^{-3.36})$$

$$2[Fe(H_2O)_6]^{3+} + 2H_2O \rightleftharpoons [Fe_2(OH)_2(H_2O)_8]^{4+} + 2H_3O^+ \qquad (K_3 = 10^{-2.91})$$

The Fe^{3+} ion at the glass surface in contact with H_2O can be expected to undergo similar hydrolysis reactions releasing $H_3O^+_{(aq)}$ which can be expected to lower the pH of the solution. This reaction can be represented by:

$$[-\overset{|}{\underset{|}{Si}}-O^- \ \ Fe(H_2O)_5]^{3+} + H_2O \rightleftharpoons [-\overset{|}{\underset{|}{Si}}-O^- \ \ Fe(H_2O)_4(OH)]^{2+} + H_3O^+, \text{ etc}$$

This reaction is most noticeable in Dalhousie fly ash which has an unusually high Fe_2O_3 content, but the pH behaviour of the Lingan ash indicates that even lower Fe_2O_3 contents may still depress the solution pH.

ORF

The Role of Na^+, K^+, Mg^{2+}, Ca^{2+}

The alkali and alkaline earth cations in the glass are largely responsible for the increase in solution pH upon leaching. This increase is largely the result of a surface reaction in which cations in the glass are exchanged for hydronium ions from the solution leaving an excess of $OH^-_{(aq)}$ with the resultant rise in pH.

The Role of SiO_2

The silicate framework of the glassy waste materials is vital for their role in cement hydration for two reasons. First, it can react with $OH^-_{(aq)}$ thereby reducing the pH; and secondly, it can act as a source of siliceous materials which can become incorporated into C-S-H type structures.

As the solution pH increases to ~9-10 as a result of cation exchange described above the silica network breaks down releasing siliceous acids. The reaction of the silicates of the network by $OH^-_{(aq)}$ and the further exchange of cations leads to a steady state during which the pH remains constant.

The last stage shows a drop in pH. This suggests that the consumption of $OH^-_{(aq)}$ during the breakdown of the silicate network continues while the exchange of cations from the fly ash particles with protons from solution is decreased. One explanation could be that an impermeable layer is formed at the glass surface impeding the process of ion exchange. The observed decrease in pH may then be caused by the consumption of OH^- for surface film formation. In addition the drop in pH could be aided by the absorption of atmospheric CO_2 in the reaction solution.

The Role of Al_2O_3

The leaching behaviour of Al_2O_3 in glass is also pH dependent.

pH<3.2: the predominant species is $Al^{3+}_{(aq)}$

pH 3.2-11.5: the stable species are Al_2O_3 and $Al(OH)_3$

pH>11.5: AlO_2^- is formed; it becomes significant above pH 14.

In addition Al can participate in the glass network like Si and aluminate groupings will presumably decompose along the same lines as silicates.

Mass and pH Changes Observed

A series of leaching experiments was carried out using various levels of glassy waste materials. In general, no simple relationship between initial mass and mass changes or between initial mass and maximum solution pH could be detected.

Changes in pH were, in general, less than what could be expected on the basis of the mass increase. Thus, a two-fold increase in mass can be expected to give a pH change of ~0.3 (=log 2). In fact, pH changes observed where usually less, suggesting that a doubling of the surface area cannot totally explain the pH behaviour. Mass changes (see Table 44) were often erratic suggesting a more complex hydration behaviour.

Finally, it is of interest to observe any changes in the surfaces of the glassy waste materials after leaching. X-ray diffraction showed no change in most of the fly ashes. Peaks indicative of $CaCO_3$ were detected for Sundance and Nanticoke fly ash and for Standard and Atlantic slag (see Table 49). The $CaCO_3$ was presumably formed in a reaction between surface $Ca^{2+}_{(g)}$ ions and dissolved CO_2. It can be seen that Atlantic slag which has a high Ca content shows a mass increase after leaching, indicative of precipitated $CaCO_3$. Thunder Bay fly ash which shows a higher than average mass decrease gives an XRD pattern depleted in the S-rich phases (Table 49).

Solution Analysis

Table 51 shows the results of DCP analysis carried out on solutions of Wabamun fly ash leached for various amounts of time. A gradual increase in the Si, Al, Ca and Mg content can be observed. It is interesting that most of the concentration of these elements in solution is already present at the 45 min. mark and that relatively little is added during the remainder of the leaching trial. The mass of the elements calculated as a percentage of the element present in Wabamun was determined as: Si: 0.31%, Al: 0.62%, Ca: 9.5%, Mg: 4.1%, Fe: negligible. Clearly, the modifiers Ca and Mg are preferentially leached over Si and Al.

7.8.3 Particle Size Effect

Curves for pH versus time for Wabamun and Dalhousie fly ashes leached in deionized H_2O (Table 46 and Fig. 46) as a function of particle size range show a clear trend.

On cursory inspection it seems that the two fly ashes behave quite differently. The Wabamun fly ash shows an increase in the maximum pH value of ~1.0 pH unit when the -400 mesh fraction is compared to the +400 mesh fraction while the Dalhousie fly ash shows the reverse behaviour, a clear drop in solution pH when the -400 mesh fraction is compared to the +400 mesh fraction. Furthermore, it was observed that the mass losses were lower for the batch with the coarser particles.

The observed behaviour reflects the relative changes in the $OH^-_{(aq)}$ and $H_3O^+_{(aq)}$ concentration for the leaching of fly ashes of different size ranges and, as a result, different exposed surface areas. In the case of Wabamun fly ash, the leaching trial on the finer particulates involves a greater exposed surface area. The result is an increase in the number of glass cations being exchanged for solution $OH^-_{(aq)}$ ions. The pH will therefore be relatively increased when compared with the coarser particulates at a certain time. The Dalhousie fly ash, on the other hand, shows an acidic reaction when dissolved in deionized H_2O. Hydrolysis of hydrated $Fe^{3+}_{(g)}$ results in the release of $H_3O^+_{(aq)}$ ions to the solution. The finer particulate fraction will expose a greater surface area to solution resulting in an increase in the amount of $H_3O^+_{(aq)}$ in solution and decrease in the pH.

It should be noted that a modest correlation between maximum solution pH and B.E.T. surface area was observed for the 11 source materials. But it should also be noted that the coincidence of a very low B.E.T. surface area for the Dalhousie fly ash which also gave a low maximum solution pH (due to compositional factors) was partially responsible for this correlation.

7.8.4 Leaching of Glassy and Redevitrified Analogues of Fly Ashes and Slags

Glassy Analogues

A series of glassy analogues had been prepared of the 11 source materials of this study for several reasons. In the first place, glassy analogues were used as admixtures for the preparation of the standard curves for the NCXRD glass content method. Secondly, these glassy analogues were prepared to gain an insight in the relation between the glassy phase of the waste materials and their hydration behaviour.

It was believed that the glassy analogues would be highly reactive. In fact, it was felt that these materials would represent the equivalent of rapidly quenched glassy waste materials. The investigation would involve a hydration study on these glassy analogues in their "as prepared" states as well as hydration studies on these analogues after they had been subjected to various heat treatment schedules. The heat treated glassy analogues were anticipated to be less reactive since the glass was partially ordered and possibly contain some crystalline materials.

The leaching behaviour of the glassy analogues was found to be very similar for the 10 source materials (Dalhousie glass could not be prepared) and very different from the parent materials. All initial pH were mildly acidic and in all cases below the starting pH of the deionized water. The pH increased with time to less acidic values and then dropped again at 24 hrs for most compositions except Nanticoke, Lakeview, Thunder Bay and Atlantic slag.

The lowering of the pH of the leachant solution indicates either adsorption of $OH^-_{(aq)}$ onto the glass surface or a hydrolysis process of surface adsorbed H_2O with the release of $H_3O^+_{(aq)}$. The similarity between the behaviour of the glassy analogues of most of the source materials suggest a general process largely independent of the overall composition of the waste materials. It was noticed that a number of the waste materials did not show a decrease in mass, although others did give a larger mass decrease then some of the parent materials when leached. A precipitate, marked phase X, was observed on four of the fly ash glasses which showed zero mass change. The phase X, of which the XRD pattern is shown in Fig. 51, was not identified. It is likely that phase X represents a reaction product of surface hydration involving solution $OH^-_{(aq)}$. The loss of $OH^-_{(aq)}$ would be responsible for the initial drop in pH observed. The subsequent rise in pH could be the result of a cation - $H_3O^+_{(aq)}$ exchange process.

It seems premature to discard the use of the glassy analogues as models for glassy waste material on the basis of these hydration experiments in deionized H_2O. Only leaching trials under more realistic conditions (high pH, etc.) will establish the validity of this approach.

Redevitrified Analogues

Redevitrification of the glassy analogues gave products that were crystalline. The redevitrified analogues were also used as admixtures for the preparation of standard curves for the NCXRD method.

Leaching studies in deionized H_2O (Table 47, Fig. 48) showed that these materials behaved similar to their glassy precursors. The pH versus time curves indicated that the pH was generally somewhat below the values observed for the glassy analogues. The mass changes were negative. It is likely that surface hydration and exchange reactions are similar to those observed for the glassy analogues.

Partially Redevitrified Analogues

Finally, a detailed pH versus time study was carried out on samples of the glassy analogues of Wabamun fly ash which had been subjected to progressive heat treatment. Curves of pH vs time show no clear trend. The pH hovers in general at ~pH=6. In fact, it can be observed that there is little overall change in the pH when the initial pH is close to 6.0. However, if the initial pH is below 6 (e.g. as for the sample subjected to nucleation at 810°C/2 hrs and for the sample nucleated at 810°C/16 hrs and crystallized at 950°C/48 hrs) then the pH will tend to increase to pH~6. It is possible that the effect observed here is attributable to a buffer system formed in the solution with time (HCO_3^-/CO_3^{2-} buffer?). The mass changes were generally negative and no clear trend was observed (Table 46).

The results of leaching trials on glassy, fully redevitrified and partially devitrified analogues of the glassy waste materials indicate that:

(a) the glassy and redevitrified analogues behave similarly.

(b) the glassy and redevitrified analogues behave differently from the "as received" source materials.

(c) on the basis of these limited experiments in deionized water there is no evidence that the glassy waste materials would show different hydration behaviour from the as received materials under conditions typical in concrete formation. Also it is not clear whether crystalline analogues would behave differently in concrete formation.

7.8.5 Leaching of Model Glasses

Using the chemical analysis data of Table 2 and the mineralogical composition of the glassy waste materials determined with the QXRD method (Table 21), the average compositions of the glassy phase of five fly ashes was determined. The results are given in Table 48 for the 7 major oxides. A series of 5 glasses was prepared with the compositions of Table 48 (see Section 5.17).

Curves for pH vs time for leaching in deionized H_2O are shown in Fig. 50. Mass changes are listed in Table 46. The pH shows an initial increase followed by a decrease. There are no substantial changes with time and it does not appear that the five model glasses behave very similarly to the parent materials.

7.9 Hydration Studies in NaOH

Hydration studies were also carried out in aqueous NaOH solutions of various initial pH values as the next step towards approaching more "realistic" systems. The results have been summarized in Fig. 53(a)-(e). Three materials have been investigated: Wabamun and Dalhousie fly ash and Standard slag.

The behaviour observed was as follows. At pH=7 the three source materials behave similarly to what was observed in the previous section (7.8.2). Wabamun rises quickly to a pH in excess of 10 while Dalhousie shows a strongly acidic pH. Standard slag reaches a pH of ~9.7 quickly and the pH drops only slightly with time.

Wabamun and Standard Slag show similar pH versus time curves at higher initial pH values. The Dalhousie curves shows a progressive increase in pH when the initial solution pH increases All three curves are similar over most of the duration of the experiment at pH=11. Dalhousie shows a slight pH drop towards the end of the 24 hr period.

It would be interesting to study the behaviour of the glassy waste material under conditions more typically found in cement hydration, i.e. pH:13-14, higher glassy waste material: solution ratios, and over longer periods of time. The results obtained so far seem to indicate that high-Fe waste materials may be effective in reducing the alkalinity. These materials may, therefore, be particularly useful for the control of alkali-aggregate reactivity.

This study was not pursued further because of the directions from the scientific monitor following the Steering Committee meeting of September 21, 1984, to concentrate all remaining efforts on glass content methodology assessment. It seems appropriate to carry out further hydration studies in subsequent phases of the program.

8. SUMMARY AND CONCLUSIONS

A substantial amount of data on nine Canadian fly ashes and two blast furnace slags have been collected under this program. The results can be summarized as follows:

(1) Chemical analysis data show that the fly ashes investigated contain low (< 5%) or intermediate CaO (5-15%) levels. The SiO_2 content varies substantially (37.1-58.6%) while the Al_2O_3 content was usually about ~21%. One fly ash, Dalhousie, had an exceptionally high iron content (38.9% Fe_2O_3) and low aluminum (12.3% Al_2O_3) and silicon content (37.1% SiO_2). The two slags showed a chemical composition common for North American blast-furnace slags.

(2) B.E.T. (triple point) surface area determinations gave values between 0.4 and 4.4 $m^2.g^{-1}$. These values are often an order of magnitude greater than the Blaine surface areas. It was concluded that the B.E.T. technique is more appropriate than the Blaine method for the determination of a representative surface area for fly ash and slag hydration.

(3) The average particle size for the source material was found to vary between 5.2 and 20.0 μm. The distributions are broad and with the exception of Dalhousie fly ash they show only one maximum.

(4) Two methods for glass content determinations have been used extensively for the source materials of this study. Quantitative X-Ray Diffraction (QXRD) was used to compute the mass percentages of α-quartz, mullite, magnetite and hematite, and the glass content by difference. Non-Crystalline X-Ray Diffraction (NCXRD) used the intensity of the amorphous hump at specified 2Θ-value of the glassy waste material of interest relative to a series of standard mixtures. The methodologies for these two techniques have developed under this program. Glass contents ranged from 53.5 to 94.5% using the QXRD method and from 42.8

to 99.3% with the MCXRD approach. The correlation of glass contents determined by the two approaches was found to be poor (r= -0.60).

(5) Several other approaches for glass content determination were addressed following input from the literature assessment. Differential Intensity X-Ray Diffraction (DIXRD) is an approach which could be a potentially useful technique. The McMaster Individual Particle Analysis can only be applied to slags. It was found that the glass contents determined with this approach varied considerably between operators although the reproducibility of the results for each operator was found to be good. Optical or electron optical examination combined with image analysis show little promise for glass content determination of fly ashes since the glassy and crystalline phases cannot be clearly distinguished.

(6) Electron optical examination (SEM) of Wabamun fly ash showed the presence of at least four types of particles: solid spheres, cenospheres, plerospheres and irregularly shaped particles. Energy Dispersive X-Ray Analysis (EDXA) showed a great deal of compositional variation between the individual particles and to a lesser extent within a particle itself. It is questionable, therefore, whether the overall composition is a good indicator for the reactivity of fly ashes in concrete hydration.

(7) An extensive structural investigation was carried out using X-ray powder diffraction on model glasses, commercial glasses and the 11 source materials of this study. The results show new light on the structural inferences made for fly ashes by Diamond (Cement and Concrete Research, 13, 459-464 (1983)). The sudden jump observed by Diamond for the diffraction maxima of fly ashes containing in excess of 20% CaO was explained on the basis of the XRD results for model glasses. It was shown that generally more than 2 diffraction maxima can be observed. The jump observed can be attributed to the emergence of another maximum becoming the dominant feature in the amorphous halo. The assignment by Diamond of the diffraction maximum for fly ashes with

CaO > 20% to a calcium aluminate glass $C_{12}A_7$ is speculative since it was shown in this study that model glasses of widely varying compositions show similar 2θ-maxima close to the 2θ-maximum of $C_{12}A_7$ glass. Finally improved correlations were found if the diffraction maxima were compared with the total modifier content of the glassy waste materials.

(8) FTIR spectra were collected for the source materials of this study as an additional means for structural characterization. The frequency maximum of the dominant silicate-aluminate stretching peak was observed to be inversely correlated with the total modifying oxide content.

(9) Hydration studies were carried out on deionized water and aqueous NaOH solutions. In H_2O most of the source materials showed a rapid rise in pH towards pH values of ~9-11 followed by a slower decline towards more neutral values. The high-Fe fly ash Dalhousie showed a drop to acidic pH values in H_2O. The maximum pH appears to be correlated with $\Sigma(SiO_2 + 2Al_2O_3 - 2Fe_2O_3)$ and not with the modifier content. The pH changes were found to be increased for a specific glassy waste material of smaller average particle size. Vitreous and redevitrified analogues of the glassy waste materials showed substantially different behaviour when leached in H_2O. The pH was generally found to drop towards more acidic values. These analogues are, therefore, not good model systems for the study of hydration behaviour in H_2O. On the other hand, they could still be useful model systems for hydration studies under more "realistic" conditions. Likewise, model glasses representative of the glassy phase of the waste materials show different hydration behaviour in H_2O when compared with these waste materials.

Limited hydration studies in aqueous NaOH solutions with pH values from 7-11 showed that a high-Fe fly ash (Dalhousie) lowered the pH values up to pH 10. High-Fe glassy waste materials could, therefore, be potentially more effective in reducing alkaline-aggregate reactivity.

(10) As far as the major objective of this program is concerned, the development of a Unified Theory for predicting the behaviour of glassy waste materials (fly ashes, silica fumes and slags) some progress has been made towards the establishment of methods for characterizing these materials and understanding the structure of these materials and their glassy phase. Specifically, the major achievements of this program have been in the following areas:

(i) Surface Area Characterization

B.E.T. analysis using Krypton rather than nitrogen was shown to be an effective means of establishing the surface area of glassy waste materials.

(ii) Glassy Content Determination

Two approaches using X-ray diffraction were developed to determine the glass contents of glassy waste materials. These techniques (QXRD and NCXRD) have the advantage over optical approaches that, potentially, they can be applied to all classes of glassy waste materials since they are independent of the ability to visually distinguish between the phases.

(iii) Structure of the Glassy Waste Materials

X-ray diffraction and FTIR spectroscopy were found to be useful techniques for the characterization of the glassy waste materials. New insights were obtained in the nature of the amorphous halo in the X-ray diffraction patterns. These insights are a refinement and improvement of the studies reported by other workers.

The results obtained to-date under this program will be extremely useful for subsequent investigations aimed at an elucidation of the hydration kinetics and mechanisms of the glassy waste materials which have been characterized in this study.

9. RECOMMENDATIONS

The following recommendations are made on the basis of the literature assessment and the results of the experimental investigations discussed in this final report:

(1) Glass Content Methodology

Two methods (QXRD and NCXRD) have been developed under this program for glass content determination. These two techniques are, in principle, applicable to all classes of glassy waste materials, i.e. fly ashes, silica fumes, and the various types of slags. It has also become clear that each of these two techniques have certain disadvantages for certain glassy waste materials. The QXRD technique may be a very time-consuming way to evaluate the glass content of a sample which has a substantial number of crystalline phases not commonly found. The NCXRD approach on the other hand, cannot be used for a material which cannot be vitrified through rapid quenching. An assessment ought to be made of the time and effort involved in developing each of these two approaches to the point where they can be used routinely for the rapid determination of glass content. This point needs particular consideration when considering the incorporation of the techniques developed under this program in Standards for use by industry.

Also, the procedures developed for the preparation of standard curves in the QXRD approach could be improved to obtain more representative crystalline phase/internal standard ranges.

The poor correlation between the QXRD and NCXRD methods for the 9 source materials evaluated by both techniques is a matter of concern. A round-robin approach involving several laboratories using the procedures described in this report may be required. Also, it is recommended to extend the number of source materials greatly to obtain a statistically more meaningful estimate of the reliability of the two approaches.

A useful extension of the program could involve a comparative study using several optical techniques (FTIR, Raman), electron optical, as well as the QXRD and NCXRD approaches for glass content determinations of blast-furnace slags. These slags have a relatively simple mineralogical make-up, often containing only one crystalline phase, and the glassy phase is homogeneous.

The Differential Intensity X-Ray Diffraction (DIXRD) method subjected to a preliminary evaluation under this program deserves further study. An evaluation of this approach could easily be included in a subsequent phase of the program since the vitreous and redevitrified analogues of 10 source materials have already been prepared.

(2) Structural Characterization

X-ray diffraction, FTIR spectroscopy and SEM/EDXA have been used successfully to characterize the 11 source materials of this study. Substantial progress was made in clarifying the nature of the diffraction maximum observed in the amorphous halo in the XRD pattern.

The observation of multiple diffraction maxima in model glasses and the dependence of the 2θ-values and the relative intensities of these maxima on composition were found to be important factors.

Further clarification could be obtained if a series of model glasses were prepared using the approach described in Section 5.17. These glasses will have the average composition of the glassy phase of fly ashes. Diffraction patterns could be collected for these glasses and diffraction maxima could be observed without the interference of accompanying crystalline phases. By including a number of high-Ca fly ashes, if necessary from U.S. sources, XRD patterns could be collected of a series of fly ashes and analogues of their glassy phases covering a wide CaO content range. This investigation would be useful in establishing how compositional factors correlate with X-ray diffraction

ORF

features. It would be helpful in showing the complexities of the systems studied and prevent premature conclusions such as those reported by Diamond.

FTIR and Raman spectroscopy could be used for future studies in clarifying structural features underlying the reactivity of the glassy waste materials. A lowering of the silicate-aluminate stretching frequency can be interpreted as evidence for a more depolymerized network which can be expected to be more reactive. FTIR data may, therefore, be supportive of reactivity data from hydration studies.

SEM/EDXA could be useful in classifying particle types and their average compositions. It would be worthwhile to determine whether certain oxides, notably CaO, Fe_2O_3 and TiO_2, show high concentrations in relatively few particles or whether they are distributed more or less evenly over all particles. The data collected for Wabamun fly ash suggest that the former description may be more representative than the latter. SEM/EDXA may then be used to classify the particles by composition, shape and size, and these data could be correlated with the hydration behaviour of fly ashes.

(3) Hydration Studies

This report provides the basic data for a comprehensive compositional, mineralogical, morphological and structural characterization of the 11 source materials studied thus far. Areas for refinement have been indicated under (1) and (2). So far, only preliminary hydration studies, mostly using H_2O, have been carried out. Further work should involve hydration studies under conditions that approximate more closely the processes in concrete formation. Interactions with alkali hydroxides and $Ca(OH)_2$ at pH~13-14 in systems containing higher glassy waste material/H_2O ratios than used thus far are a first step. The next stage would be a study on the hydration kinetics of Portland cement paste systems. SEM and thermal analysis could be used to analyze the hydration products and the unique capability at ORF developed for the extraction and analysis of pore solutions could be helpful for the interpretation of the results.

It seems that a careful study involving progressively more complex systems rather than an all-out investigation on the effect of the addition of glassy waste materials on concrete formation is more likely to increase an understanding of the fundamental processes involved. Following this approach we recommend that a study of mortar and concrete systems be postponed until a later phase of the program.

10. ACKNOWLEDGEMENTS

The authors wish to thank the members of the Steering Committee for this program, Dr. E. Douglas, Dr. M. Malhotra, Dr. P.K. Mehta, Dr. V.S. Ramachandran and Dr. D.M. Roy for their direction and helpful suggestions given during the program review meetings. The technical assistance of Mr. Patrick Betty, Mrs. Shabniz Hemraj and Ms. Pam Hollaman with the experimental work is hereby acknowledged. Thanks is also expressed to Mrs. Sally Broughton and Mrs. Diane Christie for their assistance with the preparation of this manuscript.

R.T. Hemmings

R.T. Hemmings, Ph.D.
Industrial Materials Centre

for M. van Roode, Ph.D.
Glass and Ceramics Centre

References

1. M.D. Karkhanavala and F.A. Hummel, J. Amer. Ceram. Soc., 36, 389 (1953).

2. H.P. Klug and L.E. Alexander, X-Ray Diffraction Procedures for Polycrystalline and Amorphous Materials, John Wiley & Sons, 2nd edition (1973).

3. S.M. Ohlberg and D.W. Strickler, J. Amer. Ceram. Soc., 45, 170-171 (1962).

4. J.H. Wakelin, H.S. Virgin and E. Crystal, J. Appl. Phys., 30, 1654 (1959).

5. J. Millet, R. Hammey and F. Brivot, Bull. Liaison des Labs. des Ponts et Chaussees 92, 101-104, Nov.-Dec. 1977.

6. L.E. Alexander, X-Ray Diffraction Methods in Polymer Science. John Wiley & Sons Inc., New York, 1969, Ch. 3.

7. S. Diamond, "On the Glass Present in Low-Calcium and in High-Calcium Flyashes", Cement and Concrete Research, 13, 459-464 (1983).

8. N. Valenkov and E.A. Porai-Koshits, Z. Krist., 95, 195 (1936).

9. See for example L.D. Hulett Jr., A.J. Weinberger, K.J. Northcutt and M. Ferguson, Chemical Species in Fly Ash from Coal-Burning Power Plants, Science, 210, 1356-1358 (1980).

10. R.J. Lauf, Microstructures of Coal Fly Ash Particles, Am. Ceram. Soc. Bull., 61(4), 487-490 (1982).

11. A.C. Wright and A.J. Leadbetter, "Diffraction Studies of Glass Structure", Physics and Chemistry of Glasses, Vol.17, No.5, 122-145 (1976).

12. M. Misawa, D.L. Price and K. Suzuki "The Short-Range Structure of Alkali Disilicate Glasses by Pulsed Neutron Total Scattering", J. of Non-Crystalline Solids, 37, 85-97 (1980).

13. I. Yasui, H. Hasegawa and M. Imaoka, "X-Ray Diffraction Study of the Structure of Silicate Glasses. Part I, Alkali Metasilicate Glasses. Part II, Alkali Disilicate Glasses", Physics and Chemistry of Glasses, Vol.24, No.3, 65-78 (1983).

14. S.A. Brawer and W.B. White, "Raman Spectroscopic Investigation of the Structure of Silicate Glasses I. The binary alkali silicates", J. Chem. Phys., 63(6), 2421-2432 (1975).

15. S.A. Brawer and W.B. White, "Raman Spectroscopic Investigation of the Structure of Silicate Glasses II. Soda-Alkaline Earth-Alumina Ternary and Quatenary Glasses", J. Non-Cryst. Solids, 23, 261-278 (1966).

16. See for example, J.O. Isard, "Electrical conduction in the aluminosilicate glasses", J. Soc. Glass Technol., 43, 113T (1959).

17. D.E. Day and G.E. Rindone, "Properties of Soda Alumino-silicate Glasses I. Refractive Index, Density, Molar Refractivity, and Infrared Absorption Spectra", J. Amer. Ceram. Soc., 45(10), 489-496 (1962).

18. Ibid, II. "Internal Friction", J. Amer. Ceram. Soc., 45(10), 497-504 (1962).

19. Ibid, III. "Co-ordination of Aluminum Ions", J. Amer. Ceram. Soc., 45(10), 579-581 (1962).

ORF

20. The Infrared Spectra of Minerals, V.C. Farmer ed., Mineralogical Society, Monograph 4, London, 1974.

21. A.N. Lazarev, Vibrational Spectra and Structure of Silicates, Consultants Bureau, New York, 1972.

22. K. Nakamoto, Infrared Spectra of Inorganic and Coordination Compounds, 2nd ed., Wiley Interscience, New York, 1970.

ORF

TABLES

TABLE 1

Nucleation/Crystallization Parameters*

Source	Melting Temp.(^{o}C)	DSP (^{o}C)	CTE (cm/cm/^{o}C)	Nucleation (^{o}C/hr)	Crystallization (^{o}C/hr)
Wabamun	1575	776	-	810/16 hr	950/16 hr
Sundance	1575			810/16 hr	950/16 hr
Forestburg	1575			810/16 hr	950/16 hr
Nanticoke	1575			830/16 hr	1050/4 days
Lakeview	1575			830/16 hr	1050/4 days
Lingan	1575	810		870/16 hr	950/48 hr
Dalhousie	1550				
Estevan	1575			810/16 hr	950/16 hr
Thunder Bay	1575	773	6.5×10^{-6}	830/16 hr	930/16 hr
Standard Slag	1575	777	7.3×10^{-6}	830/16 hr	950/16 hr
Atlantic Slag	1575			810/16 hr	950/16 hr

* DSP: dilatometric softening point;
CTE: coefficient of thermal expansion

ORF

TABLE 2

Composition of Fly Ashes and Granulated Blast Furnace Slags

Source	SiO_2	Al_2O_3	B_2O_3	P_2O_5	SO_3	TiO_2	Cr_2O_3	MnO_2	Fe_2O_3	SrO	CaO	MgO	Na_2O	K_2O	ZnO	PbO	C	LOI	Total
Wabamun	58.6	21.3	0.16	0.09	0.34	0.63	<0.01	0.07	3.33	-	11.1	1.80	0.57	0.67	0.007	0.005	0.51	0.77	99.3
Sundance	53.7	23.2	0.17	0.11	0.34	0.59	<0.01	0.06	3.86	-	12.5	1.36	2.03	0.55	0.009	0.008	0.49	0.39	99.0
Forestburg	52.0	21.2	0.74	0.42	0.51	0.44	<0.01	0.05	5.08	-	10.5	1.61	4.74	1.17	0.010	0.006	0.10	0.77	98.6
Nanticoke	48.8	21.5	0.14	0.27	0.96	1.00	0.01	0.04	10.6	-	5.95	1.12	0.87	0.95	0.011	0.007	6.30	7.54	98.5
Lakeview	43.7	22.7	0.17	0.33	1.66	1.11	0.02	0.04	15.7	-	3.82	1.09	0.87	1.63	0.021	0.007	7.34	9.7	100.2
Lingan	45.5	22.5	0.04	0.13	0.97	0.85	0.02	0.09	20.1	-	1.29	1.37	0.83	3.32	0.037	0.024	2.53	3.47	99.6
Dalhousie	37.1	12.3	0.04	1.55	1.77	0.60	0.01	0.25	38.9	-	4.45	0.78	0.64	1.64	0.019	0.005	0.42	1.54	100.5
Estevan	43.2	22.1	-	0.41	0.85	0.78	<0.01	0.03	3.45	0.49	13.0	3.15	8.43	0.84	-	-	0.53	0.93	97.3
Thunder Bay	41.2	21.1	-	0.64	6.84	0.93	<0.01	0.03	3.92	0.52	12.4	3.09	6.91	0.91	-	-	0.15	2.31	98.7
Standard	38.8	6.55	-	0.02	3.30	0.30	<0.01	1.19	1.30	0.04	35.1	12.1	0.37	0.47	-	-	0.76	-0.84	100.3
Atlantic	35.1	9.34	-	0.02	2.90	0.34	<0.01	0.46	0.98	0.04	40.1	9.62	0.18	0.22	-	-	0.04	-1.84	99.4

TABLE 3

Specific Gravities of the Source Materials

Source	Pycnometry as received	 after grinding	Le Chatelier Method as received	 after grinding
Wabamun	2.28	2.47	2.13	1.99
Sundance	2.15	2.44	1.99	2.89
Forestburg	2.00	2.43	1.61	2.50
Nanticoke	2.32	2.59	2.16	2.50
Lakeview	2.52	2.61	3.74	2.43
Lingan	2.60	2.76	1.82	2.66
Dalhousie	3.10	3.05	2.97	3.52
Estevan	2.49	-	-	-
Thunder Bay	2.67	-	-	-
Standard Slag	3.00	-	-	-
Atlantic Slag	2.98	-	-	-

ORF

TABLE 4

DENSITIES, PARTICLE SIZES AND SURFACE AREAS OF THE SOURCE MATERIALS

Source	Average Specific Gravity $(g.cm^{-3})^{(1)}$	From Sedigraph Analysis: Average Particle Size (µm)	From Sedigraph Analysis: % Particles <45 µm (wt.%)	From Sedigraph Analysis: Surface Area $(m^2.g^{-1})^{(2)}$	Wet Sieving Retained on No.325 Sieve	B.E.T. (Krypton) $(m^2.g^{-1})$	Blaine $(m^2.g^{-1})$
Wabamun	2.28	20.0	85.0	0.2587	42.5	2.2	0.2387
Sundance	2.15	12.0	93.5	0.3247	18.1	1.0	
Forestburg	2.00	11.0	96.5	0.5360	30.6	1.9	
Nanticoke	2.32	19.0	89.0	0.2463	39.7	3.8	
Lakeview	2.52	11.0	94.0	0.3864	21.6	4.4	
Lingan	2.60	11.0	94.0	0.3441	16.4	1.0	
Dalhousie	3.10	17.0	95.0	0.1954	17.8	0.4	0.2127
Estevan	2.49	9.2	93.0	0.5256	22.6	1.6	
Thunder Bay	2.67	5.2	99.0	0.4877	3.1	1.1	
Standard Slag	3.00	8.3	98.0	0.5362	12.6	2.5	
Atlantic Slag	2.98	6.3	99.0	0.7201	1.7	2.0	

(1) By Pycnometry;

(2) Calculated assuming spherical particle shape.

TABLE 5

Particle Size Distribution by Sedigraph Analysis -

Numerical data accompanying the Sedigraph traces
of Figure 1

(a)	Wabamun
(b)	Sundance
(c)	Forestburg
(d)	Nanticoke
(e)	Lakeview
(f)	Lingan
(g)	Dalhousie
(h)	Estevan
(i)	Thunder Bay
(j)	Standard Slag
(k)	Atlantic Slag

```
NUMBER DISTRIBUTION OF PARTICLES FROM WEIGHT DATA FOR
WAGAMUM (-149 MICRONS)

CLASS INTERVAL   AVERAGE RADIUS   WEIGHT   NUMBER OF PARTICLES   NUMBER
  (MICRONS)        (MICRONS)      PERCENT       PER GRAM         PERCENT
  0.0-   0.5         0.125          0.0         0.0E+00            0.0
  0.5-   1.0         0.375          1.0         2.0E+10           70.6
  1.0-   1.5         0.625          1.0         4.3E+09           15.2
  1.5-   2.0         0.875          1.0         1.6E+09            5.6
  2.0-   2.5         1.125          1.0         7.4E+08            2.6
  2.5-   3.0         1.375          1.0         4.0E+08            1.4
  3.0-   3.5         1.625          2.0         4.9E+08            1.7
  3.5-   4.0         1.875          1.0         1.6E+08            0.6
  4.0-   4.5         2.125          3.0         3.3E+08            1.2
  4.5-   5.0         2.375          1.0         7.8E+07            0.3
  5.0-  10.0         3.750          5.5         1.1E+08            0.4
 10.0-  15.0         6.250         22.5         9.6E+07            0.3
 15.0-  20.0         8.750          9.5         1.5E+07            0.1
 20.0-  25.0        11.250          8.5         6.3E+06            0.0
 25.0-  30.0        13.750          7.5         3.0E+06            0.0
 30.0-  35.0        16.250          7.5         1.8E+06            0.0
 35.0-  40.0        18.750          6.0         9.5E+05            0.0
 40.0-  45.0        21.250          6.0         6.5E+05            0.0
 45.0-  50.0        23.750          4.0         3.1E+05            0.0
 50.0-  55.0        26.250          3.0         1.7E+05            0.0
 55.0-  60.0        28.750          2.0         8.8E+04            0.0
 60.0-  65.0        31.250          2.5         8.6E+04            0.0
 65.0-  70.0        33.750          1.5         4.1E+04            0.0
 70.0- 100.0        42.500          2.0         2.7E+04            0.0


SURFACE AREA DETERMINATION FOR WAGAMUM (-149 MICRONS)

CLASS INTERVAL   AVERAGE RADIUS   WEIGHT        AREA
  (MICRONS)        (MICRONS)      PERCENT  FRACTION (CM↑2)
  0.0-   0.5         0.125          0.0          0.0
  0.5-   1.0         0.375          1.0        350.9
  1.0-   1.5         0.625          1.0        210.5
  1.5-   2.0         0.875          1.0        150.4
  2.0-   2.5         1.125          1.0        117.0
  2.5-   3.0         1.375          1.0         95.7
  3.0-   3.5         1.625          2.0        161.9
  3.5-   4.0         1.875          1.0         70.2
  4.0-   4.5         2.125          3.0        185.8
  4.5-   5.0         2.375          1.0         55.4
  5.0-  10.0         3.750          5.5        193.0
 10.0-  15.0         6.250         22.5        473.7
 15.0-  20.0         8.750          9.5        142.9
 20.0-  25.0        11.250          8.5         99.4
 25.0-  30.0        13.750          7.5         71.8
 30.0-  35.0        16.250          7.5         60.7
 35.0-  40.0        18.750          6.0         42.1
 40.0-  45.0        21.250          6.0         37.2
 45.0-  50.0        23.750          4.0         22.2
 50.0-  55.0        26.250          3.0         15.0
 55.0-  60.0        28.750          2.0          9.2
 60.0-  65.0        31.250          2.5         10.5
 65.0-  70.0        33.750          1.5          5.8
 70.0- 100.0        42.500          2.0          6.2

TOTAL SURFACE AREA = 2567     CM↑2 G
```

```
MBER DISTRIBUTION OF PARTICLES FROM WEIGHT DATA FOR
NDANCE

ASS INTERVAL    AVERAGE RADIUS   WEIGHT   NUMBER OF PARTICLES   NUMBER
(MICRONS)          (MICRONS)     PERCENT       PER GRAM         PERCENT
 0.0-   0.5          0.125          0.0        0.0E+00            0.0
 0.5-   1.0          0.375          0.0        0.0E+00            0.0
 1.0-   1.5          0.625          0.5        2.3E+09           26.1
 1.5-   2.0          0.875          1.5        2.5E+09           28.5
 2.0-   2.5          1.125          1.0        7.8E+08            9.0
 2.5-   3.0          1.375          2.0        8.5E+08            9.8
 3.0-   3.5          1.625          2.0        5.2E+08            5.9
 3.5-   4.0          1.875          3.0        5.1E+08            5.8
 4.0-   4.5          2.125          3.5        4.1E+08            4.6
 4.5-   5.0          2.375          2.5        2.1E+08            2.4
 5.0-  10.0          3.750         28.0        5.9E+08            6.8
10.0-  15.0          6.250         14.0        6.4E+07            0.7
15.0-  20.0          8.750         10.5        1.7E+07            0.2
20.0-  25.0         11.250          8.0        6.2E+06            0.1
25.0-  30.0         13.750          6.0        2.6E+06            0.0
30.0-  35.0         16.250          4.5        1.2E+06            0.0
35.0-  40.0         18.750          3.0        5.1E+05            0.0
40.0-  45.0         21.250          3.5        4.1E+05            0.0
45.0-  50.0         23.750          1.5        1.2E+05            0.0
50.0-  55.0         26.250          2.0        1.2E+05            0.0
55.0-  60.0         28.750          1.0        4.7E+04            0.0
60.0-  65.0         31.250          0.5        1.8E+04            0.0
65.0-  70.0         33.750          0.5        1.4E+04            0.0
70.0- 100.0         42.500          1.0        1.4E+04            0.0
```

```
URFACE AREA DETERMINATION FOR SUNDANCE

LASS INTERVAL     AVERAGE RADIUS   WEIGHT        AREA
 (MICRONS)          (MICRONS)      PERCENT  FRACTION (CM↑2)
  0.0-   0.5          0.125          0.0          0.0
  0.5-   1.0          0.375          0.0          0.0
  1.0-   1.5          0.625          0.5        111.6
  1.5-   2.0          0.875          1.5        239.2
  2.0-   2.5          1.125          1.0        124.0
  2.5-   3.0          1.375          2.0        203.0
  3.0-   3.5          1.625          2.0        171.7
  3.5-   4.0          1.875          3.0        223.3
  4.0-   4.5          2.125          3.5        229.8
  4.5-   5.0          2.375          2.5        146.9
  5.0-  10.0          3.750         28.0       1041.9
 10.0-  15.0          6.250         14.0        312.6
 15.0-  20.0          8.750         10.5        167.4
 20.0-  25.0         11.250          8.0         99.2
 25.0-  30.0         13.750          6.0         60.9
 30.0-  35.0         16.250          4.5         38.6
 35.0-  40.0         18.750          3.0         22.3
 40.0-  45.0         21.250          3.5         23.0
 45.0-  50.0         23.750          1.5          8.8
 50.0-  55.0         26.250          2.0         10.6
 55.0-  60.0         28.750          1.0          4.9
 60.0-  65.0         31.250          0.5          2.2
 65.0-  70.0         33.750          0.5          2.1
 70.0- 100.0         42.500          1.0          3.3

TOTAL SURFACE AREA = 3247    CM↑2/G
```

ORF

```
NUMBER DISTRIBUTION OF PARTICLES FROM WEIGHT DATA FOR
FORESTBURG

CLASS INTERVAL   AVERAGE RADIUS   WEIGHT   NUMBER OF PARTICLES   NUMBER
  (MICRONS)        (MICRONS)      PERCENT       PER GRAM         PERCENT
   0.0-   0.5        0.125          1.0         6.1E+11           93.0
   0.5-   1.0        0.375          1.5         3.4E+10            5.2
   1.0-   1.5        0.625          1.0         4.9E+09            0.7
   1.5-   2.0        0.875          1.5         2.7E+09            0.4
   2.0-   2.5        1.125          1.5         1.3E+09            0.2
   2.5-   3.0        1.375          1.5         6.9E+08            0.1
   3.0-   3.5        1.625          2.0         5.6E+08            0.1
   3.5-   4.0        1.875          2.0         3.6E+08            0.1
   4.0-   4.5        2.125          3.0         3.7E+08            0.1
   4.5-   5.0        2.375          2.0         1.8E+08            0.0
   5.0-  10.0        3.750         27.5         6.2E+08            0.1
  10.0-  15.0        6.250         19.5         9.5E+07            0.0
  15.0-  20.0        8.750         13.0         2.3E+07            0.0
  20.0-  25.0       11.250          6.0         5.0E+06            0.0
  25.0-  30.0       13.750          5.0         2.3E+06            0.0
  30.0-  35.0       16.250          4.5         1.3E+06            0.0
  35.0-  40.0       18.750          2.5         4.5E+05            0.0
  40.0-  45.0       21.250          1.5         1.9E+05            0.0
  45.0-  50.0       23.750          0.5         4.5E+04            0.0
  50.0-  55.0       26.250          1.0         6.6E+04            0.0
  55.0-  60.0       28.750          1.0         5.0E+04            0.0
  60.0-  65.0       31.250          0.5         2.0E+04            0.0
  65.0-  70.0       33.750          0.5         1.6E+04            0.0
  70.0- 100.0       42.500          0.0         0.0E+00            0.0


SURFACE AREA DETERMINATION FOR FORESTBURG

CLASS INTERVAL   AVERAGE RADIUS   WEIGHT      AREA
  (MICRONS)        (MICRONS)      PERCENT  FRACTION (CM↑2)
   0.0-   0.5        0.125          1.0       1200.0
   0.5-   1.0        0.375          1.5        600.0
   1.0-   1.5        0.625          1.0        240.0
   1.5-   2.0        0.875          1.5        257.1
   2.0-   2.5        1.125          1.5        200.0
   2.5-   3.0        1.375          1.5        163.6
   3.0-   3.5        1.625          2.0        184.6
   3.5-   4.0        1.875          2.0        160.0
   4.0-   4.5        2.125          3.0        211.8
   4.5-   5.0        2.375          2.0        126.3
   5.0-  10.0        3.750         27.5       1100.0
  10.0-  15.0        6.250         19.5        468.0
  15.0-  20.0        8.750         13.0        222.9
  20.0-  25.0       11.250          6.0         80.0
  25.0-  30.0       13.750          5.0         54.5
  30.0-  35.0       16.250          4.5         41.5
  35.0-  40.0       18.750          2.5         20.0
  40.0-  45.0       21.250          1.5         10.6
  45.0-  50.0       23.750          0.5          3.2
  50.0-  55.0       26.250          1.0          5.7
  55.0-  60.0       28.750          1.0          5.2
  60.0-  65.0       31.250          0.5          2.4
  65.0-  70.0       33.750          0.5          2.2
  70.0- 100.0       42.500          0.0          0.0
TOTAL SURFACE AREA = 5360     CM↑2/G
```

ORF

```
NUMBER DISTRIBUTION OF PARTICLES FROM WEIGHT DATA FOR
NANTICOKE (-149 MICRONS)

CLASS INTERVAL   AVERAGE RADIUS   WEIGHT   NUMBER OF PARTICLES   NUMBER
  (MICRONS)        (MICRONS)      PERCENT       PER GRAM         PERCENT
  0.0-   0.5         0.125          0.0         0.0E+00            0.0
  0.5-   1.0         0.375          0.0         0.0E+00            0.0
  1.0-   1.5         0.625          0.5         2.1E+09           28.3
  1.5-   2.0         0.875          2.0         3.1E+09           41.2
  2.0-   2.5         1.125          0.5         3.6E+08            4.9
  2.5-   3.0         1.375          1.5         5.9E+08            8.0
  3.0-   3.5         1.625          1.0         2.4E+08            3.2
  3.5-   4.0         1.875          1.5         2.3E+08            3.1
  4.0-   4.5         2.125          2.5         2.7E+08            3.6
  4.5-   5.0         2.375          1.5         1.2E+08            1.5
  5.0-  10.0         3.750         19.0         3.7E+08            5.0
 10.0-  15.0         6.250         12.5         5.3E+07            0.7
 15.0-  20.0         8.750         12.0         1.6E+07            0.2
 20.0-  25.0        11.250          9.5         6.9E+06            0.1
 25.0-  30.0        13.750          8.0         3.2E+06            0.0
 30.0-  35.0        16.250          8.0         1.9E+06            0.0
 35.0-  40.0        18.750          4.0         6.2E+05            0.0
 40.0-  45.0        21.250          5.0         5.4E+05            0.0
 45.0-  50.0        23.750          3.5         2.7E+05            0.0
 50.0-  55.0        26.250          2.5         1.4E+05            0.0
 55.0-  60.0        28.750          1.5         6.5E+04            0.0
 60.0-  65.0        31.250          1.5         5.1E+04            0.0
 65.0-  70.0        33.750          1.0         2.7E+04            0.0
 70.0- 100.0        42.500          1.0         1.3E+04            0.0



SURFACE AREA DETERMINATION FOR NANTICOKE (-149 MICRONS)

CLASS INTERVAL   AVERAGE RADIUS   WEIGHT        AREA
  (MICRONS)        (MICRONS)      PERCENT   FRACTION (CM↑2)
  0.0-   0.5         0.125          0.0           0.0
  0.5-   1.0         0.375          0.0           0.0
  1.0-   1.5         0.625          0.5         103.4
  1.5-   2.0         0.875          2.0         295.6
  2.0-   2.5         1.125          0.5          57.5
  2.5-   3.0         1.375          1.5         141.1
  3.0-   3.5         1.625          1.0          79.6
  3.5-   4.0         1.875          1.5         103.4
  4.0-   4.5         2.125          2.5         152.1
  4.5-   5.0         2.375          1.5          81.7
  5.0-  10.0         3.750         19.0         655.2
 10.0-  15.0         6.250         12.5         258.6
 15.0-  20.0         8.750         12.0         177.3
 20.0-  25.0        11.250          9.5         109.2
 25.0-  30.0        13.750          8.0          75.2
 30.0-  35.0        16.250          8.0          63.7
 35.0-  40.0        18.750          4.0          27.6
 40.0-  45.0        21.250          5.0          30.4
 45.0-  50.0        23.750          3.5          19.1
 50.0-  55.0        26.250          2.5          12.3
 55.0-  60.0        28.750          1.5           6.7
 60.0-  65.0        31.250          1.5           6.2
 65.0-  70.0        33.750          1.0           3.8
 70.0- 100.0        42.500          1.0           3.0

TOTAL SURFACE AREA = 2463    CM↑2/G
```

ORF

```
McEF DISTRIBUTION OF PARTICLES FROM WEIGHT DATA FOR
KEVIEW

F S INTERVAL  AVERAGE RADIUS  WEIGHT  NUMBER OF PARTICLES  NUMBER
(MICRONS)        (MICRONS)    PERCENT      PER GRAM        PERCENT
0.0-    0.5       0.125         0.5        2.4E+11          91.0
0.5-    1.0       0.375         0.5        9.0E+09           3.4
1.0-    1.5       0.625         2.0        7.8E+09           2.9
1.5-    2.0       0.875         2.0        2.8E+09           1.1
2.0-    2.5       1.125         2.5        1.7E+09           0.6
2.5-    3.0       1.375         2.5        9.1E+08           0.3
3.0-    3.5       1.625         2.0        4.4E+08           0.2
3.5-    4.0       1.875         3.0        4.3E+08           0.2
4.0-    4.5       2.125         3.5        3.5E+08           0.1
4.5-    5.0       2.375         3.5        2.5E+08           0.1
5.0-   10.0       3.750        24.0        4.3E+08           0.2
0.0-   15.0       6.250        13.5        5.2E+07           0.0
5.0-   20.0       8.750        10.0        1.4E+07           0.0
0.0-   25.0      11.250         7.5        5.0E+06           0.0
5.0-   30.0      13.750         7.0        2.6E+06           0.0
0.0-   35.0      16.250         3.0        6.6E+05           0.0
5.0-   40.0      18.750         4.5        6.5E+05           0.0
0.0-   45.0      21.250         2.5        2.5E+05           0.0
5.0-   50.0      23.750         2.5        1.8E+05           0.0
0.0-   55.0      26.250         1.5        7.9E+04           0.0
5.0-   60.0      28.750         1.0        4.0E+04           0.0
0.0-   65.0      31.250         0.0        0.0E+00           0.0
5.0-   70.0      33.750         1.0        2.5E+04           0.0
 .0-  100.0      42.500         0.0        0.0E+00           0.0


.FACE AREA DETERMINATION FOR LAKEVIEW

.SS INTERVAL   AVERAGE RADIUS   WEIGHT      AREA
MICRONS)         (MICRONS)      PERCENT  FRACTION (CM↑2)
 0.0-   0.5        0.125          0.5        476.2
 0.5-   1.0        0.375          0.5        158.7
 1.0-   1.5        0.625          2.0        381.0
 1.5-   2.0        0.875          2.0        272.1
 2.0-   2.5        1.125          2.5        264.6
 2.5-   3.0        1.375          2.5        216.5
 3.0-   3.5        1.625          2.0        146.5
 3.5-   4.0        1.875          3.0        190.5
 4.0-   4.5        2.125          3.5        196.1
 4.5-   5.0        2.375          3.5        175.4
 5.0-  10.0        3.750         24.0        761.9
10.0-  15.0        6.250         13.5        257.1
15.0-  20.0        8.750         10.0        136.1
20.0-  25.0       11.250          7.5         79.4
25.0-  30.0       13.750          7.0         60.6
30.0-  35.0       16.250          3.0         22.0
35.0-  40.0       18.750          4.5         28.6
40.0-  45.0       21.250          2.5         14.0
45.0-  50.0       23.750          2.5         12.5
50.0-  55.0       26.250          1.5          6.8
55.0-  60.0       28.750          1.0          4.1
60.0-  65.0       31.250          0.0          0.0
65.0-  70.0       33.750          1.0          3.5
70.0- 100.0       42.500          0.0          0.0

TAL SURFACE AREA = 3864    CM↑2/G
```

ORF

```
NUMBER DISTRIBUTION OF PARTICLES FROM WEIGHT DATA FOR
LINGAN (-149 MICRONS)

CLASS INTERVAL  AVERAGE RADIUS  WEIGHT  NUMBER OF PARTICLES  NUMBER
  (MICRONS)       (MICRONS)     PERCENT      PER GRAM        PERCENT
   0.0-   0.5       0.125         0.5        2.4E+11          95.3
   0.5-   1.0       0.375         0.0        0.0E+00           0.0
   1.0-   1.5       0.625         1.5        5.6E+09           2.3
   1.5-   2.0       0.875         1.5        2.1E+09           0.8
   2.0-   2.5       1.125         1.5        9.7E+08           0.4
   2.5-   3.0       1.375         3.0        1.1E+09           0.4
   3.0-   3.5       1.625         2.0        4.3E+08           0.2
   3.5-   4.0       1.875         3.0        4.2E+08           0.2
   4.0-   4.5       2.125         4.0        3.8E+08           0.2
   4.5-   5.0       2.375         2.0        1.4E+08           0.1
   5.0-  10.0       3.750        27.5        4.8E+08           0.2
  10.0-  15.0       6.250        14.5        5.5E+07           0.0
  15.0-  20.0       8.750        10.0        1.4E+07           0.0
  20.0-  25.0      11.250         7.0        4.5E+06           0.0
  25.0-  30.0      13.750         6.0        2.1E+06           0.0
  30.0-  35.0      16.250         5.0        1.1E+06           0.0
  35.0-  40.0      18.750         3.0        4.2E+05           0.0
  40.0-  45.0      21.250         2.0        1.9E+05           0.0
  45.0-  50.0      23.750         2.0        1.4E+05           0.0
  50.0-  55.0      26.250         2.0        1.0E+05           0.0
  55.0-  60.0      28.750         0.5        1.9E+04           0.0
  60.0-  65.0      31.250         0.5        1.5E+04           0.0
  65.0-  70.0      33.750         0.0        0.0E+00           0.0
  70.0- 100.0      42.500         1.0        1.2E+04           0.0


SURFACE AREA DETERMINATION FOR LINGAN (-149 MICRONS)

CLASS INTERVAL   AVERAGE RADIUS   WEIGHT       AREA
  (MICRONS)        (MICRONS)      PERCENT  FRACTION (CM↑2)
    0.0-   0.5       0.125          0.5        461.5
    0.5-   1.0       0.375          0.0          0.0
    1.0-   1.5       0.625          1.5        276.9
    1.5-   2.0       0.875          1.5        197.8
    2.0-   2.5       1.125          1.5        153.8
    2.5-   3.0       1.375          3.0        251.7
    3.0-   3.5       1.625          2.0        142.0
    3.5-   4.0       1.875          3.0        184.6
    4.0-   4.5       2.125          4.0        217.2
    4.5-   5.0       2.375          2.0         97.2
    5.0-  10.0       3.750         27.5        846.2
   10.0-  15.0       6.250         14.5        267.7
   15.0-  20.0       8.750         10.0        131.9
   20.0-  25.0      11.250          7.0         71.8
   25.0-  30.0      13.750          6.0         50.3
   30.0-  35.0      16.250          5.0         35.5
   35.0-  40.0      18.750          3.0         18.5
   40.0-  45.0      21.250          2.0         10.9
   45.0-  50.0      23.750          2.0          9.7
   50.0-  55.0      26.250          2.0          8.8
   55.0-  60.0      28.750          0.5          2.0
   60.0-  65.0      31.250          0.5          1.8
   65.0-  70.0      33.750          0.0          0.0
   70.0- 100.0      42.500          1.0          2.7

TOTAL SURFACE AREA = 3441    CM↑2/G
```

ORF

```
NUMBER DISTRIBUTION OF PARTICLES FROM WEIGHT DATA FOR
DALHOUSIE

CLASS INTERVAL   AVERAGE RADIUS   WEIGHT   NUMBER OF PARTICLES   NUMBER
  (MICRONS)        (MICRONS)      PERCENT       PER GRAM         PERCENT
  0.0-   0.5         0.125          0.5         2.0E+11           98.7
  0.5-   1.0         0.375          0.0         0.0E+00            0.0
  1.0-   1.5         0.625          0.0         0.0E+00            0.0
  1.5-   2.0         0.875          1.0         1.1E+09            0.6
  2.0-   2.5         1.125          0.5         2.7E+08            0.1
  2.5-   3.0         1.375          1.0         3.0E+08            0.1
  3.0-   3.5         1.625          2.0         3.6E+08            0.2
  3.5-   4.0         1.875          1.0         1.2E+08            0.1
  4.0-   4.5         2.125          1.5         1.2E+08            0.1
  4.5-   5.0         2.375          1.5         8.6E+07            0.0
  5.0-  10.0         3.750          9.0         1.3E+08            0.1
 10.0-  15.0         6.250         26.0         8.2E+07            0.0
 15.0-  20.0         8.750         14.0         1.6E+07            0.0
 20.0-  25.0        11.250          5.0         2.7E+06            0.0
 25.0-  30.0        13.750         13.0         3.9E+06            0.0
 30.0-  35.0        16.250          7.5         1.3E+06            0.0
 35.0-  40.0        18.750          5.5         6.4E+05            0.0
 40.0-  45.0        21.250          6.0         4.8E+05            0.0
 45.0-  50.0        23.750          2.0         1.1E+05            0.0
 50.0-  55.0        26.250          1.0         4.3E+04            0.0
 55.0-  60.0        28.750          1.0         3.2E+04            0.0
 60.0-  65.0        31.250          1.0         2.5E+04            0.0
 65.0-  70.0        33.750          0.0         0.0E+00            0.0
 70.0- 100.0        42.500          0.0         0.0E+00            0.0


SURFACE AREA DETERMINATION FOR DALHOUSIE

CLASS INTERVAL   AVERAGE RADIUS   WEIGHT        AREA
  (MICRONS)        (MICRONS)      PERCENT   FRACTION (CM↑2)
  0.0-   0.5         0.125          0.5         387.1
  0.5-   1.0         0.375          0.0           0.0
  1.0-   1.5         0.625          0.0           0.0
  1.5-   2.0         0.875          1.0         110.6
  2.0-   2.5         1.125          0.5          43.0
  2.5-   3.0         1.375          1.0          70.4
  3.0-   3.5         1.625          2.0         119.1
  3.5-   4.0         1.875          1.0          51.6
  4.0-   4.5         2.125          1.5          68.3
  4.5-   5.0         2.375          1.5          61.1
  5.0-  10.0         3.750          9.0         232.3
 10.0-  15.0         6.250         26.0         402.6
 15.0-  20.0         8.750         14.0         154.8
 20.0-  25.0        11.250          5.0          43.0
 25.0-  30.0        13.750         13.0          91.5
 30.0-  35.0        16.250          7.5          44.7
 35.0-  40.0        18.750          5.5          28.4
 40.0-  45.0        21.250          6.0          27.3
 45.0-  50.0        23.750          2.0           8.1
 50.0-  55.0        26.250          1.0           3.7
 55.0-  60.0        28.750          1.0           3.4
 60.0-  65.0        31.250          1.0           3.1
 65.0-  70.0        33.750          0.0           0.0
 70.0- 100.0        42.500          0.0           0.0

TOTAL SURFACE AREA = 1954    CM↑2/G
```

```
NUMBER DISTRIBUTION OF PARTICLES FROM WEIGHT DATA.FOR
ESTEVEN

CLASS INTERVAL   AVERAGE RADIUS   WEIGHT   NUMBER OF PARTICLES   NUMBER
  (MICRONS)        (MICRONS)      PERCENT       PER GRAM          PERCENT
  0.0-   0.5         0.125          2.0         9.8E+11            98.0
  0.5-   1.0         0.375          0.5         9.1E+09             0.9
  1.0-   1.5         0.625          1.0         3.9E+09             0.4
  1.5-   2.0         0.875          1.5         2.1E+09             0.2
  2.0-   2.5         1.125          2.0         1.3E+09             0.1
  2.5-   3.0         1.375          2.0         7.4E+08             0.1
  3.0-   3.5         1.625          4.0         8.9E+08             0.1
  3.5-   4.0         1.875          4.0         5.6E+08             0.1
  4.0-   4.5         2.125          3.0         3.0E+08             0.0
  4.5-   5.0         2.375          3.5         2.5E+08             0.0
  5.0-  10.0         3.750         28.5         5.2E+08             0.1
 10.0-  15.0         6.250         12.0         4.7E+07             0.0
 15.0-  20.0         8.750          9.5         1.4E+07             0.0
 20.0-  25.0        11.250          6.5         4.4E+06             0.0
 25.0-  30.0        13.750          6.0         2.2E+06             0.0
 30.0-  35.0        16.250          3.5         7.8E+05             0.0
 35.0-  40.0        18.750          3.0         4.4E+05             0.0
 40.0-  45.0        21.250          0.5         5.0E+04             0.0
 45.0-  50.0        23.750          2.0         1.4E+05             0.0
 50.0-  55.0        26.250          1.0         5.3E+04             0.0
 55.0-  60.0        28.750          1.0         4.0E+04             0.0
 60.0-  65.0        31.250          1.0         3.1E+04             0.0
 65.0-  70.0        33.750          1.5         3.7E+04             0.0
 70.0- 100.0        42.500          0.5         6.2E+03             0.0
```

```
SURFACE AREA DETERMINATION FOR ESTEVEN

CLASS INTERVAL   AVERAGE RADIUS   WEIGHT        AREA
  (MICRONS)        (MICRONS)      PERCENT  FRACTION (CM↑2)
  0.0-   0.5         0.125          2.0       1927.7
  0.5-   1.0         0.375          0.5        160.6
  1.0-   1.5         0.625          1.0        192.8
  1.5-   2.0         0.875          1.5        206.5
  2.0-   2.5         1.125          2.0        214.2
  2.5-   3.0         1.375          2.0        175.2
  3.0-   3.5         1.625          4.0        296.6
  3.5-   4.0         1.875          4.0        257.0
  4.0-   4.5         2.125          3.0        170.1
  4.5-   5.0         2.375          3.5        177.6
  5.0-  10.0         3.750         28.5        915.7
 10.0-  15.0         6.250         12.0        231.3
 15.0-  20.0         8.750          9.5        130.8
 20.0-  25.0        11.250          6.5         69.6
 25.0-  30.0        13.750          6.0         52.6
 30.0-  35.0        16.250          3.5         25.9
 35.0-  40.0        18.750          3.0         19.3
 40.0-  45.0        21.250          0.5          2.8
 45.0-  50.0        23.750          2.0         10.1
 50.0-  55.0        26.250          1.0          4.6
 55.0-  60.0        28.750          1.0          4.2
 60.0-  65.0        31.250          1.0          3.9
 65.0-  70.0        33.750          1.5          5.4
 70.0- 100.0        42.500          0.5          1.4

TOTAL SURFACE AREA = 5256    CM↑2/G
```

```
NUMBER DISTRIBUTION OF PARTICLES FROM WEIGHT DATA FOR
THUNDERBAY

CLASS INTERVAL  AVERAGE RADIUS  WEIGHT  NUMBER OF PARTICLES  NUMBER
  (MICRONS)       (MICRONS)     PERCENT      PER GRAM        PERCE
   0.0-   0.5       0.125         0.0        0.0E+00           0.0
   0.5-   1.0       0.375         0.5        8.5E+09          31.0
   1.0-   1.5       0.625         2.0        7.3E+09          26.8
   1.5-   2.0       0.875         0.1        1.3E+08           0.5
   2.0-   2.5       1.125         7.4        4.6E+09          17.0
   2.5-   3.0       1.375         6.5        2.2E+09           8.0
   3.0-   3.5       1.625         7.5        1.6E+09           5.7
   3.5-   4.0       1.875         7.5        1.0E+09           3.7
   4.0-   4.5       2.125         8.5        7.9E+08           2.9
   4.5-   5.0       2.375         7.0        4.7E+08           1.7
   5.0-  10.0       3.750        38.0        6.4E+08           2.4
  10.0-  15.0       6.250         6.0        2.2E+07           0.1
  15.0-  20.0       8.750         4.0        5.3E+06           0.0
  20.0-  25.0      11.250         2.0        1.3E+06           0.0
  25.0-  30.0      13.750         1.0        3.4E+05           0.0
  30.0-  35.0      16.250         0.5        1.0E+05           0.0
  35.0-  40.0      18.750         0.5        6.8E+04           0.0
  40.0-  45.0      21.250         0.0        0.0E+00           0.0
  45.0-  50.0      23.750         0.0        0.0E+00           0.0
  50.0-  55.0      26.250         0.5        2.5E+04           0.0
  55.0-  60.0      28.750         0.0        0.0E+00           0.0
  60.0-  65.0      31.250         0.0        0.0E+00           0.0
  65.0-  70.0      33.750         0.0        0.0E+00           0.0
  70.0- 100.0      42.500         0.5        5.8E+03           0.0
```

```
SURFACE AREA DETERMINATION FOR THUNDERBAY

CLASS INTERVAL  AVERAGE RADIUS  WEIGHT        AREA
  (MICRONS)       (MICRONS)     PERCENT  FRACTION (CM↑2)
   0.0-   0.5       0.125         0.0          0.0
   0.5-   1.0       0.375         0.5        149.8
   1.0-   1.5       0.625         2.0        359.6
   1.5-   2.0       0.875         0.1         12.8
   2.0-   2.5       1.125         7.4        739.1
   2.5-   3.0       1.375         6.5        531.2
   3.0-   3.5       1.625         7.5        518.6
   3.5-   4.0       1.875         7.5        449.4
   4.0-   4.5       2.125         8.5        449.4
   4.5-   5.0       2.375         7.0        331.2
   5.0-  10.0       3.750        38.0       1138.6
  10.0-  15.0       6.250         6.0        107.9
  15.0-  20.0       8.750         4.0         51.4
  20.0-  25.0      11.250         2.0         20.0
  25.0-  30.0      13.750         1.0          8.2
  30.0-  35.0      16.250         0.5          3.5
  35.0-  40.0      18.750         0.5          3.0
  40.0-  45.0      21.250         0.0          0.0
  45.0-  50.0      23.750         0.0          0.0
  50.0-  55.0      26.250         0.5          2.1
  55.0-  60.0      28.750         0.0          0.0
  60.0-  65.0      31.250         0.0          0.0
  65.0-  70.0      33.750         0.0          0.0
  70.0- 100.0      42.500         0.5          1.3
TOTAL SURFACE AREA = 4877    CM↑2/G
```

```
NUMBER DISTRIBUTION OF PARTICLES FROM WEIGHT DATA FOR
STANDARD SLAG

CLASS INTERVAL  AVERAGE RADIUS  WEIGHT  NUMBER OF PARTICLES  NUMBER
  (MICRONS)       (MICRONS)    PERCENT       PER GRAM         PERCENT
  0.0-    0.5       0.125         1.0        4.1E+11           82.8
  0.5-    1.0       0.375         4.0        6.1E+10           12.3
  1.0-    1.5       0.625         4.5        1.5E+10            3.0
  1.5-    2.0       0.875         4.0        4.8E+09            1.0
  2.0-    2.5       1.125         4.0        2.2E+09            0.5
  2.5-    3.0       1.375         3.0        9.2E+08            0.2
  3.0-    3.5       1.625         3.5        6.5E+08            0.1
  3.5-    4.0       1.875         3.5        4.2E+08            0.1
  4.0-    4.5       2.125         3.0        2.5E+08            0.1
  4.5-    5.0       2.375         3.5        2.1E+08            0.0
  5.0-   10.0       3.750        21.5        3.3E+08            0.1
 10.0-   15.0       6.250        13.0        4.3E+07            0.0
 15.0-   20.0       8.750         9.0        1.1E+07            0.0
 20.0-   25.0      11.250         6.0        3.4E+06            0.0
 25.0-   30.0      13.750         6.0        1.8E+06            0.0
 30.0-   35.0      16.250         3.5        6.5E+05            0.0
 35.0-   40.0      18.750         3.0        3.6E+05            0.0
 40.0-   45.0      21.250         2.0        1.7E+05            0.0
 45.0-   50.0      23.750         1.0        6.0E+04            0.0
 50.0-   55.0      26.250         0.5        2.2E+04            0.0
 55.0-   60.0      28.750         0.5        1.7E+04            0.0
 60.0-   65.0      31.250         0.0        0.0E+00            0.0
 65.0-   70.0      33.750         0.0        0.0E+00            0.0
 70.0-  100.0      42.500         0.0        0.0E+00            0.0
```

```
SURFACE AREA DETERMINATION FOR STANDARD SLAG

CLASS INTERVAL    AVERAGE RADIUS   WEIGHT        AREA
  (MICRONS)         (MICRONS)     PERCENT  FRACTION (CM↑2)
   0.0-    0.5        0.125         1.0        803.7
   0.5-    1.0        0.375         4.0       1070.2
   1.0-    1.5        0.625         4.5        722.4
   1.5-    2.0        0.875         4.0        458.7
   2.0-    2.5        1.125         4.0        356.7
   2.5-    3.0        1.375         3.0        218.9
   3.0-    3.5        1.625         3.5        216.1
   3.5-    4.0        1.875         3.5        187.3
   4.0-    4.5        2.125         3.0        141.6
   4.5-    5.0        2.375         3.5        147.9
   5.0-   10.0        3.750        21.5        575.3
  10.0-   15.0        6.250        13.0        208.7
  15.0-   20.0        8.750         9.0        103.2
  20.0-   25.0       11.250         6.0         53.5
  25.0-   30.0       13.750         6.0         43.8
  30.0-   35.0       16.250         3.5         21.6
  35.0-   40.0       18.750         3.0         16.1
  40.0-   45.0       21.250         2.0          9.4
  45.0-   50.0       23.750         1.0          4.2
  50.0-   55.0       26.250         0.5          1.9
  55.0-   60.0       28.750         0.5          1.7
  60.0-   65.0       31.250         0.0          0.0
  65.0-   70.0       33.750         0.0          0.0
  70.0-  100.0       42.500         0.0          0.0

TOTAL SURFACE AREA = 5362    CM↑2/G
```

```
NUMBER DISTRIBUTION OF PARTICLES FROM WEIGHT DATA FOR
ATLANTIC SLAG

CLASS INTERVAL   AVERAGE RADIUS   WEIGHT    NUMBER OF PARTICLES   NUMBER
  (MICRONS)        (MICRONS)      PERCENT       PER GRAM          PERCENT
  0.0-   0.5         0.125          3.5         1.4E+12            95.5
  0.5-   1.0         0.375          3.0         4.6E+10             3.0
  1.0-   1.5         0.625          3.5         1.1E+10             0.8
  1.5-   2.0         0.875          4.0         4.8E+09             0.3
  2.0-   2.5         1.125          4.0         2.3E+09             0.1
  2.5-   3.0         1.375          4.0         1.2E+09             0.1
  3.0-   3.5         1.625          4.0         7.5E+08             0.0
  3.5-   4.0         1.875          4.0         4.9E+08             0.0
  4.0-   4.5         2.125          3.5         2.9E+08             0.0
  4.5-   5.0         2.375          2.5         1.5E+08             0.0
  5.0-  10.0         3.750         27.0         4.1E+08             0.0
 10.0-  15.0         6.250         15.0         4.9E+07             0.0
 15.0-  20.0         8.750          9.0         1.1E+07             0.0
 20.0-  25.0        11.250          6.0         3.4E+06             0.0
 25.0-  30.0        13.750          4.0         1.2E+06             0.0
 30.0-  35.0        16.250          1.0         1.9E+05             0.0
 35.0-  40.0        18.750          1.0         1.2E+05             0.0
 40.0-  45.0        21.250          0.0         0.0E+00             0.0
 45.0-  50.0        23.750          0.0         0.0E+00             0.0
 50.0-  55.0        26.250          0.0         0.0E+00             0.0
 55.0-  60.0        28.750          0.0         0.0E+00             0.0
 60.0-  65.0        31.250          1.0         2.6E+04             0.0
 65.0-  70.0        33.750          0.0         0.0E+00             0.0
 70.0- 100.0        42.500          0.0         0.0E+00             0.0


SURFACE AREA DETERMINATION FOR ATLANTIC SLAG

CLASS INTERVAL   AVERAGE RADIUS   WEIGHT        AREA
  (MICRONS)        (MICRONS)      PERCENT   FRACTION (CM↑2)
  0.0-   0.5         0.125          3.5         2818.8
  0.5-   1.0         0.375          3.0          805.4
  1.0-   1.5         0.625          3.5          563.8
  1.5-   2.0         0.875          4.0          460.2
  2.0-   2.5         1.125          4.0          357.9
  2.5-   3.0         1.375          4.0          292.9
  3.0-   3.5         1.625          4.0          247.8
  3.5-   4.0         1.875          4.0          214.8
  4.0-   4.5         2.125          3.5          165.8
  4.5-   5.0         2.375          2.5          106.0
  5.0-  10.0         3.750         27.0          724.8
 10.0-  15.0         6.250         15.0          241.6
 15.0-  20.0         8.750          9.0          103.5
 20.0-  25.0        11.250          6.0           53.7
 25.0-  30.0        13.750          4.0           29.3
 30.0-  35.0        16.250          1.0            6.2
 35.0-  40.0        18.750          1.0            5.4
 40.0-  45.0        21.250          0.0            0.0
 45.0-  50.0        23.750          0.0            0.0
 50.0-  55.0        26.250          0.0            0.0
 55.0-  60.0        28.750          0.0            0.0
 60.0-  65.0        31.250          1.0            3.2
 65.0-  70.0        33.750          0.0            0.0
 70.0- 100.0        42.500          0.0            0.0

TOTAL SURFACE AREA = 7201     CM↑2/G
```

TABLE 6

Comparison of Concentrations of Selected Oxides from SEM/EDXA Analysis and Chemical Analysis

Oxide	SEM/EDXA		Chemical Analysis (Bulk Ash)
	Range	Average (No. of Locations)	
SiO_2	15.58-87.13	52.62 (8)	58.6
Al_2O_3	5.66-25.58	15.41 (8)	21.3
SO_3	5.11-5.38	5.19 (2)	0.34
TiO_2	2.28-11.60	6.94 (2)	0.63
FeO, Fe_2O_3	1.58-76.88 (FeO)	17.39(5) (FeO)	3.33 (Fe_2O_3)
CaO	1.80-53.16	19.43 (7)	11.1
MgO	0.59-1.78	1.34 (3)	1.80
K_2O	4.40	4.40 (1)	0.76

TABLE 7

EDXA Oxide Analysis of Wabamun Fly Ash in Cross-Section

Oxide	Location						
	A	B	3	4A	4B	4C	4D
SiO_2	26.96	70.07	51.27	66.84	55.69	63.15	49.24
Al_2O_3	4.80	7.17	31.29	15.70	14.68	20.56	16.35
TiO_2	1.50	0.48	4.86	1.71	4.06	1.60	1.91
FeO	24.78	2.75	2.27	3.08	5.78	3.03	5.31
SO_3	-	-	-	-	3.04	-	-
CaO	41.56	18.57	9.17	6.12	8.53	4.80	23.87
MgO	0.40	0.34	0.33	0.31	-	-	0.68
K_2O	-	-	0.80	6.24	7.52	6.45	2.64
MnO	-	0.17	-	-	-	-	-
Cl	-	-	-	-	0.70	0.41	-

TABLE 8

Results of Modified McMaster Individual Particle Analysis on Standard and Atlantic Slags*

Sample ID	X	S_x	S_{x-1}	$X(n)$	S_n
Operator A					
Standard Slag	87.0	13.7	13.9	84.3	2.3
(no gypsum	81.4	19.1	19.3		
plate)	84.4	17.1	17.3		
Standard Slag	75.2	20.6	20.8	75.9	2.5
(gypsum	73.2	23.0	23.3		
plate)	79.2	20.8	21.0		
Operator B					
Standard Slag	48.2	36.0	36.4	47.1	1.1
	47.6	37.0	37.3		
	45.6	34.1	34.5		
Atlantic Slag	60.8	33.5	33.8	59.7	1.8
	57.2	37.7	38.1		
	61.0	35.6	36.0		
Operator C					
Standard Slag	70.0	24.7	25.0	73.7	2.8
	76.7	18.6	18.8		
	74.3	17.1	17.2		
Atlantic Slag	69.4	26.3	26.6	68.9	1.3
	67.2	25.8	26.0		
	70.2	17.7	17.9		

* according to CSA Standard A363-M1983.

ORF

TABLE 9

Mineralogy of Canadian Fly Ashes and Slags

Source	Phases Detected (1,2)
Wabamun	Q, M
Sundance	Q, M, H
Forestburg	Q, M
Nanticoke	Q, M, H, Ma
Lakeview	Q, M, H, Ma
Lingan	Q, M, H, Ma
Dalhousie	Q, M, H, Ma
Thunder Bay	Q, $C\bar{S}$, CaS, $N_3A\bar{S}_6$
Estevan	Q
Standard Slag	Mel
Atlantic Slag	Mer

(1) Q: α-quartz, M: mullite, H: hematite, Ma: magnetitie, Mel: melilite, Mer: merwinite, $C\bar{S}$: $CaSO_4$, $N_3A\bar{S}_6$: $Na_3Al(SO_4)_3$

(2) Sillimanite ($Al_2O_3.SiO_2$) has an XRD pattern almost identical to that of mullite ($3Al_2O_3.2SiO_2$). The assignment given here was based on the relative peak intensities of the two phases.

TABLE 10

X-ray data for 4 crystalline phases and NaCl

Phase	2θ (d-spacings) [a]			
NaCl	31.7 (2.821)	45.5 (1.994)		
α-quartz	20.8 (4.26)	26.7 (3.343)		
mullite	16.4 (5.39)	40.8 (2.206)	26.0 (3.390)	
magnetite	30.1 (2.967)	35.4 (2.532)	43.1 (2.099)	56.9 (1.485)
hematite	33.3 (2.69)	35.7 (2.51)	54.2 (1.690)	

(a) 2θ - values measured at ORF
d-spacings from literature data

TABLE 11

Intensity Ratios for Four Phases and NaCl

α-quartz			mullite			magnetite			hematite		
$2\theta_Q$	$2\theta'_{NaCl}$	I_Q/I_{NaCl}	$2\theta_M$	$2\theta'_{NaCl}$	I_M/I_{NaCl}	$2\theta_{Ma}$	$2\theta'_{NaCl}$	I_{Ma}/I_{NaCl}	$2\theta_H$	$2\theta'_{NaCl}$	I_H/I_{NaCl}
20.8	31.7	1.11	16.4	31.7	0.265	30.1	31.7	0.14	33.3	31.7	4.42
26.7	31.7	6.11	26.0	31.7	0.470	35.4	31.7	2.38	35.7	31.7	3.08
20.8	45.5	3.08	35.2	31.7	0.349	43.1	31.7	0.508	54.2	31.7	2.17
26.7	45.5	15.9	16.4	45.5	0.847	57.1	31.7	0.555	33.3	45.5	8.83
			26.0	45.5	1.68	30.1	45.5	2.00	35.7	45.5	6.17
			35.2	45.5	1.12	35.4	45.5	6.67	54.2	45.5	4.33
						43.1	45.5	1.42			
						57.1	45.5	1.56			

Table 12

The Crystalline and Glass Content of Seven Canadian Fly Ashes

Fly Ash: Wabamun

Phase	$2\Theta_P$	$2\Theta'_{NaCl}$	I_P/I_{NaCl}	% Phase	% Phase
α-quartz	20.8	31.7	0.111	10.0	8.7
	26.7	31.7	0.539	8.8	
	20.8	45.5	0.250	8.1	
	26.7	45.5	1.22	7.7	
mullite	16.4	31.7	0.0434	16.4	11.5
	26.0	31.7	0.0506	10.8	
	35.2	31.7	0.0482	13.8	
	16.4	45.5	0.0978	11.5	
	26.0	45.5	0.114	6.8	
	35.2	45.5	0.109	9.7	
magnetite	-	-	-	0.0	0.0
hematite	-	-	-	0.0	0.0
LOI					0.8
Glass					79.8

...... contd.

ORF

Table 12 (continued)

The Crystalline and Glass Content of Seven Canadian Fly Ashes

Fly Ash: Sundance

Phase	$2\theta_p$	$2\theta'_{NaCl}$	I_p/I_{NaCl}	% Phase	% Phase
α-quartz	20.8	31.7	1.11	5.5	
	26.7	31.7	6.11	4.6	4.1
	20.8	45.5	3.08	2.7	
	26.7	45.5	15.9	3.5	
mullite	16.4	31.7	0.0396	14.9	
	26.0	31.7	0.063	13.4	
	35.2	31.7	0.0354	10.1	10.2
	16.4	45.5	0.0774	9.1	
	26.0	45.5	0.123	7.3	
	35.2	45.5	0.0695	6.2	
magnetite	-	-	-	-	0.0
hematite	33.3	31.7	0.0606	1.37	1.4
	33.3	45.5	0.119	1.34	
LOI					0.39
Glass					83.9

....contd.

Table 12 (continued)

The Crystalline and Glass Content of Seven Canadian Fly Ashes

Fly Ash: Forestburg

Phase	$2\Theta_P$	$2\Theta'_{NaCl}$	I_P/I_{NaCl}	% Phase	% Phase
α-quartz	20.8	31.7	0.0395	3.6	
	26.7	31.7	0.184	3.0	2.9
	20.8	45.5	0.0769	2.5	
	26.7	45.5	0.359	2.3	
mullite	16.4	31.7	0.0263	9.9	
	26.0	31.7	0.0263	5.6	
	35.2	31.7	0.0263	7.5	6.1
	16.4	45.5	0.0518	6.1	
	26.0	45.5	0.0518	3.1	
	35.2	45.5	0.0518	4.6	
magnetite	-	-	-	0.0	0.0
hematite	-	-	-	0.0	
LOI					0.8
Glass					90.2

......contd.

ORF

Table 12 (continued)

The Crystalline and Glass Content of Seven Canadian Fly Ashes

Fly Ash: Nanticoke

Phase	$2\theta_p$	$2\theta'_{NaCl}$	I_p/I_{NaCl}	% Phase	% Phase
α-quartz	20.8	31.7	0.125	11.3	8.3
	26.7	31.7	0.500	8.2	
	20.8	45.5	0.236	7.7	
	26.7	45.5	0.944	5.9	
mullite	16.4	31.7	0.0808	30.5	23.5
	26.0	31.7	0.140	29.7	
	(35.2)	(31.7)	(0.118)	(33.7)	
	16.4	45.5	0.153	18.0	
	26.0	45.5	0.263	15.7	
	(35.2)	(45.5)	(0.222)	(19.8)	
magnetite	30.1	31.7	0.0294	4.1	4.4
	(35.4)	(31.7)	(0.198)	(8.3)	
	43.1	31.7	0.0257	5.1	
	57.1	31.7	0.0367	6.6	
	30.1	45.5	0.0556	2.8	
	(35.4)	(45.5)	(0.375)	(5.6)	
	43.1	45.5	0.0486	3.4	
	57.1	45.5	0.0694	4.5	
hematite	33.3	31.7	0.121	2.7	2.1
	(35.7)	(31.7)	(0.199)	(6.4)	
	54.2	31.7	0.0368	1.7	
	33.3	45.5	0.229	2.6	
	(35.7)	(45.5)	0.375	(6.1)	
	54.2	45.5	0.0694	1.4	
LOI					7.5
Glass					54.2

.....contd.

ORF

Table 12 (continued)

The Crystalline and Glass Content of Seven Canadian Fly Ashes

Fly Ash: Lakeview

Phase	$2\theta_p$	$2\theta'_{NaCl}$	I_p/I_{NaCl}	% Phase	% Phase
α-quartz	20.8	31.7	0.102	9.2	
	26.7	31.7	0.479	7.8	6.2
	20.8	45.5	0.128	4.1	
	26.7	45.5	0.596	3.7	
mullite	16.4	31.7	0.0855	32.3	
	26.0	31.7	0.120	25.5	
	(35.2)	(31.7)	(0.0855)	(24.5)	19.8
	16.4	45.5	0.106	12.5	
	26.0	45.5	0.149	8.9	
	(35.2)	(45.5)	(0.106)	(9.5)	
magnetite	30.1	31.7	0.0684	9.6	
	(35.4)	(31.7)	(0.205)	(8.6)	
	43.1	31.7	0.0299	5.9	
	57.1	31.7	0.0427	7.7	5.6
	30.1	45.5	0.0851	4.3	
	(35.4)	(45.5)	(0.255)	(3.8)	
	43.1	45.5	0.0372	2.6	
	57.1	45.5	0.0532	3.4	
hematite	33.3	31.7	0.188	4.2	
	(35.7)	(31.7)	(0.205)	(6.7)	
	54.2	31.7	0.0726	3.3	3.1
	33.3	45.5	0.234	2.7	
	(35.7)	(45.5)	(0.266)	(4.1)	
	54.2	45.5	0.0904	2.1	
LOI					9.7
Glass					55.6

......contd.

Table 12 (continued)

The Crystalline and Glass Content of Seven Canadian Fly Ashes

Fly Ash: Lingan

Phase	$2\theta_p$	$2\theta'_{NaCl}$	I_p/I_{NaCl}	% Phase	% Phase
α-quartz	20.8	31.7	0.0581	5.2	4.0
	26.7	31.7	0.261	4.3	
	20.8	45.5	0.110	3.6	
	26.7	45.5	0.494	3.1	
mullite	16.4	31.7	0.0387	14.6	12.6
	26.0	31.7	0.0839	17.8	
	(35.2)	(31.7)	(0.0645)	(18.5)	
	16.4	45.5	0.0732	8.6	
	26.0	45.5	0.156	9.4	
	(35.2)	(45.5)	(0.122)	(10.9)	
magnetite	30.1	31.7	0.0645	9.0	6.2
	(35.4)	(31.7)	0.226	9.5	
	43.1	31.7	0.0258	5.1	
	57.1	31.7	0.0387	7.0	
	30.1	45.5	0.122	6.1	
	(35.4)	(45.5)	0.427	(6.4)	
	43.1	45.5	0.0487	3.4	
	57.1	45.5	0.0732	6.5	
hematite	33.3	31.7	0.103	2.3	1.6
	(35.7)	(31.7)	(0.226)	(7.3)	
	54.2	31.7	0.0226	1.0	
	33.3	45.5	0.195	2.2	
	(35.7)	(45.5)	(0.427)	(6.9)	
	54.2	45.5	0.0427	1.0	
LOI					3.5
Glass					72.1

.......contd.

Table 12 (continued)

The Crystalline and Glass Content of Seven Canadian Fly Ashes

Fly Ash: Dalhousie

Phase	$2\theta_p$	$2\theta'_{NaCl}$	I_p/I_{NaCl}	% Phase	% Phase
α-quartz	20.8	31.7	0.0417	3.8	
	26.7	31.7	0.250	4.1	3.2
	20.8	45.5	0.0727	2.4	
	26.7	45.5	0.436	2.7	
mullite	26.0	31.7	0.0208	4.4	
	(35.2)	(31.7)	(0.0416)	(11.9)	3.3
	26.0	45.5	0.0364	2.2	
	(35.2)	(45.5)	(0.0727)	(6.5)	
magnetite	30.1	31.7	0.198	27.7	
	(35.4)	(31.7)	(0.552)	(23.2)	
	43.1	31.7	0.0781	15.4	
	57.1	31.7	0.115	20.6	17.2
	30.1	45.5	0.345	17.3	
	(35.4)	(45.5)	(0.964)	(14.4)	
	43.1	31.7	0.136	9.6	
	57.1	31.7	0.200	12.8	
hematite	33.3	31.7	0.240	5.4	
	(35.7)	(31.7)	(0.552)	(17.9)	
	54.2	31.7	0.109	5.0	4.7
	33.3	45.5	0.345	3.9	
	(35.7)	(45.5)	(0.964)	(15.6)	
	54.2	45.5	(0.191)	4.4	
LOI					1.5
Glass					70.1

TABLE 13

Contents of Crystalline Phases and Glass in Seven Canadian Fly Ashes

Fly Ash	α-quartz	mullite	magnetite	hematite	LOI	Glass
Wabamun	8.7	11.5	-	-	0.8	79.8
Sundance	4.1	10.2	-	1.4	0.4	83.9
Forestburg	2.9	6.1	-	-	0.8	90.2
Nanticoke	8.3	23.5	4.4	2.1	7.5	54.2
Lakeview	6.2	19.8	5.6	3.1	9.7	55.6
Lingan	4.0	12.6	6.2	1.6	3.5	72.1
Dalhousie	3.2	3.3	17.2	4.7	1.5	70.1

TABLE 14

Settling Parameters

Material	Density ($g.cm^{-3}$)	Solvent	Density ($g.cm^{-3}$)	Viscosity/ $20^{o}C$ (P)	Time[a] (s)
CaF_2	3.18	Ethanol	0.7893	0.0120	14,400
mullite	3.07	"	"	"	15,500
glass[b]	2.54	"	"	"	

a: Settling time over 20 cm

b: Composition glass: CaO, 15.63%; MgO, 2.55%; SiO_2, 65.98%; Al_2O_3, 15.84%

TABLE 15

Composition of Mixtures (in g) Prepared for the Standard Curves

α-Quartz	Glass	CaF_2	Mullite	Glass	CaF_2	Magnetite	Glass	CaF_2	Hematite	Glass	CaF_2
2.000	-	1.000	3.000	-	.100	6.000	-	1.000	6.000	-	1.000
1.800	.200	1.000	2.700	.300	.100	5.500	.500	1.000	5.500	.500	1.000
1.600	.400	1.000	2.400	.600	.100	5.000	1.000	1.000	5.000	1.000	1.000
1.400	.600	1.000	2.100	.900	.100	4.500	1.500	1.000	4.500	1.500	1.000
1.200	.800	1.000	1.800	1.200	.100	4.000	2.000	1.000	4.000	2.000	1.000
1.000	1.000	1.000	1.500	1.500	.100	3.500	2.500	1.000	3.500	2.500	1.000
.800	1.200	1.000	1.200	1.800	.100	3.000	3.000	1.000	3.000	3.000	1.000
.600	1.400	1.000	.900	2.100	.100	2.500	3.500	1.000	2.500	3.500	1.000
.400	1.600	1.000	.600	2.400	.100	2.000	4.000	1.000	2.000	4.000	1.000
.200	1.800	1.000	.300	2.700	.100	1.500	4.500	1.000	1.500	4.500	1.000
.160	1.840	1.000	.250	2.750	.100	1.250	4.750	1.000	1.250	4.750	1.000
.120	1.880	1.000	.200	2.800	.100	1.500	5.000	1.000	1.000	5.000	1.000
.080	1.920	1.000	.150	2.850	.100	.500	5.500	1.000	.500	5.500	1.000
.040	1.960	1.000	.100	2.900	.100	.300	5.700	1.000	.300	5.700	1.000
.020	1.980	1.000	.050	2.950	.100	.100	5.900	1.000	.100	5.900	1.000

TABLE 16

Peaks Scanned for the Standard Curves

Phases	2Θ	2Θ-range Scanned
CaF_2	28.3	27.47 - 29.13
CaF_2	47.0	46.17 - 47.83
α-Quartz	20.8	20.0 - 21.66
α-Quartz	26.6	25.8 - 27.46
α-Quartz	50.1	49.3 - 50.96
Mullite	16.4	15.57 - 17.23
Mullite	39.2	38.37 - 40.03
Mullite	60.6	59.77 - 61.43
Magnetite	30.1	29.27 - 30.93
Magnetite	43.0	42.17 - 43.83
Magnetite	62.5	61.69 - 63.35
Hematite	24.1	23.27 - 24.93
Hematite	49.4	48.57 - 50.23
Hematite	63.9	63.12 - 64.78

ORF

TABLE 17

α-Quartz Content of 8 Canadian Fly Ashes

Fly Ash	2θ	$I_{Q,2\theta}$	2θ	$I_{F,2\theta}'$	$\frac{I_{Q,2\theta}}{I_{F,2\theta}}$	%* Quartz	Average
Wabamun	20.8	3390	28.3	11348	.2987	10.73	10.9
	26.6	19732	28.3	11348	1.7388	(12.49)	
	50.1	2306	28.3	11348	.2033	11.39	
	20.8	3390	47.0	12329	.2750	10.52	
	26.6	19732	47.0	12329	1.6005	(12.25)	
	50.1	2306	47.0	12329	.1871	11.12	
Sundance	20.8	1368	28.3	19112	.0716	4.91	4.7
	26.6	8021	28.3	19112	.4197	(6.15)	
	50.1	746	28.3	19112	.0391	4.41	
	20.8	1368	47.0	19715	.0694	5.05	
	26.6	8021	47.0	19715	.4068	(6.36)	
	50.1	746	47.0	19715	.0379	4.44	
Forestburg	20.8	760	28.3	25068	.0303	2.84	3.1
	26.6	3882	28.3	25068	.1549	(3.54)	
	50.1	504	28.3	25068	.0201	3.43	
	20.8	760	47.0	26659	.0285	2.81	
	26.6	3882	47.0	26659	.1456	(3.59)	
	50.1	504	47.0	26659	.0189	3.27	
Nanticoke	20.8	3294	28.3	10987	.2998	10.77	9.1
	26.6	18032	28.3	10987	1.8032	(1.95)	
	50.1	1467	28.3	10987	.1335	7.48	
	20.8	3294	47.0	11740	.2806	10.74	
	26.6	18032	47.0	11740	1.5359	(11.76)	
	50.1	1467	47.0	11740	0.1250	7.42	

* Values in brackets are not used for the average because of overlap with Mullite Peaks.

TABLE 17 (continued)

Fly Ash	2θ	$I_{Q,2\theta}$	2θ	$I_{F,2\theta}'$	$\frac{I_{Q,2\theta}}{I_{F,2\theta}}$	% Quartz	Average
Lakeview	20.8	2599	28.3	11102	.2342	8.38	5.5
	26.6	13456	28.3	11102	1.2120	(8.73)	
	50.1	305	28.3	11102	.0275	2.96	
	20.8	2599	47.0	12537	.2074	7.89	
	26.6	13456	47.0	12537	1.0733	(8.25)	
	50.1	305	47.0	12537	.0243	2.76	
Lingan	20.8	1388	28.3	18394	.0755	5.19	4.6
	26.6	6814	28.3	18394	.3704	(5.44)	
	50.1	434	28.3	18394	.0236	2.68	
	20.8	1388	47.0	19348	.0718	7.86	
	26.6	6814	47.0	19348	.3522	(5.53)	
	50.1	434	47.0	19348	.0224	2.60	
Dalhousie	20.8	2151	28.3	20364	.1056	11.08	12.4
	26.6	1012	28.3	20364	.4970	(10.88)	
	50.1	1706	28.3	20364	.0838	14.11	
	20.8	2151	47.0	22214	.0968	10.78	
	26.6	1012	47.0	22214	.4557	(10.66)	
	50.1	1706	47.0	22214	.0768	13.62	
Estevan	20.8	1445	28.3	11019	.1278	4.50	4.6
	26.6	5423	28.3	11019	.4797	(3.50)	
	50.1	857	28.3	11019	.0758	4.26	
	20.8	1445	47.0	11306	.1312	4.93	
	26.6	5423	47.0	11306	.4922	(3.83)	
	50.1	857	47.0	11306	.0778	4.61	

* Values in brackets are not used for the average because of overlap with Mullite Peaks.

ORF

TABLE 18

Mullite Content of 8 Canadian Fly Ashes

Fly Ash	2θ	$I_{M,2\theta}$	2θ	$I_{F,2\theta}'$	$\frac{I_{M,2\theta}}{I_{F,2\theta}'}$	% Mullite	Average
Wabamun	16.4	1317	28.3	11348	.1161	-	12.2%
	39.2	1367	28.3	11348	.1205	-	
	60.6	1004	28.3	11348	.0885	11.93	
	16.4	1317	47.0	12329	.1069	-	
	39.2	1367	47.0	12329	.1109	-	
	60.6	1004	47.0	12329	.0815	12.52	
Sundance	16.4	1059	28.3	19112	.05542	-	9.8%
	39.2	-504	28.3	19112	-.0264	-	
	60.6	643	28.3	19112	.0337	9.41	
	16.4	1059	47.0	19715	.0537	-	
	39.2	-504	47.0	19715	-.0256	-	
	60.6	643	47.0	19715	.0327	10.16	
Forestburg	16.4	188	28.3	25068	.0075	-	7.1%
	39.2	277	28.3	25068	.0111	-	
	60.6	399	28.3	25068	.0159	7.10	
	16.4	188	47.0	26659	.0071	-	
	39.2	277	47.0	26659	.0104	-	
	60.6	399	47.0	26659	.0149	7.15	
Nanticoke	16.4	2071	28.3	10987	.1885	-	17.3%
	39.2	563	28.3	10987	.0513	-	
	60.6	1397	28.3	10987	.1273	16.44	
	16.4	2071	47.0	11740	.1764	-	
	39.2	563	47.0	11740	.0480	-	
	60.6	1397	47.0	11740	.1190	18.25	

Table 18 (Continued)

Fly Ash	2θ	$I_{M,2\theta}$	2θ	$I_{F,2\theta'}$	$\frac{I_{M,2\theta}}{I_{F,2\theta'}}$	% Mullite	Average
Lakeview	16.4	3129	28.3	11102	.2819	-	25.2%
	39.2	240	28.3	11102	.0216	-	
	60.6	2080	28.3	11102	.1874	24.97	
	16.4	3129	47.0	12537	.2496	-	
	39.2	240	47.0	12537	.0192	-	
	60.6	2080	47.0	12537	.1659	25.40	
Lingan	16.4	1127	28.3	18394	.0613	-	10.4%
	39.2	-1184	28.3	18394	-.0644	-	
	60.6	666	28.3	18394	.0362	10.1	
	16.4	1127	47.0	19348	.0583	-	
	39.2	-1184	47.0	19348	-.0612	-	
	60.6	666	47.0	19348	.0344	10.70	
Dalhousie	16.4	307	28.3	20364	.0151	-	2.9%
	39.2	-1057	28.3	20364	-.0519	-	
	60.6	115	28.3	20364	.0057	3.05	
	16.4	307	47.0	22214	.0139	-	
	39.2	-1057	47.0	22214	-.0476	-	
	60.6	115	47.0	22214	.0052	2.69	
Estevan	-	-	-	-	-	-	-

TABLE 19

Magnetite Content of 8 Canadian Fly Ashes

Fly Ash	2θ	$I_{Ma,2\theta}$	$2\theta'$	$I_{F,2\theta'}$	$\frac{I_{Ma,2\theta}}{I_{F,2\theta'}}$	% Magnetite	Average
Wabamun	-	-	-	-	-	-	-
Sundance	-	-	-	-	-	-	-
Forestburg	-	-	-	-	-	-	-
Nanticoke	30.1	-968	28.3	10987	-.0882	-	4.8
	43.0	2199	28.3	10987	.2002	7.30	
	62.5	1152	28.3	10987	.1049	2.21	
	30.1	-968	47.0	11740	-.0825	-	
	43.0	2199	47.0	11740	.1874	8.10	
	62.5	1152	47.0	11740	.09813	1.83	
Lakeview	30.1	-2191	28.3	11102	-.1973	-	3.6
	43.0	1052	28.3	11102	.0948	3.35	
	62.5	-347	28.3	11102	-.0313	-	
	30.1	-2191	47.0	12537	-.1748	-	
	43.0	1052	47.0	12537	.0839	3.90	
	62.5	-347	47.0	12537	-.0277	-	
Lingan	30.1	-862	28.3	18394	-.0469	-	1.6
	43.0	428	28.3	18394	.0233	1.55	
	62.5	-119	28.3	18394	-.0070	0.43	
	30.1	-862	47.0	19348	-.0446	-	
	43.0	428	47.0	19348	.02215	2.79	
	62.5	-119	47.0	19348	-.0062	-	

Table 19 (continued)

Fly Ash	2θ	$I_{Ma,2\theta}$	$2\theta'$	$I_{F,2\theta'}$	$\frac{I_{Ma,2\theta}}{I_{F,2\theta'}}$	% Magnetite	Average
Dalhousie	30.1	835	28.3	20364	.0410	3.55	3.3
	43.0	741	28.3	20364	.0364	3.74	
	62.5	706	28.3	20364	.0347	2.88	
	30.1	835	47.0	22214	.0376	2.32	
	43.0	741	47.0	22214	.0334	5.67	
	62.5	706	47.0	22214	.0318	1.51	
Estevan	-	-	-	-	-	-	-

TABLE 20

Hematite Content of 8 Canadian Fly Ashes

Fly Ash	2θ	$I_{H,2\theta}$	$2\theta'$	$I_{F,2\theta'}$	$\frac{I_{H,2\theta}}{I_{F,2\theta'}}$	% Hematite	Average
Wabamun	-	-	-	-	-	-	-
Sundance	24.1	-61	28.3	19112	-.0032	-	
	49.4	-234	28.3	19112	-.0123	2.31	2.2
	63.9	-0.4	28.3	19112	-.00002	-	
	24.1	-61	47.0	19715	-.0031	0.24	
	49.4	-234	47.0	19715	-.0119	1.71	
	63.9	-0.4	47.0	19715	-.00002	4.70	
Forestburg	-	-	-	-	-	-	-
Nanticoke	24.1	327	28.3	10987	.0298	0.85	1.6
	49.4	-196	28.3	10987	-.0179	0.26	
	63.9	304	28.3	10987	.0277	2.96	
	24.1	327	47.0	11740	.0279	1.41	
	49.4	-196	47.0	11740	-.0168	0.71	
	63.9	304	47.0	11740	.0259	3.30	
Lakeview	24.1	-428	28.3	11102	-.0386	-	2.5
	49.4	121	28.3	11102	.01097	1.12	
	63.9	470	28.3	11102	.0424	3.48	
	24.1	-428	47.0	12537	-.0342	-	
	49.4	121	47.0	12537	.0097	1.52	
	63.9	470	47.0	12537	.0375	3.72	
Lingan	24.1	428	28.3	18394	.0233	1.18	2.6
	49.4	-239	28.3	18394	-.0130	0.81	
	63.9	119	28.3	18394	.0065	4.41	
	24.1	428	47.0	19348	.0221	2.34	
	49.4	-239	47.0	19348	-.0124	1.68	
	63.9	119	47.0	19348	.0062	5.16	

Table 20 (continued)

Fly Ash	2Θ	$I_{H,2\Theta}$	$2\Theta'$	$I_{F,2\Theta'}$	$\frac{I_{H,2\Theta}}{I_{F,2\Theta'}}$	% Hematite	Average
Dalhousie	24.1	426	28.3	26364	.0209	1.47	
	49.4	-497	28.3	26364	-.0244	0.07	3.2
	63.95	-5.8	28.3	26364	-.0003	5.88	
	24.1	426	47.0	22214	.0192	3.14	
	49.4	-497	47.0	22214	-.0224	-1.61	
	63.95	-5.8	47.0	22214	-.0003	1.02	
Estevan	-	-	-	-	-	-	-

TABLE 21

Crystalline and Glass Content of 8 Canadian Fly Ashes
(wt.%)

Fly Ash	α-quartz	Mullite	Magnetite	Hematite	LOI	Glass
Wabamun	10.9	12.2	-	-	0.8	76.1
Sundance	4.7	9.8	-	2.2	0.4	82.9
Forestburg	3.1	7.1	-	-	0.8	89.0
Nanticoke	9.1	17.3	4.8	1.6	7.5	59.7
Lakeview	5.5	25.2	3.6	2.5	9.7	53.5
Lingan	4.6	10.4	1.6	2.6	3.5	77.3
Dalhousie	12.4	2.9	3.3	3.2	1.5	76.7
Estevan	4.6	-	-	-	0.9	94.5

TABLE 22

Composition of the Mixtures (in g) Prepared for Standard Curves for Melilite and Merwinite

Melilite	Glass	CaF_2	$\frac{\text{Melilite}}{CaF_2}$	Merwinite	Glass	CaF_2	$\frac{\text{Merwinite}}{CaF_2}$
3.000	0.000	0.200	15.0	4.000	0.000	0.200	20.0
2.750	0.250	0.200	13.75	3.500	0.500	0.200	17.5
2.500	0.500	0.200	12.5	3.000	1.000	0.200	15.0
2.250	0.750	0.200	11.25	2.500	1.500	0.200	12.5
2.000	1.000	0.200	10.0	2.000	2.000	0.200	10.0
1.750	1.250	0.200	8.75	1.500	2.500	0.200	7.5
				1.000	3.000	0.200	5.0
1.500	1.500	0.200	7.50	0.750	3.250	0.200	3.75
1.250	1.750	0.200	6.25	0.600	3.400	0.200	3.00
1.000	2.000	0.200	5.00	0.500	3.500	0.200	2.50
0.750	2.250	0.200	3.75	0.400	3.600	0.200	2.00
0.500	2.500	0.200	2.50	0.300	3.700	0.200	1.50
0.250	2.750	0.200	1.25	0.200	3.800	0.200	1.00
				0.050	3.950	0.200	0.250

TABLE 23

Peaks Scanned for the Standard Curves for Melilite and Merwinite

Phases	2Θ	2Θ-range scanned
Melilite Curve		
CaF_2	46.97	46.14 - 47.80
Melilite	31.20	30.60 - 32.26
Merwinite Curve		
CaF_2	28.40	27.00 - 28.66
	55.70	55.00 - 56.66
Merwinite	31.30	30.20 - 31.86
	33.60	32.80 - 34.46

ORF

TABLE 24

Crystalline and Glass Contents of 2 Blast Furnace Slags

Sample	2θ	$I_{M,2\theta}$	$2\theta'$	$I_{F,2\theta'}$	$\frac{I_{M,2\theta}}{I_{F,2\theta'}}$	$\overline{\frac{I_{M,2\theta}}{I_{F,2\theta'}}}$	% M	$\overline{\%M}$	% Glass
Standard	31.20	1592	46.97	4987	0.3192	0.3329	11.7	11.7	88.3
(Melilite)	31.20	1794	46.97	5378	0.3336				
	31.20	1821	46.97	5266	0.3458				
Atlantic	31.30	581	28.40	996	0.583	0.448	(4.49)		
(Merwinite)	31.30	503	28.40	1464	0.344				
	31.30	560	28.40	1343	0.417				
	31.30	581	55.70	443	1.312	1.069	(3.65)		
	31.30	503	55.70	476	1.057				
	31.30	560	55.70	668	0.838				
	33.60	2298	28.40	996	2.307	1.849	12.92	11.9	88.1
	33.60	2521	28.40	1464	1.722				
	33.60	2037	28.40	1343	1.517				
	33.60	2298	55.70	443	5.187	4.511	10.80		
	33.60	2521	55.70	476	5.296				
	33.60	2037	55.70	668	3.049				

TABLE 25

XRD Data for Cordierite Non-Crystalline Scattering Method*

% Glass	Intensity Standard	I_x (1)	I_x (2)	I_x (3)	$\overline{I}_{x'}$ (Corr.)	$\overline{I}_{x'}-\overline{I}_o$
0	35923	10176	10232	10220	10209	0
10	35788	13463	13264	13258	13328	3119
20	36078	14651	14735	14683	14690	4481
30	35686	18243	18116	18227	18195	7986
40	35721	22412	22695	22470	22526	12317
50	35830	25303	25231	25302	25279	15070
60	35605	29861	29650	29852	29788	19579
70	35751	32233	31782	32018	32011	21802
80	36470	36876	36915	37257	37016	26801
90	35651	40810	40754	40849	40804	30595
100	35995	43587	43689	43442	43573	33364

* $\overline{I}_{x'}-\overline{I}_o = 3.44\times10^2 \times \%\text{Glass} - 1.29\times10^3$ $r = 0.9969$

TABLE 26

XRD Data for Wabamun Fly Ash
(Non-Crystalline Scattering Method)*

% Glass	Intensity Standard	I_x (1)	I_x (2)	I_x (3)	$\overline{I}_{x'}$ (Corr.)	$\overline{I}_{x'}-\overline{I}_o$
0	36261	8547	8565	8575	8562	0
10		11053	11062	11144	11086	2524
20		12559	12630	12591	12593	4031
30		15844	15822	15892	15853	7291
40		17746	17609	17662	17672	9110
50	35968	20278	20374	20203	20285	11723
60		22065	22113	22054	22077	13515
70		24302	24344	24286	24311	15749
80		26597	26344	26408	26450	17888
90		28094	28297	28312	28233	19671
100		30032	30017	30333	30127	21565
Fly Ash		22477	22340	22325	22381	13819

* $\overline{I}_{x'}-\overline{I}_o = 2.176\times10^2 \times \%\text{Glass} + 3.104\times10^2$ r = 0.9987

% Glass in Wabamun Fly Ash : 62.1%

ORF

TABLE 27

XRD Data for Sundance Fly Ash
(Non-Crystalline Scattering Method)*

% Glass	Intensity Standard	I_x (1)	I_x (2)	I_x (3)	$\overline{I}_{x'}$ (Corr.)	$\overline{I}_{x'}-\overline{I}_o$
0		9631	9402	9475	9503	0
10		11139	11249	11053	11147	1644
20		12889	13001	12911	12934	3431
30		14305	14550	14544	14466	4963
40		16849	16583	16572	16668	7165
50		18220	18109	18362	18230	8727
60		20179	20286	20084	20183	10680
70	35789	22282	22071	22051	22135	12632
80		23987	24175	24200	24121	14618
90		26356	26220	26141	26239	16736
100		28551	28289	28543	28461	18958
Fly Ash		23788	23649	23727	23720	14212

* $\overline{I}_{x'}-\overline{I}_o = 1.887\times10^2 \times \%\text{Glass} + 3.857\times10^2$ $r = 0.9991$
% Glass in Sundance Fly Ash : 77.4%

ORF

TABLE 28

XRD Data for Forestburg Fly Ash
(Non-Crystalline Scattering Method)*

% Glass	Intensity Standard	I_x (1)	I_x (2)	I_x (3)	$\bar{I}_{x'}$	$\bar{I}_{x'}-\bar{I}_o$
0	35574	7699	7728	7444	7624	0
10	36027	9886	9443	9335	9555	1937
20	35789	11423	11282	11521	11409	3783
30	35777	13919	13942	14265	14042	6435
40	36011	15462	15029	15423	15305	7769
50	36418	17257	17907	17819	17661	10090
60	35562	19238	19381	19869	19496	11899
70	36202	21702	22012	22290	22001	14520
80	36112	23899	23920	24088	23969	16544
90	36361	25341	25052	26217	25537	18152
100	36198	25931	26115	26194	26080	18646
Fly Ash	36140	23478	24197	23799	23825	16354

* $\bar{I}_{x'}-\bar{I}_o = 1.970\text{x}10^2$ x %Glass + $1.308\text{x}10^2$ r = 0.9969

% Glass in Forestburg Fly Ash : 82.4%

TABLE 29

XRD Data for Nanticoke Fly Ash (Non-Crystalline Scattering Method)*

% Glass	Intensity Standard	I_x (1)	I_x (2)	I_x (3)	$\bar{I}_x$	$\bar{I}_x'$ (Corr.)	$\bar{I}_x'-\bar{I}_o$
0	34811	7794	7649	7833	7759	7759	0
10	34956	9597	9590	9551	9579	9600	1841
20	34655	11119	10901	11010	11010	11193	3434
30	33969	11641	11538	11693	11624	11898	4139
40	34189	12520	12374	12357	12417	12677	4918
50	34149	12883	12816	13103	12934	13213	5454
60	34143	14962	14817	14880	14886	15340	7581
70	33559	17480	17347	17585	17471	18019	10260
80	34086	18099	18179	18313	18197	18705	10946
90	33787	20958	20792	20885	20878	21549	13790
100	33809	22525	22314	22515	22451	23172	15413
	33918						
Fly Ash	34832	19904	19979	19674	19852	19808	12049
	35087						

* $\bar{I}_x-\bar{I}_o = 1.475\text{x}10^2$ %Glass $- 3.068\text{x}10^2$ $r = 0.9854$

% Glass in Nanticoke Fly Ash : 83.8%

TABLE 30

XRD Data for Lakeview Fly Ash
(Non-Crystalline Scattering Method)*

% Glass	Intensity Standard	I_x (1)	I_x (2)	I_x (3)	$\bar{I}_x$	$\bar{I}_{x'}$ (Corr.)	$\bar{I}_{x'}-\bar{I}_o$
0	34215	9360	9509	9444	9438	9438	0
10	34100	10306	10331	10338	10325	10254	816
20	34597	10893	10705	10563	10720	10657	1219
30	34034	11558	11641	11773	11657	11696	2258
40	33963	11999	12062	11987	12028	12057	2619
50	34098	13974	13974	13845	13931	13883	4445
60	34363	14493	14606	14687	14595	14655	5217
70	33585	15658	15469	15834	15654	15884	6446
80	33654	15975	16074	16003	16017	16118	6680
90	34145	16677	16740	16788	16735	16810	7372
100	33775	18002	17951	18168	18048	18194	8756
	33903						
Fly Ash	34945	18180	18320	18457	18319	17969	8531
	34697						

---

* $\bar{I}_{x'}-\bar{I}_o = 8.85\times10^1$ %Glass $- 2.593\times10^2$ $r = 0.9933$
% Glass in Lakeview Fly Ash : 99.3%

TABLE 31

XRD Data for Lingan Fly Ash
(Non-Crystalline Scattering Method)*

% Glass	Intensity Standard	I_x (1)	I_x (2)	I_x (3)	$\bar{I}_x$	$\bar{I}_{x'}$ (Corr.)	$\bar{I}_{x'}-\bar{I}_{53.6}$
53.6	36141	15014	14809	14825	14883	14883	0
58.2	35301	14565	14567	14498	14543	14593	-290
62.9	35898	14643	14624	14665	14644	14547	-336
67.5	36022	15544	15540	15335	15473	15407	524
72.2	35728	15698	15705	15857	15753	15704	821
76.8	35936	16395	16198	16359	16307	16249	1366
81.4	35762	17190	17115	17035	17113	17047	2164
86.1	35956	17235	17313	17350	17299	17131	2248
90.7	36186	18047	18086	17940	18024	17906	3022
95.4	35728	19676	19334	19405	19472	19507	4624
100.0	35585	20706	20503	20376	20528	20559	5676
Fly Ash	35748	17635	17684	17594	17638	17625	2742

* $\bar{I}_{x'}-\bar{I}_{53.6} = 1.232\times10^{2}$ %Glass $- 7.659\times10^{3}$ r = 0.9510
% Glass in Lingan Fly Ash : 84.4%

TABLE 32

XRD Data for Estevan Fly Ash
Non-Crystalline Scattering Method*

% Glass	Intensity Standard	$I_x(1)$	$I_x(2)$	$I_x(3)$	$\bar{I}_x$, (corrected)	$\bar{I}_x - \bar{I}_o$
0	33822	5323	5413	5559	5434	0
10	33834	7456	7648	7554	7520	2086
20	33440	9076	9050	8994	9136	3702
30	33936	11128	11316	11175	11260	5826
40	34045	12678	12648	12591	12803	7369
50	34490	14692	14888	14779	14930	9496
60	33827	16223	15942	15976	16050	10616
70	33842 34223	18564	18571	18676	18716	13282
80	35051	19501	19403	19440	19895	14461
90	34160	21482	21458	21664	21761	16327
100	34205 34689	24058	24322	24259	24646	19212
Fly Ash	34223 35051	18040	18002	17984	18440	13006

* $\bar{I}_x - \bar{I}_o = 1.850\times10^2$ % Glass + 5.882×10^1 r=0.9964
% Glass in Estevan Fly Ash: 70.0%

ORF

TABLE 33

XRD Data for Thunder Bay Fly Ash
Non-Crystalline Scattering Method*

% Glass	Intensity Standard	$I_x(1)$	$I_x(2)$	$I_x(3)$	$\bar{I}_{x'}$ (corrected)	$\bar{I}_x-\bar{I}_o$
0	35581	9349	9413	9459	9381	0
10	35482	10644	10582	10737	10632	1251
20	35433	12823	12817	12958	12851	3470
30	35550	13947	13954	13791	13918	4537
40	35620	15299	15282	15378	15406	6025
50	35842	17054	17025	17248	17237	7856
60	35754	19300	19609	19562	19546	10165
70	35515	20911	20839	20899	20869	11488
80	35504	22104	22290	22160	22235	12854
90	35720	23362	23407	23626	23596	14215
100	35821	25580	25281	25449	25599	16218
Fly Ash	35696	23492	23186	23213	23405	14024

* $\bar{I}_{x'}-\bar{I}_o = 1.629\times10^2$ % Glass + 1.356×10^2 r=0.9986
% Glass in Thunder Bay Fly Ash: 86.9%

ORF

TABLE 34

XRD Data for Standard Slag
Non-Crystalline Scattering Method

% Glass	Intensity Standard	$I_x(1)$	$I_x(2)$	$I_x(3)$	$\overline{I}_x$ (corrected)	$\overline{I}_{x'}-\overline{I}_o$
0	34539	3537	3469	3524	3510	0
10	35123	4071	4095	4133	4077	570
20	34147	5262	5278	5158	5127	1617
30	34104	6106	5951	6000	5901	2391
40	34189	7309	7238	6953	7049	3539
50	34321	7946	7949	8073	7870	4360
60	34301	9441	9411	9513	9275	5765
70	34037 34256	9602	9561	9756	9451	9541
80	34114	11362	11369	11265	11195	7685
90	34706	11916	11919	11790	11823	8313
100	34653 34191	13016	12994	13104	12885	9375
Slag	34256 34114	10489	10240	10329	10161	6651

$\overline{I}_{x'}-\overline{I}_o = 9.580\times10^1$ % Glass $- 2.848\times10^2$ $r=0.9972$

% Glass in Standard Slag: 72.4%

TABLE 35

XRD Data for Atlantic Slag
Non-Crystalline Scattering Method

% Glass	Intensity Standard	$I_x(1)$	$I_x(2)$	$I_x(3)$	$\overline{I}_x$ (corrected)	$\overline{I}_{x_i}-\overline{I}_o$
0	33124	2989	2899	2980	2956	0
10	32971	4199	4238	4205	4175	1219
20	32508	6265	6239	6308	6229	3273
30	33148	7282	7222	7378	7264	4308
40	32675	8983	9102	8993	8968	6012
50	32996	10224	10512	10446	10410	7454
60	33201 32339	12232	12012	11867	11936	8980
70	33066	14278	14183	14294	14224	11268
80	32901	15293	15380	15115	15321	12365
90	33445	16458	16436	16454	16649	13693
100	33456 33160	18749	18522	18376	18695	15739
Slag	32339 33066	9626	9572	9574	9491	6535

$\overline{I}_{x_i}-\overline{I}_o = 1.571\times10^2$ % Glass $- 1.879\times10^2$ $r=0.9988$

% Glass in Atlantic Slag: 42.8%

ORF

TABLE 36

Scattering Intensities of Cordierite Glass (I_a), α-Cordierite (I_c) and a Mixture of 20% Cordierite Glass and 80% of α-Cordierite (I_u)

2θ	I_a	I_c	I_u	I_c-I_a	I_u-I_a
Standard	35483	35610	34316		
10.0	9515	20242	39669	10727	30154
10.5	9497	54058	34259	44561	24762
11.0	9525	6568	6962	-2957	-2563
11.5	9664	6219	6366	-3445	-3298
12.0	9919	6290	6585	-3629	-3334
12.5	10384	6473	6444	-3911	-3940
13.0	10675	6912	6515	-3763	-4160
13.5	10984	6645	6649	-4339	-4335
14.0	11438	7430	6999	-4008	-4439
14.5	12285	6715	6834	-5570	-5451
15.0	12891	6547	6722	-6344	-6169
15.5	13763	6906	7062	-6857	-6701
16.0	14535	10260	9074	-4275	-5461
16.5	15562	18987	10373	3425	-5189
17.0	16799	7538	7756	-9261	-9043
17.5	18118	8142	9366	-9976	-8752
18.0	19542	25688	64542	6146	45000
18.5	21306	9535	11909	-11771	-9397
19.0	23489	19405	19860	-4084	-3629
19.5	25417	11805	11398	-13612	-14019
20.0	27991	19765	13757	-8226	-14234
20.5	30705	19648	16069	-11057	-14636
21.0	33033	10908	13803	-122125	-19230
21.5	35685	46573	90730	10888	55045
22.0	38336	12514	15697	-25822	-22639
22.5	40538	9434	13373	-31104	-27165
23.0	42024	9255	13489	-32769	-28535
23.5	43526	11448	15154	-32078	-28372

TABLE 36 continued

2θ	I_a	I_c	I_u	I_c-I_a	I_u-I_a
24.0	43712	9299	13704	-34413	-30008
24.5	44015	9171	13940	-34844	-30075
25.0	43934	10895	14227	-33039	-29707
25.5	43624	39178	24008	-4446	-19616
26.0	41688	174712	77852	133024	36164
26.5	40034	34330	33853	-5704	-6181
27.0	38565	15588	16035	-22977	-22530
27.5	36616	10922	13733	-25694	-22883
28.0	34718	19057	21171	-15661	-13547
28.5	33806	61954	81137	28148	47331
29.0	31666	12689	16831	-18977	-14835
29.5	29832	97420	184773	67588	154941
30.0	28467	10072	12048	-18395	-16419
30.5	27091	19699	15226	-7392	-11865
31.0	25946	27986	18035	2040	-7911
31.5	24697	12541	11382	-12156	-13315
32.0	23314	8266	9073	-15048	-14241
32.5	22150	7919	9004	-14231	-13146
33.0	21330	21732	16317	402	-5013
33.5	20525	11795	11665	-8730	-8860
34.0	19838	23567	36978	3729	17140
34.5	19203	9708	8963	-9495	-10240
35.0	19156	22337	17601	3181	-1555
35.5	17779	15950	12146	-1829	-5633
36.0	16774	36227	18908	19453	2134
36.5	16204	16710	13660	506	-2544
37.0	16007	16192	13483	185	-2524
37.5	15783	8330	7937	-7453	-7846
38.0	16046	6992	9762	-9054	-6284
38.5	16984	18282	25567	1298	8583
39.0	14148	12842	10642	-1306	-3506
39.5	14047	12872	15931	-1175	1884
40.0	14203	14019	10856	-184	-3347
				-227,885	-155,184

TABLE 37

Scattering Intensities of Cordierite Glass (I_a), α-Cordierite (I_c) and a Mixture of 70% Cordierite Glass and 30% of α-Cordierite (I_u)

2Θ	I_a	I_c	I_u	I_c-I_a	I_u-I_a
Standard	35483	35610	34911		
10.0	9515	20242	18983	10727	9468
10.5	9497	54058	24692	44561	15195
11.0	9525	6568	8053	-2957	-1472
11.5	9664	6219	8108	-3445	-1556
12.0	9919	6290	8094	-3629	-1825
12.5	10384	6473	8282	-3911	-2102
13.0	10675	6912	8428	-3763	-2247
13.5	10984	6645	8728	-4339	-2256
14.0	11438	7430	9121	-4008	-2317
14.5	12285	6715	9246	-5570	-3039
15.0	12891	6547	9585	-6344	-3306
15.5	13763	6906	10360	-6857	-3403
16.0	14535	10260	11411	-4275	-3124
16.5	15562	18987	12955	3425	-2607
17.0	16799	7538	12452	-9261	-4347
17.5	18118	8142	14479	-9976	-3639
18.0	19542	25688	31323	6146	11781
18.5	21306	9535	16435	-11771	-4871
19.0	23489	19405	21909	-4084	-1580
19.5	25417	11805	18885	-13612	-6532
20.0	27991	19765	21464	-8226	-6437
20.5	30705	19648	24065	-11057	-6640
21.0	33033	10908	24808	-22125	-8225
21.5	35685	46573	50890	10888	15205
22.0	38336	12514	28846	-25822	-9490
22.5	40538	9434	28716	-31104	-11822
23.0	42024	9255	30674	-32769	-11350
23.5	43526	11448	31888	-32078	-11638
24.0	43712	9299	31686	-34413	-12026

ORF

TABLE 37 continued

2θ	I_a	I_c	I_u	I_c-I_a	I_u-I_a
24.5	44015	9171	32139	-34844	-11876
25.0	43934	10895	31621	-33039	-12314
25.5	43624	39178	34653	-4446	-8971
26.0	41688	174712	54582	133024	12894
26.5	40034	34330	38393	-5704	-641
27.0	38565	15588	29480	-22977	-9085
27.5	36616	10922	27437	-25694	-9179
28.0	34718	19057	28644	-15661	-6074
28.5	33806	61954	44495	28148	10689
29.0	31666	12689	25152	-18977	-6514
29.5	29832	97420	76650	67588	46818
30.0	28467	10072	21341	-18395	-7126
30.5	27091	19699	21856	-7392	-5235
31.0	25946	27986	21919	2040	-4027
31.5	24697	12541	18691	-12156	-6006
32.0	23314	8266	19270	-15048	-4044
32.5	22150	7919	16655	-14231	-5495
33.0	21330	21732	19500	402	-1830
33.5	20525	11795	16559	-8730	-3966
34.0	19838	23567	23083	3729	3245
34.5	19203	9708	14795	-9495	-4408
35.0	19156	22337	18738	3181	-418
35.5	17779	15950	15387	-1829	-2392
36.0	16774	36227	17256	19453	482
36.5	16204	16710	15244	506	-960
37.0	16007	16192	14526	185	-1481
37.5	15783	8330	12363	-7453	-3420
38.0	16046	6992	13288	-9054	-2758
38.5	16984	18282	18208	1298	-1224
39.0	14148	12842	12686	-1306	-1462
39.5	14047	12872	14761	-1175	714
40.0	14203	14019	12947	-184	-1256
TOTAL				-227,885	-123,522

TABLE 38

Scattering Intensities of Wabamun Fly Ash Glass (I_a) its Redevitrified Analogue (I_u) and Wabamun Fly Ash (I_u)

2Θ	I_a	I_c	I_u	I_c-I_a	I_u-I_a	
Standard						
10.0	7904	6436	7733	-1468	-171	
10.5	7957	6750	7678	-1207	-279	
11.0	7687	5435	7629	-2252	-58	
11.5	7604	5287	7780	-2317	176	
12.0	7777	5255	8006	-2522	229	
12.5	7901	5105	7891	-2796	-10	
13.0	8239	5134	8169	-3105	-70	
13.5	8156	7004	8301	-1152	145	
14.0	8462	5109	8490	-3353	28	
14.5	8561	4662	9056	-3899	495	
15.0	9096	5018	9166	-4078	70	
15.5	9593	4763	9789	-4830	196	
16.0	10221	4670	12477	-5551	2256	
16.5	10901	4596	12010	-6305	1109	
17.0	11592	4746	13848	-6846	2256	
17.5	12853	5868	12200	-6985	-653	
18.0	13744	6900	13047	-6844	-697	
18.5	14937	6340	14303	-8597	-634	
19.0	16309	7792	15123	-8517	-1186	
19.5	17769	5870	16072	-11899	-1697	
20.0	19248	6532	17865	-12716	-1383	
20.5	20731	11340	28353	-9391	7622	*
21.0	22126	17926	20790	-4200	-1336	*
21.5	23575	125113	23061	101538	-514	*
22.0	25040	52819	21414	27779	-3626	*
22.5	25820	16306	21125	-9514	-4695	*
23.0	26732	10926	21452	-15806	-5280	
23.5	27189	23732	21744	-3457	-5445	*
24.0	26966	24272	21353	-2694	-5613	*
24.5	27141	13514	20648	-13627	-6493	

ORF

TABLE 38 (continued)

2θ	I_a	I_c	I_u	I_c-I_a	I_u-I_a	
25.0	26986	7869	21139	-19117	-5847	
25.5	26063	14823	23074	-11240	-2989	
26.0	25454	11650	36178	-13804	10724	*
26.5	25247	13350	36464	-11897	11217	*
27.0	23841	9701	20643	-14140	-3198	*
27.5	22935	53516	19919	30581	-3016	*
28.0	22306	63031	19511	40725	-2795	*
28.5	21273	16461	18242	-4812	-3031	
29.0	20324	9764	17744	-10560	-2580	
29.5	19616	13309	17344	-6307	-2272	
30.0	18789	12634	16968	-6155	-1821	
30.5	18016	19887	16568	1871	-1448	
31.0	17344	14550	18191	-2794	847	*
31.5	16457	12474	15440	-3983	-1017	
32.0	16021	9321	15601	-6700	-420	
32.5	15509	7346	15983	-8163	474	
33.0	14572	13114	24677	-1458	10125	*
33.5	14086	12725	15493	-1361	1407	
34.0	13499	6536	12314	-6963	-1185	
34.5	13107	6879	11841	-6228	-1266	
35.0	12601	11141	15101	-1460	2500	
35.5	12104	40334	12784	28230	680	
36.0	11567	15204	11525	3637	-42	*
36.5	11055	10609	14855	-446	3800	
37.0	10711	9731	11340	-980	629	
37.5	10395	8310	9844	-2085	-551	
38.0	11211	7314	9565	-3897	-1646	
38.5	11149	6858	9030	-4291	-2119	
39.0	9884	6613	10925	-3271	1041	
39.5	9683	7761	12184	-1922	2501	
40.0	9823	6436	10347	-3387	524	
TOTAL				-88,988	-16,032	

ORF

TABLE 39

Glass Contents Determined with the Differential Intensity Method

	Cordierite		Wabamun
	A	B	
% Glass (known)	20	70	?
Integral Index (C_i)	0.681	0.542	0.180
Crystallinity (C_i)%	68.1	54.2	18.0
% Glass (C_i)	31.9	45.8	82.0
Correlation Index (C_c)	0.795	0.278	-0.0104 (0.164)
Correlation Coefficient (r)	0.722	0.772	-0.0508 (0.529)
Crystallinity (C_c)%	79.5	27.8	-1.0 (16.4)
% Glass (C_c)	20.5	72.2	101.0 (83.6)

ORF

TABLE 40

Specific Gravities of Three Fly Ashes and Analogues Determined by Pycnometry

Fly Ash	Specific Gravity Fly Ash	Specific Gravity Glassy Analogue	Specific Gravity Crystalline Analogue
Wabamun	2.47	2.67	2.68
Sundance	2.44	2.65	2.73
Forestburg	2.43	2.77	2.80

TABLE 41

Composition (wt.%) and Diffraction Maxima ($2\Theta_{Imax}$) of Glasses in the Na_2O-SiO_2, $CaO-SiO_2$, $CaO-Al_2O_3$, $Na_2O-CaO-SiO_2$ and $CaO-Al_2O_3-SiO_2$ Systems

Sample	Na_2O	CaO	Al_2O_3	SiO_2	$2\Theta_{Imax}$	
1	20.00	-	-	80.00	22.5	
2	30.00	-	-	70.00	24.5,	30.4
3	32.00	-	-	68.00	24.5,	31.4
4	34.00	-	-	66.00	24.5,	31.4
5	36.00	-	-	64.00	24.4,	32.0
6	38.00	-	-	62.00	24.5,	32.5
7	40.00	-	-	60.00	24.5,	32.5
8	50.00	-	-	50.00	34.0	
9	-	48.28	-	51.72	30.0	
10	15.00	15.00	-	70.00	25.5,	29.0
11	20.00	20.00	-	60.00	23.0,	31.0
12		49.04	8.92	42.04	30.2	
13		49.84	18.12	32.04	30.2	
14		50.66	27.63	21.71	30.6	
15		51.51	37.46	11.04	30.8	
16		52.38	47.62	-	31.2	
17		48.53	51.47	-	31.0	

ORF

TABLE 42

Composition (wt%) and Diffraction Maximum ($2\theta_{Imax}$) of Commercial Glasses

Serial No.	Glass Name	Components							$2\theta_{Imax}$
		SiO_2	Al_2O_3	Na_2O	B_2O_3	CaO	MgO	K_2O	Degree
1	Pyrex Test Tube Glass	81.0	2.0	3.8	13.0	-	-	0.2	21.6
2	Window Glass	73.0	1.0	17.0	-	6.0	3.0	-	24.0
3	Corning Slide Glass			Not analyzed					
4	Fused Silica Glass	100.0							21.3
5	Container Glass	74.9	0.8	15.2	-	5.5	3.6	-	24.0

TABLE 43

XRD $2\theta_{Imax}$ for 9 Fly Ashes, 2 Slags and Their Glassy Analogues

Source	$2\theta_{Imax}$	$2\theta_{Imax}$(glass)	CaO (wt.%)	$\Sigma CaO + MgO + Na_2O + K_2O$ (mol/100g)
Wabamun	23.2	24.5	11.1	0.259
Sundance	23.4	25.3	12.5	0.295
Forestburg	25.4	25.7	10.5	0.316
Nanticoke	23.0	24.0	5.95	0.158
Lakeview	24.0	24.2	3.82	0.126
Lingan	24.4	25.5	1.29	0.106
Dalhousie	23.8	-	4.45	0.127
Estevan	29.0	26.4	13.0	0.455
Thunder Bay	25.4	26.0	12.4	0.419
Standard Slag	30.6	29.5	35.1	0.937
Atlantic Slag	30.8	28.4	40.1	0.959

ORF

TABLE 44

Mass Changes Observed for Fly Ashes and Slags after Leaching for 24 hrs in Deionized Distilled H_2O

Fly Ash/ Slag	Initial Mass (g)	Final Mass (g)	Change (g)	% Change
Wabamun	1.00	.86	-.14	-16.28
	2.00	1.77	-.23	-13.00
	4.00	3.70	-.30	- 8.11
	8.00	7.76	-.24	- 3.09
Sundance	1.00	.93	-.07	- 7.53
Forestburg	1.00	.94	-.06	- 6.38
Nanticoke	1.00	.95	-.05	- 5.26
Lakeview	1.00	.97	-.03	- 3.09
	2.00	1.89	-.11	- 5.82
	4.00	3.83	-.17	- 4.44
	8.00	7.68	-.32	- 4.17
Lingan	1.00	.96	-.04	- 4.17
Dalhousie	1.00	.94	-.06	- 6.38
	2.00	1.91	-.09	- 4.71
	4.00	3.76	-.24	- 6.38
	8.00	7.63	-.37	- 4.85
Estevan	1.00	0.96	-0.04	-4
	2.00	1.96	-0.04	-2
	4.00	3.65	-0.35	-8.8
	8.00	7.86	-0.14	-1.8
Thunder Bay	1.00	0.93	-0.07	-7
	2.00	1.79	-0.21	-11
	4.00	3.28	-0.72	-18
	8.00	7.30	-0.70	-8.8

ORF

TABLE 44 (continued)

Fly Ash/ Slag	Initial Mass (g)	Final Mass (g)	Change (g)	% Change
Standard	1.00	0.93	-0.07	-7
	2.00	1.88	-0.12	-6
	4.00	3.97	-0.03	-0.8
	8.00	8.01	+0.01	+0.1
Atlantic	1.00	1.12	+0.12	+12
	2.00	2.10	+0.10	+5
	4.00	4.08	+0.10	+2
	8.00	7.91	-0.09	-1

TABLE 45

Summary of Observations Made During Leaching of Fly Ashes and Slags

Source Material	Initial pH (H_2O)	Initial Temperature (°C)	Maximum pH (time)	Final pH (24 hrs)	pH change when mass is doubled
Wabamun	7.2	23.5	10.60-11.20 (30 min)	8.85-10.60	0.15-0.20
Sundance	6.2	24.0	11.05 (20 min)	8.05	-
Forestburg	6.2	24.0	10.50 (15 min)	7.95	-
Nanticoke	6.2	24.0	11.20 (20 min)	8.60	-
Lakeview	6.9	25.0	10.35-10.95 (15-30 min)	8.20-9.85	0.20
Lingan	6.2	24.0	8.85 (45 min)	7.85	-
Dalhousie	6.9	24.5*	~7.30 (24 hrs)	~7.30	0.10
Estevan	6.3	-	10.55-11.20 (30-40 min)	8.90-10.70	0.20
Thunder Bay	7.6	-	9.00-9.20 (15 min)	8.05-8.60	0.10-0.40
Standard Slag	6.9	-	9.85-10.60 (25 min-3 hrs)	9.30-10.45	0.10-0.30
Atlantic Slag	6.7	-	10.60-10.85 (3-5 hrs)	10.30-10.60	0.10

* A temperature raise to 28°C was observed during this experiment for 2-4g sample.

ORF

TABLE 46

Mass Changes Observed of Various Derived Materials During Leaching in Deionized H_2O

Series	Fly Ash/Slag	Initial Mass (g)	Final Mass (g)	Change (g)	% Change
Particle Size Study	Wabamun -400 mesh	1.00	0.94	-0.06	-6
	+400 mesh	1.00	1.00	0.00	0
	Dalhousie -400 mesh	1.00	0.92	-0.08	-8
	+400 mesh	1.00	0.99	-0.01	-1
Glassy Analogues	Wabamun glass	1.00	1.00	0	0
	Sundance glass	1.00	1.00	0	0
	Forestburg glass	1.00	1.00	0	0
	Nanticoke glass	1.00	1.00	0	0
	Lakeview glass	1.00	0.93	-0.07	7
	Lingan glass	1.00	1.00	0	0
	Estevan glass	1.00	0.75	-0.25	-25
	Thunder Bay glass	1.00	0.87	-0.13	-13
	Standard glass	1.00	0.78	-0.22	-22
	Atlantic glass	1.00	0.91	-0.09	-9
Redevitrified Glasses	Wabamun red.	1.00	0.93	-0.07	-7
	Sundance red.	1.00	0.99	-0.01	-1
	Forestburg red.	1.00	0.99	-0.01	-1
	Thunder Bay red.	1.00	0.96	-0.04	-4
	Atlantic red.	1.00	0.93	-0.07	-7
Controlled Heat Treatment	Wabamun 810°C/1 hr	1.00	1.00	0	0
	" " /2 hr	1.00	0.92	-0.08	-2
	" " /4 hr	1.00	0.89	-0.11	-11
	" " /8 hr	1.00	0.99	-0.01	-1
	" " /24 hr	1.00	0.98	-0.02	-2

ORF

TABLE 46 (continued)

Series	Fly Ash/Slag	Initial Mass (g)	Final Mass (g)	Change (g)	% Change
	Wabamun 810°C/16 hrs				
	& 950°C/1 hr	1.00	0.93	-0.07	-7
	& 950°C/2 hr	1.00	0.96	-0.04	-4
	& 950°C/4 hr	1.00	0.93	-0.07	-7
	& 950°C/8 hr	1.00	0.98	-0.02	-2
	& 950°C/24 hr	1.00	0.99	-0.01	-1
	& 950°C/48 hr	1.00	0.89	-0.11	-11
Model Glasses	Wabamun 1	1.00	0.94	-0.06	-6
	Nanticoke 1	1.00	1.00	-0.06	-6
	Lakeview 1	1.00	0.98	-0.02	-2
	Dalhousie 1	1.00	0.94	-0.06	-6
	Estevan 1	1.00	0.94	-0.06	-6

TABLE 47

Summary of Observations Made During Leaching of Fly Ash and Slag Derivatives

Source Material	pH H_2O	Initial pH	Maximum pH (time)	Final pH (24 hrs)
Wabamun Glass	6.20	4.15	5.35 (4 hrs)	4.70
Sundance Glass	6.20	4.25	5.75 (4 hrs)	5.05
Forestburg Glass	6.20	4.20	5.35 (4 hrs)	4.80
Nanticoke Glass	6.00	5.00	5.90 (1.5 hr)	5.90
Lakeview Glass	6.00	4.50	5.80 (3 hrs)	5.80
Lingan Glass	6.20	4.45	5.20 (7 hrs)	4.65
Estevan Glass	6.45	4.50	6.55 (3 hrs)	5.40
Thunder Bay Glass	6.45	5.45	6.70 (30 min)	6.60
Standard Glass	6.45	6.40	7.10 (2.5 hrs) 7.15 (6.5 hrs)	6.70
Atlantic Glass	6.45	5.50	6.55 (4 hrs)	6.70
Wabamun Red.	6.40	2.90	3.65 (6.5 hrs)	3.60
Sundance Red.	6.40	4.10	6.00 (4 hrs)	5.70
Forestburg Red.	6.40	3.90	5.60 (4.5 hrs)	5.40
Thunder Bay Red.	7.00	4.50	6.00 (55 min)	6.20
Atlantic Red.	7.00	5.20	7.35 (2.5 hrs)	6.90

ORF

TABLE 48

Chemical Compositions of Five Model Glasses*

Glass ID	SiO_2	Al_2O_3	Fe_2O_3	$\Sigma(SiO_2+Al_2O_3+Fe_2O_3)$	CaO	MgO	Na_2O	K_2O	$\Sigma(CaO+MgO+Na_2O+K_2O)$
Wabamun 1	59.62	16.82	4.44	80.88	14.94	2.42	0.81	0.94	19.11
Nanticoke 1	47.98	29.17	7.03	84.18	10.55	1.93	1.58	1.76	15.82
Lakeview 1	59.13	8.75	18.06	85.94	7.22	2.09	1.71	3.04	14.06
Dalhousie 1	32.34	13.80	43.70	89.84	6.09	1.08	0.81	2.17	10.15
Estevan 1	43.08	24.67	3.91	71.66	14.51	3.57	9.38	0.89	28.35

* Based on difference between known bulk chemical composition and assigned crystalline phases from XRD analysis.

ORF

TABLE 49

XRD Patterns of Selected Materials Subjected to Leaching in Deionized Water

Source	Comments
Wabamun fly ash	no change
Sundance fly ash	$CaCO_3$ ppt
Forestburg fly ash	no change
Nanticoke fly ash	$CaCO_3$ ppt
Lakeview fly ash	no change
Lingan fly ash	no change
Dalhousie fly ash	no change
Estevan fly ash	no change
Thunder Bay fly ash	$C\bar{S}$, CaS, $NA\bar{S}$ removed
Standard slag	$CaCO_3$ ppt
Atlantic slag	$CaCO_3$ ppt
Wabamun fly ash glass	phase X
Sundance fly ash glass	phase X
Forestburg fly ash glass	phase X
Nanticoke fly ash glass	no change
Lakeview fly ash glass	no change
Lingan fly ash glass	phase X
Dalhousie fly ash glass	-
Estevan fly ash glass	no change
Thunder Bay fly ash glass	no change
Standard slag glass	no change
Atlantic slag glass	no change

TABLE 50

Results of DCP Analysis on Leaching Solutions of 1.00 g of Wabamun Fly Ash

Sample ID	Description (leaching time)	pH	Si	Al	Fe	Ca	Mg
				$(mg.L^{-1})$			
84-1546	blank	7.8	<0.1	<0.02	<0.02	<0.1	<0.02
84-1547	0 min	7.8	0.45	1.2	<0.02	15	0.33
84-1548	45 min	10.0	2.0	2.4	<0.02	26	0.52
84-1549	4 hrs	9.6	2.2	2.2	<0.02	28	0.72
84-1550	24 hrs	9.7	3.4	2.8	<0.02	30	0.73

ORF

TABLE 51

Glass Content Values (%) Determined by Various Methods

Source Material	McMaster Method	QXRD Method	NCXRD Method	Avg. of QXRD/NCXRD	DIXRD Method	Image Analysis
Wabamun	NA	76.1	62.1	69.1	82.0(C_i) 101.0(C_c) 83.6(C_c*)	93.4
Sundance	NA	82.9	77.4	80.2		
Forestburg	NA	89.0	82.4	85.7		
Nanticoke	NA	59.7	83.8	71.8		
Lakeview	NA	53.5	99.3	76.4		
Lingan	NA	77.3	84.4	80.8		
Dalhousie	NA	76.7	-	76.7		
Estevan	NA	94.5	70.0	82.2		
Thunder Bay	NA	-	86.9	86.9		
Standard Slag	47.1-84.3	88.3	72.4	80.4		
Atlantic Slag	59.7-68.9	88.1	42.8	65.5		

* Determined by omitting non-corresponding XRD peaks for the computation of C_c.

ORF

TABLE 52*

Regions of absorption (cm^{-1}) corresponding to metal-oxygen stretching for tetrahedral and octahedral co-ordination

Metal ion (X)	XO_4 Isolated	XO_4 Condensed	XO_6 Isolated	XO_6 Condensed
Si^{4+}	800-1000	900-1200	-	800-950
Ge^{4+}	700-800	800-900	~500	550-650
Ti^{4+}	650-800	-	400-500	-
Al^{3+}	700-850	700-900	350-500	500-650
Fe^{3+}	550-650	550-750	300-400	400-550
Zn^{2+}	400-500	-	<300	~400
Mg^{2+}	500-550	-	300-450	350-480
Co^{2+}	400-450	-	-	300-400
Li	400-500	400-600	-	<300

* from reference 20

ORF

TABLE 53*

Vibrational frequencies (cm^{-1}) of atomic groups in minerals containing oxygen

Group	Stretch	Bend	Group	Stretch	Bend
xOH	3750-2000	1300-400	$Se^{VI}O_4$	920-830	~420
H_2O	3660-2800	1690-1590	$Cr^{VI}O_4$	870-700	~350
NH_4	3330-2800	1500-1390	$W^{VI}O_4$	850-740	~320
CO_3	1600-1300	900-670	$W^{VI}O_6$ (c)	900-700	
HCO_3	1700-1200	900-600	$Mo^{VI}O_4$	850-740	~320
NO_3	1500-1200	850-700	$Mo^{VI}O_6$ (c)	1000-750	
NO_2	1400-1200	800-700	VO_4	915-730	~400
BO_3 (i)	1300-1200	800-600	AsO_4	850-730	~400
(c)	1500-1200	800-600	$Se^{IV}O_3$	820-700	~400
BO_4 (i,c)	1200-950	550-450	AlO_4 (c)	900-700	
SO_4	1200-1100	680-600	TiO_4 (i)	800-650	~350
PO_4 (i)	1050-950	600-550	GeO_4 (i)	800-700	~400
(c)	1300-850	600-550	(c)	900-800	
H_nPO_4	1300-800	600-550	GeO_6 (c)	650-550	
SiO_4 (i)	1000-800	550-450			
(c)	1200-900	800-400			
SiO_6 (c)	950-600				

(i) Isolated polyhedra;
(c) condensed polyhedra
* from reference 20

ORF

TABLE 54

Intensity Maximum of the 1300-750 cm^{-1} Band and Modifier Contents

Source	νSi-O (cm^{-1})	CaO (wt.%)	Σ(CaO+MgO +Na_2O+K_2O) (mol/100g)
Wabamun	1075	11.1	0.259
Sundance	1044	12.5	0.295
Forestburg	1018	10.5	0.316
Nanticoke	1080	5.95	0.158
Lakeview	1085	3.82	0.126
Lingan	1065	1.29	0.106
Dalhousie	1080	4.45	0.127
Estevan	928	13.0	0.455
Thunder Bay	1016	12.4	0.419
Standard Slag	946	35.1	0.937
Atlantic Slag	957	40.1	0.959

ORF

TABLE 55

Leaching in H_2O: Correlation Between pH and Compositional Parameters or Physical Properties*

r	Maximum pH of Fly Ashes Only	"As Received" Samples Fly Ashes and Slags
CaO (wt.%)	0.43	0.24
$\Sigma(Na_2O+K_2O+MgO+CaO)$ (mol %)	0.28	0.20
SiO_2 (wt.%)	0.72	0.51
Al_2O_3 (wt.%)	0.77	0.30
Fe_2O_3 (wt.%)	-0.79	-0.76
$\Sigma(SiO_2+2Al_2O_3-2Fe_2O_3)$ (mol %)	0.86	0.73
Glass Content	-0.21	-0.27
Surface Area (B.E.T.)	0.56	0.55
Average Particle Diameter	0.21	0.11

* Correlation coefficients

ORF

FIGURES

Figure 1

Particle Size Distribution by Sedigraph Analysis - Sedigraph Traces

(a) Wabamun
(b) Sundance
(c) Forestburg
(d) Nanticoke
(e) Lakeview
(f) Lingan
(g) Dalhousie
(h) Estevan
(i) Thunder Bay
(j) Standard
(k) Atlantic

ORF

PARTICLE SIZE DISTRIBUTION

SAMPLE IDENTIFICATION WABAMUN -14%cc

Density 2 28 g/cc LIQUID A-11 Density .751 g/cc Viscosity 1.437 cp

Preparation 30 SEC USB

DATE NOV 15/84

BY B SMITH

TEMPERATURE 31 °C

RATE 901.4 START DIA. 100 μm

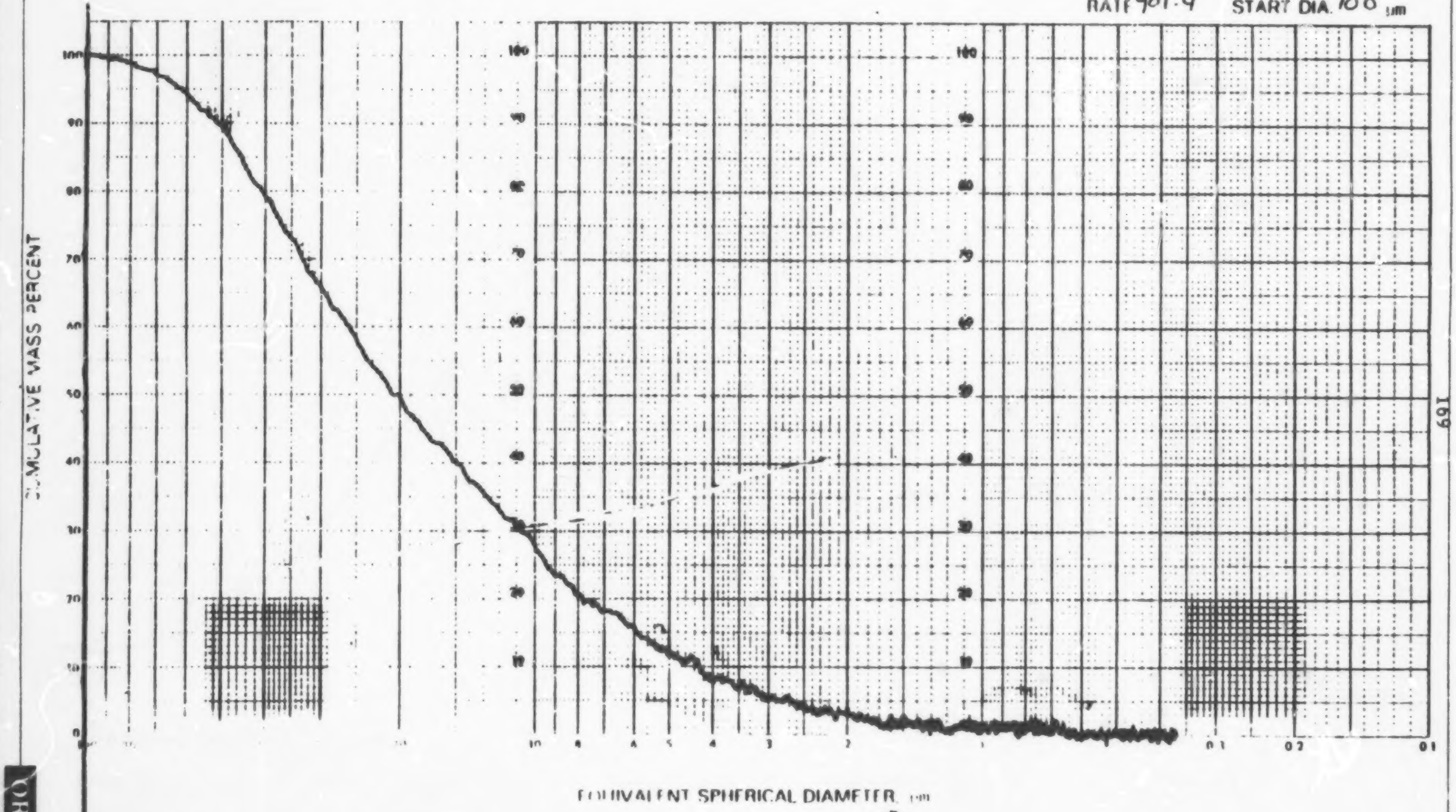

micromeritics

ORF

PARTICLE SIZE DISTRIBUTION

SAMPLE IDENTIFICATION SUNDANCE -14/9u

Density 2.15 g/cc LIQUID A-11

Preparation 30 SEC USB.

Density .751 g/cc Viscosity 1.437 cp

DATE Nov15/84

BY B Smith.

TEMPERATURE 31 °C

RATE 825 START DIA. 102 μm

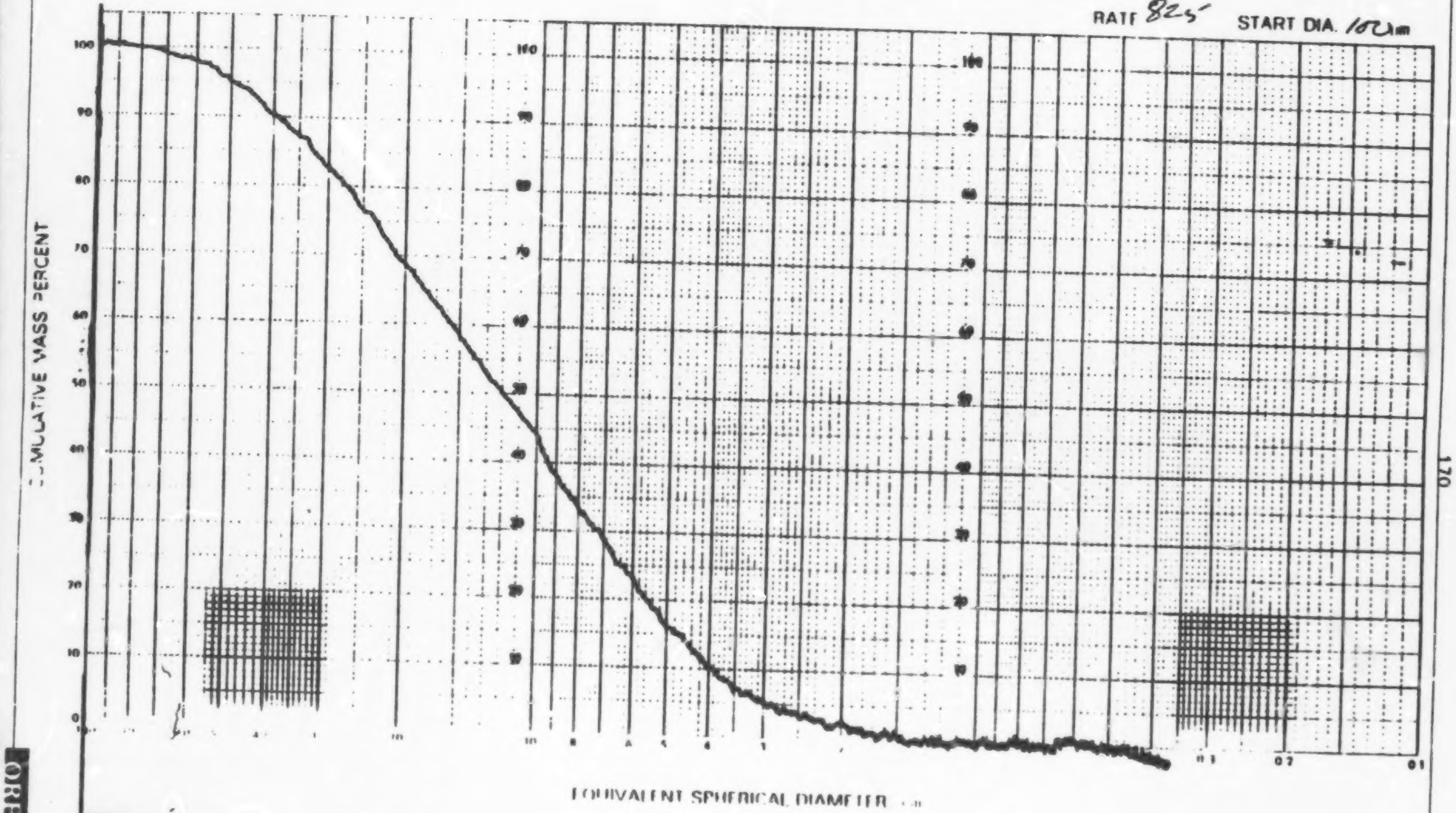

micromeritics
instrument corporation

PARTICLE SIZE DISTRIBUTION

SAMPLE IDENTIFICATION FOREST BURG		DATE Nov15T84
ρ Density 2.60 g/cc LIQUID A-11	Density .751 g/cc Viscosity 1.437 p	BY C. Smith
Preparation 30 SEC UB.		TEMPERATURE 31 °C
		RATE 756 START DIA/100 µm

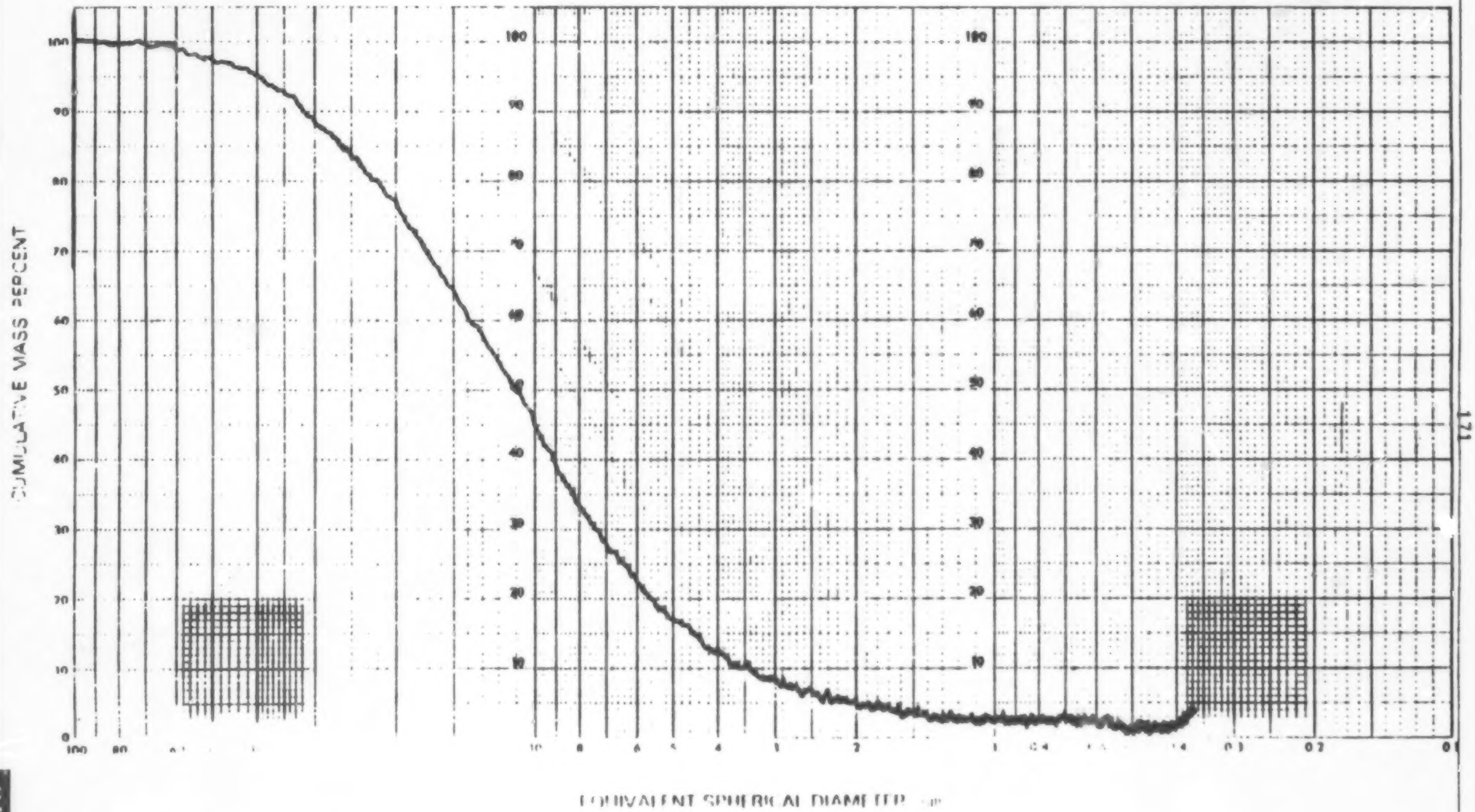

ORF

micromeritics

PARTICLE SIZE DISTRIBUTION

SAMPLE IDENTIFICATION NANTICOKE -149µ

Density 2.32 g/cc LIQUID A-11 Density .751 g/cc Viscosity 1.437 cp

Preparation

DATE Nov15/84

BY BSmith

TEMPERATURE 31 °C

RATE 925 START DIA. 100 µm

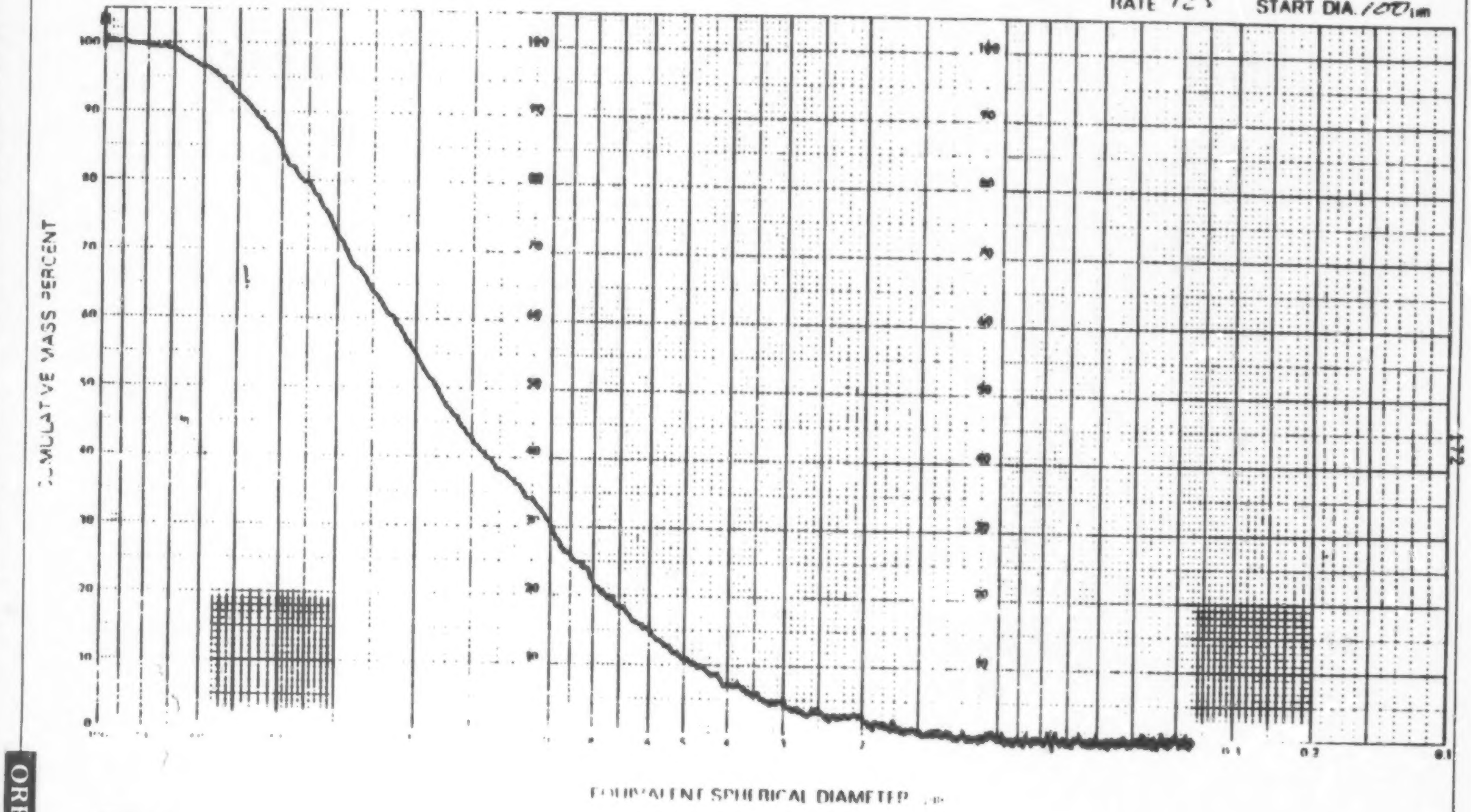

ORF

PARTICLE SIZE DISTRIBUTION

SAMPLE IDENTIFICATION LAKEVIEW

DATE NOV 14/84

Density 2.52 g/cc LIQUID A-11

Density .751 g/cc Viscosity 1.437 cp

BY BSmith

Preparation 30 Sec U.S.B.

TEMPERATURE 31 °C

RATE 845 START DIA. 90 µm

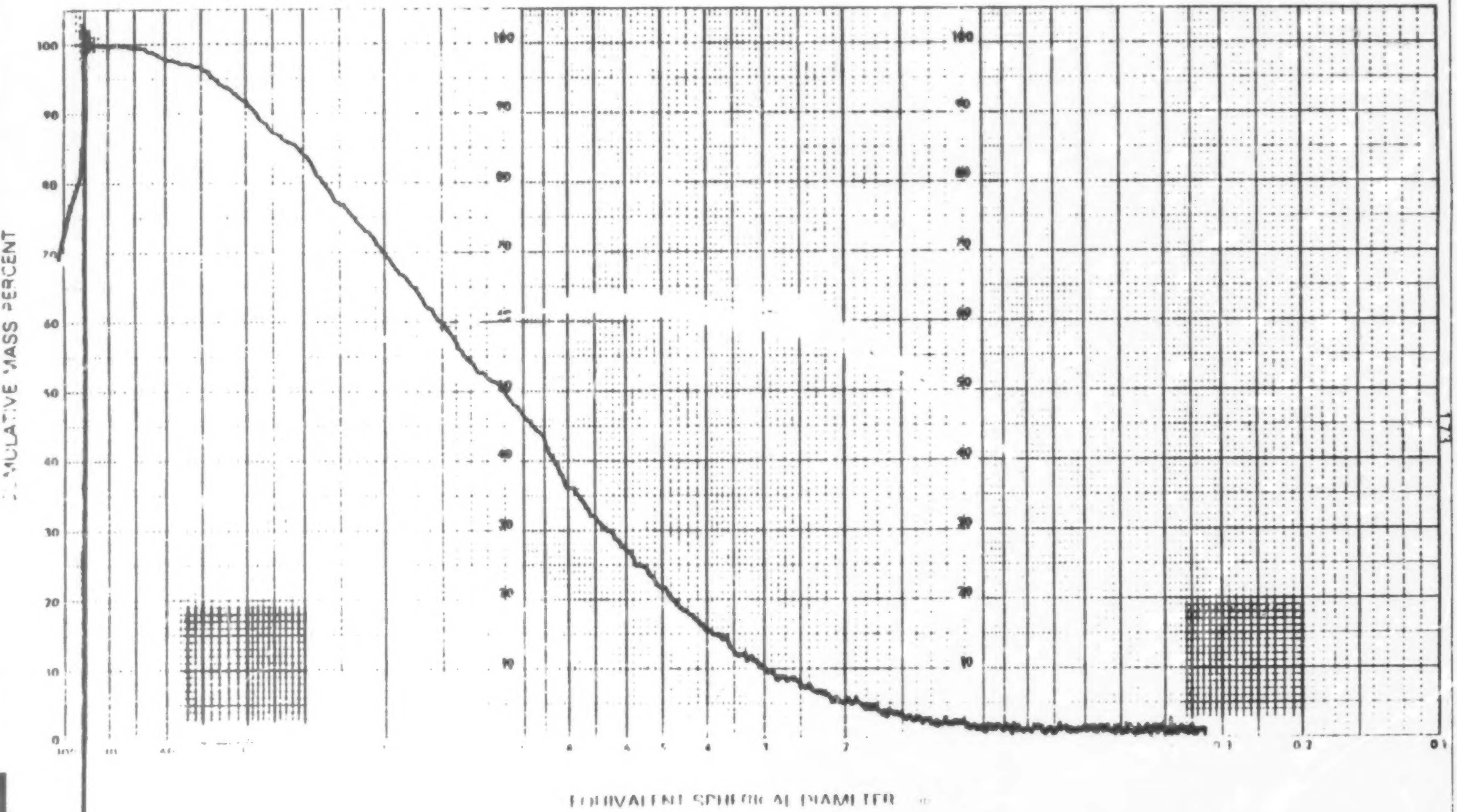

micromeritics

ORF

PARTICLE SIZE DISTRIBUTION

SAMPLE IDENTIFICATION LINGAN -149μ

Density 2.60 g/cc   LIQUID A-11   Density .751 g/cc   Viscosity 1.437 cp

Preparation 30SEC USB.

DATE Nov 15/84

BY B Smith.

TEMPERATURE 31 °C

RATE 883   START DIA. 90 μm

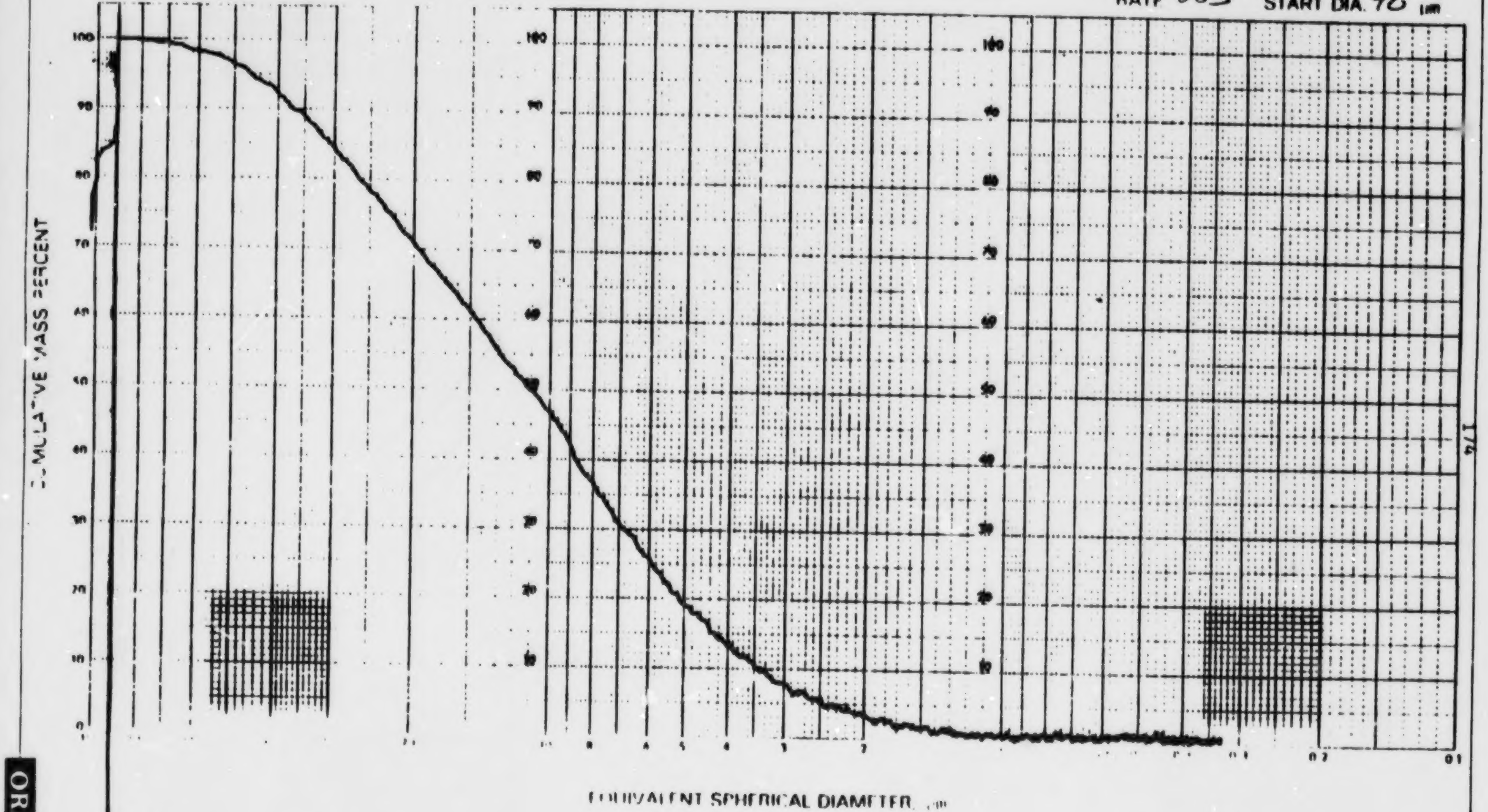

micromeritics inc
instrument corporation

ORF

PARTICLE SIZE DISTRIBUTION

SAMPLE IDENTIFICATION DAL HOUSIE

Density 3.10 g/cc LIQUID A-11

Preparation 30 SEC USB.

Density .751 g/cc Viscosity 1.437 cp

DATE Oct 15/84

BY C.SMITH

TEMPERATURE 31 °C

RATE 886 START DIA. 80 µm

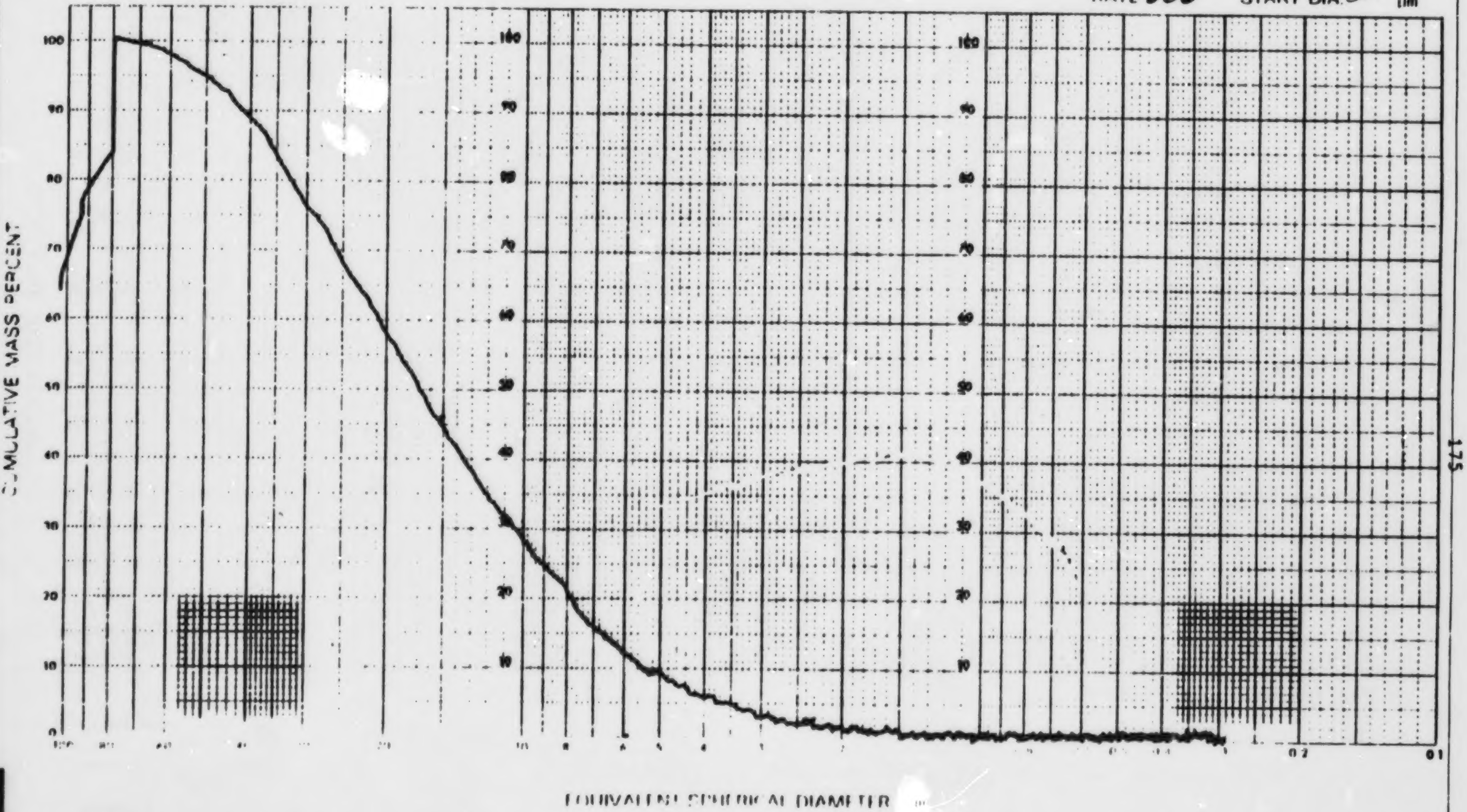

micromeritics

PARTICLE SIZE DISTRIBUTION

SAMPLE IDENTIFICATION ESTEVEN.

Density 2.49 g/cc LIQUID A-11 Density 0.750 g/cc Viscosity 1.410 cp

Preparation 30sec USB

DATE July 11/84

BY B Smith.

TEMPERATURE 31 °C

RATE 847 START DIA. 90 μm

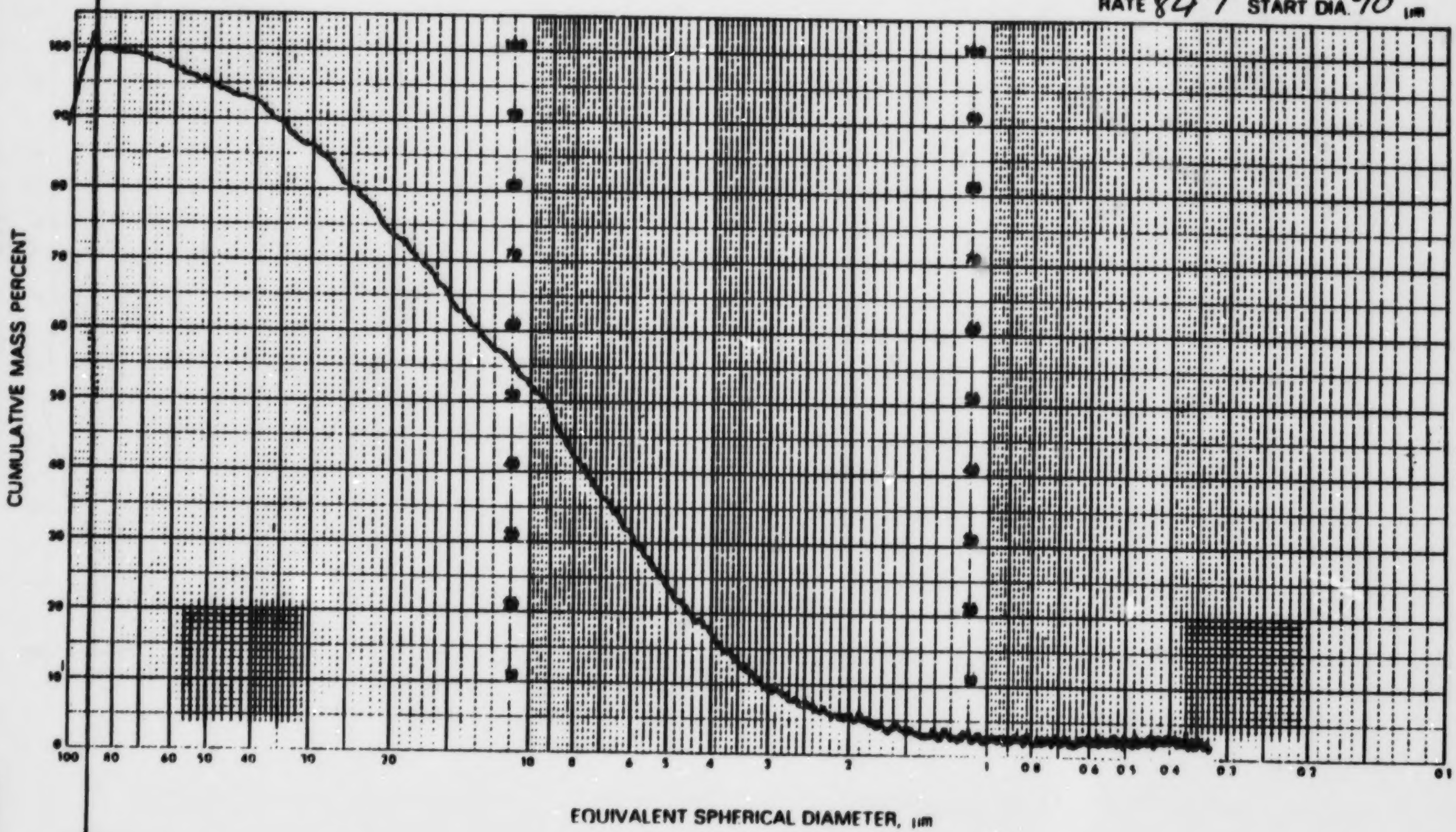

micromeritics
instrument corporation

ORF

PARTICLE SIZE DISTRIBUTION

SAMPLE IDENTIFICATION THUNDER BAY.

DATE JUL 10/84

Density g/cc LIQUID A-11

Density 2.750 g/cc Viscosity 1410 cp

BY

Preparation 30 sec USB.

TEMPERATURE 31 °C

RATE 934 START DIA. 90 µm

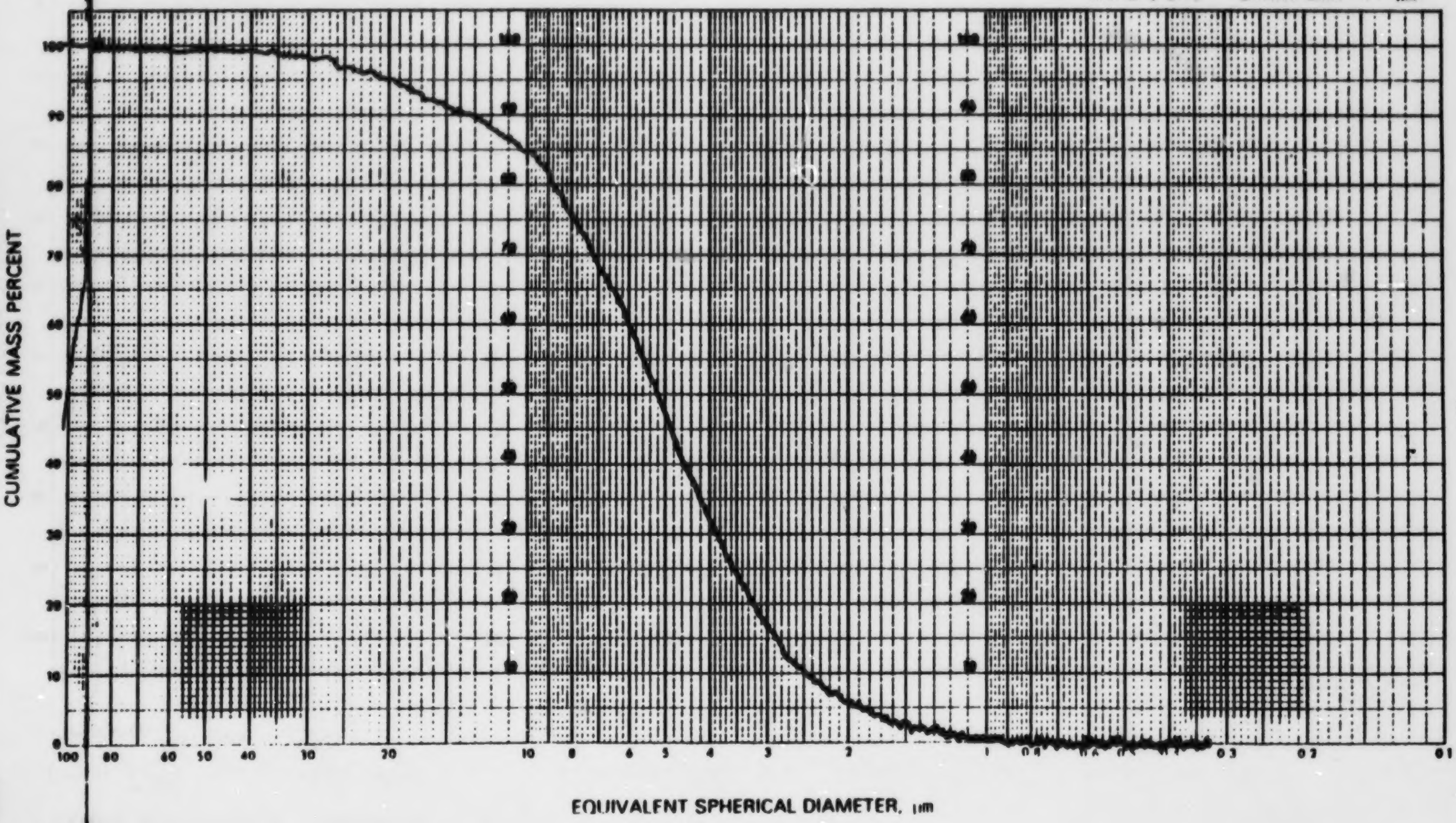

micromeritics
instrument corporation

PARTICLE SIZE DISTRIBUTION

SAMPLE IDENTIFICATION Standard Slag.

Density 2.99 g/cc LIQUID A-11 Density .950 g/cc Viscosity 1.410 cp

Preparation 30 sec USB.

DATE July 11 84

BY B Smith.

TEMPERATURE 31 °C

RATE 864 START DIA 80 um

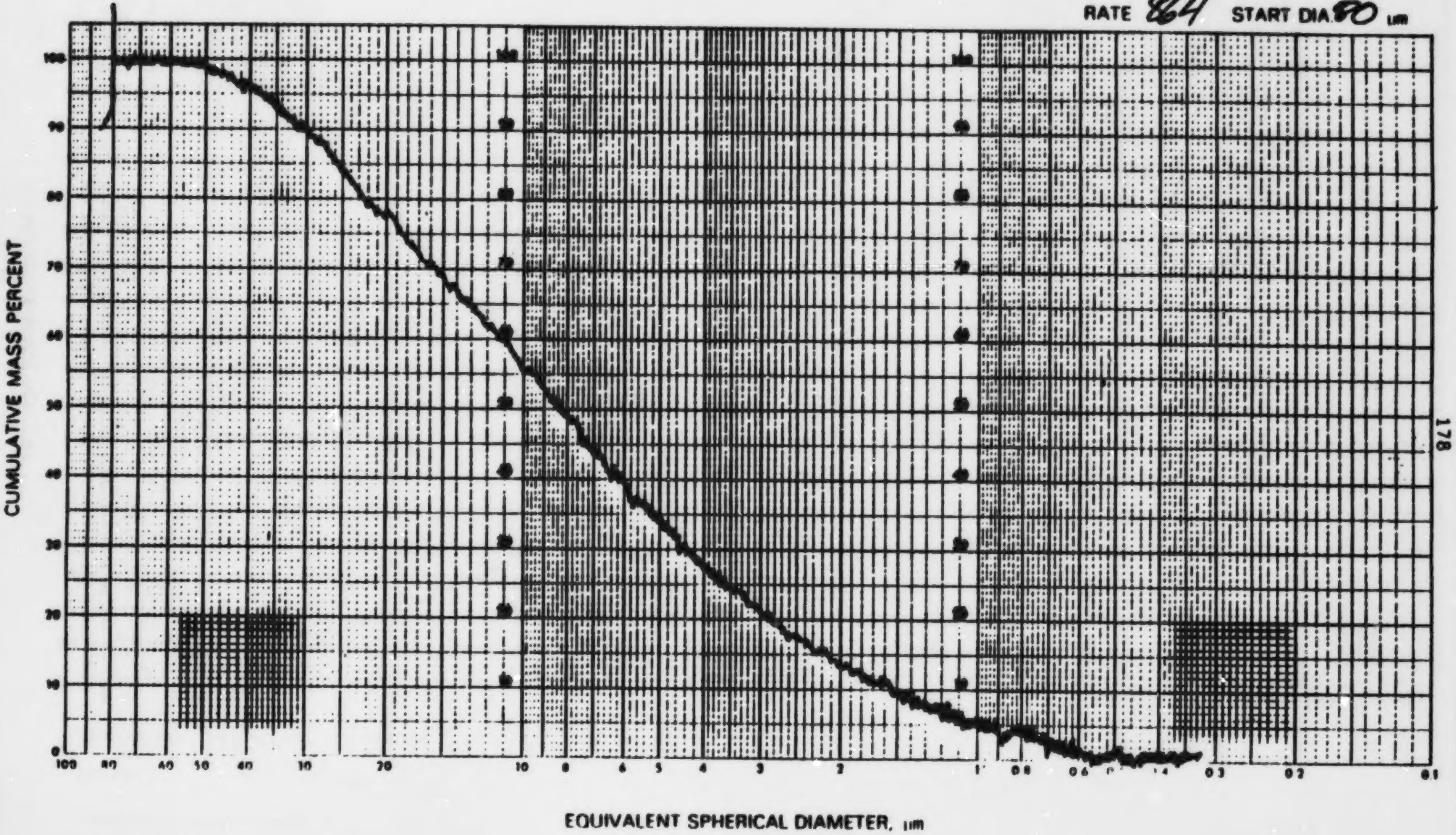

micromeritics
instrument corporation

PARTICLE SIZE DISTRIBUTION

SAMPLE IDENTIFICATION ILMENITE Slag

DATE JULY 11/84.

Density g/cc LIQUID A-11 Density 0.750 g/cc Viscosity 1.410 cp

BY B Smith.

Preparation 30 sec U.S.B.

TEMPERATURE 31 °C

RATE 356 START DIA. 90 um

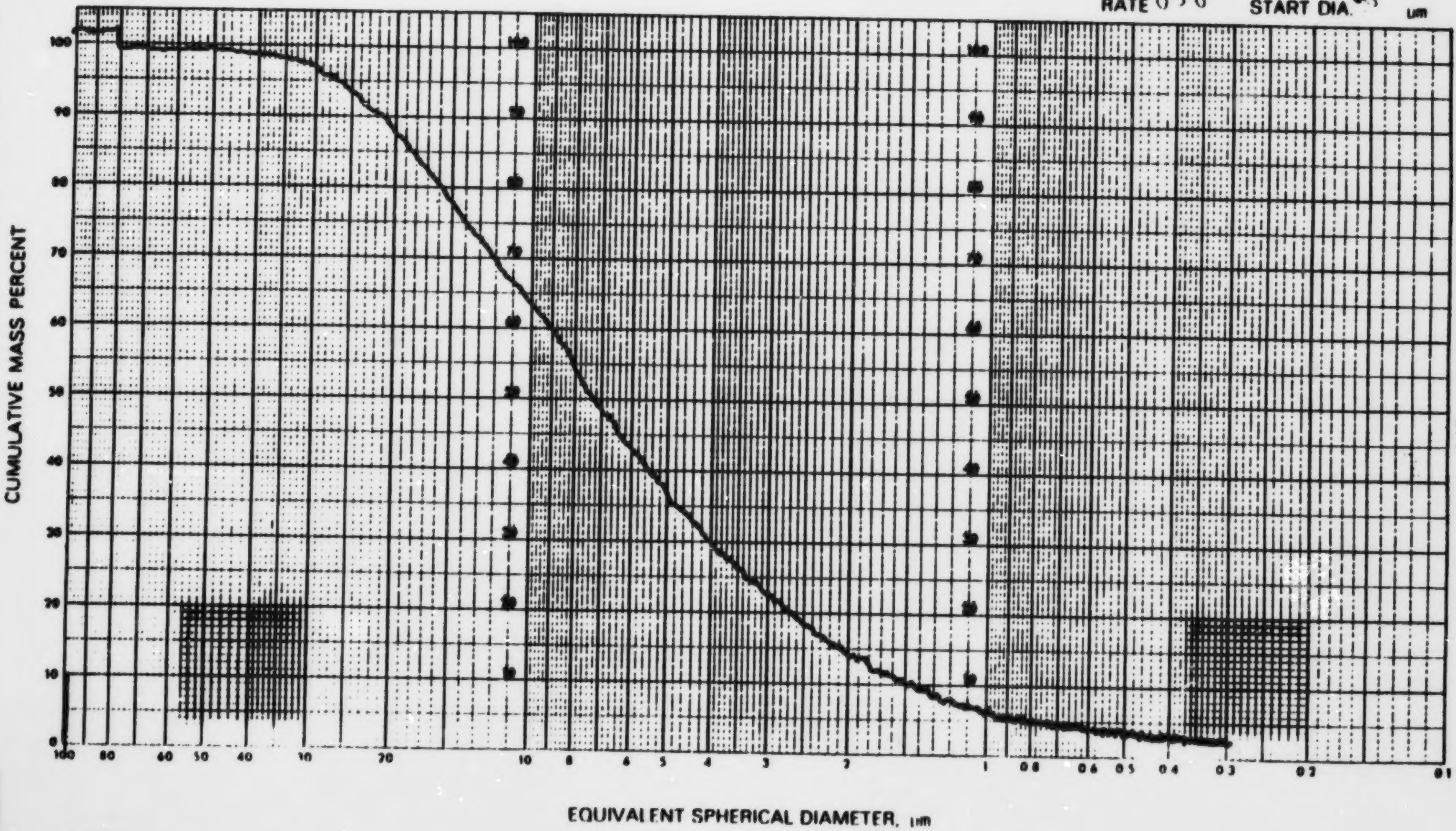

micromeritics instrument corporation

ORF

Figure 2

Particle Size Distribution by Sedigraph Analysis - Histograms

(a) Wabamun
(b) Sundance
(c) Forestburg
(d) Nanticoke
(e) Lakeview
(f) Lingan
(g) Dalhousie
(h) Estevan
(i) Thunder Bay
(j) Standard
(k) Atlantic

ORF

HISTOGRAMS FOR WABAMUM (-149 MICRONS)

AVERAGE PARTICLE SIZE = 20 MICROMETRES

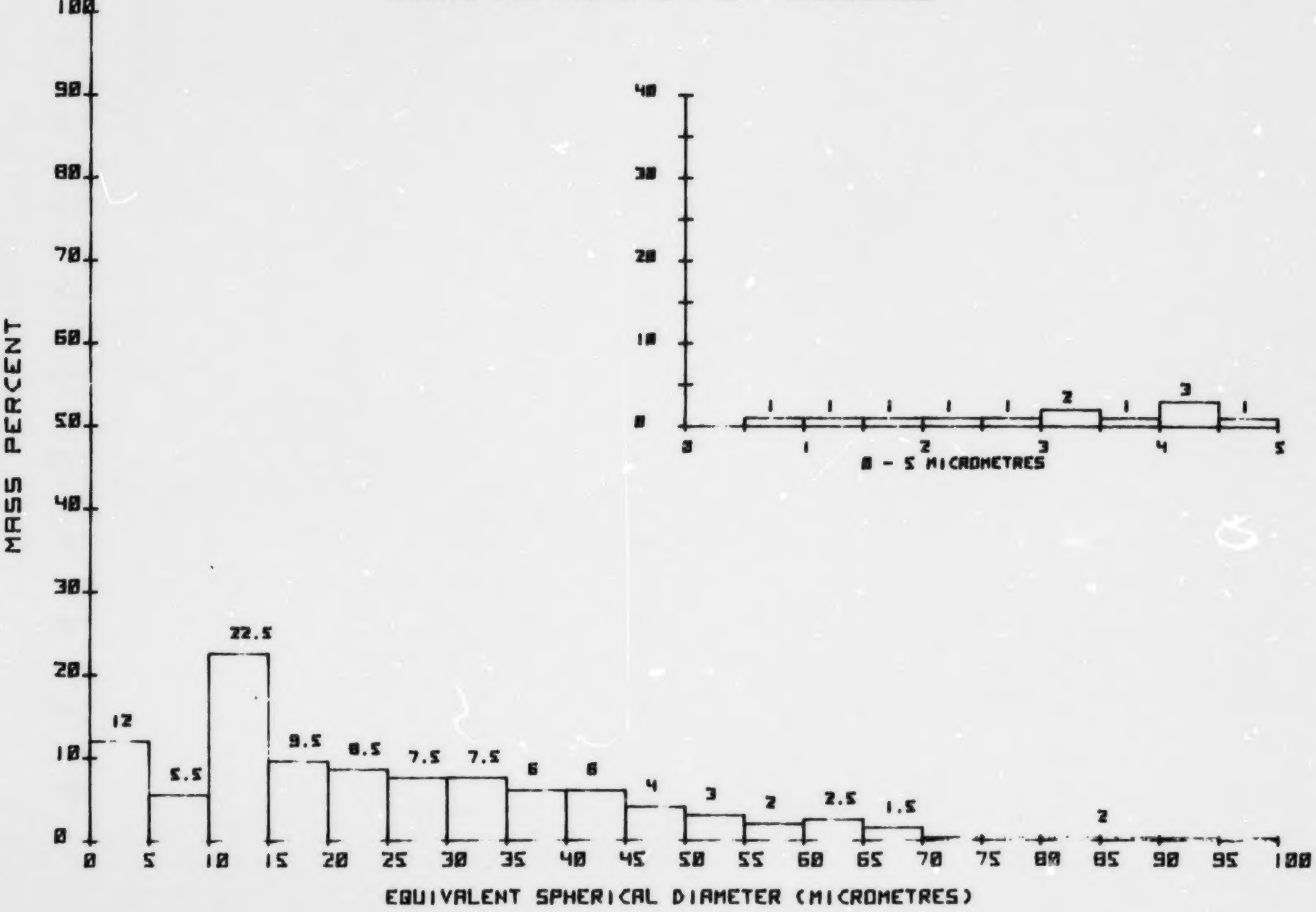

HISTOGRAMS FOR SUNDANCE

AVERAGE PARTICLE SIZE = 12 MICROMETRES

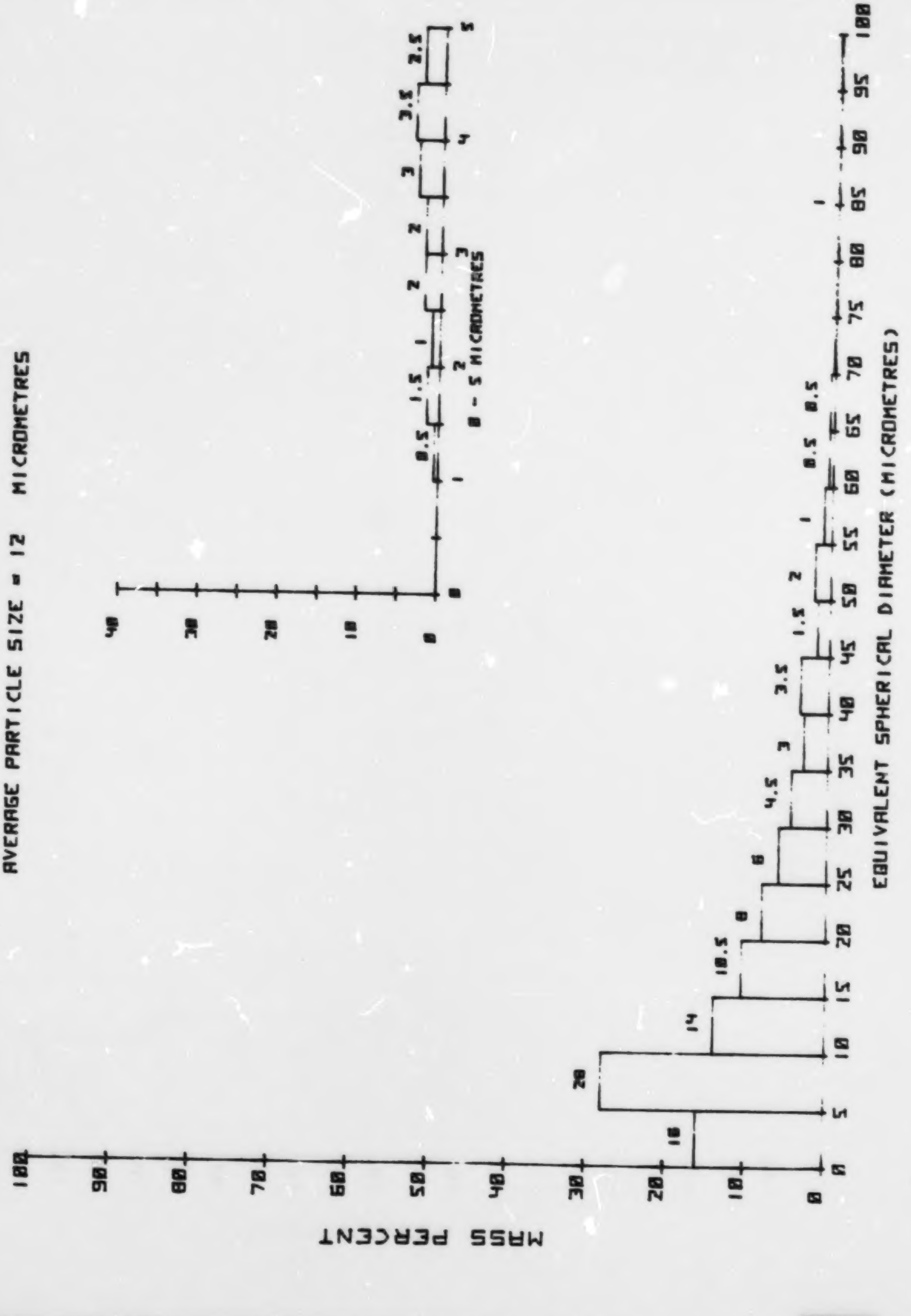

HISTOGRAMS FOR FORESTBURG

AVERAGE PARTICLE SIZE = 11 MICROMETRES

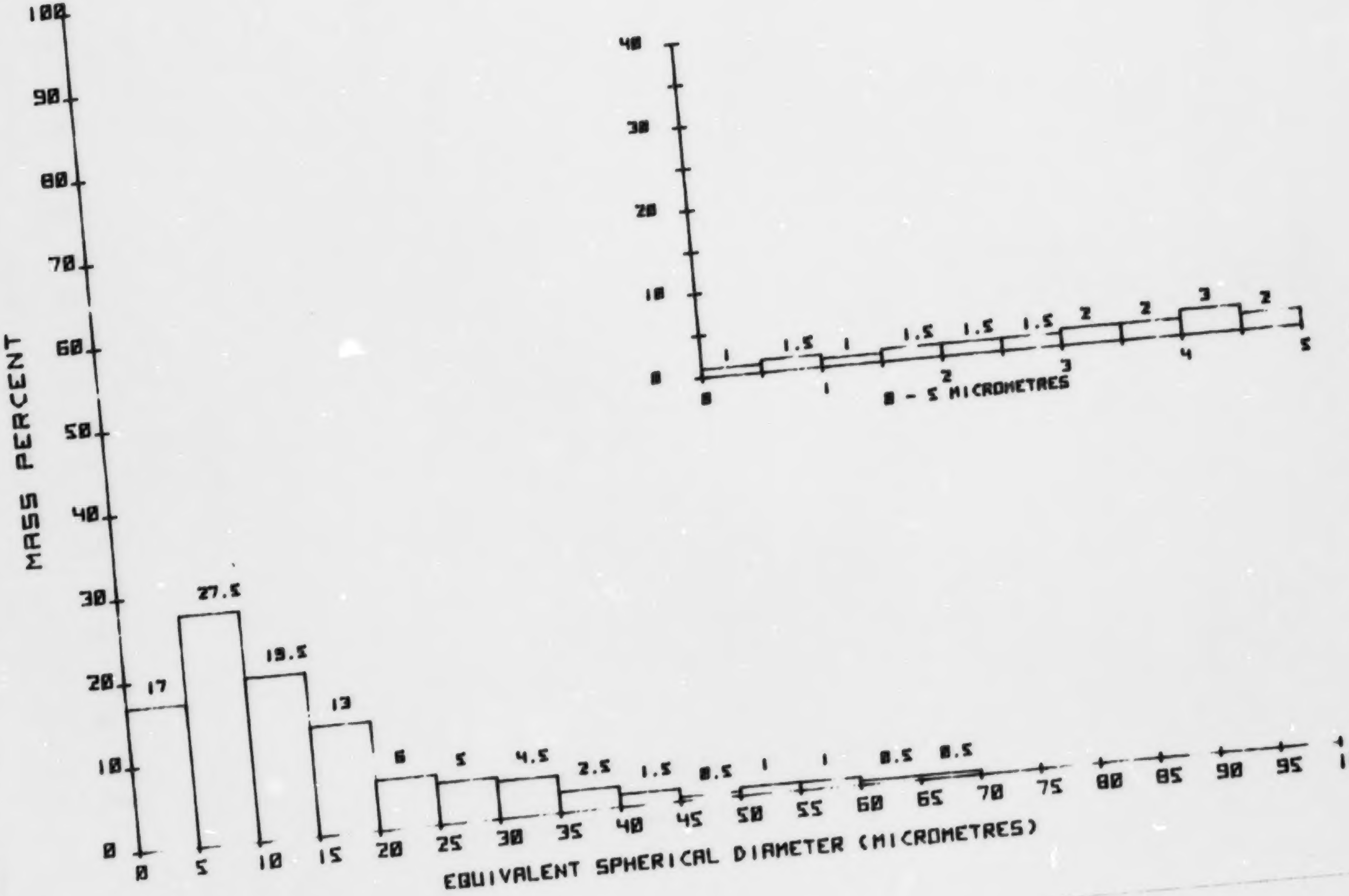

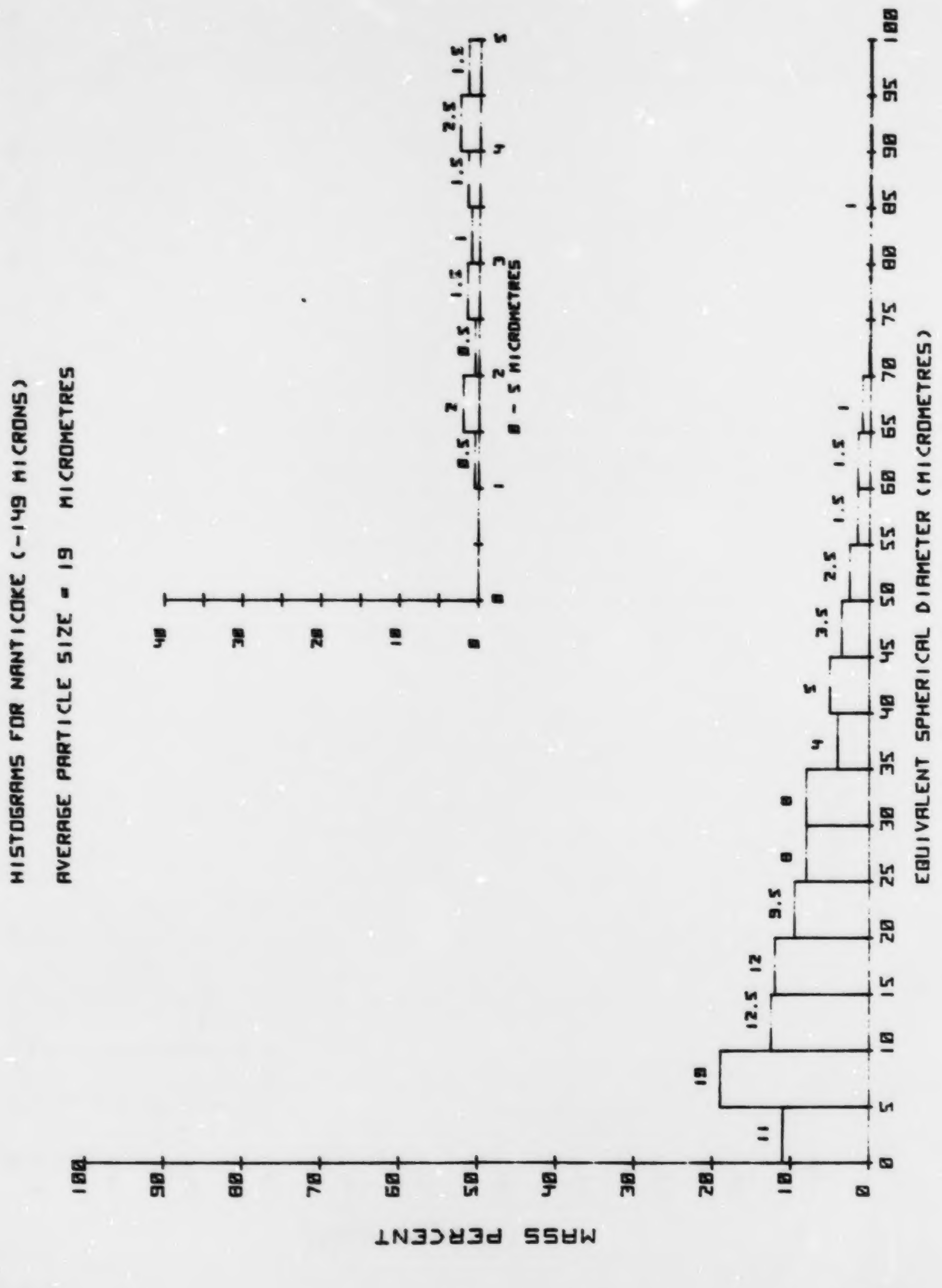

HISTOGRAMS FOR NANTICOKE (-149 MICRONS)

AVERAGE PARTICLE SIZE = 19 MICROMETRES

HISTOGRAMS FOR LAKEVIEW

AVERAGE PARTICLE SIZE = 11 MICROMETRES

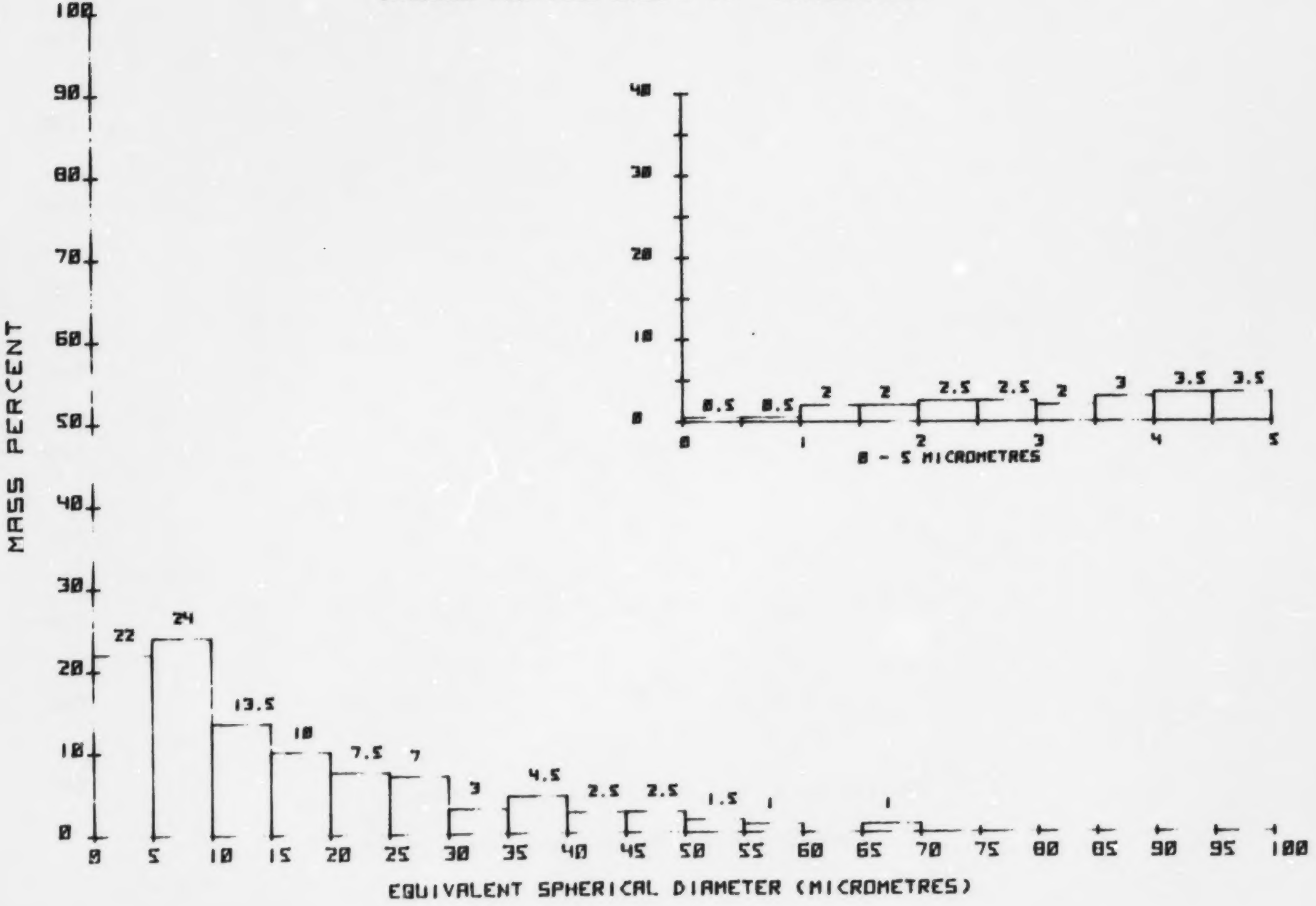

HISTOGRAMS FOR LINGAN (-149 MICRONS)

AVERAGE PARTICLE SIZE = 11 MICROMETRES

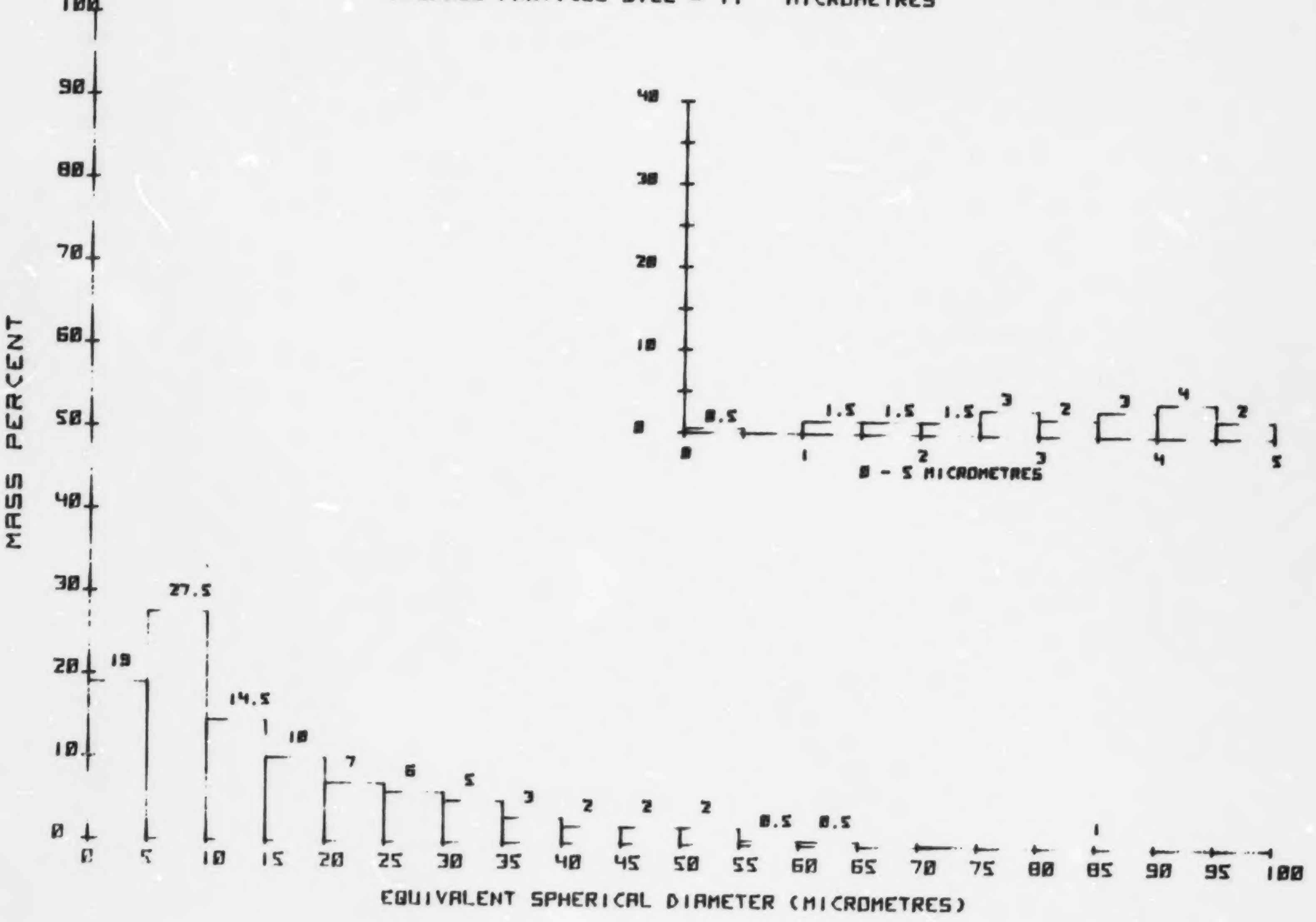

HISTOGRAMS FOR DALHOUSIE

AVERAGE PARTICLE SIZE = 17 MICROMETRES

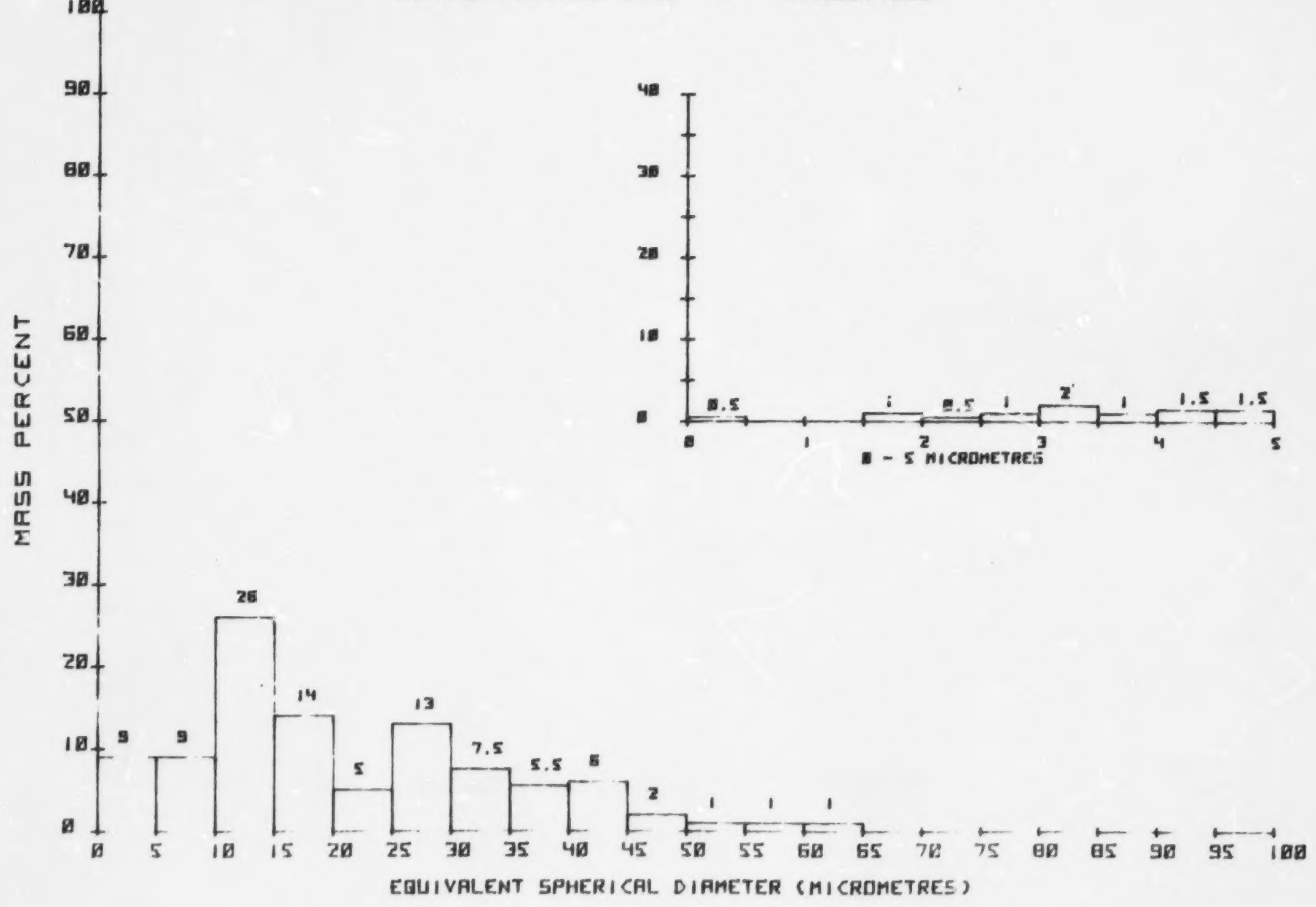

HISTOGRAMS FOR ESTEVEN

AVERAGE PARTICLE SIZE = 9.2 MICROMETRES

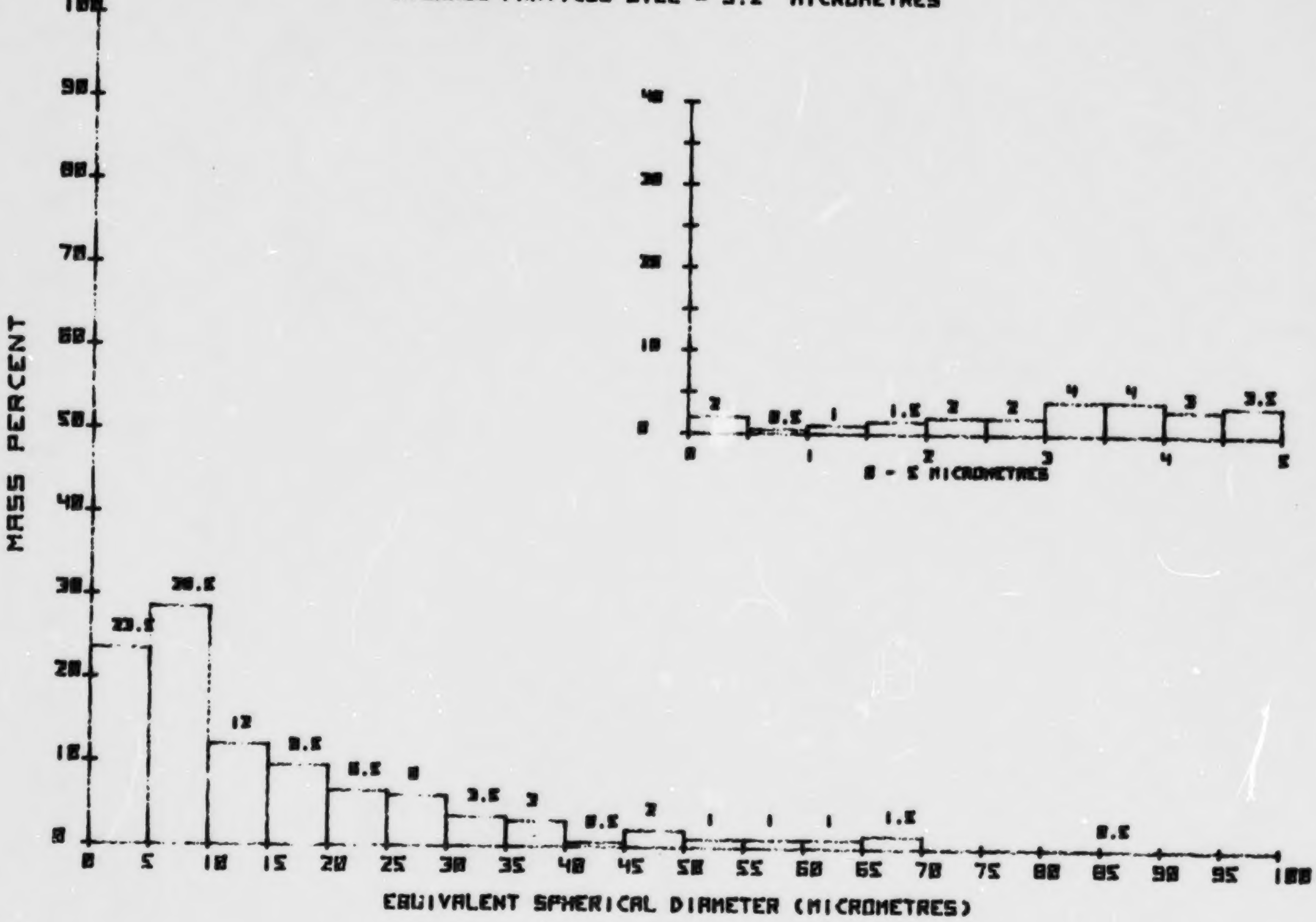

EQUIVALENT SPHERICAL DIAMETER (MICROMETRES)

HISTOGRAMS FOR THUNDERBAY

AVERAGE PARTICLE SIZE = 5.2 MICROMETRES

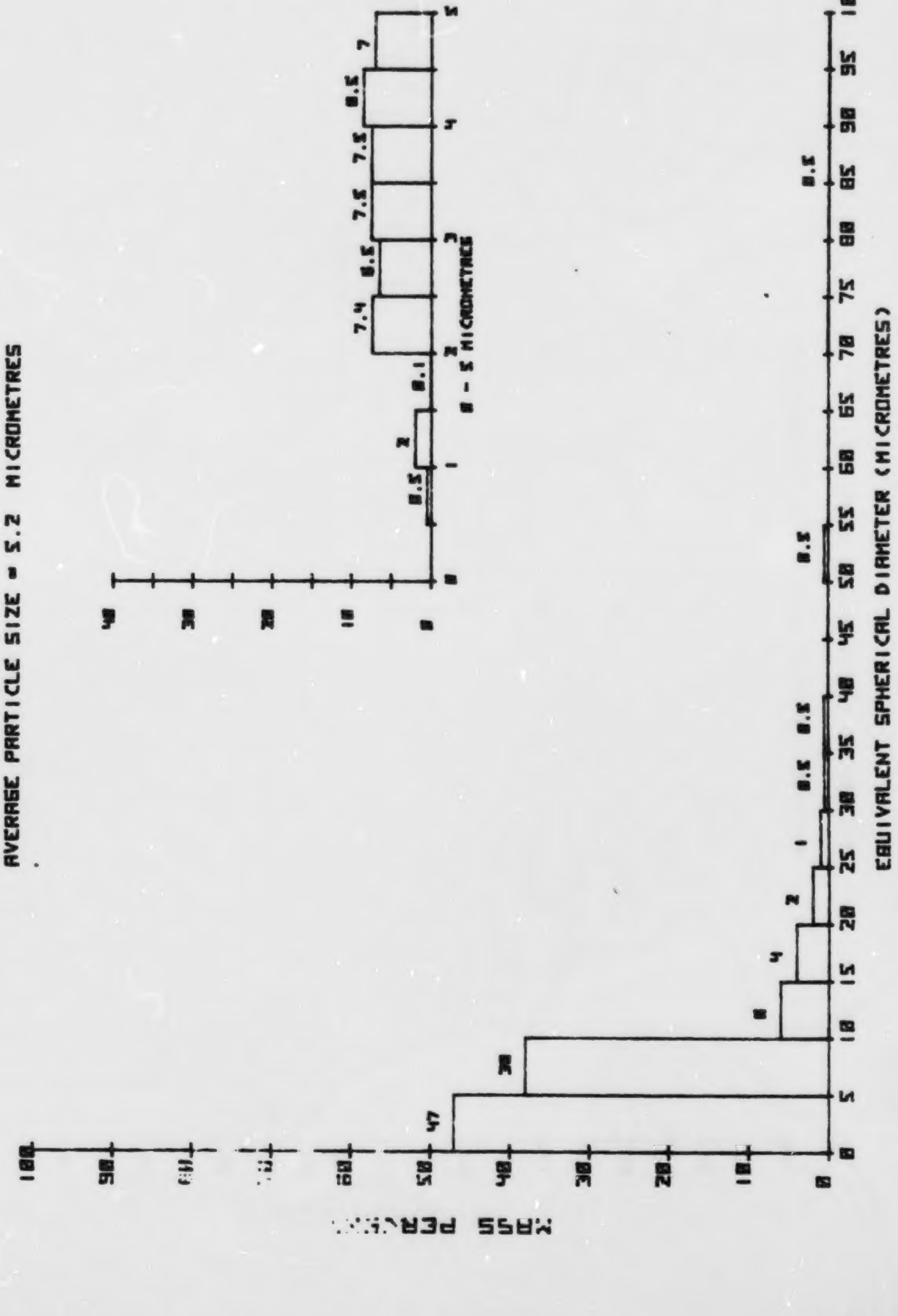

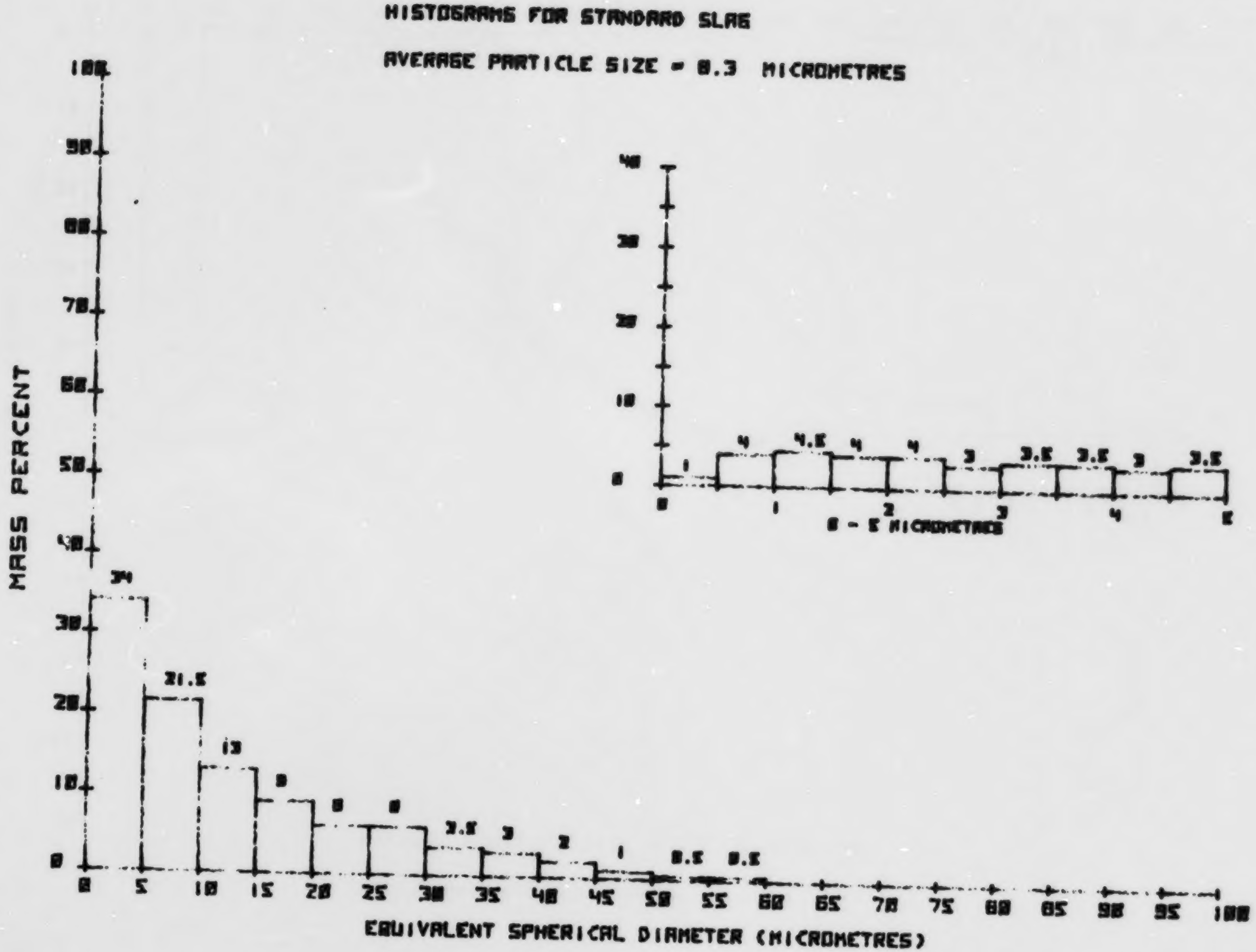

HISTOGRAMS FOR STANDARD SLAG

AVERAGE PARTICLE SIZE = 8.3 MICROMETRES

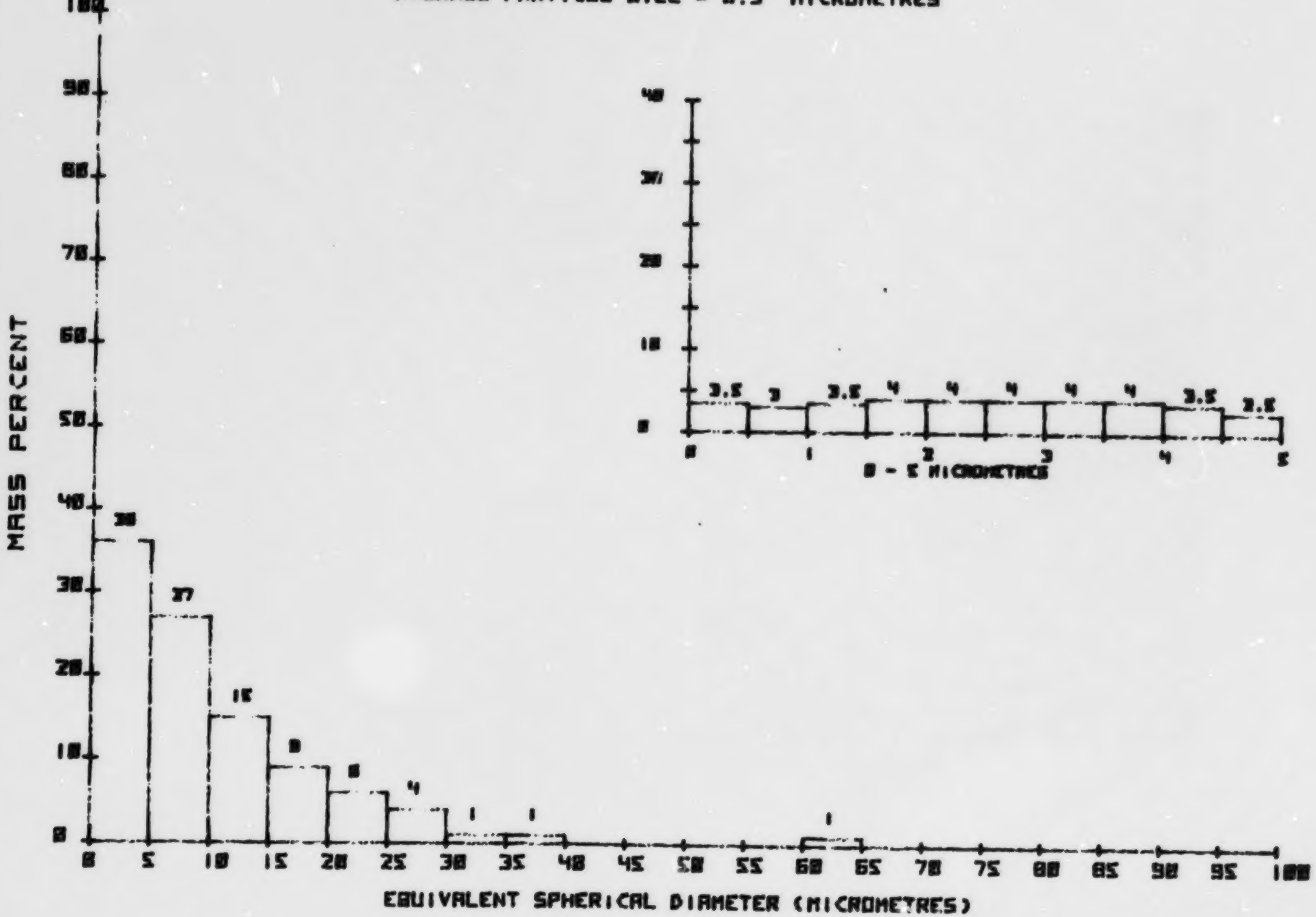

HISTOGRAMS FOR ATLANTIC SLAG

AVERAGE PARTICLE SIZE = 6.3 MICROMETRES

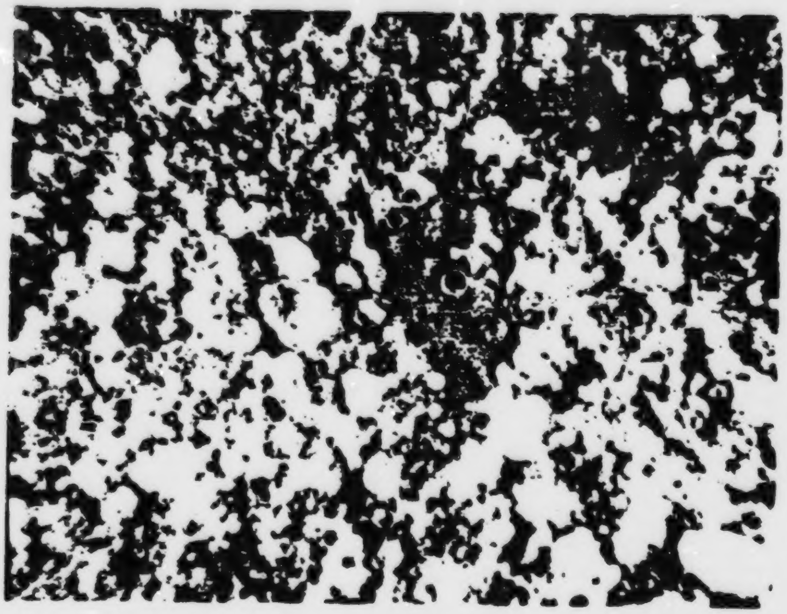

Fig. 3

Optical micrograph (magnification 137x)

[illegible]

A	
iO_2	63.31
$_2O_3$	20.62
O	13.73
eO	1.74

B	
iO_2	65.68
l_2O_3	20.92
O	1.80
O_2	11.60

C	
iO_2	87.13
$_2O_3$	8.47
O	4.40

D	
SiO_2	29.77
Al_2O_3	12.62
CaO	44.53
SO_3	5.38
FeO	3.76

E	
SiO_2	27.04
Al_2O_3	9.93
CaO	53.16
SO_3	5.11
FeO	2.97

H	
SiO_2	15.58
Al_2O_3	5.66
CaO	[illegible]
[illegible]	[illegible]

Fig. 4(a) SEM micrograph of Wabamun fly ash in an elvacite medium (magnification 20μ)

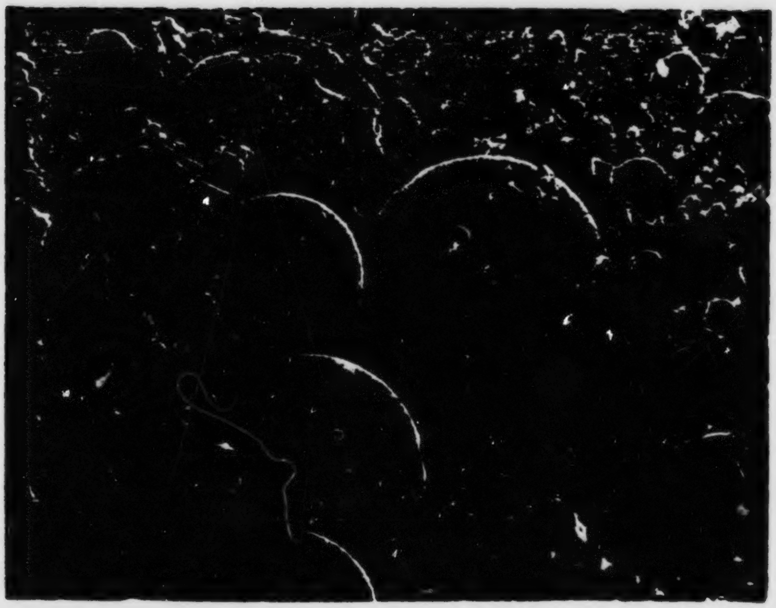

Fig. 4(b) Detail of 4(a) (magnification 10μ

Figure 5

EDXA Analysis for Selective

Locations (A-H) on Figure 4(a)

Location A

E.D. X-Ray Spectra Job Number 84907 Date MARCH 27/84

Scale 2K Seconds 300 kV 15 Specimen: Wabamun (3) Region: Client: M. Van Roode Company G.+C.

Location # Trace # Colour

Comments:- Wabamun (3) A

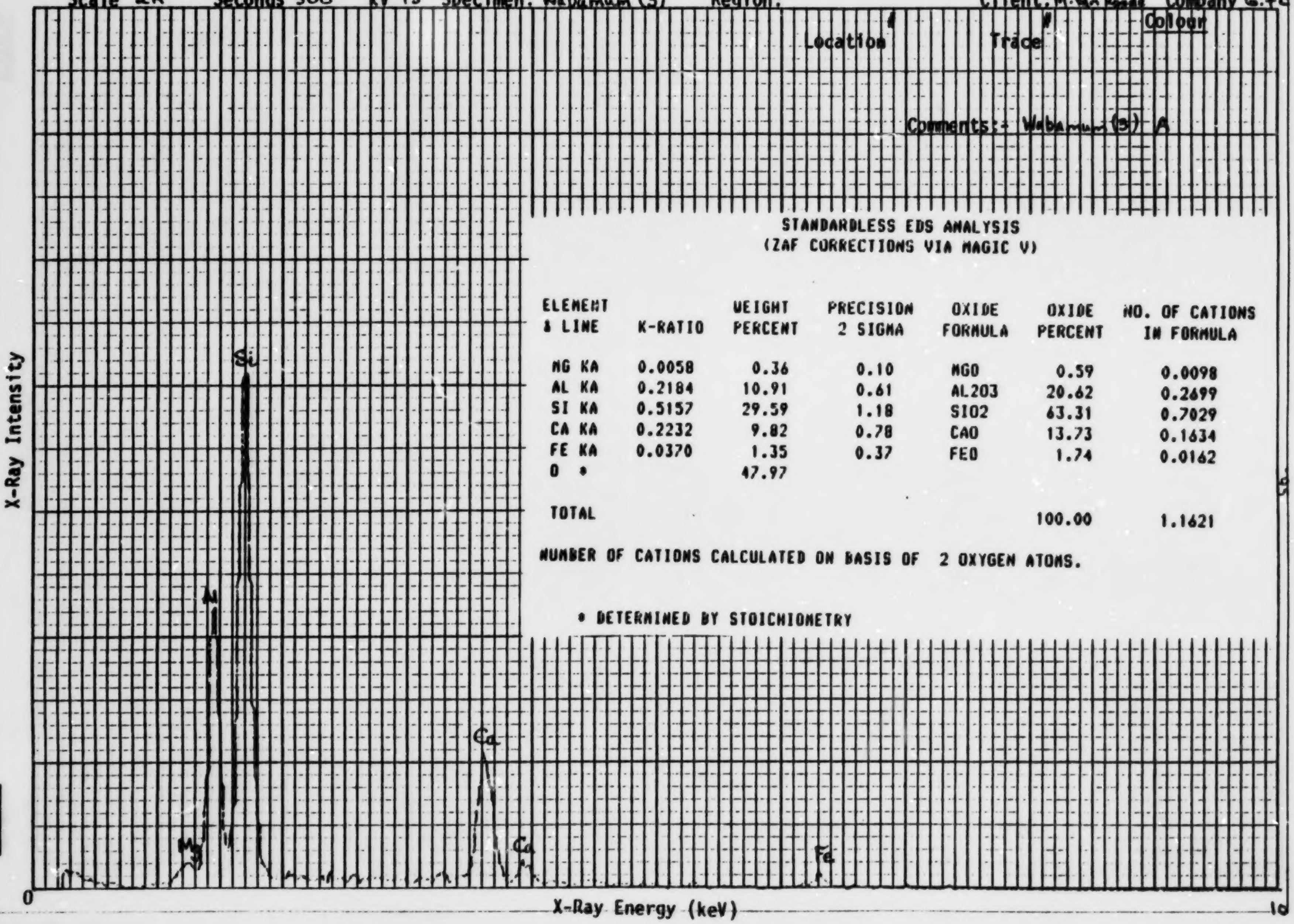

STANDARDLESS EDS ANALYSIS
(ZAF CORRECTIONS VIA MAGIC V)

ELEMENT & LINE	K-RATIO	WEIGHT PERCENT	PRECISION 2 SIGMA	OXIDE FORMULA	OXIDE PERCENT	NO. OF CATIONS IN FORMULA
MG KA	0.0058	0.36	0.10	MGO	0.59	0.0098
AL KA	0.2184	10.91	0.61	AL203	20.62	0.2699
SI KA	0.5157	29.59	1.18	SIO2	63.31	0.7029
CA KA	0.2232	9.82	0.78	CAO	13.73	0.1634
FE KA	0.0370	1.35	0.37	FEO	1.74	0.0162
O *		47.97				
TOTAL					100.00	1.1621

NUMBER OF CATIONS CALCULATED ON BASIS OF 2 OXYGEN ATOMS.

* DETERMINED BY STOICHIOMETRY

Location B

E.D. X-Ray Spectra

Job Number 84907 Date March 27/84

Scale 2K Seconds 300 kV 15 Specimen: Wabamum(3) Region:

Client: M. Van Roode Company G+C.

Location #

Trace #

Colour

Comments: Wabamum(3) B

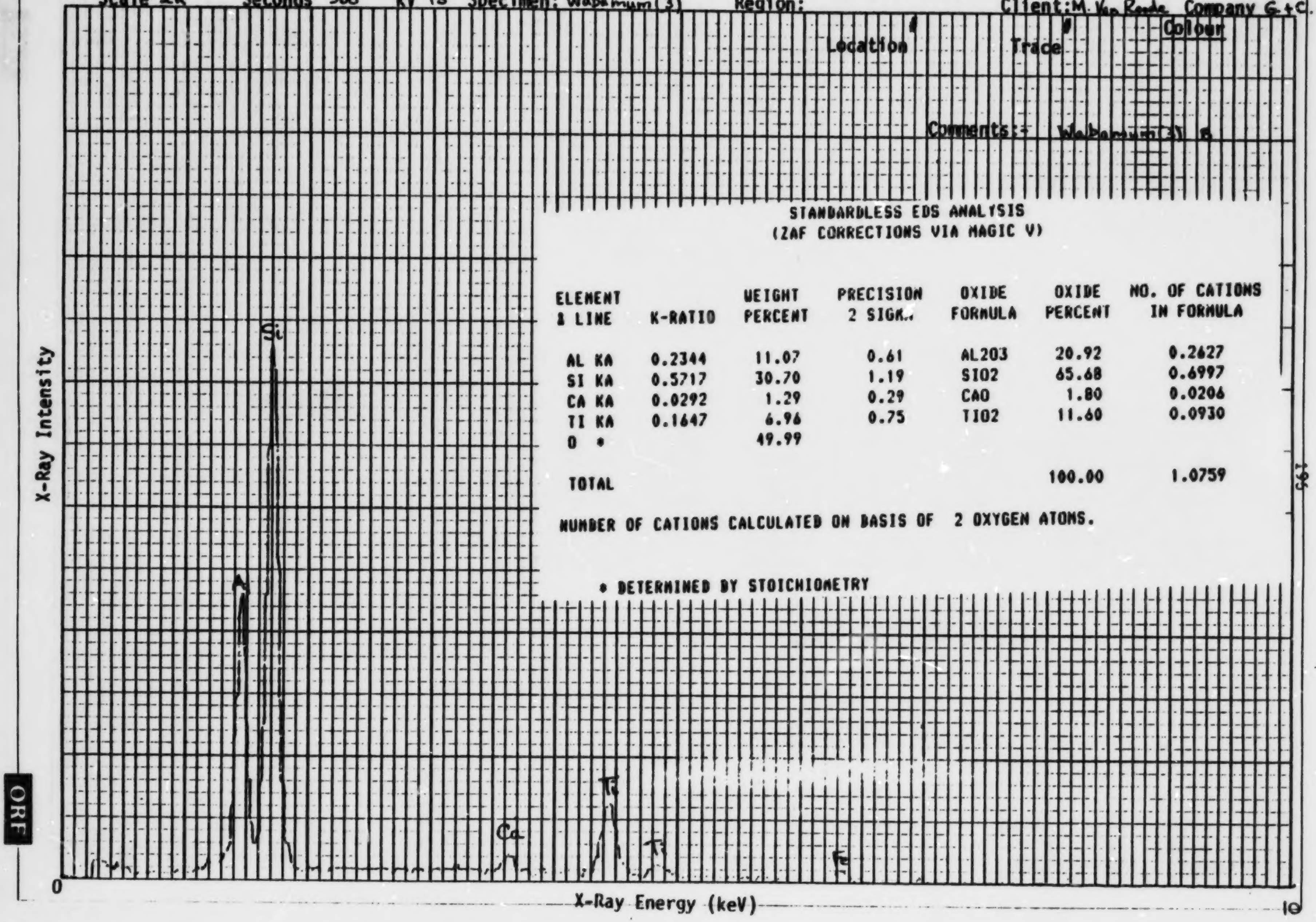

STANDARDLESS EDS ANALYSIS
(ZAF CORRECTIONS VIA MAGIC V)

ELEMENT & LINE	K-RATIO	WEIGHT PERCENT	PRECISION 2 SIGMA	OXIDE FORMULA	OXIDE PERCENT	NO. OF CATIONS IN FORMULA
AL KA	0.2344	11.07	0.61	AL2O3	20.92	0.2627
SI KA	0.5717	30.70	1.19	SIO2	65.68	0.6997
CA KA	0.0292	1.29	0.29	CAO	1.80	0.0206
TI KA	0.1647	6.96	0.75	TIO2	11.60	0.0930
O *		49.99				
TOTAL					100.00	1.0759

NUMBER OF CATIONS CALCULATED ON BASIS OF 2 OXYGEN ATOMS.

* DETERMINED BY STOICHIOMETRY

Location C

E.D. X-Ray Spectra

Job Number 84907 Date March 27/84

Scale 2K Seconds 300 kV 15 Specimen: Wabamun (3) Region:

Client: M. VanRoode Company G.+C.

Location # Trace # Colour

Comments:- Wabamun (3) C

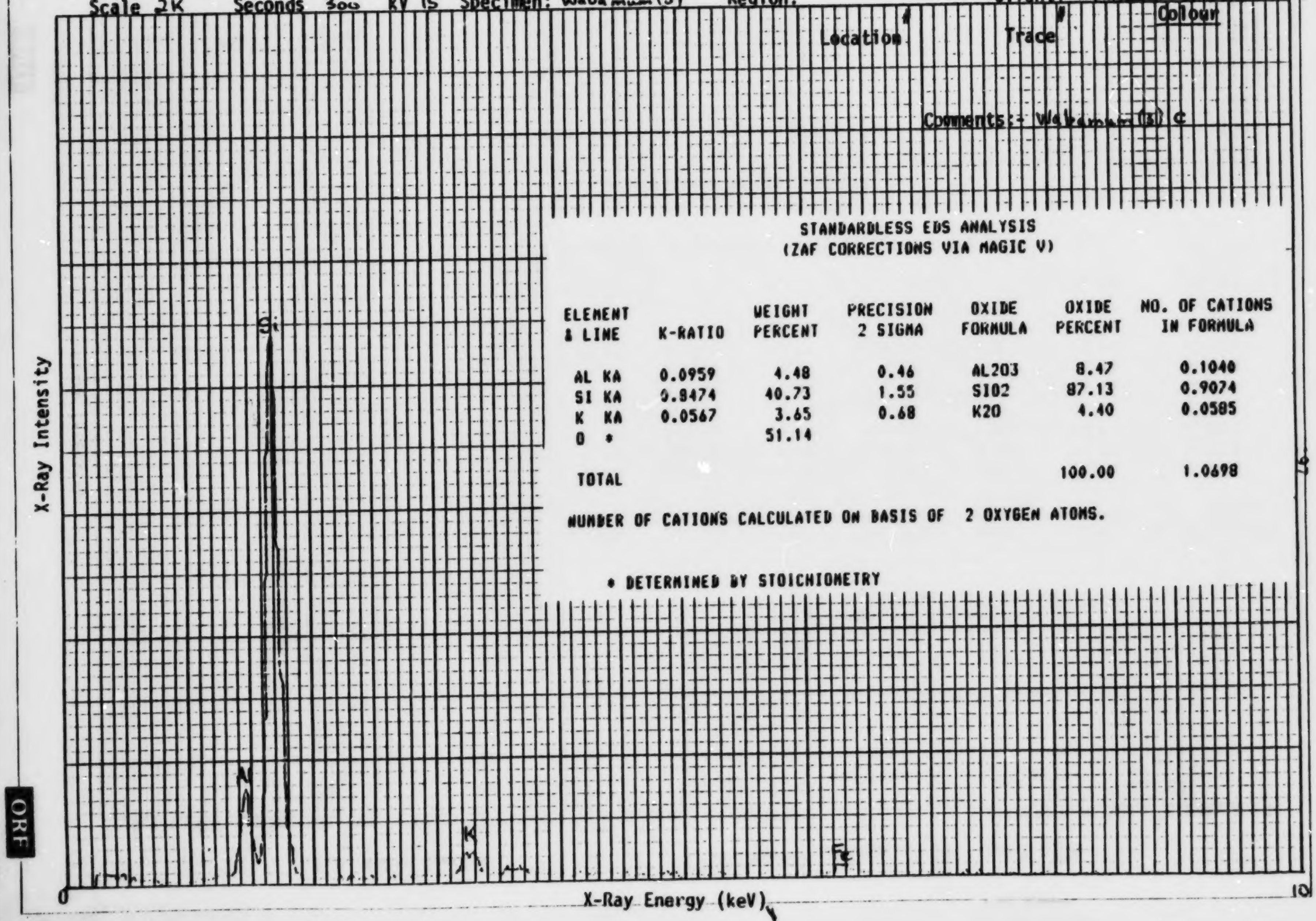

STANDARDLESS EDS ANALYSIS
(ZAF CORRECTIONS VIA MAGIC V)

ELEMENT & LINE	K-RATIO	WEIGHT PERCENT	PRECISION 2 SIGMA	OXIDE FORMULA	OXIDE PERCENT	NO. OF CATIONS IN FORMULA
AL KA	0.0959	4.48	0.46	AL2O3	8.47	0.1040
SI KA	0.8474	40.73	1.55	SIO2	87.13	0.9074
K KA	0.0567	3.65	0.68	K2O	4.40	0.0585
O *		51.14				
TOTAL					100.00	1.0698

NUMBER OF CATIONS CALCULATED ON BASIS OF 2 OXYGEN ATOMS.

* DETERMINED BY STOICHIOMETRY

Location D

E.D. X-Ray Spectra

Job Number 84907 Date March 27/84

Scale 2K Seconds 300 kV 15 Specimen: Wabamun(3) Region: Client: M. VanRoode Company G.+C.

Location # Trace # Colour

Comments:- Wabamun(3) D

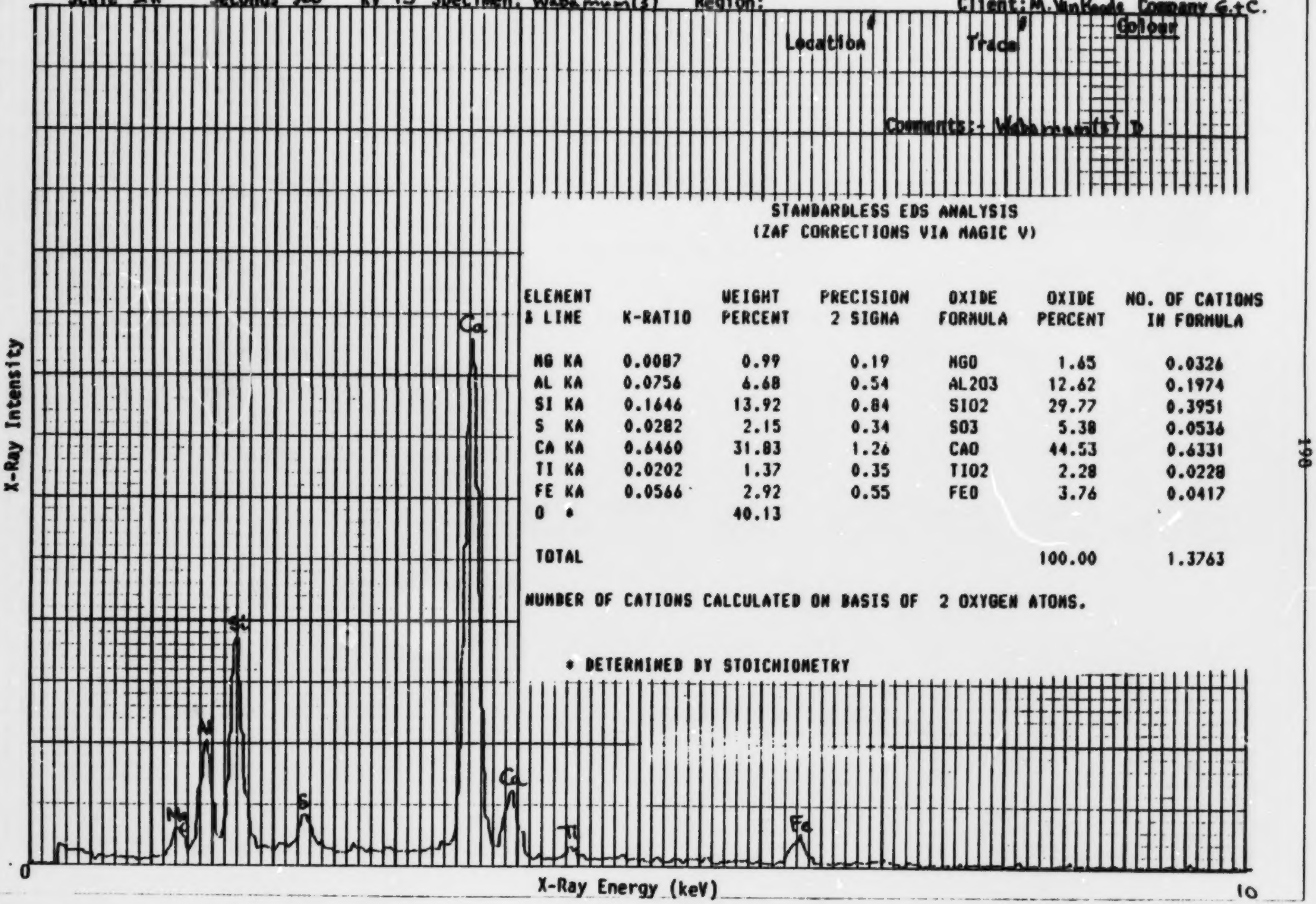

STANDARDLESS EDS ANALYSIS
(ZAF CORRECTIONS VIA MAGIC V)

ELEMENT & LINE	K-RATIO	WEIGHT PERCENT	PRECISION 2 SIGMA	OXIDE FORMULA	OXIDE PERCENT	NO. OF CATIONS IN FORMULA
MG KA	0.0087	0.99	0.19	MGO	1.65	0.0326
AL KA	0.0756	6.68	0.54	AL2O3	12.62	0.1974
SI KA	0.1646	13.92	0.84	SIO2	29.77	0.3951
S KA	0.0282	2.15	0.34	SO3	5.38	0.0536
CA KA	0.6460	31.83	1.26	CAO	44.53	0.6331
TI KA	0.0202	1.37	0.35	TIO2	2.28	0.0228
FE KA	0.0566	2.92	0.55	FEO	3.76	0.0417
O *		40.13				
TOTAL					100.00	1.3763

NUMBER OF CATIONS CALCULATED ON BASIS OF 2 OXYGEN ATOMS.

* DETERMINED BY STOICHIOMETRY

Location E

E.D. X-Ray Spectra

Job Number 84907 Date March 27/84

Scale 2K Seconds 300 kV 15 Specimen: Wabamum (3) Region: Client: M. VanRoode Company G.+C.

Location # Trace # Colour

Comments: - Wabamum (#3) E

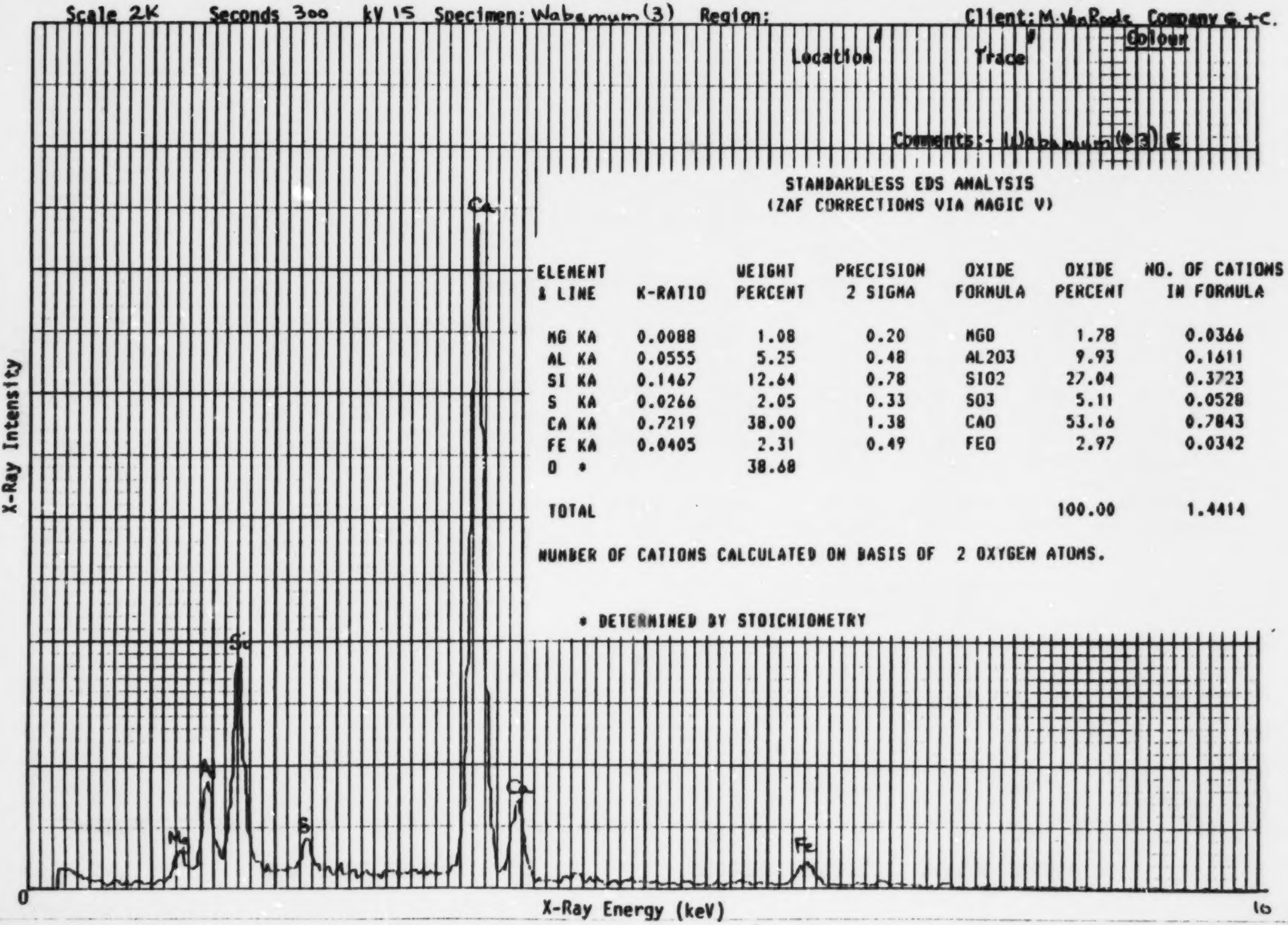

STANDARDLESS EDS ANALYSIS
(ZAF CORRECTIONS VIA MAGIC V)

ELEMENT & LINE	K-RATIO	WEIGHT PERCENT	PRECISION 2 SIGMA	OXIDE FORMULA	OXIDE PERCENT	NO. OF CATIONS IN FORMULA
MG KA	0.0088	1.08	0.20	MGO	1.78	0.0366
AL KA	0.0555	5.25	0.48	AL203	9.93	0.1611
SI KA	0.1467	12.64	0.78	SI02	27.04	0.3723
S KA	0.0266	2.05	0.33	S03	5.11	0.0528
CA KA	0.7219	38.00	1.38	CAO	53.16	0.7843
FE KA	0.0405	2.31	0.49	FEO	2.97	0.0342
O *		38.68				
TOTAL					100.00	1.4414

NUMBER OF CATIONS CALCULATED ON BASIS OF 2 OXYGEN ATOMS.

* DETERMINED BY STOICHIOMETRY

Location F

E.D. X-Ray Spectra

Job Number 84907 Date March 27/84

Scale 2K Seconds 300 kV 15 Specimen: Wabamum(3) Region: Client: M. Van Rode Company G.T.C.

Location Trace Colour

Comments:- Wabamum(3) F

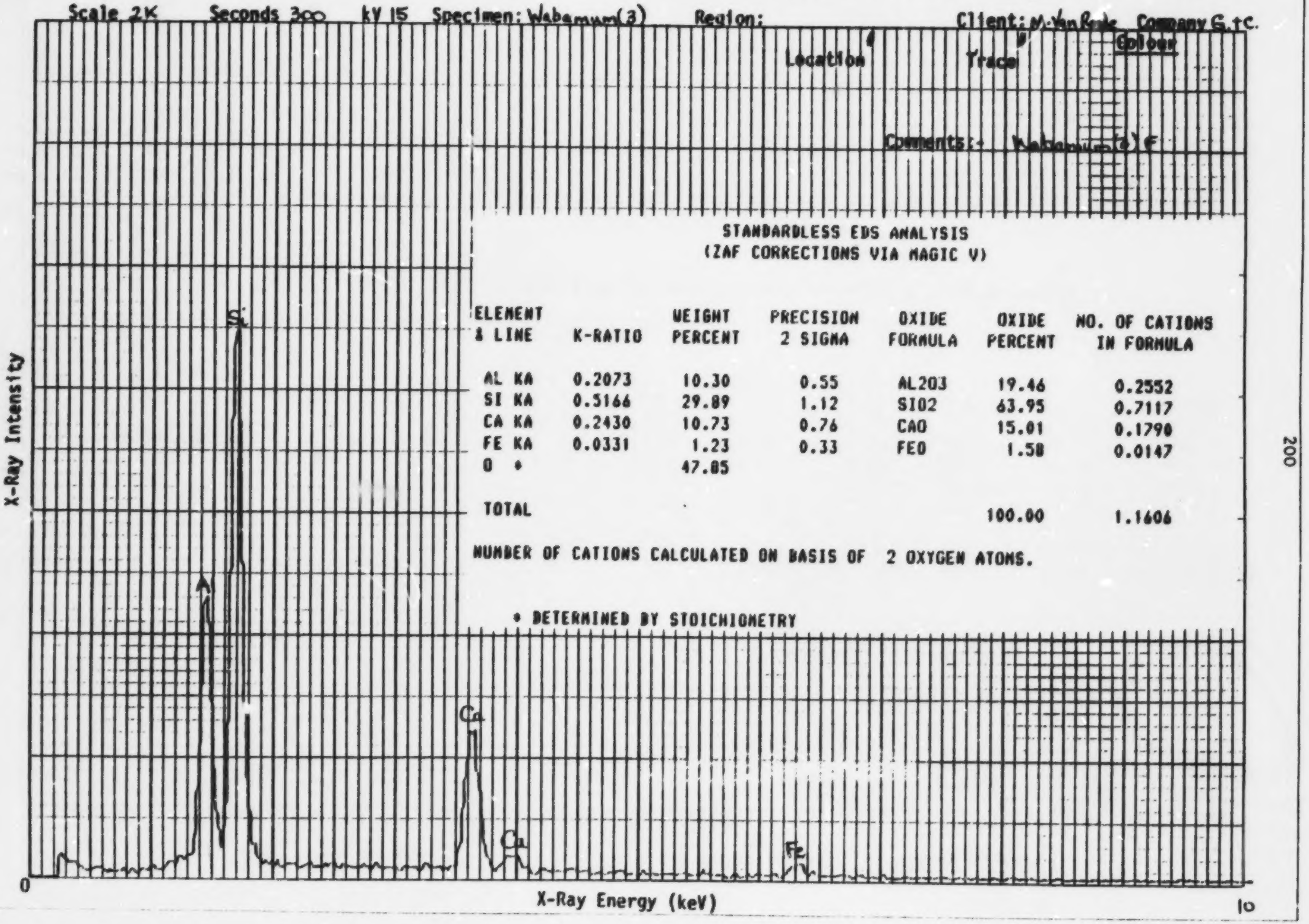

STANDARDLESS EDS ANALYSIS
(ZAF CORRECTIONS VIA MAGIC V)

ELEMENT & LINE	K-RATIO	WEIGHT PERCENT	PRECISION 2 SIGMA	OXIDE FORMULA	OXIDE PERCENT	NO. OF CATIONS IN FORMULA
AL KA	0.2073	10.30	0.55	AL2O3	19.46	0.2552
SI KA	0.5166	29.89	1.12	SIO2	63.95	0.7117
CA KA	0.2430	10.73	0.76	CAO	15.01	0.1790
FE KA	0.0331	1.23	0.33	FEO	1.58	0.0147
O *		47.85				
TOTAL					100.00	1.1606

NUMBER OF CATIONS CALCULATED ON BASIS OF 2 OXYGEN ATOMS.

* DETERMINED BY STOICHIOMETRY

ORF

Location G

E.D. X-Ray Spectra

Job Number 84907 Date March 27/84

Scale 2K Seconds 300 kV 15 Specimen: Wabamun(3) Region: Client: M. Van Rode Company G.+C.

Location # Trace # Colour

Comments:- Wabamun(3) G

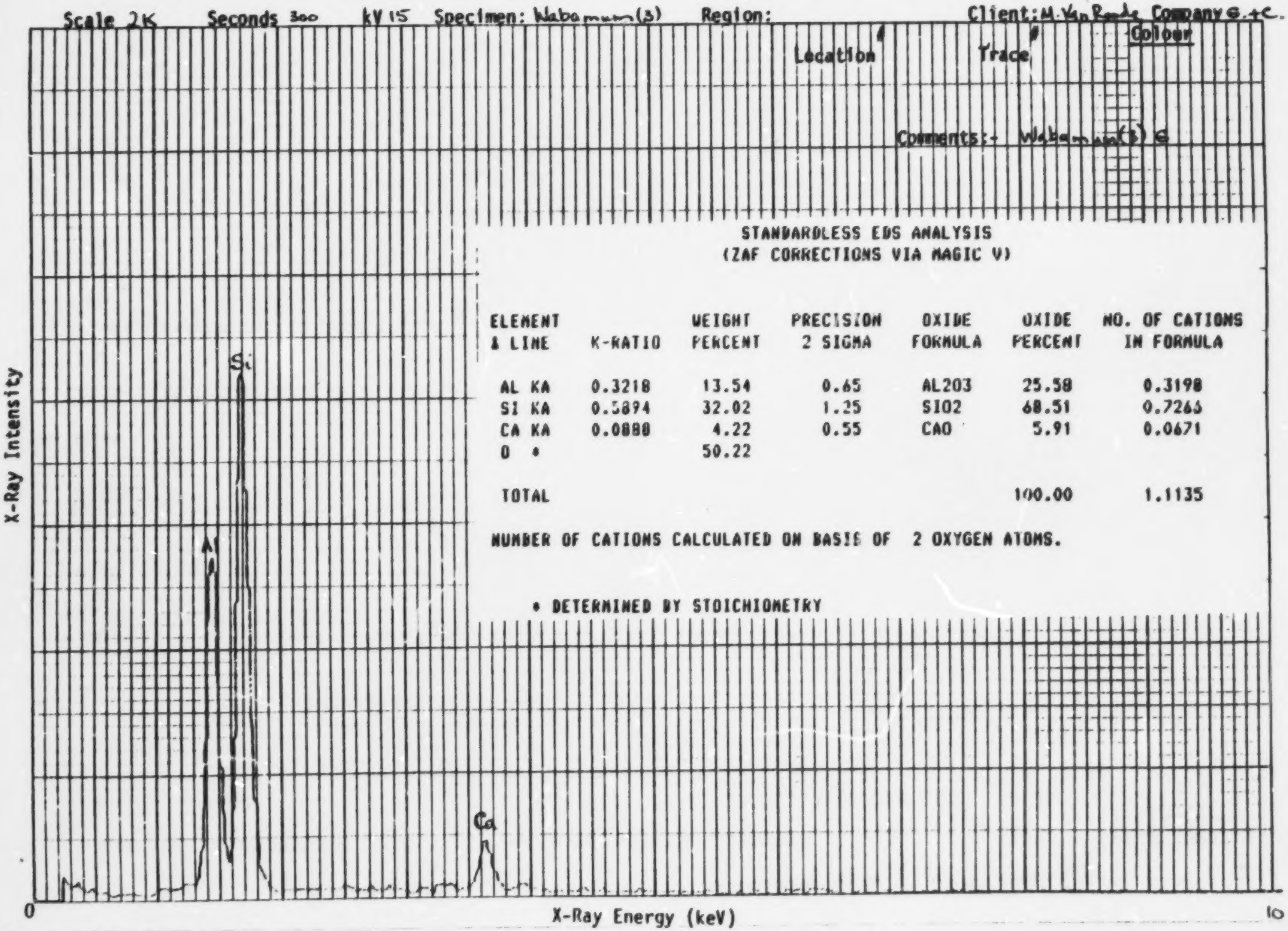

STANDARDLESS EDS ANALYSIS
(ZAF CORRECTIONS VIA MAGIC V)

ELEMENT & LINE	K-RATIO	WEIGHT PERCENT	PRECISION 2 SIGMA	OXIDE FORMULA	OXIDE PERCENT	NO. OF CATIONS IN FORMULA
AL KA	0.3218	13.54	0.65	AL2O3	25.58	0.3198
SI KA	0.5894	32.02	1.25	SIO2	68.51	0.7265
CA KA	0.0888	4.22	0.55	CAO	5.91	0.0671
O *		50.22				
TOTAL					100.00	1.1135

NUMBER OF CATIONS CALCULATED ON BASIS OF 2 OXYGEN ATOMS.

* DETERMINED BY STOICHIOMETRY

ORF

Location H

E.D. X-Ray Spectra

Job Number 84907 Date March 27/84

Scale 2K Seconds 300 kV 15 Specimen: Wabamum(3) Region:

Client: M. Van Rode Company G.+C.

Location # Trade # Colour

Comments:- Wabamum(3) H

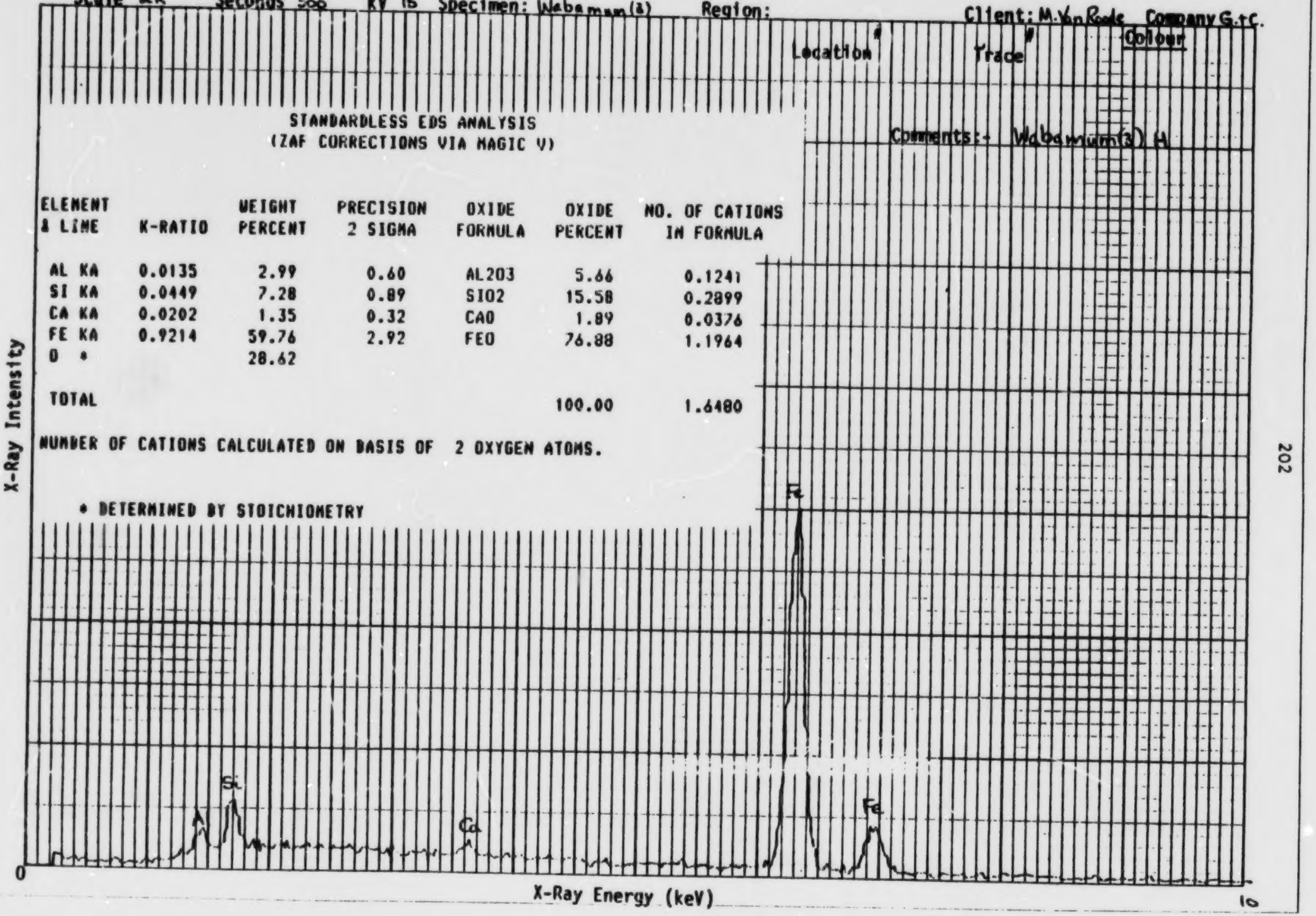

STANDARDLESS EDS ANALYSIS
(ZAF CORRECTIONS VIA MAGIC V)

ELEMENT & LINE	K-RATIO	WEIGHT PERCENT	PRECISION 2 SIGMA	OXIDE FORMULA	OXIDE PERCENT	NO. OF CATIONS IN FORMULA
AL KA	0.0135	2.99	0.60	AL203	5.66	0.1241
SI KA	0.0449	7.28	0.89	SI02	15.58	0.2899
CA KA	0.0202	1.35	0.32	CAO	1.89	0.0376
FE KA	0.9214	59.76	2.92	FEO	76.88	1.1964
O *		28.62				
TOTAL					100.00	1.6480

NUMBER OF CATIONS CALCULATED ON BASIS OF 2 OXYGEN ATOMS.

* DETERMINED BY STOICHIOMETRY

Figure 6

CROSS SECTION OF WABAMUN FLY ASH AFTER ION ETCHING

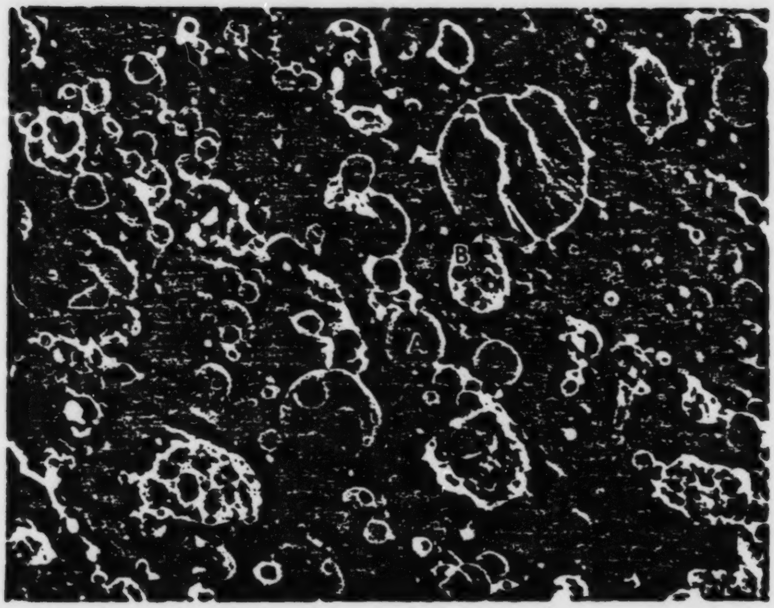

A	
SiO_2	29.93
Al_2O_3	4.80
FeO	24.73
CaO	41.55

B	
SiO_2	73.07
Al_2O_3	7.17
Fe	2.75
CaO	16.57

(A) SECONDARY ELECTRON MODE

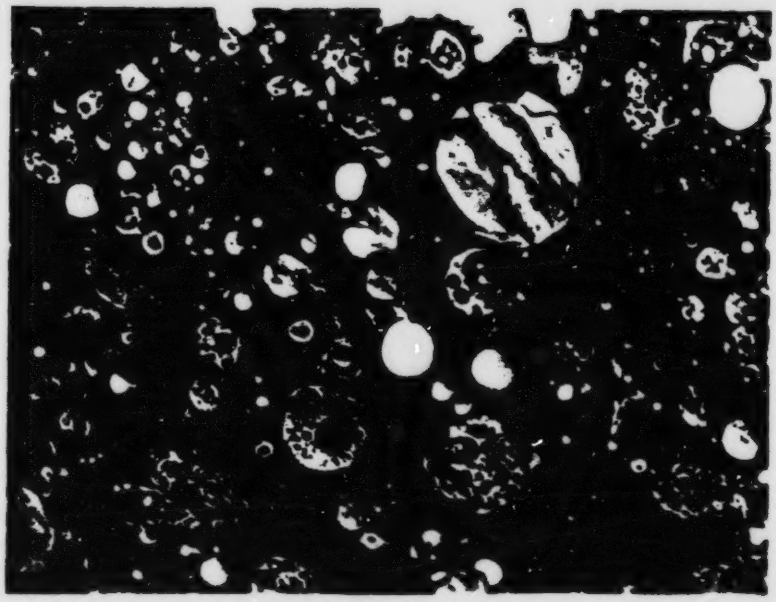

(B) BACK-SCATTER MODE

	3
SiO_2	51.27
Al_2O_3	31.29
TiO_2	4.86
FeO	2.27
CaO	9.17

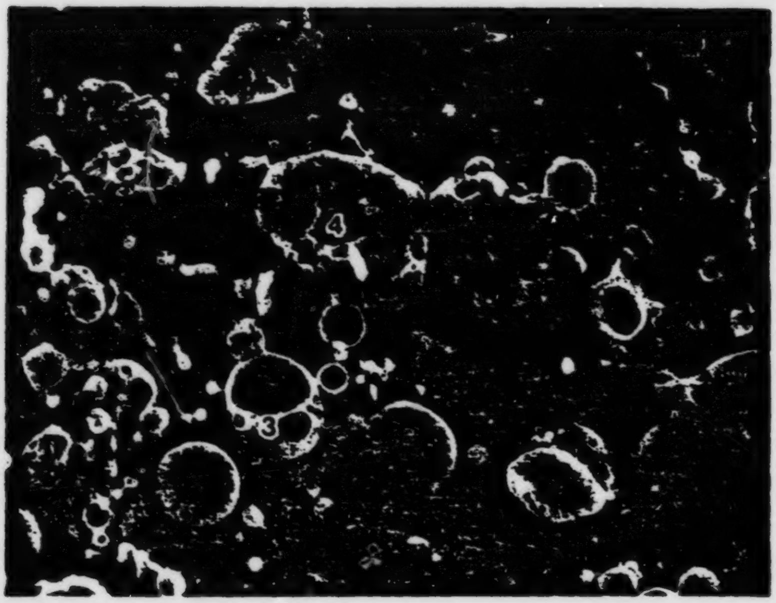

(A) Secondary electron mode

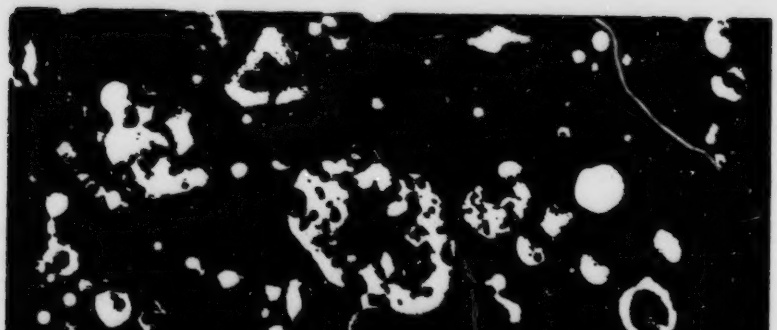

(B) Back-scatter mode

Figure 7 Cross Section of Wabamun Fly Ash After Ion Etching

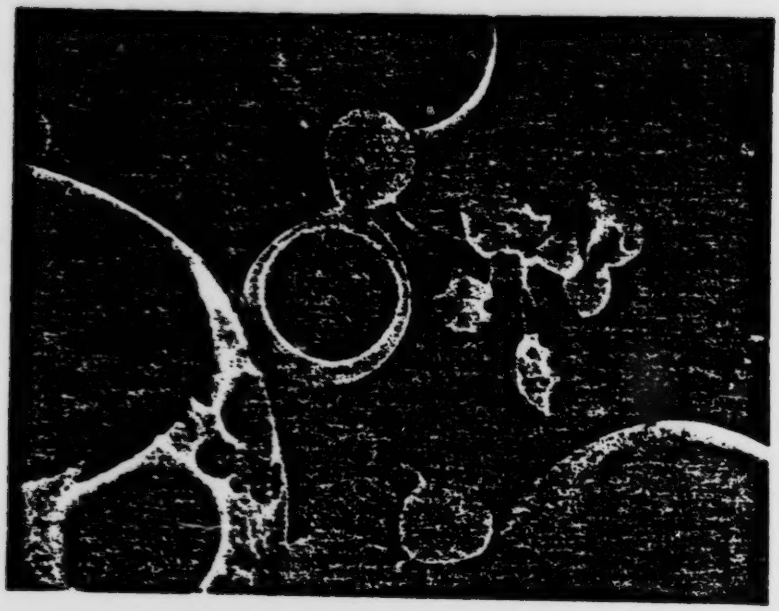

(A) Secondary electron mode

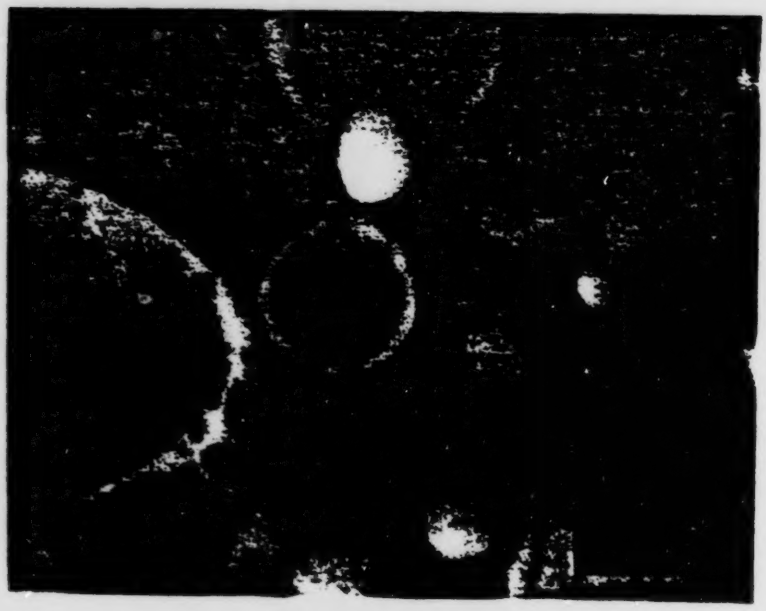

(B) Back-scatter mode

Figure 8 SEM micrograph of Location 3 in Figure 7 at higher magnification.

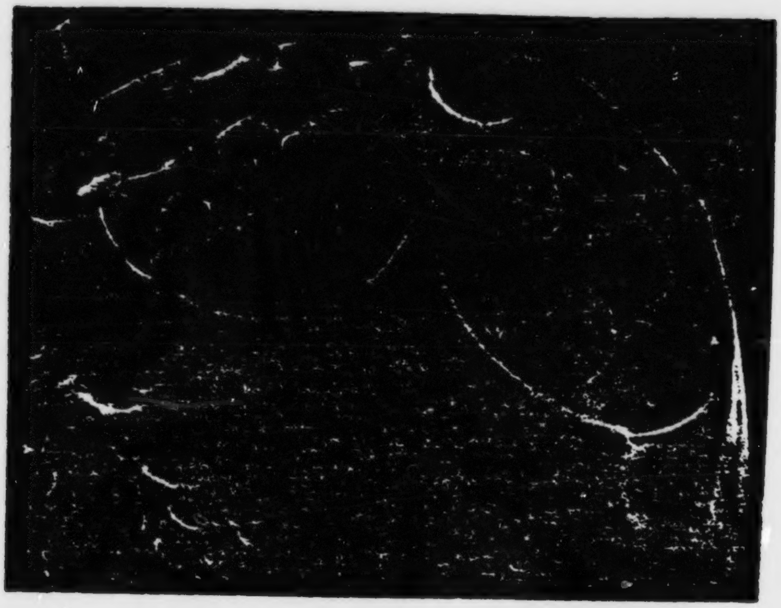

(A) Secondary electron mode

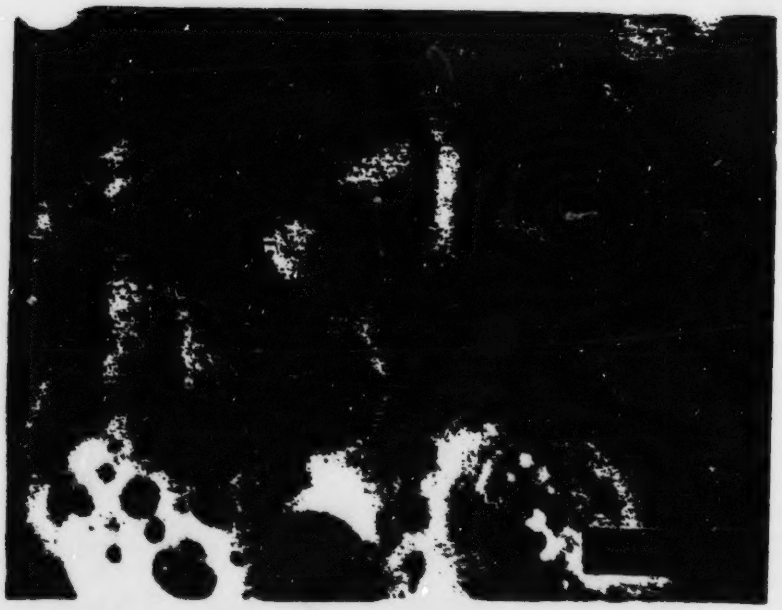

(B) Back-scatter mode

Figure 9 SEM micrograph of a plerosphere

4A

SiO_2	56.84
Al_2O_3	15.70
TiO_2	1.71
FeO	3.08
CaO	6.12
K_2O	6.24

4C

SiO_2	53.1[illegible]
Al_2O_3	20.5[illegible]
TiO_2	1.5[illegible]
FeO	3.[illegible]3
CaO	4.8[illegible]
K_2O	6.4[illegible]

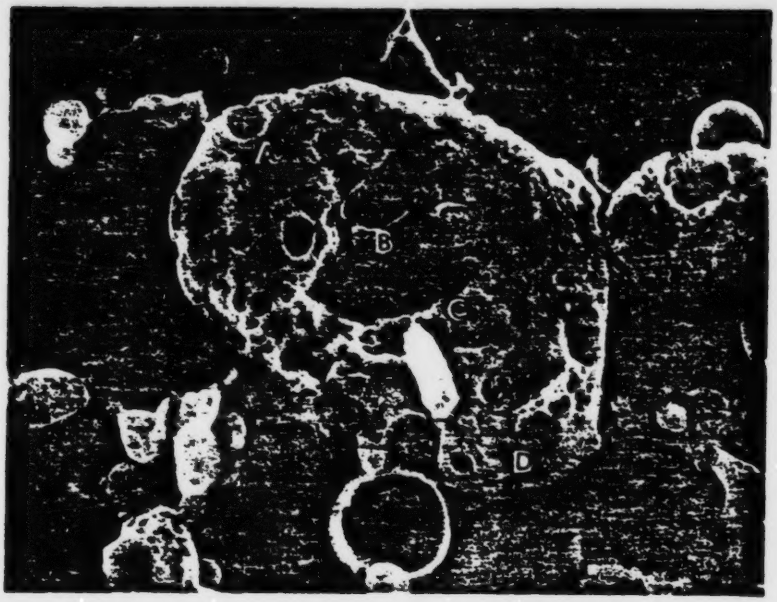

4B

SiO_2	55.69
Al_2O_3	14.68
TiO_2	4.06
FeO	5.78
SO_3	3.04
CaO	8.53
K_2O	6.24

4D

SiO_2	49.24
Al_2O_3	16.35
TiO_2	1.31
FeO	5.31
CaO	23.87
K_2O	2.64

(A) Secondary electron mode

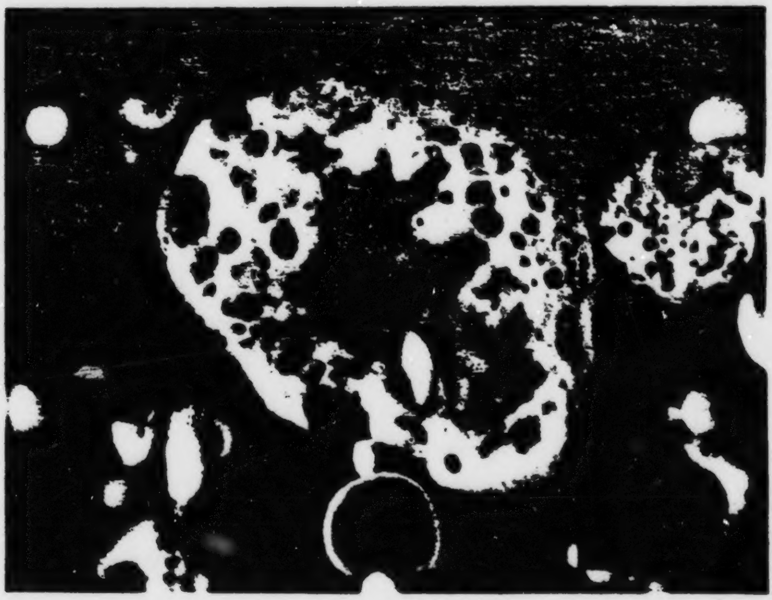

(B) Back-scatter mode

Figure 10 SEM micrograph of Location 4 in Figure 7 at higher magnification

XRD PATTERNS FOR CORDIERITE GLASS-α- CORDIERITE MIXTURES FOR GLASS CONTENT DETERMINATION (QXRD METHOD)

(A) 100% GLASS (B) 75% GLASS (C) 50% GLASS

(D) 25% GLASS (E) 0% GLASS

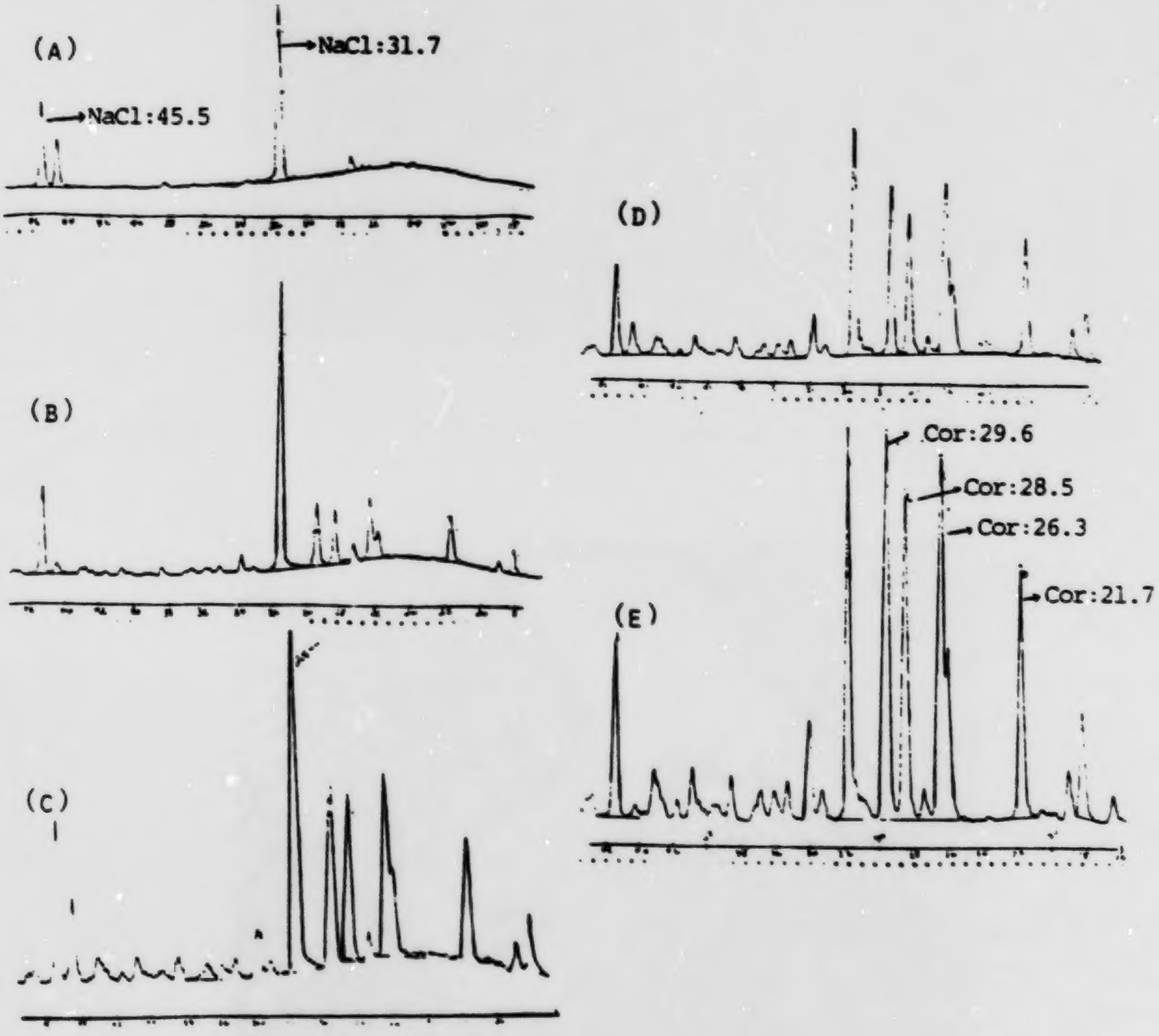

Figure 11

ORF

Figure 12

Intensity Ratios for Cordierite Glass-α-Cordierite Mixtures versus Glass Content (QXRD Method)

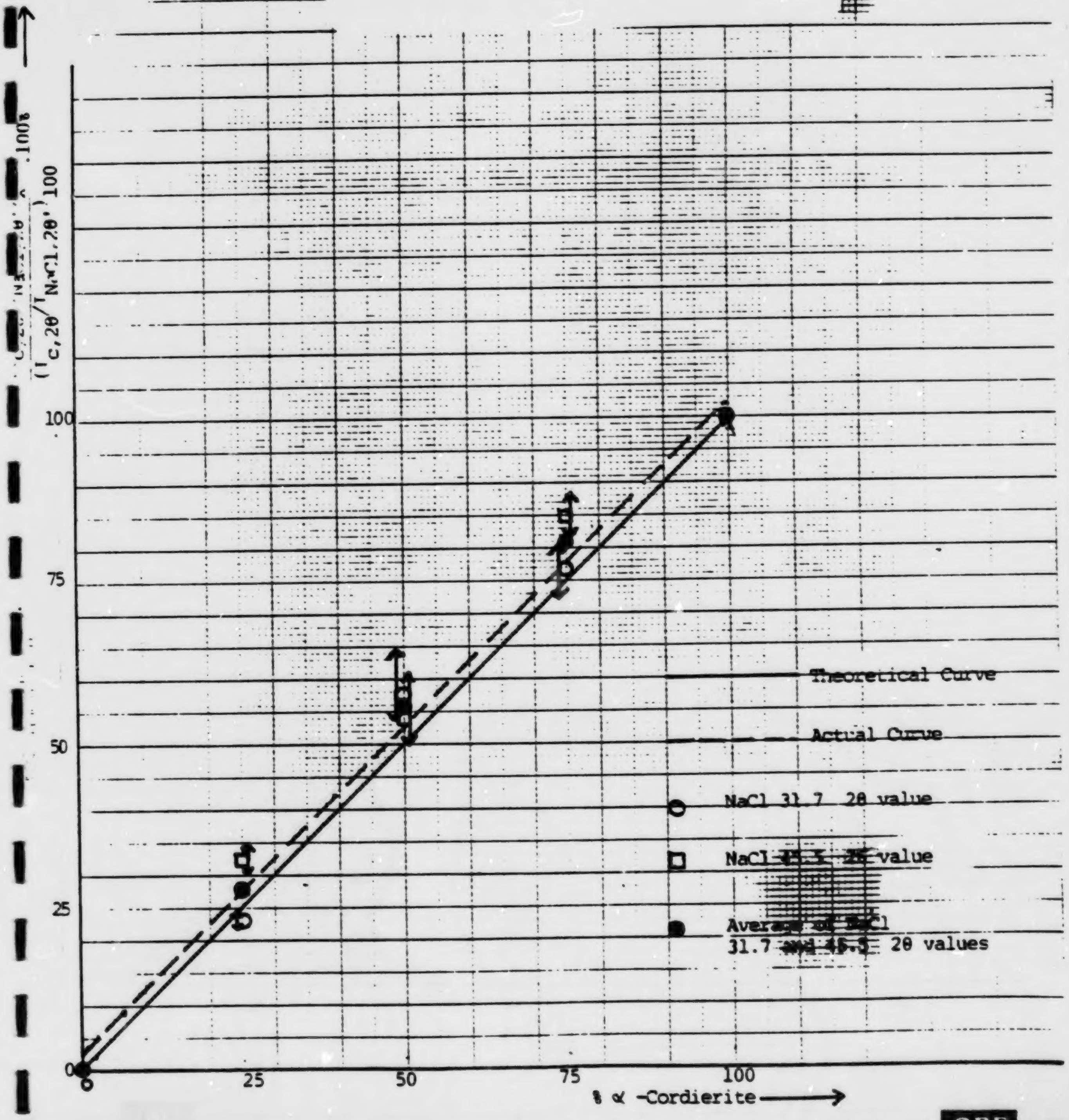

Figure 13a. Standard Curve for α-Quartz $2\theta=20.8$, $2\theta'=28.3$

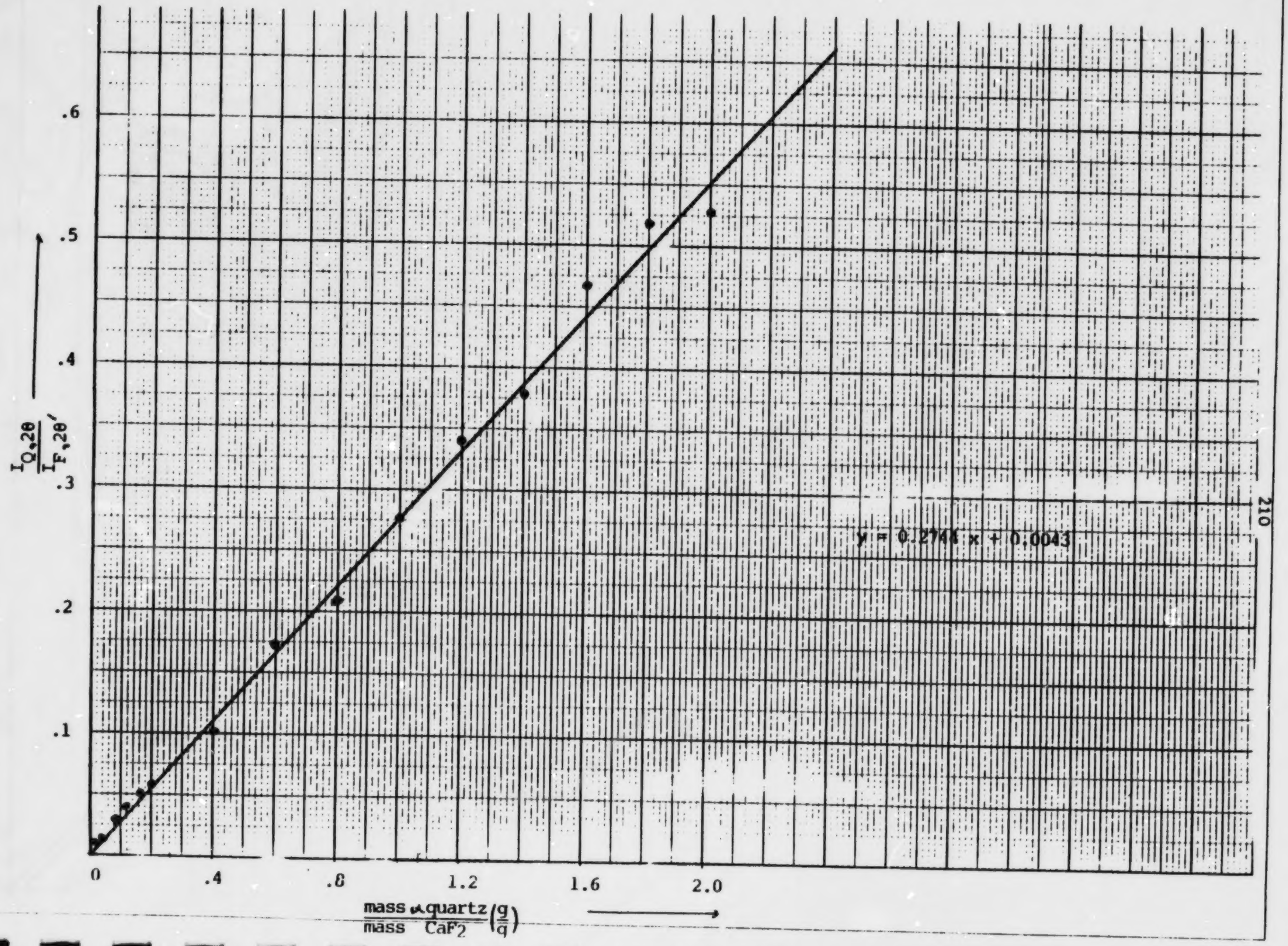

ORF

Figure 13b, Standard Curve for α-Quartz 2θ=26.6, 2θ'=28.3

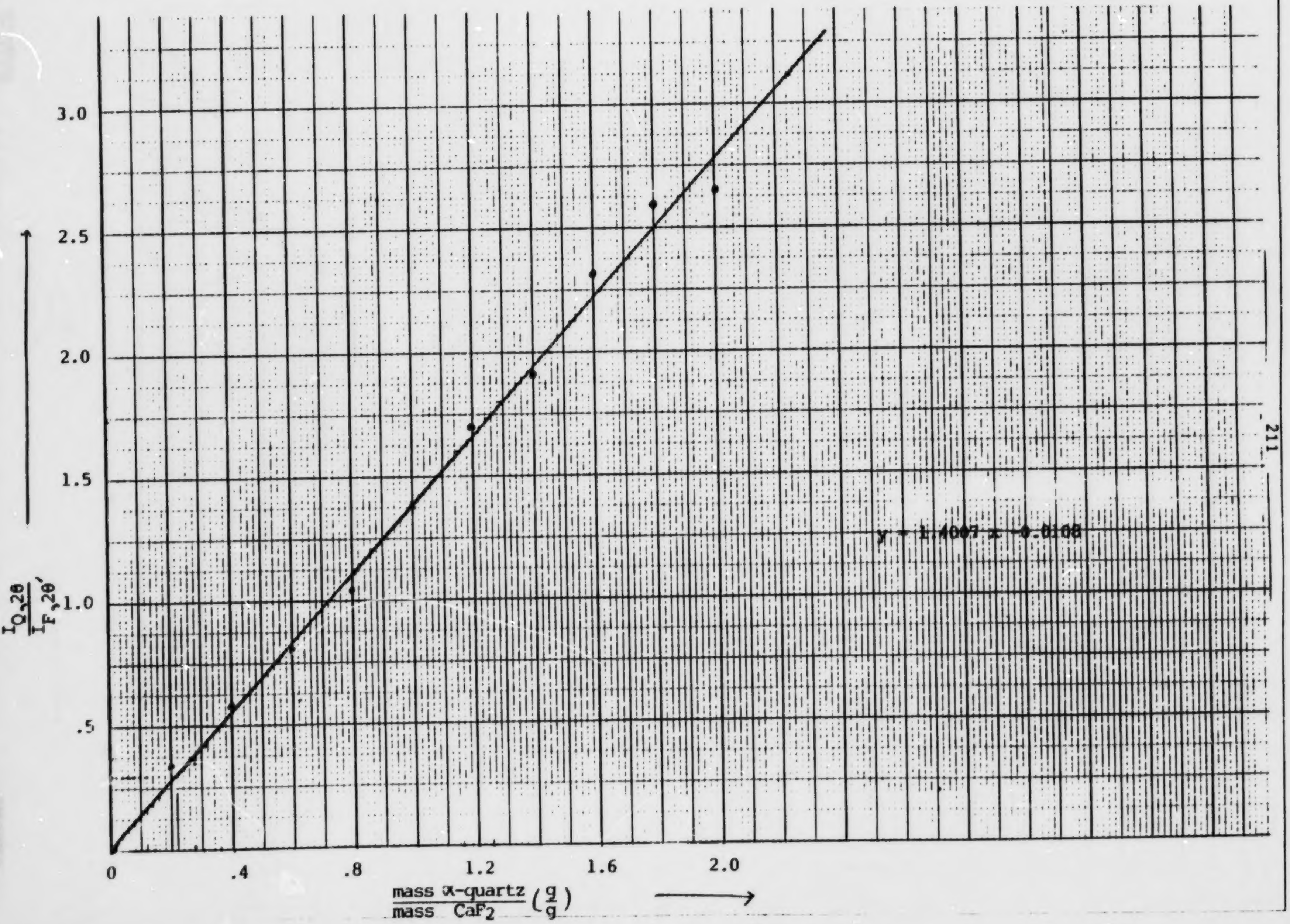

Figure 13c. Standard Curve for α-Quartz 2θ = 50.1, 2θ' = 28.3

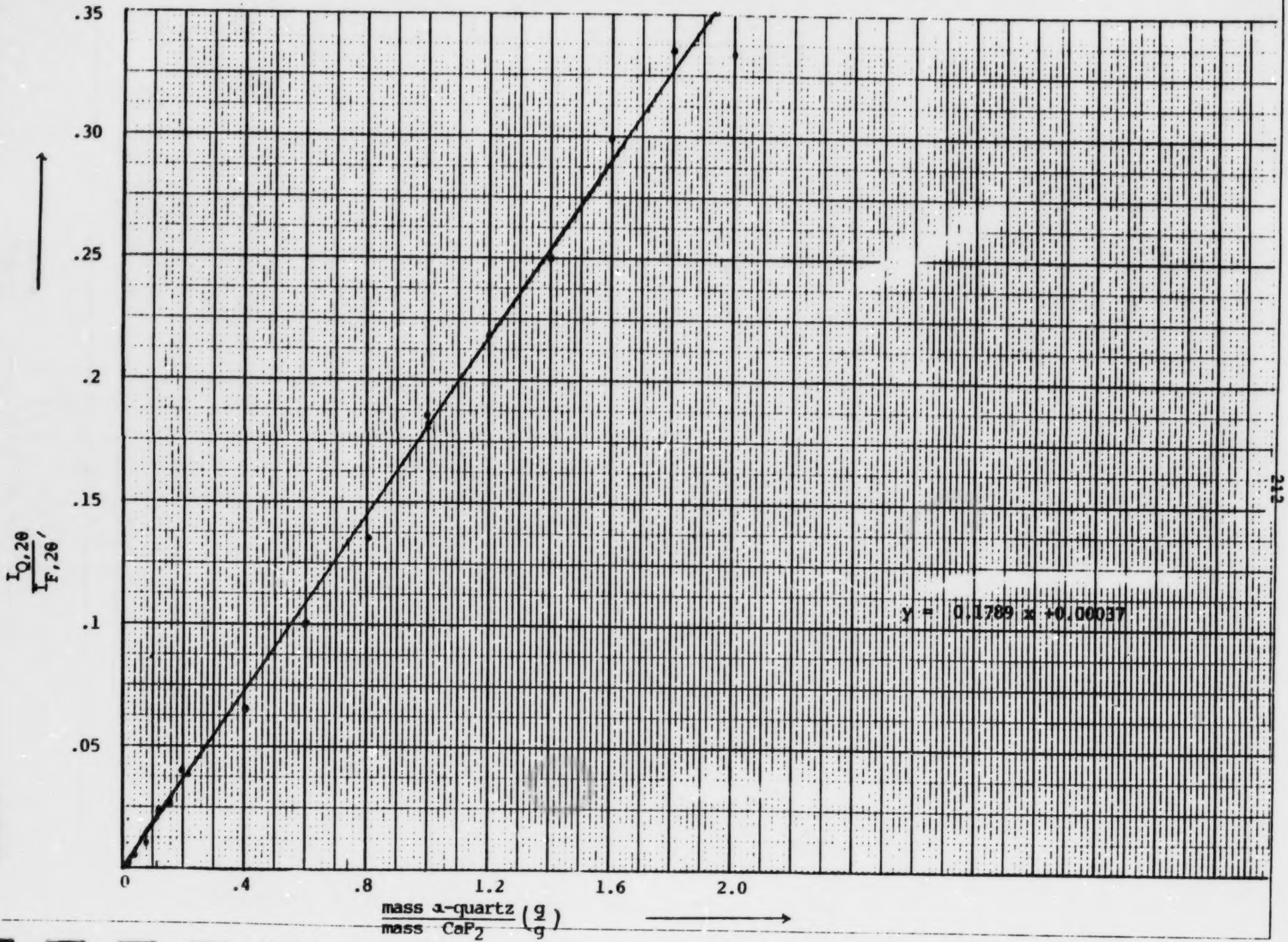

Figure 13d. Standard Curve for α-Quartz 2θ = 20.8, 2θ' = 47.0

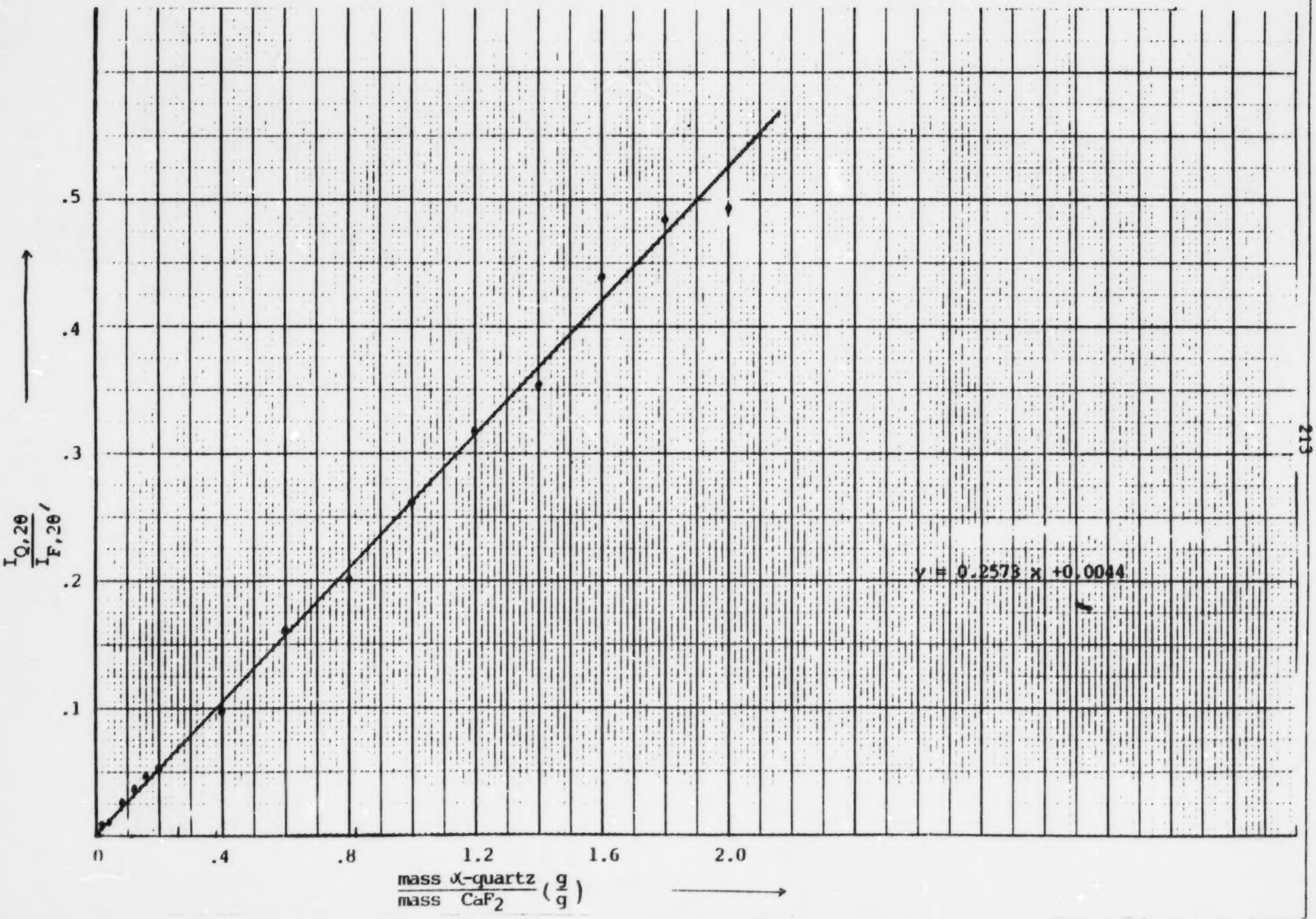

Figure 13e. Standard Curve for α-Quartz $2\theta = 26.6$, $2\theta' = 47.0$

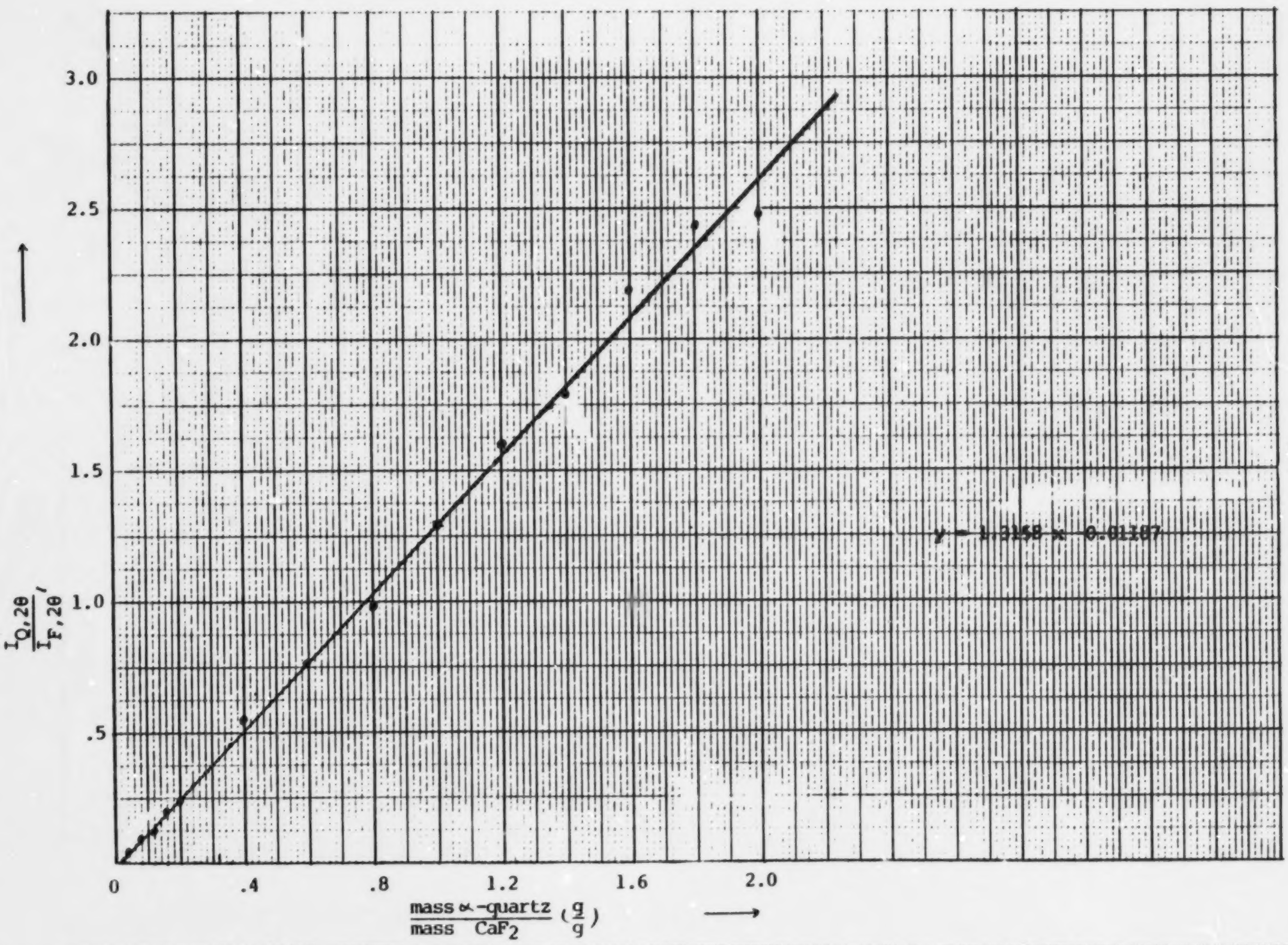

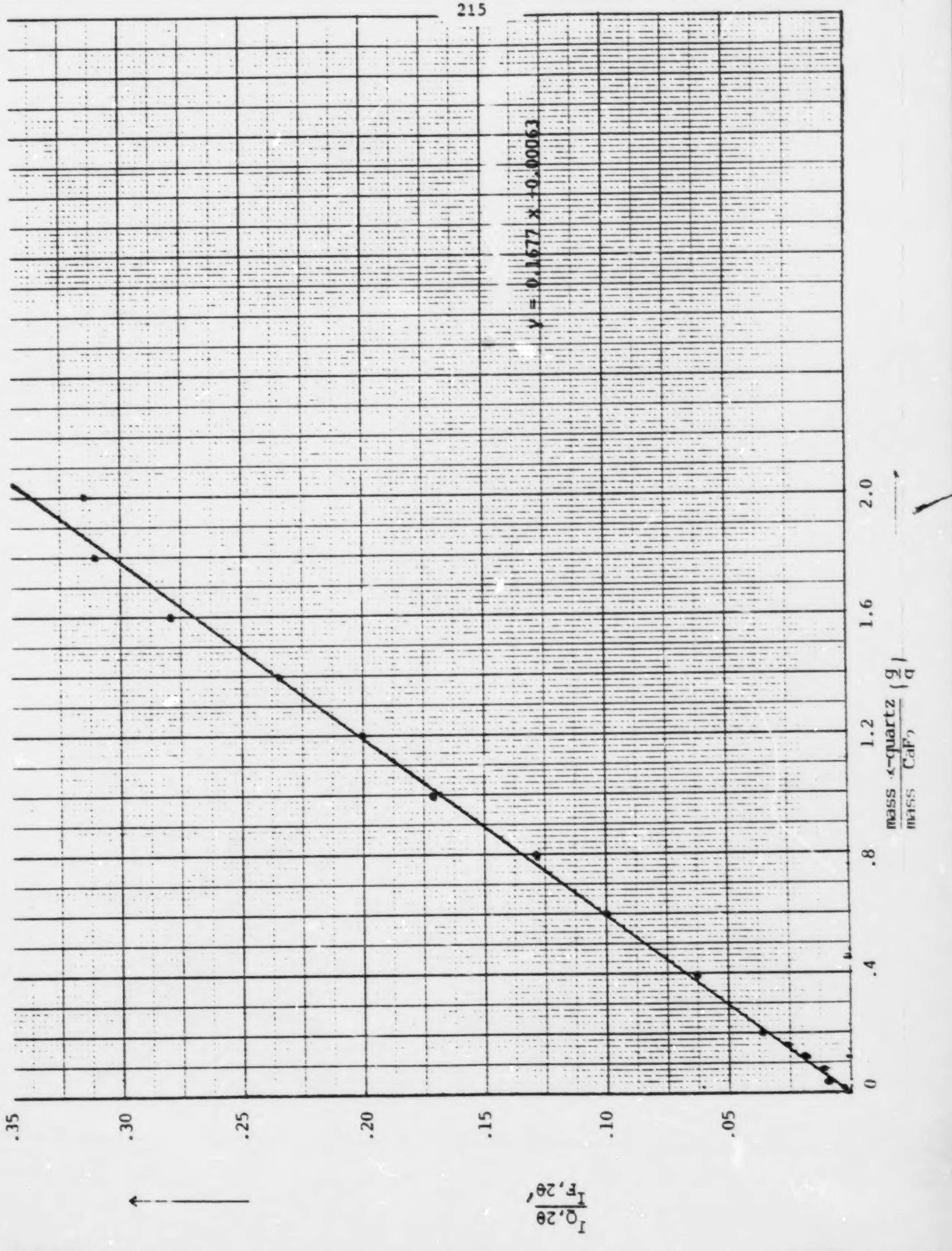

Figure 13f. Standard Curve for α-Quartz 2θ = 50.1, 2θ' = 47.0

Figure 14a. Standard Curve for Mullite $2\theta=16.4$, $2\theta'=28.3$ Low Mass Ratio

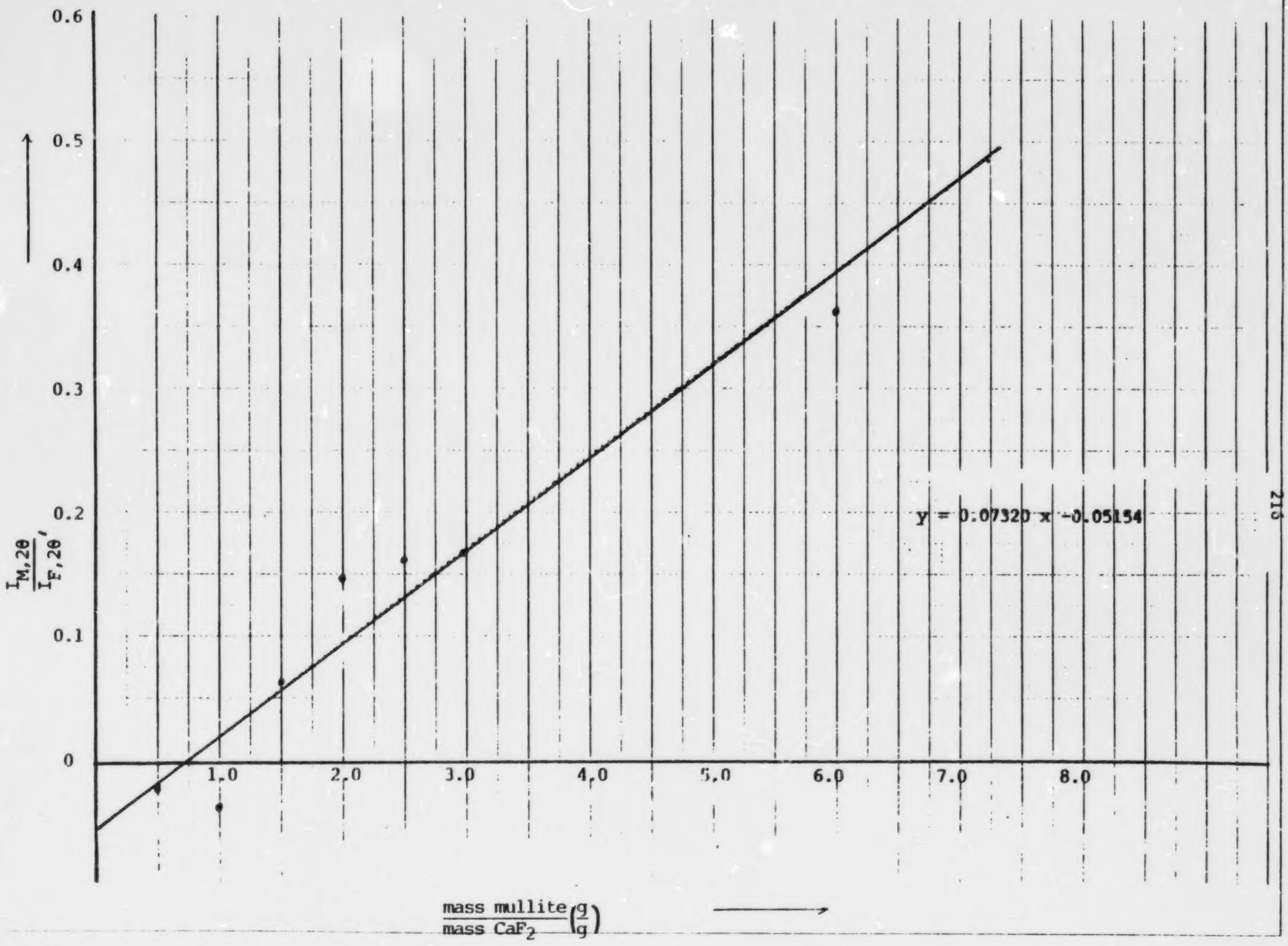

Figure 14b. Standard Curve for Mullite 2θ=16.4, 2θ'=28.3 High Mass Ratio

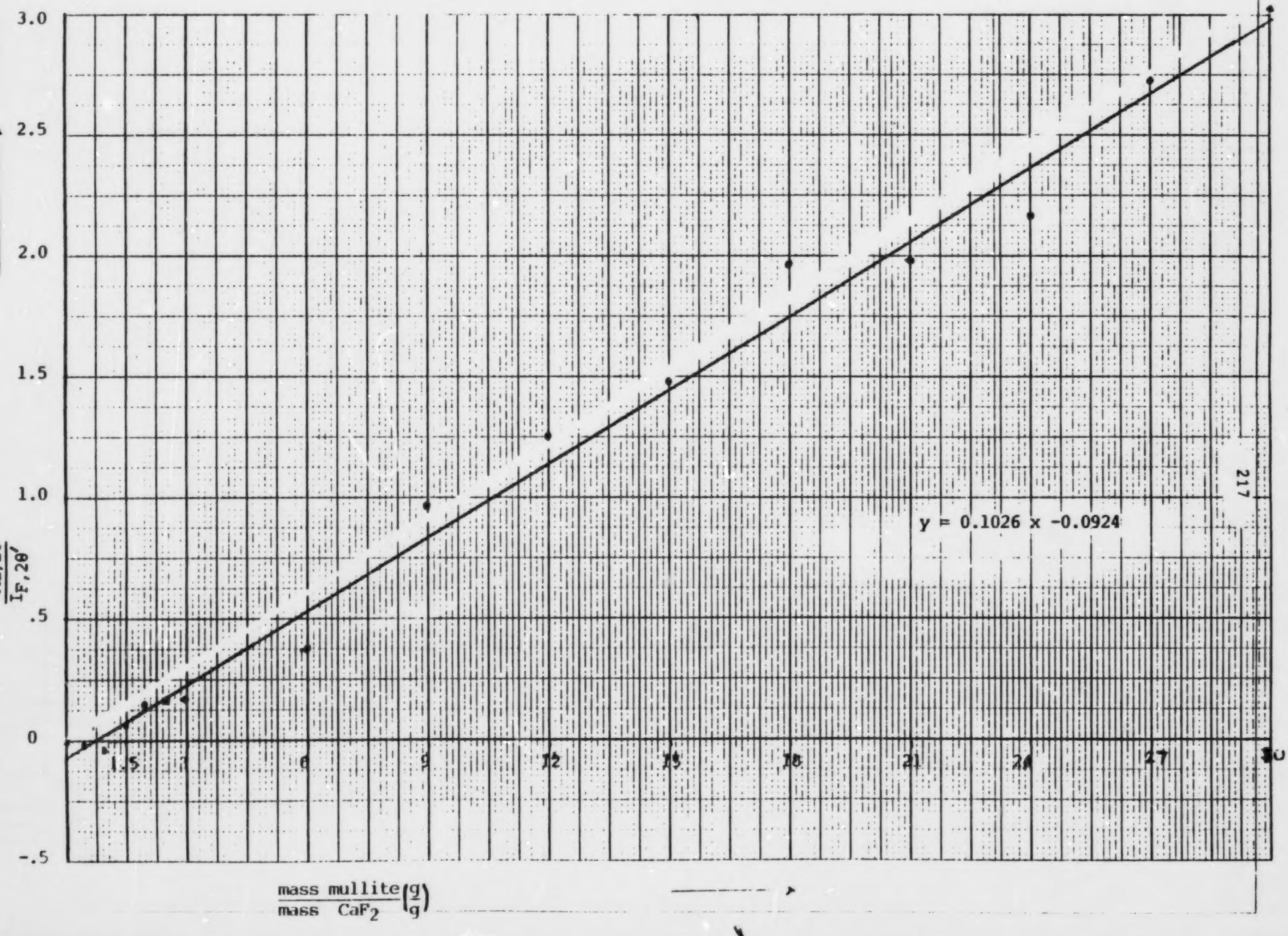

Figure 14c. Standard Curve for Mullite 2θ=60.6, 2θ'=28.3 Low Mass Ratio

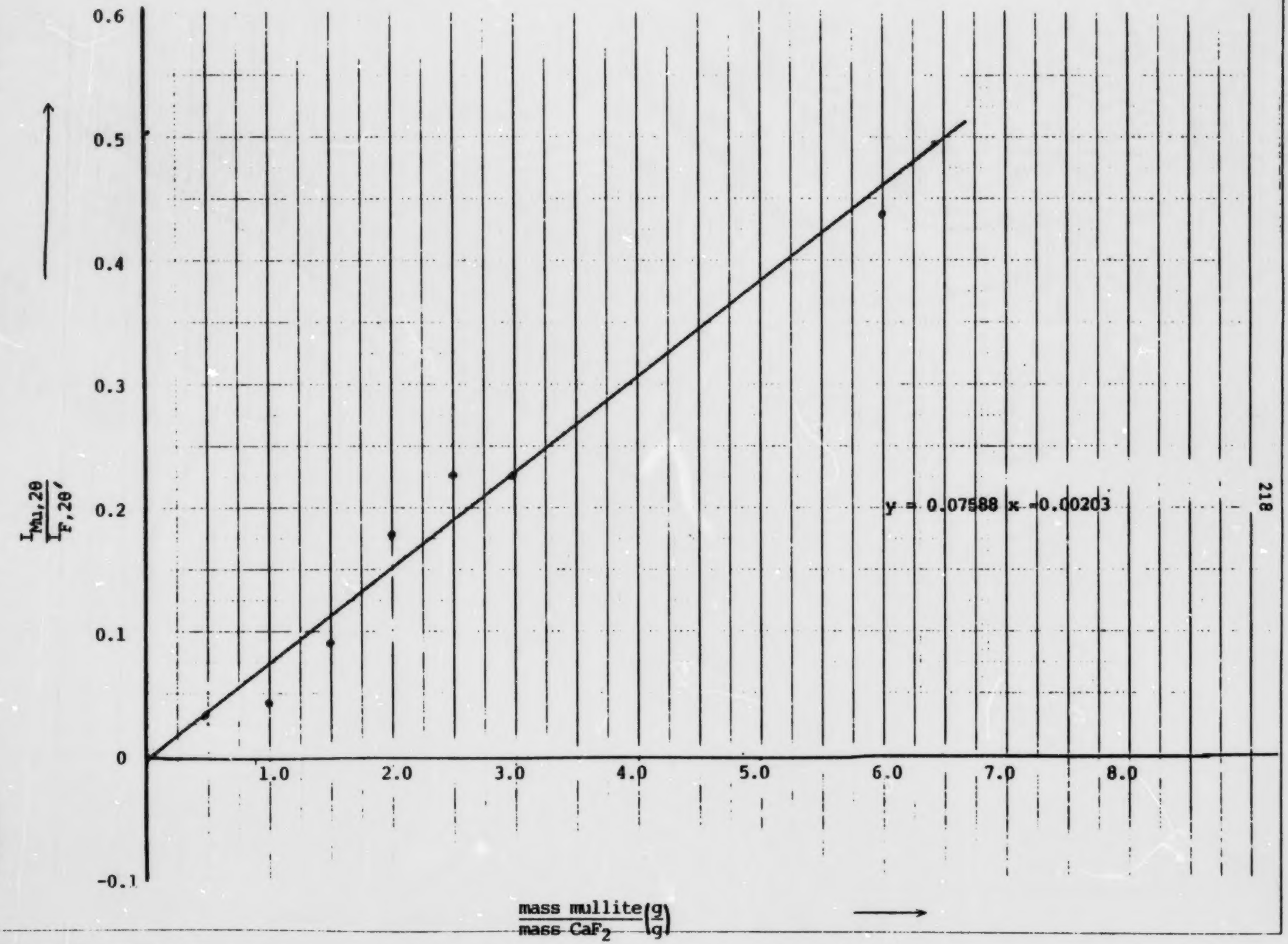

Figure 14d. Standard Curve for Mullite 2θ=60.6, 2θ'=28.3 High Mass Ratio

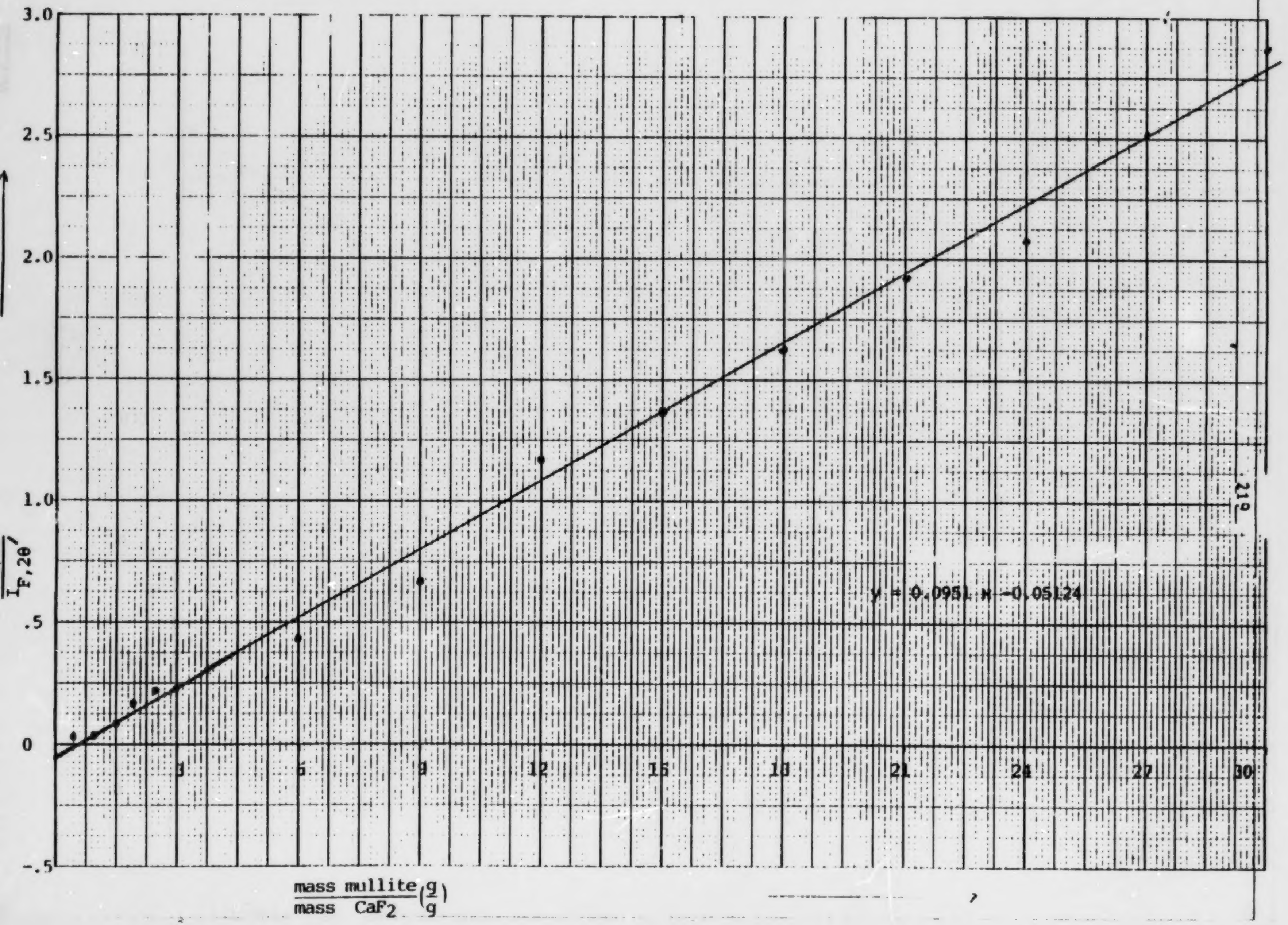

Figure 14e. Standard Curve for Mullite 2θ=16.4, 2θ'=47.0 Low Mass Ratio

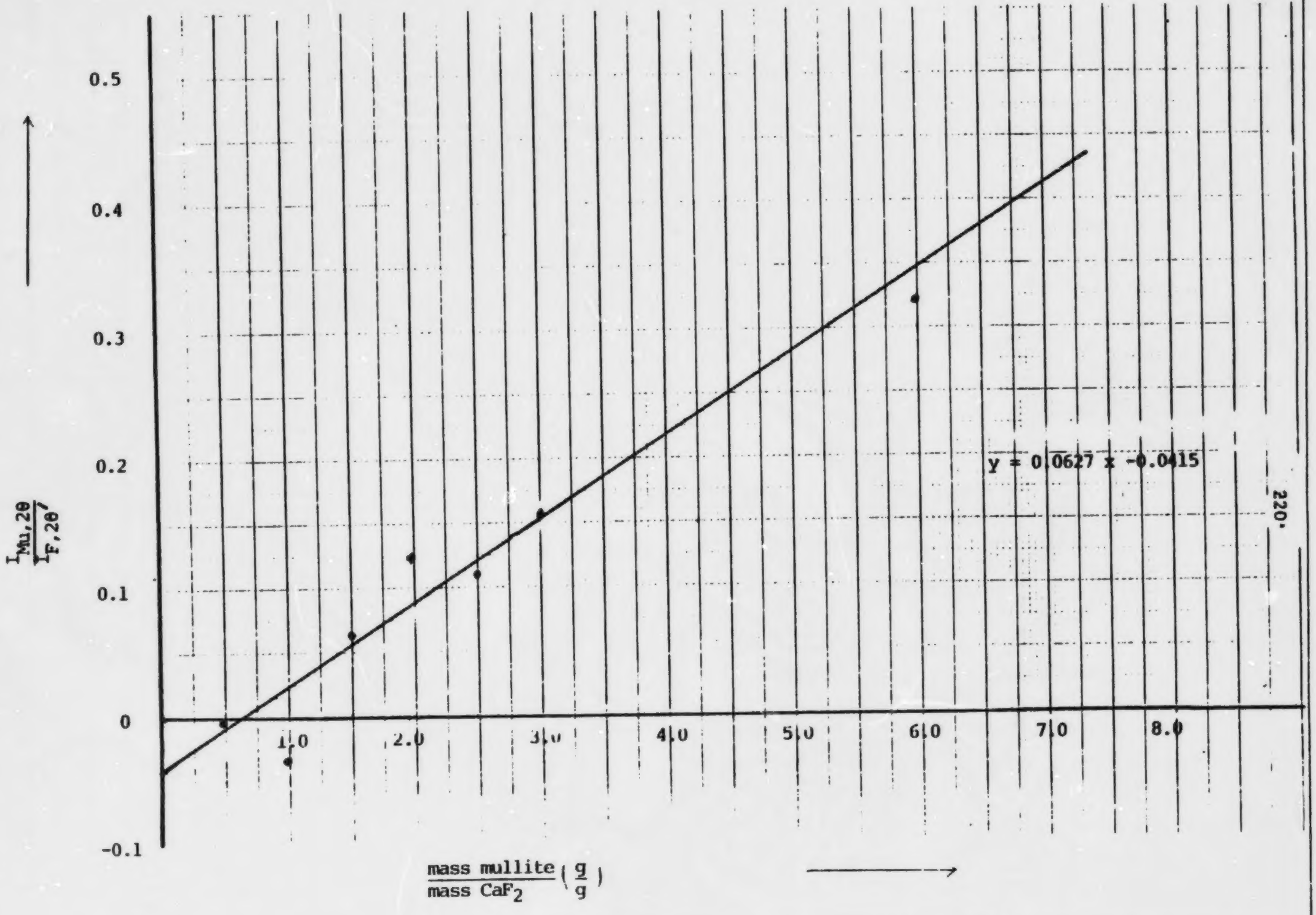

ORF

Figure 14f. Standard Curve for Mullite 2θ=16.4, 2θ'=47.0 High Mass Ratio

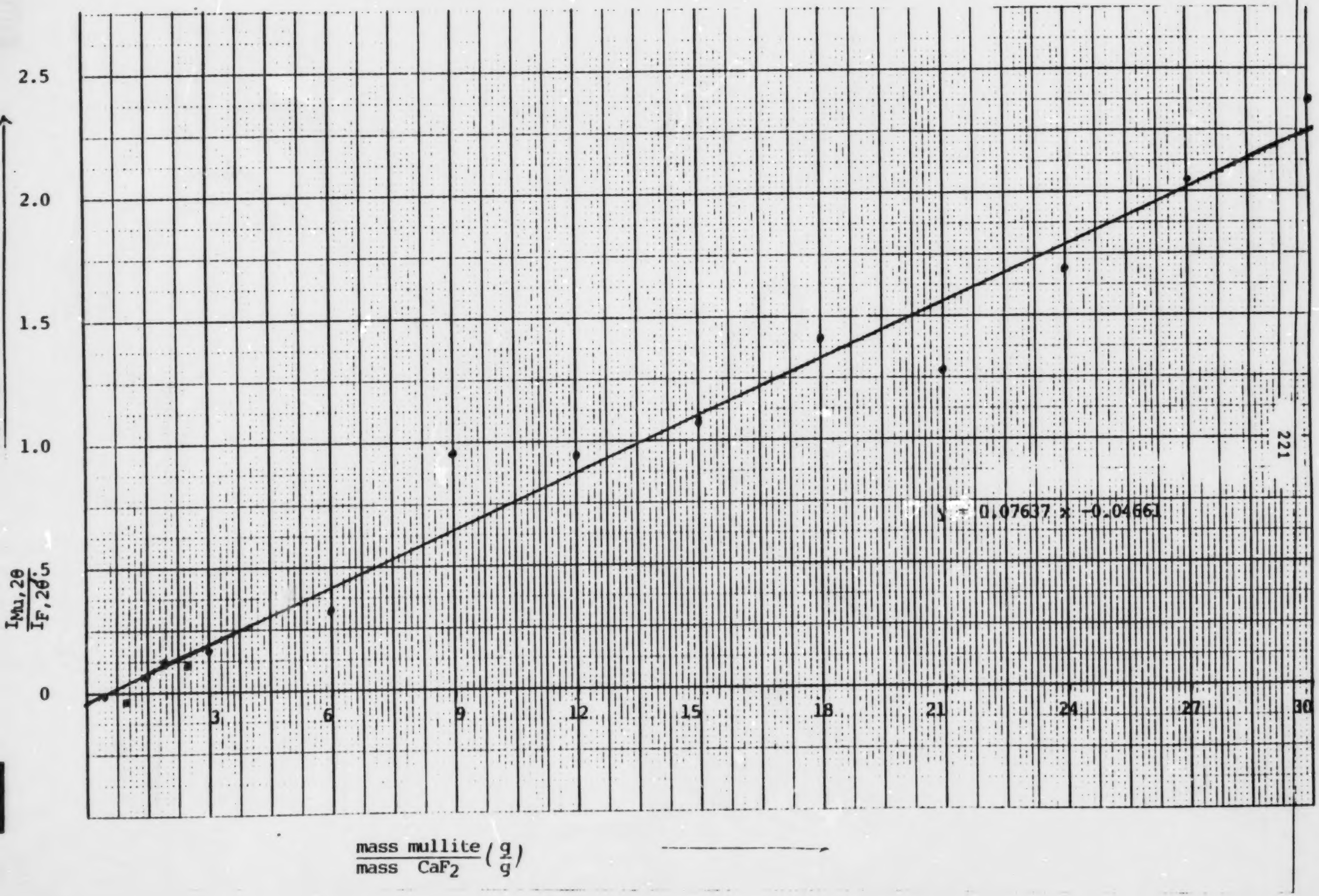

Figure 14g. Standard Curve for Mullite 2θ=60.6, 2θ'=47.0 Low Mass Ratio

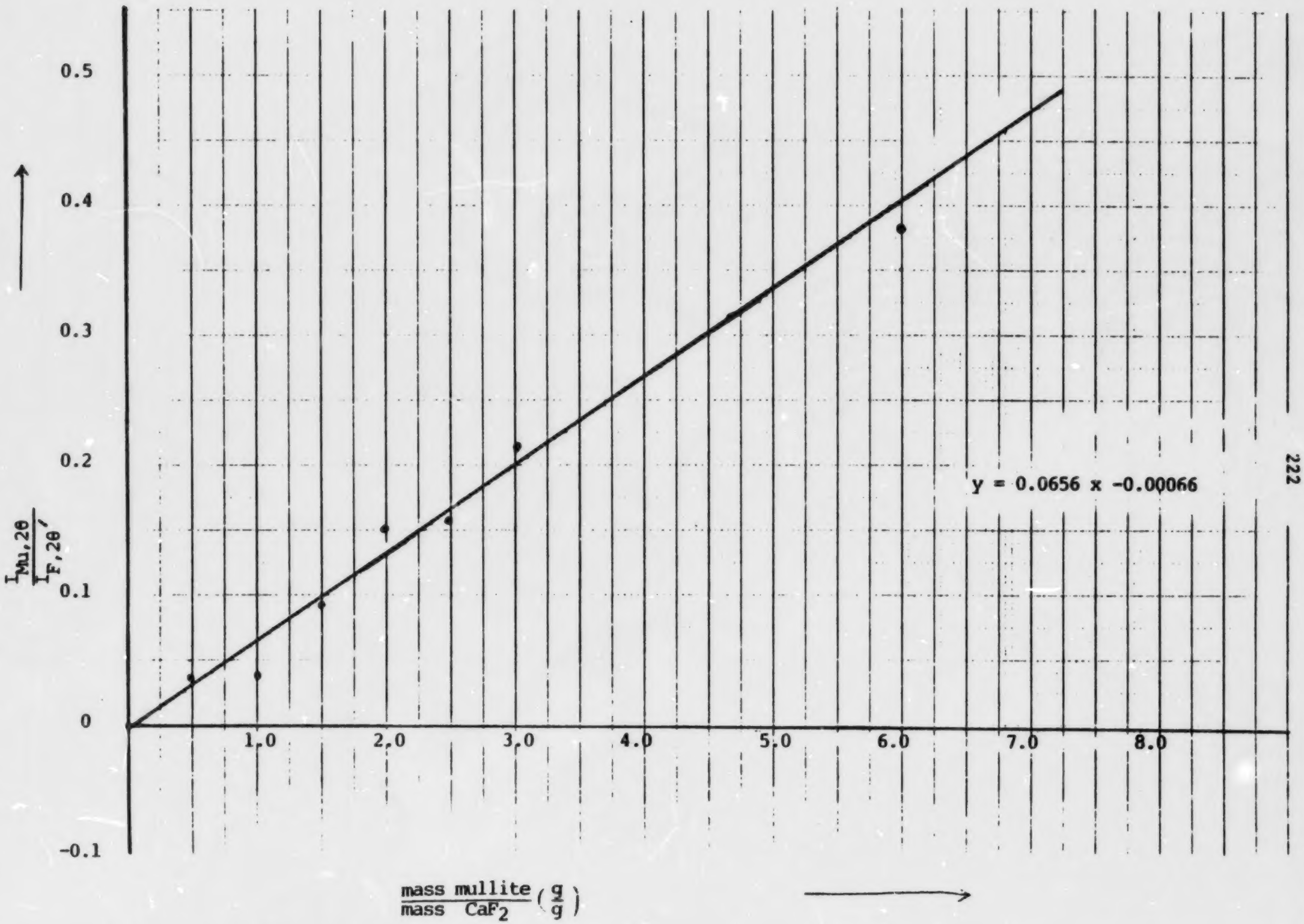

Figure 14h. Standard Curve for Mullite 2θ=60.6, 2θ'=47.0 High Mass Ratio

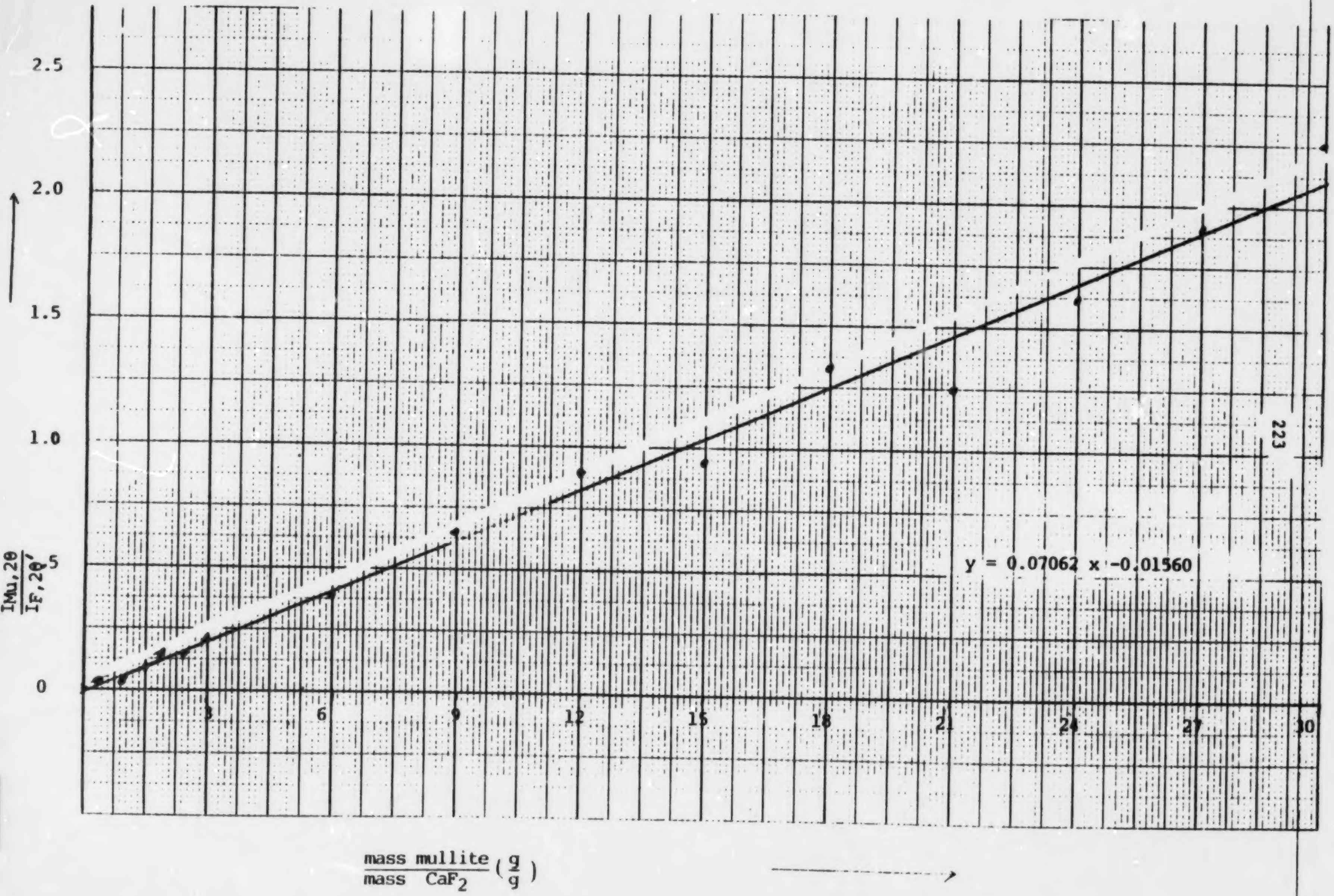

Figure 15a. Standard Curve for Magnetite 2θ=30.1, 2θ'=28.3

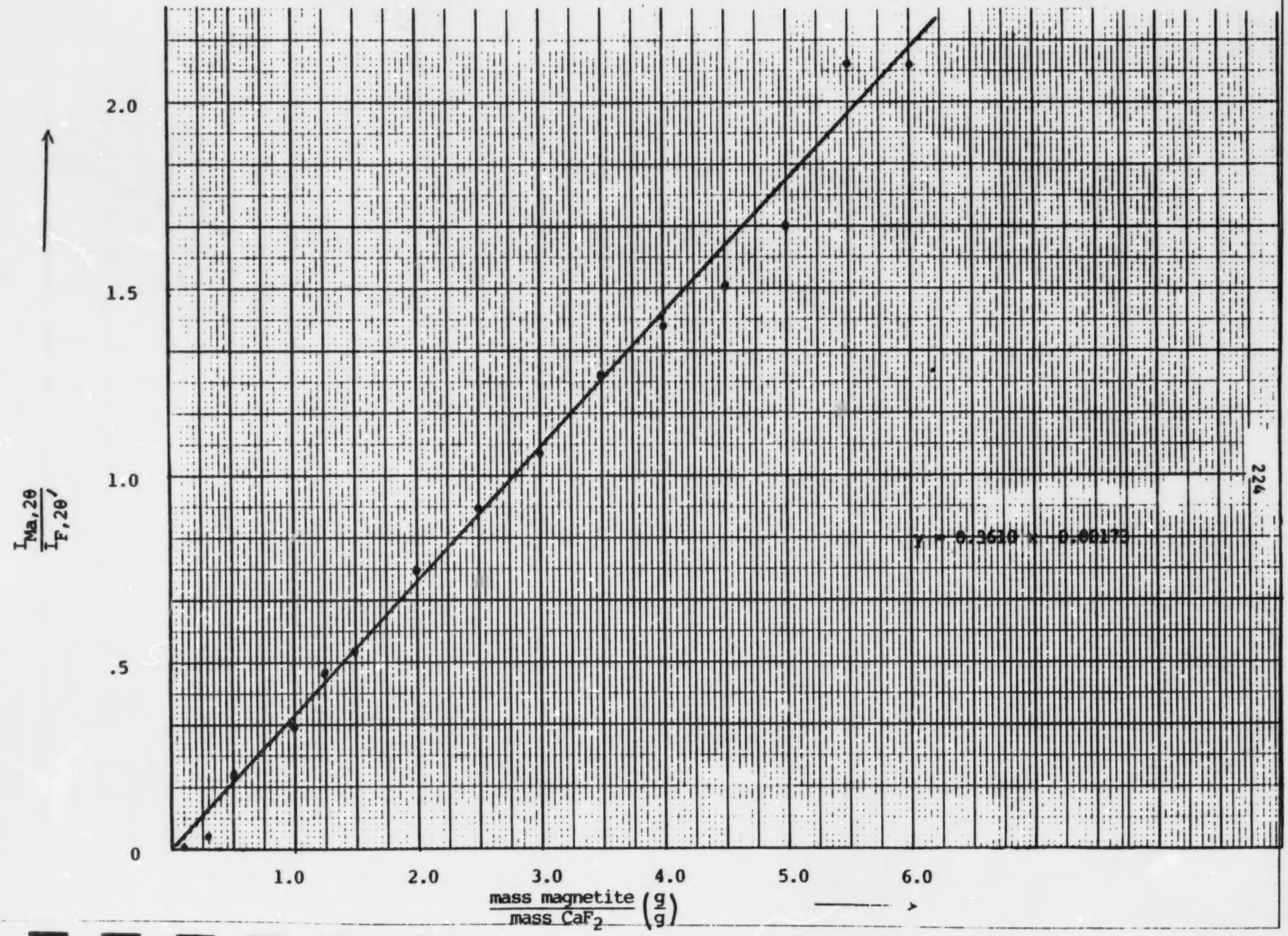

Figure 15b. Standard Curve for Magnetite $2\theta=43.0$, $2\theta'=28.3$

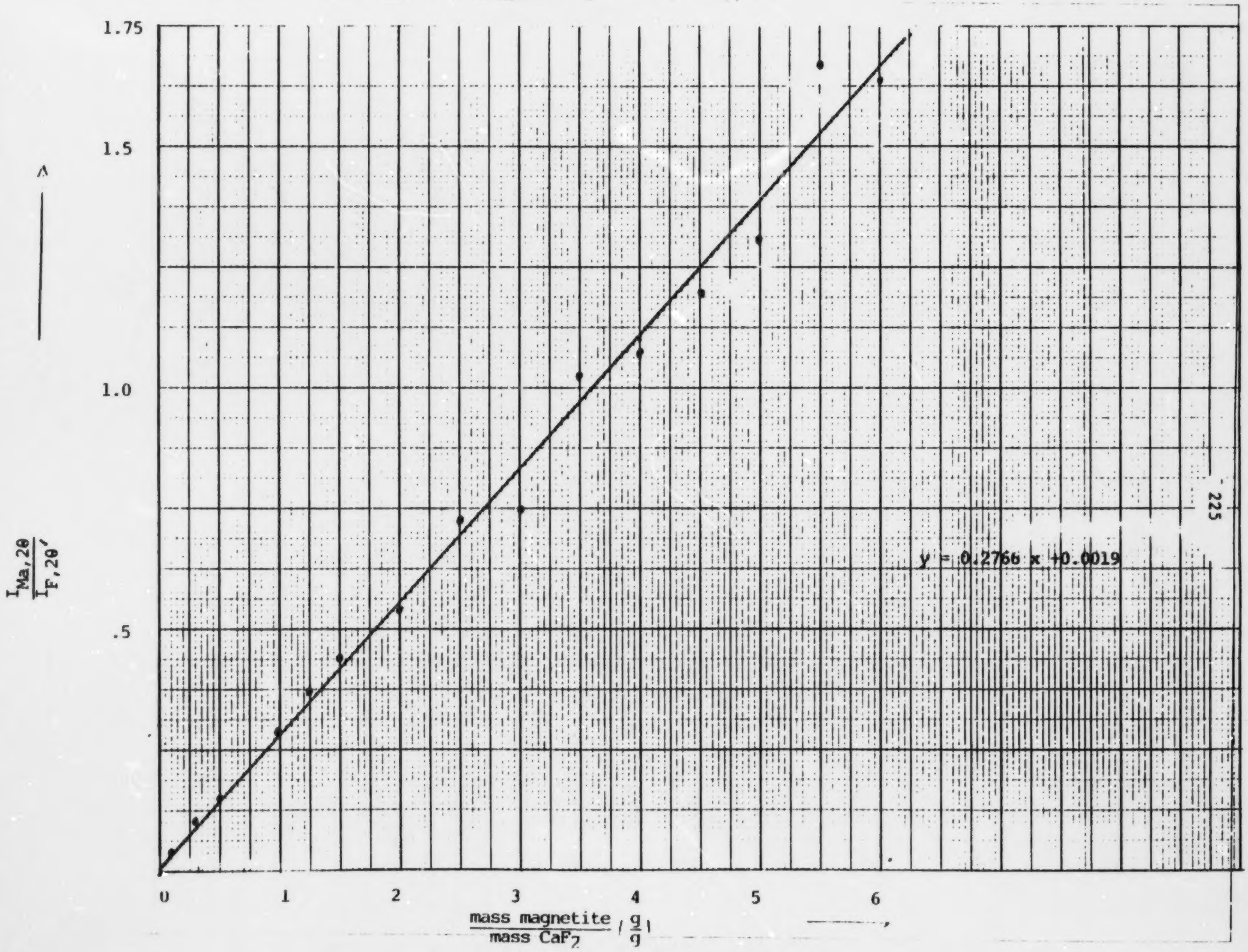

Figure 15c. Standard Curve for Magnetite 2θ=62.5, 2θ'=28.3

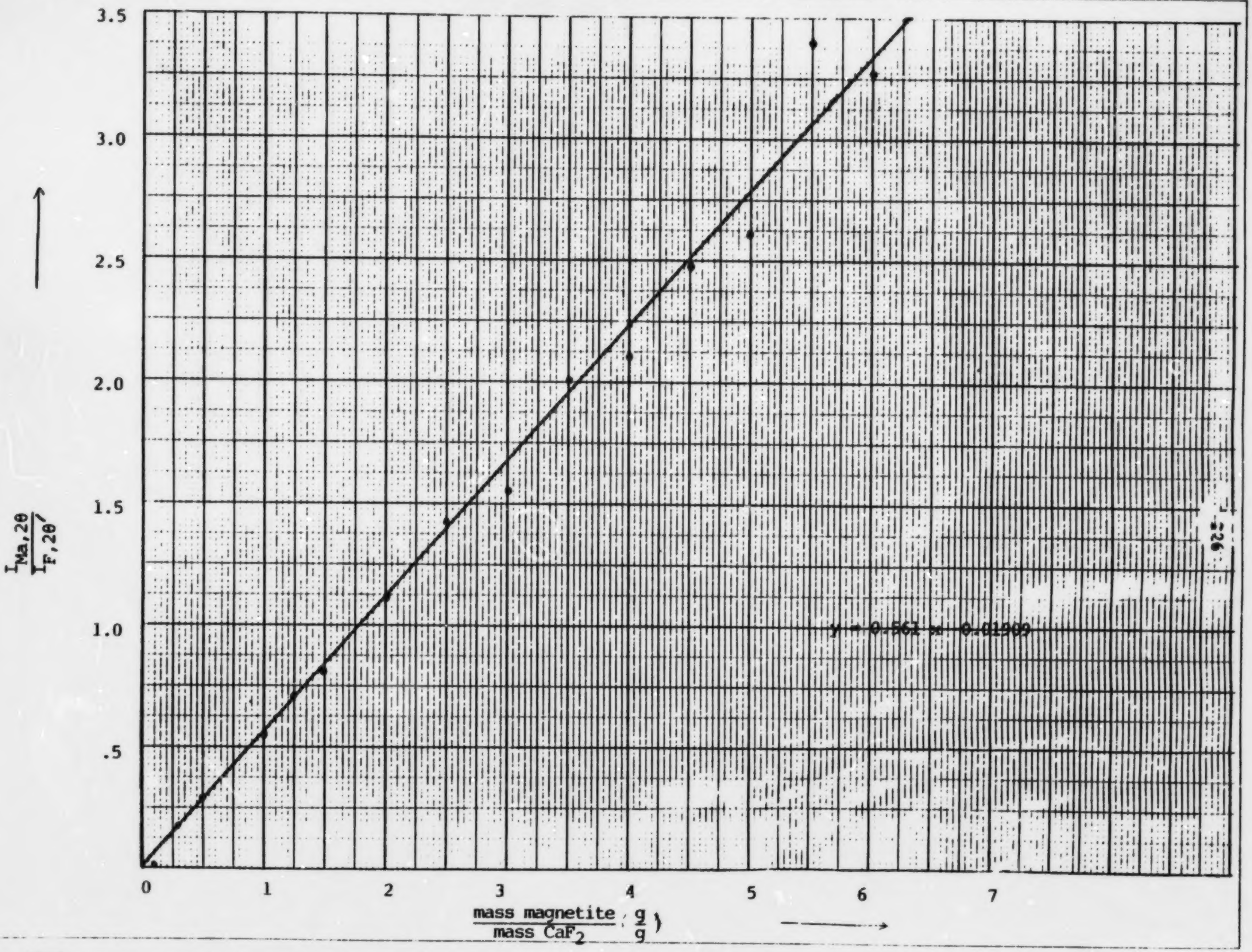

Figure 15d. Standard Curve for Magnetite 2θ=30.1, 2θ'=47.0

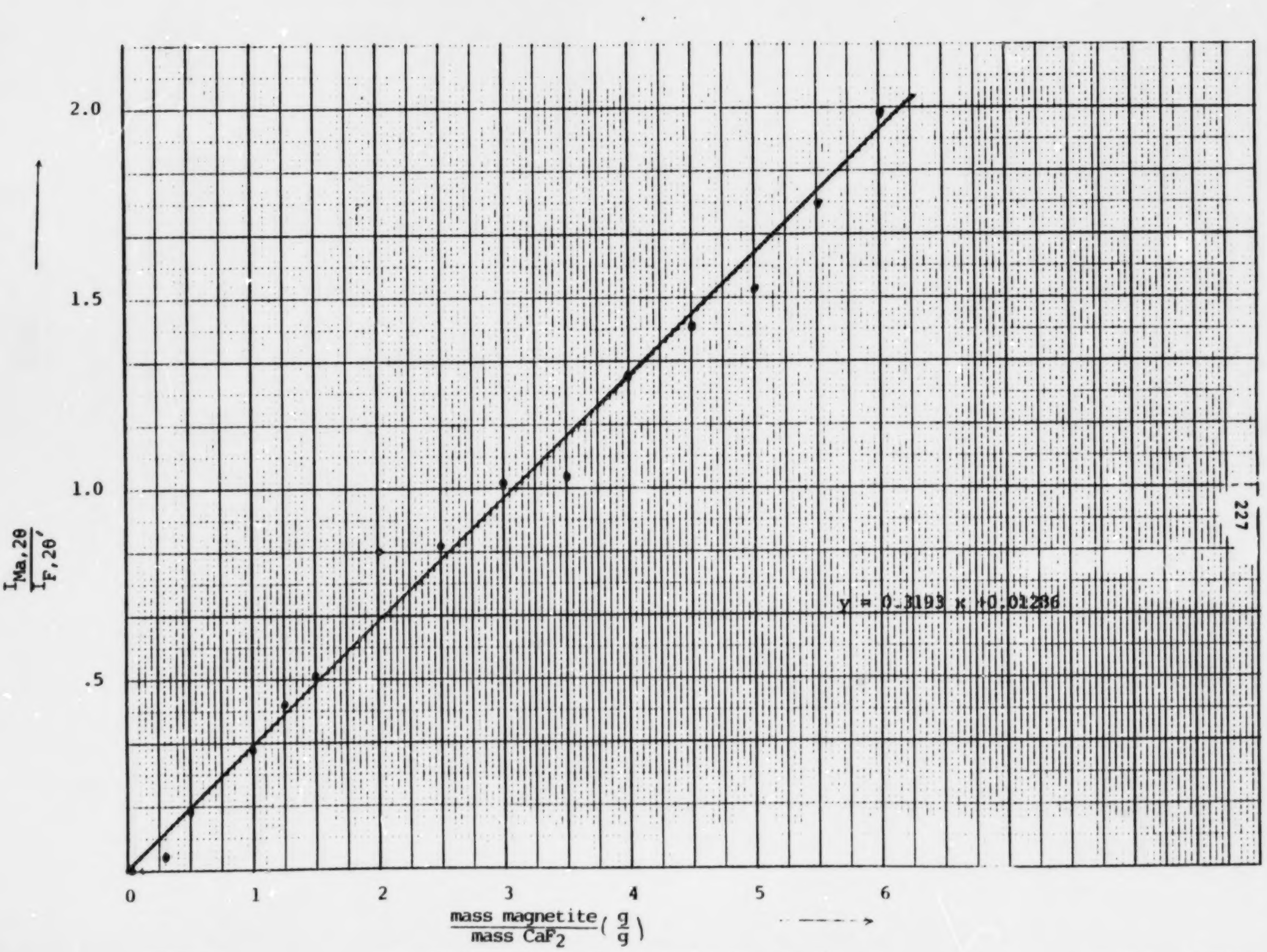

Figure 15e. Standard Curve for Magnetite 2θ=43.0, 2θ'=47.0

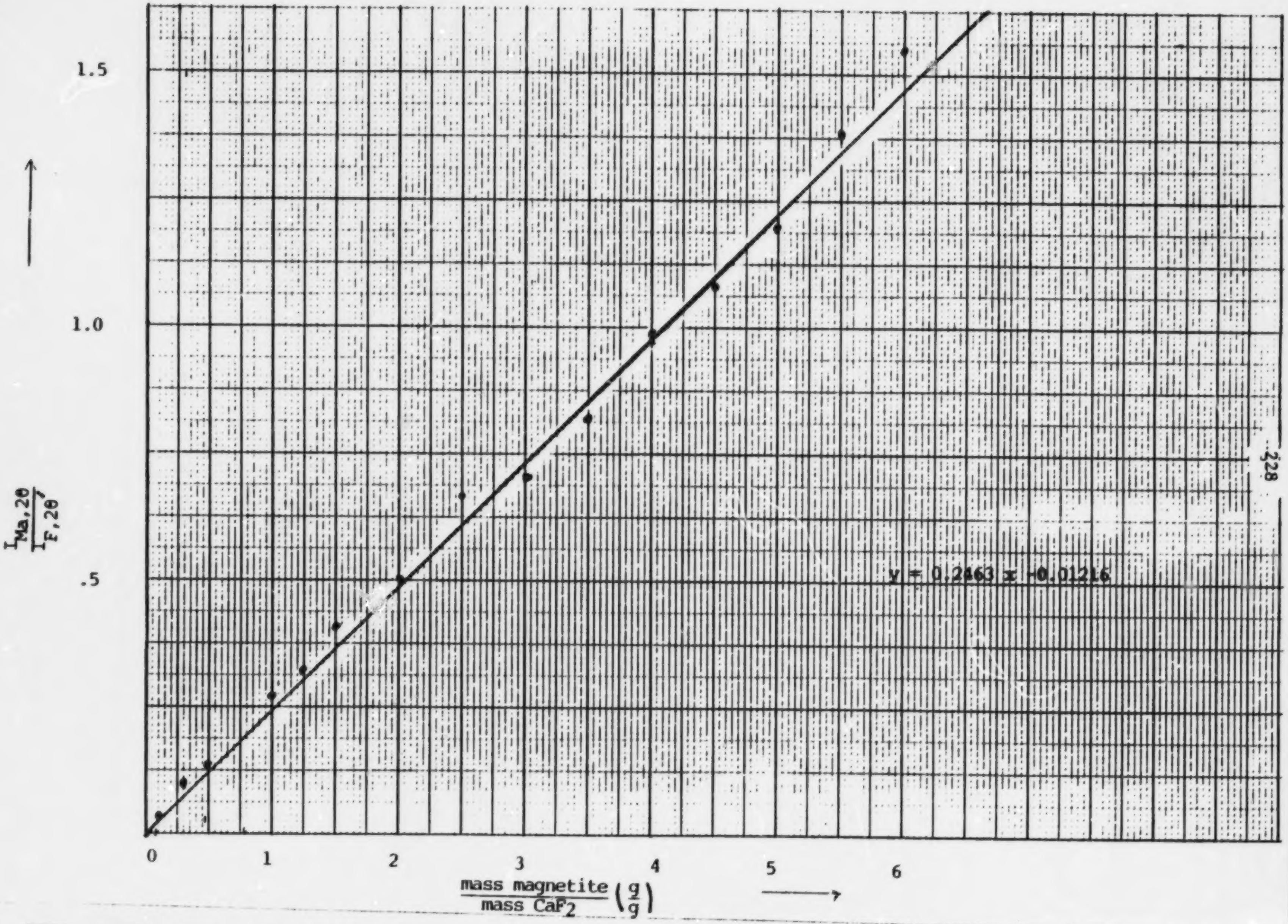

Figure 15f. Standard Curve for Magnetite 2θ=62.5, 2θ'=47.0

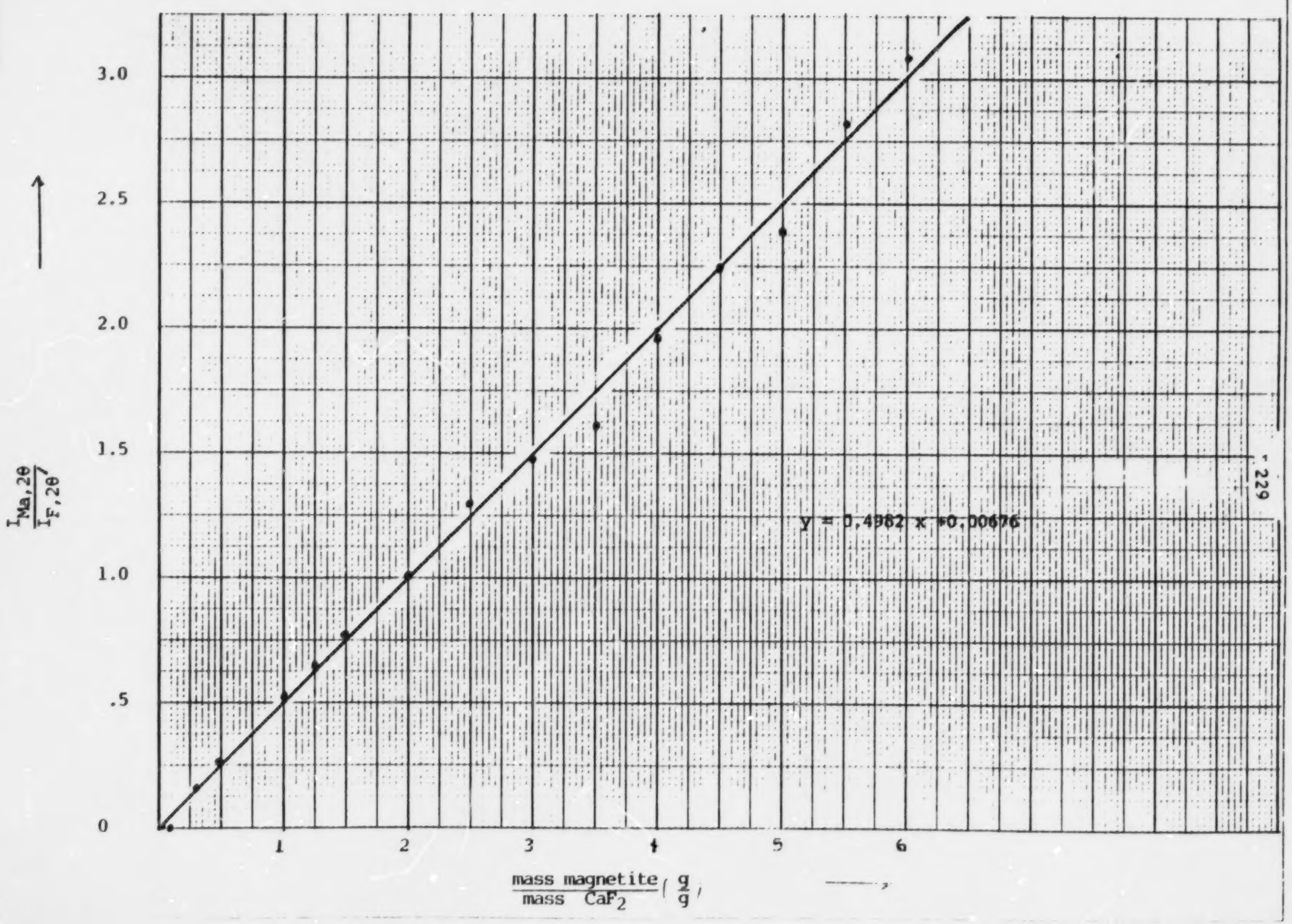

Figure 16a. Standard Curve for Hematite 2θ=24.1, 2θ'=28.3

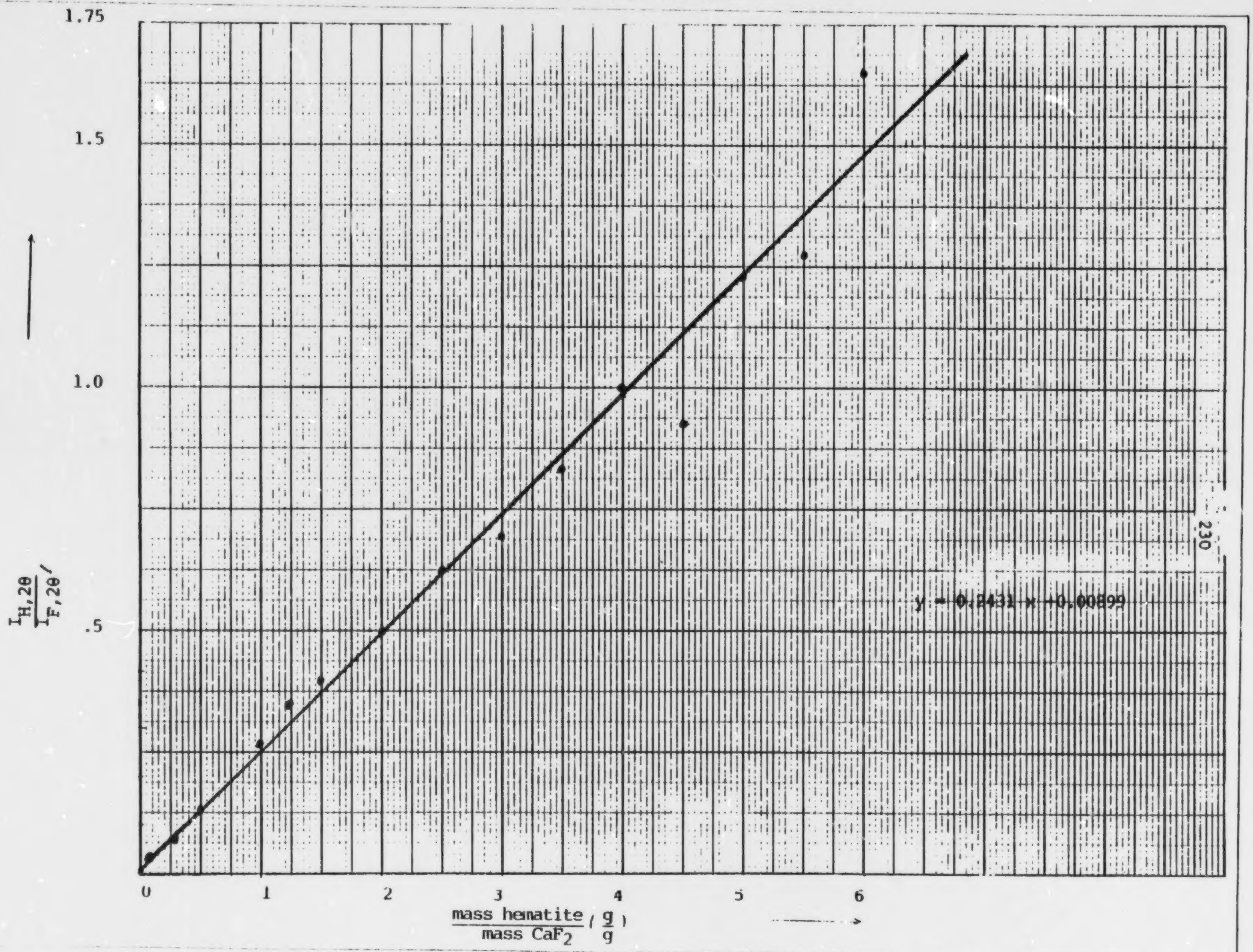

Figure 16b. Standard Curve for Hematite $2\theta=49.4$, $2\theta'=28.3$

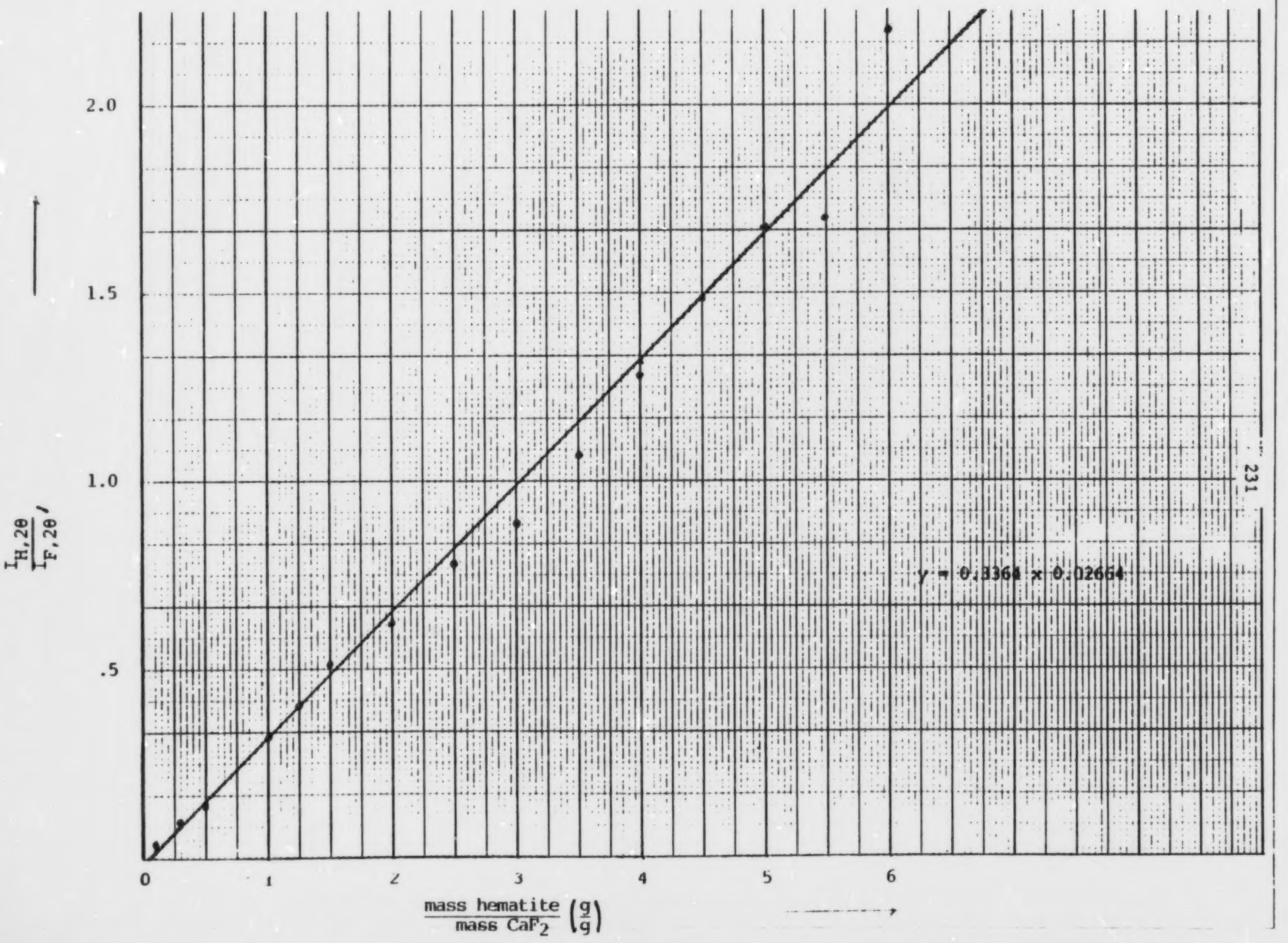

Figure 16c. Standard Curve for Hematite 2θ=63.9, 2θ'=28.3

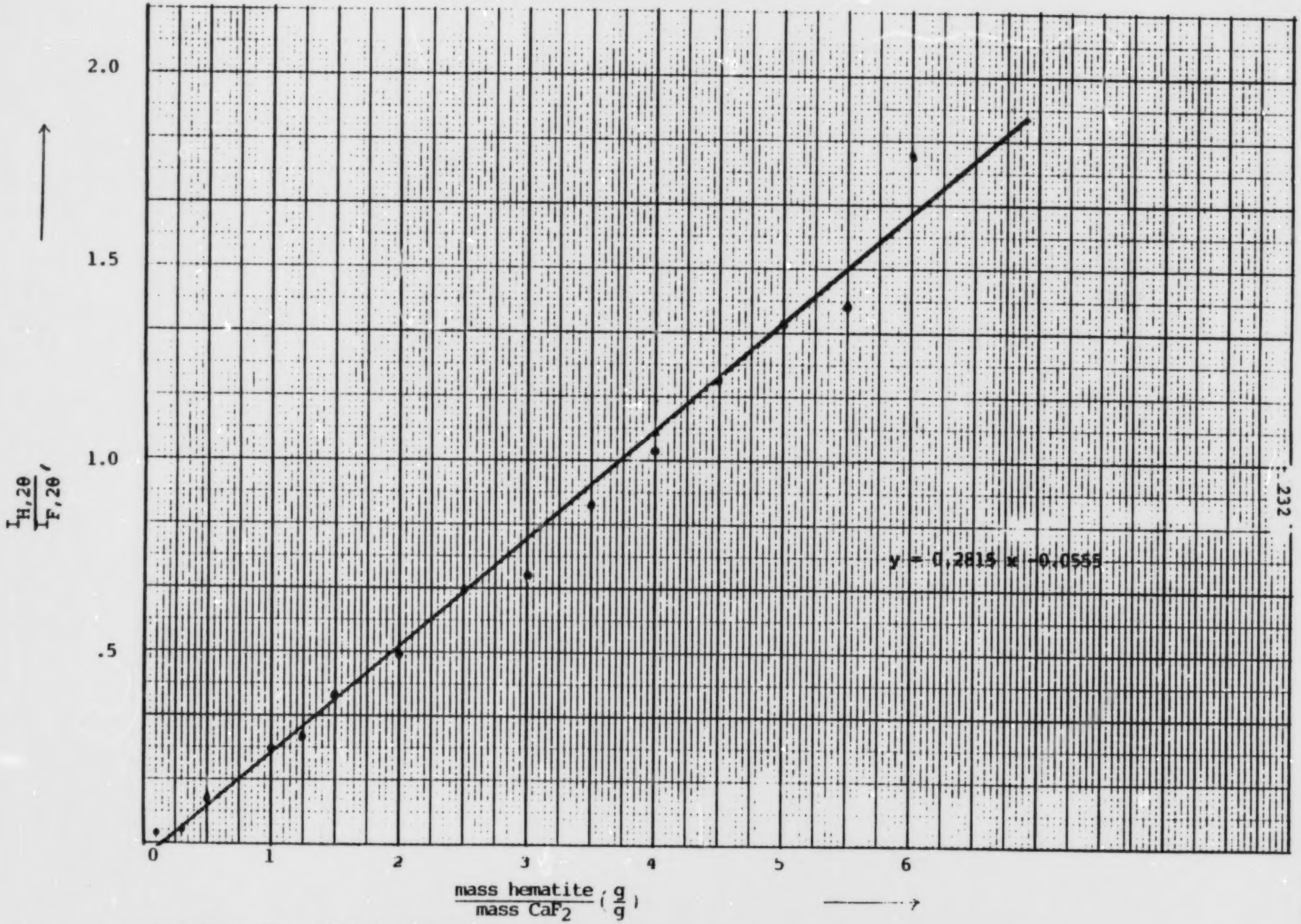

ORF

Figure 16d. Standard Curve for Hematite 2θ=24.1, 2θ'=47.0

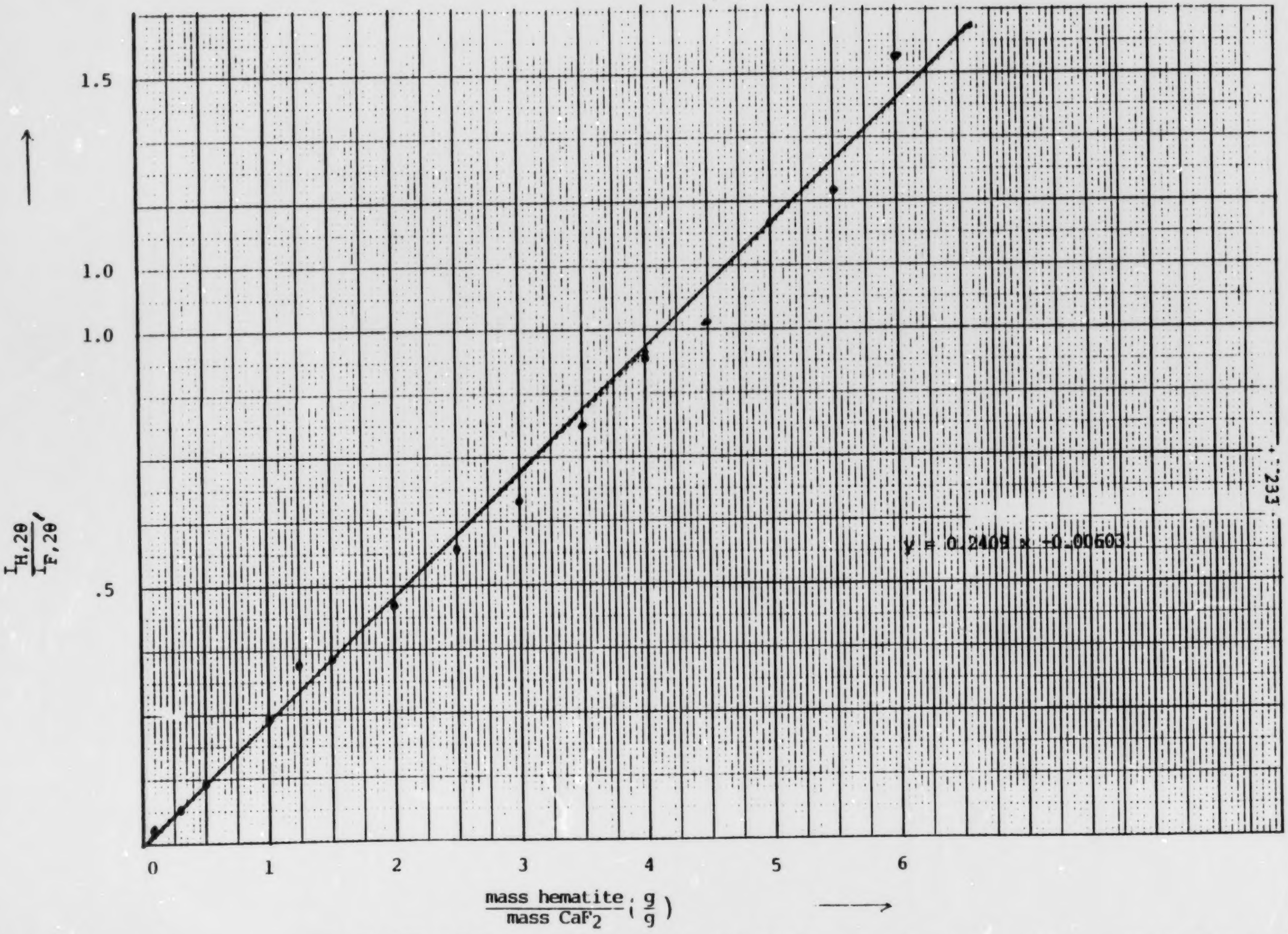

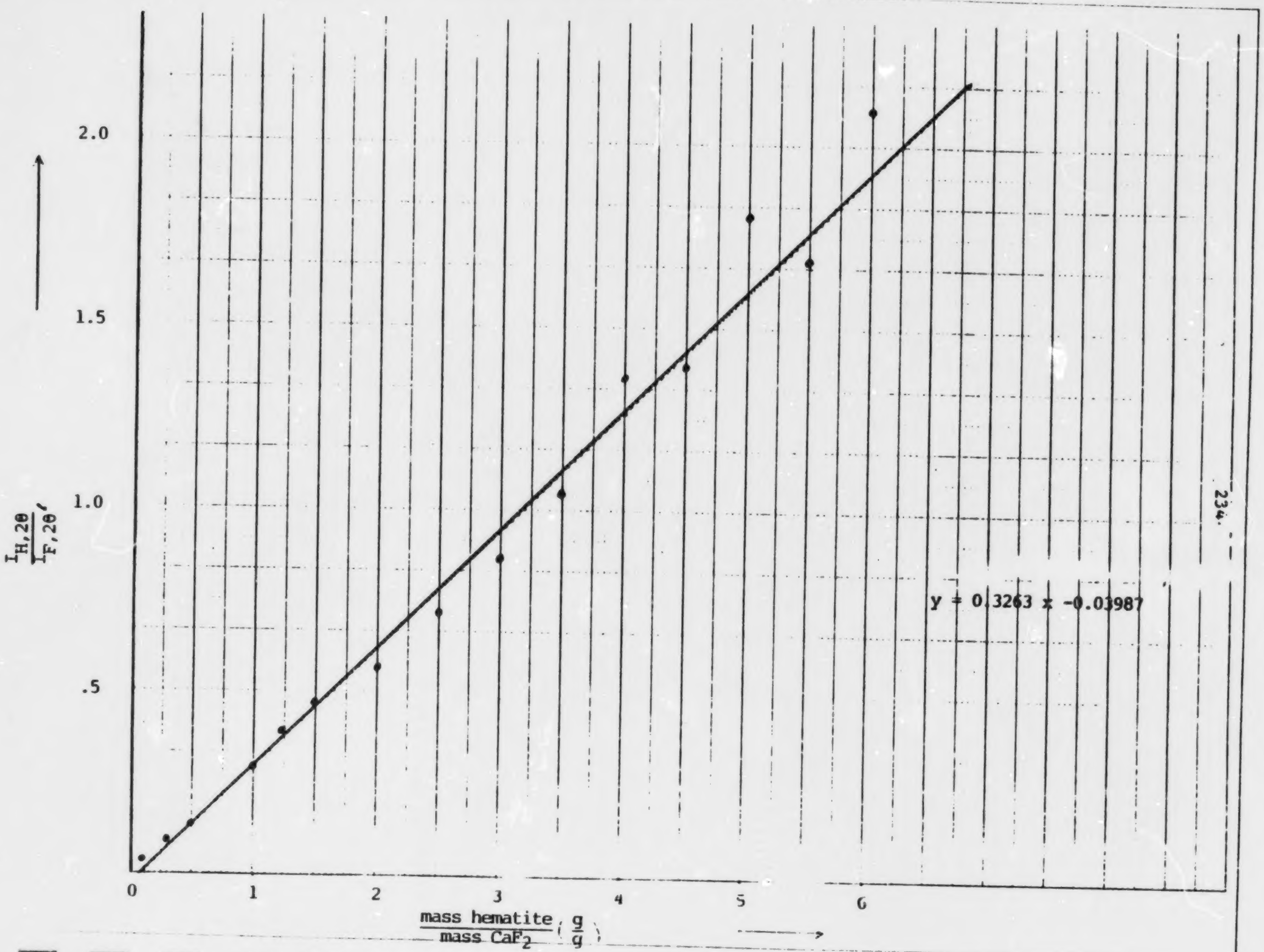

Figure 16e. Standard Curve for Hematite 2θ=49.4, 2θ'=28.3

Figure 16f. Standard Curve for Hematite 2θ=63.9, 2θ'=47.0

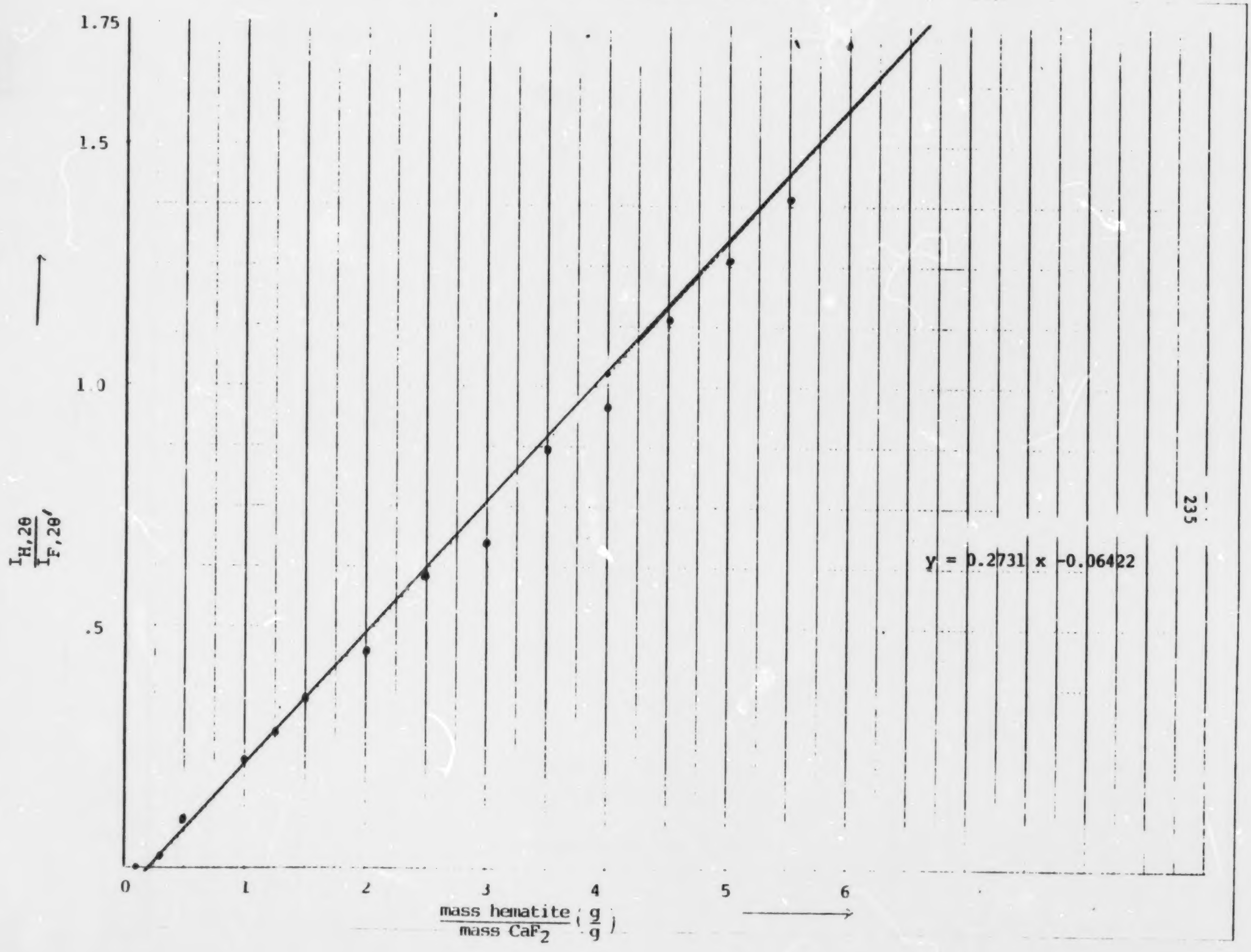

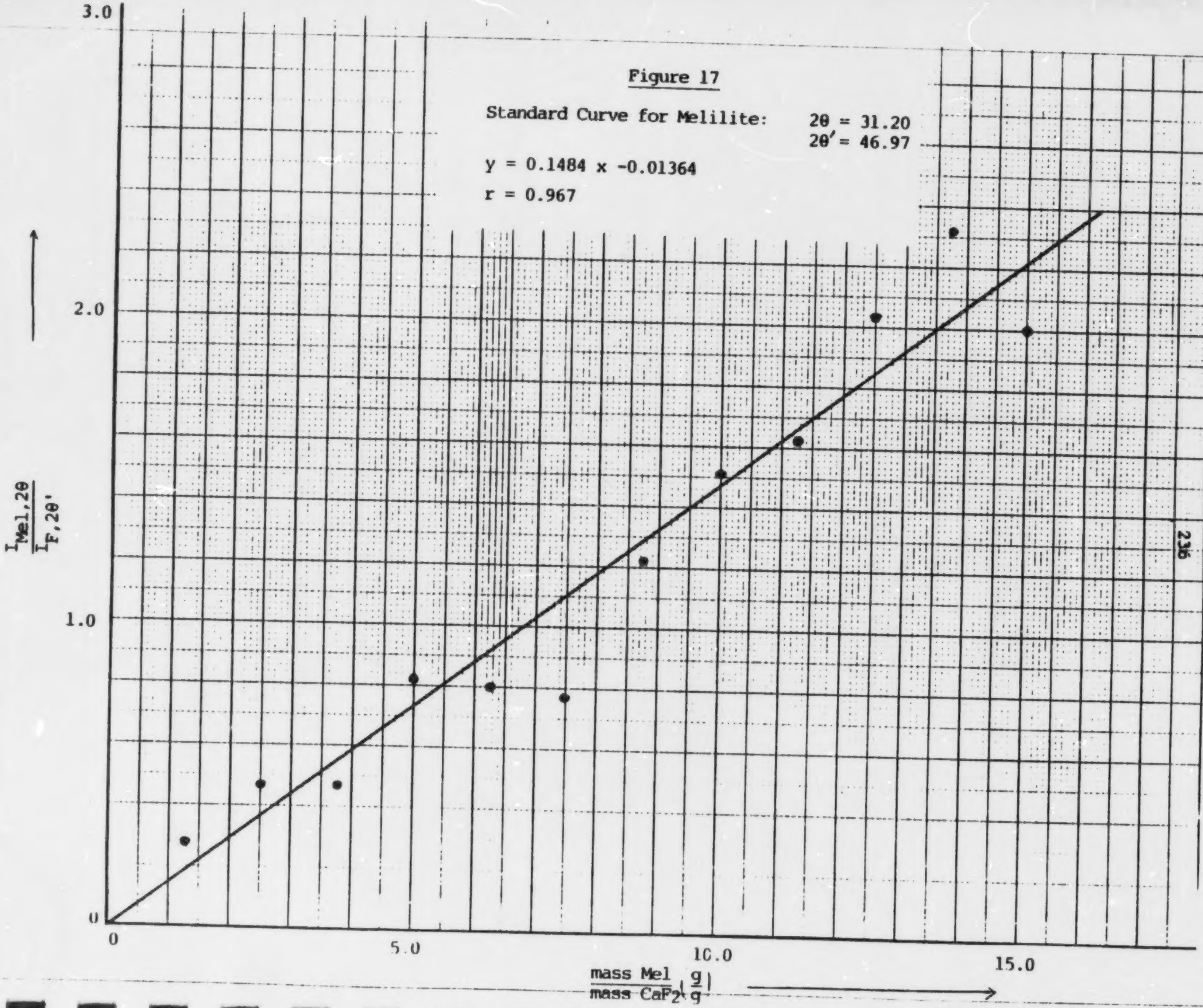

Figure 17

Standard Curve for Melilite:

$2\theta = 31.20$
$2\theta' = 46.97$

$y = 0.1484\ x - 0.01364$
$r = 0.967$

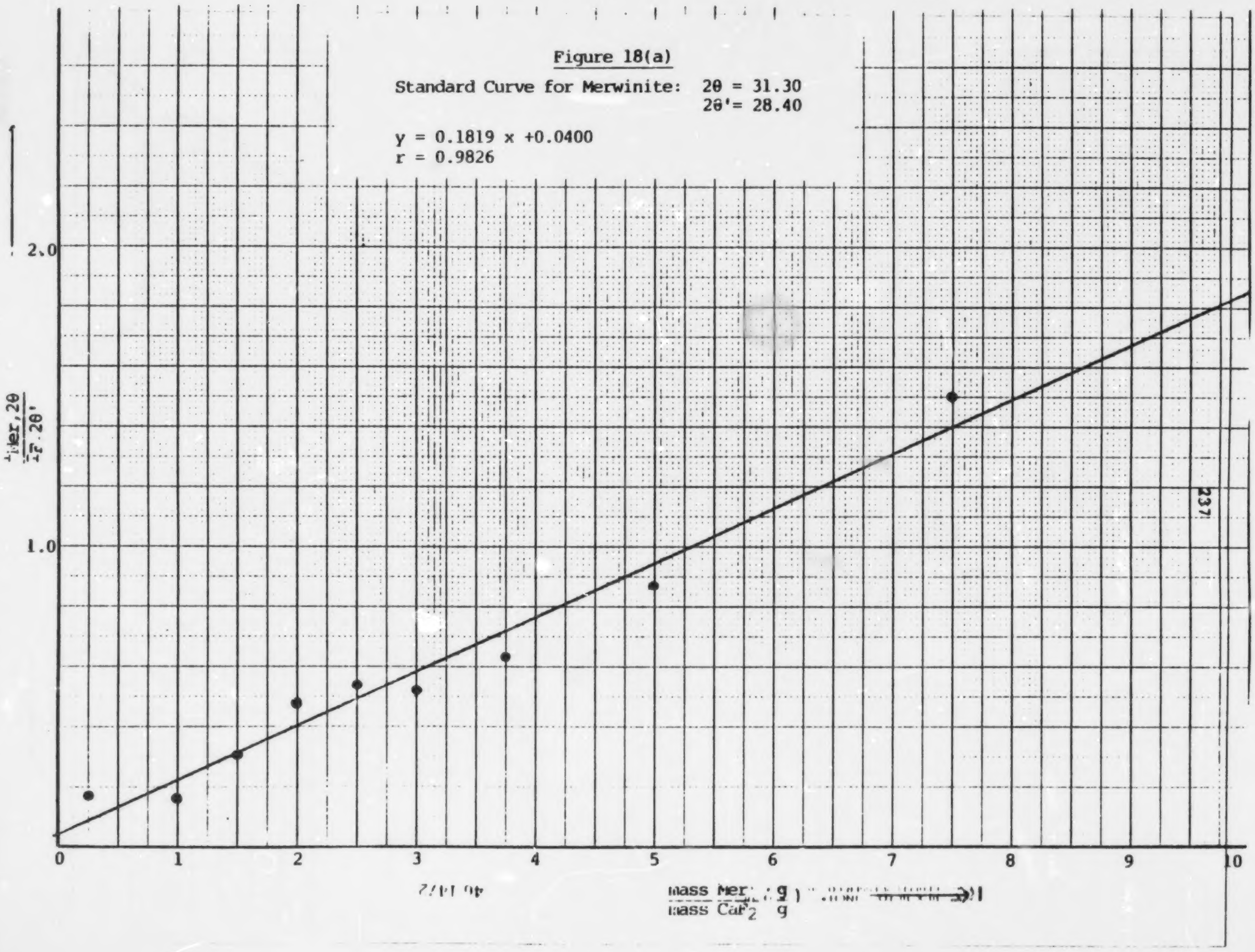

Figure 18(a)

Standard Curve for Merwinite: 2θ = 31.30
2θ'= 28.40

$y = 0.1819 x + 0.0400$
$r = 0.9826$

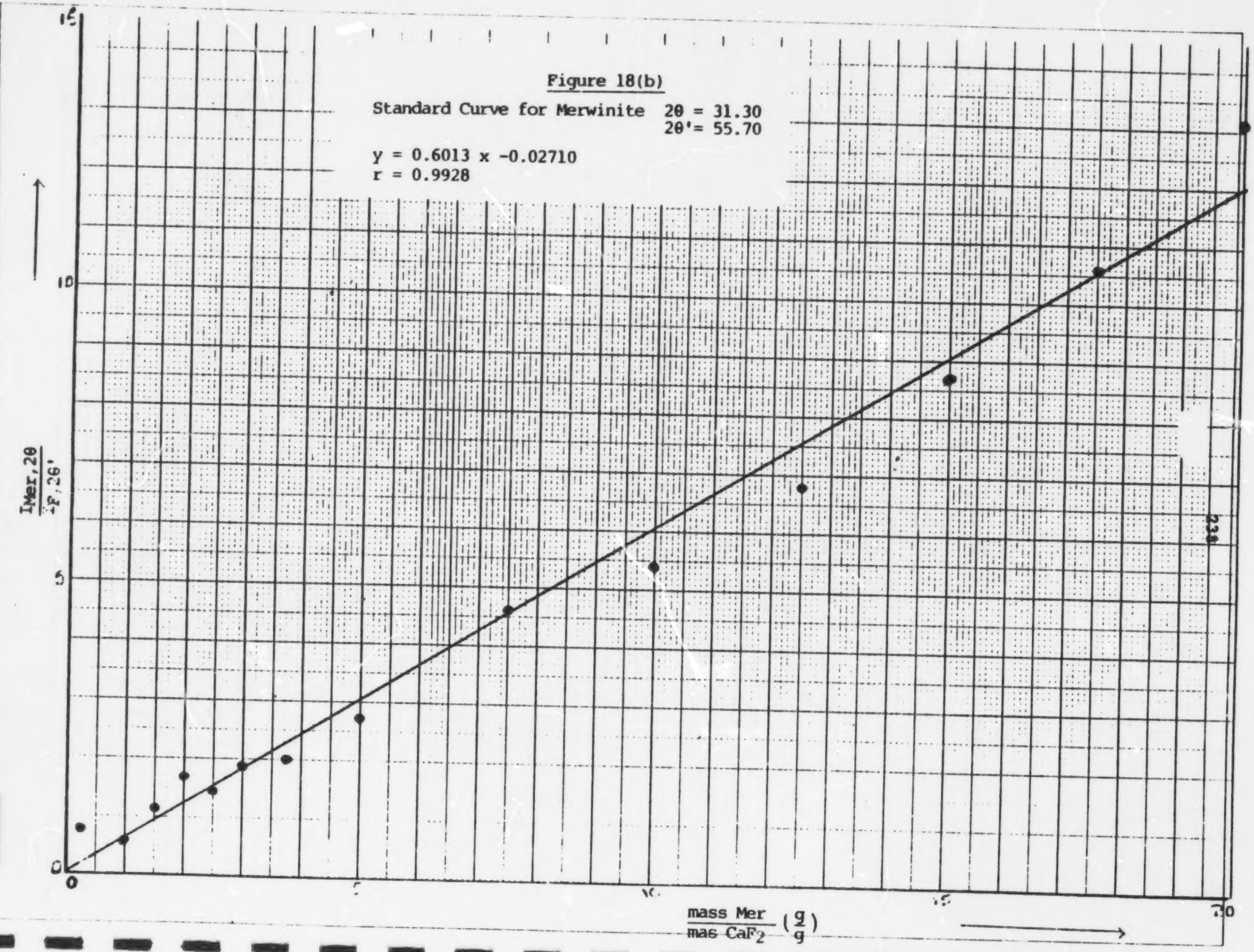

Figure 18(b)

Standard Curve for Merwinite $2\theta = 31.30$
$2\theta' = 55.70$

$y = 0.6013x - 0.02710$
$r = 0.9928$

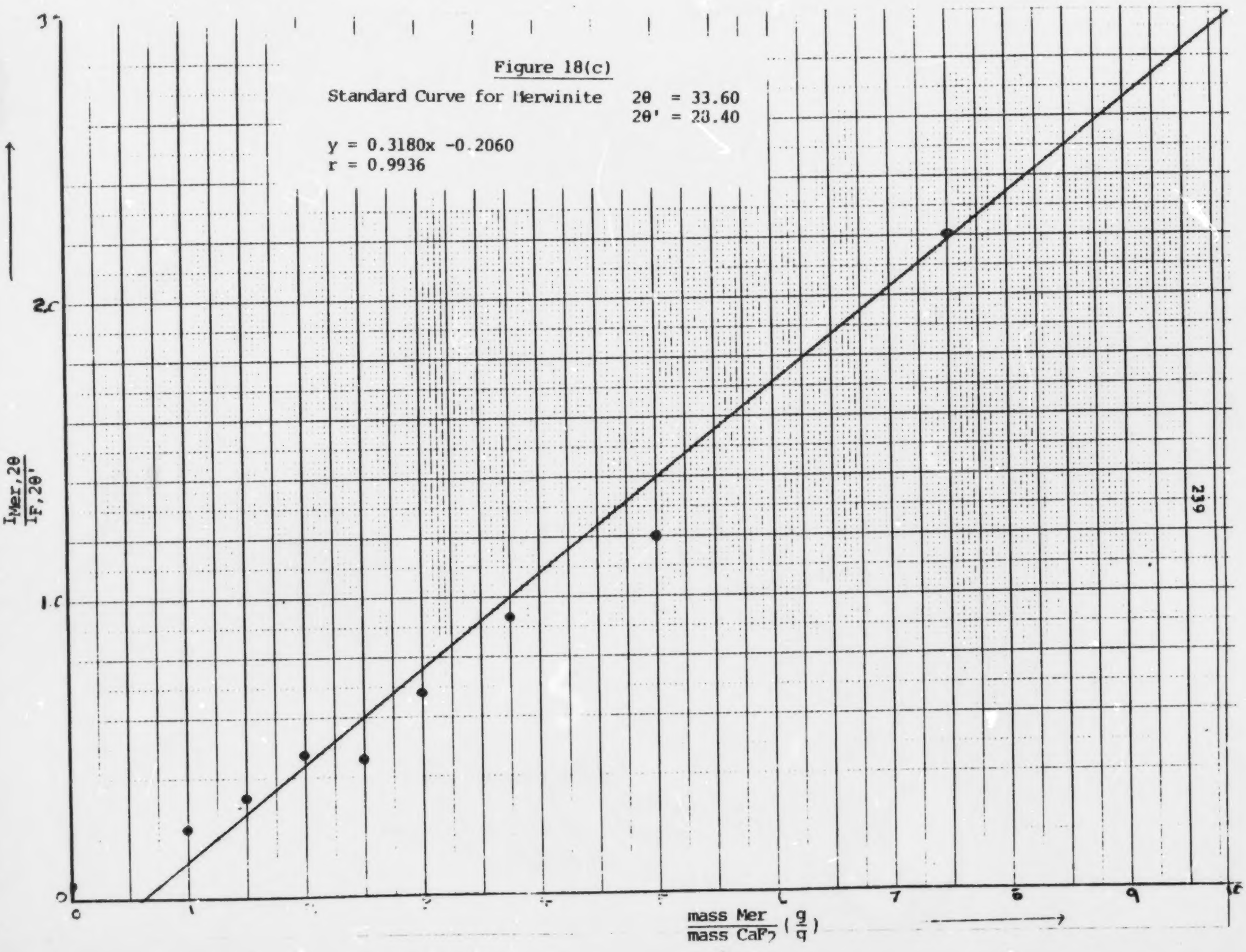

Figure 18(c)

Standard Curve for Merwinite 2θ = 33.60
2θ' = 28.40

$y = 0.3180x - 0.2060$
$r = 0.9936$

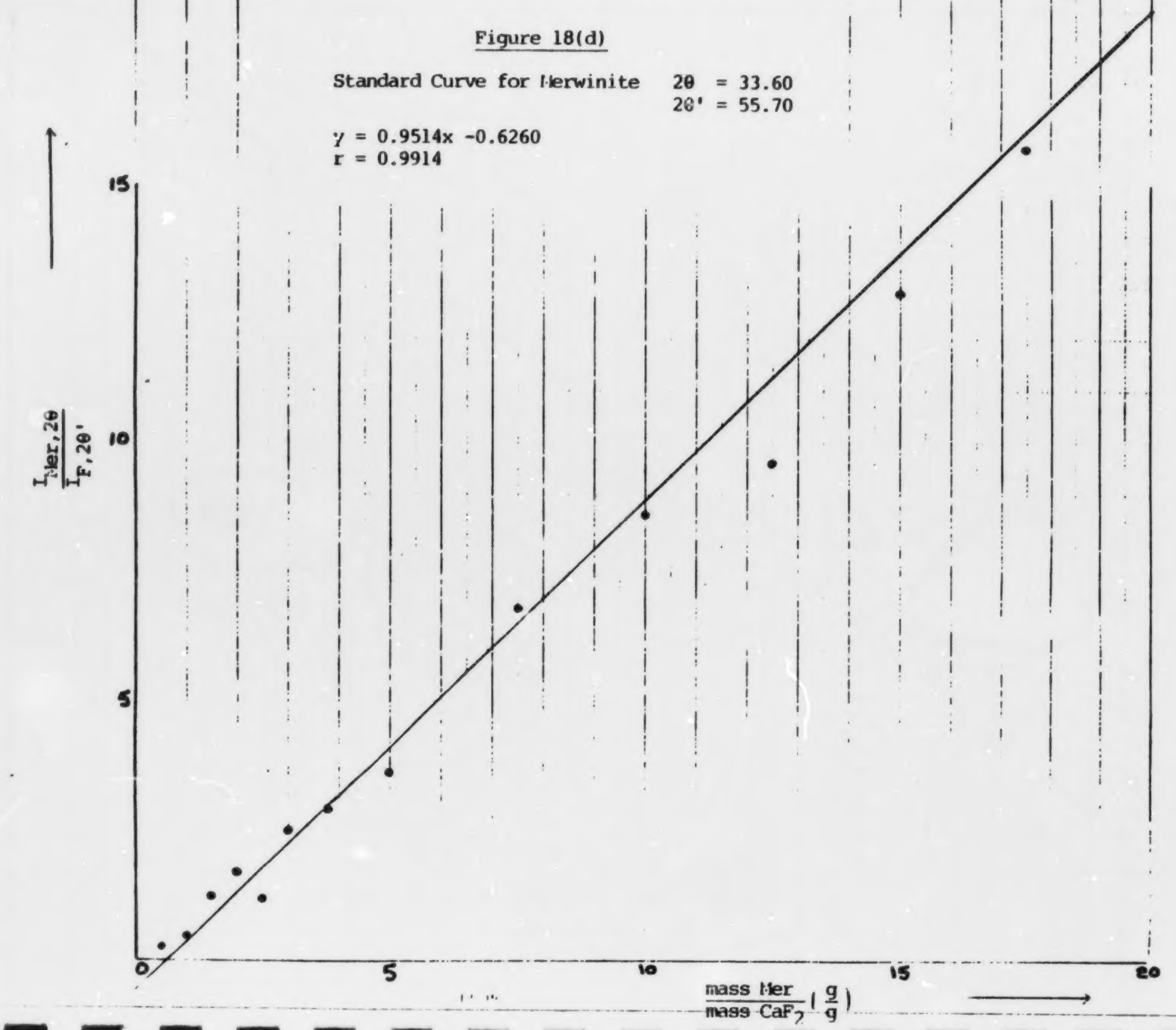

Figure 18(d)

Standard Curve for Merwinite

XRD Patterns for Cordierite glass-α-Cordierite Mixtures for Glass Content Determination (XRD Non-Crystalline Scattering Method)

(A) 100% glass (B)75% glass (C)50% glass (D)25% glass
(E) 0% glass

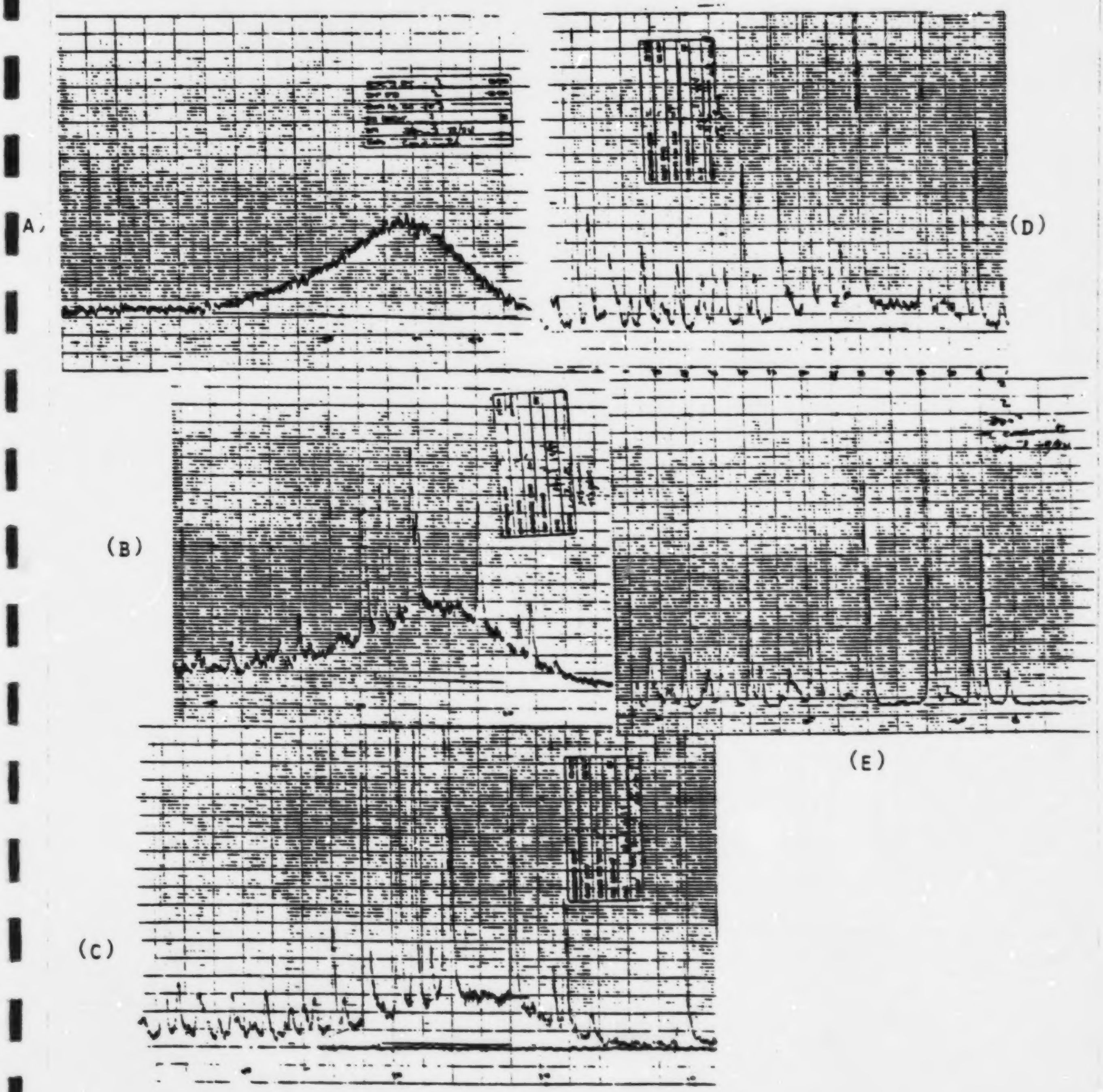

Figure 19

Intensity Ratio of Glassy Halo at 24° 2θ versus Glass Content for Cordierite Glass- α-Cordierite Mixtures

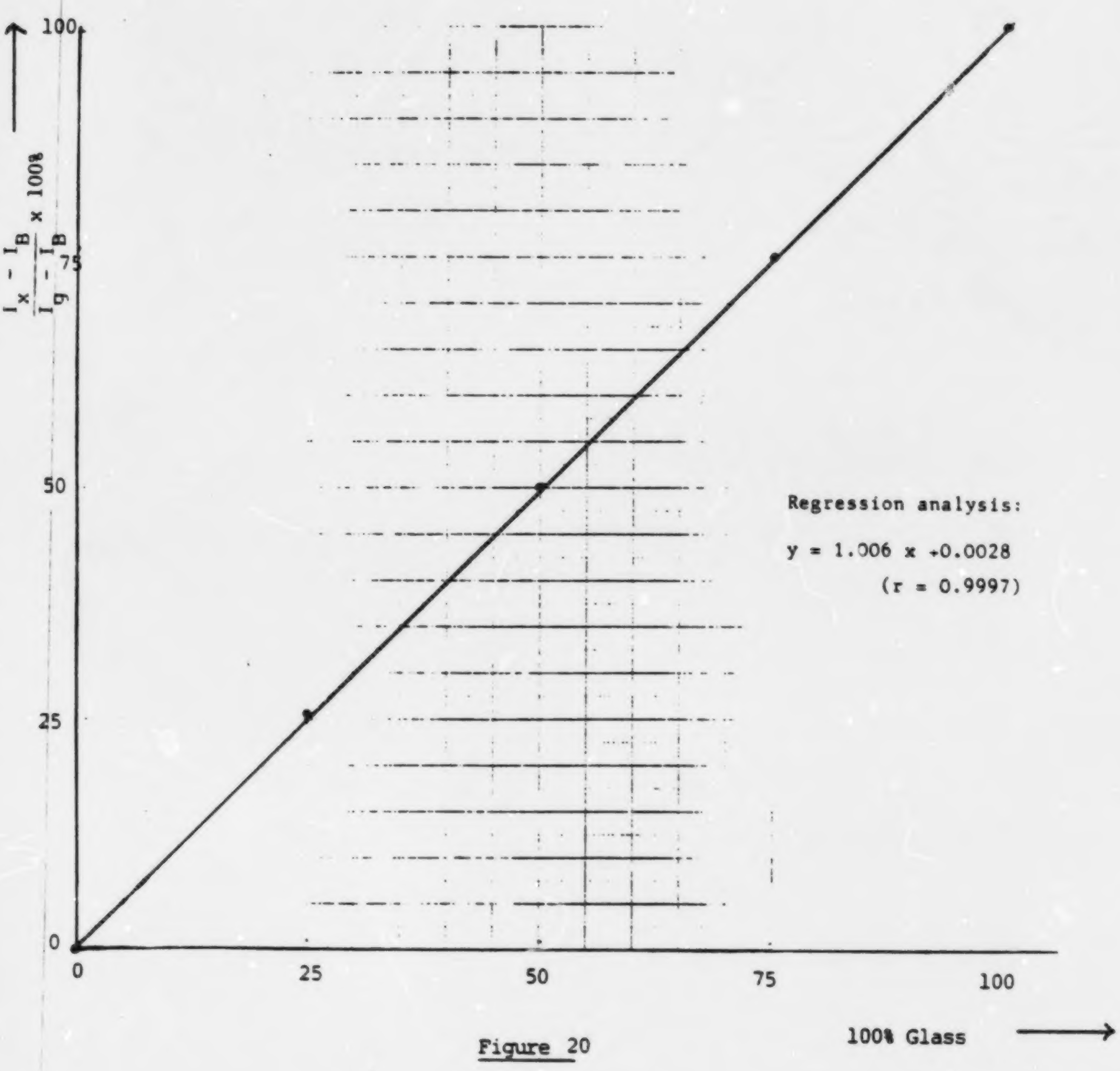

Regression analysis:

$y = 1.006\,x + 0.0028$

$(r = 0.9997)$

Figure 20

ORF

Figure 21 XRD Patterns of Mixtures of Vitrified and Redivitrified Forestburg Flyash

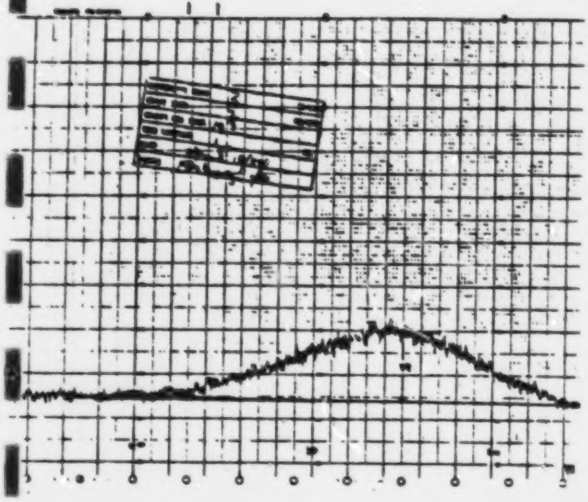

(a) 100% Glass

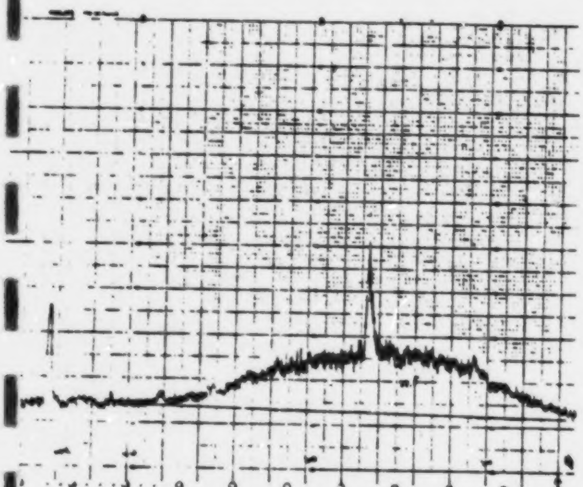

(b) Forestburg Flyash

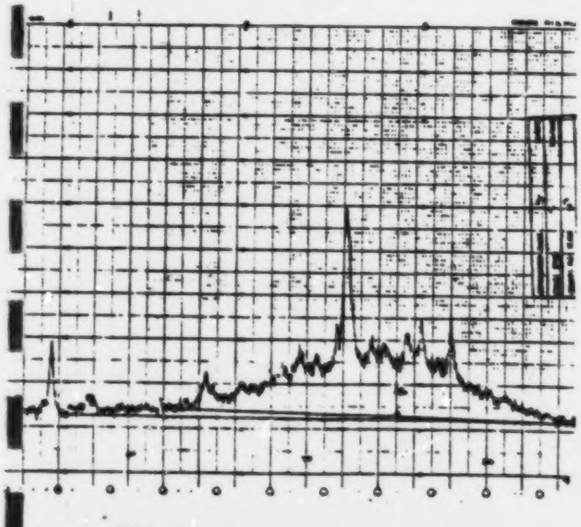

(c) 75% Glass

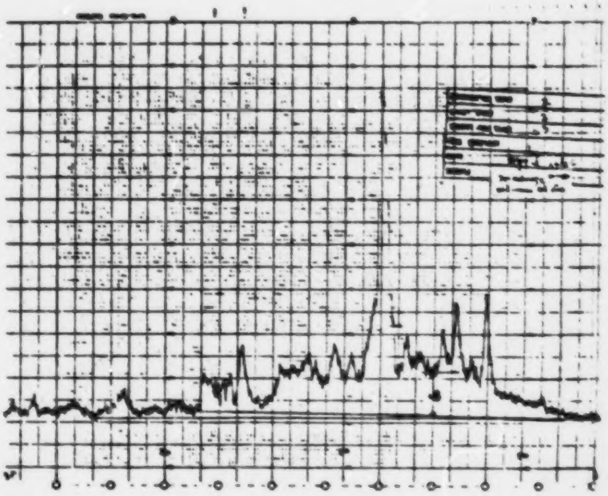

(d) 50% Glass

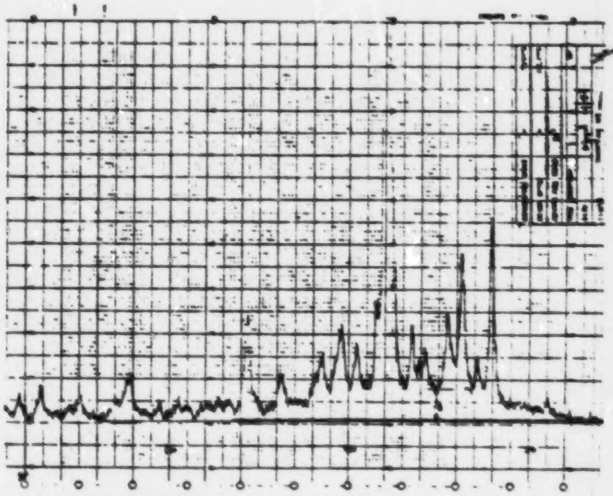

(e) 25% Glass

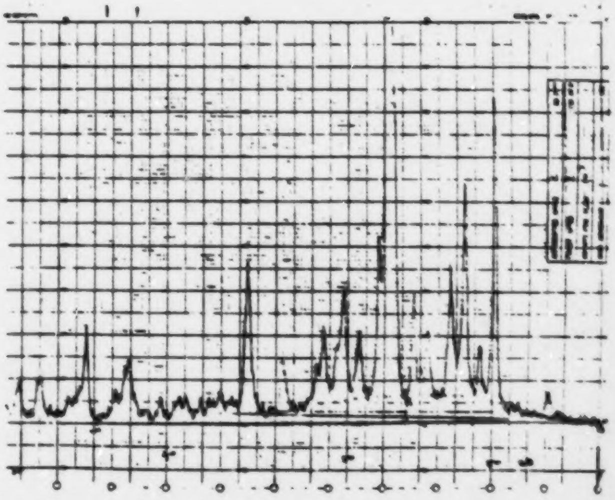

(f) 0% Glass

Intensity Ratio of Glassy Halo at 25° 2θ versus Glass Content for Forestburg Glass and Redevitrified Glass Mixtures

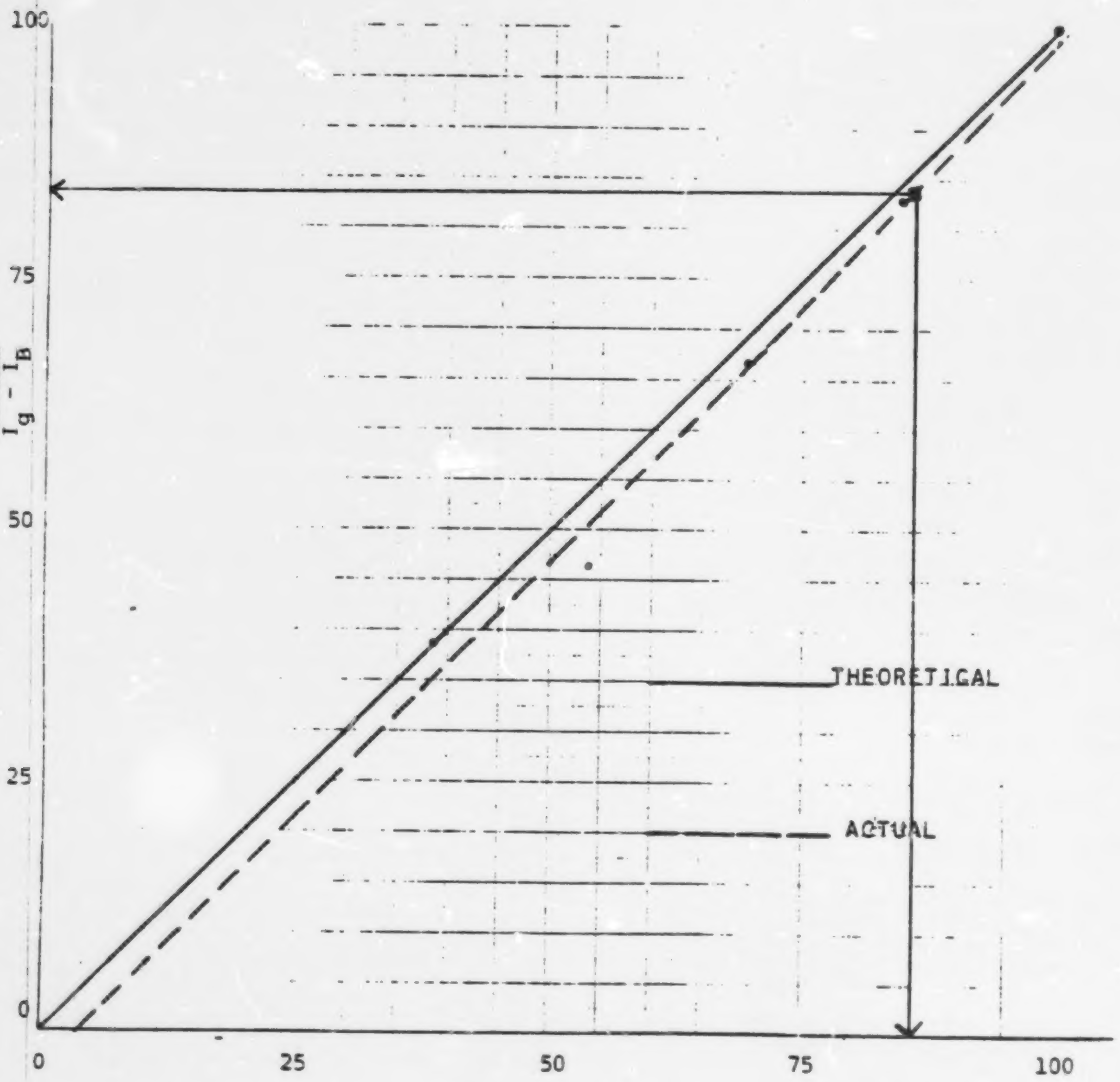

Figure 22

Figure 23 Scattering Intensity $\bar{I}_x - \bar{I}_o$ at $2\theta = 24^o$ vs. Glass Content for Cordierite Glass - Cordierite Mixtures.

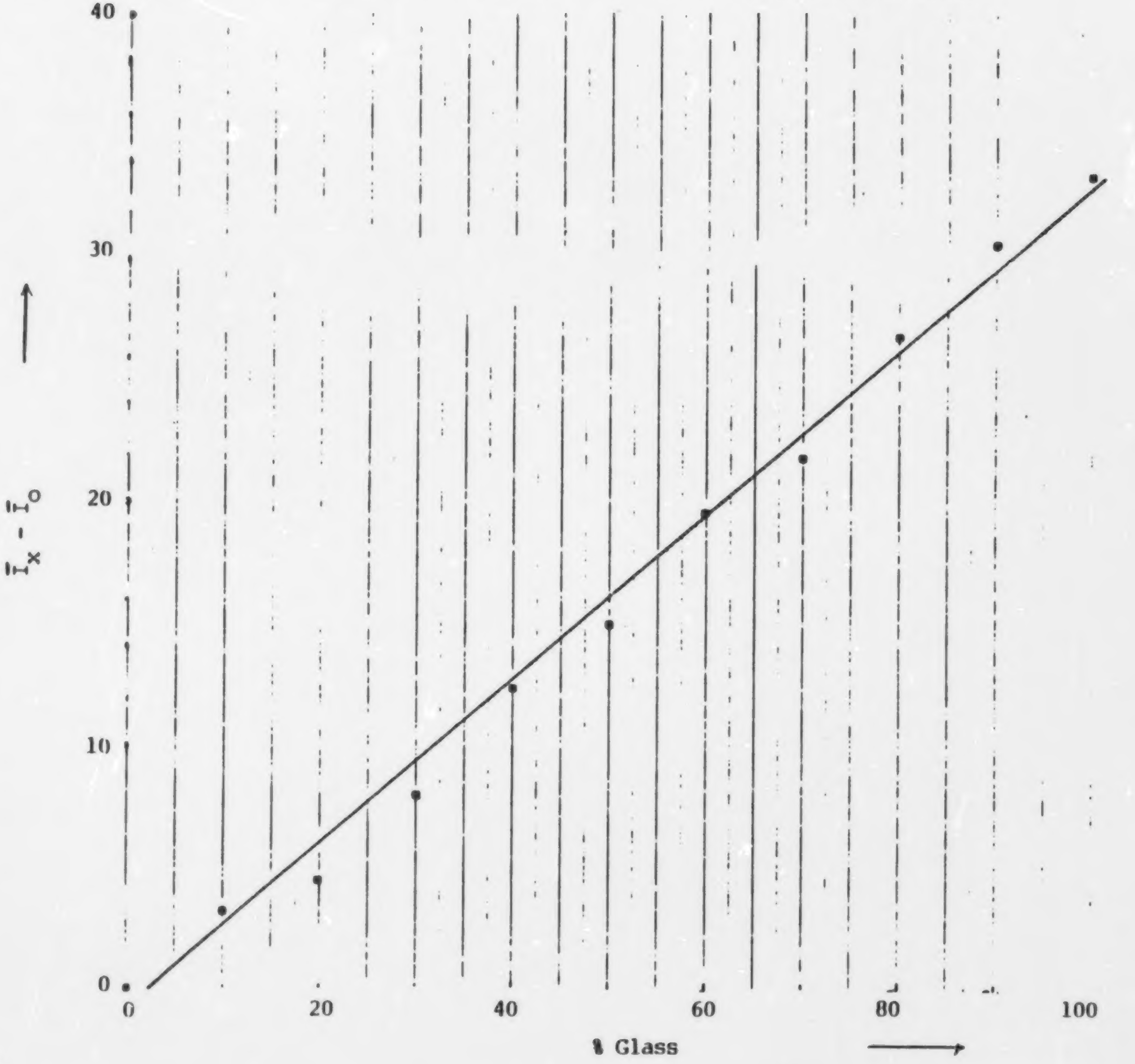

Figure 24 Scattering Intensity $\bar{I}_x-\bar{I}_o$ at $2\theta=25^o$ vs. Glass Content for Wabamun Fly Ash

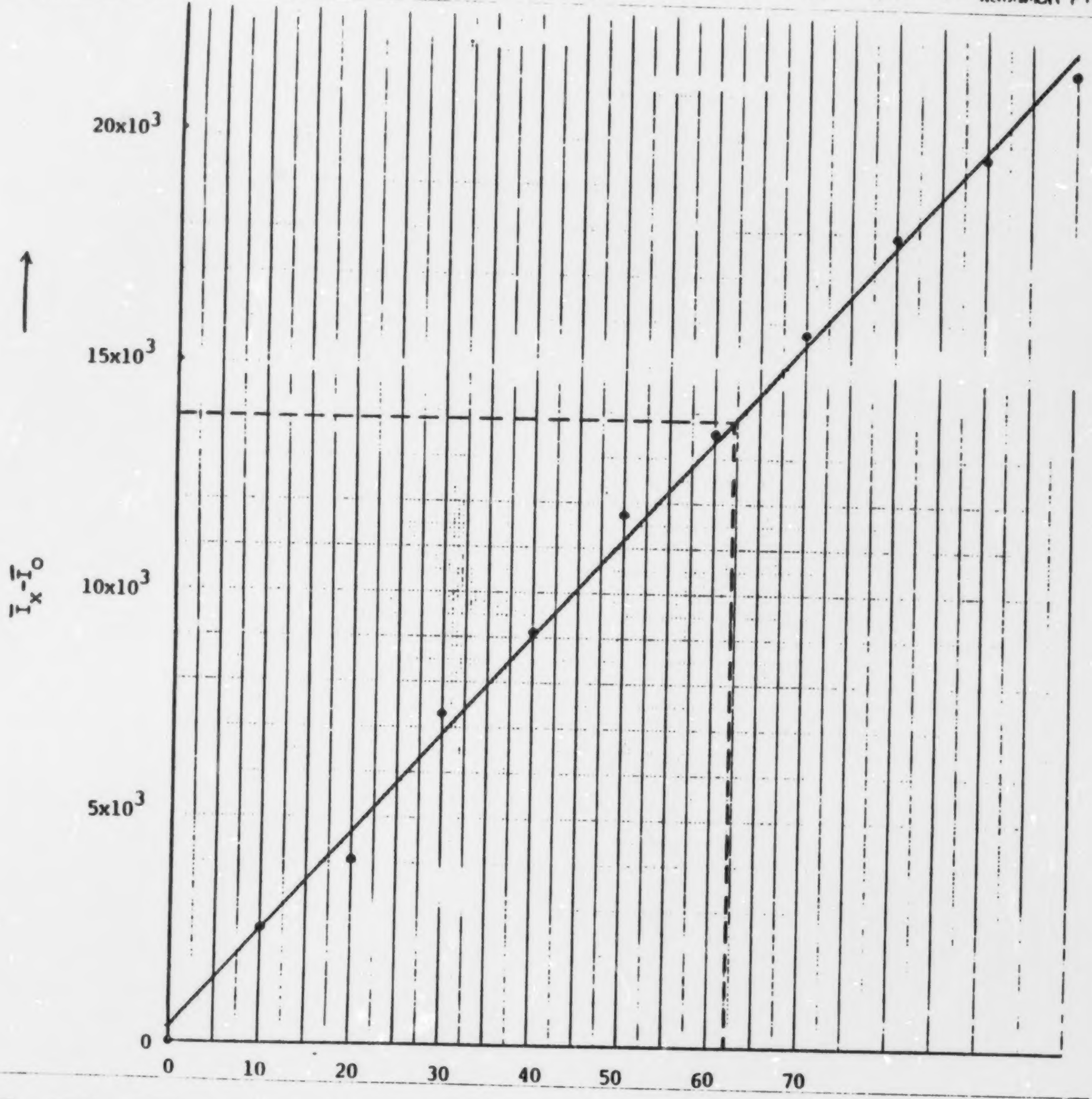

Figure 25. Scattering Intensity $\overline{I}_x-\overline{I}_o$ at 2θ=25° vs. Glass Content for Sundance Fly Ash

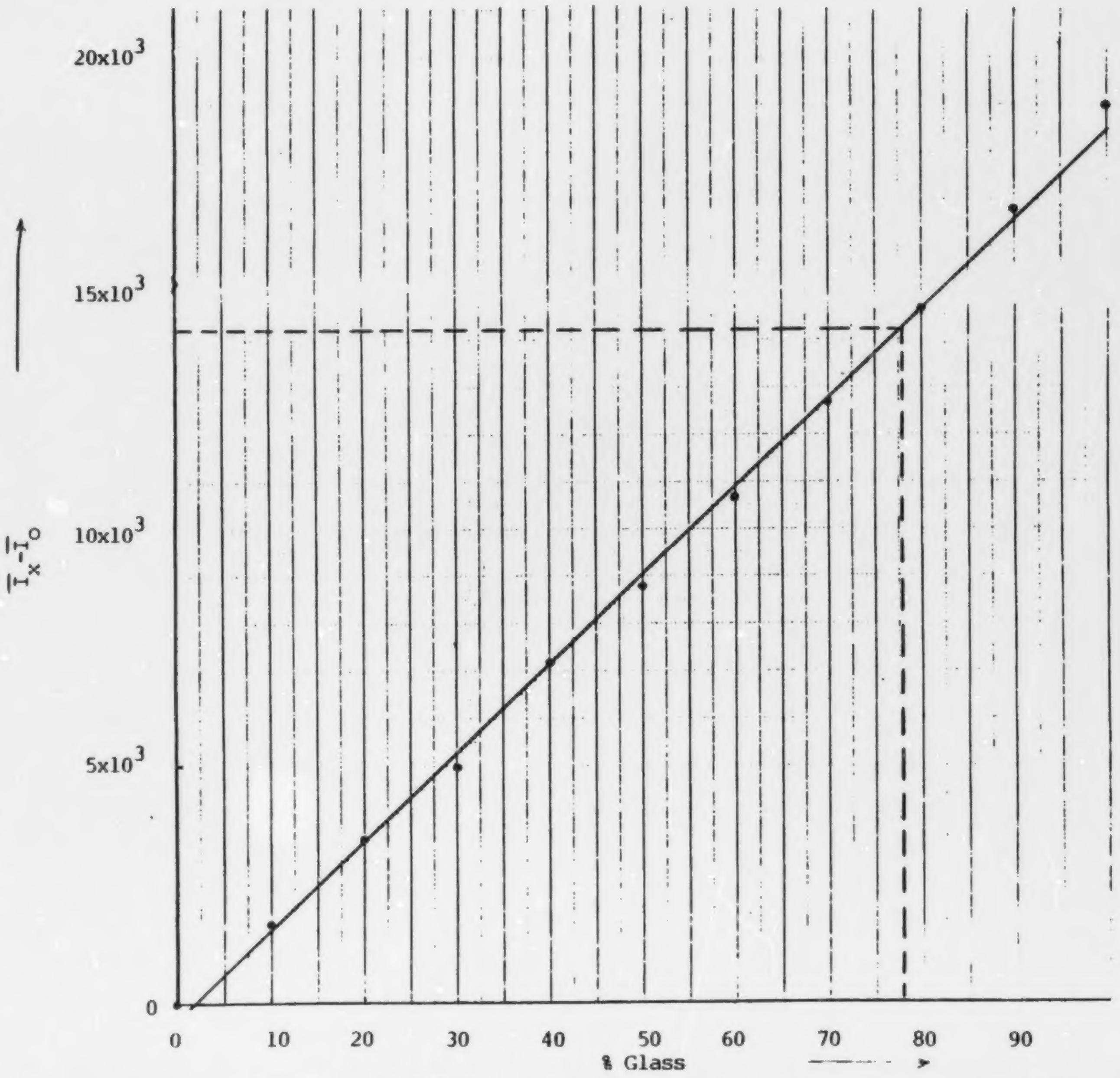

Figure 26. Scattering Intensity $\bar{I}_x - \bar{I}_o$ at $2\theta = 25^{\circ}$ vs. Glass Content for Forestburg Fly Ash

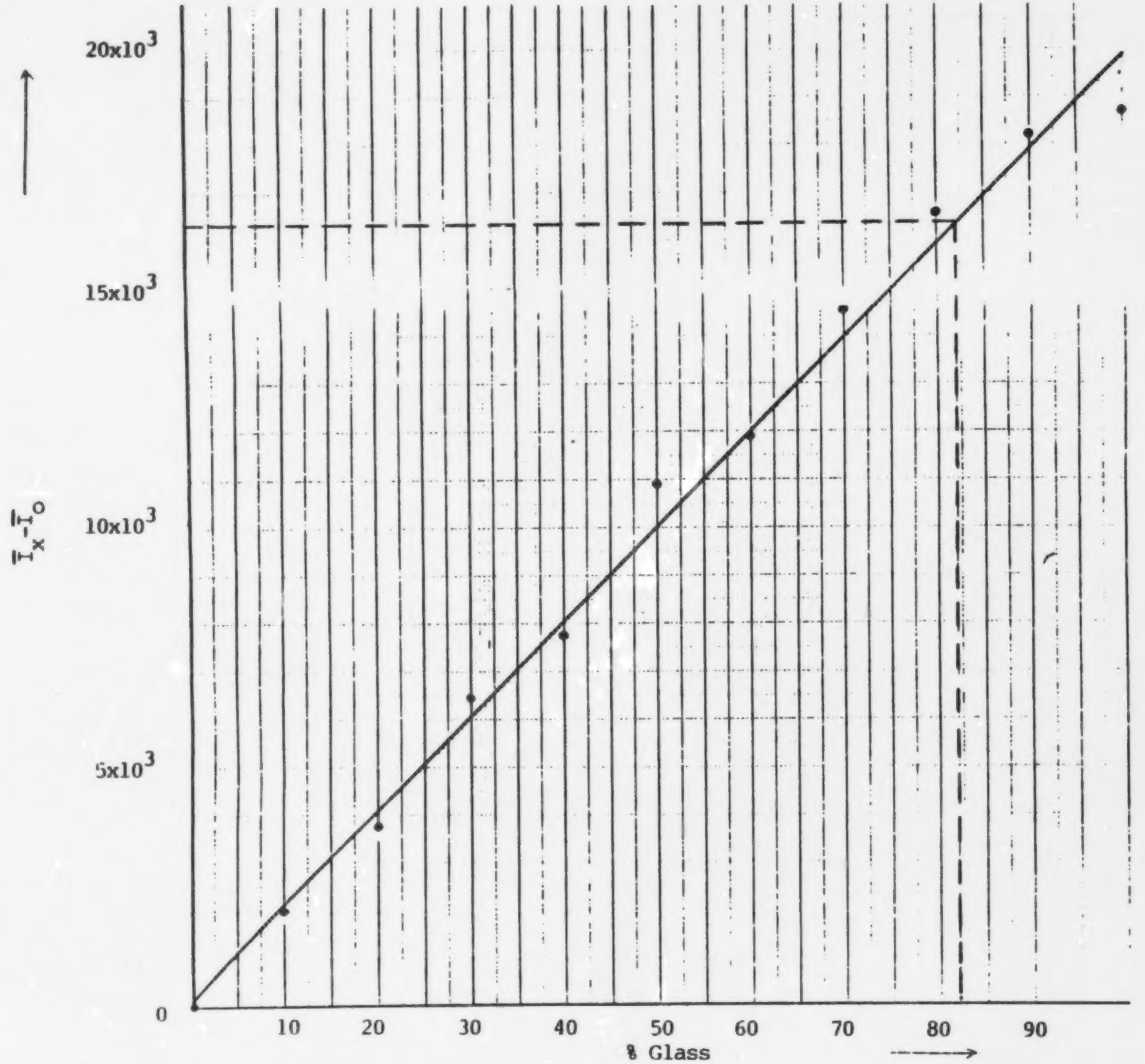

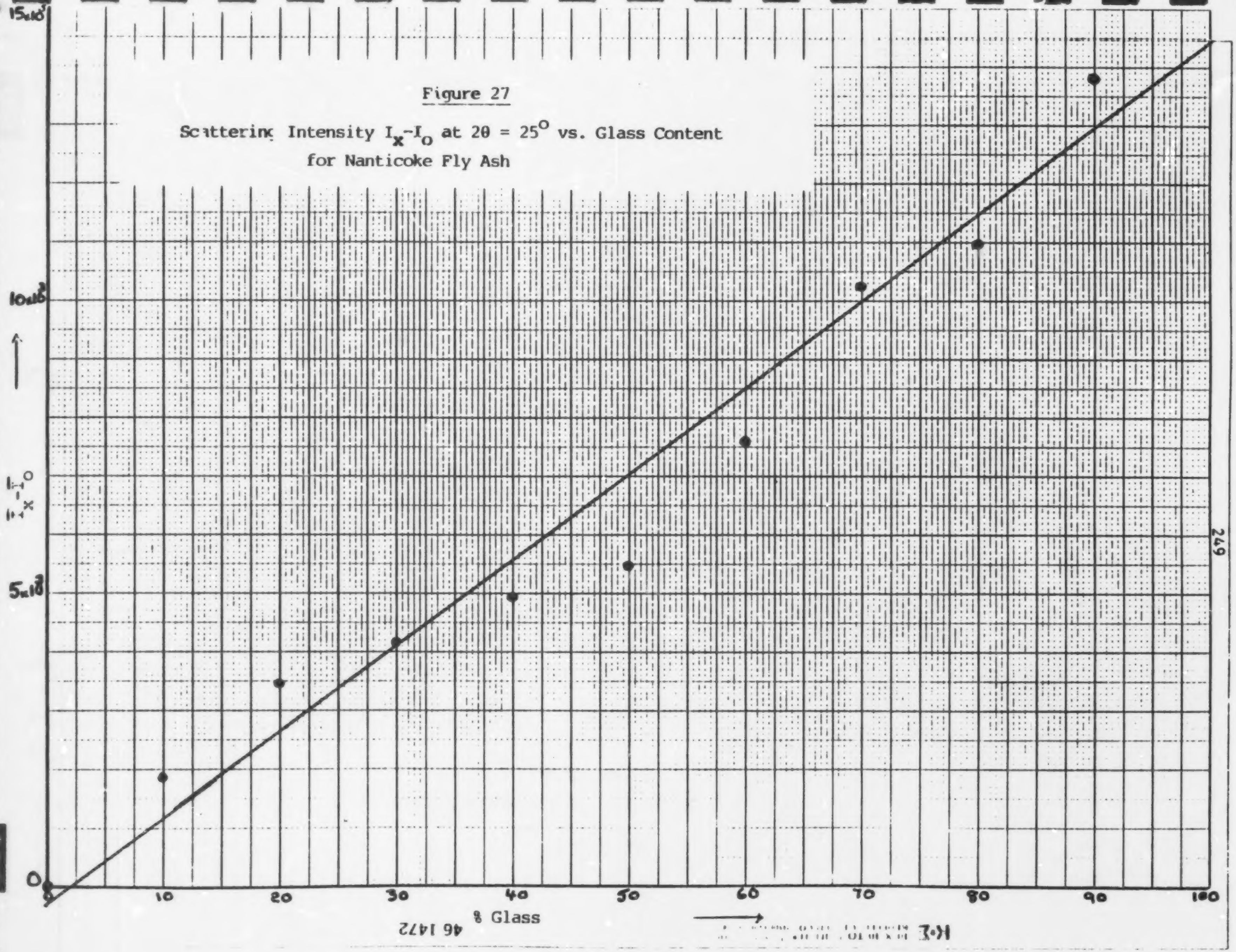

Figure 27

Scattering Intensity $I_x - I_o$ at $2\theta = 25^\circ$ vs. Glass Content for Nanticoke Fly Ash

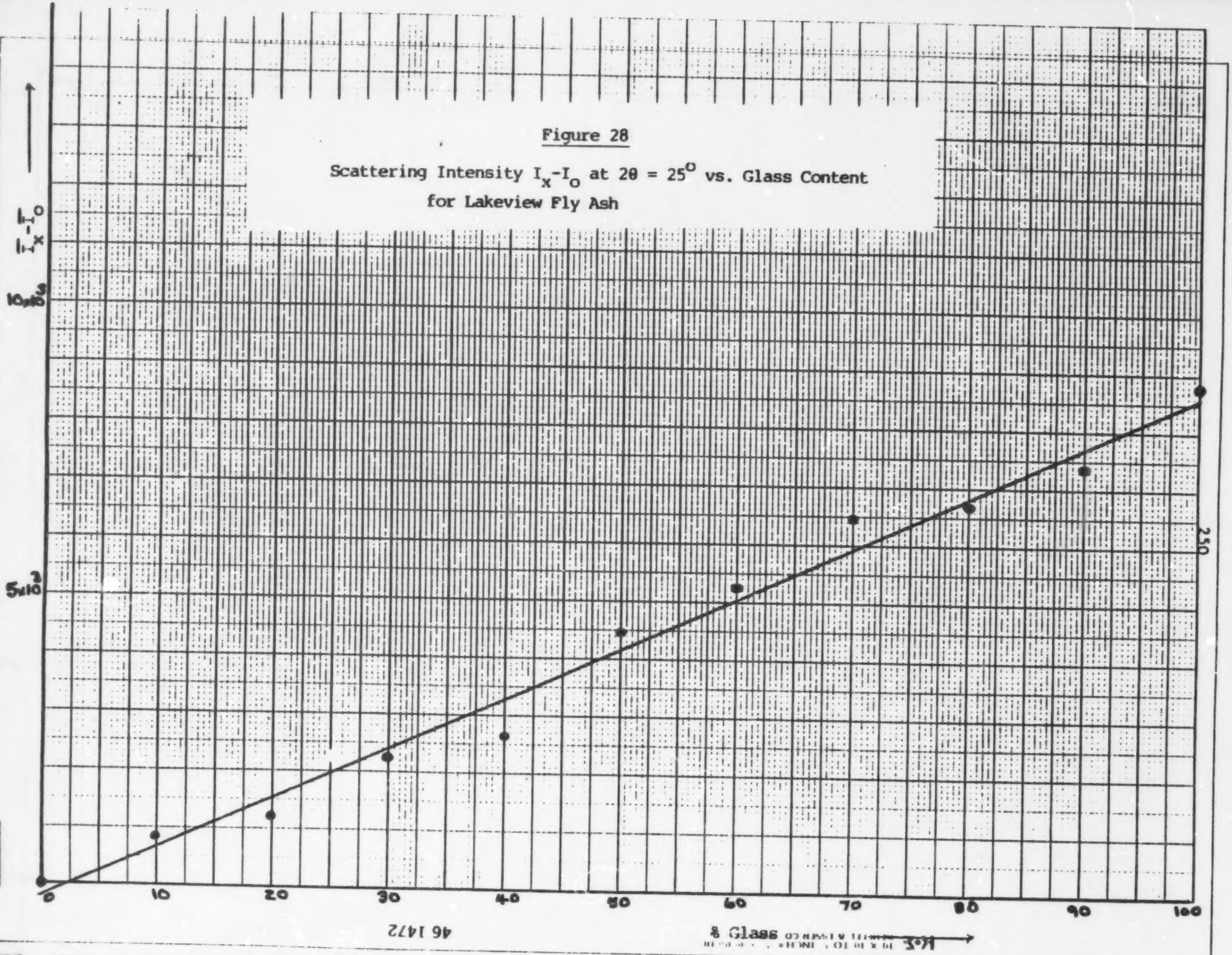

Figure 28

Scattering Intensity I_x-I_o at $2\theta = 25^{\circ}$ vs. Glass Content for Lakeview Fly Ash

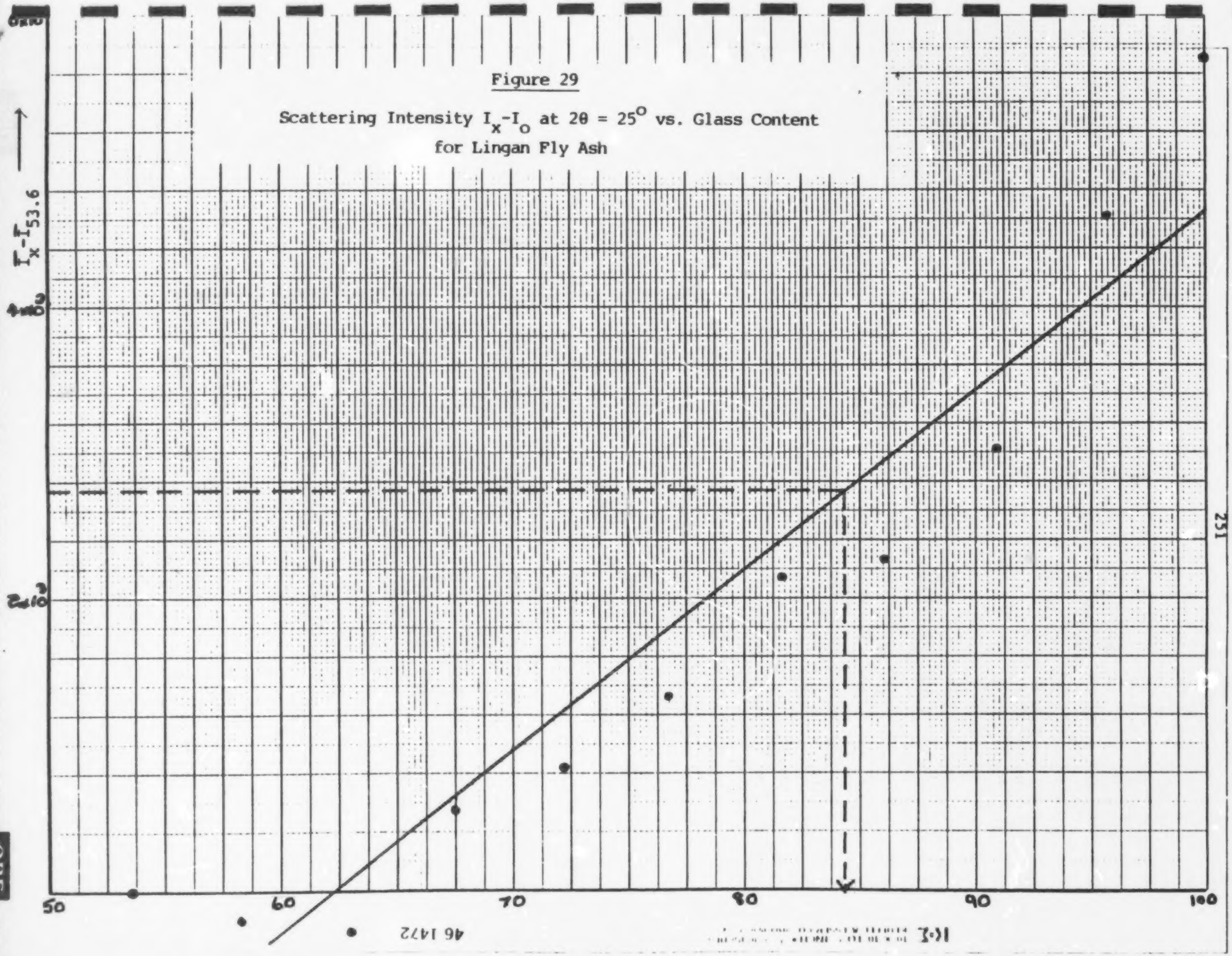

Figure 29

Scattering Intensity $I_x - I_o$ at $2\theta = 25^o$ vs. Glass Content for Lingan Fly Ash

Figure 30

Scattering Intensity, $\overline{I}_x - \overline{I}_o$, at $2\theta=25^\circ$ vs. Glass Content for Estevan Fly Ash.

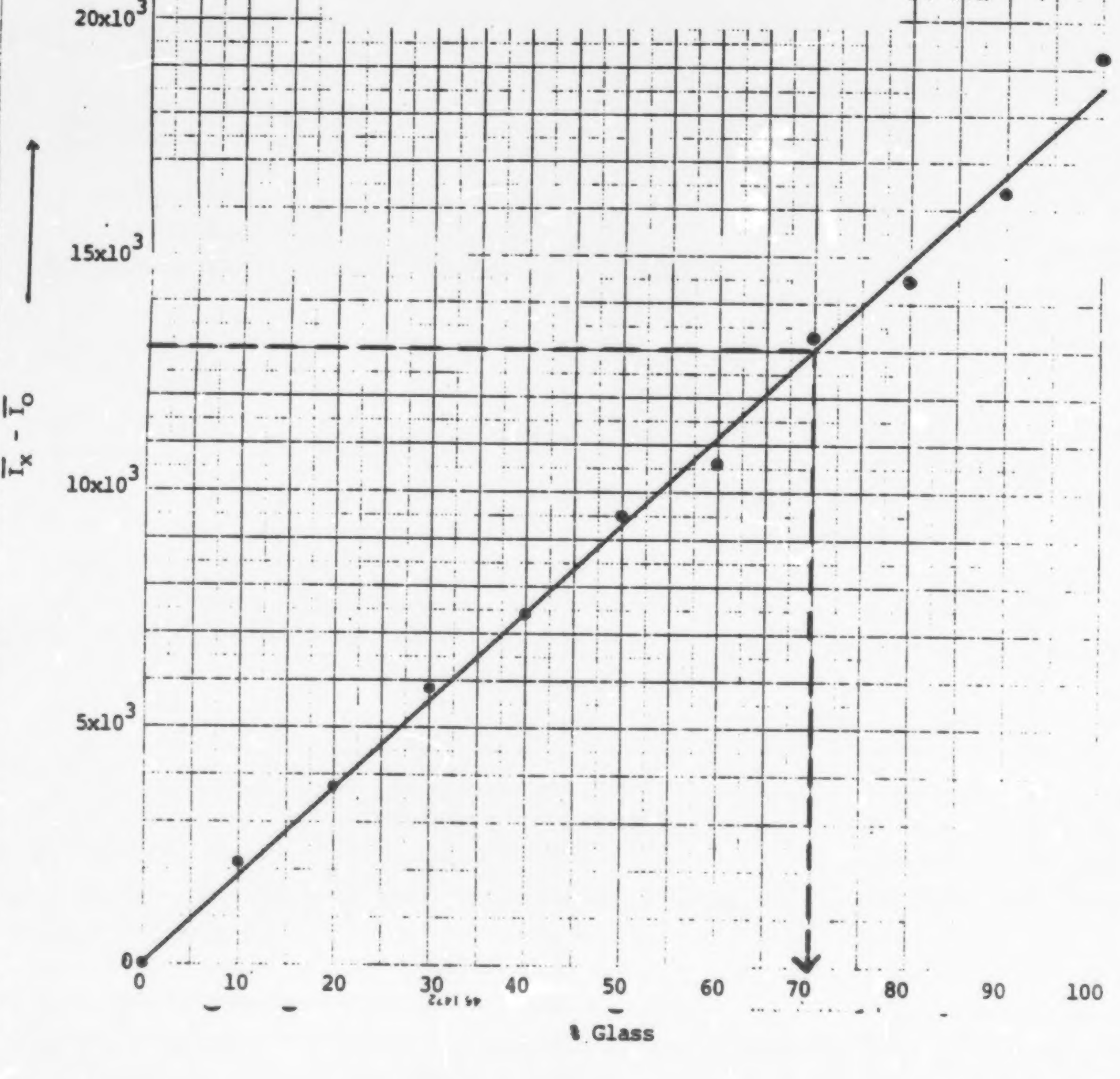

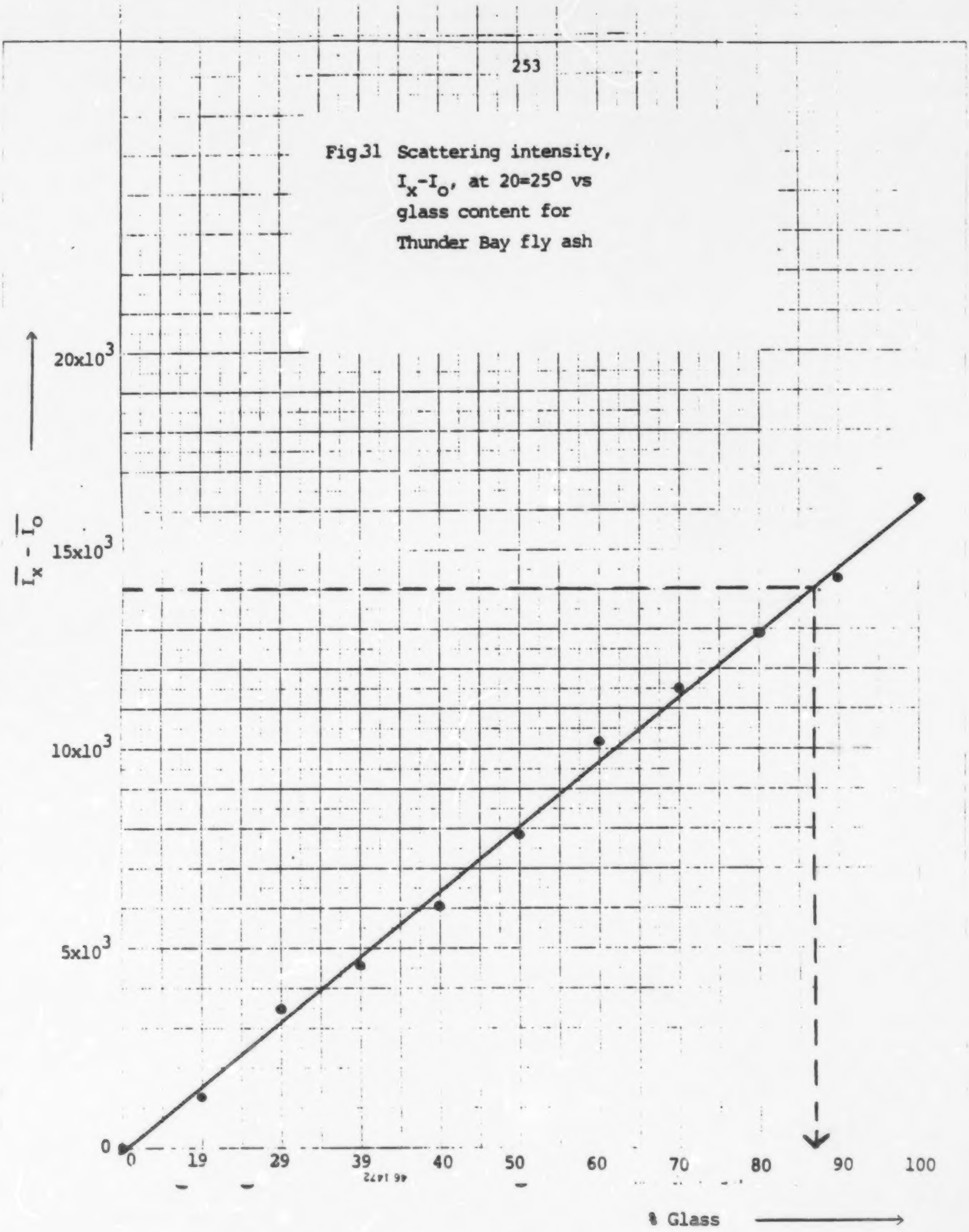

Fig.31 Scattering intensity, I_x-I_o, at 20=25° vs glass content for Thunder Bay fly ash

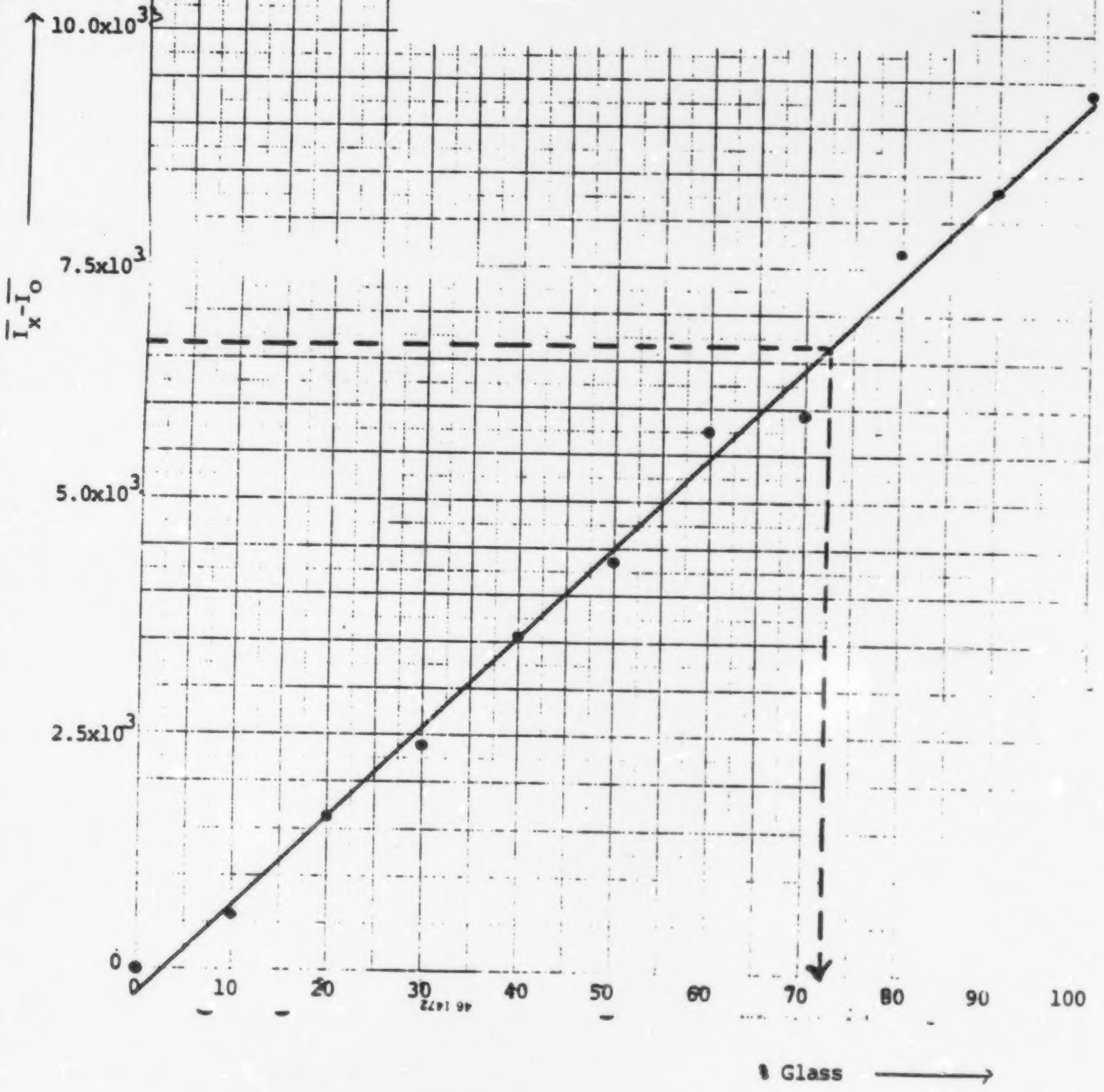

Fig.32 Scattering intensity, $\overline{I}_x-\overline{I}_o$, at $2\theta=25^\circ$ vs. glass content for Standard slag.

ORF

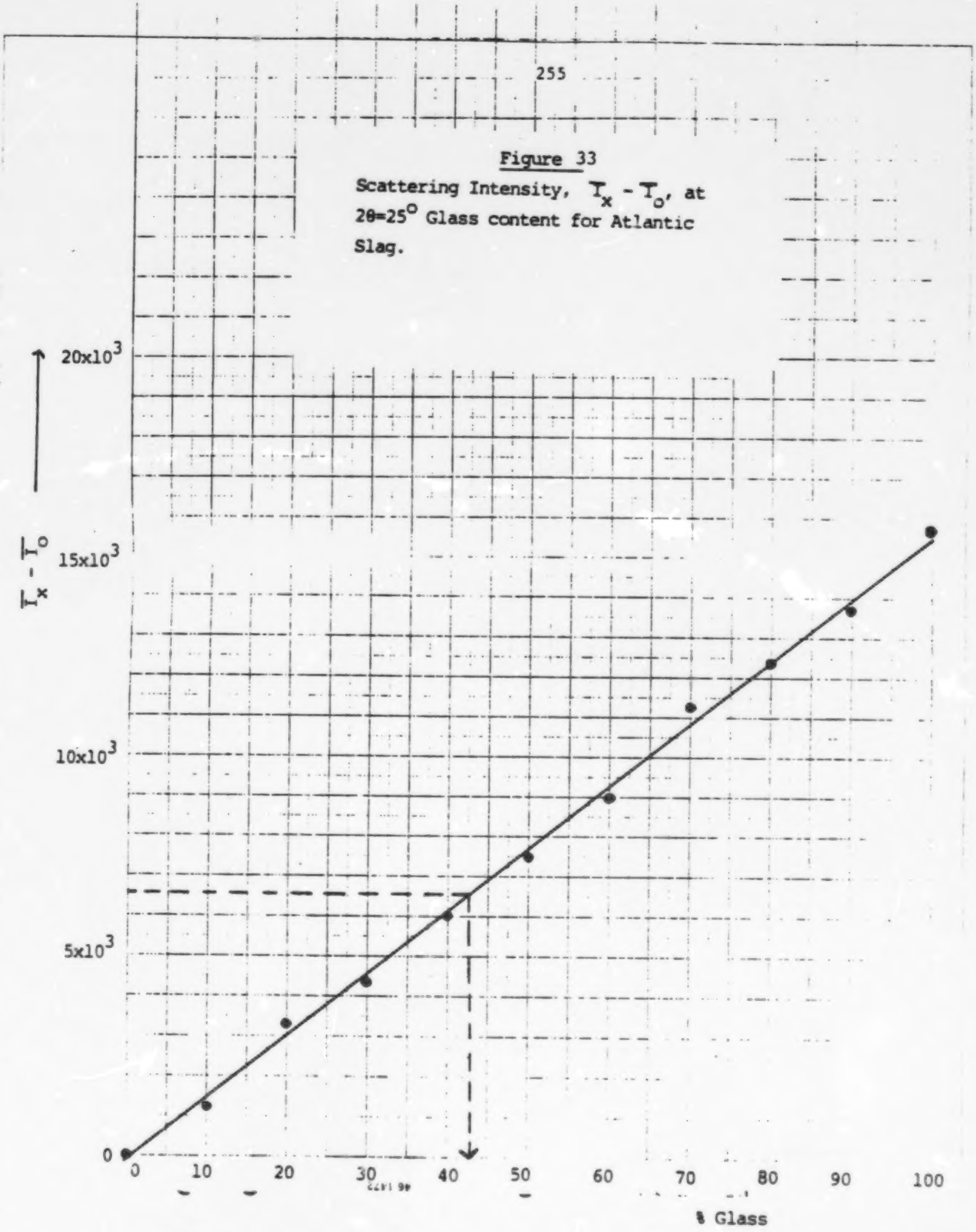

Figure 33

Scattering Intensity, $T_x - T_o$, at $2\theta=25^{\circ}$ Glass content for Atlantic Slag.

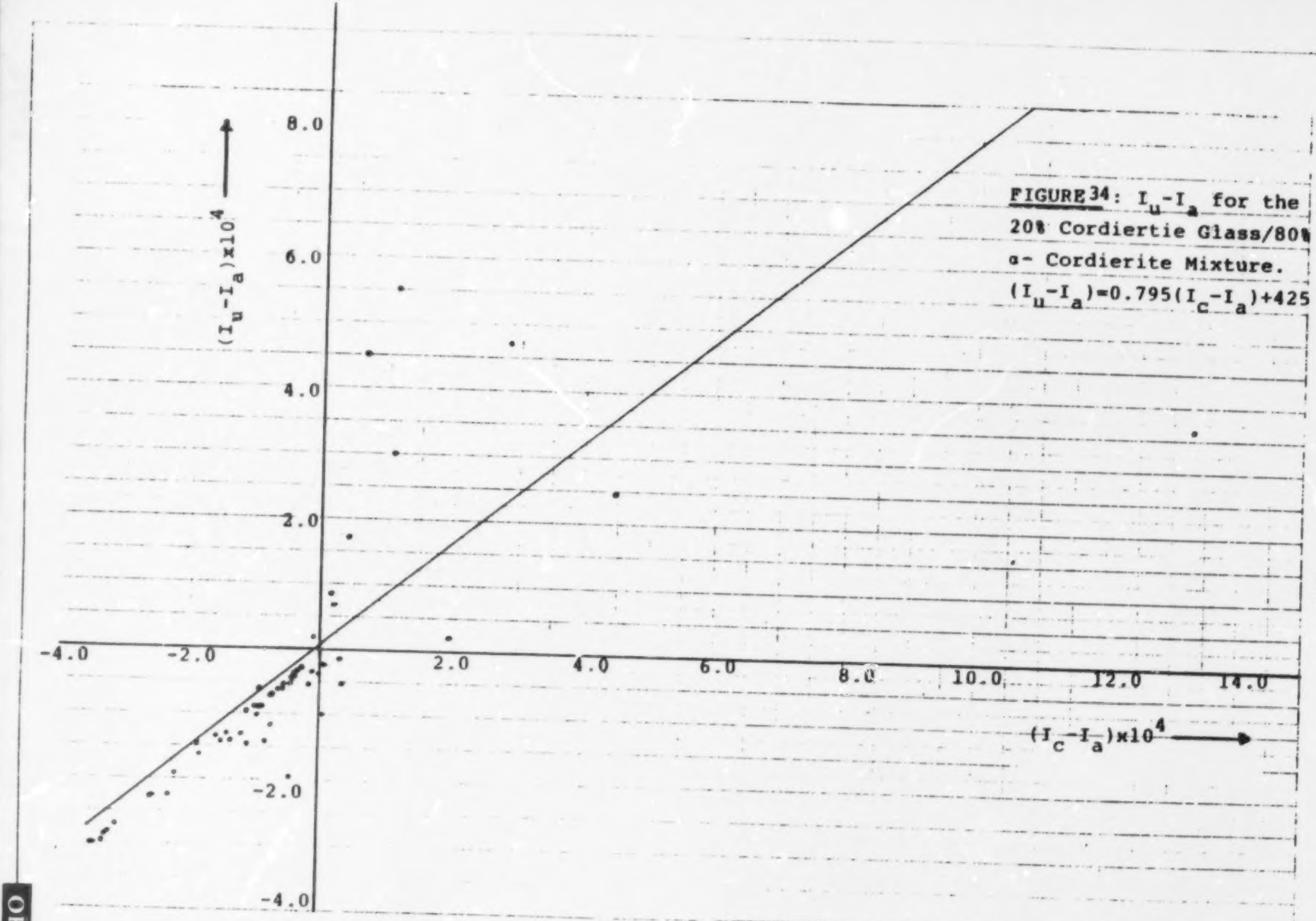

FIGURE 34: $I_u - I_a$ for the 20% Cordiertie Glass/80% α- Cordierite Mixture.
$(I_u - I_a) = 0.795(I_c - I_a) + 425$

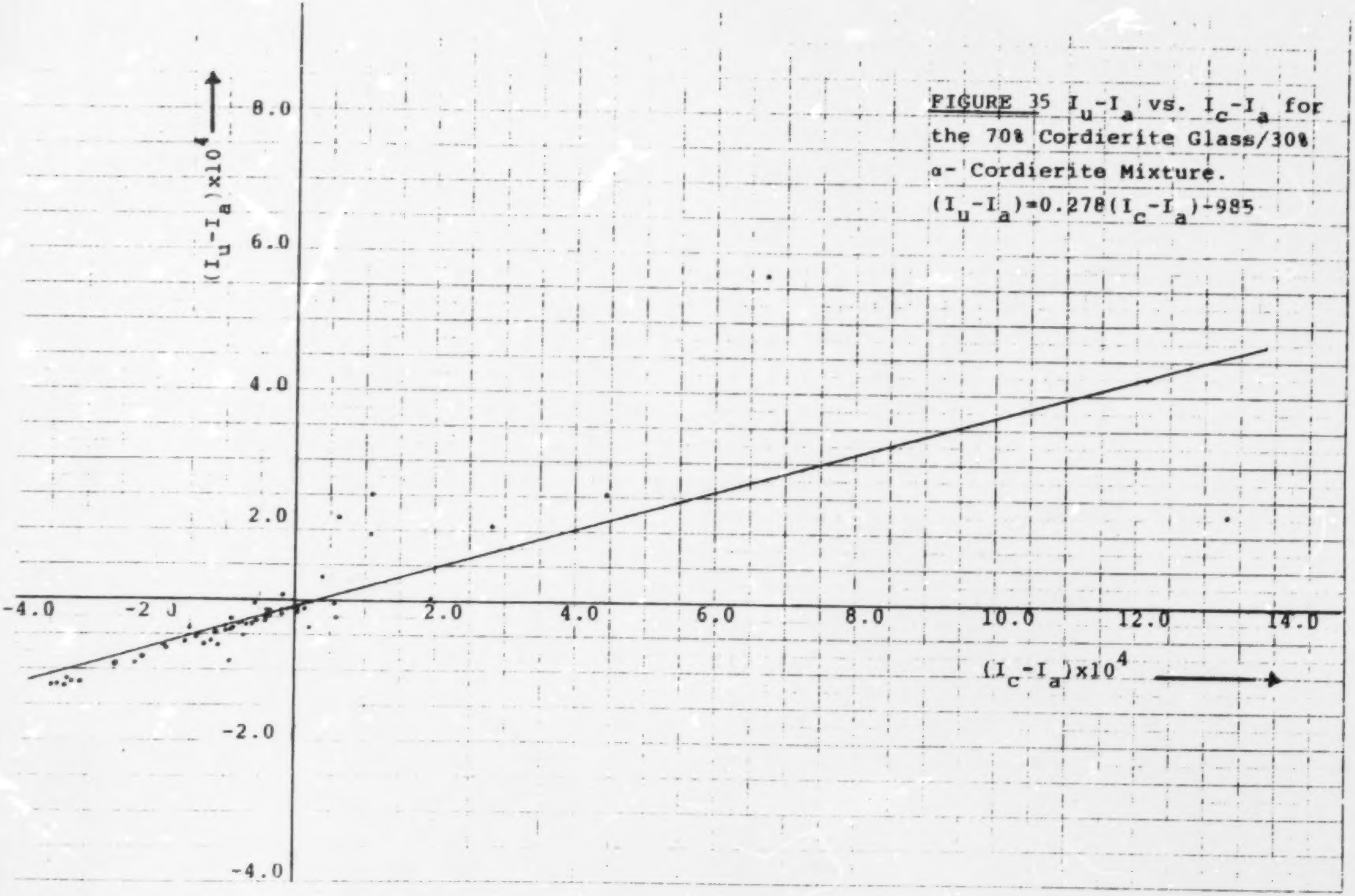

FIGURE 35 $I_u - I_a$ vs. $I_c - I_a$ for the 70% Cordierite Glass/30% α- Cordierite Mixture.
$(I_u - I_a) = 0.278(I_c - I_a) - 985$

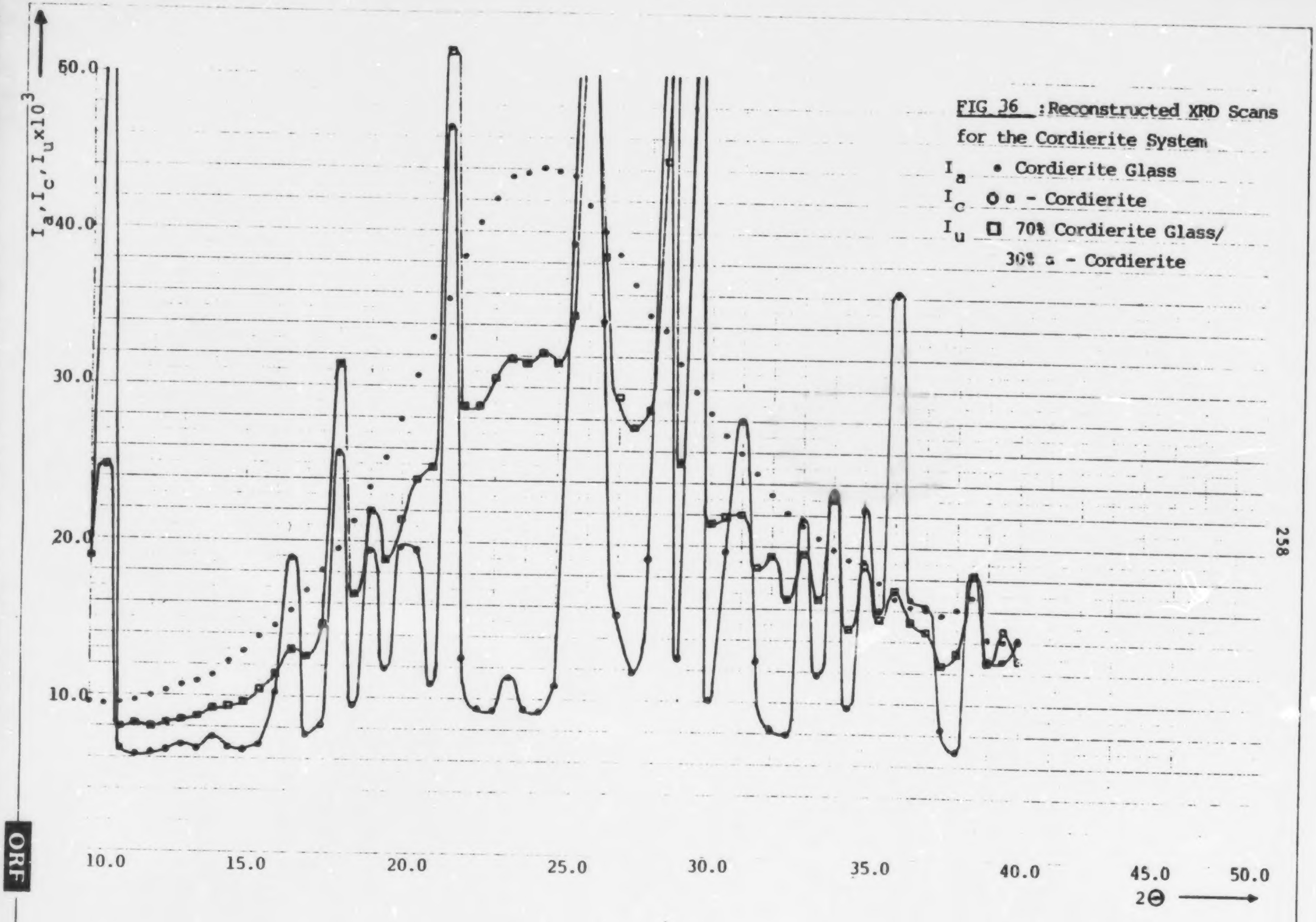

FIG 36 : Reconstructed XRD Scans for the Cordierite System

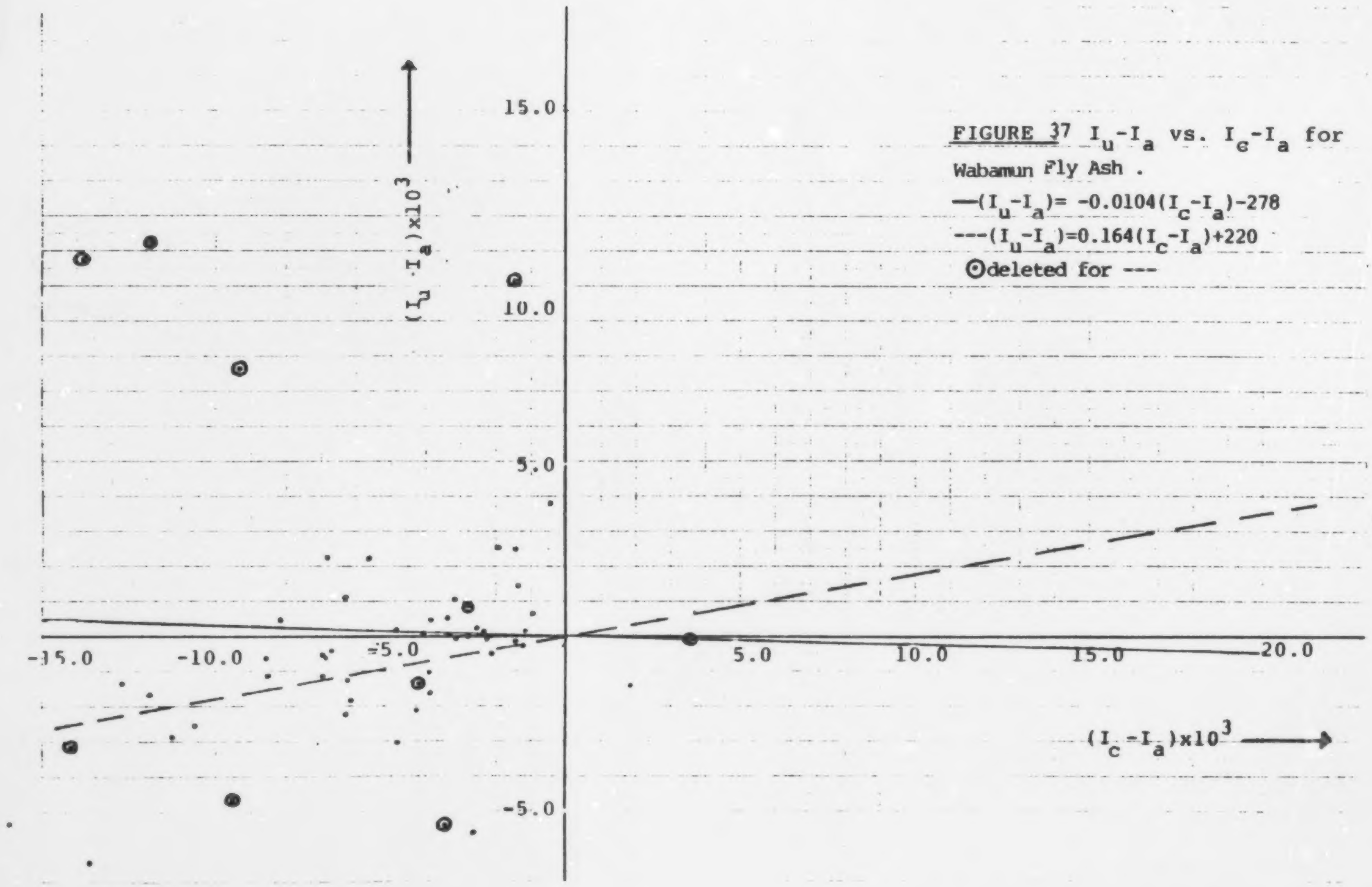

FIGURE 37 I_u-I_a vs. I_c-I_a for Wabamun Fly Ash .

—$(I_u-I_a) = -0.0104(I_c-I_a)-278$

---$(I_u-I_a)=0.164(I_c-I_a)+220$

⊙deleted for ---

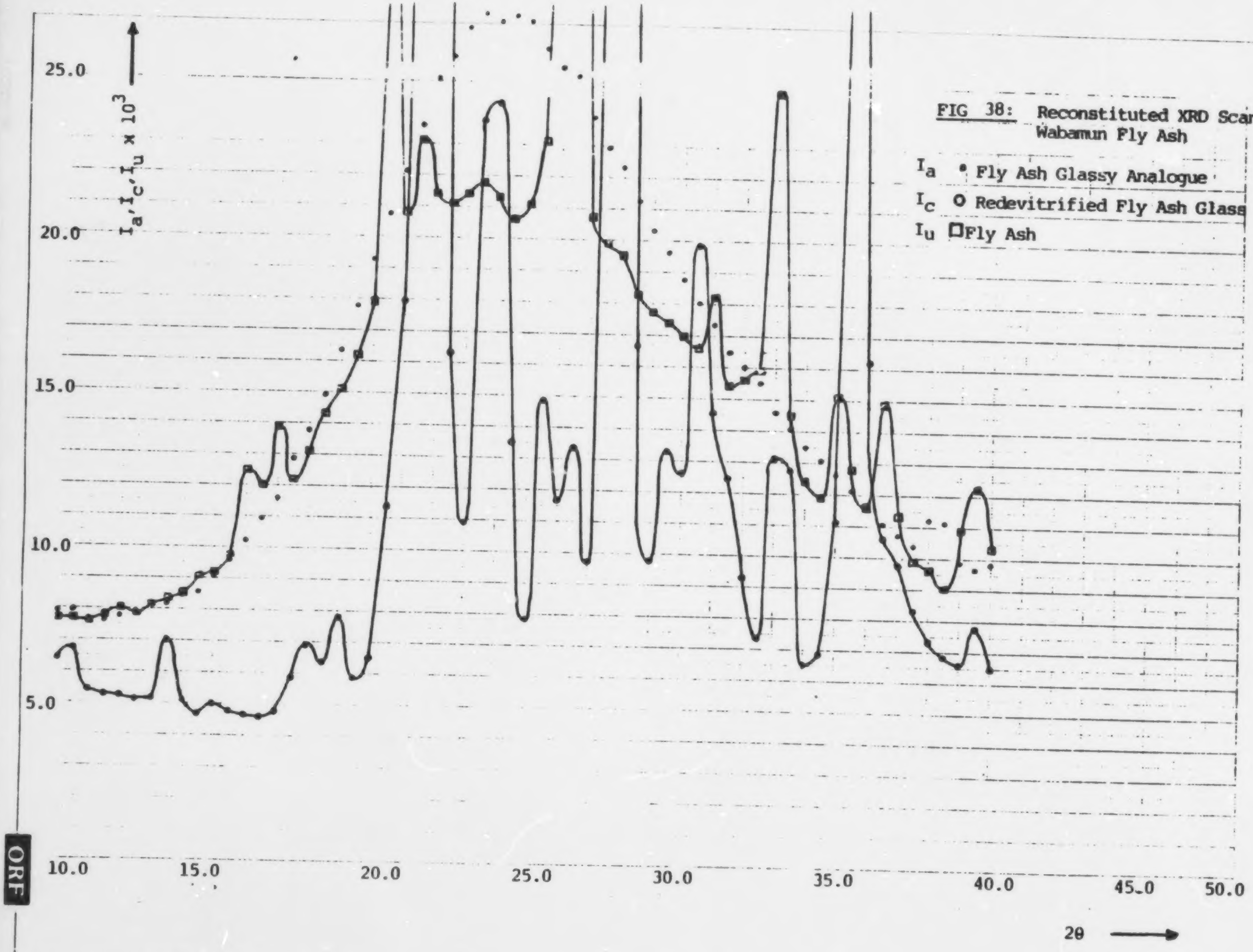

FIG 38: Reconstituted XRD Scans Wabamun Fly Ash

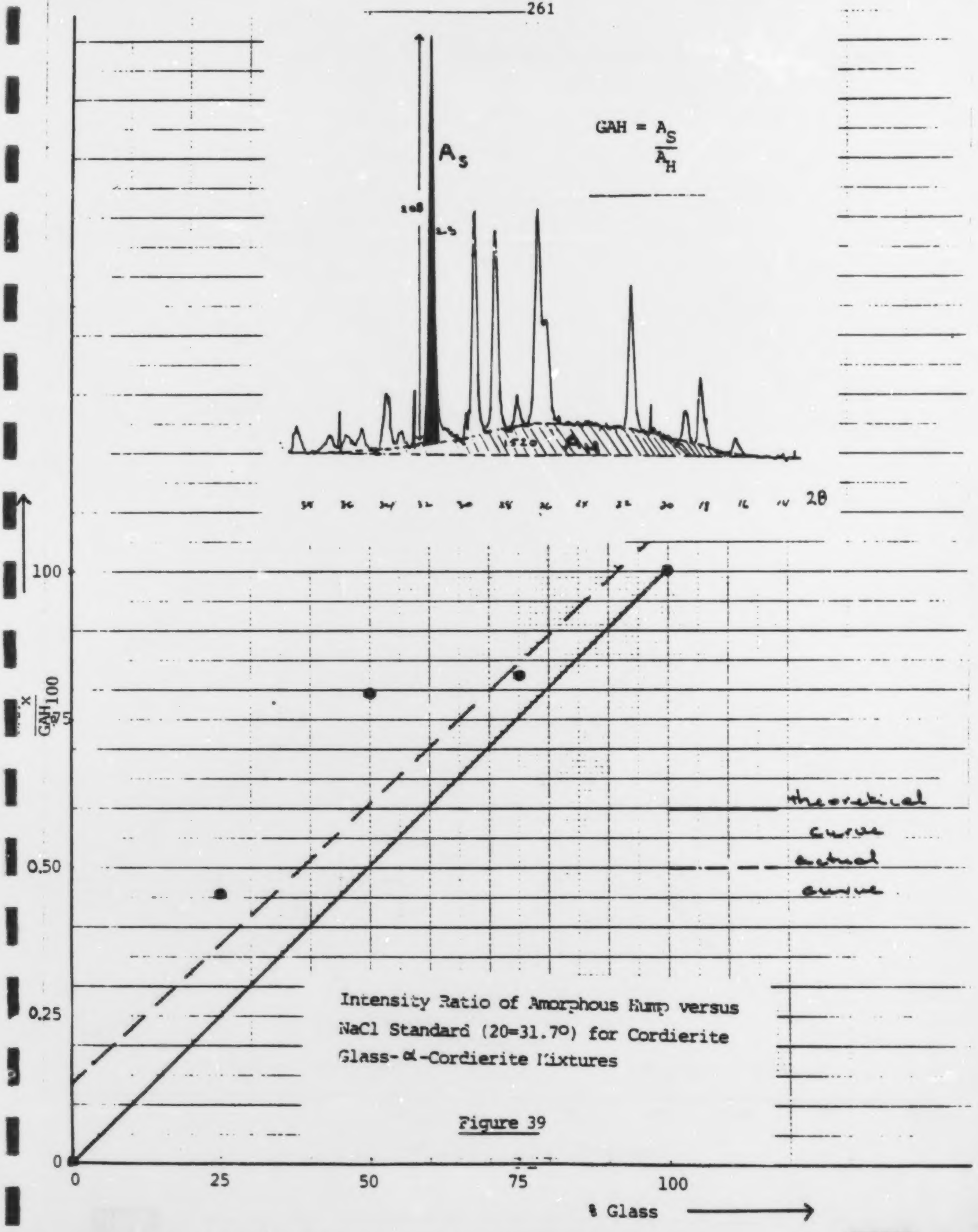

Intensity Ratio of Amorphous Hump versus NaCl Standard (2θ=31.7°) for Cordierite Glass-α-Cordierite Mixtures

Figure 39

Figure 40 X-Ray Diffraction Patterns of Glasses in Na_2O-SiO_2 System

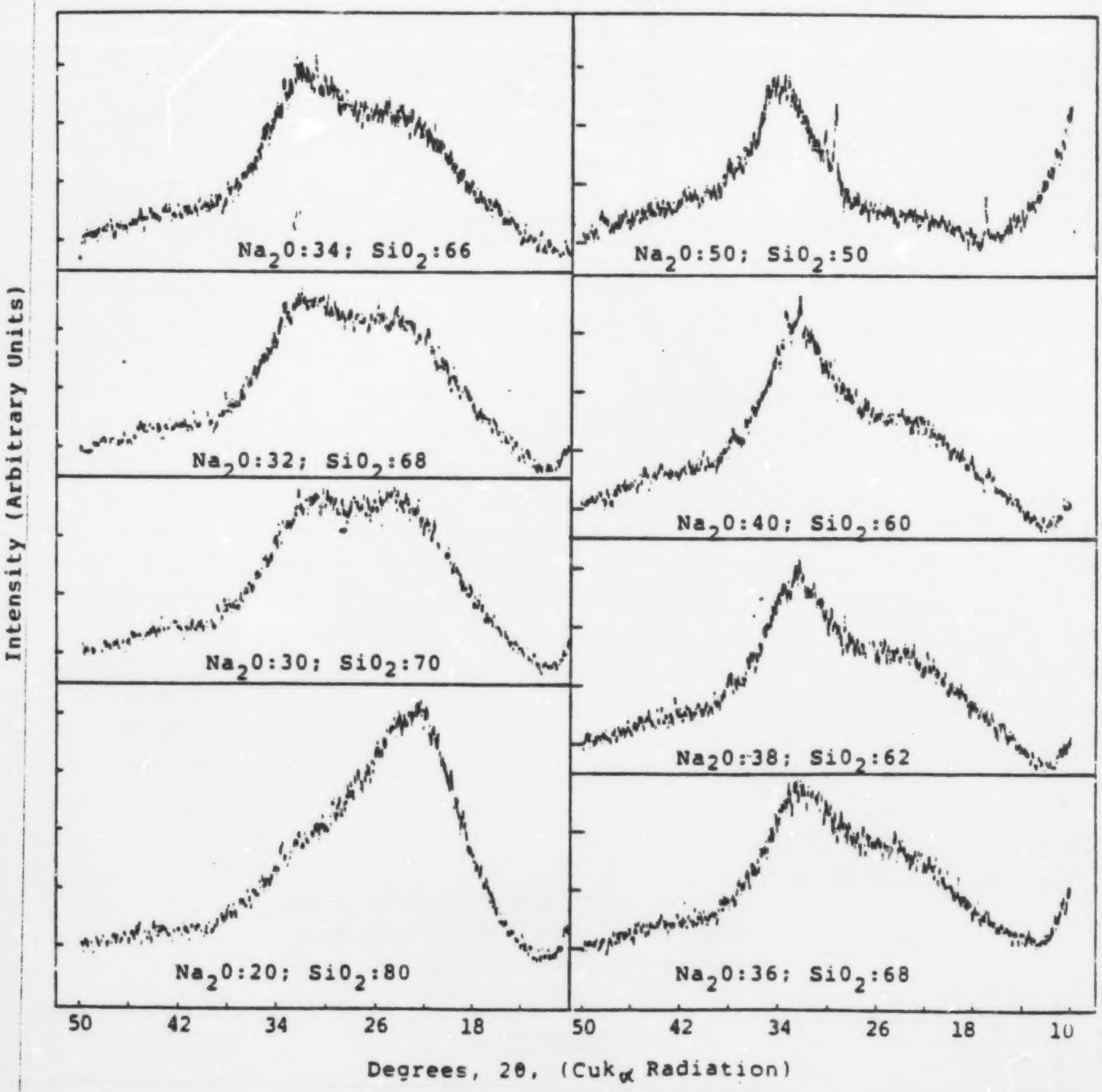

ORF

Figure 41 X-Ray Diffraction Patterns of Glasses in $Na_2O-CaO-SiO_2$ and other systems.

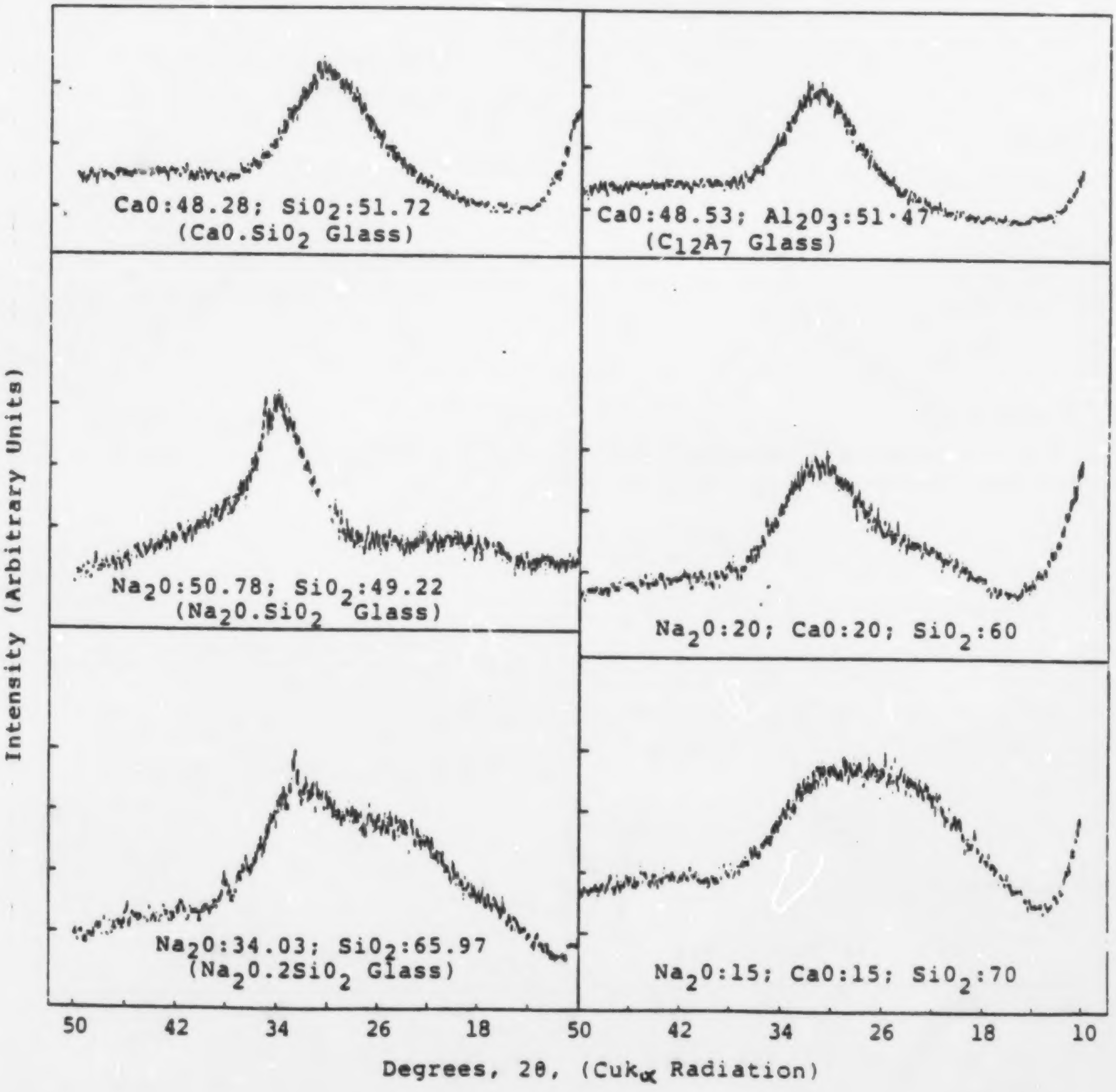

Figure 42 X-ray Diffraction Patterns of Some Commercial Glasses

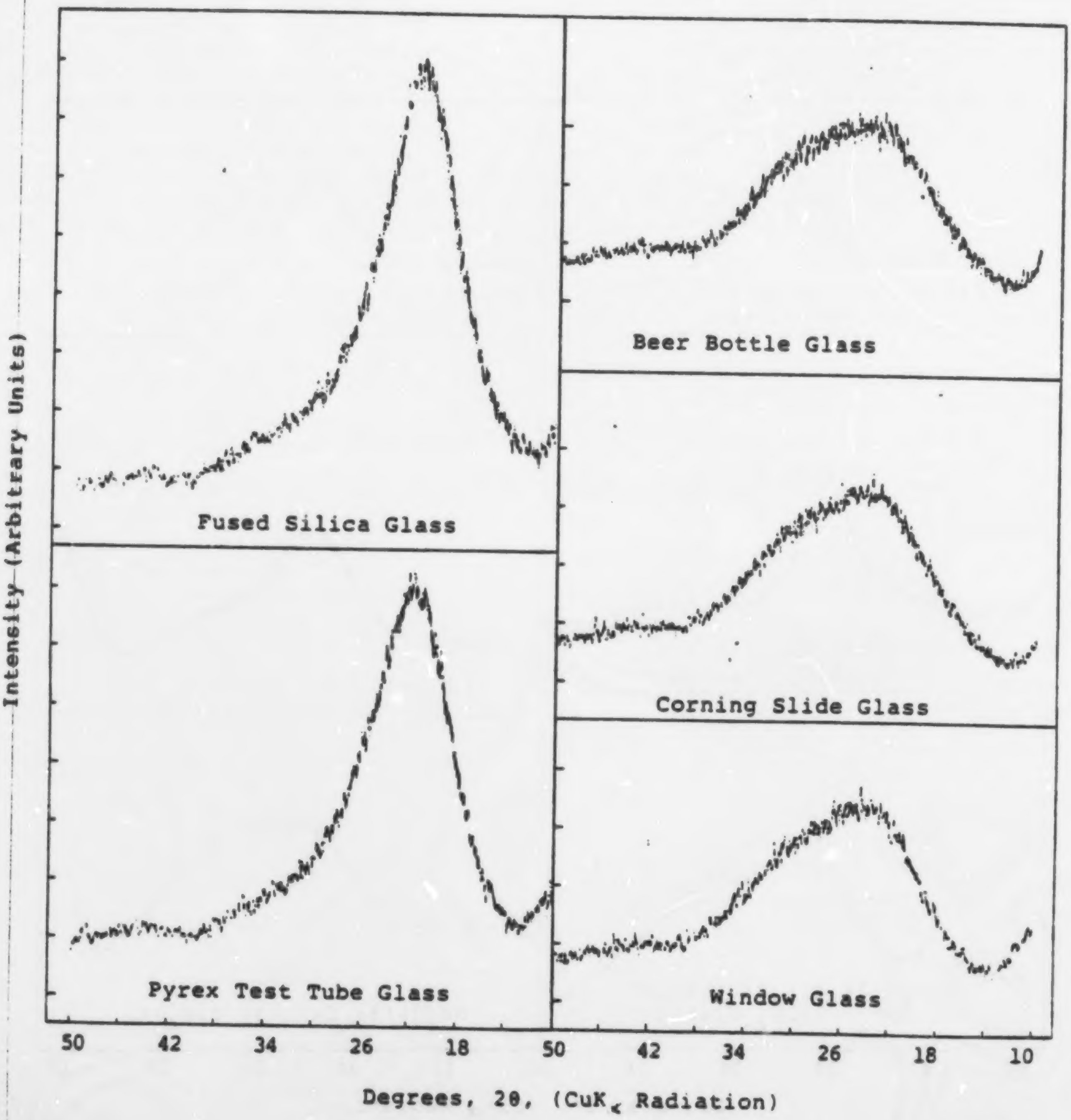

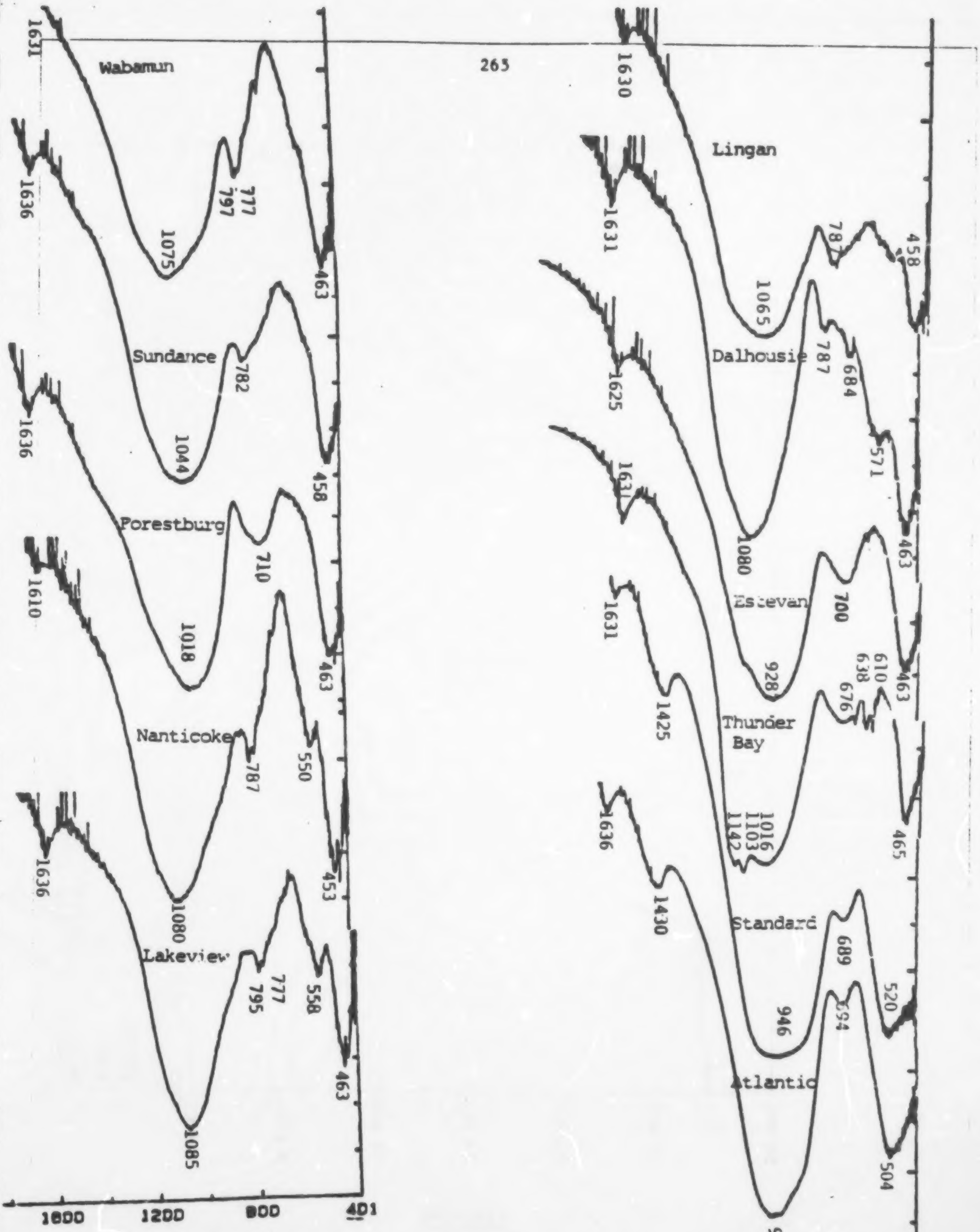

Figure 43
FTIR Spectra of Fly Ashes and Slags.

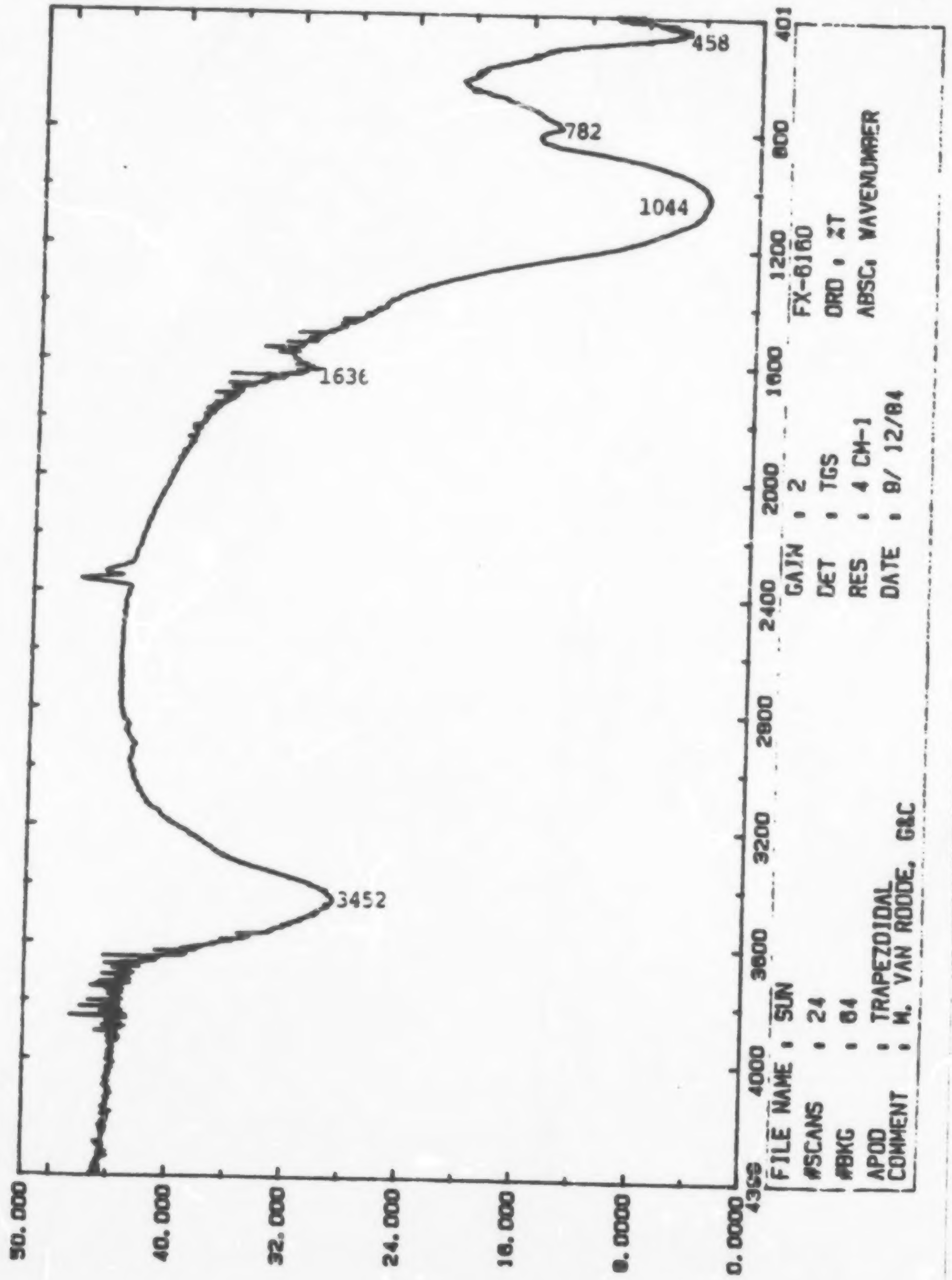

Figure 44

FTIR spectrum of Sundance fly ash in the 4000-400 cm^{-1} range.

FIGURE 45: pH versus Time Curves for the leaching of Fly Ashes and Slags in Dionized Distilled H_2O

(a) Nanticoke, Sundance, Forestburg, Lingan: 1 g/250 mL

(b) Wabamun: 1,2,4 and 8 g/250 mL

(c) Dalhousie: 1,2,4 and 8 g/250 mL

(d) Lakeview: 1,2,4 and 8 g/250 mL

(e) Thunder Bay: 1,2,4 and 8 g/250 mL

(f) Estevan: 1,2,4 and 8 g/250 mL

(g) Atlantic: 1,2,4 and 8 g/250 mL

(h) Standard: 1,2,4 and 8 g/250 mL

● 1 g/250 mL
○ 2 g/250 mL
□ 4 g/250 mL
△ 8 g/250 mL

Leaching of 7 Flyash in deionized water. PH vs Time

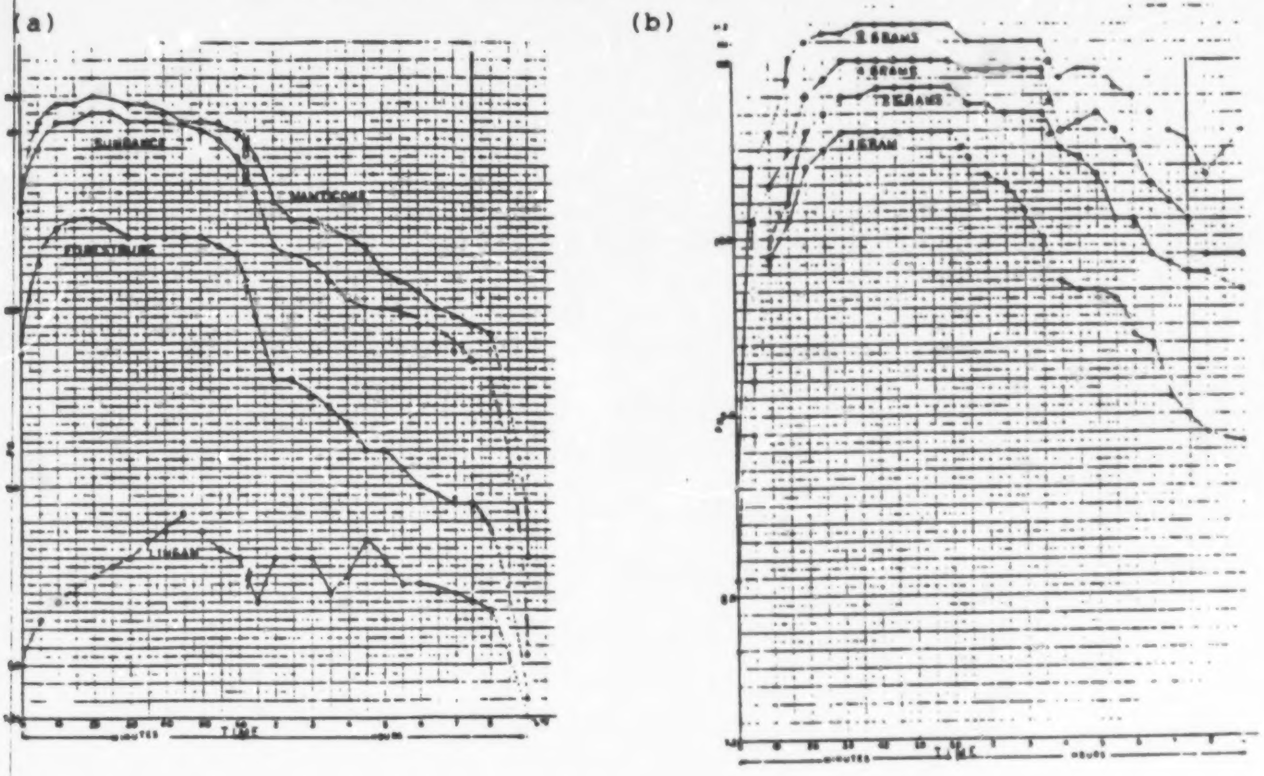

WABAMUN

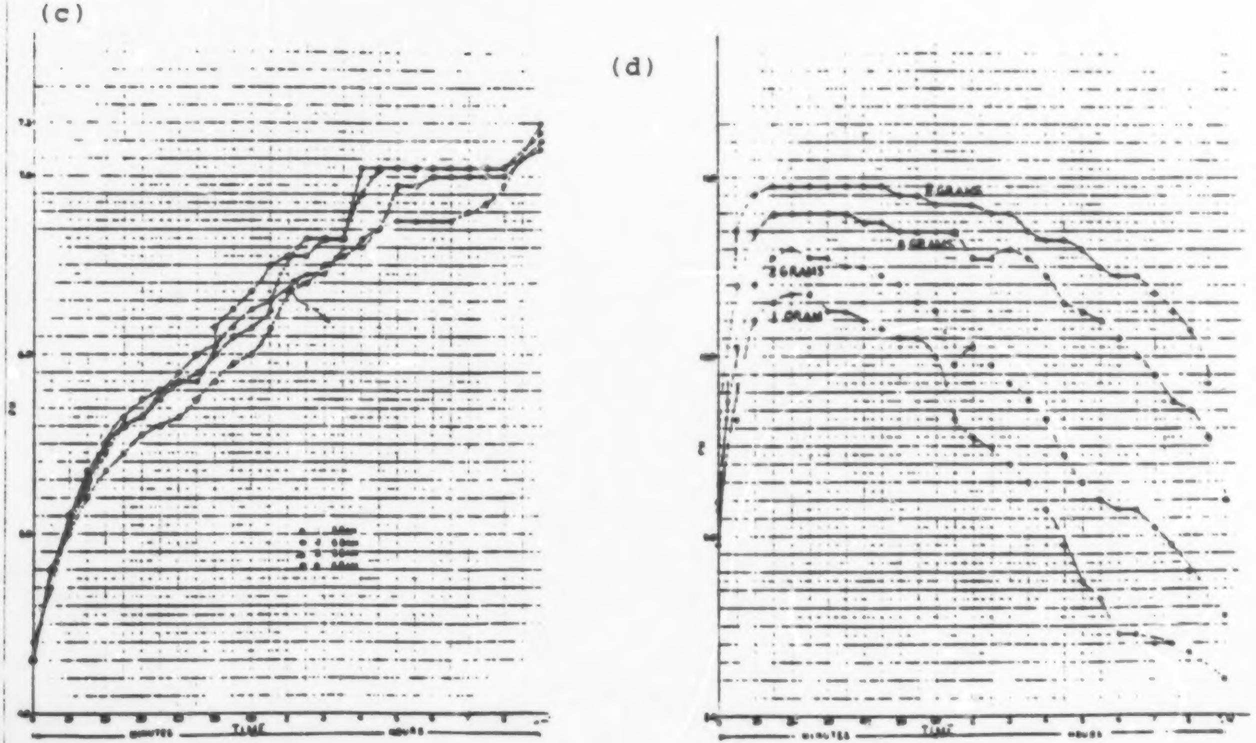

DALHOUSIE

LAKEVIEW

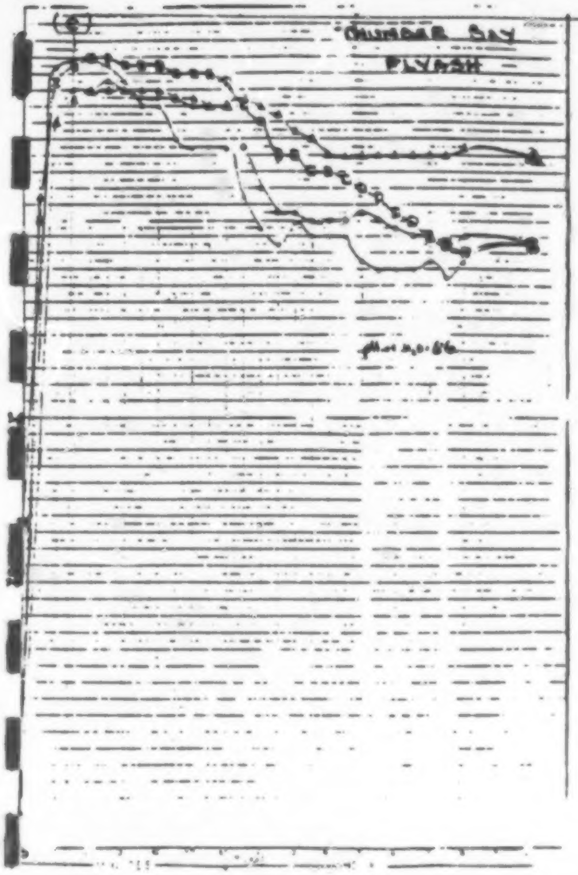
(e)
THUNDER BAY
FLYASH
pH of H2O = 6.6
MINUTES
TIME

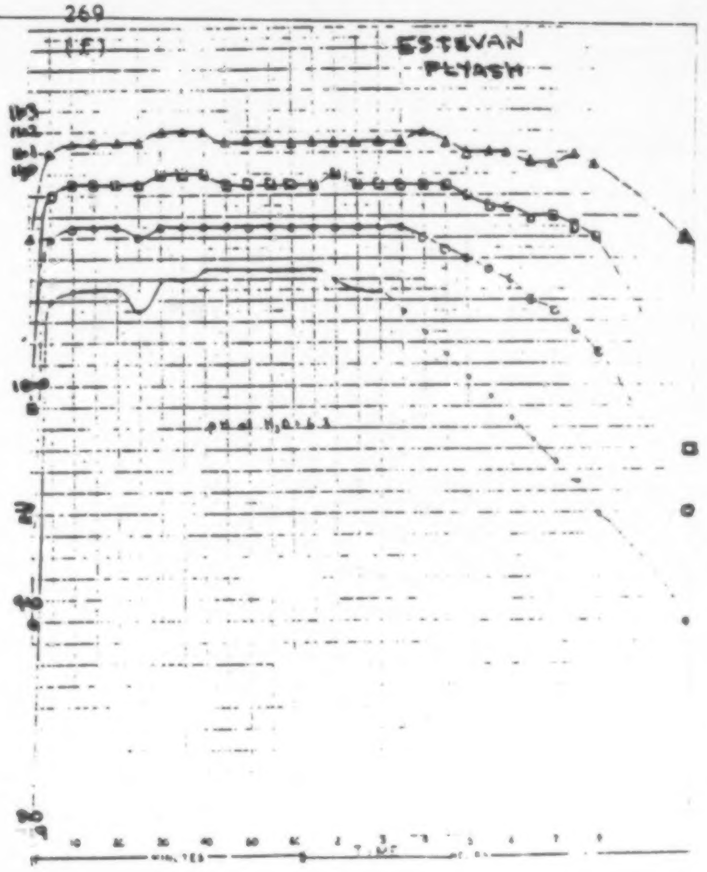
(F)
ESTEVAN
FLYASH
10.3
10.2
10.1
10.0
pH of H2O = 6.3
pH
9.0
10
20
30
40
50
60
2
3
4
5
6
7
8
MINUTES
TIME

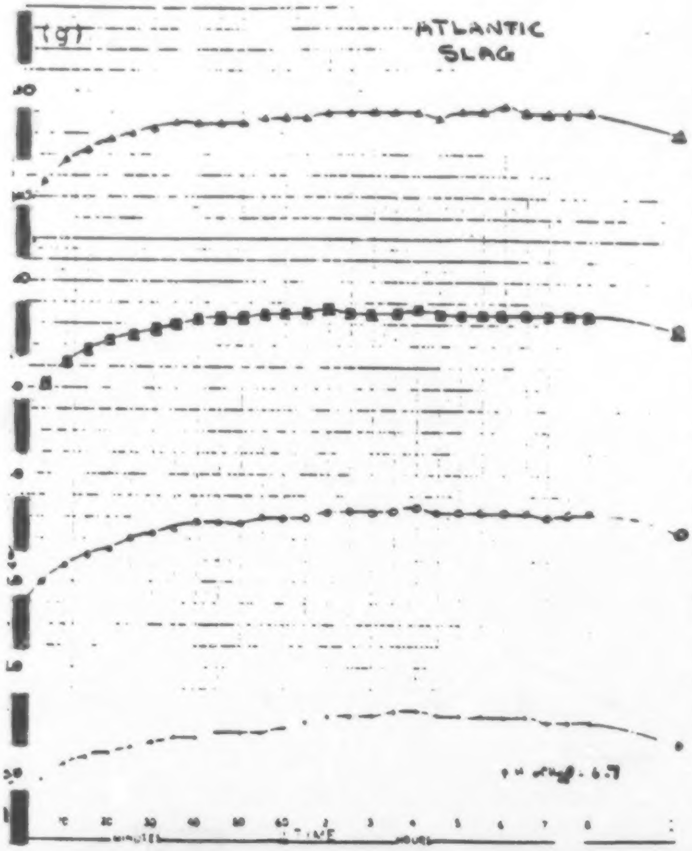
(g)
ATLANTIC
SLAG
pH of H2O = 6.7
10
20
30
40
50
60
2
3
4
5
6
7
8
MINUTES
TIME
HOURS

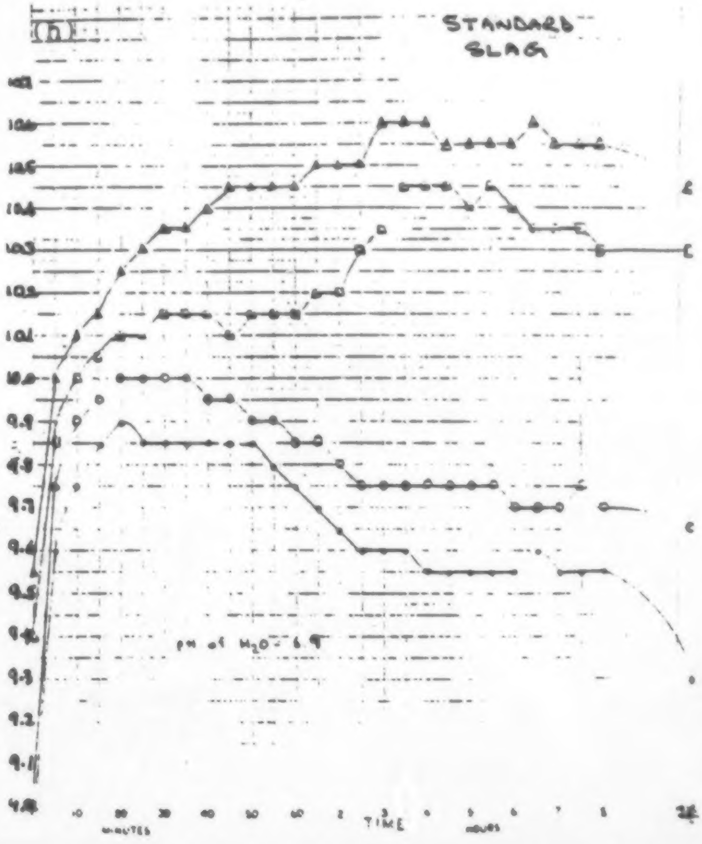
(h)
STANDARD
SLAG
10.7
10.6
10.5
10.4
10.3
10.2
10.1
10.0
9.9
9.8
9.7
9.6
9.5
9.4
9.3
9.2
9.1
9.0
pH of H2O = 6.9
10
20
30
40
50
60
2
3
4
5
6
7
8
24
MINUTES
TIME
HOURS

FIGURE 46:
PH versus Time Curve for two fly ashes of different particle size ranges.

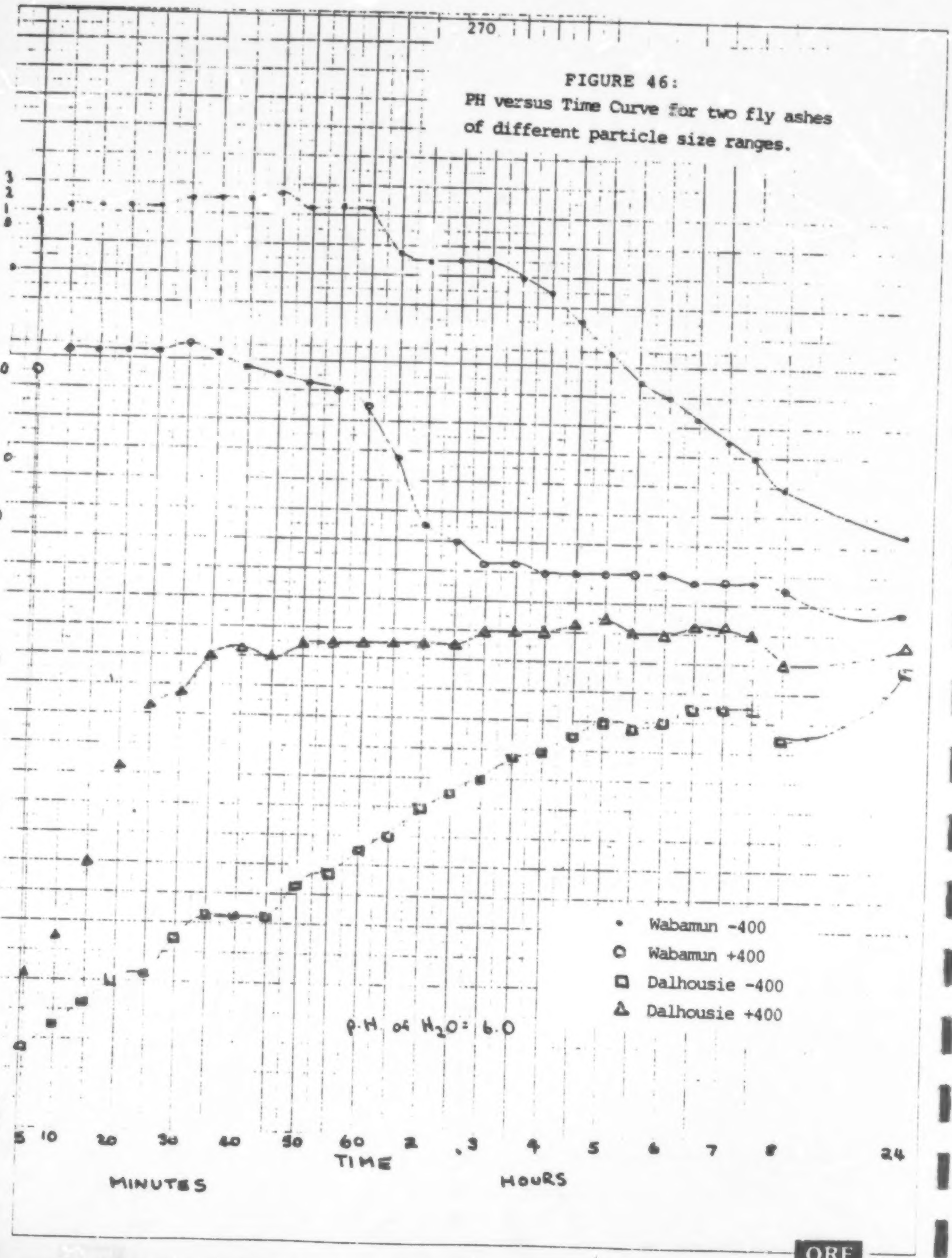

FIGURE 47: pH versus Time Curves for the Leaching of Glassy Analogues of Fly Ashes and Slags

(a)	○	Wabamun
	△	Sundance
	□	Forestburg
	x	Nanticoke
	●	Lakeview
	v	Lingan
(b)	●	Estevan
	○	Thunder Bay
	△	Standard
	□	Atlantic

FIGURE 47: pH versus Time Curves for the leaching of glassy analogues of fly ashes and slags.

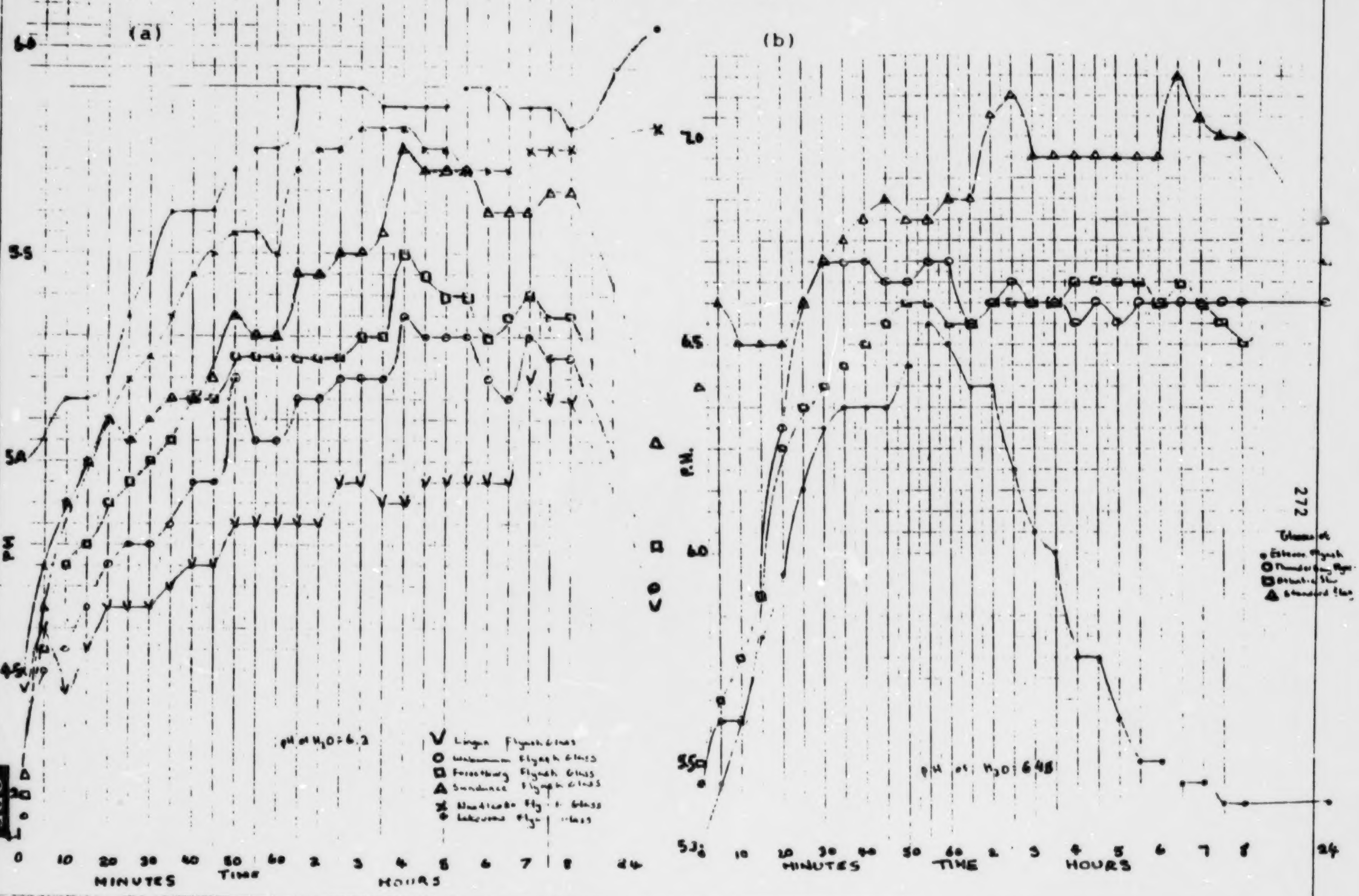

FIGURE 48: pH versus Time Curves of Redevitrified Analogues of Fly Ashes and One Slag

(a) ● Wabamun

△ Sundance

○ Forestburg

(b) ● Thunder Bay

○ Atlantic

ORF

FIGURE 48: pH versus Time curves of redevitrified analogues of fly ashes and one slag.

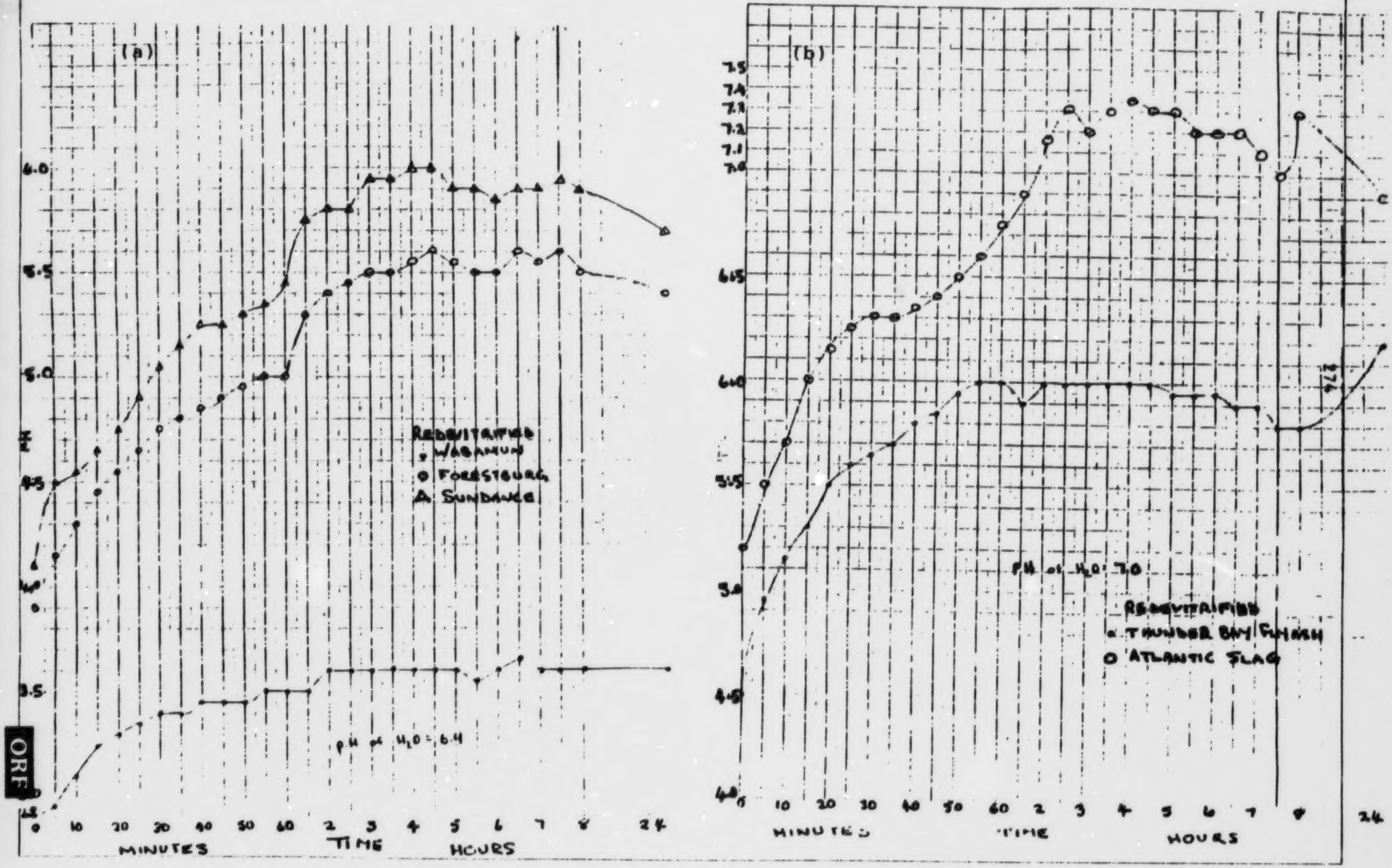

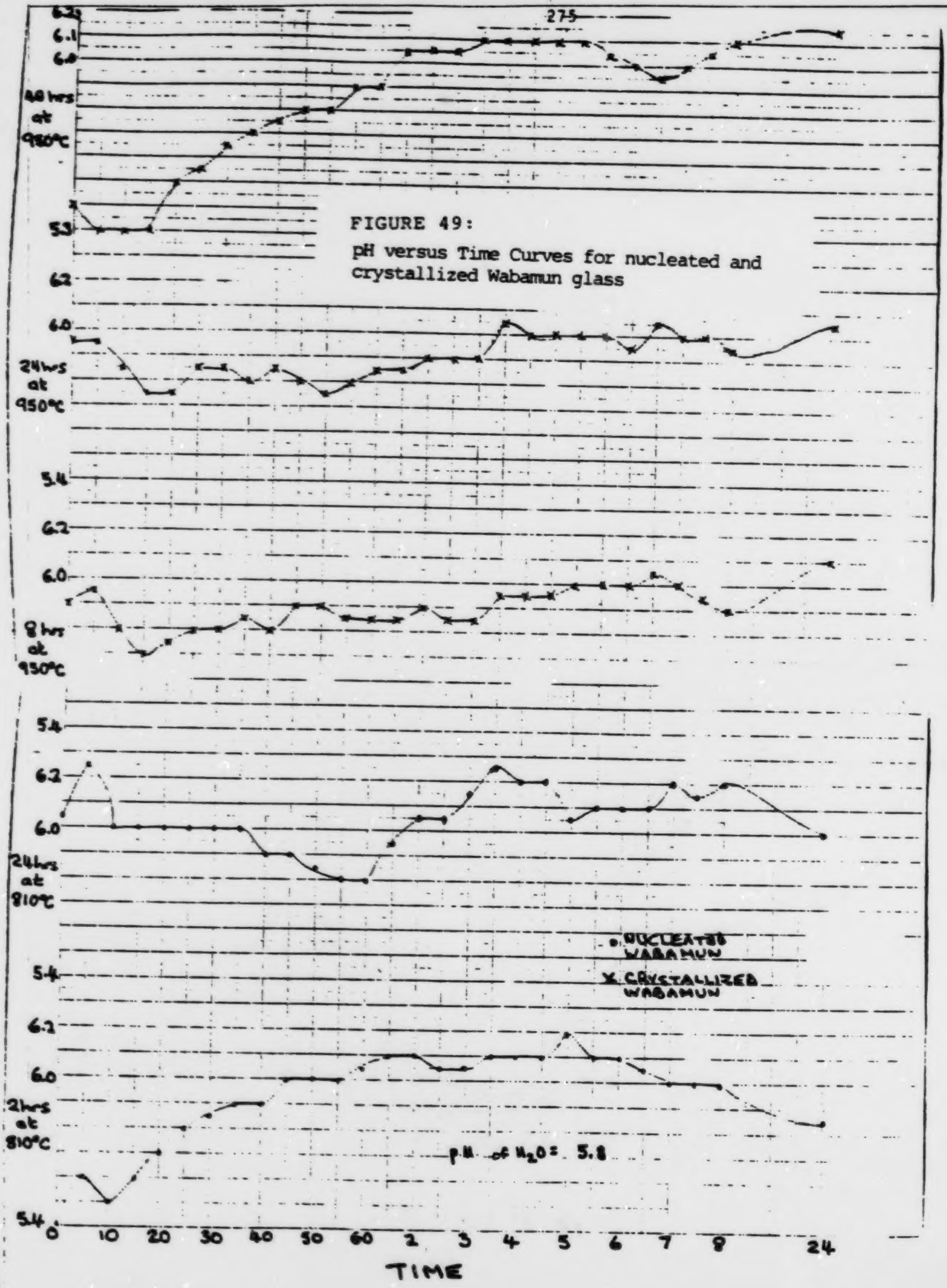

FIGURE 49:
pH versus Time Curves for nucleated and crystallized Wabamun glass

FIGURE 50:
PH versus Time curves of synthetic glasses with compositions similar to those of the glassy phases of five fly ashes.

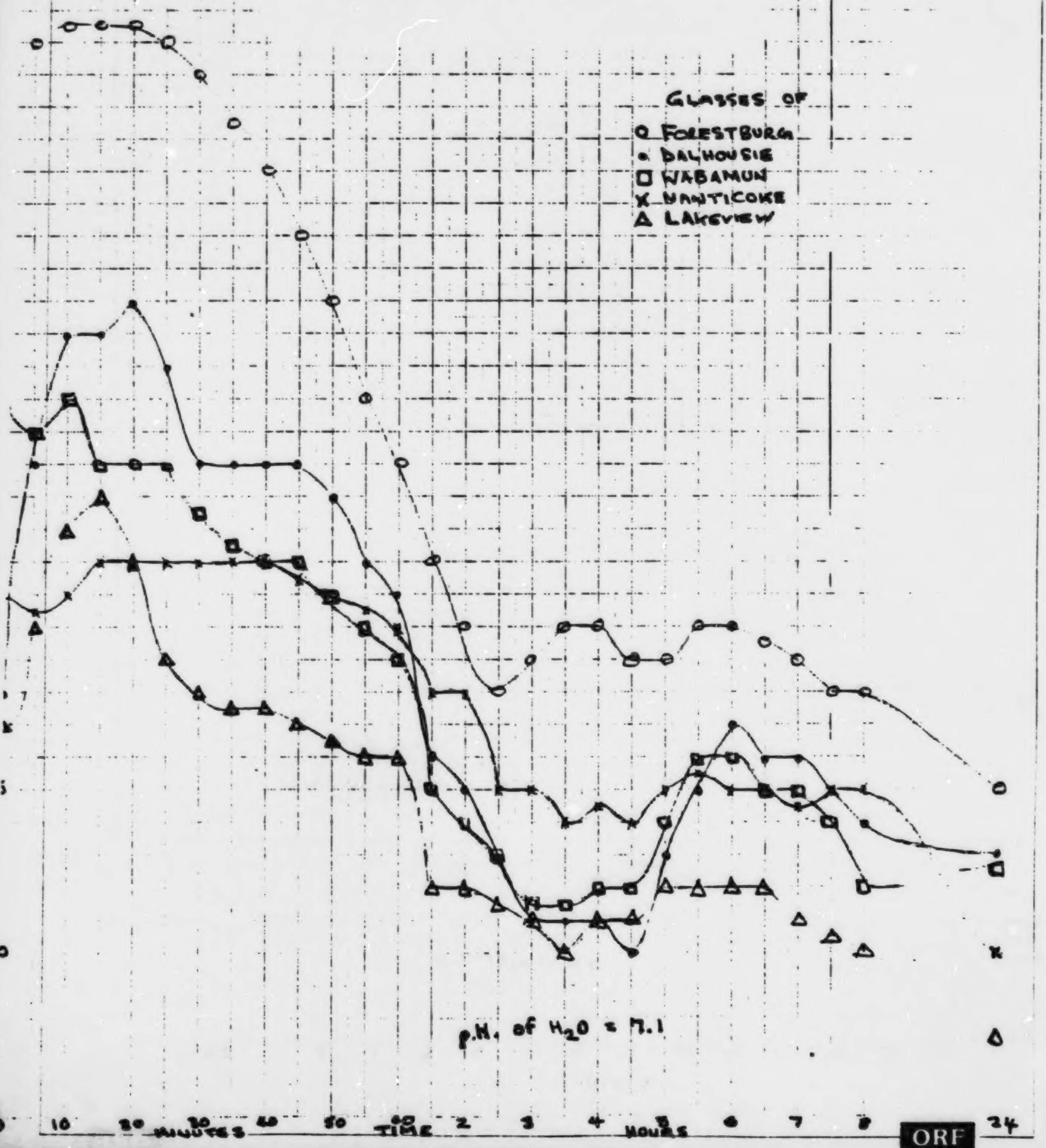

FIGURE 51: XRD pattern of leached Sundance fly ash glass.

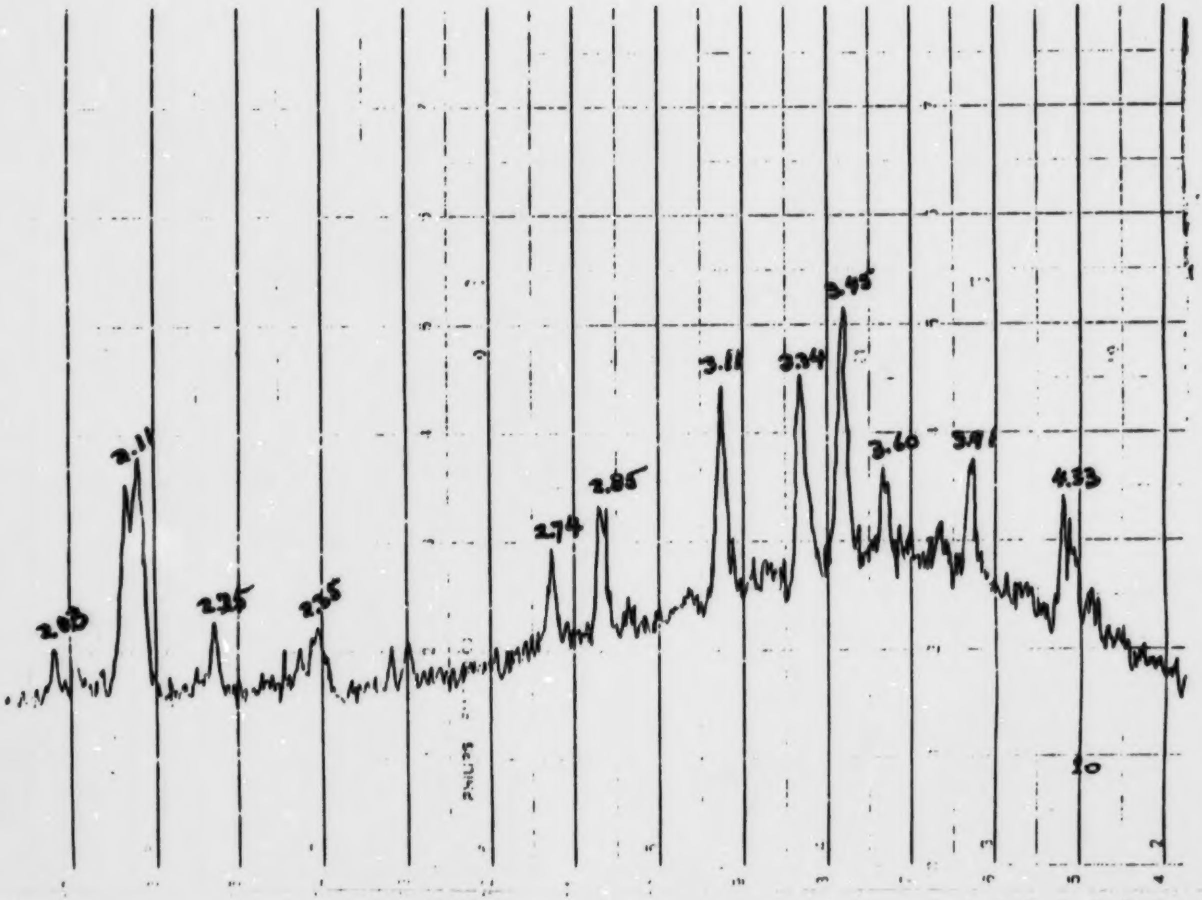

FIGURE 52: XRD patterns of Wabamun fly ash glass.

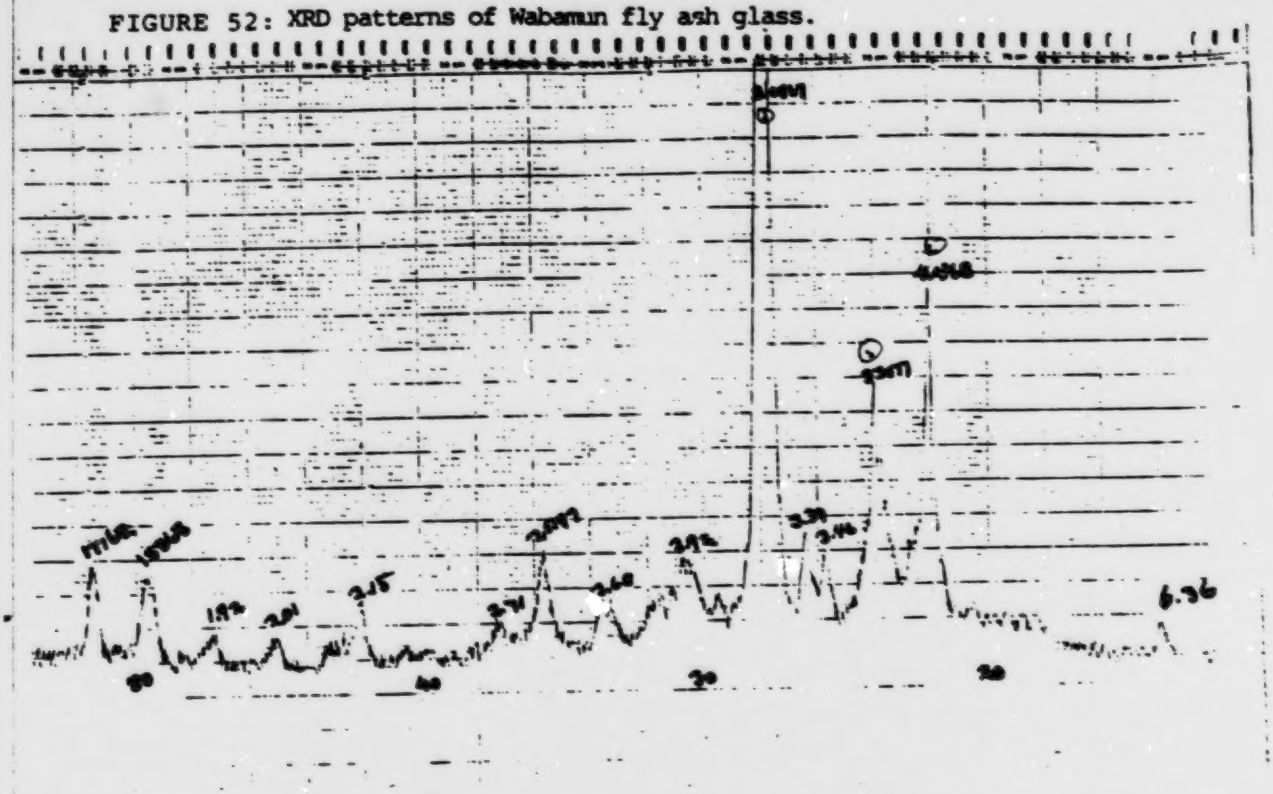

(a) nucleated at 810°C/16 hrs and crystallized at 950°C/2 hrs.

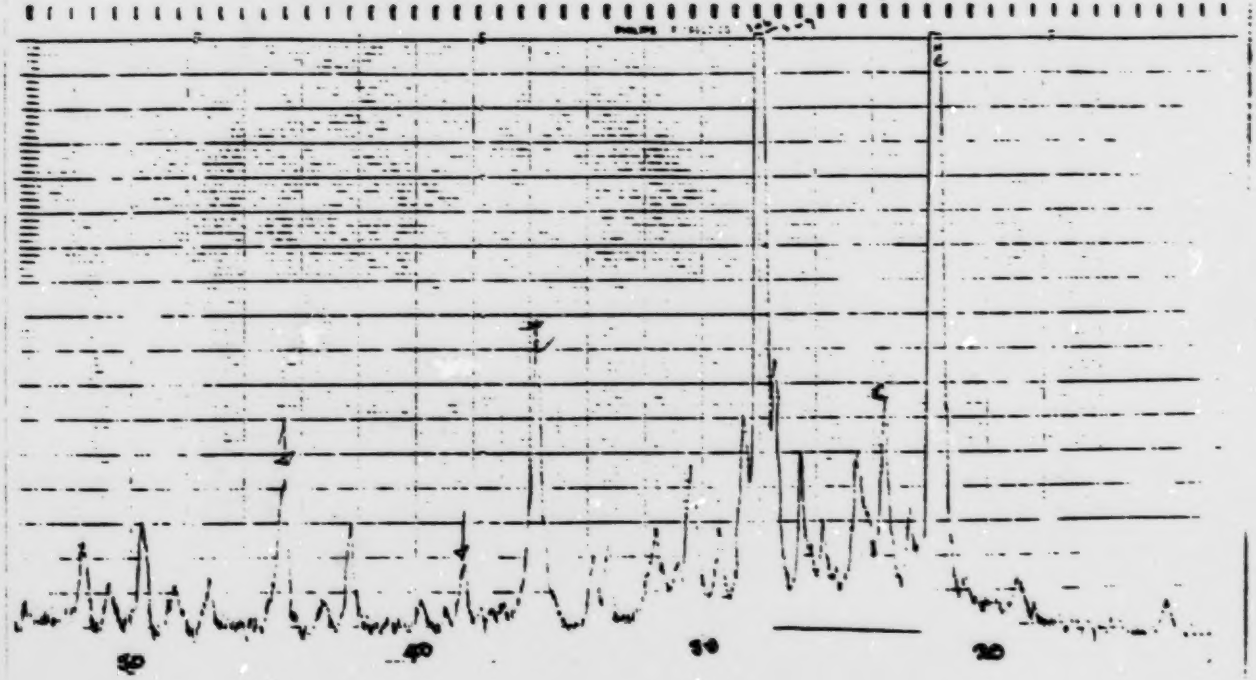

(b) nucleated at 810°C/16 hrs and crystallized at 950°C/48 hrs.

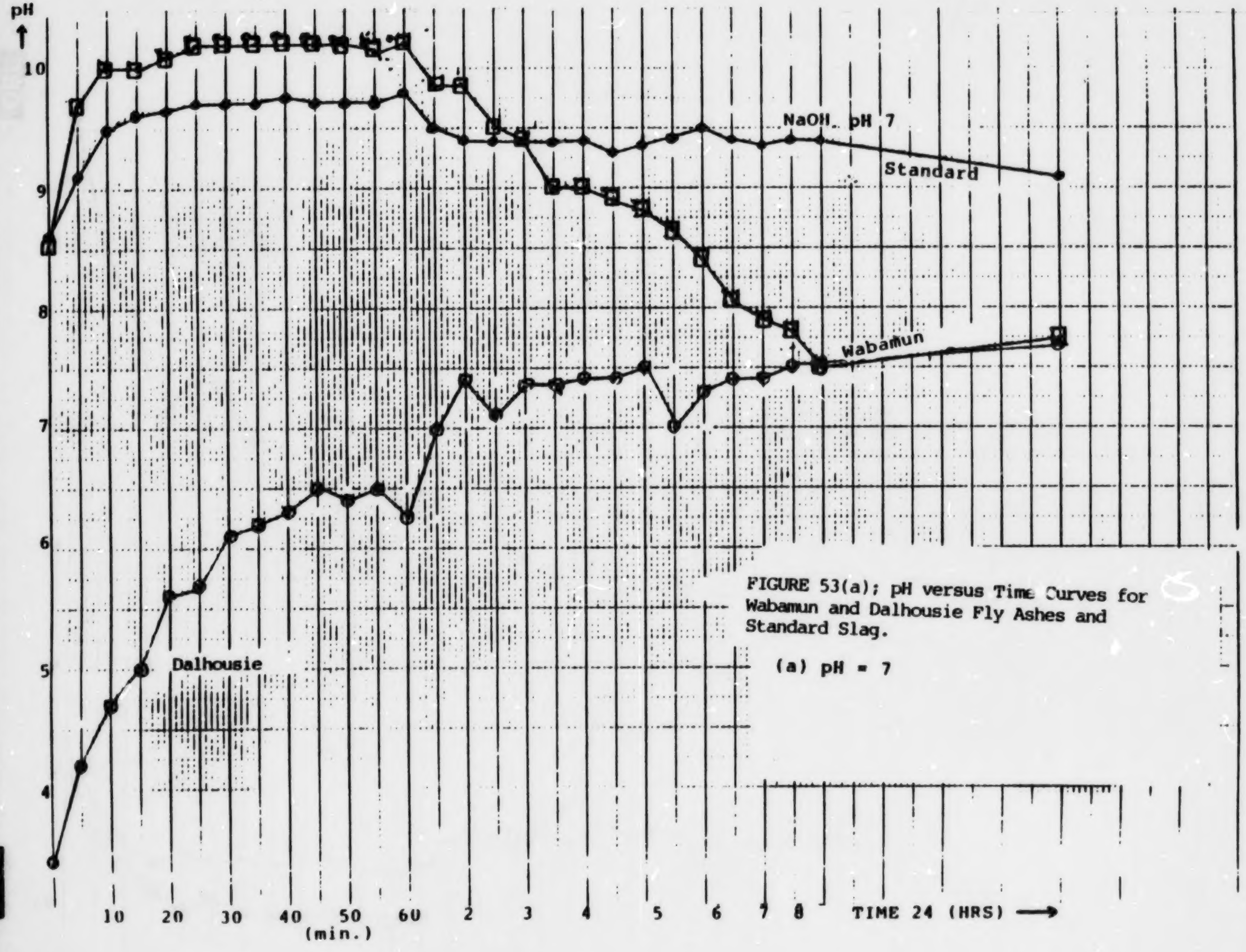

FIGURE 53(a); pH versus Time Curves for Wabamun and Dalhousie Fly Ashes and Standard Slag.

(a) pH = 7

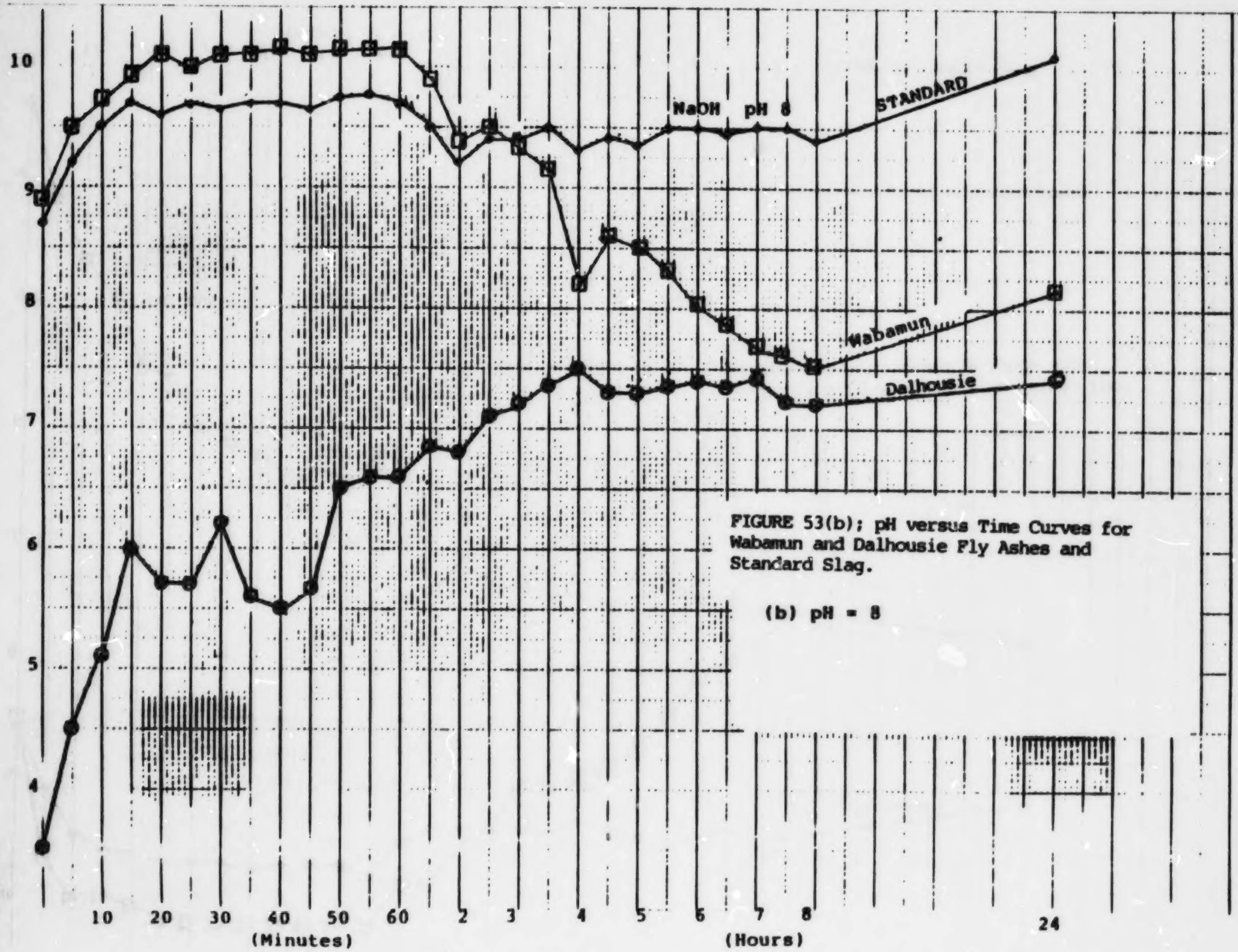

FIGURE 53(b); pH versus Time Curves for Wabamun and Dalhousie Fly Ashes and Standard Slag.

(b) pH = 8

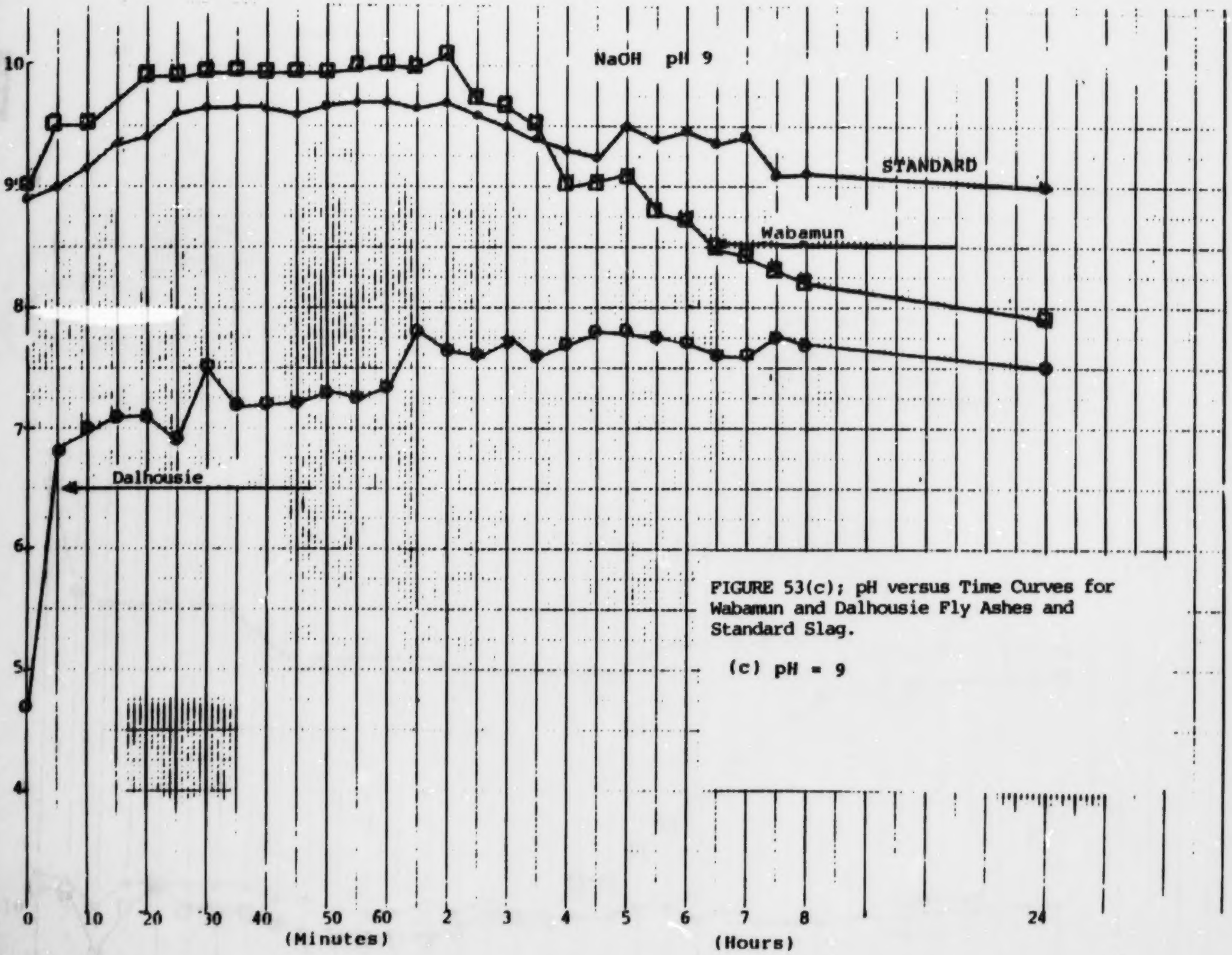

FIGURE 53(c); pH versus Time Curves for Wabamun and Dalhousie Fly Ashes and Standard Slag.

(c) pH = 9

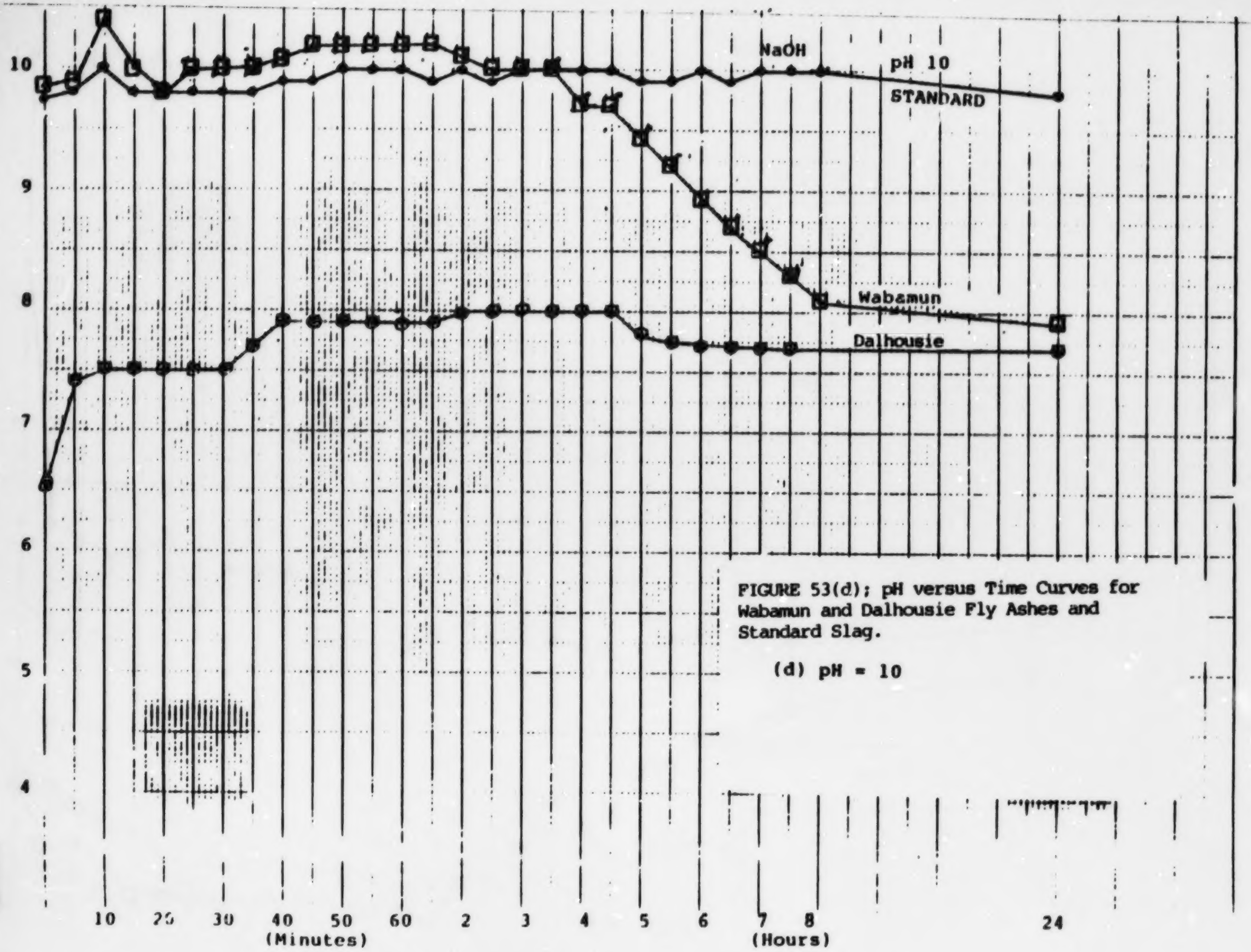

FIGURE 53(d); pH versus Time Curves for Wabamun and Dalhousie Fly Ashes and Standard Slag.

(d) pH = 10

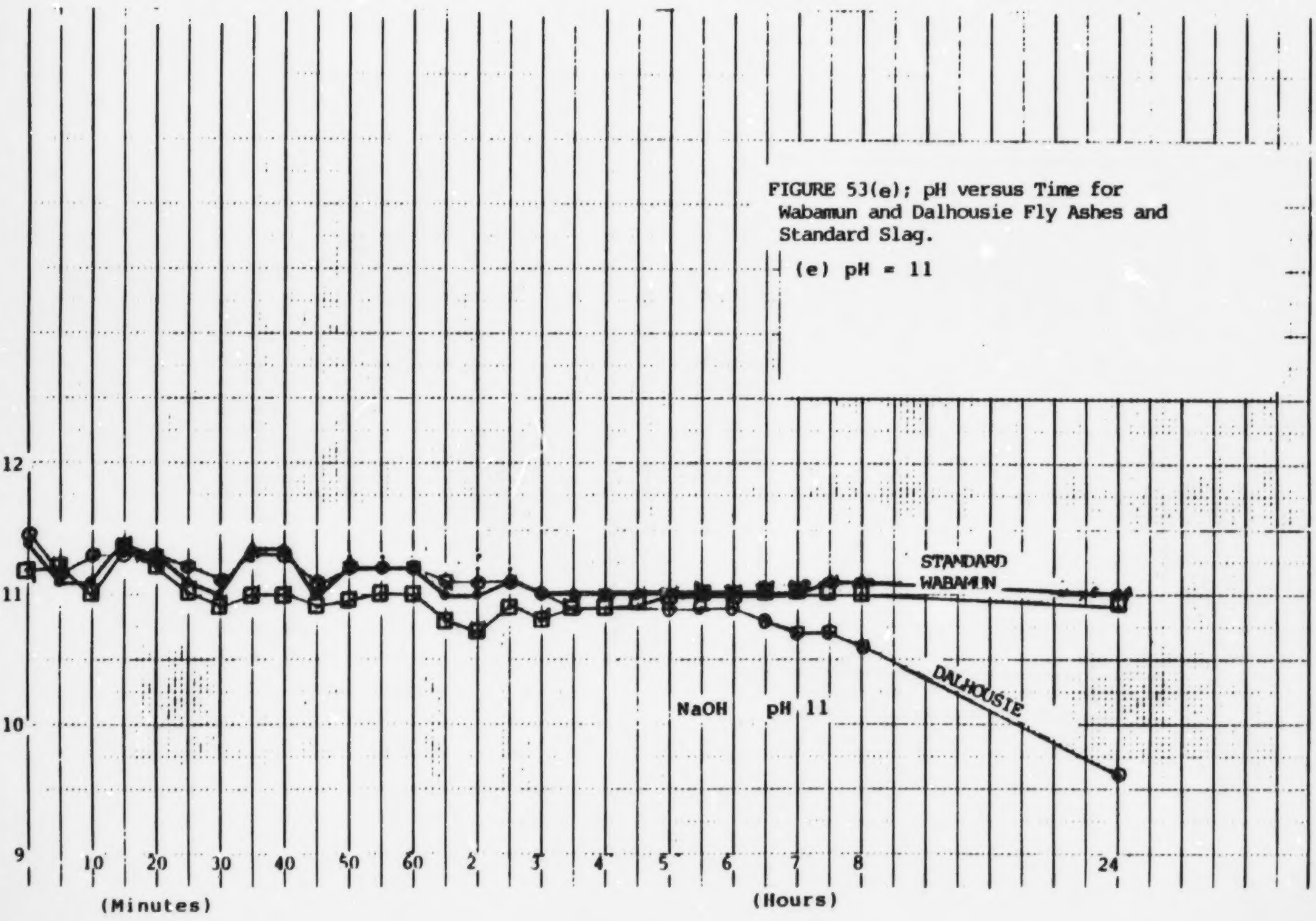

FIGURE 53(e); pH versus Time for Wabamun and Dalhousie Fly Ashes and Standard Slag.

(e) pH = 11

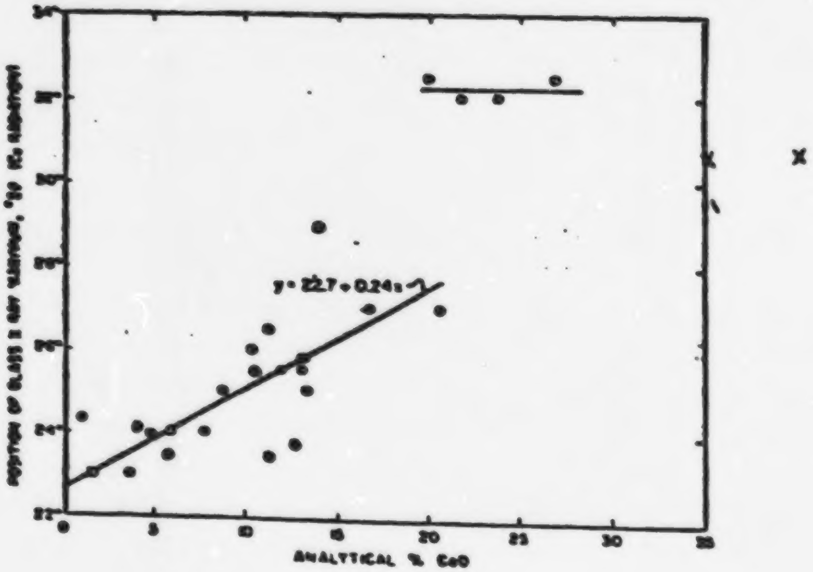

Positions of Glass X-ray Maxima vs Analytical CaO Contents for 16 Flyashes.

From Sidney Diamond,
Cement and Concrete Research
13, 459-464 (1983)

Figure 54 (from ref.7)

○ Data from ref. 7
● Fly Ash data from this study
x Slag data from this study

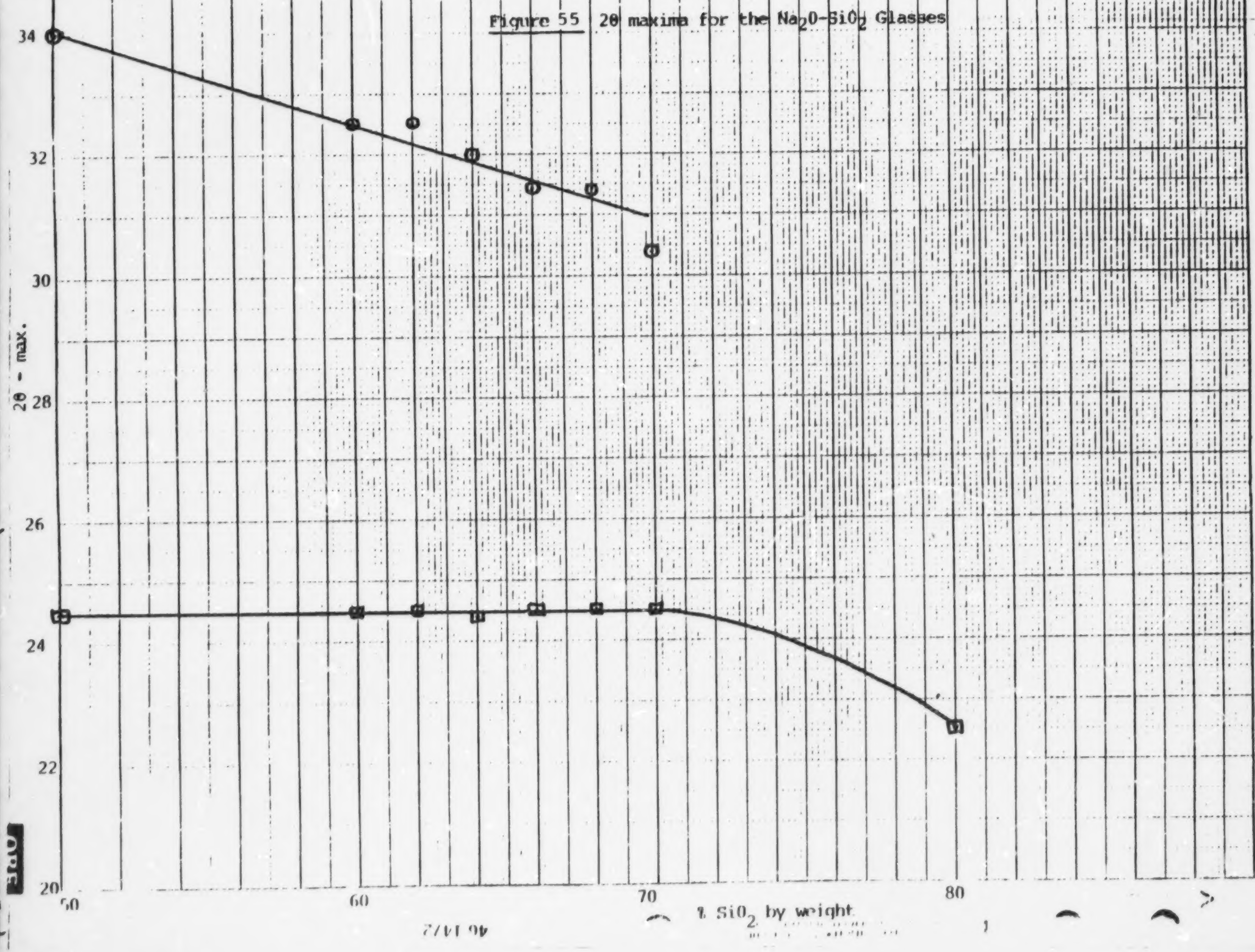

Figure 55 2θ maxima for the Na_2O-SiO_2 Glasses

APPENDIX A

APPENDIX A

Minutes of the Meeting of the Steering Committee held January 16, 1984, and September 21, 1984 at the Ontario Research Foundation

EMR FLYASH

(61-10178)

Development of a Unified Theory for Predicting the Behaviour of Glassy Waste Products (fly ash, silica fume, slags) in Concrete and to Develop New Compositions for Offshore Applications

Meeting of the Steering Committee, Jan. 16, 1984,
Ontario Research Foundation, Mississauga, 2:30 - 4.45 p.m.

Present: Dr. G. Carette, EMR CANMET
Dr. H. Chen, CCL
Dr. C. Gibbons, ORF
Dr. R. Hemmings, ORF
Mr. S. Johar, ORF
Dr. R.A. Kuntze, ORF - attended part of the meeting
Dr. M. Malhotra, EMR CANMET
Dr. P.K. Mehta, UC Berkeley
Dr. M.K. Murthy, ORF
Dr. V.S. Ramachandran, NRC
Dr. D.M. Roy, Penn State
Dr. M. van Roode, ORF

1. Dr. Malhotra outlined that the inhouse work of EMR is currently primarily devoted to the development of concrete technology. Contract work currently underway is aimed at achieving two objectives. The first aim is the gathering of engineering data on the use of pozzolans in controlling alkaline-aggregate reactivity. This work is being undertaken by Canada Cement Lafarge. The second objective is to carry out a fundamental study which will elucidate the basic mechanisms that determine the behaviour of waste materials, such as fly ashes, slags and silica fume in concrete formation.

This study, for which the contract was awarded to ORF, will also focus on the development of methodology for establishing the glassy content of these waste materials.

2. Dr. Murthy noted that ORF can make a significant contribution to new developments in concrete technology for high-performance applications. The Foundation has a track record in building materials research and development and testing and contract work has been carried out in the area of fly ash characterization and utilization. This factor combined with the expertise and capabilities in glass science, unique in Canada, form a strong basis for the fundamental study currently underway.

3. Dr. Kuntze expressed his appreciation to the Steering Committee for their assistance in defining ORF programs and projects in the area of advanced materials development. There can be a substantial pay off if this project can be linked to the real needs for the development of high-performance materials for structures to be used in exploration in the Arctic and other offshore areas.

4. Dr. van Roode described the objectives of the EMR Flyash program, the development of a unified theory for predicting the behaviour of glassy waste materials in concrete products and the development of new compositions of concrete for offshore applications on the basis of this new unified theory. These objectives are envisioned to be realized in a multiphase program with the emphasis during Phase I on a kinetic-mechanistic study to elucidate the reactions of the glassy waste materials with leaching media. Vital elements in this study are methodology for establishing the glass content, determination of composition and structure of the glassy portion, hydration kinetics, mechanisms and energetics, the effect of various devitrification schedules and the role of particle size distribution and surface area of the glassy waste materials.

5. Dr. Mehta commented on the X-ray study reported by S. Diamond which showed a dependency of the 2θ value of maximum intensity on the CaO content of the glass. The assignment of this 2θ value is not unambiguous because of interference of peaks of the crystalline phases with those of the glassy phases in the XRD spectrum. Moreover, the correlation of the higher 2θ maximum with a $C_{12}A_7$ glassy phase is rather speculative. Dr. van Roode showed data of work carried out at ORF that indicated that calcium silicate as well as some soda silicates produce a maximum at the higher 2θ value observed by Diamond. Dr Hemmings showed data which demonstrated that the correlation between 2θ and CaO reported by Diamond is rather poor for Canadian fly ashes. A better correlation is found between the maximum 2θ value and the combined total of all glass network formers in the fly ashes of a single rank.

6. Dr. Malhotra emphasized that the development of a rapid and simple test for the determination of glassy content of the waste materials is an essential element of the program. Dr. Ramachandran recommended that density fractionation may be useful as a technique to establish the glassy content of the fly ashes.

   Dr. van Roode presented data illustrating the potential of the method of Ohlberg and Stricker for the determination of the glassy content of fly ashes.

7. The members of the Steering Committee commented on the provisional outline of major tasks and subtasks presented by Dr. van Roode. Dr. Mehta suggested to delete silica fume and non-ferrous slags from the list of materials for consideration at this stage of the program. A good core set of samples for this study would include three Canadian fly ashes with CaO contents of 1-5%, 5-10%, 15-20%, respectively, and one U.S. fly ash containing 20-25% CaO. Dr. Malhotra proposed that six fly ashes would be selected on the basis of chemical analysis data and two blast furnace slags, a granulated and a pelletized specimen. Dr. Roy recommended that the selection of fly ashes should be governed by the maximum 2θ values in the XRD spectra.

8. Dr. Mehta stated that it was more important to select good flyashes for the hydration study than to consider synthetic glassy analogues because of substantial differences in shape and surface structure of the two classes of materials. The remelting and subsequent devitrification of flyashes was also objectionable for these reasons. Dr. Murthy emphasized the merits of the vitrification-devitrification route for an understanding of the role of the glassy phase in the hydration kinetic mechanistic study.

9. Dr. Murthy stated that the comments of the meeting would be incorporated in a revised work statement to be forwarded to the Steering Committee for feedback. Dr. van Roode will make arrangements with Dr. Carette to collect the samples of glassy waste materials from EMR.

10. The next meeting of the Steering Committee was scheduled for Monday, June 4, 1984, at ORF.

Mark van Roode
Research Scientist

Minutes of the EMR Fly Ash Program Review Meeting

Held Friday September 21, 1984,
10:30 a.m. - 3:00 p.m. at the
Ontario Research Foundation, Mississauga, Ontario

Present:

Dr. H. Chen	Canada Cement Lafarge Ltd
Dr. E. Douglas	Energy, Mines & Resources, (CANMET)
Dr. C.S. Gibbons	Ontario Research Foundation
Dr. R.T. Hemmings	Ontario Research Foundation
Mr. S. Johar	Ontario Research Foundation
Dr P.K. Mehta	University of California, Berkeley
Dr. D. Roy	Materials Research Laboratory, Penn State
Dr. M. van Roode	Ontario Research Foundation

1. Dr. van Roode reviewed the program objectives and major areas of work outlined at the meeting of the Steering Committee on January 16, 1984. The four major areas are: glass content methodology assessment, determination of composition and structure of the glassy waste materials, a study of the hydration behaviour of synthetic analogues of the glassy waste materials, a study of hydration kinetics and mechanism of the glassy waste materials. It was recommended that 6 Canadian fly ashes and 2 blast-furnace slags be characterized and evaluated.

   The major achievements to-date were reviewed.

   i) Literature Assessment.

      (a) Sources, availability and compositions of glassy waste materials - completed.
      (b) Methodology for glass content determination - completed.
      (c) Hydration kinetics - 75% completed.

ii) Glass Content Methodology and Assessment.

(a) Quantitative X-Ray Diffraction - completed for 8 fly ashes.

(b) Non-Crystalline Scattering Methods - One technique based on the optimum intensity of the non-crystalline scattering was evaluated and used to determine the glassy content of 5 fly ashes and two blast-furnace slags. Another X-ray technique (Amorphous Hump) was rejected. A third approach (Differential Intensity) is currently being evaluated.

(c) Techniques based on optical and electron microscopy in conjunction with image analysis showed little promise for glass content determinations.

iii) 9 Canadian fly ashes and 2 blast-furnace slags have been characterized by chemical and mineralogical composition, particle size distribution, surface area determination, X-ray diffraction, Fourier Transform Infrared spectroscopy and scanning electron microscopy in conjunction with energy dispersive analysis.

iv) Hydration studies have been carried out in H_2O on all "as received" glassy waste materials and on their glassy and redevitrified analogues. The effect of particle size was also addressed. Studies in NaOH were carried out as well for selected materials.

2. Dr. Douglas commented on the glass content data presented by Dr. van Roode. The low glass content measured for the Atlantic Slag measured by the Non-crystalline scattering method is a matter of concern. Also, efforts in the program should be directed towards completing the glass content study. In particular, an effort should be made to determine the glass contents of the slags using the quantitative X-ray technique. Dr. Douglas expressed concern about the information that could be obtained from the hydration studies given the time and funds available.

3. Dr. Mehta expressed doubt about whether any efforts for the remainder of the program should be directed towards hydration kinetics and mechanism. The results obtained to-date suggest that there is not a single method which can be used to determine glass contents of all fly ashes and slags. Dr. Mehta recommended that the remaining funds and time available should be used to complete the glass content methodology assessment. In particular, an attempt should be made to fill in the gaps in the glass content table.

4. Dr. Chen presented the engineering data of the Canfarge study on the hydration kinetics of glassy waste materials. Dr. Roy wondered how the results of the various glass content techniques correlated with the Canfarge data.

5. Dr. Mehta and Dr. Roy questioned the premise that a high glass content would contribute to the strength development in concretes incorporating glassy waste materials. Dr. Mehta referred to a Montebello paper which indicated that the high-Ca fly ashes which are not particularly glassy appear to be strength-developing. Dr. Roy indicated that in some cases the crystalline phases are the most reactive.

6. Dr. Douglas summarized the concensus of the Steering Committee concerning the directions of the remainder of the program. Efforts should be concentrated on completing as much of the glass content work as possible within the constraints of time and budget. Dr. Douglas pointed out that the publication of any results of the work carried out under this program had to await review of the data and approval by the Scientific Moniter.

M. van Roode

APPENDIX B

APPENDIX B

WORK STATEMENT

Development of a Unified Theory for Predicting the Behaviour of Glassy Waste Products (fly ash, silica fume, slags) in Concrete and to Develop New Compositions for Offshore Applications

M. van Roode

February 16, 1984

TABLE OF CONTENTS

		Page
1.	INTRODUCTION	B1
2.	Determination of the Glassy Content	B1
3.	Glass Composition and Structure	B2
4.	Hydration Study of Synthetic Analogues	B4
5.	Hydration Studies of the Glassy Waste Materials	B6
6.	Analysis and Correlation of Results	B6

1. INTRODUCTION

This revised work statement for the EMR Flyash project (Development of a Unified Theory for Predicting the Behaviour of Glassy Waste Products (fly ash, silica fume, slags) in Concrete and to Develop New Compositions for Offshore Applications) reflects the directions outlined by the Steering Committee for the project at its meeting of January 16, 1984 at the Ontario Research Foundation. The meeting was particularly helpful in that it stressed a systematic approach taking into account the complexity of the systems of this study. In particular compositional variations in fly ashes as a result of the process of its formation need to be considered. This work statement was prepared with these factors in mind.

The following stepwise approach is used here to elucidate the basic mechanisms that determine the behaviour of glassy waste materials, such as fly ashes, slags and silica fume in concrete.

(a) The determination of the glassy content of the waste material.
(b) The determination of the composition and structure of the glassy portion of the waste material.
(c) A study of the hydration behaviour of synthetic analogues of the waste material.
(d) A study of hydration kinetics, mechanisms and energetics of the glassy waste material.

The Steering Committee recommended that six Canadian fly ashes representative of a broad range of compositions and two blast furnace slags be selected for this study. In particular, the calcium content should be considered in selecting the fly ash compositions.

2. Determination of the Glassy Content

The behaviour of fly ashes, slags and silica fumes in concrete formation is largely attributable to their glassy nature. The determination of the glassy content of these materials is, therefore, the first major task in the project. There is currently no simple technique by which the glass content of fly ashes, slags and silica fumes can be determined. These materials may contain a glassy and several crystalline phases, the particle size distribution varies over a broad range, and the history of formation of the particles suggests that glass content (and composition and structure) may vary considerably between particles.

Practically, in concrete formation it is important to quantify the average behaviour of the glassy waste materials. The emphasis, therefore, will be to develop a simple method for the determination of the average glassy content. There are several potentially promising approaches to this problem:

(a) Determination of the glassy content from the non-crystalline scattering in the x-ray diffraction pattern of the glassy waste material.

(b) Determination of the glassy content from the crystalline scattering in the x-ray diffraction pattern of the glassy waste material.

(c) Determination of the glassy content by image analysis of SEM or optical micrographs of cut sections of a mounted or pressed sample of the glassy waste material.

(d) Determination of the glassy waste content by selective leaching of the vitreous fraction of the glassy waste material.

These four approaches and others as determined from the literature assessment will be investigated as to their applicability for fly ashes and/or slags.

3. Glass Composition and Structure

Having determined the glass content of the waste material the composition and structure of the glassy portion needs to be established since these parameters will determine the reactivity during the hydration process. Past workers have often referred to a glassy waste material in terms of its overall composition or stressed the content of a particular component, e.g. CaO. A recent study by Diamond [Cement and Concrete Research, 13, 459 (1983)] is an example of this approach. However, since the devitrification process will immobilize certain components of the glassy waste material in preference to others it is important to develop methodology for the estimation of the elemental composition of the glassy portion of the waste material. The following approaches are considered for this purpose:

(a) The crystalline scattering method will give a quantitative estimate of the amounts of the major crystalline phases. The elemental content of the glassy phase could be determined by substracting the elemental content of the combined crystalline phases from the overall composition of the glassy waste material.

(b) Selective leaching of the glassy phase with HF or HF/HCl solutions and chemical analysis of the leachates.

(c) X-ray dispersive analysis (EDXA) of the glassy phase of the waste material.

The elemental composition of the glassy phase of the fly ash or slag largely determines its structure. Broadly speaking the glass scientist distinguishes two categories of components in a glassy system. Network formers such as SiO_2, Al_2O_3 or B_2O_3 form the backbone of the three dimensional structure that give a glass its strength. Modifiers, e.g. the alkali and alkaline earth oxides, PbO and ZnO break up the network structure through the formation of non-bridging oxygens. The modifiers, therefore, soften the glass, improve its workability but lower its chemical durability. The latter factor is of prime importance for understanding the hydration behaviour of a glassy waste material.

The elemental composition of the glassy phase will determine the ratio of network formers to modifiers in the glass which is the first step to understanding glass structure.

There are a number of established techniques at the disposal of the glass scientist for probing glass structure.

(a) Differential Scanning Calorimetry (DSC) and Differential Thermal Analysis (DTA) can be used to analyze the thermal history of a glass and its softening point (DSP).

(b) Thermal expansion measurements can be used to determine the coefficient of thermal expansion and DSP. The latter parameters are indicative of the strength of the glass network.

(c) Viscosity measurements also provide valuable information regarding the strength of the glass network.

(d) Raman spectroscopy can be used to establish the presence of specific functional groups in a glass.

(e) X-ray diffraction can be used to interpret glass structure on the basis of an analysis of the glassy halo in the powder pattern.

The above techniques will be considered for the elucidation of the glass structure of the fly ashes and slags.

4. Hydration Study of Synthetic Analogues

Following the determination of the glassy content, glass composition and structure a series of synthetic analogues of the fly ashes and slags will be prepared for a hydration study. It is important to gain an understanding of the hydration behaviour of the glassy portion of the waste materials separately and then correlate the findings with the hydration behaviour of the waste materials as a whole.

It is fully realized at this point that the synthetic analogues only represent the average composition and structure of the glassy waste material. There are a number of important parameters, such as compositional variations for particles of various size ranges, specific particle shapes and the distribution of the glassy and crystalline phases which by necessity have to be approximated at this point of the investigation. However, the use of model systems to study the behaviour of more complex "real-life" situations is a valid approach in this case.

In preparing the synthetic analogues the following guidelines will be used:

(a) The composition should be representative of the compositions of the glassy phases found in the selected Canadian fly ashes and/or slags.

(b) The particle size distribution should be chosen with the particle size distributions of the selected fly ashes and slags in mind.

(c) The surface area should reflect the surface area of the glassy waste material for which it is an analogue.

Using the above guidelines the synthetic analogues can be prepared in several ways:

(a) From the chemically pure batch materials.

(b) From the original source material through a process of controlled devitrification.

Both techniques will be used for the analogue preparation.

The conditions of the hydration study will be varied to enable an evaluation of the key factors in the behaviour of the glassy waste materials in concrete formation. Leaching will be carried out with H_2O, alkali hydroxides and aqueous $Ca\ (OH)_2$. Reagent concentrations, pH and temperature will be varied. Enthalpy changes will be monitored by calorimetry. Changes in the glass surface/leached layer will be investigated by electron optical techniques.

5. Hydration Studies of the Glassy Waste Materials

The hydration study of the model systems should give an insight in the behaviour of the glassy phase of the glassy waste materials during concrete formation. The methodology developed under 4 will now be applied to the study of the "real-life" fly ashes and slags selected for this study.

The hydration investigation will be carried out along similar lines. The leaching solutions will be H_2O, alkali hydroxide solutions and aqueous $Ca(OH)_2$. Solution parameters will be varied to cover a range of concentrations, temperatures and pH values. Enthalpy changes will be monitored by calorimetry.

6. Analysis and Correlation of Results

The findings of the experimental work described under 2-5 will be analyzed and correlated. The conclusions reached will form the basis for a theoretical framework from which the behaviour of glassy waste products in concrete formation can be predicted. The relationships between glassy content, composition and structure of the glassy phase and hydration kinetics, mechanisms and energetics will be established.

M. van Roode

APPENDIX C

APPENDIX C

LITERATURE ASSESSMENT

TABLE OF CONTENTS

Page

CHAPTER 1: SOURCES, AVAILABILITY AND COMPOSITIONS OF GLASSY WASTE MATERIALS

1.1 Introduction C1
1.2 Blast Furnace Slag C1
1.3 Steel Making Slags C3
1.4 Non-Ferrous Slags C6
1.5 Fly ash C7
1.6 Silica Fume C8
References C12

CHAPTER 2: GLASS CONTENT METHODOLOGY

2.1 Introduction C14
2.2 Methodology for Glass Content Determination C14
2.3 X-Ray Techniques C16
  2.3.1 Quantitative X-Ray Determination (QXRD Method) C16
  2.3.2 Non-Crystalline Scattering Methods C17

2.4 Optical Techniques C21
  2.4.1 McMaster Individual Particle Analysis C21
  2.4.2 South African Optical Procedure C21
  2.4.3 Parker and Nurse Optical Method C21
  2.4.4 Rheinhausen Optical Method C21
  2.4.5 Optical Mineralogical Composition C22

2.5 Spectroscopic Techniques C22
  2.5.1 Automated Ultra-Violet Reflectance Method C22
  2.5.2 Rheinhausen Ultra-Violet Method C22
  2.5.3 Infrared Techniques C23
  2.5.4 Nuclear Magnetic Resonance C24

2.6 Electron-Optical Techniques C24
2.7 Solution Techniques C25

TABLE OF CONTENTS (contd)

Page

2.8 Density Method C25
2.9 Differential Thermal Analysis C26
2.10 Selection of Glass Content Methodology C26
References C29

CHAPTER 3: HYDRATION KINETICS AND MECHANISMS OF GLASSY WASTE MATERIALS

3.1 Introduction C33
3.2 Kinetics and Mechanism of Cement Hydration C33
3.2.1 Cement Hydration C34
3.2.2 Kinetics of Portland Cement Hydration C36
3.2.3 A Model for Cement Hydration C40

3.3 Slag Hydration C43
3.3.1 Blast Furnace Slags C43
3.3.2 Assessment of Results C57
3.3.3 Non-Ferrous Slags C62

3.4 Fly Ash Hydration C63
3.5 Assessment of Results C72
References C75

CHAPTER 1

SOURCES, AVAILABILITY AND COMPOSITIONS OF GLASSY WASTE MATERIALS

1.1 INTRODUCTION

The annual production of glassy waste materials (slags, fly ashes and silica fumes) in Canada is about 12.5 million tonnes. A breakdown over the various categories is given in Table 1.1.

TABLE 1.1

Annual Production of Glassy Waste Materials in Canada

Type	Quantity($\times 10^6$ tonnes)	Ref.
Iron blast furnace slags	2.84	(1)
Steel slags	3.22	(1)
Non-ferrous slags	3.73	(1)
Fly ash	2.5	(2)
Silica fume	0.2	(3)

1.2 Blast Furnace Slag

Slags result from the fusion of fluxing stone, gangue and fuel ash during the pyroprocessing of metallic ores. The first report on the utilization of slags surfaced in 1862 when Langens discovered that iron blast furnace slag, granulated from the molten state by quenching in water possessed good cementing properties (4). Since then slags have been used in Europe to reduce the energy consumed in making concrete.

Table 1.2 lists the sources and quantities of slags produced in Canada annually (5).

TABLE 1.2

Sources and Quantities of Iron Blast
Furnace Slags in Canada (5)

Source No.	Location	Quantities (tonnes/year)
F1	Sydney, N.S.	172,000
F2	Sault Ste.Marie, Ont.	1,100,000
F3	Hamilton, Ont.	660,000 (220,000 pelletized)
F4	Hamilton	907,000
	Total	2,839,000

The approximate chemical compositions of the slags of Table 1.2 are listed in Table 1.3.

TABLE 1.3

Approximate Chemical Compositions of Canadian Iron Blast Furnace Slags (5)

Source No.	Percentage Oxides (by mass)						
	CaO	MgO	SiO_2	Al_2O_3	Total Fe	FeO	Fe_2O_3
F1	44	12	33	10.3	0.8	1.0	1.1
F2	38	19	38	8.2	-	-	0.6
F3	38.9	10.3	38.9	7.8	-	0.5	-
F4	30-40	10-20	35-45	5-9	1.0	-	-

Of the blast furnace slag up to 200,000 tonnes per year is pelletized for use as a lightweight aggregate or after grinding, as a supplementary cementing material.

Figure 1.1 shows the section of the system $CaO-SiO_2-Al_2O_3$-(10% MgO) which covers the main field of equilibrium compositions for blast furnace slags produced in North America (6). The equilibrium compositions are in the region of melilite solid solutions, intermediate in composition between akermanite (C_2MS_2) and gehlenite (C_2AS).

Four general classes of blast furnace slag may be distinguished.

(a) Air cooled, largely crystalline slag. Traditionally this type has been used as aggregate or granular base material.

(b) Foamed or expanded slag is used as a light-weight aggregate. This type is no longer used in Canada because of the air pollution problems caused by H_2S during foaming.

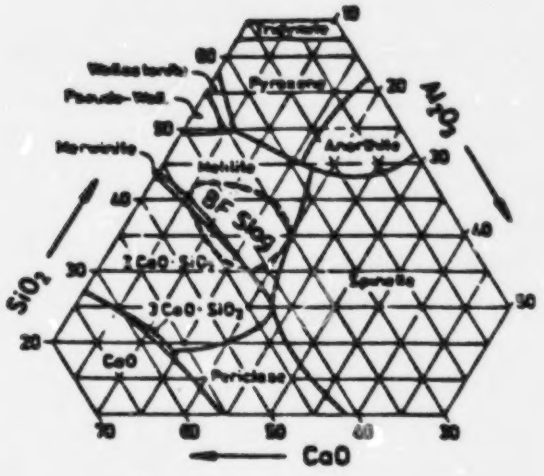
Tridymite
Wollastonite
Pseudo-Woll.
Pyroxene
Anorthite
Merwinite
Melilite
BF Slag
2 CaO · SiO$_2$
3 CaO · SiO$_2$
Spinelle
CaO
Periclase
SiO$_2$
Al$_2$O$_3$
CaO
10
60
50
40
30
20
20
30
40
50
70
60
50
40
30

Main field of chemical compositions of blast furnace slags with 10% MgO

Figure 1.1 (6)

(c) Granulated slag, formed when molten slag is rapidly quenched with water. This is the primary source of slags used for hydraulic cements in Europe, Japan and the U.S.

(d) Pelletized slag is produced by expanding molten blast furnace slag under water sprays and passing the resulting pyroplastic material over a spinning drum. Pellets are formed because of surface tension when the broken slag is carried through the air.

1.3 Steel Making Slags

Sources and quantities of steel slags in Canada are listed in Table 1.4.

TABLE 1.4

Sources and Quantities of Steel Slags in Canada

Source No.	Location	Quantities (tonnes/year)
S1	Sydney, N.S.	127,000
S2	Montreal, Quebec	5,400
S3	Montreal, Quebec	9,000
S4	Contrecoeur, Quebec	227,000
S5	Contrecoeur, Quebec	16,000
S6	Sault St. Marie, Ontario	635,000
S7	Welland, Ontario	27,000
S8	Burlington, Ontario	36,000
S9	Hamilton, Ontario	640,000
S10	Whitby, Ontario	455,000
S11	Hamilton, Ontario	500,000
S12	Hamilton, Ontario	450,000
S13	Selkirk, Manitoba	14,000
S14	Regina, Saskatchewan	65,000
S15	Edmonton, Alberta	10,000
S16	Vancouver, B.C.	6,000
	Total	3,222,400

The approximate compositions are listed in Table 1.5.

TABLE 1.5

Approximate Chemical Compositions of Canadian Steel Slags (5)

Source No.	Percentage Oxides (by mass)						
	CaO	MgO	SiO_2	Al_2O_3	Total Fe	FeO	Fe_2O_3
S1	10-50	2-3	11-29	2-8	8-40	-	-
S2	37.5	9.9	33.3	6.9	0.9	-	-
S3	40-46	-	12-14	-	-	15-25	-
S4	40	15	20	5	-	20	-
S5	44.3	7.0	18.7	5.6	16	-	-
S6	36.7	7.4	13.6	1.6	-	-	21.9
S7	40-55	5-15	25-50	0-5	1-10	-	-
S8	41.6	7.3	15.9	3.9	12.5	-	-
S9	46.0	6.7	13.6	0.9	-	24.1	-
S10	47	11	23	10	2.5	-	-
S11	25-38	8-15	8-16	1-3	16-29	12-24	5-17
S12	44-53	5-9	14-22	0.7-1.6	8	15	6-12
S13	40-50	5-10	10-20	5-10	7-20	-	-
S14	40	7	15	9	20	-	-
S15	35	15	20	5	8	-	-
S16	45	-	14	-	2	-	-

As can be seen from Table 1.5 the composition of steel-making slags varies widely and these materials are generally not utilized for their hydraulic activity. They are either returned to the blast furnace for recovery of iron or are used for highway base or granular fill.

More recently, the introduction into the Basic Oxygen Process (BOP) converter of a prefired flux containing CaO, Al_2O_3, MgO and Fe_2O_3 has been claimed to produce a homogeneous, low free-lime slag (7). Classical BOP slags are largely crystalline and contain P_2O_5

stabilized β-calcium orthosilicate ($2CaO.SiO_2$), ferrites (e.g. $2CaO.Fe_2O_3$), calcium phosphate ($3CaO.P_2O_5$), wustite, FeO and (Ca, Fe, Mn, Mg)O solid solutions. They contain negligible amounts of vitreous material and their hydraulic activity is low. Hydraulic activity in the modified process is achieved bringing the Al_2O_3 content up to 6 to 10% which produces enough of a compound with nominal formula $4CaO.Al_2O_3.Fe_2O_3$ to give a useful level of hydraulic properties.

1.4 Non-Ferrous Slags

The sources of non-ferrous slags in Canada are the copper, nickel and lead industries. Table 1.6 lists the sources and quantities produced.

TABLE 1.6

Sources and Quantities of Copper, Nickel and Lead Smelting Slags in Canada (8)

Source No.	Location	Metal	Quantities (tonnes/year)
1	Noranda, Quebec	Cu	474,000
2	Noranda, Quebec	Ni	252,000
3	Murdochville, Quebec	Cu	308,000
4	Falconbridge, Ontario	Cu, Ni	600,000
5	Coppercliff, Ontario	Cu	145,000
6	Coppercliff, Ontario	Ni	1,451,000
7	Thompson, Manitoba	Ni	464,000
8	Flin Flon, Manitoba	Cu	-
9	Kamloops, B.C.	Cu	-
10	Belledune, N.B.	Pb	127,000
11	Trail, B.C.	Pb	159,000
			3,728,000

Selected approximate compositions for the non-ferrous slags of Table 1.6 are listed in Table 1.7.

TABLE 1.7

Approximate Chemical Compositions of Canadian Non-Ferrous Slags

Source No.	Percentage Oxides (by mass)				
	CaO	MgO	SiO_2	Al_2O_3	Fe_2O_3
1	1.3	1.8	33.8	6.2	51.6
3	5	1	40	4	42.9
4	1.8	2.0	38	5.7	52.9
5	1.5	1.2	35	5	58.6
6	2.2	2.4	37	5.6	52.9
7	2.3	5.4	40	6.1	45.3
10	14.5	-	19.6	2.1	47.1
11	14	2	26	6	42.9

Regardless of the different process types that have been utilized the slags in Table 1.7 are remarkably similar in composition. Their compositions may be represented by the CaO-SiO_2-FeO system (see Figure 1.2). The non-ferrous slags contain a glass phase, fayalite (Fe_2SiO_4) and minor quantities of magnetite (Fe_3O_4) (9).

1.5 Fly Ash

Fly ash is the generic term which describes the fraction of the residue remaining after the combustion of pulverized coal in power-generating stations. Table 1.8 lists the production and utilization figures for coal ash on a world wide basis (2). It can be seen that of the 2.6 million tonnes of coal ash produced in Canada in 1977 only 27.1% was utilized. In 1981 a total of 21 coal fired thermal generating stations produced about 3.7 million tonnes of ash, including 2.5 million tonnes of fly ash (2). The location of the principal coal- burning generating stations in Canada is given in Figure 1.3

TABLE 1.8

PRODUCTION/UTILIZATION STATISTICS FOR COAL ASH: MAJOR ASH USES IN THE WORLD (1977)*

		U.S.A.	POLAND	UNITED KINGDOM	FED. REP. GERMANY	GERMAN DEM. REP.	CANADA	WORLD
	ASH PRODUCTION:							
	Total ash produced ($x10^3$ tonnes)	61,495	15,000	12,336	15,000	15,000	2,626	278,443
	Total ash utilized ($x10^3$ tonnes)	9,079	5,512	5,070	3,413	2,475	711	31,605
	% Ash production utilized	14.8	36.7	41.1	22.7	16.5	27.1	11.4
	END USE:			---(Percent of utilized ash)---				
1.	Structural fill	24.3	0.2	44.8	5.8	--	75.9	18.3
2.	Portland cement replacement	15.8	9.1	--	9.1	--	18.3	17.7
3.	Addition to Portland cement	4.1	1.8	0.6	--	24.2	0.3	12.9
4.	Road stabilizer	4.7	38.1	--	--	1.6	--	10.1
5.	Aerated concrete block	--	18.1	32.2	--	1.0	--	5.8
6.	Blasting and roofing grit+	14.9	--	--	7.8	--	--	5.1
7.	Asphalt mineral filler	1.3	--	--	29.3	--	?	3.7
8.	Cement raw material	5.3	--	--	4.6	--	--	3.2
9.	Lightweight aggregate¶	2.8	?	6.0	--	9.1	--	2.5
10.	Bricks and ceramics	--		--	6.9	3.4	--	1.8
11.	All other uses§	26.9	32.7	16.4	36.6	60.6	5.2	30.1

+ boiler and cyclone slag;
¶ bottom ash and sintered (Lytag) ash; § agriculture, fillers, ice control, mineral extraction, mineral wool, grout, etc.

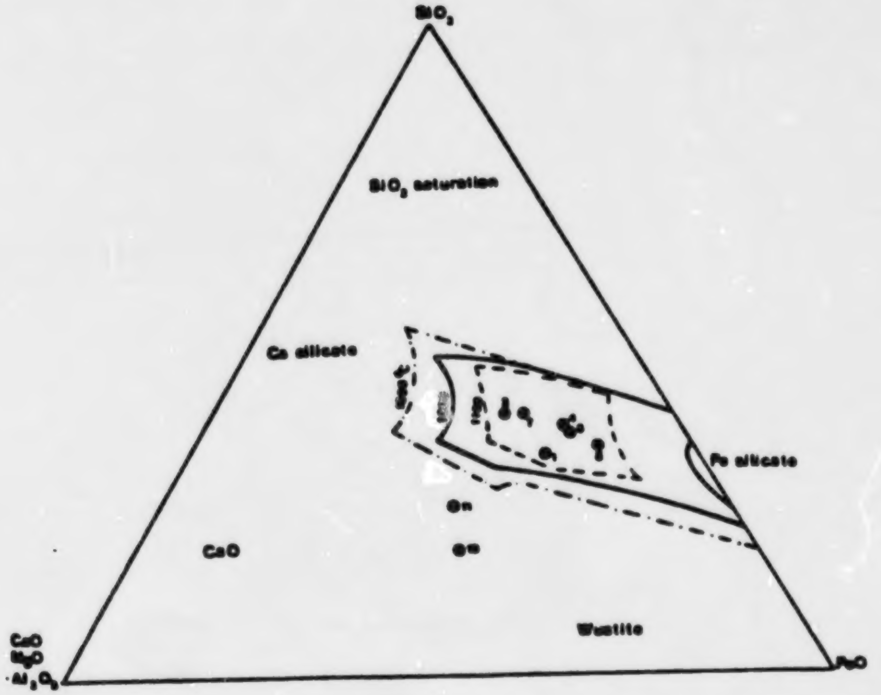

Figure 1.2
The System Ca-SiO_2-FeO (1)

Figure 1.4 shows concentration ranges for the major chemical components of coal ashes. It can be seen that the major differences between the coal ashes derive from the origin of the coal used. Bituminous coals tend to produce ashes that have relatively high Fe_2O_3 and low CaO contents. On the other hand, subbituminous and lignitic coals have relatively low Fe_2O_3 and high CaO contents.

1.6 Silica Fume

Silica fume and ferrosilicon dusts are by-products of the manufacture of silicon metal and ferrosilicon alloys, respectively. These solids are produced through the oxidation of escaping SiO gas at the top of the open furnace. It has been estimated that about 500,000 tons of silica fume are available in the Western World and Japan (11). An estimate for the U.S. and Canada gives a total annual production of 205,000 tonnes of silica fume with SiO_2 content in excess of 70% (12).

THE LOCATION OF CANADIAN COAL-BURNING GENERATING STATIONS*

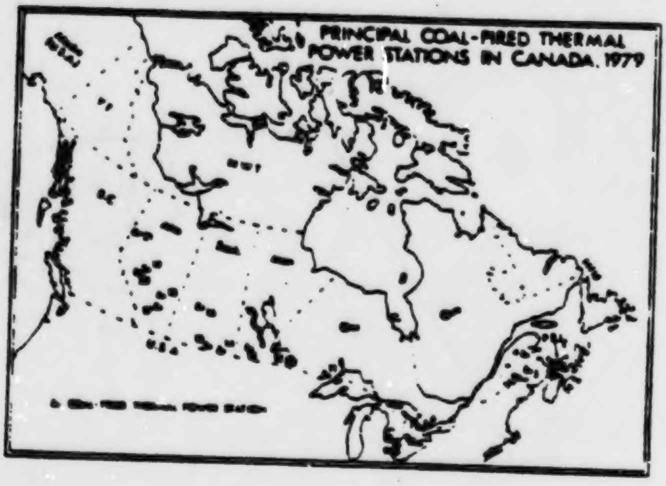
PRINCIPAL COAL-FIRED THERMAL POWER STATIONS IN CANADA, 1979

Legend:

1. Glace Bay, Lingan
2. Trenton
3. Harrison Lake
4. Dalhousie, Chatham
5. Grand Lake
6. R.L. Hearn
7. Lakeview
8. Nanticoke
9. J.C. Keith
10. Lambton
11. Thunder Bay
12. Selkirk
13. Brandon
14. Estevan
15. Boundary Dam
16. Queen Elizabeth
17. Drumheller
18. Battle River
19. Wabamun
20. Sundance
21. H.R. Milner

* Source: J.A. Aylsworth and W.J. Wevland, "Coal and Coke", Canadian Minerals Yearbook, pp125-138, Energy, Mines and Resources Canada (1979).

Figure 1.3 (2)

ORF

CONCENTRATION RANGES FOR THE MAJOR CHEMICAL OMPONENTS OF COAL ASHES

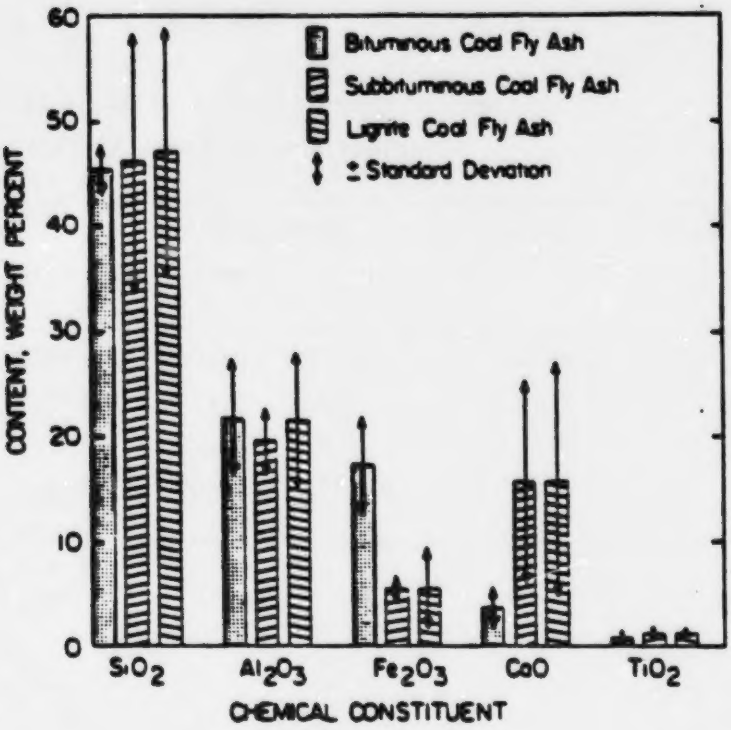

Figure 1.4 (2)

Table 1.9 lists the chemical composition of silica fume from various locations.

TABLE 1.9

Chemical Composition of Silica Fume from Various Sources (mass %) (12)

Component	Australian	US/Canada		Norway	
		Min.	Max.	Ferro-silicon	Silicon-metal
SiO_2	88.60	63.30	96.00	86-92	94-98
Al_2O_3	2.44	0.10	5.45	0.2-0.6	0.1-0.4
Fe_2O_3	2.56	0.10	12.20	0.1-1.0	0.02-0.15
C	3.00	1.75	10.00	0.8-3.0	0.2-2.0

References

1. E.E. Berry, "The Cementitious Properties of Slags - A Critical Review", Contract of the Department of Energy, Mines and Resources, Canada (CANMET) (March, 1982).

2. E.E. Berry, R.T. Hemmings and J.S. Burns, "Coal Ash in Canada: Volume 1, Ash as a Potential Resource", Canadian Electrical Association, Report G195 (August 16, 1982).

3. J. Wolfsiefer, Study for the U.S. and Canada, Internal Norcem Report (March, 1979).

4. F.M. Lea, "The Chemistry of Cement and Concrete", Chemical Publishing Co., New York (1971).

5. R.K. Collings and S.S.B. Wang, Mineral Waste Resources of Canada Report No. 7 - Ferrous Metallurgical Wastes, CANMET REPORT 80-19E, Energy Mines and Resources Canada (May, 1980).

6. H.G. Smolczyk, Slag Structure and Identification of Slags, Proceedings of the 7th Int. Congr. Chemistry of Cement, Paris 1(111), 3-17 (1980).

7. M. Conjeaud, C.M. George and F. Sorrentino, A new steel slag for cement manufacture: Mineralogy and hydraulicity, Cement and Concrete Research 11, 85-102 (1981).

8. R.K. Collings and S.S.B. Wang, Personal Communication in ref. 1.

9. I. Gaballah, F. Jeannot, L.C. Dufour and Gleitzer, Reactivite de l'aluminate et du silicate de fer dans des reactions d'oxydo-reduction, Silicates Ind. 41, 427-438 (1976).

10. J.R. Baragano and P. Rey, The study of a non-traditional pozzolan: Copper slag, Proc. 7th Int. Congr. Chemistry of Cements, Paris Paper III - 37 (1980).

11. P. Jahren, Experience with Addition of Silica to Concrete, NIF - Air Pollution Seminar, Trondheim (May, 1981).

12. P. Jahren, Use of Silica Fume in Concrete, Fly Ash Silica Fume, Slag and Other Mineral By-Products in Concrete Vol. II, Publication SP-79, American Concrete Institute, Detroit, V.M. Malhotra, Editor, pp.625-642 (1983).

CHAPTER 2

GLASS CONTENT METHODOLOGY

2.1 Introduction

To predict the behaviour of glassy waste products in concrete formation the properties of these waste products ought to be established. The literature surveyed revealed that the following properties of these materials are worthy of further consideration:

(a) glass content and quality,
(b) glass composition and structure,
(c) particle size distribution,
(d) surface area.

These four properties determine to a large extent the reactivity of the glassy waste materials in concrete hydration. In this chapter the methodology for the determination of glass content, will be surveyed and its usefulness for this project will be assessed.

2.2 Methodology for Glass Content Determination

A number of studies have addressed the importance of glass content of slags for the strength of slag-concrete. Schwiete and Dolbor (1) modified quenching conditions for each of 30 slags and found that the predominant factor affecting strength was glass content. Slags with 30 to 40% glass could still be employed, however. Smolczyk (2) did not find a linear relationship between glass content and strength and Demoulian et al.(3) reported that the strengths of slags with glass contents in excess of 95% were reduced.

The degree to which glass content can be measured with precision is doubtful, however, and the results between various techniques are not always in agreement with each other. The various methods of glass content determination in slags have been reviewed by Hooton (4).

Table 2.1 lists the various methods of glass content determination reported for glass-ceramics, polymers, slags and other waste materials.

TABLE 2.1

Techniques for Glass Content Determination

Technique	Used for	Ref.
1. X-Ray Techniques		
- QXRD Method	mineral dusts, portland cement, coal ashes, slags, glass-ceramics.	4-8, 10-12
- Amorphous Intensity Method	glass-ceramics	13
- Amorphous Hump Method	pozzolans	4, 14, 15
- Amorphous-Crystalline Method	polymers	16
- Differential Intensity Method	polymers	17
2. Optical Techniques		
- McMaster Individual Particle Analysis	slags	4, 11, 18
- South African Optical Procedure	slags	19
- Parker and Nurse Method	slags	20
- Rheinhausen Optical Method	slags	21
- Optical Mineralogical Composition	slags	22
3. Spectroscopic Techniques		
- Automated UV Reflectance	slags	23, 24
- Reinhausen UV method	slags	21, 24
- Infrared Method	polymers, slags, fly ashes	9, 25-28
- NMR method	polymers	9
4. Electron-Optical Techniques	glass-ceramics, fly ashes	29, 30, 31
5. Solution Method	fly ashes	32, 33
6. Density Method	polymers	9

2.3 X-Ray Techniques

X-ray diffraction techniques have been used to determine the glassy or crystalline contents of such diverse materials as mineral dusts (5), Portland cement (6), coal ashes (7), slags (4), glass-ceramics (8) and polymers (9). All methods are essentially based on the assumption that the crystalline and non-crystalline components of a material make distinguishable contributions to the scattering intensity of its XRD pattern.

Broadly speaking, two approaches have been used. In the first one, the percentages of each of the crystalline phases is determined from the crystalline scattering and the glass content is computed by difference. The second approach involves the calculation of the glass content directly from the non-crystalline scattering. Both approaches can be used, in principle, for the determination of the glass content of glassy waste materials.

2.3.1 Quantitative X-Ray Determination (QXRD Method)

In a sample containing glassy and crystalline phases, the mass fraction of each crystalline phase can be determined by measuring peak intensities at selected 2θ-values as ratios to the peak intensity of an added internal standard. This technique has been used extensively for the quantitative determination of the crystalline phases in mineral dusts (5), Portland cement (6), coal ashes (7), slags (4) and glass-ceramics (8). The method which can give an accuracy of ±5% has been described in detail by Klug and Alexander (10). Crucial to the success of the method are the following factors:

(a) A chemically stable internal standard with several strong diffraction lines in the XRD pattern free of interference from the crystalline phases to be identified.

(b) A particle size less than 5 μm.

(c) The preparation of standard curves to improve accuracy.

(d) Sufficient counting time and/or repeated scanning to improve accuracy.

Provided the major crystalline phases can be identified this technique is particularly useful since it enables the calculation of glass content by difference and the quantitative estimation of the composition of the glassy phase by subtraction of the elemental content of the crystalline phases from the overall composition.

Simons and Jefferey (7) used the QXRD technique to determine the crystalline and glass content of a number of pulverized fuel ashes from U.K. and U.S. sources. Glass contents calculated varied from 52 to 87%.

Hooton and Emery reported glass contents between 10 and 100% for a number of commercial slags from various sources using the QXRD technique (11).

Mehta has used the QXRD technique in a semi-quantitative manner to indicate the magnitude of the content of various crystalline phases in 11 U.S. fly ashes (12).

2.3.2 Non-Crystalline Scattering Methods

A number of variants exist on this approach in which the non-crystalline scattering is determined either in conjunction with or without an added internal standard. The crystalline scattering may be considered as well.

a. Amorphous Intensity Method

In this approach the glass content is calculated by comparing the intensity of the amorphous halo at a suitable 2θ-value between sample to be analyzed and a standard which is fully vitreous. The technique in this form has been used for the determination of the glass and crystalline content of single-phase glass-ceramics (13). The accuracy claimed was ±5% or better. The method requires the preparation of fully vitreous and crystalline analogues with the same overall composition as the waste material.

b. Amorphous Hump Method

In another variant the glass content is estimated by comparing the area of the amorphous halo with the area of a selected peak of an added internal standard. This approach referred to as the "Amorphous Hump Method" (4) has been used to determine the glass content of pozzolans (4).

Since the position and area of the hump depends on the composition of the glass a series of standard glasses of a range of compositions are required. Also, as pointed out by Mather (15), the use of copper radiation on iron also causes a halo due to secondary iron emissions. No calibration curves are required for this method.

c. Amorphous-Crystalline Scattering Method

This technique, which can be used if a 100% amorphous standard is not available, has been reported for polymers. For the method to be applicable (a) samples with a considerable range of crystallinity must be available, and (b) it must be possible to draw an acceptable demarcation line between the crystalline and amorphous scattering over some angular interval that encompasses the principal amorphous halo.

Figure 2.1 shows the principle of the method which has been applied to several organic polymers (16). The crystalline intensity (I_c) is taken as the area above the curve ACD, while the amorphous intensity (I_a) is the area between the curves AED and BCD. Conversely the intensity at a specified 2Θ-value (e.g. $I_{a,2\Theta}$) can be taken to represent the amorphous scattering. The crystalline content is then calculated from:

- the regression curve based on I_c and I_a
- the regression curve based on I_c and $I_{a,2\Theta}$
- from I_a values alone as described under (a) above.

In general, good agreement has been found between the methods listed above. The advantage of this method is that there is no need for vitreous and crystalline analogues of the glassy waste material under consideration.

Figure 2.1 (from Ref. 16)

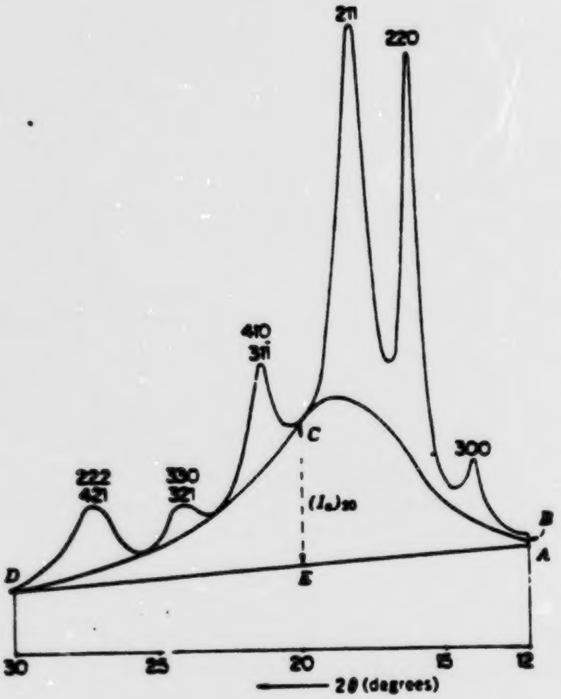

(a)

X-Ray scattering curve of a partially crystalline isotactic polystyrene specimen (Challa, Hermans, and Weidinger)

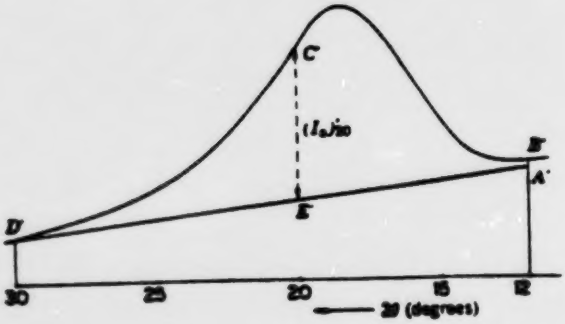

(b)

X-Ray scattering curve of a fully amorphous isotactic polystyrene specimen (Challa, Hermans, and Weidinger)

ORF

d. Differential Intensity Method

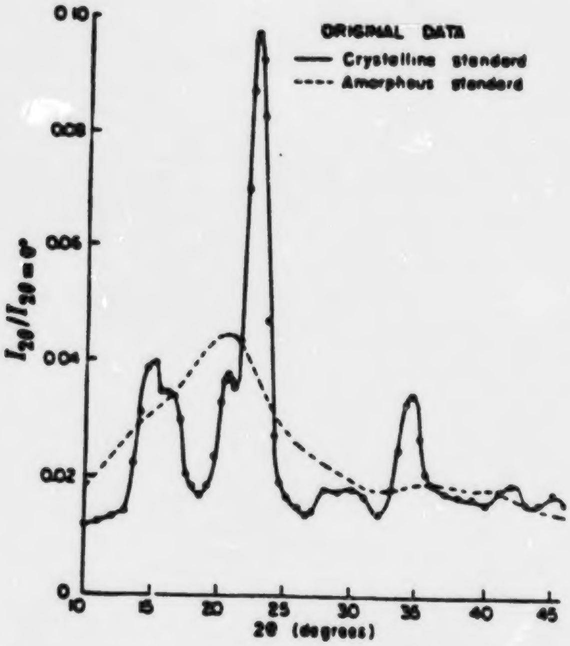

X-Ray intensity curves of the crystalline and amorphous standards used for the analysis of cotton cellulose. (Wakelin, Virgin, and Crystal)

Figure 2.2 (From ref. 17)

The method devised by Wakelin et al.(17) for polymers is based on the calculation of an integral or correlation crystallinity index.

$$\text{Integral Index:}\quad C_i = \frac{\sum_{2\theta_o}^{2\theta_m}(I_u-I_a)}{\sum_{2\theta_o}^{2\theta_m}(I_c-I_a)}$$

$$\text{Correlation Index:}\quad (I_u-I_a) = C_c\,(I_c-I_a) + B$$

where: I_u : intensity of sample at designated 2θ-values
I_a : intensity of the amorphous polymorph over the 2θ-range
I_c : intensity of the crystalline polymorph over the 2θ-range.

The intensity values are measured over small 2θ-increments (e.g. 0.5^o).

ORF

2.4 Optical Techniques

Techniques using optical microscopy are based on statistical counting of glassy and crystalline particles. A number of variants have been developed for slags.

2.4.1 McMaster Individual Particle Analysis

This procedure originally developed by Emery et al. (18) was modified by Hooton and Emery (11) to distinguish between clear glassy particles, birefringent crystalline particles and opaque, milky particles. Well washed, -65 µm/+45 µm grains, immersed in ethylene glycol are observed under cross-polarized light at 400 x magnification. The glass particles do not transmit cross-polarized light while most crystalline materials do and tend to glow due to birefringence. The method was found to correlate well with the QXRD method for slags.

2.4.2 South African Optical Procedure

This cross-polarized light procedure has been adopted in Canada by Standard Slag Cement Co. (19). This method uses the -65 µm/+45 µm fraction of ground slag immersed in camphor oil. The opaque particles are assumed to be glass, orange translucent particles are crystalline. At least 4 or 5 counting areas need to be scanned. This method was found to be highly insensitive to changes in glass content.

2.4.3 Parker and Nurse Optical Method

The original method published in 1949 (20) is currently employed in a modified form by Frodingham Cement Company in Britain. Grains, -90 µm/+53 µm, of slag immersed in bromoform are examined by transmitted light at 200 x magnification using an eyepiece with a graticula. The percentage of opaque particles is subtracted from 100 to obtain the percentage glass.

2.4.4 Rheinhausen Optical Method

This method was developed at the Rheinhausen Institute for Blast Furnace Slags, Rheinhausen, W. Germany. A polished section is made of -60 µm/+40 µm ground slag bedded into a plastic material polished in plastic. The polished sample is etched with 1% alcoholic HNO_3 and HF vapour. An integration occular is used to count the vitreous and crystalline components. The method has been described by Schroder (21).

2.4.5 Optical Mineralogical Composition

The method was developed by Steyn (22) in South Africa to identify and quantify each crystalline phase in slags with the glass content obtained by difference. The samples after mounting are subjected to 10 successive grinding and polishing stages. Linear traverses are made in seven stages with six different etchants being used. The method is more accurate than the Rheinhausen Optical method but extremely tedious.

2.5 Spectroscopic Techniques

Several techniques have been developed to determine the glass content of slags, polymers, etc. using ultraviolet and vibrational spectroscopy.

2.5.1 Automated Ultra-Violet Reflectance Method

This method described by Foster (23) employs an ultra-violet (uv) spectrophotometer fitted with a solid sample chamber. The technique measures the percentage of emission at 590 nm compared to a standard arbitrarily assigned a value of 100% glass. The method is employed by the Dravo Lime Company in the U.S. to assess the slag cement used in its Calcilox sludge stabilization process. Since the standard may actually contain less than 100% glass, glass contents in excess of 100% are sometimes observed by this method. The largest number ever assigned to a slag by this method was 165% (23).

Hooton and Emery reported that this technique, although able to identify slags of low glass content, may give erroneous results for slags with higher glass contents (19). A further drawback may be the interference with the UV radiation due to minor oxide contents (24).

2.5.2 Rheinhausen Ultra-Violet Method

This method was described by Schroder (21). A preliminary study of this technique, using a portable UV light source, showed this procedure to be more qualitative in nature. The technique also poses a hazard to the eyes of the operator. As with the Automated UV Reflectance Method minor oxide staining may cause interference (24).

2.5.3 Infrared Techniques

Although infrared absorption is not a good measure of long range order, or crystallinity, certain infrared bands of polymers can be specifically related to the configuration states of molecular chains. Various workers have been able to relate the intensities of specific infrared bands to the amorphous fraction of polymers (9, 25-27).

Table 2.3 gives a comparison between the percentage crystallinity of a series of poly(ethylene terephtalate) samples measured by density, X-ray and infrared methods.

TABLE 2.3 (from Ref. 26)

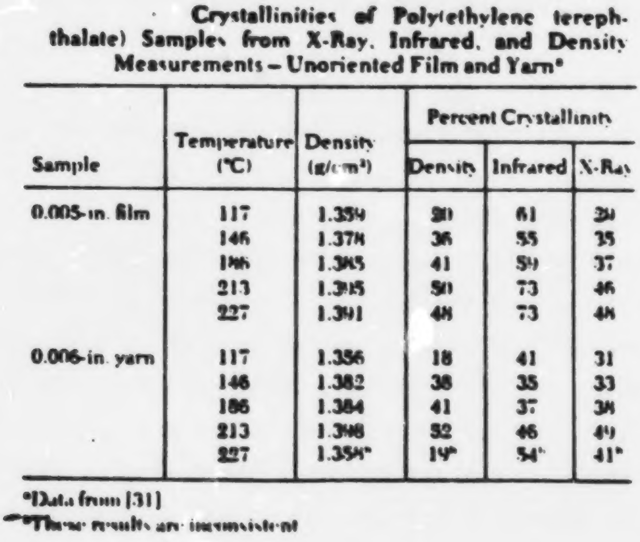

Crystallinities of Poly(ethylene terephthalate) Samples from X-Ray, Infrared, and Density Measurements – Unoriented Film and Yarn[a]

Sample	Temperature (°C)	Density (g/cm³)	Percent Crystallinity		
			Density	Infrared	X-Ray
0.005-in. film	117	1.359	20	61	29
	146	1.378	36	55	35
	186	1.385	41	59	37
	213	1.395	50	73	46
	227	1.391	48	73	48
0.006-in. yarn	117	1.356	18	41	31
	146	1.382	38	35	33
	186	1.384	41	37	38
	213	1.398	52	46	49
	227	1.358[b]	19[b]	54[b]	41[b]

[a] Data from [31]

[b] These results are inconsistent

Dougherty (28) reported the use of an infrared technique in conjuction with an internal standard to calculate the glass content of slags and fly ashes. The method was reported to give good correlation with other techniques for slags but poor correlation for fly ashes.

2.5.4 Nuclear Magnetic Resonance

The possibility of measuring degree of crystallinity of polymers by the nuclear/magnetic/resonance (NMR) method is based on the fact that when the frequency of molecular motion equals or exceeds approximately 10^4 s^{-1} the resonance curve is narrowed. Under these conditions the NMR absorption consists of a superposition of a narrow resonance and a broad resonance. The narrow and broad components are resolved graphically, and the ratio of the areas of the narrow and broad components is taken as equal to the ratio of the amounts of rapidly moving polymer and relatively stationary polymer. On the assumption that the rapidly and slowly moving portions represent amorphous and crystalline regions, respectively, a numerical value can be assigned to the crystalline fraction.

This technique which gave results for organic polymers in good agreement with XRD data may not be useful for inorganic glasses because of the measuring temperature requirement which has been found to be in excess of the glass transition temperature for organic polymers (9).

2.6 Electron-Optical Techniques

Electron-microscopy for determining the percent crystallinity of glass-ceramics is well known. Carrier (29) described an SEM technique in which the glassy phase of a partially devitrified glass-ceramic is selectively etched leaving the crystalline phase in relief. The volume percent of the crystalline material can be determined by areal analysis, lineal analysis or point counting on electromicrographs. The technique is more complex for glass-ceramics with more than one crystalline phase. Several solvents may be required to preferentially etch the various phases, leaving an often complex relief. the method is applicable if the crystal size is in excess of 0.1 µm. The glass content is obtained by difference.

Doherty and Leombruno (30) describe a TEM technique for the determination of the crystalline phases in a glass-ceramic using a selected area diffraction technique and dark-field micrography. Amorphous material can be photographed by placing an aperture in the amorphous halo and taking a photograph of the area underneath it.

TEM can also be used to study the glassy and crystalline phases in even the smallest (sub-micron) fly ash particle (31). However, a substantial amount of development work will be required to adapt these methods for routine glass content determinations of materials as complex as fly ashes.

2.7 Solution Techniques

Hulett et al. (32,33) have described a technique by which the fly ash can be quantitatively separated into three matrices: glass, mullite-quartz and magnetic spinel. The method involves size-fractioning and magnetic separation. The iron containing spinels and oxides are removed from the aluminosilicate residue by treatment with concentrated HCl. The glass phase is removed from the non-magnetic phases by etching with 1% HF, leaving behind a mullite-quartz rich residue. The method is potentially useful since it will enable a calculation of the glass content and the composition of the glassy phase.

2.8 Density Method

Crystallization in a system is accompanied by an increase in density. The glass content by volume can be represented by:

$$X_{a,v} = \frac{\rho_c - \rho}{\rho_c - \rho_a}$$

ρ_c : crystalline density
ρ_a : amorphous
ρ : density of the unknown sample

The glass content by mass is given by

$$X_{a,m} = \frac{\rho a}{C} \quad \frac{(\rho c - \rho)}{(\rho c - \rho a)}$$

This method, which has been used for polymers (9), requires that the densities of a fully vitreous sample, a fully re-devitrified sample and the unknown sample can be determined. The results agree well with those determined by XRD techniques (26) as can be seen from Table 2.3.

It is implicit in this method that:

- the density of the amorphous phase is the same in the fully vitreous and unknown sample;
- no pores exist in the fully vitreous and unknown specimens.

It is unlikely that these conditions will apply rigorously for glassy waste materials. This is particularly true for fly ashes which contain substantial proportions of hollow spherical particles (cenospheres).

2.9 Differential Thermal Analysis

This method has been used in Germany and South Africa in relationship to hydraulic properties but with little success (24, 34). The method is based on measuring the area of the slag devitrification exotherm (800-900°C) for a known weight of sample. Unfortunately, each mineral has its own exotherm (35) and the results change with the chemical composition of the slag.

2.10 Selection of Glass Content Methodology

For the purposes of determining the glass content of the different types of glassy waste materials the following criteria have been used:

- The technique must be applicable to slags, fly ashes and glassy waste materials.
- The technique must be accessible and inexpensive.
- The technique should not require elaborate preparation and handling techniques.

Applying these selection criteria to the techniques described in the previous sections the following conclusions have been reached:

(a) XRD Techniques

All 5 XRD techniques listed in Table 2.1 are potentially applicable for the determination of the glass content in glassy waste materials. The QXRD technique has the added advantage that it provides a route by which the glass composition can be calculated as well.

(b) Optical Techniques

The optical techniques have limited value only since they are based on the ability to separate glassy and crystalline particles. This condition is invalid for fly ashes where the crystalline phases are embedded in the glassy matrix.

(c) Spectroscopic Techniques

The UV methods are unlikely to be useful because of the interference of colouring oxides. The NMR method is probably not useful because of the requirement to perform measurements close to the softening point of the glass. The latter technique also requires access to expensive NMR equipment. The Infrared technique may prove to be useful provided that vibrational frequencies common to all components of a complex system such as a fly ash can be found.

(d) Electron-Optical Techniques

SEM is probably not very useful because of the small crystallite size in fly ashes. TEM may be useful if a way can be found to examine a representative sample of the glassy waste material.

(e) Solution Method

This method ranks with the QXRD technique as one of the potentially more useful methods since it has been applied to fly ashes and it can give glass composition as well as glass content.

(f) Density Method

The density method is worthwhile investigating because of its simplicity. The requirement is, however, that a fully vitreous and devitrified analogue of the glassy waste material can be prepared. The density technique resembles in this respect the non-crystalline scattering techniques.

(g) DTA Method

This method appears to have limited applicability to homogeneous materials, such as slags.

The techniques worthy of consideration are listed in Table 2.4.

TABLE 2.4

Method of Glass Content Determination which are potentially applicable

QXRD Method
Amorphous Intensity Method
Amorphous Hump Method
Amorphous-Crystalline Scattering Method
Differential Intensity Method
Infrared Method
TEM Technique
Solution Technique
Density Technique

References

1. H.E. Schwiete and F. Dolbor, "The effect of cooling conditions and the chemical composition on the hydraulic properties of haematitic slags", Forschungs-bericht des Landes Nordrhein - Westfalen, No. 1186 (1983).

2. H.G. Smolczyk, Slag Structure and Identification of Slags, Proceedings of the 7th Int. Congr, Chemistry of Cement, Paris, 1(III), 3-17 (1980).

3. E. Demoulian, P. Gourdin, F. Hawthorn and C. Vernet, "Influence of slag chemical composition and texture on their hydraulicity", Proc. 7th Int. Congr. Chemistry of Cement, Paris, 2(III), 89-94 (1980).

4. R.D. Hooton, "Pelletized Slag Cement: Hydraulic Potential and Autoclave Reactivity", Ph.D Thesis, (Civil Engineering), McMaster University, Hamilton, Ontario, Canada (1981).

5. e.g. G.L. Clark and D.H. Reynolds, Ind. Eng. Chem., Anal. Ed., 8, 36 (1936).

6. K.H.L. Sehlke, "X-Ray Diffraction as a Method of Determining the Portland Cement Content of Mixtures of Portland Cement and Milled Granulated Blast Furnace Slag", Cement & Lime Manufacturer, XL, 4, 57-62 (1967).

7. H.S. Simons and J.W. Jeffery, "An X-Ray Study of Pulverised Fuel Ash", J. Appl. Chem. 10, 328-336 (1960).

8. J.P. Williams, G.B. Carrier, H.J. Holland, F.J. Farncomb, "The Determination of the Crystalline Content of Glass-Ceramics", J. Materials Science, 2, 513-520 (1967).

9. L.E. Alexander, X-Ray Diffraction Methods in Polymer Science, John Wiley & Sons Inc., New York; 1969, Chapter 3.

10. H.P. Klug and L.E. Alexander, "X-Ray Diffraction Procedures for Polycrystalline and Amorphous Materials", John Wiley & Sons (1954).

11. R.D. Hooton and J.J. Emery, Glass Content Determination and Strength Development Predictions for Blast Furnace Slag, Proc. of the CANMET/ACI First Int. Conf. on the Use of Fly Ash, Silica Fume, Slag and other Mineral By-Products in Concrete, Montebello, Quebec, Canada (1983). Paper SP 79-50, pp.943-962.

12. P.K. Mehta, Testing and Correlation of Fly Ash Properties with Respect to Pozzolanic Behaviour, Electric Power Research Institute Project 1260-26, Final Report, Jan. 1984.

13. S.M. Ohlberg & D.W. Strickler, "Determination of Percent Crystallinity of Partly Devitrified Glass by X-Ray Diffraction", J. Amer. Ceram. Soc., 45, 170-171, (1962).

14. J. Millet, R. Hammey and F. Brivot, Dosage de la phase vitreuse dans les materiaux pouzzolaniques, Bull. Liaison des labs. des Ponts et Chaussees, 92, 101-104 (Nov.-Dec. 1977).

15. K. Mather, Member of ASTM Committee C.I. Personal Communication (August 23, 1974) in ref. 4.

16. G. Challa, P.H. Hermans and A. Weidinger, Makromol. Chem., 56, 169 (1962).

17. J.H. Wakelin, H.S. Virgin and E. Crystal, J. Appl. Phys., 30, 1654 (1959).

18. J.J. Emery, C.S. Kim and R.P. Cotsworth, Base stabilization using pelletized blast furnace slag, J. of Testing and Evaluation 4(1), 94-100 (1976).

19. R.D. Hooton and J.J. Emery, Determining the Glass Content of Vitrified Blast Furnace Slags, paper presented at the Int. Conf. on Slags and Blended Cements, Mons, Belgium, Sept. 7-11 (1981).

20. T.W. Parker and R.W. Nurse, Investigations on Granulated Blast Furnace Slags for the Manufacture of Portland-Blast Furnace Cement, National Building Studies, Technical Paper J.O.S.I.R., HSMO, London (1949).

21. F. Schroder, Slags and Slag Cements, Proceedings of the Fifth Int. Symposium on the Chemistry of Cement, Tokyo, 4, 149-199 (1968).

22. J.G.D. Steyn, The identification, mode of occurrence, and quantitative determination of crystalline phases in granulated blast furnace slags, Mineralogical Magazine, 37(289), 578-587 (1965).

23. J.R. Foster, Private Communications, 1978, 1979, 1980, In ref. 4.

24. W. Schramli, The characterization of blast furnace slags by means of differential thermal analysis, Zement-Kalk-Gips 15(4), 140-147 (1963).

25. R.G.J. Miller and H.A. Willis, J. Polymer Sci., 19, 485 (1956).

26. G. Farrow and I.M. Ward, Polymer, 1, 330 (1960).

27. H. Hendus and G. Schnell, Kunststoffe, 51, 69 (1961).

28. K. Dougherty, Slag Chemistry Characterization and Potential Uses. Paper presented at the Slag Cements Symposium. March 12-14, 1984. Penn. State University.

29. G.B. Carrier, Electron Microscopic Technique for Determining the Percent Crystallinity of Glass-Ceramic Materials, J. Am. Ceram. Soc., 47(8), 365-367 (1974).

30. P.E. Doherty and R.R. Leombruno, Transmission Electron Microscopy of Glass-Ceramics, J. Am. Ceram. Soc., 47(8), 368-370 (1974).

31. R.J. Lauf, Microstructures of Coal Fly Ash Particles, Bull. Am. Ceram. Soc., 61(4), 487-490 (1982).

32. L.D. Hulett and A.J. Weinberger, Some Etching Studies of the Microstructure and Composition of Large Aluminosilicate Particles in Fly Ash from Coal-Burning Power Plants, Env. Sci. and Techn., 14(8), 965-970 (1980).

33. L.D. Hulett Jr., A.J. Weinberger, K.J. Northcutt and M. Ferguson, Chemical Species in Fly Ash from Coal-Burning Power Plants, Science, 210, 1356-1358 (1980).

34. P. Terrier, Research into the hydraulicity of granulated blast furnace slags, CILAMS Information, 8(1), 1-6 (1973).

35. J.E. Kruger, Contributions to the knowledge of the characteristics of vitreous blast furnace slag with a high magnesia content, D.S. thesis, University of Pretoria, R.S.A., 175 pp. (1976).

ORF

CHAPTER 3

HYDRATION KINETICS AND MECHANISMS OF GLASSY WASTE MATERIALS

3.1 Introduction

Figure 3.1 is the schematic of the $CaO-Al_2O_3-SiO_2$ phase diagram showing the simplified composition ranges of glassy waste materials (slags, fly ashes and silica fumes) as well as that of Portland cement. Evidently, the nominal composition ranges of these materials vary a great deal. However, their properties in concrete formation are very similar (see Table 3.1). Thus, it is likely that a common factor exists which is responsible for the similarity in behaviour of these materials. It is the intent of this chapter to survey the factors that govern the hydration behaviour of the glassy waste materials in cement and concrete formation as well as the interaction with H_2O, alkali hydroxides and $Ca(OH)_2$.

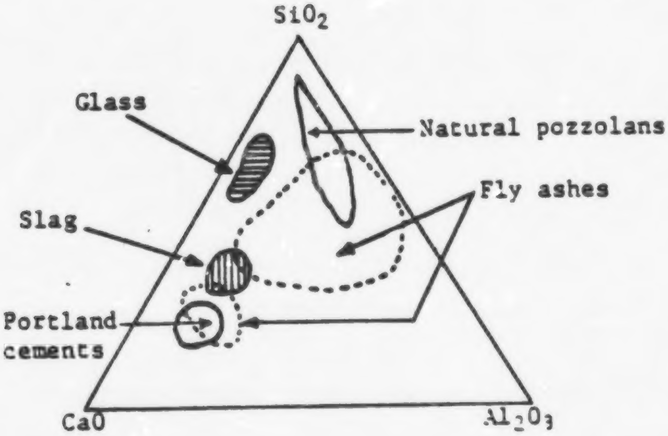

Fig. 3.1

Schematic of the System $CaO-Al_2O_3-SiO_2$ (1)

3.2 Kinetics and Mechanism of Cement Hydration

The literature on the hydration of Portland cement is extensive since full coverage would be outside the scope of this review only the main factors have been outlined here.

3.2.1 Cement Hydration

The chemical and mineralogical composition in a typical Portland cement is given in Table 3.1.

TABLE 3.1

Composition and Mineralogy of a Typical Portland Cement (2)

Oxide	Percent	Compound*	Percent
CaO	62.8	C_3S	50.1
SiO_2	20.4	C_2S	20.8
Al_2O_3	5.9	C_3A	10.8
Fe_2O_3	2.9	C_4AF	8.9
MgO	1.4		
SO_3	2.13	Fineness (Blaine) 3,620 cm^2/g	

* Calculated according to ASTM C150 (3)

The classical picture which describes the hydrolysis and hydration of Portland cement is as follows (4).

With the water-cement ratios customarily used in cement pastes, mortars, and concretes, tricalcium silicate hydrolyzes, that is, breaks down to a calcium silicate of lower basicity, to form $2CaO.SiO_2$ and release the excess lime as calcium hydroxide, $Ca(OH)_2$. The latter precipitates out as crystals from the supersaturated $Ca(OH)_2$ solution produced by the rapid rate of hydrolysis of tricalcium silicate. At these same water-cement ratios, very little hydrolysis of dicalcium silicate takes place.

Both the dicalcium silicate originally present in the cement and that resulting from hydrolysis of the high lime compounds combine directly with water in a process called hydration. At normal temperature the resulting compound is probably $2CaO.SiO_2.2H_2O$. Due to uncertainty in the nature of the compound with respect to chemical composition and nature of crystallinity the hydration products are generally represented as C-S-H*. A simple overall representation of C_3S hydration is;

$$C_3S \xrightarrow{H_2O} C\text{-}S\text{-}H + nCa(OH)_2$$

C_3A* also has hydraulic properties like C_3S. Pure C_3A reacts with water as represented by the following equation:

$$\begin{array}{lcl} 2C_3A + 21H_2O & \rightarrow & C_4AH_{13} + C_2AH_8 \\ & & \text{(hexagonal hydrates)} \\ & & \qquad\downarrow \\ & & 2C_3AH_6 + 9H_2O \\ & & \text{(cubic hydrates)} \end{array}$$

In the cement, the C_3A reaction is modified due to the presence of $CaSO_4.2H_2O$ as follows:

$$\underset{}{C_3A} + \underset{\text{(gypsum)}}{3C\bar{S}H_2} + 26H_2O \longrightarrow \underset{\text{(Ettringite)}}{C_3A.3C\bar{S}.H_{32}}$$

$$C_3A.3C\bar{S}.H_{32} + 2C_3A + 4H_2O \longrightarrow \underset{\text{(monosulphate)}}{3C_3AC\bar{S}.H_{12}}$$

The ettringite is associated with the early setting characteristics of the cement (6). A summary of the hydration process (5) in terms of the formation of new chemical species is given in Fig. 3.2.

Conventional cement chemistry short-hand

* C = CaO

S = SiO_2

H = H_2O

$3CaO.Al_2O_3 = C_3A$

$CaSO_4.2H_2O = CSH_2$

ORF

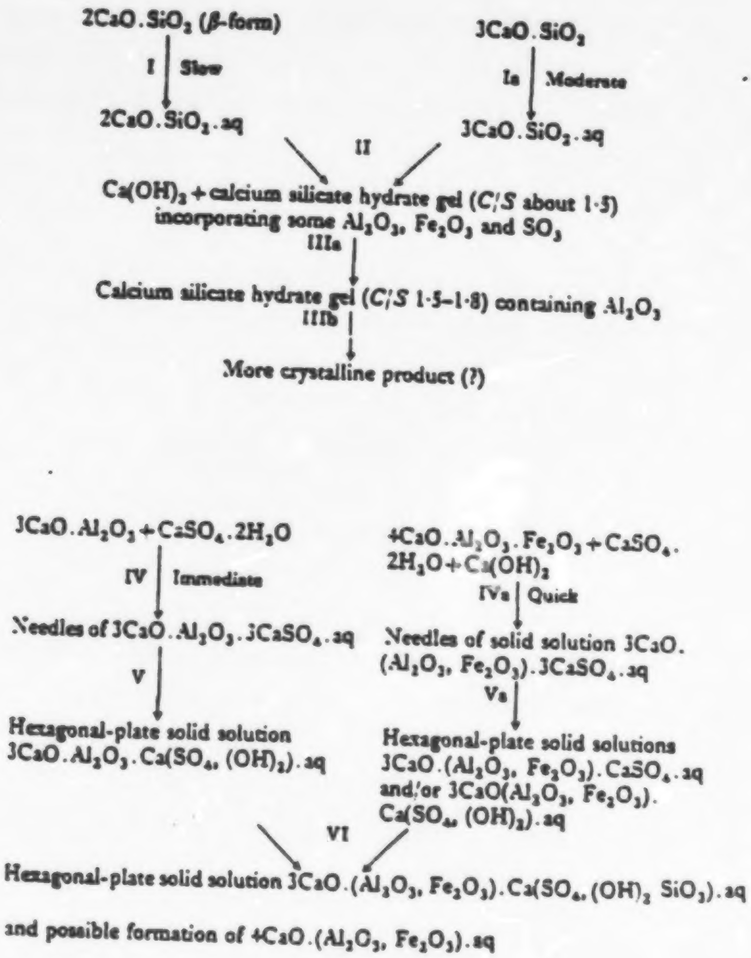
2CaO.SiO₂ (β-form)
I Slow
2CaO.SiO₂.aq
3CaO.SiO₂
Ia Moderate
3CaO.SiO₂.aq
II
Ca(OH)₂ + calcium silicate hydrate gel (C/S about 1·5) incorporating some Al₂O₃, Fe₂O₃ and SO₃
IIIa
Calcium silicate hydrate gel (C/S 1·5–1·8) containing Al₂O₃
IIIb
More crystalline product (?)
3CaO.Al₂O₃ + CaSO₄.2H₂O
IV Immediate
Needles of 3CaO.Al₂O₃.3CaSO₄.aq
V
Hexagonal-plate solid solution 3CaO.Al₂O₃.Ca(SO₄, (OH)₂).aq
4CaO.Al₂O₃.Fe₂O₃ + CaSO₄.2H₂O + Ca(OH)₂
IVa Quick
Needles of solid solution 3CaO.(Al₂O₃, Fe₂O₃).3CaSO₄.aq
Va
Hexagonal-plate solid solutions 3CaO.(Al₂O₃, Fe₂O₃).CaSO₄.aq and/or 3CaO(Al₂O₃, Fe₂O₃).Ca(SO₄, (OH)₂).aq
VI
Hexagonal-plate solid solution 3CaO.(Al₂O₃, Fe₂O₃).Ca(SO₄, (OH)₂ SiO₂).aq
and possible formation of 4CaO.(Al₂O₃, Fe₂O₃).aq

Fig. 3.2 Schematic Summary of the Hydration Processes for Portland Cement (5)

3.2.2 Kinetics of Portland Cement Hydration

The literature on the rate of hydration of the Portland cement has been summarized by Lea (5). The rate of hydration of the individual compounds present in the cement, can be monitored directly by X-ray diffraction or by electron microscopy. The rates of hydration of $3CaO.SiO_2$, $2CaO.SiO_2$ and other compounds present in Portland cement are shown in Figures 3.3, 3.4 and 3.5, respectively.

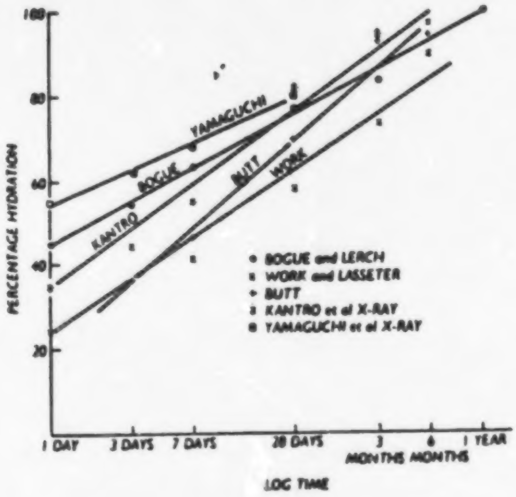

Fig. 3.3 Rates of hydration of $3CaO.SiO_2$ pastes (5)

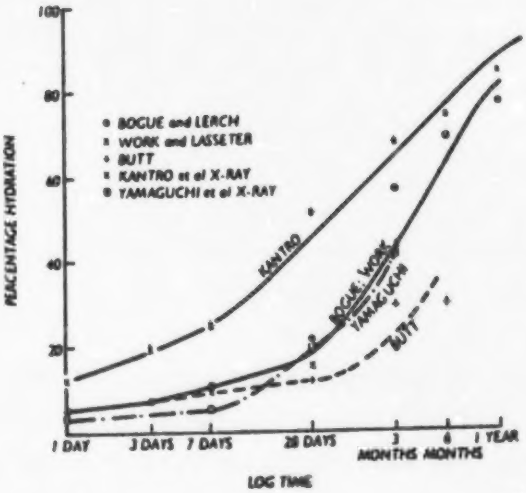

Fig. 3.4 Rates of hydrations of $2CaO.SiO_2$ pastes (5)

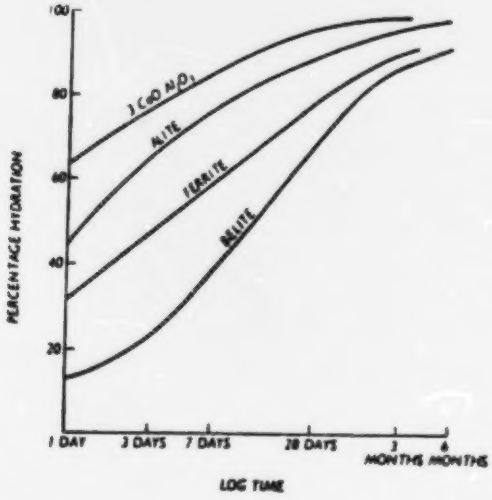

Fig. 3.5 Rates of hydration of other compounds in a Portland cement (5)

Rate equations for hydration have been proposed (5). The first assumption is that the reaction rate is initially controlled by the solid-water reaction,

$$\frac{dy}{dt} = k \quad \text{or} \quad y = kt \qquad \ldots(1)$$

where y and k are the hydrated layer thickness and a proportionality constant, respectively.

Once a coating of sufficient thickness is formed the rate will become controlled by diffusion of water through the hydrated layer. Assuming that this diffusion rate is inversely proportional to the thickness of the layer,

$$\frac{dy}{dt} = \left(\frac{1}{y}\right) \times k \quad \text{or} \quad y^2 = 2kt \qquad \ldots(2)$$

ORF

Cement hydration has been treated (2) as a reaction of the first order, i.e.

$$\frac{dc}{dt} = -kC \qquad \ldots(3)$$

Where C represents the amount of unhydrated material present. However, the experimental data indicate two slopes in the line obtained by plotting log C vs. t, suggesting two rate constants. The first is 10-15 times greater than the second. The lower rate of reaction after some time is attributed to the change in the structure and adherence of the gel coatings to the cement particles. This behaviour in many ways resembles that observed in glasses where a rapid initial process, directly proportional to the time lapsed is followed by a slower diffusion controlled process.

Due to the presence of many chemical compounds and their polymorphs, the hydration of cement involves many overlapping physical and chemical changes that are difficult to discern. In view of this, C_3S, the major phase present in the Portland cement is generally chosen for fundamental studies on kinetics and mechanism of hydration.

Recently, Stewart and Bailey (7) have reported microstructural studies on the hydration products of three C_3S polymorphs (triclinic, trigonal and monoclinic). C/S ratio, rate of heat evolution, structure of C-S-H and the morphology of the hydration products were monitored as a function of time. The heat evolution profiles are shown in Figures 3.6. These authors concluded that in the early stages, less than one day, there are distinct differences between the products on the surfaces of grains of different crystal structures but later all three appear similar. The difference in early stages was attributed to the presence of foreign ions. It is known that OH^- is one of the most important reactants in C-S-H formation, but this parameter was not monitored by Stewart et al. (7).

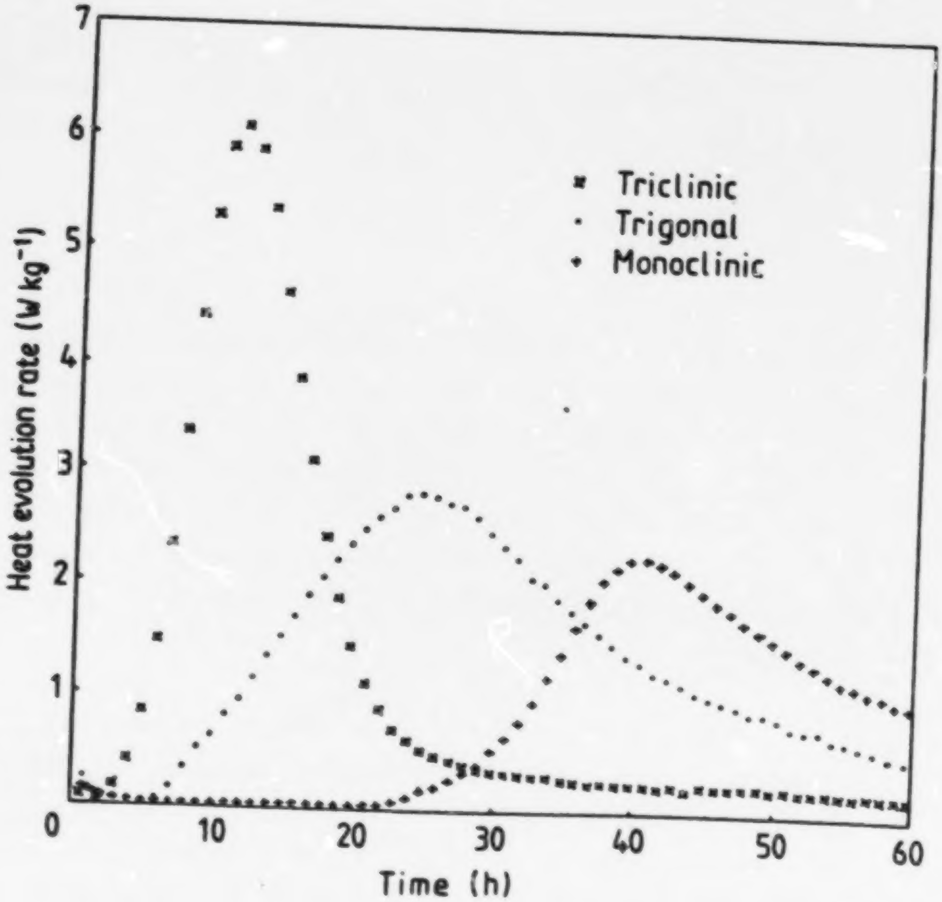

Fig. 3.6 Heat Evolution Profiles of Three C_3S Samples (7)

Since cement is a multiphase material and also, since the process of cement hydration is not a simple reaction, homogeneous kinetics cannot be applied (8).

3.2.3 A Model for Cement Hydration

The following synopsis of cement hydration has been extracted from the work of Berry (9) and Skalny et al (10).

Most of the engineering properties of Portland cement are based on the formation of C-S-H, an amorphous product of colloidal dimensions which comprises 60 to 70% of the solid part of the fully hydrated cement paste. Four types of C-S-H have been distinguished by electron microscopy. The most important for cement hydration are types I and III.

Type I. Acicular fibres up to 2 cm in length, predominantly formed at early hydration ages for high w/c pastes.

Type III. Irregularly equant or flattened particles often less than 0.3 µm across. This form predominates in mature pastes.

The C/S ratio of C-S-H varies from close to 3.0 at the commencement of hydration to reach a final value of 1.4 to 1.8 in the mature paste.

The second major product of cement hydration, $Ca(OH)_2$ (CH), fills the void space as the water is consumed. It is non-cementitious and apart from a desirable minimum quantity of CH in the mature paste, it is deleterious to the cementitious bonding of paste.

The elevated long term strength observed for pozzolanic and slag cements has been attributed to the progressive reduction of CH in such mature pastes by reaction with SiO_2 to form C-S-H.

Figure 3.7 shows a hydration mechanism poposed by Glasser et al. (11). The progress of the paste hydration is readily followed by the heat evolution curve obtained by calorimetric measurements (see Figure 3.8). The following stages can be discerned in the hydration process.

(a) Initially, immediately upon contact with water a rapid exchange of ions occurs leading to an increase in the concentration of Ca^{2+}, Na^+, K^+, aluminate, sulfate and OH^- in solution. This process is largely exothermic and ettringite is formed.

(b) Next, during the so-called induction period in which the rate of heat evolution decreases nucleation and growth of C-S-H and CH follow.

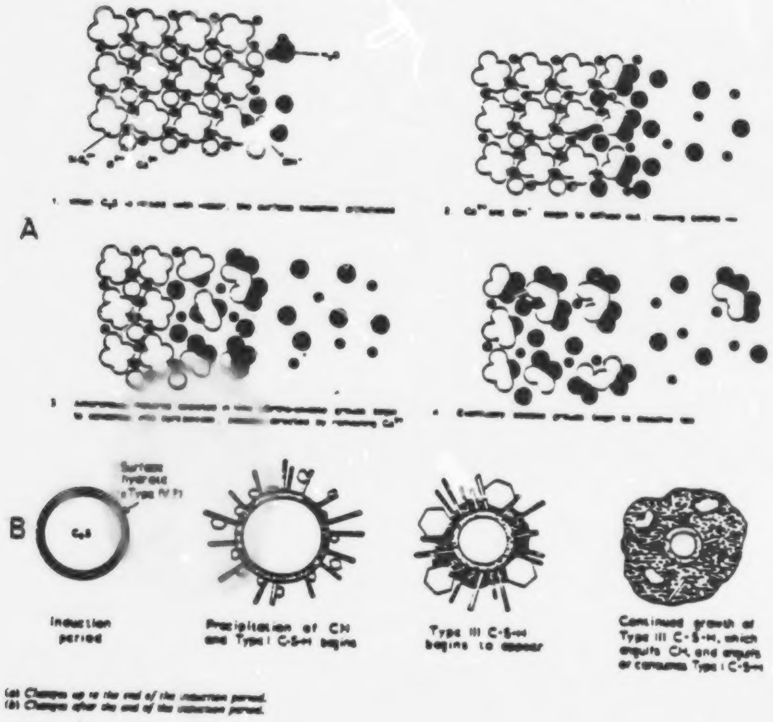
A
B
C₃S
Surface hydrate (Type IV ?)
Induction period
Precipitation of CH and Type I C-S-H begins
Type III C-S-H begins to appear
Continued growth of Type III C-S-H, which engulfs CH, and engulfs or consumes Type I C-S-H
(a) Changes up to the end of the induction period.
(b) Changes after the end of the induction period.

Fig. 3.7 C_3S hydration mechanism proposed by Glasser (11)

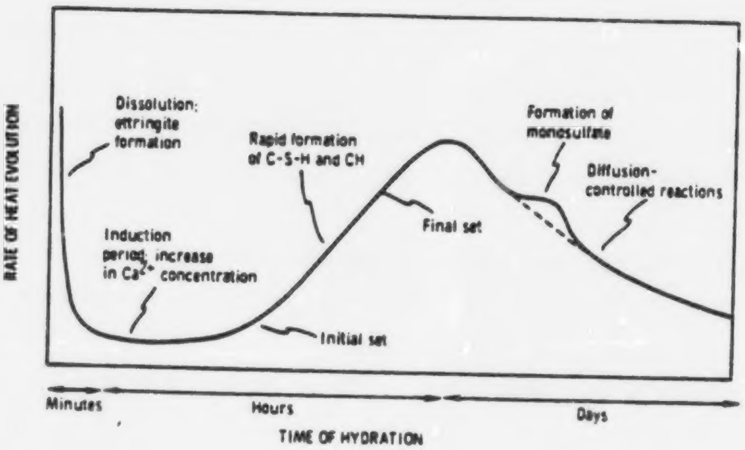

Fig. 3.8 Schematic representation of the heat evolution from Portland cement hydration.

(c) C_3S dissolution accelerates upon depletion of Ca^{2+} in solution, heat is evolved, overall paste porosity decreases and more solid phase precipitates. Ettringite becomes converted to the mono-sulphate form as SO_4^{2-} is depleted in solution.

(d) Throughout the final stages, diffusion controlled formation of C-S-H and CH continues and some polymerization of silicates may occur.

It is noteworthy that there is a remarkable similarity in the composition and nature of the products of reaction formed from materials as diverse as Portland cement, pozzolans, ferrous and non-ferrous slags upon reaction with water. The formation of C-S-H is common to all these systems. The major point of difference is that the mature pastes from pozzolan or slag hydration contain less $Ca(OH)_2$. Also, the pore distribution in pozzolan and slag cements is substantially reduced when compared with control cements.

3.3 Slag Hydration

Typical chemical compositions of Canadian blast-furnace slags, steel slags and non-ferrous slags were shown in Chapter 1 of this survey (Tables 1.2 - 1.4)(9). It can be seen that there is considerable difference between the compositions of the various types of slags.

3.3.1 Blast Furnace Slags

The hydraulicity of slags has been reviewed by Keil (18), Kramer (19), Schroder (20), Satarin (21), Smolczyk (22), Hooton (17) and Berry (9). In the discussion of slag hydration gives below we will follow the classification of relevant parameters given by Hooton (17).

(a) The Degree of Vitrification (Glass Content):

Mills stated that the latent hydraulicity of quenched slag is generally considered to originate from the perched Arrhenius energy level of its amorphous structure when compared with a crystalline structure of similar compositions (23). This implies that both glass content (or level of divitrification) and the free energy associated with the degree of molecular disorder affects the slag hydraulicity.

Concerning the former factor, Schwiete and Dolbor who modified quenching conditions for over 30 slags found that glass content was the predominant factor affecting strength (24). Hooton and Emery (25) correlated glass content, composition, Blaine fineness and other parameters with 7, 28 and 91 day hydraulic indices and concluded that glass content is the most influential parameter although the correlation coefficients ($R<0.7$) are not highly significant. Other researchers, such as Smolczyk (22) did not find a linear glass content-strength relationship and Demoulian et al (26) observed a reduction in strength when the slags had glass contents in excess of 95%. These workers found that merwinite (C_3MS_2) crystallization would actually enhance slag reactivity. Smolczyk (22) also suggested that because of encapsulation in reactive finely ground slag glass, small crystals will not be detrimental to glass strength.

As far as the second factor, the free energy associated with the degree of disorder is concerned, Fierens and Poswick (27, 28) point out that the glass quality is a critical factor. More quickly quenched slags were found to be more reactive, presumably because of fewer defects in the glass structure. More recent research by these authors, however, showed the trend to be less clear on industrial slags (29). Fierens et al. also reported that aging deteriorated hydraulic activity in three year old gehlenite due to a progressive deactivation of the surface centres of excitation.

(b) Chemical Composition:

The effect of chemical composition on slag reactivity was reviewed by Schroder (20) and Hooton (17). Chemical composition influences both the degree of vitrification achievable upon quenching as well as the solubility and, thus the hydraulicity of the slag during hydration.

The view generally held is that a high CaO content coupled with higher Al_2O_3 contents under otherwise identical conditions increases the hydraulic activity of slags (17, 19, 20, 30-35). It has become clear over the years that the lime content must be considered in relation to the concentration of other oxides. For example, Smolczyk (22) stated that the so-called acid slags (C/S<1.0) which were previously considered to be of poor quality (18,19), were reactive when the low CaO contents were coupled with increased MgO and Al_2O_3 contents.

The literature of MgO on hydraulicity is conflicting. D. Heyl (36) when increasing simultaneously the MgO content from 8 to 12% and the C/S ratio from 1.2 to 1.3 did not find an improvement in quality. On the other hand, Oelschlager (37) found an improvement in strength by increasing the MgO content (up to 10%) with constant basicity. This author found the C/S ratio to be more important for strength than the MgO content. Janowski (38) reported that slags rich in MgO (Al_2O_3<11%) gave better strength than slags rich in lime. Schillak (39) noted that MgO in up to 7% of the vitreous phase is inoccuous provided the slag contains more than 12% Al_2O_3. Schwiete and Kuhle recommend an increase in the Al_2O_3/SiO_2 ratio for slag-cements made from granulated slags with higher MgO contents (40). In general, most recent studies have shown that MgO affects hydraulicity in a beneficial manner (22). Early concerns about the formation of periclase which could result in unsoundness have been diminished by the use of South African slags with up to 20% MgO with no adverse effects (41-43).

The favourable effect of higher Al_2O_3 contents has been reported by several authors (24,38,39,44,45). Given equal basicity an increase in Al_2O_3 content increases strength. However, it is likely that the strength increase attributed to increasing Al_2O_3 content is sometimes partly due to calcium hydroxide activation (17,46). The increased $Ca(OH)_2$ demand at increased Al_2O_3 contents may even be the result of pozzolanic rather than hydraulic reactivity.

The detrimental effect of higher FeO contents on slag quality were attributed to troubles in the blast furnace run by Sopora (47).

The effect of minor oxides on reactivity is not clear. Solacu and Balta who studied the influence of manganese and of sulfur on the hydraulicuty of slags of the system C-M-A-S found varying effects of Mn an S on hydraulicity (48). The adverse effect is especially noticeable when these elements are present in the same quantity leading to the formation of MnS. The detrimental effect of MnO was also noticed with slags of low basicity and low Al_2O_3 content (30). Keil and Gille (49) found that synthetic glasses composed of only the four major oxides, C-M-A-S, did not exhibit the same reactivity trends as industrial slags. On the other hand it was reported that the reactivity of C-A-S glasses was similar to that of slags (32).

Compositional Moduli:

A large number of compositional moduli have been proposed to predict optimum slag compositions. Table 3.2 gives a listing compiled from summaries by Hooton (17), Keil (18), Schroder (20), Lea (5), Terrier (50), Gupta (51) and Kruger (43). Many of these moduli are derived from the basicity ratios used in the blast furnace operations to judge the melting conditions. It has been argued that these moduli have only limited or doubtful value, either on account of the method used or due to the properties of the material (20).

Indices M1-M3 simply reflect basicity ratios in the slag. M3 has been used in conjunction with M4 to evaluate slags for cements in the USSR (52). M5 was used in Germany prior to 1942. The value of M5 had to be at least unity. More recently M5 has been replaced by M6 which is still contained in the German standard DIN 1164 (1967) and which was adopted in the Canadian CSA A363-M77 preliminary standard. The modulus M6 is required to be larger than 1.4 in Japan (21). The basis for M11 lies in the network theory of glass structure of W.H. Zachariasen. Up to 10% of Al_2O_3 are supposed to be built into the SiO_4 tetrahedral network structure while the excess occurs as network modifiers.

Hooton and Emery (25) used hydraulic indices to correlate strength with glass content and chemical composition (see Table 3.3). In multiple

TABLE 3.2

Compositional Moduli to Predict Optimum Slag Compositions

Modulus	Reference
M1 = C/S	17, 18, 25
M2 = (C+M)/S	17, 18
M3 = (C+M)/(S+A)	17, 18, 25, 52
M4 = A/S	17, 52
M5 = (C+M+0.33A)/(S+0.67A)>1.0	17
M6 = (C+M+A)/S≥1.0 or 1.4 (Japan)	17, 21, 25
M7 = (C+CS+0.5M+A)/(S+MnO)>1.5	17, 18
M8 = 20+C+A+0.5 M-2S	
slag quality: M8<12, medium	17, 53
12<M8<16, good	
M8>16, very good	
M9 = $(C+M+A)/(S+F+(MnO)^2)$	22, 25
M10 = $(C+0.5M+A)/(S+F+(MnO)^2)$	17, 47
M11 = (C+0.9A)/(S+0.1A)	17, 24, 43
M12 = (C+1.4M+0.56A)/S	17, 54
M13 = (6C+3A)/(7S+4M)	17, 55
M14 = 0.38 (Glass Content)(M5-0.72)+75.0	17, 56

TABLE 3.3

Hydraulic Indices

Time	Hydraulic Index	R	SE
7 days	HI7 = 0.688 (glass) + 3.03 (CaO) -7.97 (SiO_2) -14.24 (Mn)+177.1	0.943	±7.4
7 days	HI7 = 0.682 (glass) + 216.5 (C/S)-239.5	0.916	±8.6
7 days	HI7 = 0.580 (glass) + 153.8 (C+M+A)/S -243.0	0.916	±8.7
28 days	HI28 = 1.105 (glass) -7.08 (SiO_2)+251.0	0.811	±15.9
91 days	HI91 = 1.143 (glass) -6.92 (SiO_2)+254.0	0.711	±18.6

regression analysis the glass content is the most significant parameter for the hydraulic indices at 7, 28 or 91 days. Some simple oxides (CaO, MnO?) improve the correlations in some cases but in multiple regression analysis the glass content was obtained in all the best correlations. Table 3.4 shows simple correlation coefficients between the hydraulic indices, major oxides and several compositional moduli.

TABLE 3.4

Simple Correlation coefficients (25)

	Hydraulic Indices		
Parameter	7 Day	28 Day	91 Day
Glass	0.414	0.667	0.647
CaO	0.465	0.030	0.252
SiO_2	-0.654	-0.262	-0.266
Al_2O_3	0.644	-0.301	0.404
MgO	-0.334	0.019	-0.204
K_2O	-0.497	-0.349	0.199
S_T	-0.355	-0.187	-0.323
Mn_T	-0.067	-0.004	-0.048
Fe_T	-0.067	-0.04	-0.047
Blaine Fineness	0.224	0.193	0.134
C/S	0.692	0.199	0.291
$\frac{(C+M+A)}{S}$	0.752	0.343	0.327
$\frac{(C+M+A)}{(S+F+Mn^2)}$	0.747	0.344	0.332
$\frac{C+M}{S+A}$	-0.012	-0.001	-0.123

Tanaka et al. (75) studied the potential hydraulicity of granulated blast-furnace slag cement. The authors found a positive correlation between hydration activity and vitrification ratio (glass content) and basicity and a negative correlation with TiO_2 content. The composition and multiple correlation coefficients are shown in Tables 3.5 and 3.6, respectively.

(c) Mineralogical Composition

As discussed earlier under (a) in this section there is a notion amongst several investigators that glass content and glass quality are significant factors affecting slag hydraulicity. Direct and latent slag hydraulicity are observed for granulated and vitreous blast furnace slags (9). Both of these are predominantly glassy. There is also evidence, however, that the extent and nature of the crystallinity has a relationship to slag hydraulicity.

The crystalline compounds found in devitrified slag are mainly the melilite solid solutions series with end members akermanite (C_2MS_2) and gehlenite (C_2AS) with lesser amounts of monticellite (CMS), diopside (CMS_2), merwinite (C_3MS_2) and others (17).

Some workers considered that these minerals are inert towards water (5,20). However, there is also evidence of direct or latent hydraulicity for some of these.

Keil and Gille concluded that the equilibrium mineral composition could not be used to evaluate the hydraulic properties of the glass (49). This approach had no advantage over using the relations with oxide composition according to Nurse (32).

Several workers have established a relationship between strength development and melilite composition. Of the end members Kondo and Ueda considered akermanite more than latently hydraulic while gehlenite and the solid solution were considered latently hydraulic (57).

Akatsu established a relationship between slag reactivity and akermanite content (58). The beneficial effect of metastable merwinite crystallization on slag reactivity has also been noticed (20,43).

(d) Particle Size/Surface Area

It has been established that the average particle size and exposed surface area of blast furnace slag correlates with strength. In practice these parameters are determined by slag fineness of grinding (17). The optimum fineness for Canadian pelletized slags was found to be 400 m^2/kg Blaine (59). The correlation with Blaine fineness is not a simple one but rather a complex interplay with slag content of the concrete and chemical composition (5,20).

(e) Activation of Slags

For the majority of blast furnace slags significant hydration occurs only when activators are present. The activators most commonly used are: calcium hydroxide, Portland cement, gypsum or mixtures of portland cement and gypsum. Other activators used are sodium carbonate, sodium or potassium hydroxide, sodium silicate (Na_2SiO_3) and calcium chloride (9,17).

The hydration products in hydrated blast furnace slag cements are according to Nurse and Schroder (9,20,32):

- a tobermorite type C-S-H phase,
- an ettringite type C-A-S phase,
- hexagonal calcium aluminum hydrate or a solid solution of tetracalcium aluminate mono-sulphate hydrate,
- $Ca(OH)_2$.

Teoreanu et al.(62) reported on the phases produced by hydration of slags in the presence of lime and gypsum and in the presence of lime and sodium silicate.

The hydration products of slags in the presence of lime and gypsum are C-S-H (tobermorite), ettringite, gehlenite (after 7 days) which transformed to hydrogarnets. The hydration products in the lime/sodium silicate system are tobermorite-gel, gehlenite hydrate and calcium sodium hydrosilicates.

Regourd (73) reported the presence of a "pseudomorphic" slag hydrate, enriched in MgO and Al_2O_3 compared to clinker hydrates, which is formed inside the original slag particle in slag cement.

Mechanism of Hydration in the Presence of Activators:

The original theory of D'Ans and Eick (61) envisioned an initial release from the slag grain surface, followed by the formation of impermeable acidic surface films through the reaction of water with the Al_2O_3 and SiO_2. Additional $Ca(OH)_2$ was required to remove these films and enable continued hydration. The role of $Ca(OH)_2$ was considered to be catalytic in the original theory but more recently it is believed that the lime itself reacts since substantial quantities are being consumed.

Kondo and Ueda (57) studied the formation of surface films on gehlenite glass (C_2AS) in water and found a poorly permeable coating of approximate composition ASH_6, 0.2 µm thick. The solution compositions after repeated extractions are shown in Figure 3.9. Figure 3.10 shows the solution composition following the accelerated hydration upon the addition of $Ca(OH)_2$ to the system. It can be seen that the Al_2O_3 and SiO_2 extracted from the glass is significantly higher when lime is used.

Abo-El-Enein and coworkers (63) hydrated slag-lime pastes (20 wt.% $Ca(OH)_2$) of low porosity (water/solid ratio of 0.20). The composition of the granulated blast-furnace slag was: CaO: 44.0%, SiO_2: 34.3%, Al_2O_3: 15.5%, MgO: 3.4%. During the early stage of the hydration process (3 days) a high-lime product was formed (molar C/S+A ratio: 2.51-2.56). The C/S+A ratio dropped to 1.55 after 90 days hydration and then increases to a value of 1.71 after 180 days hydration. Since the C/STA ratio in the slag is 1.08 it is surmized that the free lime in the solution reacts with the components of the slag source of CaO. Kruger (43), on the other hand, found no significant difference between lime and Portland cement in its effect on slag hydration reactions.

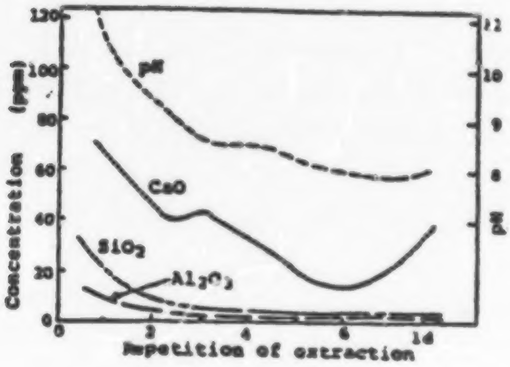

Fig. 3.9 Solution compositions from repeated water extraction of C_2AS glass (57)

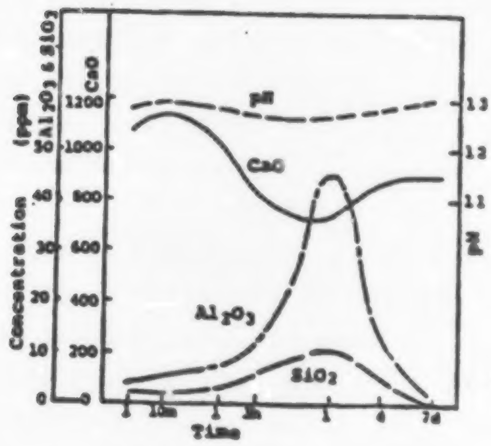

Fig. 3.10 Solution compositions from repeated extraction of C_2AS glass with 2 moles $Ca(OH)_2$ (57)

Several studies have addressed the relationship between the crystalline components of the slags and the effect of activators but there is no unanimity about the effect of certain activators on specific phases. For example, Keil and Gille (49) observed that akermanite glasses were reactive in pure water while Teoreanu and Georgescu (60) found akermanitic systems to be inert.

Controversy also exists about the effect of CaO in relation to its source; Keil and Gille (49) observed a beneficial effect on strength when lime was used on gehlenite but not on akermanite. The reverse was found when Portland cement was the source of the Ca.

Tanaka et al.(74) studied the hydration mechanism of remelted industrial blast furnace slag and a melilite mixture (C_2AS/C_2MS_2 molar ratio: 7/3) in $Ca(OH)_{2(aq)}$ suspension and in Portland cement paste. Fig. 3.11 shows the surface of the hydrated remelted-slag in $Ca(OH)_{2(aq)}$ suspension after 28 days. Two types of hydrates could be distinguished, a card-house like hydrate enriched in Mg and Al compared to the unhydrated remelted slag and a Ca-enriched C-S-H gel with much less Mg and Al (Fig. 3.12 shows the EDXA spectra). The authors suggest that the Ca-rich C-S-H gel is produced around a $Ca(OH)_2$ particle by combination with silicate ions liberated from the glassy slag structure.

Hydration of a Portland cement mixture is different in that the hydrated surface of the slag glass cannot be distinguished from that of the paste. A schematic is shown in Fig. 3.13. Only the "inner hydrated layer" of either regular pores or close-packed equant grains is formed at 20°C after 14 days. At 28 days, the "skeleton layer" of well crystallized dense hydrate is formed. Both layers are formed at one day curing at 80°C. As time progresses the "inner layer" expands at the expense of the "skeleton layer" which simultaneously penetrates deeper into the glass surface.

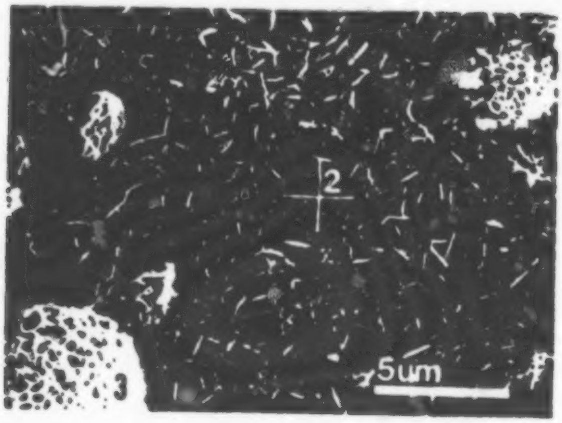

Surface of hydrated remelted-slag in $Ca(OH)_2$ aq. suspension (28 days, 80°C)

Fig. 3.11 (74)

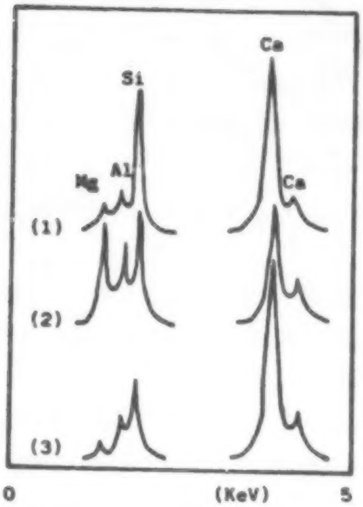

X-ray spectra of Ca,Al,Si and Mg on the position (2 and 3) labelled in Fig. 3
1:unhydrated remelted-slag 2:card-house like hydrate
3:spherical aggregate

Fig. 3.12 (74)

Fig. 3.13 (74)

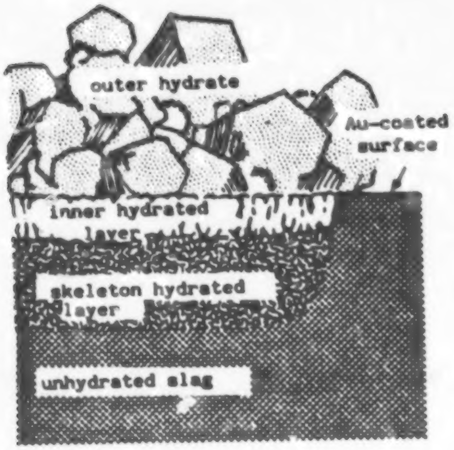
outer hydrate
Au-coated surface
inner hydrated layer
skeleton hydrated layer
unhydrated slag

Schematic hydrated structure of glassy slag in portland cement paste

TABLE 3.5 (74)

Relative content of four elements (Ca, Mg, Al and Si) in hydrated and unhydrated layer by EDXA (1 year, 20°C)

Specimen	Composition & mole ratio	unhydrated layer	skeleton hydrated layer	inner hydrated layer	outer hydrate
Remelted-salg	CaO	47	45	49	56
	MgO	5	11	7	7
	SiO_2	34	31	32	29
	Al_2O_3	15	13	11	9
	C/S	1.48	1.56	1.64	2.07
	A/S	0.26	0.25	0.20	0.18
	M/S	0.22	0.53	0.33	0.36
Melilite	CaO	42	45	51	63
	MgO	4	7	5	3
	SiO_2	29	30	31	27
	Al_2O_3	25	18	14	8
	C/S	1.55	1.45	1.76	2.50
	A/S	0.51	0.35	0.26	0.17
	M/S	0.21	0.35	0.24	0.17

TABLE 3.6 (74)

Chemical composition of glassy specimens (%)

Specimen	SiO_2	Al_2O_3	Fe_2O_3	CaO	MgO	Na_2O	K_2O
Remelted-slag	33.8	15.3	0.5	43.9	5.0	0.2	0.3
Melilite	28.6	26.0	0.1	40.6	4.4	-	-

Table 3.5 shows the chemical composition of the various zones in the slag-cement and melilite-cement paste. The compositions of the samples are given in Table 3.6. It is concluded that:

- the MgO content of the skeleton hydrated layer is increased
- the C/S ratio increases gradually in going from the unhydrated glass to the "outer hydrate"
- the A/S ratio decreases in going from the unhydrated glass to the "outer hydrate".

The authors propose the following mechanism for the hydration process of glassy slag in Portland cement paste.

(1) The surface of a glassy slag embedded in a cement paste is predominately occupied by the hydrates produced from the cement at early stage, because the rate of slag hydration is slower than that of the cement. In addition, the aqueous phase near the slag surface is in the supersaturated state filled with Ca^{++} ion and alkali metal ion liberated from the cement.

(2) The surface of the glassy slag is attacked by the alkali activator, such as Ca^{++} ion and alkali metal ion, and then converts to the "inner hydrated layer" consisting of well-crystallized hydrates which were formed by drawing Ca^{++} ion from the cement. The "latent hydraulic property" of glassy slag can be explained by the above phenomena.

(3) The diffusion of Ca^{++} ion from the outside aqueous phase to the inside of "inner hydrated layer" becomes slow after the formation of the "inner hydrated layer". Reversely, the dissolution of Ca^{++} and Al^{+++} ions from the unhydrated slag to the aqueous phase becomes considerable. These ions would be bound in the "inner hydrated layer" and are carried partially to the outside aqueous phase. Thus, the "skeleton hydrated layer" can also be regarded as the shell structure which is formed after exit of the dissolved ions from the glassy slag.

(4) At a later stage, "skeleton hydrated layer" converts gradually to "inner hydrated layer" by the supply of Ca^{++} ion from both the outside and unhydrated slag.

Nagataki et al.(75) related the potential hydraulicity of granulated blast-furnace slag sand to the structure of the hydrated layers formed on the surface of slag sand particles. The authors noticed the formation of a hydration layer on the slag sand surface which was thought to be different in composition and structure for cement paste and aggregate portions. It was found that a thinner hydration layer with a high C/Si ratio is formed around slag sand in contact with $Ca(OH)_2$. The slag sand not in contact with $Ca(OH)_2$ has a thicker hydration layer with a relatively low C/S ratio, even lower than in the slag sand particles themselves.

3.3.2 Steel Making Slags

Steel slags are generally not considered as sources of hydraulic materials since,

(a) their composition varies over a wide range, and
(b) they are largely crystalline and contain only negligible quantities of vitreous material.

Most steel slags are returned to the blast furnace for recovery of iron or are used as highway base or granular fill. Recently a process has been developed to produce homogeneous, low free-lime slags with hydraulic activity (64-66). The summary of the hydration properties given here is based on the paper by Conjeaud et al.(66).

The major crystalline components in steel making slags produced by the Basic Oxygen Process, P_2O_5-stabilized $2CaO.SiO_2$, ferrites (such as $2CaO.Fe_2O_3$), $3CaO.P_2O_5$, wustite, FeO and (Ca, Fe, Mn, Mg)O solid solutions, hydrate only slowly or are chemically inert.

Figure 3.14 shows the rate of hydration of calcium-aluminoferrites as a function of alumina content. It can be seen that the rate of hydration increases with the Al_2O_3/Fe_2O_3 ratio.

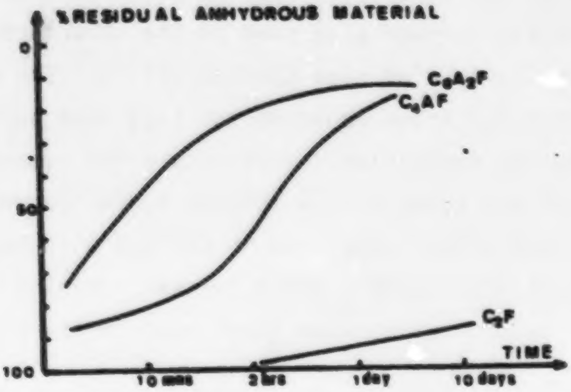

Fig. 3.14 Rate of Hydration of calcium-aluminoferrites as a function of alumina content (66)

The authors studied hydraulicity by isothermal calorimetry. Figure 3.15 shows compressive strength as a function of heat evolved for neat slag - 5N NaOH samples at 24 hrs. A heat evolution of 20 Kcal/g is necessary if the slag is to display useful hydraulic behaviour. Figure 3.16 shows that such behaviour is observed for an Al_2O_3 content of about 15%. This compares with an Al_2O_3 content of 6% calculated on theoretical grounds. The latter implies the transformation of calcium ferrite into calcium alumino ferrite ($4CaO.Al_2O_3.Fe_2O_3$).

The authors subsequently produced hydraulic slags by adding CAM Flux, a synthetic slagging agent to the steel making slags. The compositions used for hydration studies are listed in Table 3.7.

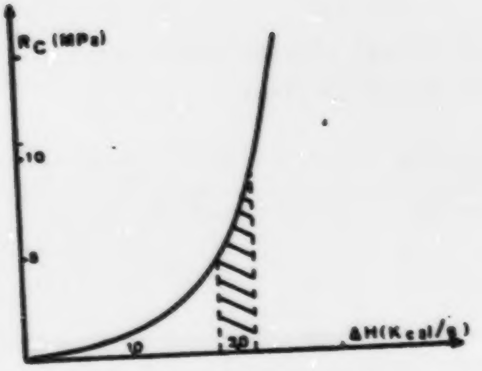

Relationship between compressive strength and heat evolution of alumina doped LD slag pastes

Fig. 3.15 (66)

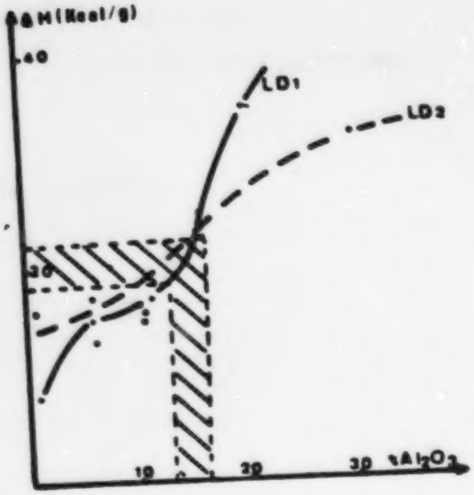

Relationship between hear evolution and alumina content of laboratory LD slags

Fig. 3.16 (66)

TABLE 3.7

Compositions of semi-industrial LD slags

Slag :	T_1	T_2	F_{1A}	F_{1B}	F_{2A}	F_{2B}
SiO_2	9.55	10.75	7.75	9.0	10.25	10.7
CaO	44.4	43.7	43.4	45.8	40.6	42.65
Al_2O_3	0.95	1.3	10.2	11.4	6.5	9.15
MgO	10.45	6.25	5.8	7.2	14.5	10.85
MnO	4.36	4.99	3.10	3.82	3.91	3.91
P_2O_5	2.40	3.95	2.15	2.25	2.5	1.8
Fe^{++}	19.7	18.35	17.9	12.6	16.25	14.75
Fe^{+++}	8.6	10.7	10.15	8.7	4.8	6.15
Fe^{++}/Fe^{+++}	2.3	1.7	1.75	1.45	3.4	2.4
Free CaO	10.8	3.3	4.2	3.8	4.55	1.8
TiO_2	0.21	0.19	0.34	0.60	0.39	0.53
TOTAL	100.6	100.18	100.99	101.37	99.6	100.49
From test N°	1	2	3	4	5	6

Table 3.8 lists the calculated mineralogical composition of the semi-industrial LD slags.

TABLE 3.8

Calculated mineralogical composition of semi-industrial LD slags

Slag :	T_1	T_2	F_{1A}	F_{1B}	F_{2A}	F_{2B}
C_2S - C_3P %	31 - 6	32 - 9	22 - 5	27 - 5	30 - 5	32 - 4
Ferrite %	16	19	32	27	15	19
(Ca-Fe-Mn-Mg)O %	47	40	24	26	42	34
C_3A %			17	15	8	11

Table 3.9 shows loss on ignition as a measure of hydration (6 hrs, 1, 2, 7 and 28 days).

TABLE 3.9

Combined water in semi-industrial slags after various periods of hydration

Sample	6 hours	1 day	2 days	7 days	28 days
T_1	7.6 %	11.8 %	11.8 %	13.0 %	17.1 %
T_2	5.2 %	8.3 %	9.4 %	11.1 %	14.9 %
F_{1A}	12.3 %	12.9 %	14.3 %	14.6 %	17.5 %
F_{2A}	10.4 %	10.2 %	10.7 %	13.2 %	17.2 %
Industrial LD slag	6.3 %	7.7 %	10.0 %	13.6 %	17.0 %

It can be seen that the aluminous slags react much more rapidly initially. The semi-industrial slags with lower Al_2O_3 content hydrate slower initially but their water fixation catches up after 28 days, except for the fluorspar fluxed slag (T_2) which remains lower.

Slags T_1 and T_2 and the industrial slags form $Ca(OH)_2$ and a calcium ferrite hydrate: $4CaO.Fe_2O_3(H_2O)_x$. The latter compound reacts rapidly with CO_2 from the atmosphere to give calcium mono-carbo ferrite hydrate which has a structure similar to calcium mono-carbo aluminate hydrate.

ORF

The aluminous slags gave rise to $Ca(OH)_2$ and cubic calcium aluminate hydrate ($3CaO.Al_2O_3.6H_2O$) which reacted with CO_2 to give calcium mono-carbo aluminate hydrate while no more calcium alumino-ferrite was detectable after 6 hrs of reaction.

Fig. 3.17 shows the heat evolution upon hydration of a high-alumina (F1A) and low-alumina (T1) slag. The high-alumina slag gives a much higher heat evolution in contact with water.

The heat evolution of various slags in contact with 5N NaOH are shown in Fig. 3.18.

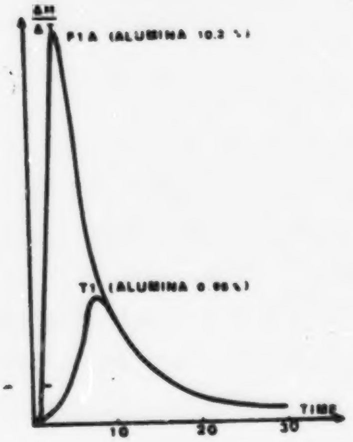

Fig. 3.17
The effect of alumina content on the rate of heat evolution of semi-industrial LD slags in contact with water.

F_{1A}, F_{2A}, T_1 - semi-industrial slags
BF - Blast Furnace Slag
LD_1, LD_2 - industrial LD slag

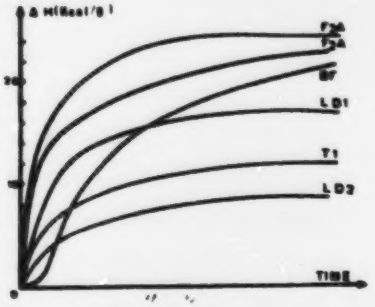

Fig. 3.18
Heat evolution from various slags in contact with NaOH solution.

Again the high-alumina slags (F1A, F2A) show the highest AH values.

Hydration in the presence of $CaSO_4$ was found to yield calcium (mono-or-tri) sulpho-aluminate hydrate from the alumino-ferrite. In low-Al_2O_3 LD slags the ferric ions may replace the majority of trivalent

ORF

aluminum. However, this reaction is extremely low for low-Al_2O_3 ferrites. The reaction is rapid in aluminous slags where the tri-sulpho compound (ettringite) is formed in substantial amounts after 24 hrs.

$$C_6A_2F + 3CH + 9CSH_2 + 75H \rightarrow 3(C_6A_{0.67}F_{0.33}S_3H_{32})$$

3.3.3 Non-Ferrous Slags

Canadian non-ferrous metallurgical slags, although derived from different processes, have similar compositions with CaO, 1.3-14.5%; MgO, 0-5.4%; SiO_2, 19.6-40%; Al_2O_3, 2.1-6.2%; Fe_2O_3, 42.9-58.6%. Copper and nickel slags contain a glass phase, fayalite and minor amounts of magnesite (67,68).

(a) Glassy Nature

Most data are available from studies by Thomas (69,70), Laneuville (70,71) and Baragano and Rey (68). The hydraulic activity is attributed to pozzolanic reactions with sources of $Ca(OH)_2$. Quench-cooled Cu-reverberatory furnace slag (CRFS) and Pb-blast furnace slag (LBFS) were good pozzolans while LBFS stockpiled for up to 30 years and copper converted slag (CCS), slowly cooled, were found to be unreactive (69,70). The data point to the importance of vitrification for pozzolanic activity.

(b) Chemical Composition and Activators

Work carried out by Laneuville (72) on granulated nickel slags failed to show a correlation between HCl soluble SiO_2, Al_2O_3 and Fe_2O_3 measured during curing of Portland cement slag mortars and compressive strength. However, a correlation was found between compressive strength of lime mortars at 7 days and the sum of soluble $SiO_2 + Al_2O_3$ for a vitreous nickel slag, a poorly granulated slag and a fly ash sample. $Ca(OH)_2$ and C-S-H were found to be the main hydration products.

Work by Baragano and Rey (68) on copper slags activated by lime showed the formation of calcium silicate hydrates of undetermined C/S ratio at 28 days curing time. At later stages better crystallized C-S-H was detected, together with a C_4FH_x type ferrite hydrate and 4% unreacted lime.

3.4 Fly Ash Hydration

As discussed for the various slags, cementitious hydrates are not only formed from the hydration of Portland cement minerals but by any natural and industrial materials capable of providing the components known to form the calcium silicate hydrates, calcium aluminate hydrates, calcium sulfo-aluminate hydrates, calcium alumino ferrite hydrates or calcium sulfo-aluminate-ferrite hydrates.

Crystalline minerals, commonly found in fly ashes, such as quartz, mullite ($3Al_2O_3.2SiO_2$) or sillimanite do not react with lime at room temperature. However, sileceous and aluminous materials in fly ashes are largely present in non-crystalline form. Given their small particle size the fly ashes can hydrate at a slow rate in alkaline solutions to furnish silica and alumina for reaction with lime leading to the formation of cementitious products.

(a) Chemical Composition, Mineralogy and Glassy Nature

There exists an intricate relationship between glass content, glass composition, overall composition, and particle shape of fly ashes. It is useful to start with a classification of fly ashes into a high-Ca (15-35%) and low-Ca (<5%) categories. The first category is the product of the combustion of lignite and subbituminous coals, the latter results from the combustion of anthracitic and bituminous coals.

The high-Ca fly ashes generally contain small quantities of C_3A as the principal crystalline mineral. This is also the most reactive mineral in Portland cement. Other minerals detected in trace amounts are

$C_4A_3\bar{S}$, $C\bar{S}$, CaO and MgO (76). Crystalline quartz, mullite and iron oxide may be detected as well. The high-Ca fly ashes are often categorized under Class C since their percentage of major non-calcium oxides although in excess of 50% is relatively low. The crystalline phases in a high-Ca fly ash are often reactive, imparting cementitious behaviour witnessed by quick-setting behaviour, and rapid formation of C_4AH_{13}, $C_4A\bar{S}H_{18}$, and ettringite.

Because of the high Ca-content, the Class C fly ashes have a composition and reactivity of their glassy phase which can be considered to resemble those of the calcium alumino-silicate glass phase in granulated blast-furnace slags. It has been found that Portland cement high-Ca fly ashes mixtures show hydration properties similar to those of Portland cement granulated blast furnace slag mixtures.

The low-Ca fly ashes, on the other hand, contain high proportions of alumino silicate glass. The principal crystalline phases are α-quartz, mullite, sillimanite, hematite and magnetite (77,78). These crystalline phases, often encapsuled within solid glassy spheres are non-reactive unlike the crystalline phases of the high-Ca fly ashes. The low-Ca fly ashes often qualify as class F, their combined percentage of major non-calcium oxides being generally in excess of 70%.

(b) Particle Size/Surface Area

Fly ashes consist of largely vitreous spheres of sizes from under 1 µm to as large as 100 µm although most of the material is under 20 µm (75). There is some evidence that high-Ca fly ashes show a finer particle size distribution than low-Ca fly ashes (78).

Blaine surface areas are typically of the order of 200-300 m^2/kg Blaine but BET (single point) nitrogen adsorption values have been found in the range 1,650-2,670 m^2/kg suggesting a high degree of surface irregularity including numerous surface pores and free carbon (78).

(c) Particle Composition and Shape

Unlike granulated slags where the particles have a uniform glass composition throughout a sample, fly ash particles show great variation in chemical composition and mineralogical composition. Particle shapes very considerably although several categories may be distinguished. Lauf (80) and Fisher et al.(81) have grouped fly ash particles into seven categories:

(1) Solid glass spheres, mostly transparent but may be partially devitrified. Small gas bubbles may be present.

(2) Coke particles, irregularly shaped and generally >300 µm.

(3) "Cenospheres" and "plerospheres" are hollow particles, cenospheres are empty while plerospheres contain smaller particles inside.

(4) "Magnetite" spheres, highly reflective and optically isotropic. The light phase is a spinel, similar but not identical to magnetite; possibly a ferrite. The dark phase is optically anisotropic, possibly mullite. They have been referred to as "ferrospheres". Their size is typically <22 µm.

(5) "Dermaspheres" containing striking radial inhomogeneities indicative of the deposition of a glassy layer on a pre-existing crystalline nucleus.

(6) Irregular silicate masses representing imperfect plerospheres or agglomerations thereof.

(7) Other crystalline aggregates, generally spherical, sometimes with a very thin but incomplete outer glassy layer.

ORF

(d) Factors in Hydration

Since fly ash particles vary considerably in chemical and mineralogical composition within a sample no simple hydration mechanism along the lines proposed for blast-furnace slag by Tanaka et al (74) for example, can be poposed.

Instead the generalized picture for the activity of mineral admixtures to concrete poposed by Mehta will be presented here (76). According to Mehta the main effects associated with the pozzolanic and cementitious reactions of Portland cement-mineral admixture hydration are:

- Strength and permeability of hardened concrete,
- Resistance to thermal cracking,
- Alkali-silica expansion,
- Sulfate attack.

Strength and Permeability:

It is often found that the addition of a mineral admixture to Portland cement lessens the water demand in concrete formation. The effect of the addition, of a particle size distribution typically of the order of 1 to 20 µm, can be anticipated to reduce the volume of voids in a concrete mixture. The result is that less water is required to produce a cement of a given consistency.

Thus, Berry and Malhotra (82) report that a 30% substitution of fly ash for cement was found to reduce the water requirement by about 7% at constant slump. In some cases, however, an increase in water demand is observed. This has been noted for coarse fly ashes, fly ashes with high loss-on-ignition (>10%), or for mineral admixtures of extremely fine particle size, such as condensed silica fume or rice husk ash.

Mehta (76) lists two factors which adversely affect both strength and impermeability of concrete. These are:

- the presence of large voids in the hydrated cement paste,
- the microcracks at the aggregate-cement transition zone.

The effect of the addition of a mineral admixture to the hydrated cement paste will be to decrease the number of large voids. It has been found that the volume of large voids (>100 µm) but not the total porosity of the hydrated paste was inversely correlated with strength (83). The mechanism of pore refinement, however, is not entirely clear. Regourd et al.(84) observed that compared to the C-S-H phase in hydrated Portland cements, a less compact C-S-H is found in well-hydrated Portland pozzolan cements. Thus, the increase in strength and impermeability is explained by the conversion of high density phases and large voids to low density products and small voids.

The transition phase between the aggregate and hydrated cement paste is generally less dense than the paste and contains a great number of plate-like $Ca(OH)_2$ crystals with c-axis perpendicular to the aggregate surface. Two properties of the transition phase are important, thickness and the degree of orientation of the calcium hydroxide crystals. It has been observed (85) that the addition of a silica fume or a lignite fly ash reduced the degree of orientation of the calcium hydroxide crystals while the addition of a condensed silica fume also decreased the thickness of the transition phase. The latter also reduced the consistency and setting time of the mortar. A bituminous coal fly ash, on the other hand, increased both the thickness of the transition phase and the degree of orientation at the same hydration age (28 days). The consistency and setting characteristics of the mortar were not affected in this case. It was concluded that silica fume or lignite fly ash can be expected to show better mechanical properties than the corresponding products to which bituminous ash was added.

Thermal Cracking:

The replacement of Portland cement by fly ash has been found to improve durability by reducing thermal cracking. The reduction in temperature rise is often proportional to the replacement level. At the same time, the heat of hydration of the portland cement can be utilized to increase the rate of reaction of the mineral admixture.

In this respect, it is worthwhile to point out that high-Ca fly ashes may not be as effective as low-Ca fly ashes in reducing heat of hydration since the former have self-cementing properties and thereby contribute to early heat evolution (86).

Sulfate Attack:

A correlation has been observed between the sulfate resistance of cement and its Al_2O_3 content. It has been noticed that a fly ash of relatively low Al_2O_3 content (15%) exhibited strength gain of 8% while a high-Al_2O_3 fly ash (30%) exhibited as 23% strength loss in an accelerated test to evaluate sulfate resistance (87). Similar trends have been observed for the sulfate resistance of high-Al_2O_3 European and low-Al_2O_3 American blast-furnace slags (88).

Alkali-Silica Reactions:

Expansion and cracking in concrete is caused by the reaction between the alkaline solution of a high-alkali Portland cement (>0.6% Na_2O eq.) and certain forms of silica in aggregate. The replacement of part of the portland cement by a mineral admixture is effective in reducing the alkali-silica reaction presumably because the amount of available alkali has been reduced. It is also possible that the mineral admixtures compete with the aggregate for the alkali released since they themselves contain substantial amounts of silica and have a fine particle size and high surface area when compared with the aggreates.

Thus, according to Berry and Malhotra (82) a 75% reduction in expansion is achieved when 36 to 48% of the volume of high-alkali Portland cement was replaced by fly ash.

On the other hand, Mehta (87) and Diamond (88) observed that the addition of some high-Ca fly ashes containing large amounts of soluble alkali sulfates may increase rather than decrease the alkali-silica activity.

Corrosion of Steel in Concrete:

Corrosion of steel in concrete is usually initiated by a reduction of the alkalinity of the cement paste by atmospheric CO_2. The presence of about 20% $Ca(OH)_2$ in hydrated Portland cement ensures the reserve basicity required for the protection of steel. It is believed that about 25% reactive silica in a Portland-pozzolan mixture is enough to consume all available $Ca(OH)_2$ from Portland cement hydration.

Other workers (87,89) reject the relationship between the resistance to carbonation of concrete and the amount of calcium hydroxide in the pore solutions since mature portland cement paste contain little or no calcium. Mehta (90) proposes, therefore, that the resistance to carbonation is caused by physical factors, such as the permeability of the cement paste, instead. Thus, Mammohan and Mehta (90) found that cements containing 10, 20 or 30% fly ash pore size refinement led to a drastic drop in permeability from $11\text{-}13 \times 10^{-11}$ to 1×10^{-11} $cm.s^{-1}$ during the 28 to 90 day curing period.

Thus, Mehta (76) acknowledges that cementitious and pozzolanic reactions associated with by-product mineral admixtures may decrease the amount of free lime present in the cement paste on one hand but that the decrease in permeability, on the other hand may improve the overall resistance to CO_2 attack.

It seems that an assessment of the factors involved in corrosion and steel in concrete should take the following factors into consideration:

(a) OH^- Content: a reduction in alkalinity increases the likelihood of corrosion. This reduction may be caused by,

- CO_2 from the atmosphere,
- consumption by reactive silica in mineral admixtures.

Pore refinement will reduce the amount of accessible atmospheric CO_2 (favourable). However, the consumption of OH^- by reactive silica in mineral admixtures seems unfavourable.

(b) Ca^{2+} Content: The free lime is immobilized through incorporation into low-density C-S-H in the presence of fly ash. The SiO_2 for this reaction is liberated through degradation of the fly ash by OH^-. Thus, the presence of fly ash can act to (i) liberate reactive SiO_2 (ii) consume Ca^{2+}.

(c) Water Content: Presumably the corrosive action on steel takes place in aqueous solution made less alkaline by the dissolution of CO_2. The lesser water content requirement for fly ash concrete may, by itself, reduce the amount of CO_2 taken up and, thereby, lessen the corrosive action as a result.

A study of pozzolanic activity usually follows one or two approaches:

- The pozzolanic activity is evaluated from the strength development of mortar or concrete mixtures made with Portland cement-pozzolan mixtures.

- The rate of disappearance of $Ca(OH)_2$ or the rate of strength development in $Ca(OH)_2$-pozzolan pastes is followed.

Pozzolanic activity has often been correlated with specific surface area, chemical analysis, and heat treatment. Chatterji et al (90) compared the strength development characteristics and the pozzolanic activity of highly porous natural pozzolans and silica fume, as well as a fly ash and an inert control sample. The main point of interest was to compare the pozzolanic activity of the silica fume with a high effective specific surface area with that of the natural pozzolans which have a similar measured specific surface area but a much lower effective specific surface area because of high porosity. It was found that all high activity pozzolans had consumed $Ca(OH)_2$ to the same extent, in spite of their varying specific surfaces.

A consideration of the data leads to the following observations:

(i) There is very little difference between the $Ca(OH)_2$ content at 1 day for the various admixtures. Thus, at this time relatively little of the overall $Ca(OH)_2$ has been consumed.

(ii) At 3 days all admixtures show roughly the same $Ca(OH)_2$ content which is ~30% lower than that of the control.

(iii) At 28 days the high-surface area admixtures show considerably less $Ca(OH)_2$ (40-50% less) than the control and low-surface area mixtures.

It is concluded that:

(i) a substantial amount of the $Ca(OH)_2$ is not consumed (~50%) (the authors do not take this into account).

(ii) short term specific surface area is not critical.

(iii) long term (28 d) specific surface area is a dominant factor.

Chatterji et al (90) proposes that a layer of initially formed reaction products on the pozzolan grains plays a dominant role in their reaction with $Ca(OH)_2$. We do not see evidence for this. Rather it appears that the initial effect of the admixture is slow (-1 d) but becomes progressively more important. The high-surface area admixtures are particularly reactive between 1-10 d.

Costa and Masazza (91) investigated the effect of fineness of fly ashes on the strength development, lime released and heat of hydration of pozzolanic cements. It was found that the amount of free lime decreases when fly ash has been added to the Portland cement. The decrease in free lime content compared with a portland cement control increases with the fineness of the fly ash.

3.5 Assessment of Results

The major conclusions of the research on the hydration of slags and fly ashes reported to-date are:

(a) There is no unanimity concerning the issue as whether glass content is correlated with glass strength (24,25) or not (22,26).

(b) There is evidence that rapidly quenched slags are more reactive than slowly cooled slags (27-29). Aging of the slag is detrimental.

(c) Slag hydraulicity can be correlated with chemical composition. Slag hydraulicity was found to increase with increasing CaO content, particularly when the Al_2O_3 content is increased as well (17,19,20,30-35). CaO can be partially substituted by MgO and Al_2O_3 content (22). Most recent studies have shown that MgO affects slag hydraulicity in a beneficial manner.

(d) The use of moduli for the establishment of optimum glass composition has only limited value.

(e) Of the major crystalline components, akermanite is found to be more hydraulic than gehlenite or melilite solid solutions.

(f) Increasing the fineness of grinding affects strength in a beneficial manner, presumably because of increase surface area.

(g) For most blast-furnace slags hydration occurs only in the presence of activators. Strength development results from the formation of tobermorite phases (C-S-H). The effect arises from direct combination of the activator with components of the slag rather than through catalysis. The activator supplies Ca (Portland cement, lime, gypsum, $CaCl_2$), while the SiO_2 is provided through the breakdown of the slag through OH^- from $Ca(OH)_2$, NaOH or KOH. The Ca can also be supplied from the slag itself. Other, aluminum and sulphate based phases are also formed in the hydration process.

(h) The Al_2O_3 content appears to be the major favourable factor in the hydration of steel making slag. Useful hydraulic behaviour has been observed for an al_2O_3 content of about 15% (66). The rate of hydration of calcium-alumino-ferrites increases with the Al_2O_3/Fe_2O_3 ratio.

(i) Vitrification has been found to be a major factor for hydraulic activity of non-ferrous slags (69,70). A correlation was observed between compressive strength of lime-mortars (7d) and the sum of soluble SiO_2 and Al_2O_3 for a vitreous nickel-slag.

(j) The major mineral phases in low-Ca fly ashes (<5% CaO), α-quartz, mullite, sillimanite, hematite and magnetite are non-reactive in hydration. The high-Ca fly ashes, however, do contain reactive crystalline phases such as C_3A, C_4A_3S, CS, CaO and MgO. The hydration properties of Portland cement - high Ca fly ash mixtures resemble those of Portland cement - granulated blast furnace slag mixtures.

(k) The volume of large voids (>100 μm) is a major factor affecting concrete strength. The addition of fly ash will reduce the volume of these voids and, thereby, improve strength (83).

(l) It was found that surface area is probably the most important property affecting the strength of concrete (79).

(m) The degree of orientation of the $Ca(OH)_2$ crystals is reduced by the addition of lignitic fly ashes. The perpendicularity of the plate-like $Ca(OH)_2$ crystals are known to affect strength adversely. Thus, the addition of lignitic fly ashes can be expected to improve strength. Bituminous fly ashes are not as effective in this respect (85).

(n) Bituminous (low-Ca) fly ashes on the other hand can be expected to be more effective than sub-bituminous and lignitic fly ashes (high-Ca) in reducing heat of hydration and, thereby, diminishing the effects of thermal cracking. The self-cementing properties of high-Ca fly ashes will increase the heat of hydration (86).

(o) Low-Al_2O_3 fly ashes (<15%) are likely to increase strength under sulfate attack while high-Al_2O_3 fly ash (30%) will give lower sulfate resistance.

(p) Expansions resulting from alkali-silica reactions are generally reduced when Portland cement is partially replaced by fly ash. The alkali, presumably, reacts with the SiO_2 of the fly ash. On the other hand, high-Ca fly ashes may increase alkali-silica activity since they may contain large amounts of soluble alkali silicates.

(q) The presence of fly ash in concrete may affect the occurrence of corrosion both positively and negatively. The lowering of the alkalinity through the reaction of OH^- with the fly ash SiO_2 and the immobilization of the free lime through incorporation in low-density C-S-H phases will lower the resistance of steel to corrosion. The reduction in permeability and reduced H_2O content, on the other hand, will improve the resistance to corrosion.

References

1. G.M. Idorn, "Application of Flyash in the Cement and Concrete Industries", EPRI Internal Report (1981).

2. D. Ravina, "Flyash Concrete under Hot Water Conditions", Efect of Flyash Incorporation in Cement and Concrete, Proceedings, Symposium N, Materials Research Society, Annual Meeting, Boston, Mass. Nov. 16-18 (1981).

3. ASTM C150-84, Standard Specification for PORTLAND CEMENT, 1984 Annual Book of ASTM Standards, Vol. 04.02 Concrete and Mineral Aggregates.

4. R.F. Blanks and H.L. Kennedy, The Technology of Cement and Concrete, Vol.I. John Wiley & Sons Inc. (1955).

5. F.M. Lea, The Chemistry of Cement and Concrete, Chemical Publishing Co., New York (1971).

6. J. Skalny and J.E. Brophy, "Hydration of Portland and Blended Cements" Paper presented Intl. Conf. Slag and Blended Cements, Birmingham, Alabama, 18-19 Feb. (1982).

7. H.R. Stewart and J.E. Bailey, "Microstructural Studies of the Hydration Products of Three Tricalcium Silicate Polymorphs" Journal of Materials Science, 18, 3686-3694 (1983).

8. D.M. Roy and G.M. Idorn "Hydration, Structure and Properties of Blast Furnace Slag Cements, Mortars and Concrete" ACI Journal, 444-457 (1982).

9. E.E. Berry, The Cementitious Properties of Slags - A Critical Review, Final Report CANMET Project No. 410104, Energy, Mines and Resources, Canada (March, 1982).

10. J. Skalny, I. Jawed and H.F.W. Taylor, Studies on Hydration of Cement-recent developments, World Cem. Techn., 183-195 (1978).

ORF

11. L.S.D. Glasser, E. Lachowski, K. Mohan and H.F.W. Taylor, Paste Hydration of C_3S. Paper presented at the 80th Annual Meeting of the American Ceramic Society, Detroit, Michigan (May 6-11, 1978).

12. P.K. Mehta, "Sulphate Resistance of Blended Portland Cements containing Pozzolans and Granulated Blast Furnace Slag", Proc. V Int. Symp. Durability of Concrete, Monterrey, Mexico, March 1981.

13. D. Manmohan, and P.K. Mehta, "Influence of Pozzolanic, Slag and Chemical Admixtures on Pore Size Distribution and Permeability of Hardened Cement Pastes", Cement, Concrete and Aggregates, 3,63-67, 1981.

14. P.K. Mehta and O.E. Gjov, "Properties of Portland Cement Concrete Containing Fly Ash and Condensed Silica Fume", in press.

15. P.K. Mehta, "Studies on Blended Portland Cements Containing Santorin Earth", Cem. and Concr. Res. 11,507-518, 1981.

16. R.F. Feldman, "Pore Structure Formation During Hydration of Fly-Ash and Slag Cement Blends", paper presented at Materials Res. Soc. Annual Meeting, Boston 16-19 Nov, 1981.

17. R.D. Hooton, "Pelletized Slag Cement: Hydraulic Potential and Autoclave Reactivity" Ph.D. Thesis, McMaster University, Hamilton, Ontario (1981).

18. F. Keil (1954), "Slag Cements", Proceedings of the Third International Conference on the Chemistry of Cement. London (1952), 530-571.

19. W. Kramer (1962), Blast-furnace slags and slag-cements, Proceedings of the Fourth International Symposium on the Chemistry of Cement, Washington, D.C. (1960), 2,957-973.

20. F. Schroder (1969). Slags and Slag cements. Proceedings of the Fifth International Symposium on the Chemistry of Cement, Tokyo (1968), 4,149-199.

21. V. Satarin (1974). Slag portland cement, Preprint, The Sixth Intern. Congress on the Chemistry of Cement, Moscow, 1974, 51pp.

22. H.G. Smolczyk (1980). Slag structure and identification of slags, Proceedings of the Seventh International Congress on the Chemistry of Cement, Paris (1980), 1(III), 3-17.

23. R.H. Mills, The case for separate grinding and batching of blast furnace slag and portland cement, Proceedings of a Seminar on Energy and Resource Conservation in the Cement and Concrete Industry, Ottawa, Paper 3.3, 1-3 (1976).

24. H.E. Schwiete and F. Dolbor, The effect of the cooling conditions and the chemical composition on the hydraulic properties of haematitic slags (in German), Forschungsbericht des Landes Nordrhein - Westfalen, No.1186 (1963).

25. R.D. Hooton and J.J. Emery, Glass Content Determination and Strength Development Predictions for Vitrified Blast Furnace Slag, Paper SP79-50 presented at the 1st Intl. Conf. on the Use of Fly Ash, Silica Fume, Slag and Other Mineral By-Products in Concrete, Montebello, Canada, July 31-Aug. 5, 1983.

26. E. Demoulian, P. Gourdin, F. Hawthorn and C. Vernet, Influence of slags chemical composition and texture on their hydraulicity (in French), Proc. of the Seventh Int. Cong. on the Chemistry of Cement, Paris, 1980, Vol.2(III), 89-94.

27. P. Fierens and P. Poswick, Etude Cinetique de l'hydration de laitiers synthetiques, Silicates Ind., 235-245 (1977).

28. P. Fierens, P. Poswick and J.P. Verhaegen, Influence du traitment thermique sur les characteristiques des centres excites de constituants de laitiers de hauts-fourneaux, Silicates Ind., 253-258 (1975).

29. P. Fierens, P. Poswick and J.P. Verhaegen, Influence du traitment thermique de la gehlenite sur la vitesse de son hydration en milieu alcalin, Silicates Ind., 401-406 (1976).

30. I.I. Kholin and S.M. Royak, Slag Cements in the USSR, Proc. of the Fourth Intl. Symposium on the Chemistry of Cement, Washington 1960, U.S. Dept. of Commerce, National Bureau of Standards, Monograph 43, Vol.II, 1057-1065.

31. F. Keil, Hochofenschlacke, 2. Aufl. Dusseldorf, Verlag Stahleisen (1963).

32. R.W. Nurse, Slag Cements in H.W.F. Taylor's "The Chemistry of Cements", Vol.2, 36-37, Academic Press, London and New York (1964).

34. P. Javelle and P. Ponteville, Characteristiques et emplois des laitiers de hauts fourneaux, Association technique de la Siderurgie Francaise, Comm. des Ingenieurs de Hauts Fourneaux, IRSID, VSP 66-RL 04 (Fevrier 1966).

35. J.C. Yang, Chemistry of slag-rich cements, Proc. of the Fifth Int. Symp. on the Chemistry of Cement, Tokyo 4,296-309 (1969).

36. D. Heyl, Einflub des MgO-Gehaltes der Schlacke auf die Betriebdaten des Hochofens, insbesondere auf die Entschwefelung, Diplom-Arbeit, Bergakademie Clausthal, TH (1959).

37. A. Oelschlager, Hochofenschlacke uit hohem Magnesium-oxydgehalt fur die Herstellung von Huttenzementen, Silikattechn. 15,288-292 (1964).

38. J. Janowski, Gesichtpunkte fur die Verwendbarkeit von Hochofenschlacken zur Zementherstellung, Cement-Wapno-Gips 16, 89-97 (1961) in Polish.

39. A. Schillak, die Verbesserung der hydraulischen Eigenschaften von Hochofenschlacken durch Aktivierung der Schlacken und Auznutzung ihrer Abfallwarme, Bergakademie 11, 594-599 (1959).

40. H.E. Schwiete and K.H. Kuhle, Uber die Moglichkeiten der Verwendung von Hochofenschlacken mit hohem MgO-Gehalten fur die Zementerzeugung, Vortrag beim VDEh "Ausschuss fur Verwertung der Hochofenschlacke" (24 October, 1967).

41. N. Stutterheim, "Properties and uses of high magnesia portland cement concretes", Journal of the American Concrete Institute, 56, 1027-1045 (1960).

42. J.G.D. Steyn, "The identification, mode of occurrence and quantitative determination of crystalline phases in granulated blast furnace slag", Mineralogical Magazine, 35, 108-117 (1965).

43. J.E. Kruger, "Contributions to the Knowledge of the characteristics of vitreous blast-furnace slag with a high magnesia content", D.S. Thesis, Univ. of Pretoria, R.S.A. 175pp (1976).

44. H. Sopora, Die Zementschlacken der DDR, Baustoffind. 7(4), 114-118 (1964).

45. M. Venuat, Recherches sur quelques laitiers particuliers, Rev. Mat. Const., 602, 494-502 (1965).

46. R. Kondo, Discussion of: Blast-furnace slags and slag cements (by W. Kramer). Proceedings of the Fourth Int. Symposium on the Chemistry of Cement, Washington D.C. 2, 973-975 (1960).

47. H. Sopora, Bewertung von Hochofenschlacken fur die Zementherstellung im Betriebslaboratorium, Silikattechn. 10(7), 361-363 (1959).

48. S. Solacolu and P. Balta, Les proprietes hydrauliques des laitiers des haut fourneau dy systeme $MgO-CaO-Al_2O_3-SiO_2$ contenant du manganese et du soufre, Rev. Mat. Constr., 583, 95-110 (1964).

49. F. Keil and F. Gille, Hydraulische eigenschaften basischer glaser mit der chemischen zusammensetzung der gehlinit und akermanits, Zement-Kalk-Gips 2, 229-232 (1949).

50. P. Terrier, Research into the hydraulicity of granulated blast-furnace slags (in French). ILAMS Informations 8(1), 1-6 (1973).

51. R.P. Gupta, Utilization of pelletized slags, M. Eng. Thesis, McMaster University (1976).

52. A. Komar, Building Materials and Components (Eng. transl.) Mir Publishers, 490pp, Moscow (1974).

53. J.C. De Langavant, Considerations theoretiques sur la nature du laitier de cimenterie. Revue des Materiaux de Construction et de Travaux Publics 401, 381-411, 425 (1949).

54. M. Cheron and C. Lardinois, The role of magnesia and alumina in the hydraulic properties of granulated blast furnace slags, Proc. of the Fifth Int. Symp. on the Chemistry of Cement, Tokyo 4, 277-285 (1969).

55. R.D. Coale, C.W. Wolhuter, P.R. Jochens and D.D. Howat, "Cementitious Properties of Metallurgical Slags", Cement and Concrete Research, 3, 81-92 (1973).

56. T.W. Parker and R.W. Nurse, Investigations on granulated blast-furnace slags for the manufacture of portland blast-furnace cement, National Building Studies, Techn. Paper 3, D.S.I.R, HSMO, London (1949).

57. R. Kondo and S. Ueda, Kinetics and mechanisms of the hydration of cements, Proceedings of the Fifth Int. Symposium on the Chemistry of Cement, Tokyo 1968, 2, 203-248 (1969).

58. K. Akatsu, I. Ikeda and K. Sadatsume, Practical properties of slag cement prepared with a series of glasses of the gehlenite-akermanite system. Review of the 32nd Mtg of the Cement Ass. of Japan, 57-58 (1978).

59. J.J. Emery, R.P. Cotsworth and R.D. Hooton, Pelletized blast furnace slag. Proceedings of a Seminar on Energy Resource Conservation in the Cement and Concrete Industry, Ottawa, Paper 4.1, 1-23 (1976).

60. I. Teoreanu and M. Georgeseu, The behaviour of synthetic and industrial blast-furnace slags in the presence of activators (in German), Zement-Kalk-Gips 27(6), 308-312 (1974).

61. J. D'Ans and H. Eick, Investigations on the setting process of hydraulic blast furnace slag, Zement-Kalk-Gips 7, 449-459 (1954).

62. I. Teoreanu, M. Georgescu and A. Puri, Hydrated phases in slag-water-activator systems, Proc. 7th Int. Conf. Chemistry of Cement, Paris, paper III-99 (1980).

63. S.A. Abo-El-Enein, M. Daimon, S. Ohsawa and R. Kondo, "Hydration of Low Porosity Slag-Lime Pastes", Cement and Concrete Research, 4, 299-312 (1974).

64. F. Sorrentino and C.M. George, "Etude de l'hydration des laitiers d' acierie L.D.", Silicates Ind., 42, 249-254 (1977).

65. C.M. George and F. Sorrentino, Valorization of basic oxygen steel slags, Proc. 7th Int. Congr. Chemistry of Cements, Paris, Paper III-140 (1980).

66. M. Conjeaud, C.M. George and F. Sorrentino, "A new steel slag for cement manufacture: Mineralogy and hydraulicity", Cement and Concrete Research, 11, 85-102 (1981).

67. I. Gaballah, F. Jeannot, L.C. Dufour and Gleitzer, Reactivite de l'aluminate et du silicate de fer dans des reactions d' oxydo-reduction, Silicates Ind., 41, 427-438 (1976).

68. J.R. Baragano and P. Rey, The study of a non-traditional pozzolan: Copper Slag, Proc. 7th Int. Congr. Chemistry of Cements, Paris. Paper III-37 (1980).

69. E.G. Thomas, Cemented fill practice and research at Mount Isa, Austral. Inst. Min. and Metall. Proc. No. 240, 33-51 (1971).

70. E.G. Thomas, A review of cemented agents for hydraulic fill, Austral. Inst. Min. and Metall. Jubilee Symp. Mine Filling, Mount Isa: 65-73 (1973).

71. J. Laneuville, Can. Patent 963482 (St. Lawrence Cement Co.) June 14, 1972.

72. J. Laneuville, The hardening of nickel slags, Proc. Int. Congr. Chemistry of Cements, Paris. Paper III-52 (1980).

73. M. Regourd, Structure and Behaviour of Slag Portland Cement Hydrates, The 7th Int. Symposium on the Chemistry of Cement, Paris. Vol. I, III-2/10 (1980).

74. H. Tanaka, Y. Totani and Y. Saito, Structure of Hydrated Glassy Blast furnace Slag in Concrete, Paper SP79-51, presented at the 1st International Conf. on the Use of Fly Ash, Silica Fume, Slag and Other Mineral By-Products in Concrete, Montebello, Canada, July 31-Aug.5,1983.

75. S. Nagataki, M. Takada and E. Sakai, Relation Between Hydration of Slag Sand and Mechanical Properties of Concrete, Paper SP79-57, presented at the 1st Int. Conf. on the Use of Fly Ash, Silica Fume and Other Mineral By-Products in Concrete, Montebello, Canada, July 31-Aug. 5, 1983.

76. P.K. Mehta, Pozzolanic and Cementitious By-products as Mineral Admixtures for Concrete - A Critical Review, Paper SP 79-1, presented at the 1st Int. Conf. on the Use of Fly Ash, Silica Fume and Other Mineral By-Products on Concrete, Montebello, Canada, July 31-Aug. 5, 1983.

77. S. Diamond, The Characterization of Fly Ashes, Proc. of the Symp. on Effects of Fly Ash Incorporation in Cement and Concrete, Materials Research Soc. Ed. S. Diamond, 12-13 (1981).

78. B. Montureux, H. Hornain, E. Gautier and M. Regourd, Comparison of the Reactivity of Different Pozzolans, Proc. 7th Int. Cong. on the Chemistry of Cement, Paris, 3, 110-115 (1980).

79. P.K. Mehta, Testing and Correlation of Fly Ash Properties with Respect to Pozzolanic Behaviour, Electric Power Research Institute Research Project 1260-26, Final Report, Jan. 1984.

80. R.J. Lauf, Microstructures of Coal Fly Ash Particles, Am. Ceram. Soc. Bull., 61(4), 487-490 (1982).

81. G.L. Fisher, B.A. Prentice, D. Silberman, J.M. Ondov, A.H. Biermann, R.C. Ragaini and A.R. McFarland, "Physical and Morphogical Studies of Size-Classified Coal Fly Ash", Environ. Sci. Technol., 12(4), 447-451 (1978).

82. E.E. Berry and V.M. Malhotra, "Fly Ash for Use in Concrete - A Critical Review", ACI Journal, 2(3), 59-73 (1982).

83. P.K. Mehta, "Studies of Blended Cements Containing Santorin Earth", Cement and Concrete Research, 11(4), 507-518 (1981).

84. M. Regourd, B. Mortureux and E. Gautier, Hydraulic Reactivity of Various Pozzolans, Proceedings, Fifth Int. Symp. on Concrete Technology, University of Nuevo Leon, Mexico, 1-14 (March, 1981).

85. A. Charles-Gilbergues, J. Grandet and J. Ollivier, Modifications in the Cement Paste-Aggregate Interfacial Region Due to Addition of Fly Ash or Silica Fume in Portland Cement Mortar. Personal comm. in ref. 76.

86. S. Diamond and F. Lopez-Flores, Comparative Studies of the Effect of Lignitic and Bitumuous Fly Ashes in Hydrated Cement Systems, Proceedings, Symposium on Fly Ash. Incorporation in Cement and Concrete, Materials Research Society, Ed: S. Diamond, 112-113 (1981).

ORF

87. P.K. Mehta, Performance Tests for Sulfate Resistance and Alkali-Silicate Reactivity of Hydraulic Cements, Durability of Building Materials and Components, ASTM STP 691, 336-345 (1980).

88. S. Diamond, "Effects of Two Danish Fly Ashes on Alkali Contents of Pore Solutions of Cement-Fly Ash Pastes", Cement and Concrete Research, 11, 383-394 (1981).

89. F. Massazza, Structure of Pozzolans and Fly Ash, and the Hydration of Pozzolanic and Fly Ash Cements - General Report, Proceedings, 7th Int. Congr. on the Chemistry of Cements, Paris 4, 85-96 (1980).

90. S. Chatterji, M. Collepardi and G. Moriconi, Pozzolanic Property of Natural and Synthetic Pozzolans: A Comparative Study, Proceedings, 1st Int. Conf. on the Use of Fly Ash, Silica Fume, Slag and Other Mineral By-Products on Concrete, Montebello, Canada, July 31-Aug. 5, 1983, Paper SP 79-10, 1, 221-233 (1983).

91. U. Costa and F. Massazza, Some Properties of Pozzolanic Cements Containing Fly Ashes, Proceedings, 1st Int. Conf. on the Use of Fly Ash, Silica Fume, Slag and Other Mineral By-Products in Concrete, Montebello, Canada, July 31-Aug. 5, 1983. Paper SP 79-11, 1, 235-254 (1983).

ORF

POOR
QUALITY
ORIGINAL